Fisheries New Zealand
Tini a Tangaroa

Characterisation and a length-based assessment model for scampi (*Metanephrops challengeri*) on the Mernoo Bank (SCI 3)

New Zealand Fisheries Assessment Report 2019/61

I.D. Tuck

ISSN 1179-5352 (online)
ISBN 978-1-99-000874-0 (online)

October 2019

New Zealand Government

Requests for further copies should be directed to:

Publications Logistics Officer
Ministry for Primary Industries
PO Box 2526
WELLINGTON 6140

Email: brand@mpi.govt.nz
Telephone: 0800 00 83 33
Facsimile: 04-894 0300

This publication is also available on the Ministry for Primary Industries websites at:
http://www.mpi.govt.nz/news-and-resources/publications
http://fs.fish.govt.nz go to Document library/Research reports

TABLE OF CONTENTS

EXECUTIVE SUMMARY

Tuck, I.D. (2019). Characterisation and a length-based assessment model for scampi (*Metanephrops challengeri*) on the Mernoo Bank (SCI 3).

***New Zealand Fisheries Assessment Report 2019/61.* 248 p.**

A stock assessment of the Mernoo Bank (SCI 3) scampi stock has been undertaken through MPI project SCI2017-02. This work has further modified and developed an existing model for this stock, which is based on previous assessment models for other scampi stocks. Survey catchability priors were revised, with developments also relevant to other scampi assessments, and the assessment was accepted by the Shellfish Fishery Assessment Working Group (SFAWG).

A fishery characterisation was undertaken, and a CPUE index was estimated for the stock, incorporating spatial and temporal components in the fishery. The earliest model for this stock incorporated considerable depth and spatial structure, and, following preliminary investigations, the SFAWG recommended the development of a three-area three-stock model, fitting annual CPUE indices and photographic and trawl survey indices to each area. Sensitivity to natural mortality and process error on the CPUE indices were investigated as part of this model, for which MCMCs were generated with M fixed at 0.2 and 0.25. All models provided broadly consistent stock trajectories and current stock status estimates, with median estimates of SSB_{2017}/SSB_0 combined across the three stocks ranging from 62% to 78%. All models estimated a series of above average YCSs in the mid to late 1990s, below average YCSs during the 2000s, and above average YCS in more recent years, consistent with recent increases in CPUE and survey indices. Projections out to 2021 suggested that SSB would remain well above 40% SSB_0 with future catches up to 20% higher than the current TACC.

1. INTRODUCTION

This study reports a fishery characterisation for the Mernoo Bank (SCI 3) scampi stock and applies a previously developed Bayesian, length-based, two-sex population model to this stock. The first attempt at developing a length-based population model for any scampi stock was conducted for SCI 1 (Cryer et al. 2005), which was implemented using the general-purpose stock assessment program CASAL v2.06 (Bull et al. 2004). This model for SCI 1 was developed further and the same model structure was also applied to SCI 2 in a later project (Tuck & Dunn 2006). The model was first applied to the SCI 3 stock in 2011 (Tuck 2013), although the SCI 3 assessment was not accepted by the Shellfish Fishery Assessment Working Group (SFAWG) until 2016 (Tuck 2016b). The current study used CASAL v 2.30 (Bull et al. 2012), incorporating developments in the model implementation and structure based on suggestions raised at the MFish-funded Scampi Assessment Workshop (Tuck & Dunn 2009), and at subsequent Ministry for Primary Industries SFAWG meetings. Assessments for all the main scampi stocks have been accepted in recent years using this general model structure (Tuck 2015; Tuck 2016a; Tuck 2016b).

We describe the available data and how they were used, the parameterisation of the model, and model fits and sensitivities. This report fulfils Ministry for Primary Industries project SCI2017-02 "*Stock assessment of scampi*"; the objective of this project was to conduct a stock assessment, including estimating yield for SCI 3 in the 2017–18 fishing year (1 October 2017 to 30 September 2018).

1.1 The Mernoo Bank (SCI 3) scampi fishery

Scampi is fished all around New Zealand, in nine fishery management areas (Figure 1). The SCI 3 fishery is one of New Zealand's four main scampi fisheries (the others being SCI 1, SCI 2 and SCI 6A), and over the last 5 fishing years (2012–13 to 2016–17) has contributed an average of 334 tonnes annually. The average catch from the previous 5 years (2007–08 to 2011–12) was 247 tonnes, and 300 tonnes in the five years before that. The total landed catch in 2016–17 (344 tonnes) was comparable to that in 2015–16, and slightly lower than 2014–15 (Figure 2). The Total Allowable Commercial Catch (TACC) for SCI 3 is 340 tonnes, and the total TACC for all management areas is 1231 tonnes.

The spatial distribution of the targeted scampi fishing within SCI 3 is focussed in an area on the western end of the Chatham Rise, and straddles the boundary between the old Quota Management Area (QMA) 3 and QMA 4W (Figure 3). Prior to introduction into the Quota Management System (QMS) in 2004, the management area boundary between the Mernoo Bank and the Chatham Rise (QMA 3 and QMA 4) fisheries was reviewed on the basis of information on average catch rates, trends in CPUE, average size, sex ratio, bathymetry, and bycatch amount and composition (Cryer 2000) resulting in changes being introduced on 1 October 2004. The fishery parameters examined were generally similar between QMA 3 and QMA 4W but less similar for QMA 4E, and hence the former two areas were combined into SCI 3. This study also suggested that it may be appropriate to separate the Mernoo Bank / western Chatham Rise fishery from the rest of QMA 3 (Canterbury and Otago coastline), because the deep water between the two areas is a natural break between the populations; this suggestion was not adopted by managers. Minimal scampi fishing (less than 1% of SCI 3 scampi catches) takes place outside the main Mernoo Bank / western Chatham Rise area.

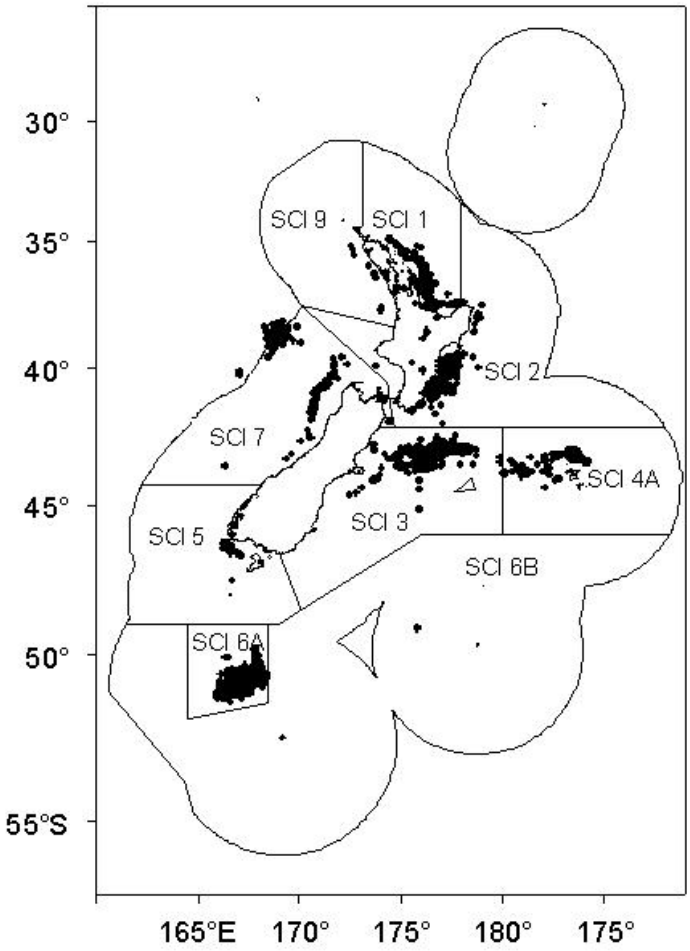

Figure 1: Spatial distribution of the scampi fishery since 1988–89. Each dot shows the midpoint of one or more tows recorded on Trawl Catch Effort Processing Return (TCEPR) forms with scampi as the target species.

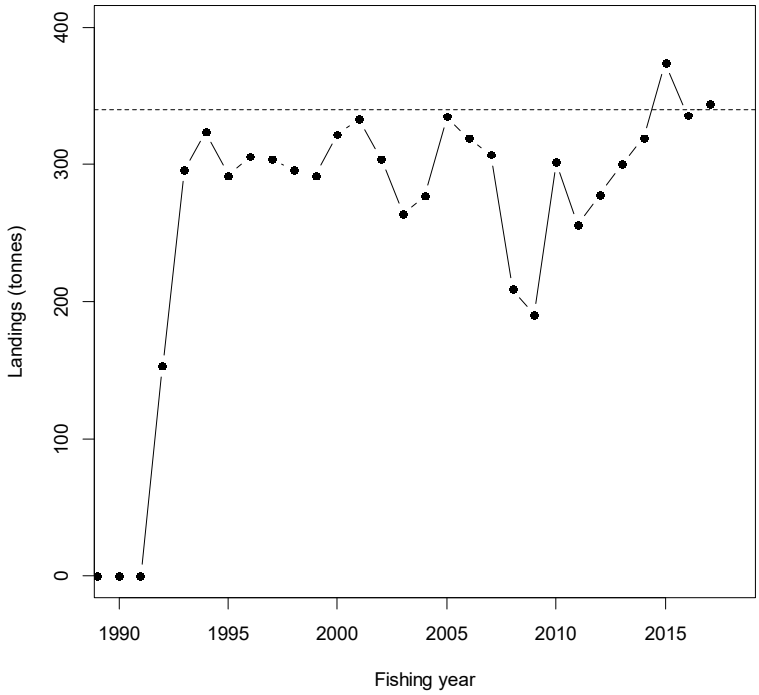

Figure 2: Time series of scampi landings from SCI 3 by fishing year (Monthly Harvest Return data). The dashed line indicates the 340 t TACC that was introduced on 1 October 2004.

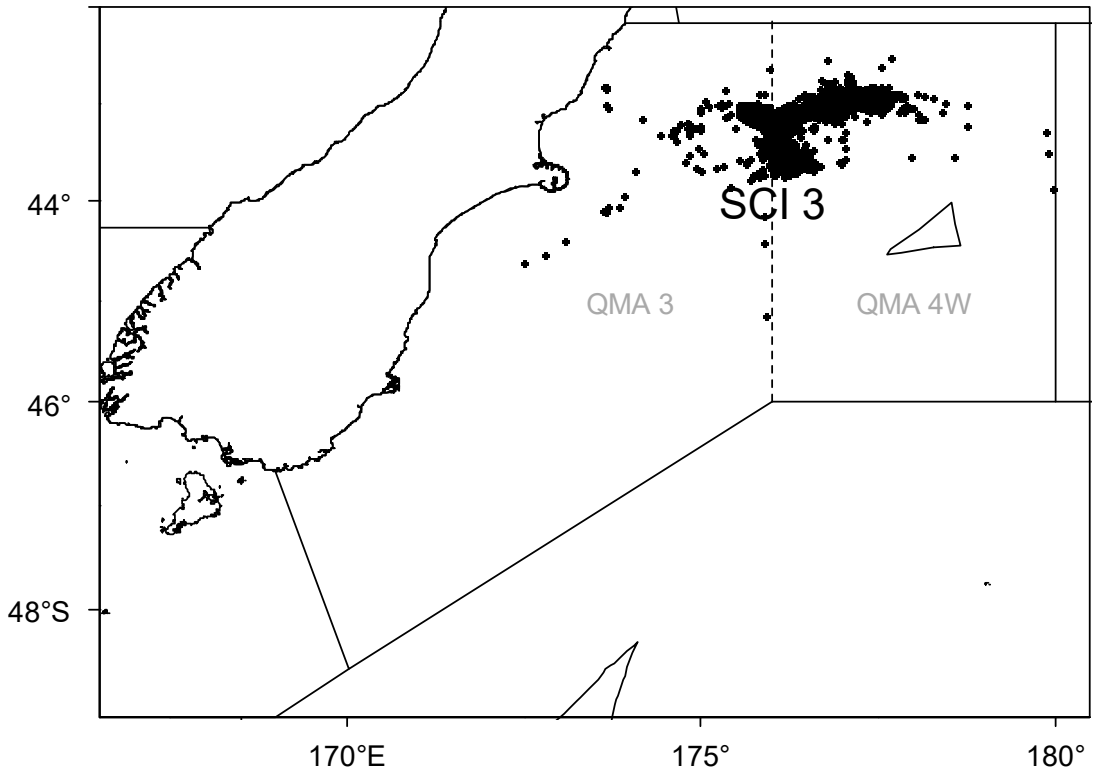

Figure 3: Spatial distribution of the scampi fishery within management area SCI 3 since 1988–89. Each dot shows the mid-point of one or more tows recorded on TCEPR with scampi as the target species. Previous (prior to the 2004–05 fishing year) scampi management areas QMA 3 and QMA 4W are also shown. The boundary between QMA 3 and QMA 4W was 176º E.

The changes to the management area boundaries mean that different parts of the SCI 3 area have different management histories. Until entry into the QMS (1 October 2004), the QMA 3 area was managed under a competitive catch limit. Individual quotas were introduced for QMA 4 in 1992–93 (allocated on the basis of the permit holders' catch in 1991–92), and maintained until October 2001 when all scampi fisheries were managed with competitive catch limits. Since October 2004, all scampi fisheries have been managed with individual quotas.

Previous fishery characterisations have been undertaken for this area; by Cryer & Coburn (2000) as separate areas (QMA 3 and QMA 4W) and by Tuck (2009; 2013; 2016b) as SCI 3. The more recent studies identified two separate fisheries within the SCI 3 fishery, one of which showed a distinct spatial shift over time (Tuck 2009).

2. FISHERY CHARACTERISATION AND DATA

2.1 Commercial catch and effort data

Scampi fishers have consistently reported catches on the Trawl Catch, Effort, and Processing Return (TCEPR) form since its introduction in 1989–90, providing a very valuable record of catch and effort on a tow-by-tow basis.

Data were extracted from the MPI TCEPR database (extract 11364), based on a request for all events from all trips where scampi (SCI) was the nominated target species, or was reported in the catch (384 754 events). From these events, 99.87 % of SCI catch was taken from SCI target events, and so only these 126 628 events were retained. Errors in TCEPR records are reducing in frequency over time, but do occur, and the raw records were groomed in the following manner. For each record, the reported data were used to estimate the duration of the trawl shot, the distance between the start and finish locations, and the midpoint between the start and finish locations. Tows with zero scampi catch were excluded (3% of SCI target events, with no trend in occurrence over time). All tows that recorded zero hours tow duration (but some scampi catch) were reset to the median tow duration for the trip. All tows with a tow distance greater than 50 km were reset to the median of the midpoint of tows on the same day, adjacent days, or the trip, depending on available data. The SCI 3 data were then extracted from this full data set on the basis of latitude and longitude. All analysis was conducted on the basis of the current management area boundaries.

Subsequent analyses were conducted on this "groomed" version of the data set (33 025 records), representing well over 99% of all scampi landings taken from SCI 3. This data set is considered to be the most appropriate to investigate patterns in the fishery, because it represents the targeted scampi fishery, and latitude and longitude data are available for spatial aspects of the analysis. Characterisations prior to Tuck (2015) have used a slightly different grooming approach, details of which are provided in Tuck (2009). Comparisons of unstandardised CPUE data for the earlier and revised grooming approaches have previously been examined (Tuck 2014). The revised grooming slightly reduces the estimated CPUE prior to 2003 (due to rounding of the haul duration data), but the medians of the annual values appear identical after this.

The distribution of fishing activity within the SCI 3 area over time is presented in Figure 4 and Figure 5. Following some exploratory fishing, the SCI 3 fishery started in 1991–92 to the east within what was then QMA 4W, but fishing started to the west in QMA 3 the following year, with the distribution of activity remaining relatively constant for a few years. In the early 2000s, the activity within QMA 4W spread further to the west, adjacent to the area fished within QMA 3, and this overall pattern continued until the 2003–04 fishing year. Following introduction to the QMS, the vessels active in SCI3 had access to all the previously fished areas (QMA 4W and QMA 3), and the pattern of effort shifted, with minimal effort having targeted scampi in the old QMA 3 area (to the west of 176° E) since this time, and effort

developing to the south of the western part of the old QMA 4W. On the basis of the patterns observed within the fishery in this main area, three sub-areas have been identified (Figure 6), each of which shows different historical fishing patterns (Table 1; Figure 7). Total annual landings for the fishery as a whole, and the subareas identified in Figure 6, and the percentage by the target scampi fishery, are presented in Table 1. Landings match the distribution of effort, with a clear shift out of subarea MO (the original QMA 3) and into MW (the western part of the original QMA 4W) in the 2004–05 fishing year. The landings data also show patterns hidden within the effort maps, with landings from MN (the eastern part of QMA 4W) reducing between 2006–07 and 2009–10, but increasing again, and reducing in MW, from 2010–11. Over 97% of the targeted scampi catch has been reported from these main areas in any year, and over 99% over all years. Boxplots of the unstandardised CPUE (Figure 8) show reasonably similar patterns over time between areas (although with slight differences in the timing of peak catch rates), with catch rates initially increasing to the late 1990s or early 2000s, declining to about 2008, and then showing an increase in the most recent years (where data are available).

Table 1: Reported commercial landings (tonnes) from the 1991–92 to 2016–17 fishing years for SCI 3, catch estimated from scampi target fishery, and breakdown by spatial areas identified in Figure 6.

		Target	%	Catch (t)			% of total			% of target
Fishing year	Landings (MHR)	catch (TCEPR)	SCI target	MN	MO	MW	MN	MO	MW	catch in main areas
1991–92	153	160	105%	155	0	2	97%	0%	2%	98%
1992–93	296	298	101%	210	81	2	71%	27%	1%	98%
1993–94	324	312	96%	250	59	2	80%	19%	1%	100%
1994–95	292	293	100%	226	65	1	77%	22%	0%	100%
1995–96	306	304	99%	225	75	2	74%	25%	1%	100%
1996–97	304	307	101%	217	73	15	71%	24%	5%	100%
1997–98	296	299	101%	214	60	25	71%	20%	9%	100%
1998–99	292	274	94%	209	58	4	76%	21%	1%	99%
1999–00	322	293	91%	215	71	5	74%	24%	2%	100%
2000–01	333	313	94%	200	71	42	64%	23%	13%	100%
2001–02	304	278	92%	191	67	20	69%	24%	7%	100%
2002–03	264	225	85%	132	59	33	59%	26%	15%	100%
2003–04	277	236	85%	176	55	5	74%	23%	2%	100%
2004–05	335	312	93%	184	0	128	59%	0%	41%	100%
2005–06	319	291	91%	106	2	182	37%	1%	63%	100%
2006–07	307	278	90%	52	0	225	19%	0%	81%	100%
2007–08	209	176	84%	75	0	101	43%	0%	57%	100%
2008–09	190	170	89%	70	0	100	41%	0%	59%	100%
2009–10	302	278	92%	82	0	196	30%	0%	70%	100%
2010–11	256	236	92%	181	0	55	77%	0%	23%	100%
2011–12	278	257	92%	191	0	65	74%	0%	25%	100%
2012–13	267	240	90%	200	0	32	83%	0%	14%	97%
2013–14	319	301	94%	257	0	40	85%	0%	13%	99%
2014–15	374	348	93%	292	0	48	84%	0%	14%	98%
2015–16	336	311	93%	284	0	26	91%	0%	8%	100%
2016–17	344	316	92%	290	0	20	92%	0%	6%	98%

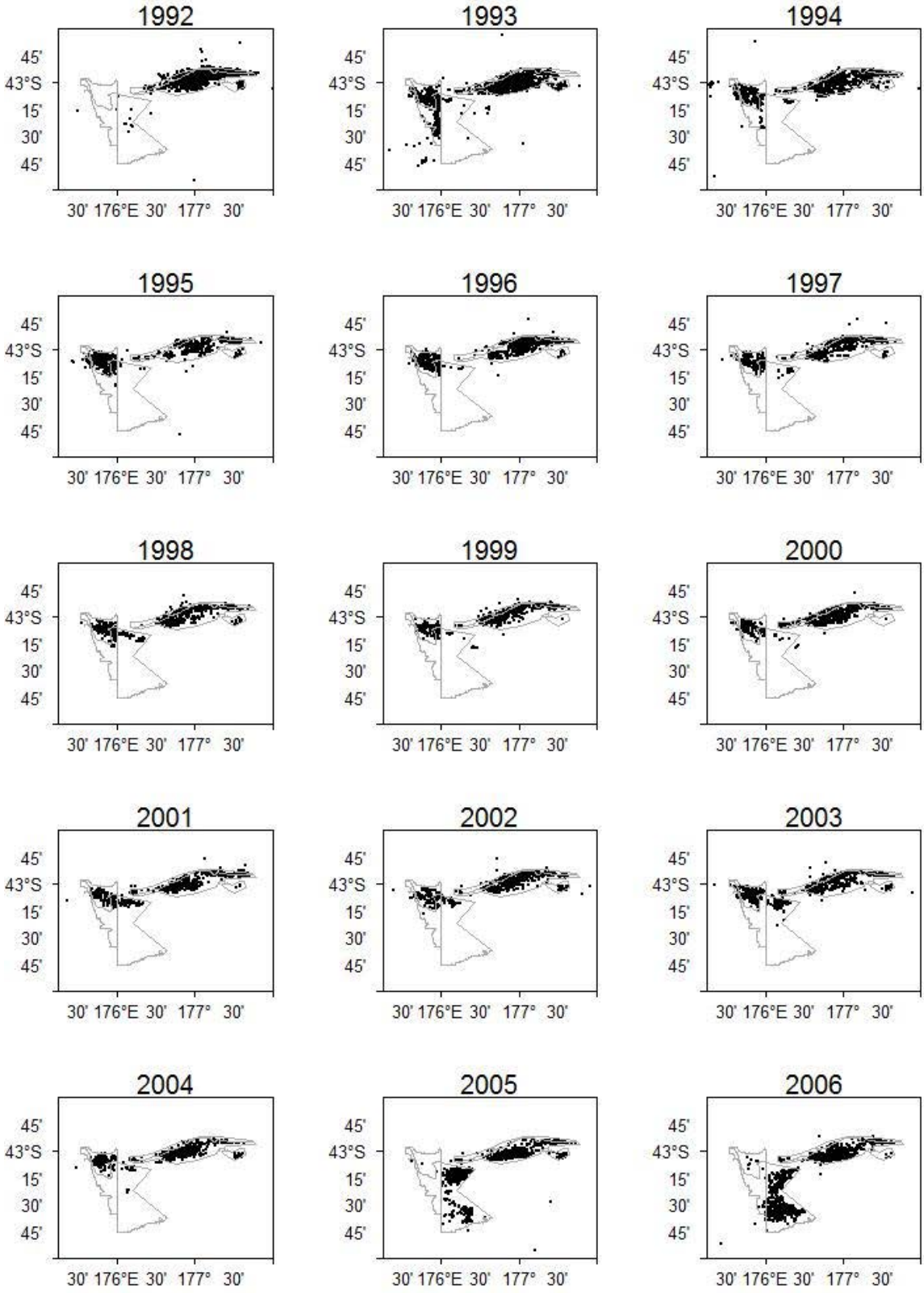

Figure 4: Spatial distribution of the main area of the SCI 6A scampi trawl fishery from 1991–92 to 2005–06. Each dot represents the midpoint of one or more tows reported on TCEPRs. Plots are labelled by their final year, i.e., 1992 represents the 1991–92 fishing year. The general area covered by the plots is indicated within Figure 5.

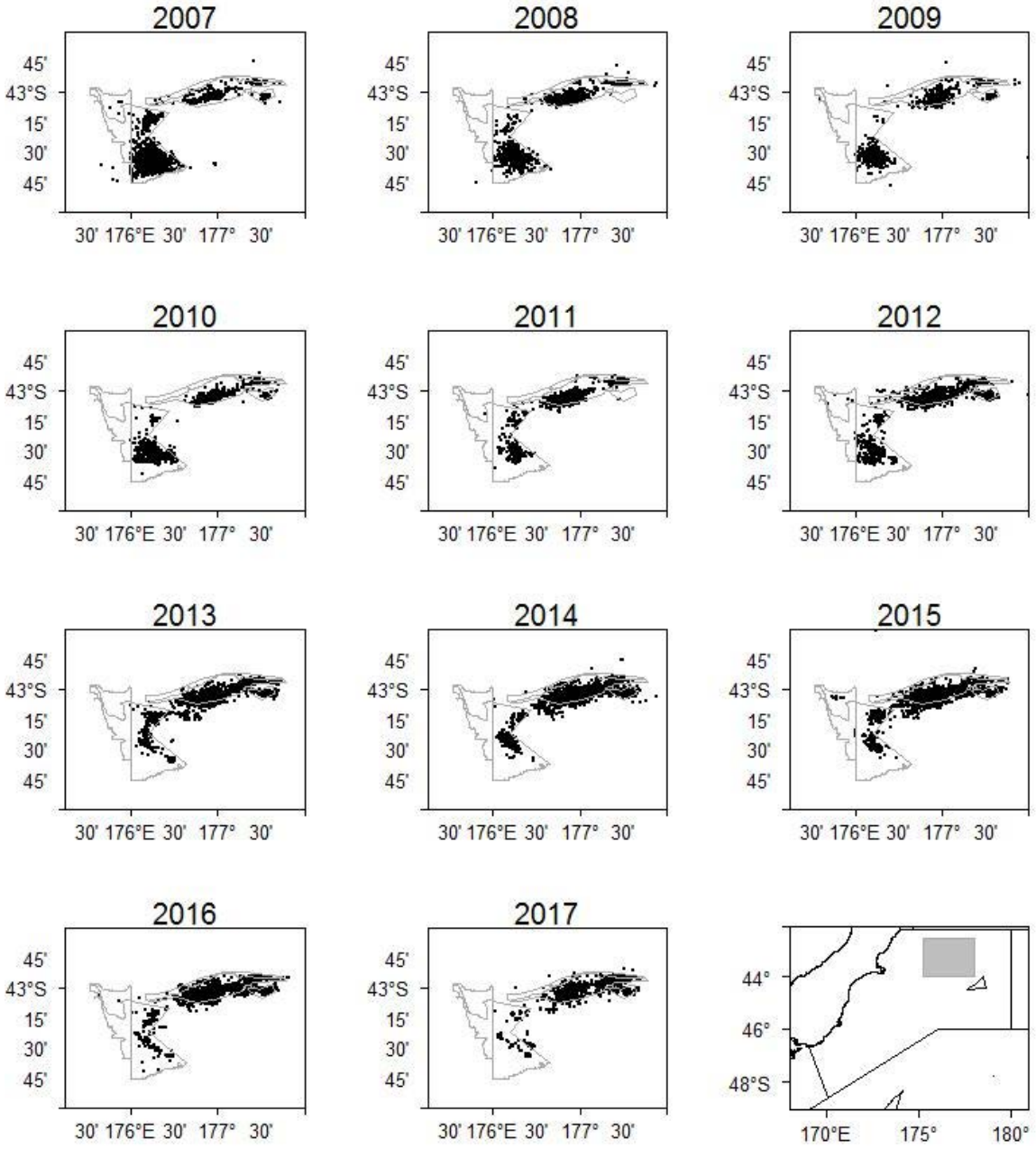

Figure 5: Spatial distribution of the main area of the SCI 3 scampi trawl fishery from 2006–07 to 2016–17. Each dot represents the midpoint of one or more tows reported on TCEPRs. Plots are labelled by their final year, i.e., 1992 represents the 1991–92 fishing year. The general area covered by the plots is indicated by the shaded box in bottom right plot.

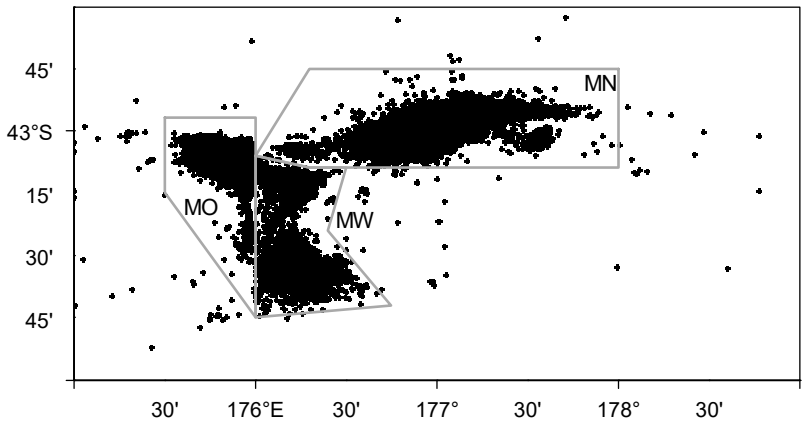

Figure 6: Sub-areas of SCI 3 used for fine-scale analysis of catch and effort. Each dot represents the mid-point of one or more tows reported on a TCEPR.

The monthly breakdown of effort and catch by subarea and fishing year (Figure 9) shows clear differences between the subareas. Subarea MN was previously managed within QMA 4W and was only managed with competitive catch limits between 2001–02 and 2003–04. During this period, catches only occurred in October, but prior to and since this time, fishing has been distributed throughout the year. Subarea MW was also previously managed within QMA 4W, and only had competitive catch limits between 2001–02 and 2003–04. Fishing was relatively sporadic prior to the competitive catch limit period, focussed in October during this period, and has been spread throughout the year since 2004–05 (with some indication of increased activity towards the end of the fishing year). Subarea MO was managed with competitive catch limits until 2004–05. Fishing was consistently focussed in October throughout this period, and there has been minimal activity in this subarea since 2004–05.

The pattern of activity in relation to depth has remained reasonably constant over time within subareas (Figure 10, Figure 11), although there is evidence of a slight shift (by about 20 m) of activity within subarea MN, with fishing prior to 2003 deeper than fishing after 2009. The depth of fishing varies between subareas, with catches from MN predominantly from the 330–400 m depth range, from MW from the 350–400 m depth range, and MO predominantly between 400–450 m. The overall shallowing of scampi fishing in SCI 3 (Figure 11) reflects the reduced activity in subarea MO.

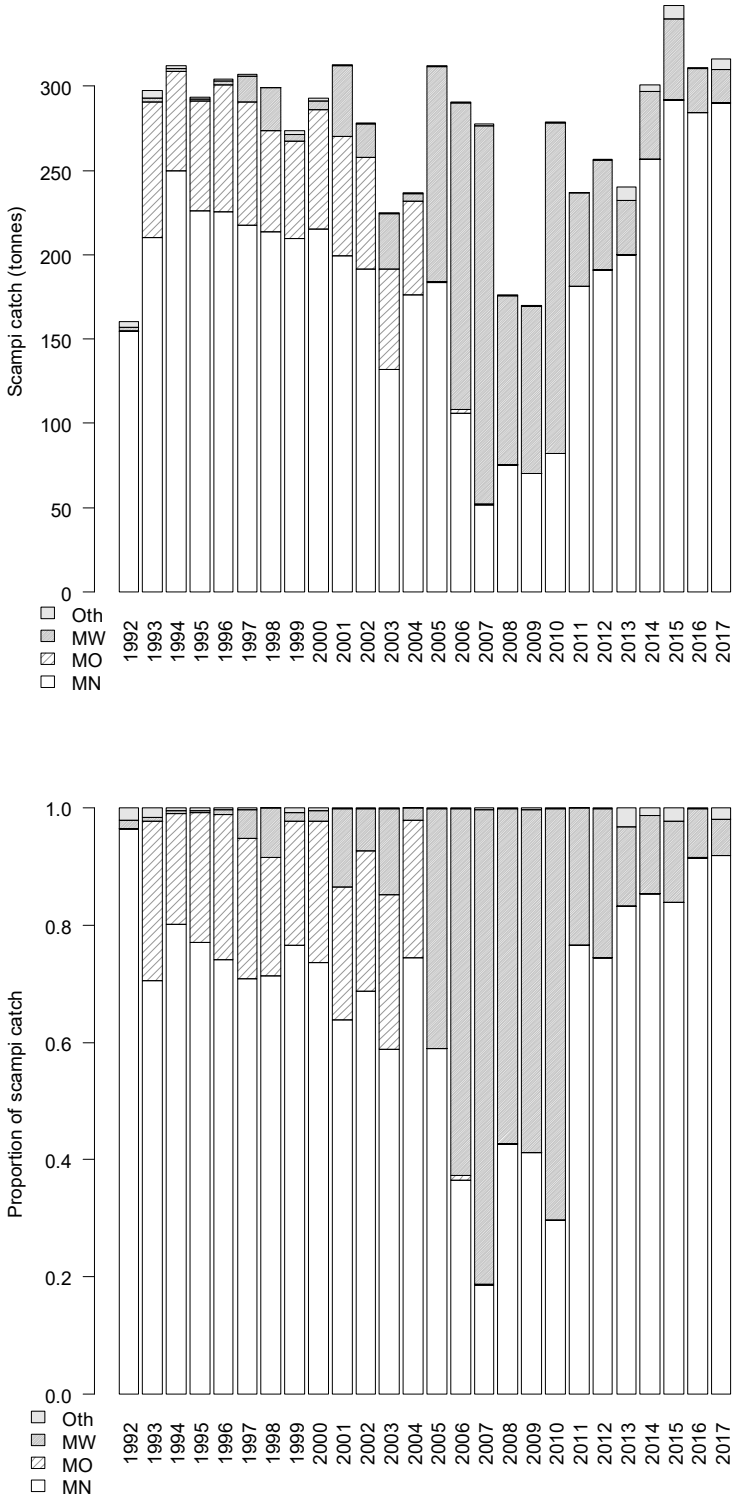

Figure 7: Barplots of scampi catch (upper plot) and catch proportion (lower plot) from SCI 3 by subarea and fishing year.

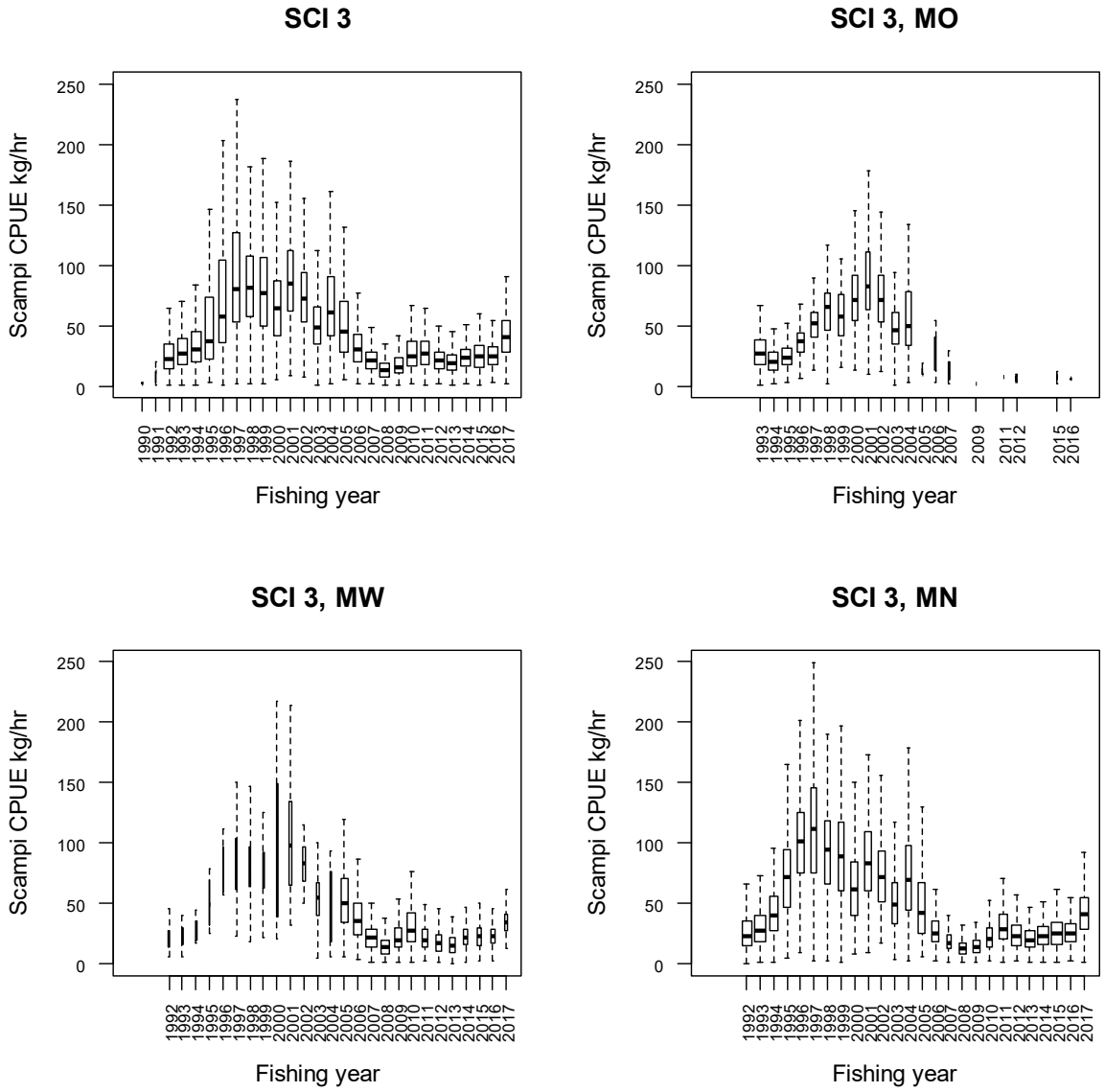

Figure 8: Boxplot (with outliers removed) of individual observations from TCEPR of unstandardised catch rate (catch (kg) divided by tow effort (hours towed, hr)) with tows of zero scampi catch excluded, by fishing year for the SCI 3 fishery, and for the three subareas identified in Figure 6. Box width is proportional to the square root of the number of observations. The solid line within each box represents the median value; the upper and lower ends of the box are the upper and lower quartiles; and the dashed lines extend out to the upper and lower adjacent values, the largest (smallest) value less (greater) than or equal to the upper (lower) quartile plus (minus) 1.5 times the interquartile range.

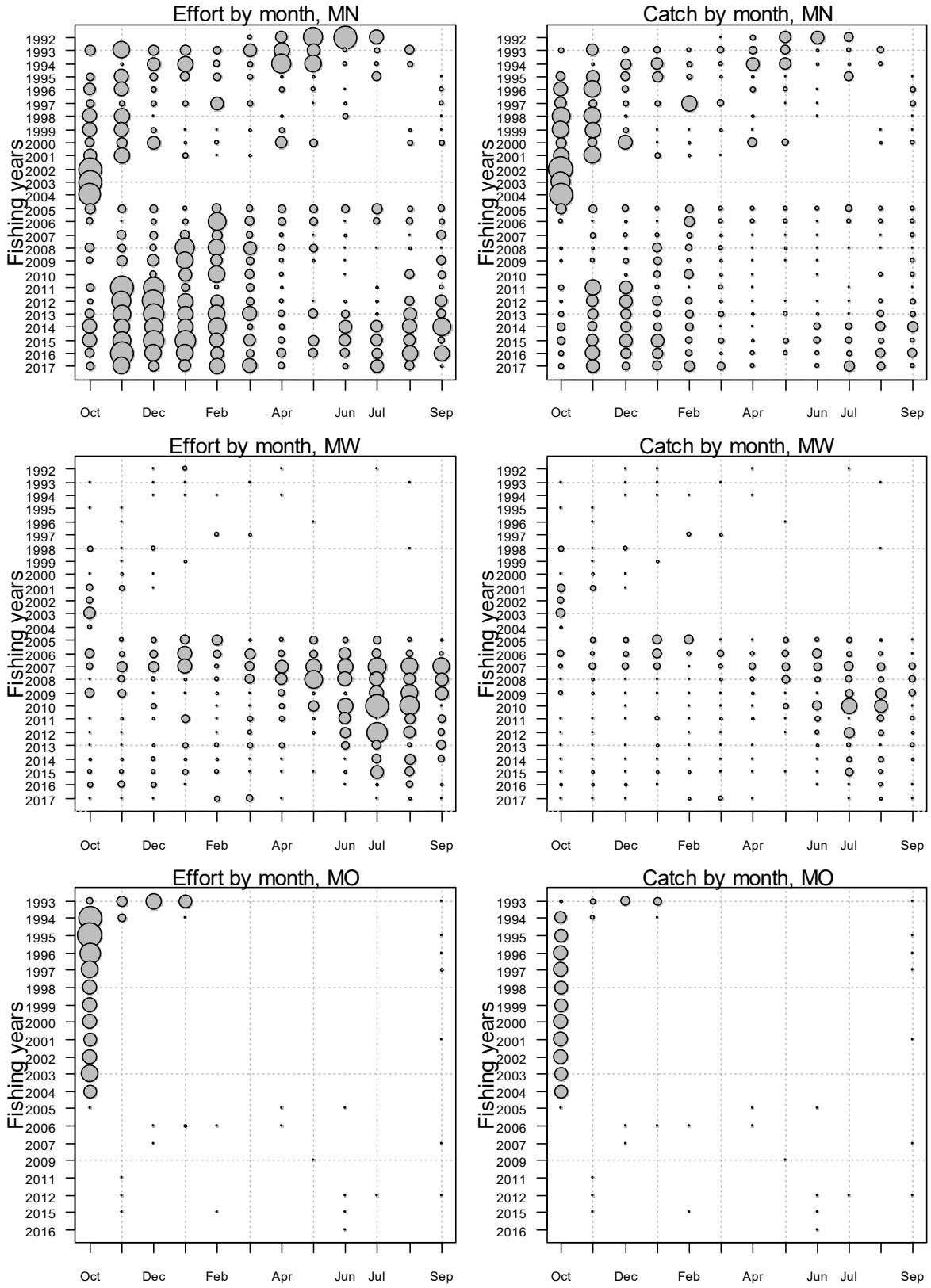

Figure 9: Monthly pattern of fishing effort (left column) and scampi catch (right column) in the scampi targeted fishery by fishing year and subarea of SCI 3. The area of the circles is proportional to the hours fished (largest circle represents 2629 hours) and the scampi catch (largest circle represents 191 tonnes), with consistent scales used for each data type.

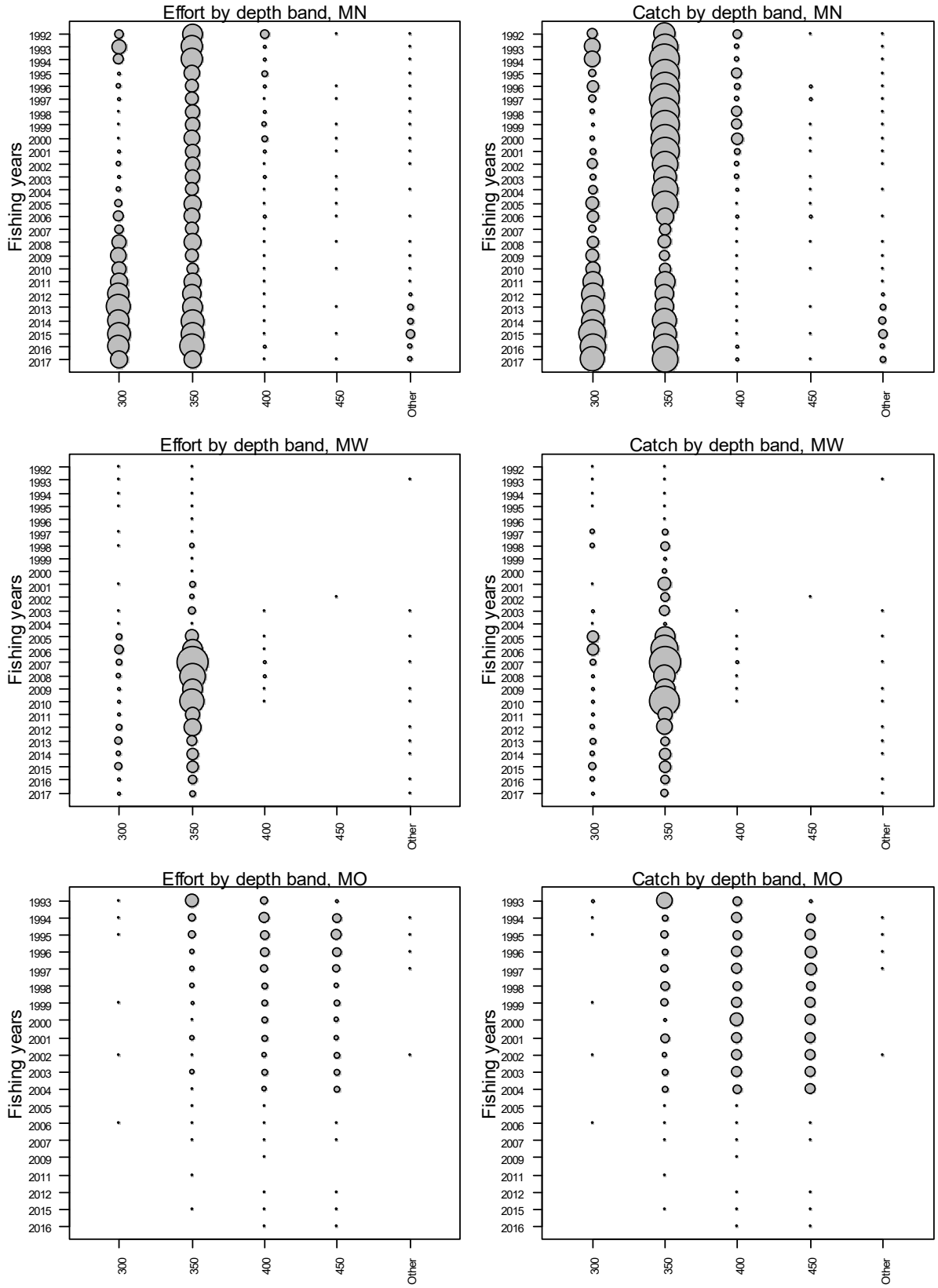

Figure 10: Annual pattern of fishing effort (left column) and scampi catch (right column) in the scampi targeted fishery by 50-m depth band and fishing year for each of the subareas of SCI 3. The area of the circles is proportional to the hours fished (largest circle represents 9515 hours) and the scampi catch (largest circle represents 209 tonnes), with consistent scales used for each data type. Depth bands are represented by their lower bound, i.e., 300 represents 300–350 m band. "Other" represents catches outside the 300–500 m depth range.

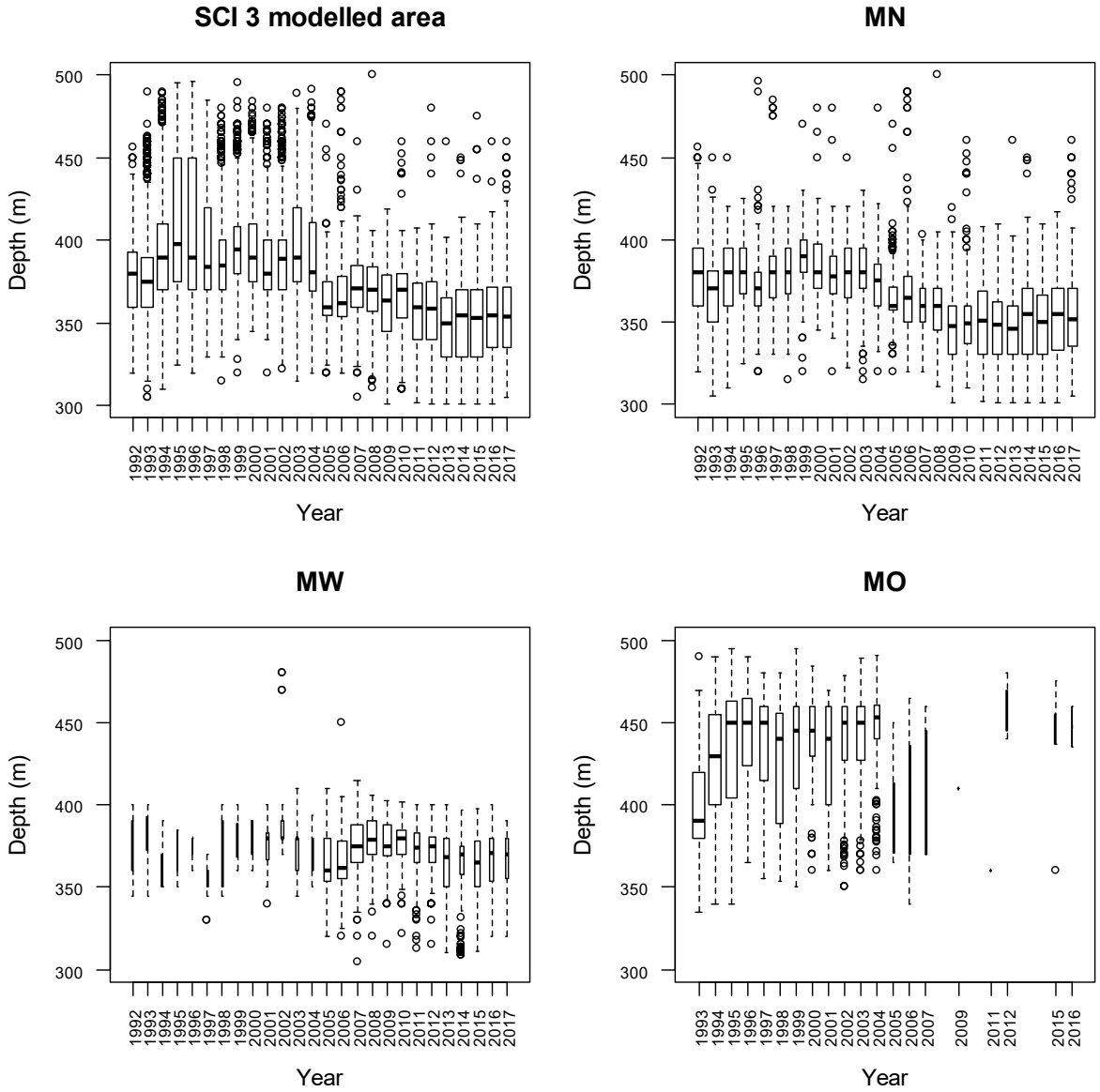

Figure 11: Boxplot of individual observations from TCEPR data of scampi targeted fishing depth with tows of zero scampi catch excluded, by fishing year for the SCI 3 fishery, and for the three subareas identified in Figure 6. Box width is proportional to the square root of the number of observations. The solid line within each box represents the median value; the upper and lower ends of the box are the upper and lower quartiles; and the dashed lines extend out to the upper and lower adjacent values, the largest (smallest) value less (greater) than or equal to the upper (lower) quartile plus (minus) 1.5 times the interquartile range.

2.2 Scampi stock structure

Stock structure of scampi in New Zealand waters is not well known. Preliminary electrophoretic analyses (Smith 1999) suggested that scampi in SCI 6A are genetically distinct from those in other areas, and there is substantial heterogeneity in samples from SCI 1,SCI 2, and SCI 4A. Work in South Africa on the similar species, *Metanephrops mozambicus*, using mitochondrial DNA suggests that there is limited gene exchange between populations, even along the same coast (Zacarais 2013). A more recent New Zealand study amplified and sequenced DNA from the mitochondrial CO1 gene and nuclear ITS-1 region, and found that *M. challengeri* from the Auckland Islands region are genetically distinct

from those inhabiting the Chatham Rise, and those collected from waters off the eastern coast of the North Island (Verry 2017). This study concluded that there appears to be gene flow among the sampling sites off the eastern coast of the North Island and on the Chatham Rise, but some isolation by distance was detected, suggesting that some of these populations may be demographically uncoupled. The abbreviated larval phase of *Metanephrops* species may lead to low rates of gene mixing.

2.3 Seasonal patterns in scampi biology

Previous development of the length-based model for scampi has shown that determination of appropriate time steps for the model is important in fitting to length and sex ratio data in particular (Tuck & Dunn 2006; Tuck & Dunn 2009; Tuck & Dunn 2012). Scampi inhabit burrows and are not usually vulnerable to trawling when they withdraw to their burrow. Catchability varies between the sexes on a seasonal basis as a result of sex-specific moulting and reproductive behaviour, which leads to seasonal changes in the sex ratio of catches (Bell et al. 2013).

Current knowledge of the timing of scampi biological processes in SCI 3 is summarised in Table 2 (revised from Tuck 2010). From patterns in the proportion of soft (post moult) animals (Figure 12), ovigerous females (Figure 13), and egg stage observed in commercial catches (Figure 14), mature female moulting appears to be focussed around October and November, just after the hatching period (July–August). Hatching has been recorded at various times through the year and appears to vary between stocks (Wear 1976; K. Heasman, Cawthron, pers. com.). Mating occurs after the females have moulted, while the shell is still soft, and new eggs are spawned onto the pleopods in December–January.

The combination of different biological processes for males and females leads to different relative availabilities of the two sexes through the year, resulting in the pattern of sex ratio (displayed as proportion males) shown in Figure 15. Males are generally less abundant than females in catches between January and June (male catches being reduced during their moulting period), with males dominating from July to December.

On the basis of our understanding of the timing of biological processes for scampi in this area and the seasonal pattern in sex ratio, it was decided to shift the model year to 1st July to 30th June, slightly in advance of the New Zealand fishing year (1st October to 30th September). The previous assessment model for SCI 3 (Tuck 2016b) had a model year from 1st August to 31st July, and two time steps: 1. August to December (when males dominate in catches), 2. January to July (when females dominate). Catch composition data from observer sampling (see Section 3.6.1) have historically been quite sparse in the winter months in this fishery, and new data collected since the last assessment suggests that July samples are more similar to time step 1 than time step 2, and so the revised approach adopted here shifts the start date of time step 1, and the end date of time step 2, one month forward (Table 3).

Table 2: Summary of scampi biological processes for SCI 3. Revised from Tuck (2010) and more recent survey data (NIWA, unpublished data).

	Jan	Feb	Mar	Apr	May	Jun	Jul	Aug	Sep	Oct	Nov	Dec
Male moult		X	?	X								
Female moult										X	X	
Mating										X	X	
Eggs spawn											X	X
Eggs hatch								X	X			

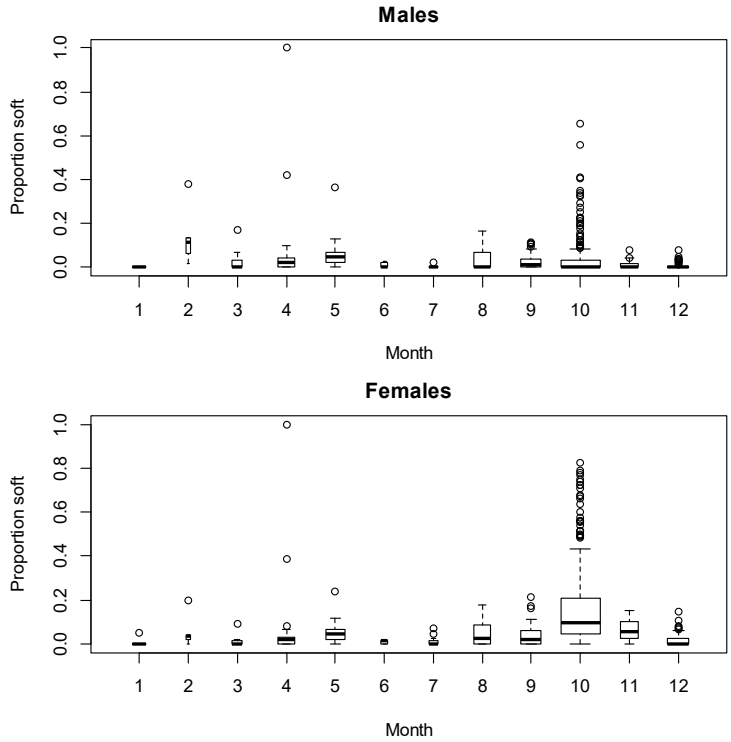

Figure 12: Boxplots of proportions of soft animals (post moult) by sex and month, as recorded by observer sampling in SCI 3, where month 1 is January. Box widths are proportional to the square root of the number of observations for that month. The solid line within each box represents the median value; the upper and lower ends of the box are the upper and lower quartiles; and the dashed lines extend out to the upper and lower adjacent values, the largest (smallest) value less (greater) than or equal to the upper (lower) quartile plus (minus) 1.5 times the interquartile range. Outliers (values beyond the adjacent values) are shown as open circles.

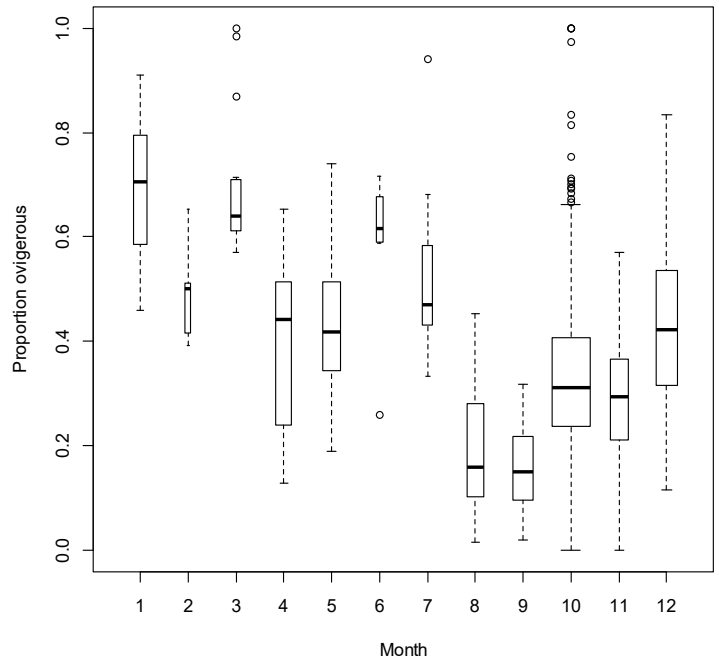

Figure 13: Boxplots of proportions of ovigerous females by month, as recorded by observer sampling in SCI 3. Box widths are proportional to the square root of the number of observations for that month. The solid line within each box represents the median value; the upper and lower ends of the box are the upper and lower quartiles; and the dashed lines extend out to the upper and lower adjacent values, the largest (smallest) value less (greater) than or equal to the upper (lower) quartile plus (minus) 1.5 times the interquartile range. Outliers (values beyond the adjacent values) are shown as open circles.

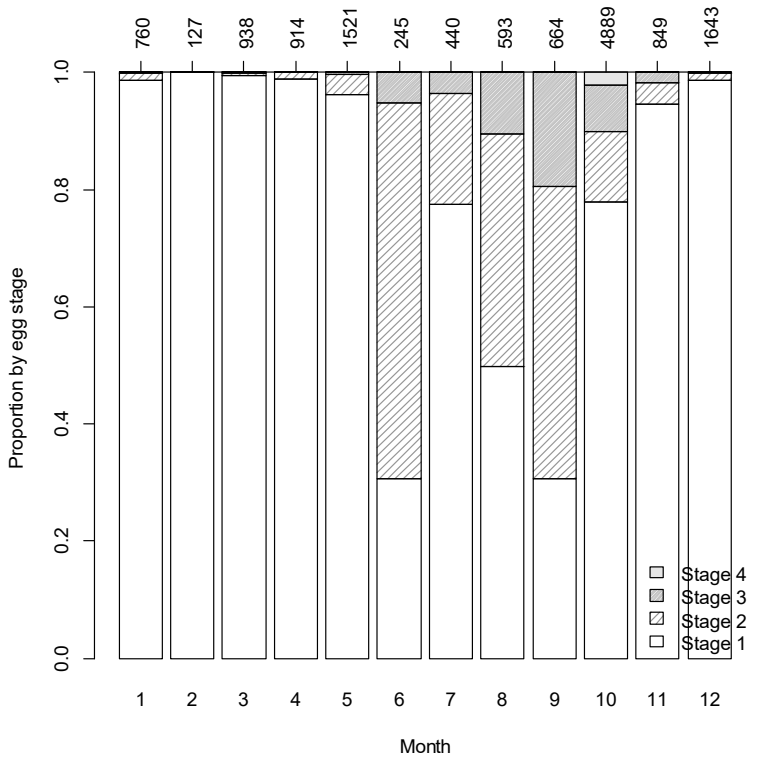

Figure 14: Barplots of the proportion of ovigerous females by egg stage and month, from observer sampling in SCI 3. Total numbers by month are provided along the top of the plot.

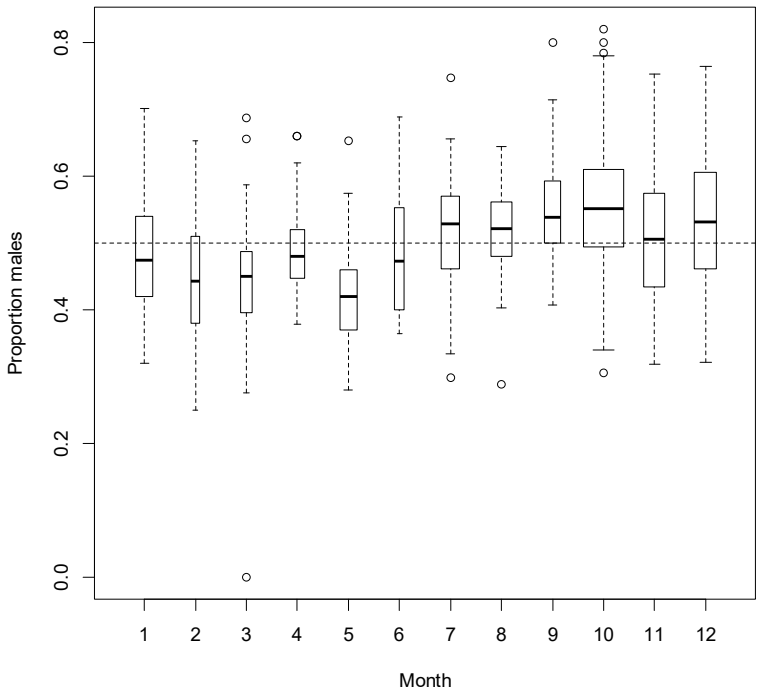

Figure 15: Boxplots of proportions of males in catches by month from observer sampling in SCI 3. Box widths are proportional to the square root of the number of observations. The solid line within each box represents the median value; the upper and lower ends of the box are the upper and lower quartiles; and the dashed lines extend out to the upper and lower adjacent values, the largest (smallest) value less (greater) than or equal to the upper (lower) quartile plus (minus) 1.5 times the interquartile range. Outliers (values beyond the adjacent values) are shown as open circles.

Table 3: Annual cycle of the population model for SCI 3, showing the processes taking place at each time step, their sequence in each time step, and the available observations. Fishing and natural mortality that occur within a time step occur after all other processes, with 50% of the natural mortality for that time step occurring before and 50% after the fishing mortality.

Step	Period	Process	Proportion in time step
1	July–December	Maturation	1.0
		Growth (both sexes)	
		Natural mortality	0.5
		Fishing mortality	From TCEPR
2	January–June	Recruitment	1.0
		Natural mortality	0.5
		Fishing mortality	From TCEPR

2.4 Standardised CPUE indices

2.4.1 Core vessels

A plot of vessel activity (number of scampi targeted tows recorded) over time is presented for the modelled area of SCI 3 (MN, MO and MW) in Figure 16. While 26 vessels have targeted scampi in the region, ten vessels were active through most of the first decade of the fishery, with some dropping out and others starting at around this time. Four vessels (E, H, J, and P) have been active in the region almost continuously through the history of the fishery, but new entrants to the fishery (A, O, and T) have contributed reasonable catches in recent years.

Figure 17 (upper plot) shows the proportion of the total catch (over the history of the fishery) in relation to the number of years the vessels contributing that catch have been active in the fishery. In previous scampi CPUE standardisations (Tuck 2016b; Tuck 2016a; Tuck 2017), a cut-off of 10 years of activity has been selected to identify core vessels and, on the basis of this, eleven vessels (D, E, F, G, H, I, J, L, P, Q, and Y) are selected, contributing 85% of scampi catches over the history of the fishery. A cut-off of 5 years activity would introduce an additional vessel into the core vessels (vessel O), and increase the contribution of the core set to 90%. The lower plot of Figure 17 shows the proportion of catch accounted for in each year by vessels active for over 5 or 10 years. Through most of the fishery the two lines are identical (i.e., vessels active for 5 years have also been active for 10 years), and other than the 1991–92 to 1993–94 and 2002–03 to 2003–04 periods, the core vessels have accounted for over 90% of targeted scampi catches in each year; often over 99%. Since 2012, the introduction of new vessels to the fishery has meant that the annual proportion of landings contributed by vessels active for over 10 years has steadily fallen and had dropped to 53% in 2017. If vessels active for over 5 years are considered, the core vessel contribution remains over 90% from 2012 to 2015, but the activity of other new vessels (A and T) in the most recent years decreases the core vessel contribution to 78% in 2017.

The pattern of activity for the potential core vessels is shown in Figure 18. Vessels E, H, J, and P have been active throughout the history of the fishery. Vessels D, I, and L were consistently active up until 2003, and D and L have been sporadic visitors since then, whereas I has been consistently active since 2013. Vessels F and G were active from 1992 to 2009, whereas vessel Q has been active in the region since 1997, vessel Y was active between 2003 and 2013, and vessel O has been active since 2012. The core vessels provide good temporal overlap, although at the subarea level (Figure 19) coverage is poor at the start (MN) and end (MO) of the series. Core vessels active over ten years provide 28 162 events in the modelled area up to the end of June 2017, and vessel O (active for 6 years) provides a further 1509 events, to give a total of 29 671 events.

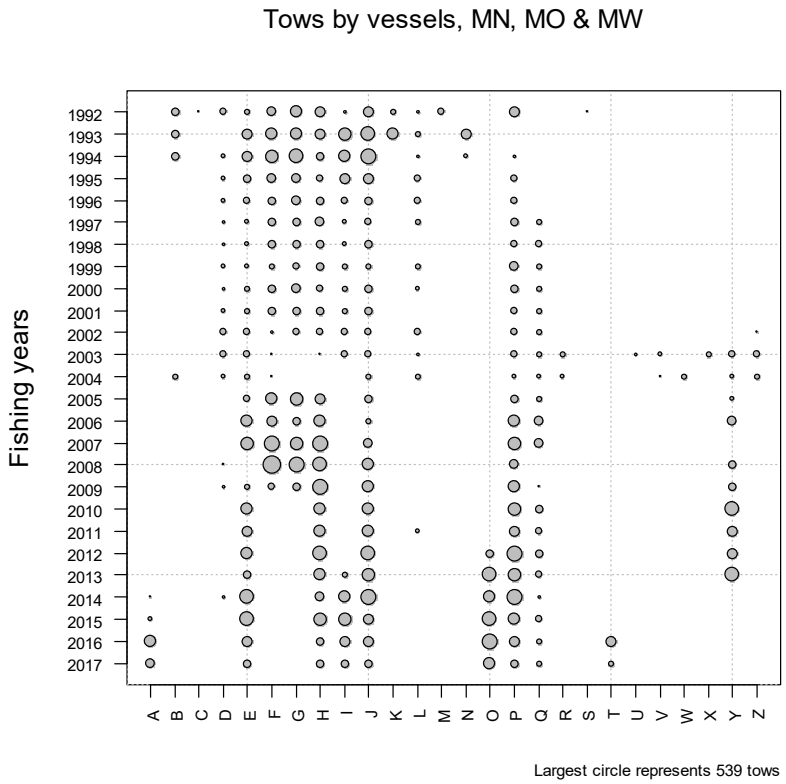

Figure 16: The annual pattern of fishing activity by vessel for the modelled area of SCI 3. The area of each circle is proportional to the number of tows recorded.

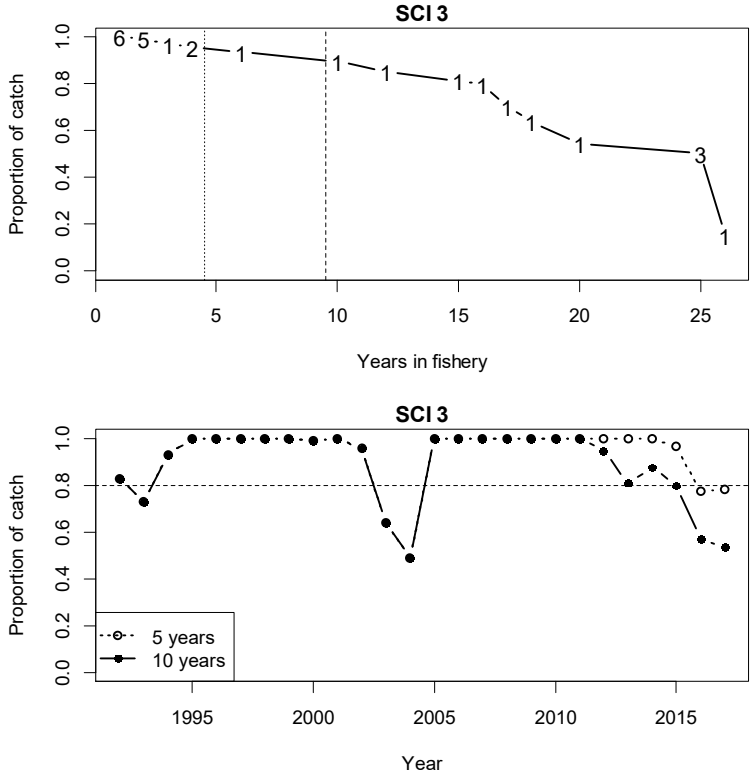

Figure 17: Catch breakdown by vessel for SCI 3. Upper plot: proportion of total scampi catch (all years) plotted against the number of years the vessels reporting that catch have been active in the fishery. Numbers indicate number of vessels active for that duration. Vertical dotted line represents cut-off for core vessels. Lower plot: proportion of annual catch reported by vessels active in the fishery for 5 and 10 years.

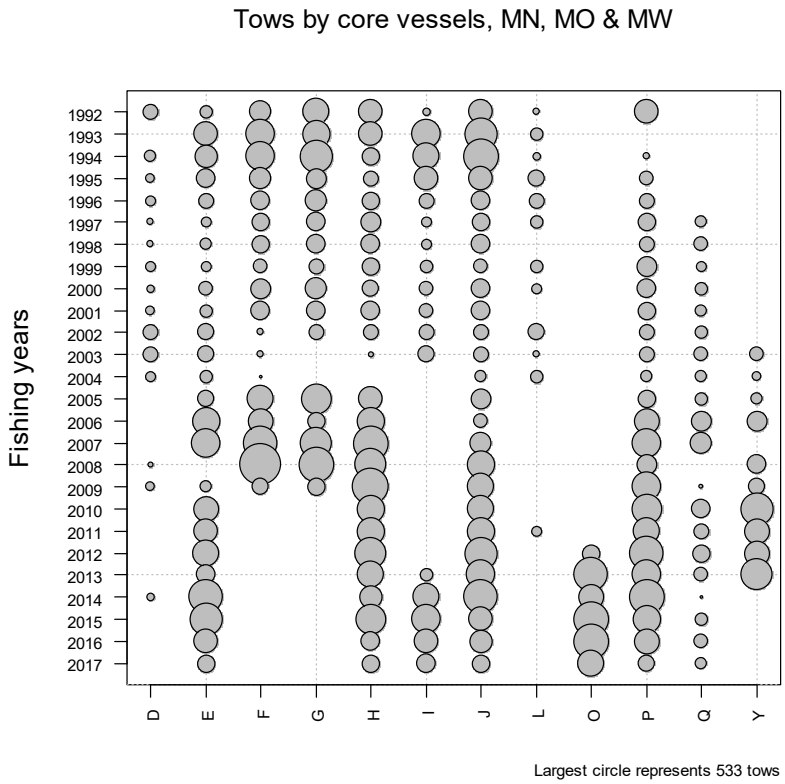

Figure 18: Core vessel pattern of fishing activity by vessel and fishing year for the modelled area of SCI 3. The area of each circle is proportional to the number of tows recorded. Vessel O was only active for 5 years and is not included in the "vessels active for over 10 years" set.

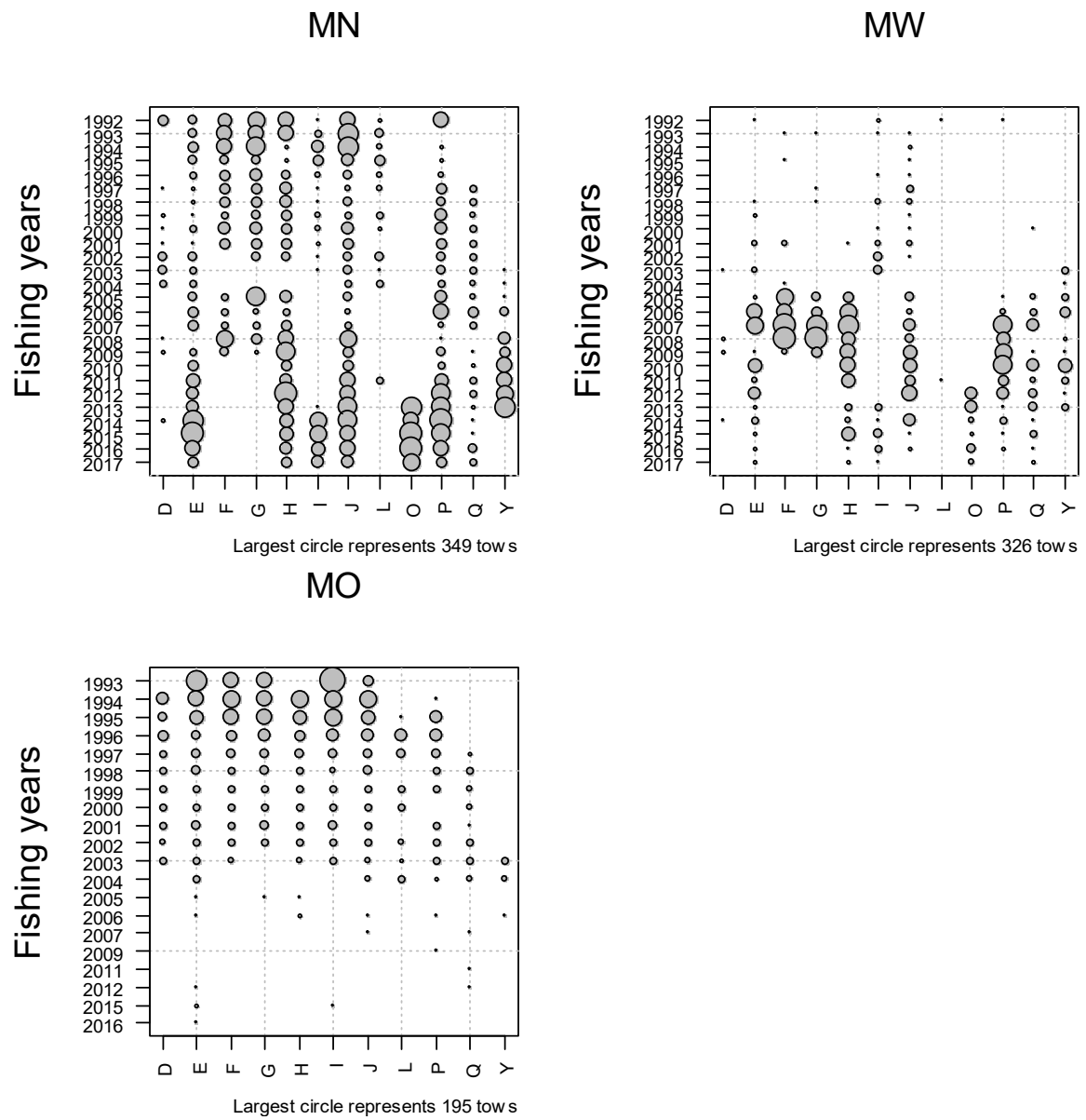

Figure 19: Core vessel pattern of fishing activity by vessel and fishing year for the three subareas of SCI 3. The area of each circle is proportional to the number of tows recorded. Vessel O was active for 5 years and is not included in the "vessels active for over 10 years" set.

2.4.2 Exclusion of poorly sampled time periods

Following the approach previously applied for SCI 3 (Tuck 2013), events occurring during time steps that were barely fished by the core vessels were excluded from the standardisation of the CPUE, on the basis that a small number of tows in an area, or at a particular time, may not provide a good index of abundance. Records were excluded from the CPUE standardisation when there were fewer than 5 tows recorded by core vessels within a time step in a year (Figure 20). In addition, because the fishing in the MO subarea has been largely focussed in October (time step 1), there are few records from time step 2 (January to June), and these data have also been excluded from the standardisation.

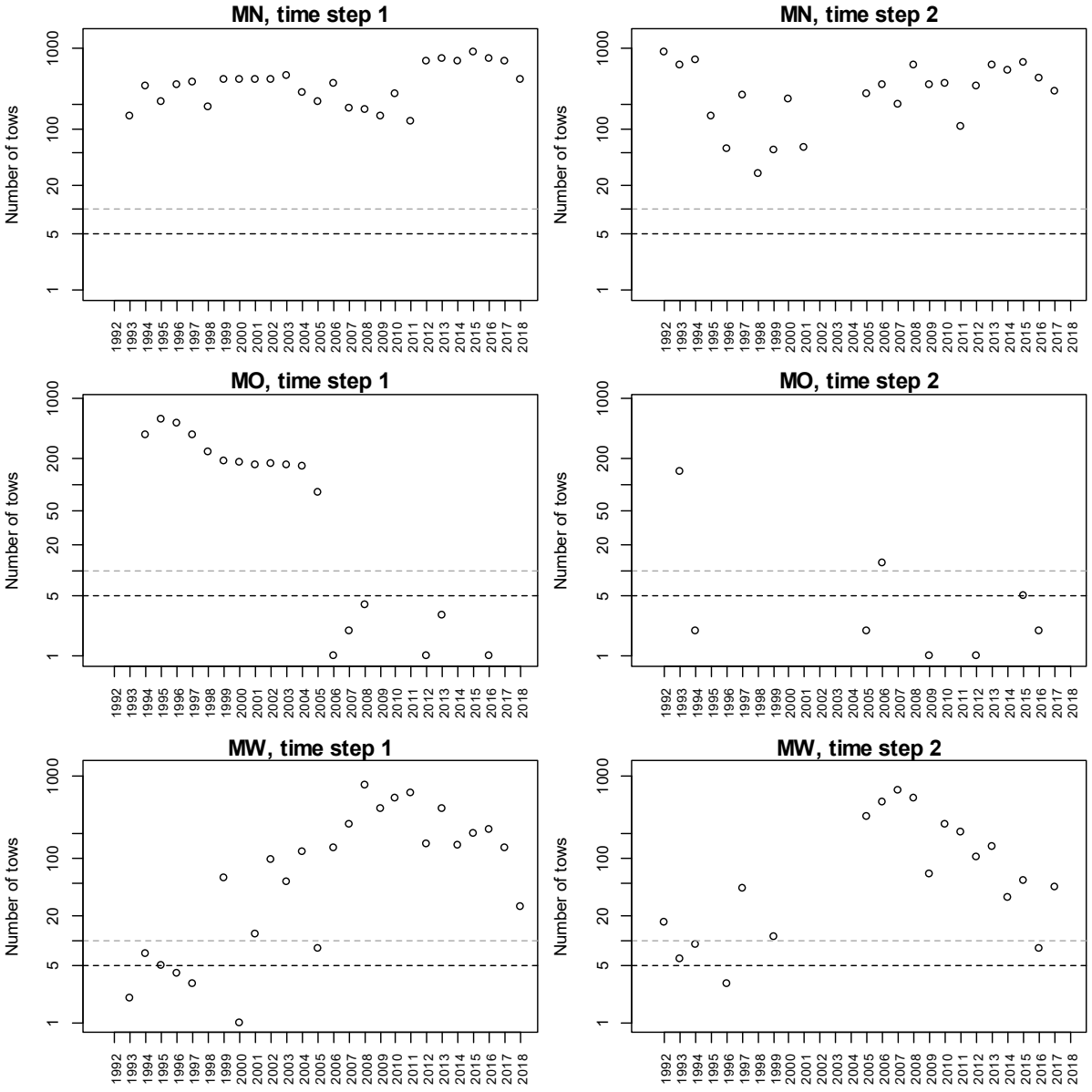

Figure 20: Numbers of commercial tows available within the core vessel dataset by time step and fishing year for SCI 3. Dashed lines represent arbitrary cut-offs at 5 and 10 tows.

2.4.3 Calculation of abundance indices

Standardisation of the CPUE data to calculate abundance indices was initially conducted using data from the twelve vessels active in the fishery for over 5 years. These were then compared with indices calculated from the eleven vessels active in the fishery for over 10 years.

Individual event records from the twelve core vessels were used to generate abundance indices. Within the previous preliminary assessment of SCI 3, a three-stock model was developed, with separate abundance indices fitted for each time step in each subarea (Tuck 2013).The SFAWG suggested a general simplification of the scampi assessment model structure, and in the more recent SCI 3 assessment, a single CPUE index was calculated for each of the subareas (Tuck 2016b). Therefore, an initial model was examined allowing for the potential of model year×subarea×time step interactions. Scampi catch of core vessels was modelled using a year index (forced), model time step, subarea, vessel, time of day, state of moon, depth, fishing duration, and trawl gear parameters.

The time of day of each tow was calculated in relation to nautical dawn and dusk (time when the sun is 12 degrees below the horizon in the morning and evening), as calculated by the *crepescule* function of the *maptools* package (Bivand & Lewin-Koh 2019) in R (R Development Core Team 2018). Individual tows were characterised on the basis of whether they included dawn (shot before dawn, hauled after dawn and before dusk), day (shot after dawn, hauled before dusk), dusk (shot before dusk, hauled after dusk and before dawn), or night (shot after dusk and hauled before dawn). Longer tows including more than one period (i.e., shot before dusk and hauled after dawn) were excluded from this part of the analysis, which resulted in the exclusion of 56 records by the core vessels fishing in SCI 3.

Individual hauls were also categorised in terms of moon phase, on the assumption that tidal current strength at the sea floor will be related to the lunar cycle. Tows were categorised by their date in relation to the lunar cycle, using the *lunar4* and *lunar8* functions within the *lunar* package (Lazaridis 2014) in R.

Within the core vessels identified, three have changed gear configuration (twin rig to triple rig) in recent years, and two have changed engine power over the history of the fishery. Engine power was fitted within the model as a third order polynomial, and gear configuration as a two-level factor (twin or triple rig). Gear configuration for a particular vessel and date was determined on the basis of information provided by the fishing industry as to when vessels changed from twin to triple, and all tows after this date are defined as triple rig. It is acknowledged that vessels may change configuration within a trip depending on gear damage or fishing conditions, but it is unclear how reliably this has been recorded on TCEPR forms in the past (as effort width). Preliminary examination of the data for the core vessels suggested that the values recorded were generally realistic and, following some minor grooming, "effort width" was also offered as a third order polynomial term to the model.

In addition, examination of the data for SCI 3 (Tuck 2013) identified a distinct shift in trawl duration between 2002–03 and 2006–07 (from about 5 hours to 7 hours). This shift (in SCI 3) was fleet-wide and associated with a modification to the top of the trawl to reduce the bycatch (John Finlayson, Sanford Ltd., pers. comm.), enabling vessels to fish for longer on each tow. Box plots of tow duration over time have been examined for each of the core vessels identified for SCI 3 (Figure 21) and show, for the vessels active at the time, a relatively rapid shift in trawl duration around the mid-2000s, from roughly 5 to 7 hours. For each vessel, the timing of the gear modification was estimated from examination of tow durations in SCI 3 and fitted as a two level factor in the model.

Catch indices were derived using generalised linear modelling (GLM) procedures (Vignaux 1994; Francis 1999), using the statistical software R. The response variable in the GLM was the natural logarithm of scampi catch. The fishing year (combined with any time step or depth strata for the index) was entered as a categorical covariate (explanatory) term on the right-hand side of the model. Standardised CPUE abundance indices (canonical) were derived from the exponential of the fishing year covariate terms as described in Francis (1999). A total of 28 879 fishing events by the twelve core vessels in the modelled area, during the modelled period, were available.

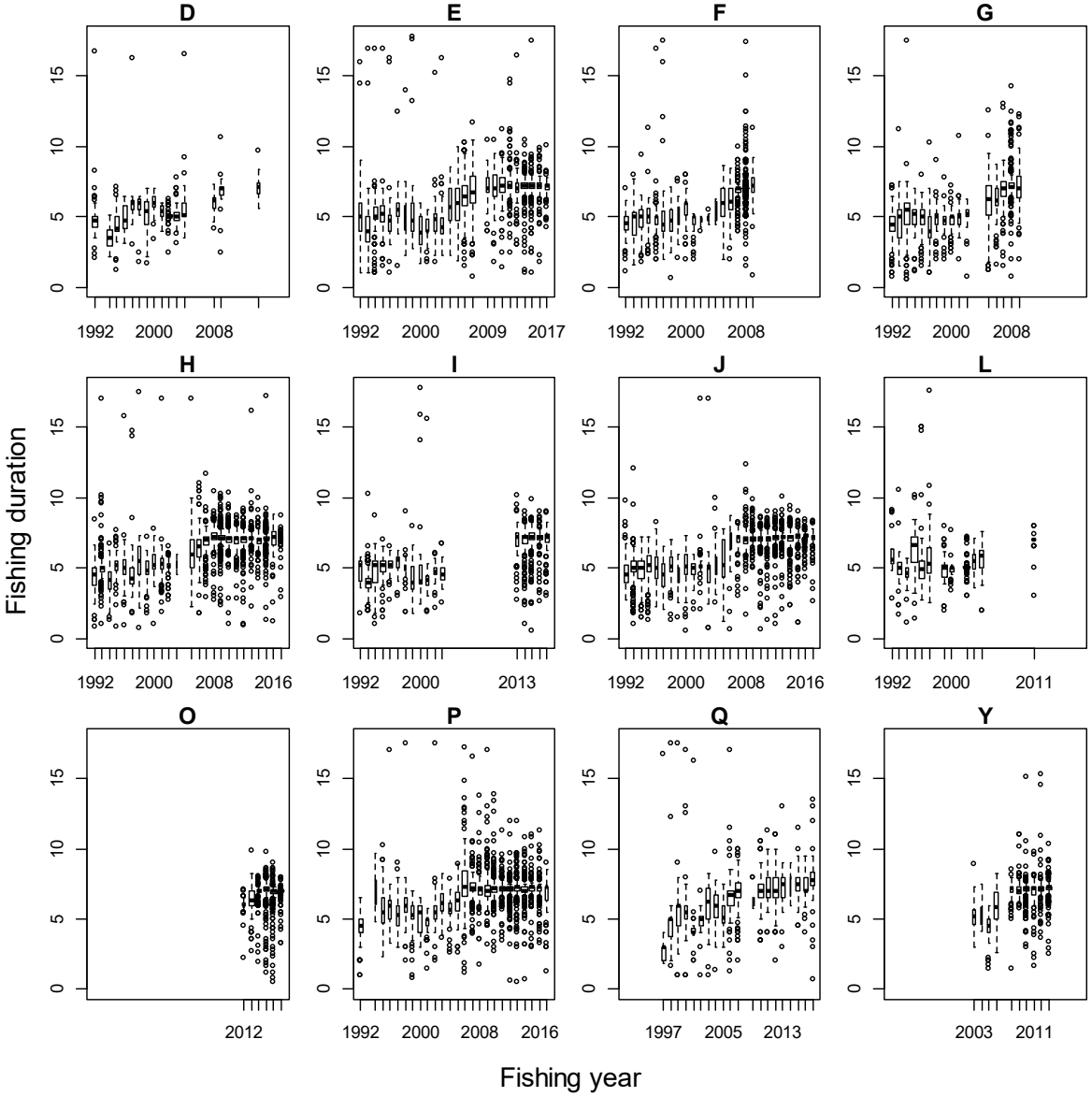

Figure 21: Box plots of tow duration (hours) for scampi targeted fishing in SCI 3 for the twelve core vessels identified. Box widths are proportional to the square root of the number of observations.

To accommodate a non-linear relationship with the response variable (log catch), the continuous variables (effort, engine power, gear width) were "offered" to the GLMs as third order polynomials. Vessel, depth (binned into the 50 m survey strata), time of day, moon phase, twin or triple rig, and bycatch modification were "offered" to the GLMs as factors. Some effects (e.g., gear width) were represented by more than one term, and the model was allowed to select which (if any) were retained. A forward-fitting, stepwise, multiple-regression algorithm was used to fit GLMs to groomed catch, effort, and characterisation data. The stepwise algorithm generates a final regression model iteratively and uses a simple model with a single predictor variable, fishing year (forced), as the initial or base model. The reduction in residual deviance relative to the null deviance is calculated for each additional term added to the base model. The term that results in the greatest reduction in residual deviance is added to the base model if this results in an improvement in residual deviance of more than 1%. The algorithm repeats this process, updating the model, until no new terms can be added. Diagnostic plots for the final models are presented in Appendix 1 (Bentley et al. 2012).

Preliminary investigations into different error distributions (comparing log-normal, gamma, and Weibull), using the model selection process described above to select terms to be retained in a minimum adequate model, identified that the gamma distribution provided a slight improvement in the distribution of residuals. This error distribution was used for calculation of the indices reported below. Diagnostic plots for the three compared error distributions, and for the final standardisation model, are presented in Appendix 1.

2.4.4 Final CPUE index

Stepwise regression analysis of the dataset with the full model to estimate the CPUE indices for SCI 3 resulted in an initial model with model_year (forced), time of day, subarea, vessel, fishing_duration, model_step, and second order interactions between model_year and subarea, and model_year and model_step retained (Table 4). The model explained 55% of the variation in the data. Depth was not retained within the model, either as a separate term, or as part of an interaction, suggesting that it does not contribute much to explaining the deviance in the catch.

Table 4: Analysis of deviance table for initial standardisation model (including year:time step interations) selected by stepwise regression for SCI 3. TOD is time of day.

	Df	Deviance explained	Additional deviance explained (%)
NULL			
model_year	25	4425.5	32.64
TOD	3	764.5	5.64
subarea	2	556.4	4.10
vessel	11	384.7	2.84
poly(fishing_duration, 3)	3	291.0	2.15
model_step	1	222.6	1.64
model_year:subarea	33	510.1	3.76
model_year:model_step	21	336.3	2.48

A second model was examined combining model_year and subarea into a single term, which explained 53% of the variation in the data, and also retained time of day, vessel, fishing_duration and model_step (Table 5). Predicted CPUE (for vessel H with a 7-hour fishing duration) from the model matched the pattern observed in the unstandardised data for each of the subareas (Figure 22), and the SFAWG agreed to use this standardised CPUE analysis for the abundance index.

Table 5: Analysis of deviance table for final standardisation model selected by stepwise regression for SCI 3. TOD is time of day.

	Df	Deviance explained	Additional deviance explained (%)	Overall influence (%)*
NULL				
model_year_subarea	60	5591.2	41.23	
TOD	3	744.1	5.49	3.56
vessel	11	335.3	2.47	2.72
poly(fishing_duration, 3)	3	256.3	1.89	9.11
model_step	1	227.9	1.68	6.38

* Overall influence as in table 1 of Bentley et al. (2012).

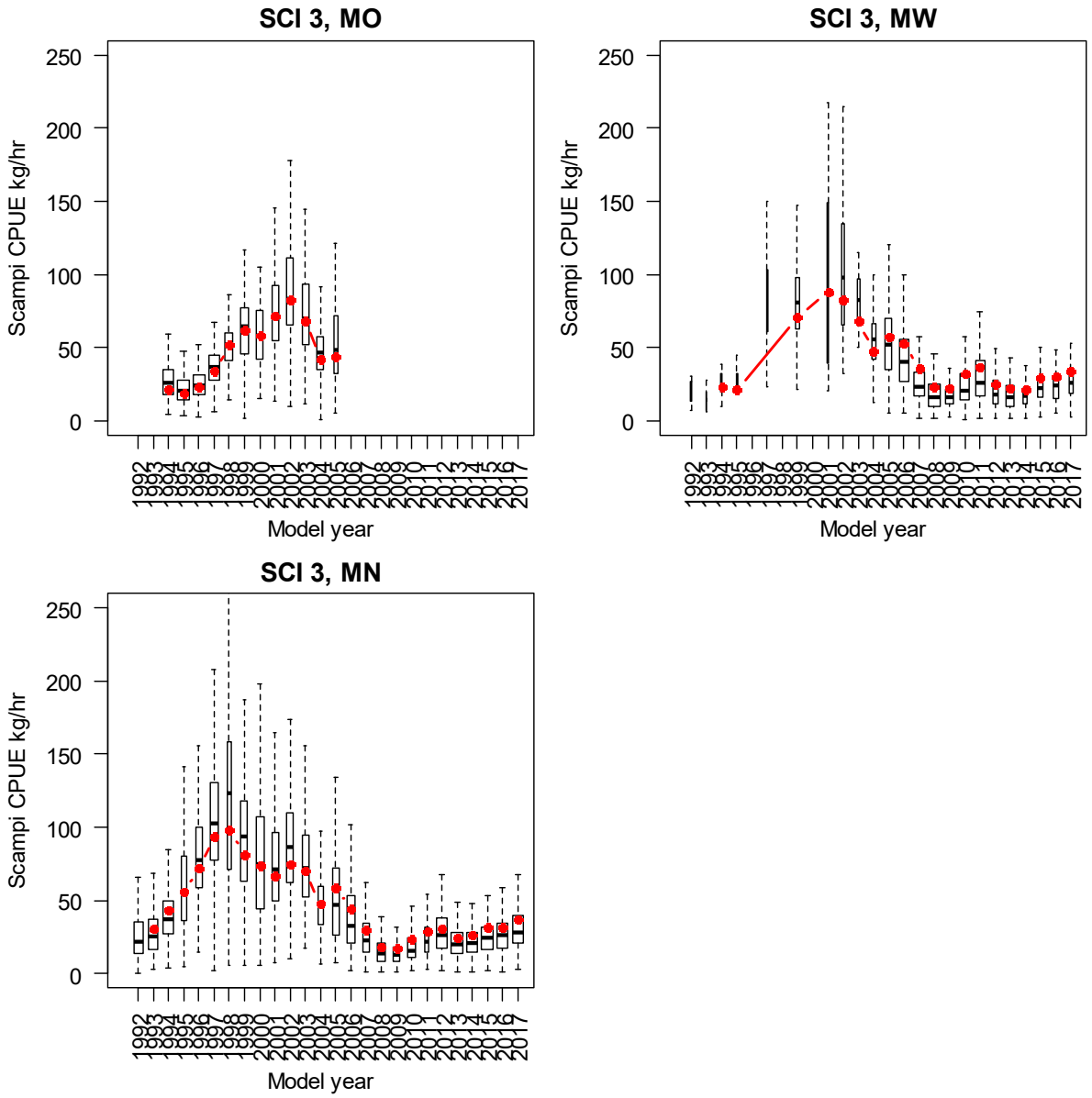

Figure 22: Annual standardised CPUE by area predicted (for vessel H for a 7-hour tow) from the final model (red dots) and boxplots of unstandardised CPUE. Box widths are proportional to the square root of the number of observations. The solid line within each box represents the median value; the upper and lower ends of the box are the upper and lower quartiles; and the dashed lines extend out to the upper and lower adjacent values, the largest (smallest) value less (greater) than or equal to the upper (lower) quartile plus (minus) 1.5 times the interquartile range.

3. MODEL STRUCTURE

3.1 Seasonal and spatial structure, and the model partition

The model partitions scampi by area (MN, MO, and MW), stock (one stock per area), sex, and length class. The model assumes that the three subareas are completely separate and that there is no movement, either by adults or recruitment, between them. Only limited recaptures have been made from the tagged scampi released in SCI 3, but recaptures from other New Zealand stocks suggest very limited movement (Cryer & Stotter 1999; Tuck et al. 2009), and this is supported by acoustic tracking of both the European scampi *Nephrops norvegicus* (albeit in shallower waters) and *Metanephrops challengeri* (Chapman et al. 1974; Tuck et al. 2015b). Larval development of scampi appears to be partially abbreviated (compared with similar shallow water species), in that there only appears to be one larval stage, with a

duration of three to four days (Wear 1976). The post-larvae appear to be benthic orientated (Wear 1976), and it has therefore been assumed that there is little potential for larval exchange between the subareas. Genetic studies on *Metanephrops mozambicus* support this (Zacarais 2013). By assessing the three areas within the same model, catches, survey indices, and length distributions can be specific to each area, but other parameters (growth, natural mortality, selectivity, catchability) can be shared.

Growth between length classes is determined by sex-specific, length-based growth parameters. Individuals enter the partition by recruitment and are removed by natural mortality and fishing mortality. The model's annual cycle is based on the fishing year and is divided into the two time-steps described above (on basis of Table 2). The choice of two time steps was based on the current understanding of scampi biology and sex ratio in catches. Note that model references to "year" within this report refer to the fishing year as described above (August to July) and are labelled as the most recent calendar year, e.g., the model_year "1998–99" is referred to as "1999" throughout. Previous models for SCI 3 included spatial structure (Tuck 2013) and, given the distinct changes in exploitation patterns in the area, the SFAWG considered that this should be maintained, but the temporal structure of the model has been simplified.

The model uses capped logistic length-based selectivity curves for commercial fishing and research trawl surveys, which vary with sex and time step. Although the sex ratio data suggest that the relative catchability of the sexes varies through the year (hence the model time structure adopted), there is no reason to suggest that assuming equal availability, selectivity at size would be different between the sexes. Therefore the two sex selectivity implementation developed within CASAL for previous scampi assessments (Tuck & Dunn 2012) was applied. This allows the L_{50} (size at which 50% of individuals are retained) and a_{95} (size at which 95% of individuals are retained) selectivity parameters to be estimated as single values shared by both sexes in a particular time step, but allows for different availability between the sexes through estimation of different a_{max} (maximum level of selectivity) values for each sex. The burrow-based photographic survey abundance indices are not sex specific, and a standard logistic length-based selectivity curve is applied.

3.2 Biological inputs

3.2.1 Growth

Recent scampi assessments have generally estimated growth within the model from tag recapture data (Tuck & Dunn 2012; Tuck 2015; Tuck 2016a; Tuck 2017). Although trawl surveys in SCI 3 (2009, 2010, 2013, and 2016) have released tagged scampi, returns have been very low, and there are insufficient data to estimate growth.

As an alternative, the previous SCI 3 model used a simple (one area) model to estimate growth and then fixed this in more complex models, also examining sensitivity to faster and slower growth (Tuck 2013). The SFAWG suggested that growth could potentially be estimated within the model without tagging data (fitting to the length composition and abundance data), and preliminary investigations suggested that this was feasible, so this approach was adopted.

3.2.2 Maturity

Female maturity can be estimated from gonad staging or the presence of eggs on the pleopods. Gonad stages are recorded from research survey catches (although only on scampi that were not tagged and released). The presence and development stage of eggs on pleopods are recorded from research survey and observer sampling. No data are available for the maturity of male scampi, so their maturity ogive was assumed to be identical to that of females, although studies on *N. norvegicus* in Europe have suggested that male maturity may occur at a larger size (although possibly the same age) than females (Tuck et al. 2000). Maturity is not considered to be a part of the model partition, but the proportion of mature females in each length class was fitted within the model based on a logistic ogive with a binomial

likelihood (Bull et al. 2012). The proportion mature was modelled as a function of length within a GLM framework, with a quasibinomial distribution of errors and a logit link (McCullagh & Nelder 1989),

$$P.mature = a + b * Length$$

which equates to the logistic model. The model was weighted by the number measured at each length. After obtaining estimates for the parameters a and b, the length at which 50% are mature (L_{50}) was calculated from:

$$L_{50} = -\frac{a}{b}$$

with selection range (SR) calculated from:

$$SR = \frac{(2.\ln(3))}{b}$$

The L_{50} estimate for the SCI 3 data was 43.2 mm, with a selection range a_{10} to a_{90} of 6.5 mm (Figure 23).

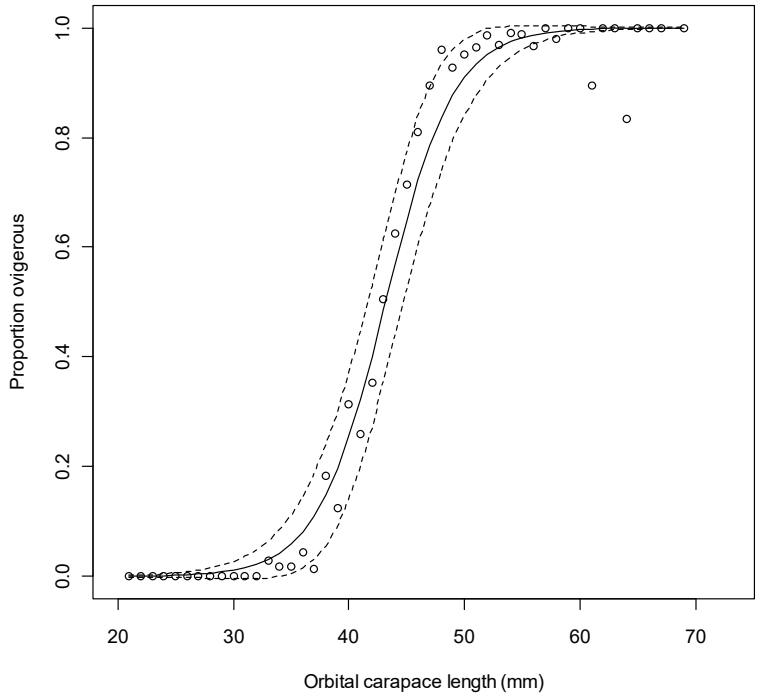

Figure 23: Proportions of female scampi carrying eggs (ovigerous) at length, from sampling in January to March period, just after the spawning period. Solid line represents the logistic curve fitted to the data (L_{50} of 43.2 mm and selection range of 6.5 mm). Dashed line represents plus or minus one Standard Error.

3.2.3 Natural mortality

The instantaneous rate of natural mortality (M) has not been estimated directly for any scampi species, but estimates have been made (0.2–0.25) based on the estimate of the K parameter from a von Bertalanffy growth curve (Cryer & Stotter 1999) using a correlative method (Pauly 1980; Charnov et al. 1983). Morizur (1982) used length distributions from 'quasi-unexploited' *Nephrops* stocks to obtain estimates for annual M of 0.2–0.3. The values most commonly assumed for assessment of *Nephrops*

stocks in the Atlantic is 0.3 for males and immature females, and 0.2 for mature females (assumed less vulnerable to predation during the ovigerous period) (Bell et al. 2006). For New Zealand scampi, *M* has previously been fixed at 0.2 (Tuck & Dunn 2012), or both 0.2 and 0.3 (Tuck 2014). Within the current assessment, preliminary models were explored where *M* was estimated, but the SFAWG requested only models with *M* fixed at 0.2 and 0.25. The instantaneous natural mortality rate is assumed to be the same for both sexes for *Metanephrops*.

3.3 Catch data

Data for the model were collated over the spatial and temporal strata as defined in the model structure. Catches in the modelled area represent over 99% of scampi catches from SCI 3. Details of catches by fishing year, subarea and time step, are provided in Table 6.

Table 6: Estimated landed catch (t) from SCI 3, by subarea and time step.

Fishing year	MN_1	MN_2	MW_1	MW_2	MO_1	MO_2
1991	0.00	0.00	0.00	0.00	0.00	0.00
1992	0.00	123.57	0.05	1.92	0.00	0.00
1993	30.98	106.78	0.54	0.35	0.00	25.65
1994	103.15	186.32	1.57	1.32	55.13	0.49
1995	63.61	61.22	0.71	0.00	58.16	0.00
1996	164.54	23.31	1.00	1.37	65.31	0.00
1997	202.07	114.09	1.00	15.11	75.11	0.00
1998	103.42	5.70	0.05	0.00	73.29	0.00
1999	207.67	9.34	25.48	3.67	60.21	0.00
2000	200.03	60.35	0.40	0.00	57.90	0.00
2001	155.01	18.88	5.44	0.00	70.50	0.00
2002	180.63	0.00	41.89	0.00	70.83	0.00
2003	191.00	0.00	20.00	0.00	67.00	0.00
2004	132.01	0.00	32.96	0.00	59.43	0.00
2005	176.00	66.09	4.86	86.29	55.40	0.09
2006	117.59	66.18	41.18	120.28	0.09	1.96
2007	39.96	27.02	61.68	104.44	0.17	0.00
2008	24.61	61.12	120.16	51.45	0.37	0.00
2009	14.03	39.56	49.23	8.36	0.00	0.01
2010	30.43	58.87	91.17	47.97	0.00	0.00
2011	23.50	17.20	147.76	29.96	0.00	0.00
2012	163.79	51.33	25.49	11.11	0.05	0.02
2013	140.00	75.00	54.00	13.00	0.00	0.00
2014	125.00	75.00	19.00	3.00	0.00	0.00
2015	182.00	120.00	37.00	9.00	0.00	0.00
2016	171.71	87.85	39.61	0.69	0.03	0.08
2017	196.44	118.89	25.37	12.32	0.00	0.00

3.4 CPUE indices

The annual CPUE indices estimated within the standardisation (see Figure 22) were fitted within the model as abundance indices. There has been considerable discussion on whether CPUE is proportional to abundance for scampi (Tuck 2009), with rapid increases in both CPUE and trawl survey catch rates for a number of stocks in the early to mid-1990s (and changes in sex ratio in trawl survey catches) initially being considered related to changes in catchability. Later analysis (Tuck & Dunn 2009) suggested that the observed changes in sex ratio were related to slight changes in the survey timing in relation to the moult cycle. Similar patterns in CPUE are observed over the same period for rock lobster *Jasus edwardsii* (Starr 2009; Starr et al. 2009), and scampi in SCI 3 (Tuck 2013), which may suggest broad- scale environmental drivers influencing crustacean recruitment. The CPUE patterns for SCI 1 are mirrored by trawl survey catch rates, suggesting that they do not reflect increases in catchability from fisher learning. Although not considered appropriate for use as an index in the model (Tuck 2013), a scampi abundance index generated from the Chatham Rise middle depths (*R.V. Tangaroa*) trawl survey (Tuck in prep) shows a very similar temporal pattern to the standardised CPUE indices for SCI 3, also supporting the suggestion that the increases in scampi catch rate observed during the 1990s reflect scampi abundance, rather than changes in catchability.

The standardised CPUE index was fitted using the approach of Clark & Hare (2006), as recommended by Francis (2011). This approach fits lowess smoothers with different degrees of smoothing (Figure 24

to Figure 26) and uses the residuals from each fit to estimate the CV. Examination of the individual series suggested that different CVs might be appropriate for different areas, but there was no reason to believe that the reliability of the index varied between subareas and, from visual examination of the fits, the SFAWG determined that a CV of 0.20 was appropriate for the CPUE series for each subarea.

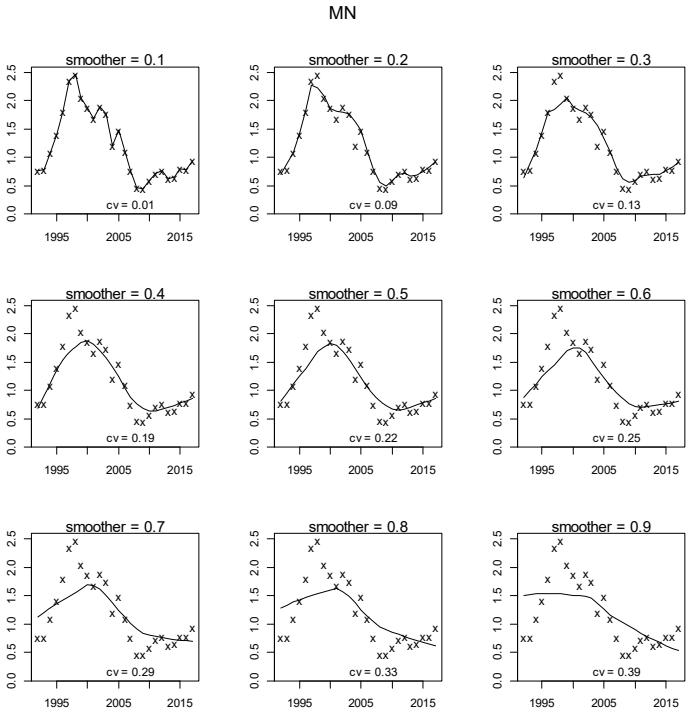

Figure 24: Fits of lowess smoothers to the standardised CPUE index for the MN subarea.

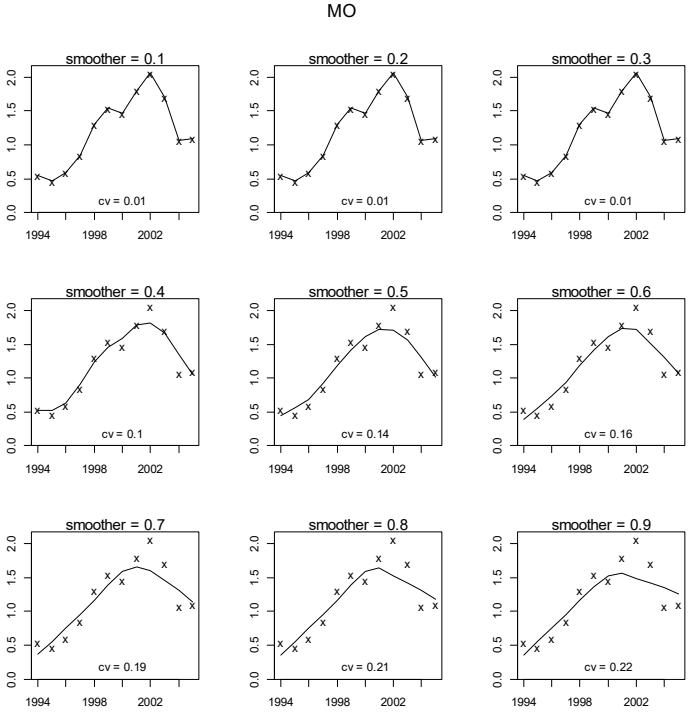

Figure 25: Fits of lowess smoothers to the standardised CPUE index for the MO subarea.

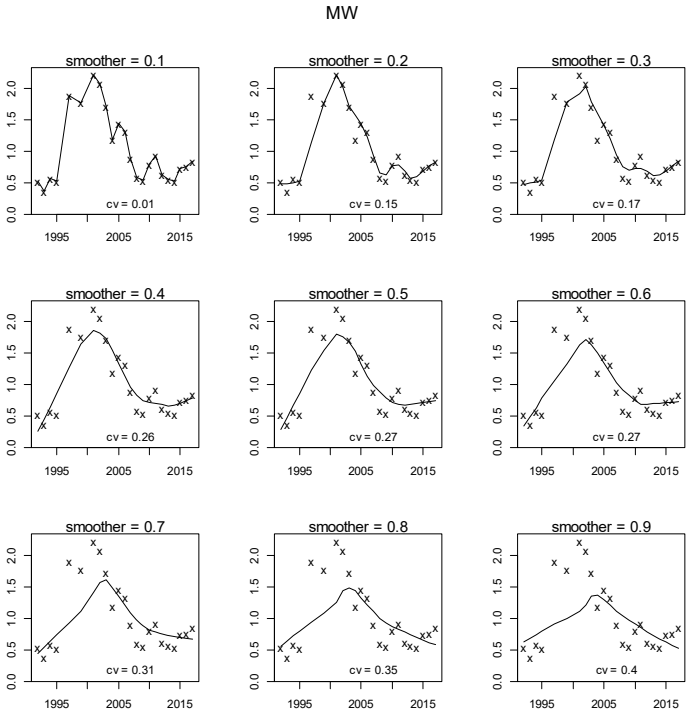

Figure 26: Fits of lowess smoothers to the standardised CPUE index for the MW subarea.

3.5 Research survey indices

Trawl and photographic surveys have been undertaken from the RV *Kaharoa* in August and November 2001, and October 2009, 2010, 2013 and 2016 (Cryer et al. 2003; Tuck et al. 2011; Tuck et al. 2015a; Tuck et al. in press). In 2001, pre- and post-fishery surveys were conducted in the MO subarea (the fishery occurring over a few weeks in October). This survey was for the QMA 3 management area and did not cover the MN and MW subareas. The more recent surveys were for the SCI 3 management area and covered all three subareas.

3.5.1 Photographic surveys

Photographic surveys of SCI 3 have been conducted in 2001, 2010, 2013 and 2016 (Cryer et al. 2003; Tuck et al. 2011; Tuck et al. 2015a; Tuck et al. in press). The surveys provide two indices of scampi abundance, one based on major burrow openings and one based on visible scampi. Both indices are subject to uncertainty, either from burrow detection and occupancy rates (for burrow-based indices) or emergence patterns (for visible scampi-based indices) (Tuck et al. 2015b). The burrow index has been used to date within assessments for SCI 1, SCI 2, and SCI 3 (Tuck & Dunn 2012; Tuck 2013; Tuck 2016b; Tuck 2016a). In SCI 6A, scampi appear to spend less time in burrows (Tuck et al. 2007), and the visible scampi index has been used (Tuck & Dunn 2012; Tuck 2015; Tuck 2017). Scaled survey estimates (by survey strata and subarea) are provided for scampi burrows in Table 7 and Figure 27. Details of the estimation of the catchability priors are provided in Section 3.7.

Table 7: Time series of photographic survey major burrow opening abundance (millions) and CV for SCI 3 by subarea.

Model year	MN		MW		MO	
	Abundance	CV	Abundance	CV	Abundance	CV
2002					224.0	0.09
2010	109.2	0.09	112.2	0.13	54.4	0.15
2011	179.1	0.06	126.8	0.12	72.0	0.11
2014	308.4	0.08	140.0	0.10	144.1	0.11
2017	373.8	0.05	221.6	0.14	152.1	0.10

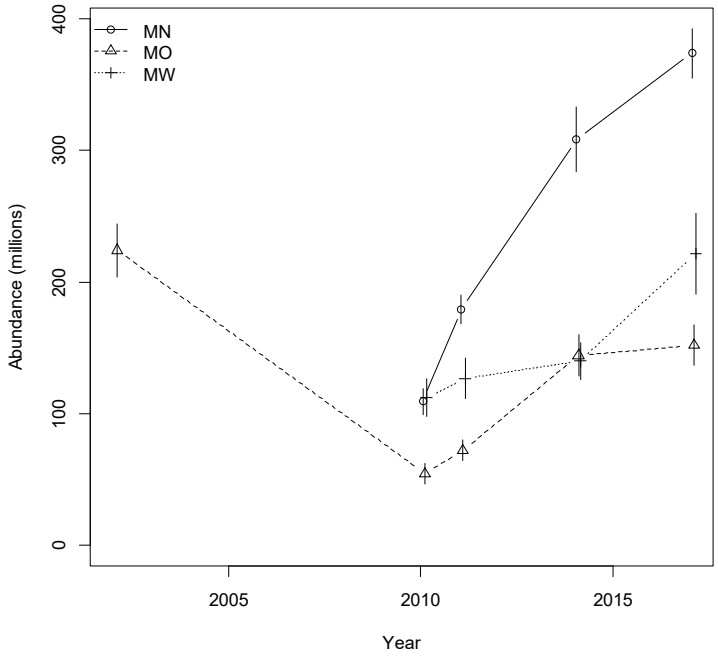

Figure 27: Time series of photographic survey major burrow opening abundance (millions) and CV for SCI 3 by subarea.

3.5.2 Trawl surveys

Stratified random trawl surveys of scampi in SCI 3 were conducted in conjunction with photographic surveys described above. Trawl catch rates from scampi surveys have been scaled up to strata to provide the relative biomass estimates given in Table 8 and Figure 28. The biomass indices were used in the assessment model. Research trawl data are also available from a Chatham Rise middle depths trawl survey time series (using *R.V. Tangaroa*), but this survey targets hoki (*Macruronus novaezelandiae*), hake (*Merluccius australis*), and ling (*Genypterus blacodes*) across the whole region, with station coverage being low within the main scampi fishery areas, and the trawl gear used is not considered appropriate for sampling scampi. Details of the estimation of the catchability priors are provided in Section 3.7.

Table 8: Time series of trawl survey scampi biomass (tonnes) and CV for SCI 3 by subarea.

	MN		MW		MO	
Year	Biomass	CV	Biomass	CV	Biomass	CV
2002					272.5	0.24
2010	82.3	0.25	295.0	0.36	40.2	0.37
2011	199.1	0.07	347.0	0.06	49.0	0.11
2014	246.9	0.06	177.0	0.30	126.5	0.27
2017	454.7	0.20	318.8	0.19	139.6	0.14

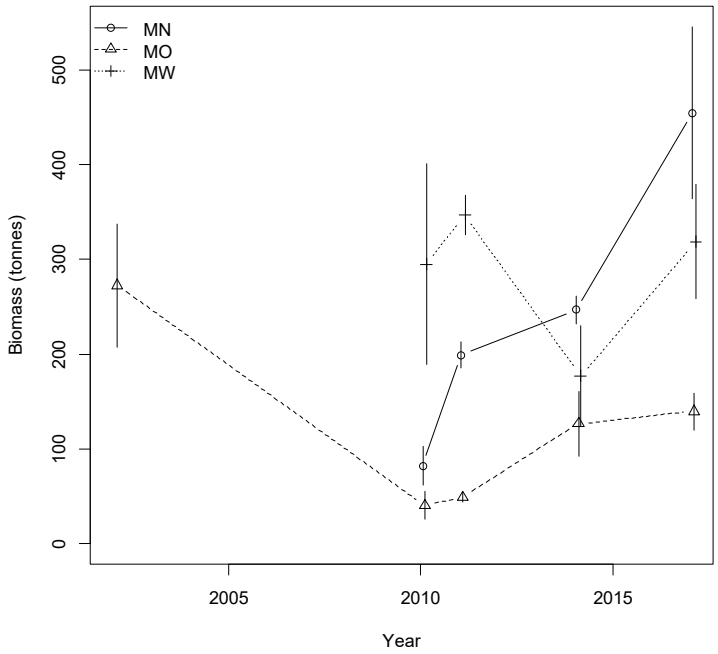

Figure 28: Time series of trawl survey scampi biomass (tonnes) and CV for SCI 3 by subarea.

3.6 Length distributions

3.6.1 Commercial catch length distributions

Government scientific observers have collected scampi length frequency data from scampi-targeted fishing on commercial vessels in SCI 3 since 1991–92. The numbers of tows by subarea and time step for which length data are available are presented by fishing year in Table 9.

Table 9: Numbers of scampi observer length frequency samples from SCI 3, by model year, subarea, and time step (TS).

	MN		MO		MW		No.
Model year	TS 1	TS 2	TS 1	TS 2	TS 1	TS 2	trips
1991/92					1		1
1992/93	15	31					3
1993/94	34	46	50				8
1994/95	23	18	50				3
1995/96	5		12				1
1996/97							0
1997/98	20		13		6		2
1998/99	23		19				4
1999/00	22		6		5		2
2000/01	17		17		1		1
2001/02	8		29		7		5
2002/03	52		18		3		5
2003/04	52		21				4
2004/05	10				18		2
2005/06						7	1
2006/07	25				17	20	4
2007/08	10	7			14	41	4
2008/09		2				11	1
2009/10	9				48		2
2010/11	54	14			17		5
2011/12		4					1
2012/13	46				9	12	2
2013/14	5	11				3	2
2014/15	10	23				4	1
2015/16	3		2		102		2
2016/17	3	29				3	3

Examination of data from other scampi fisheries has suggested that the size composition of catches may vary with depth (Tuck 2015) and so patterns in the sex ratio and mean size from the scampi observer length frequency data were examined using multivariate tree regression (using the R package *mvpart*). Data were analysed for each year separately at the observed tow level, with response variables regressed on the explanatory variables month and depth bin. Pruning was conducted to give the tree with the smallest cross-validated relative error. No consistent depth splits were identified, and the temporal splits were consistent with those already proposed for the model structure (see Table 2). It was therefore considered unnecessary to stratify the length sampling by depth.

Proportional length distributions (and associated CVs) were calculated using CALA (Francis et al. 2016), using the approaches previously implemented in NIWA's *Catch-at-Age* software (Bull & Dunn 2002). Plots of the proportional length distribution are shown by year by time step in Figure 29 to Figure 38.

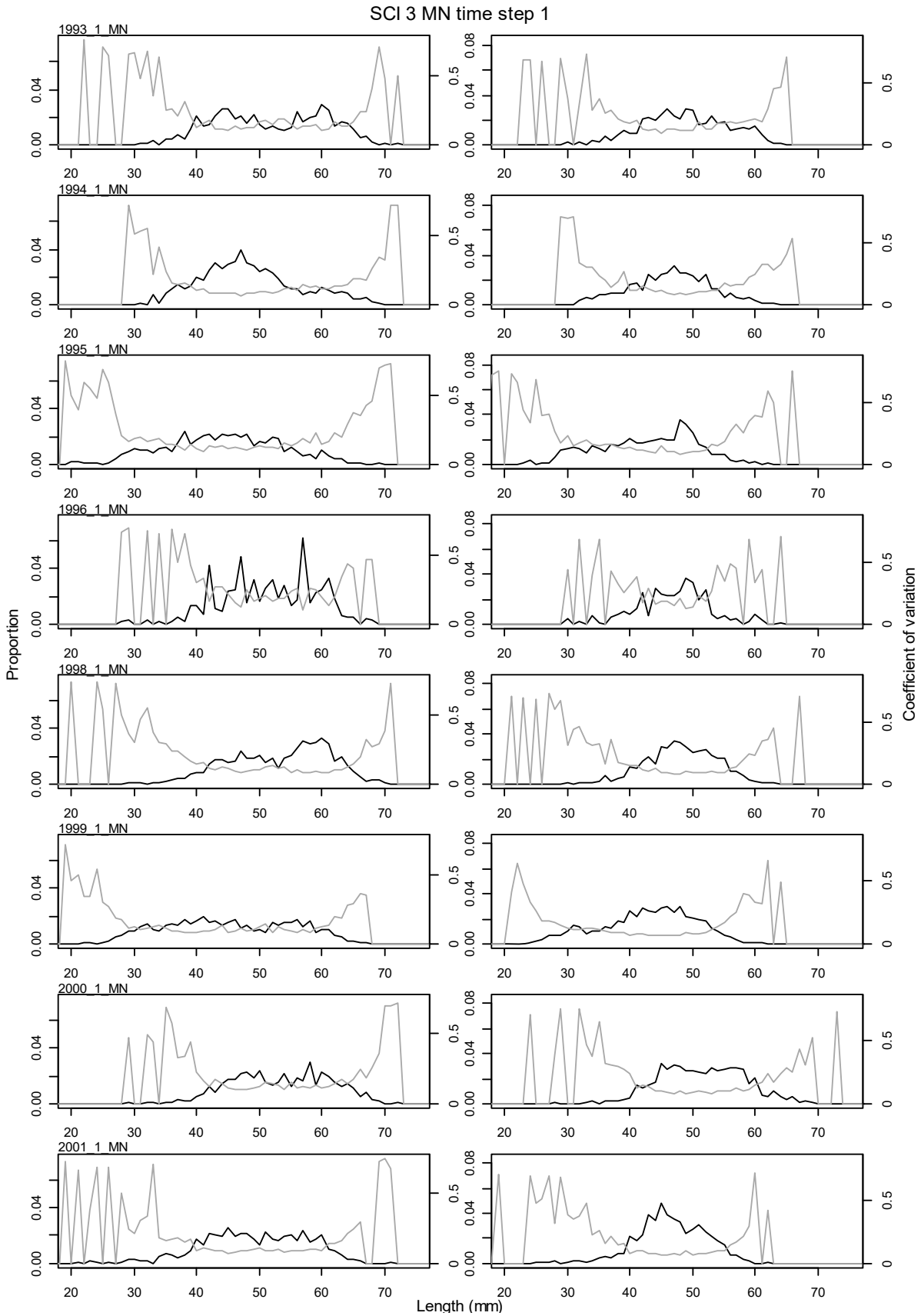

Figure 29: Proportional length frequency distributions (black line) and CVs (grey line) for commercial catches by model year and time step 1 for subarea MN of SCI 3. Males plotted on left, females on right.

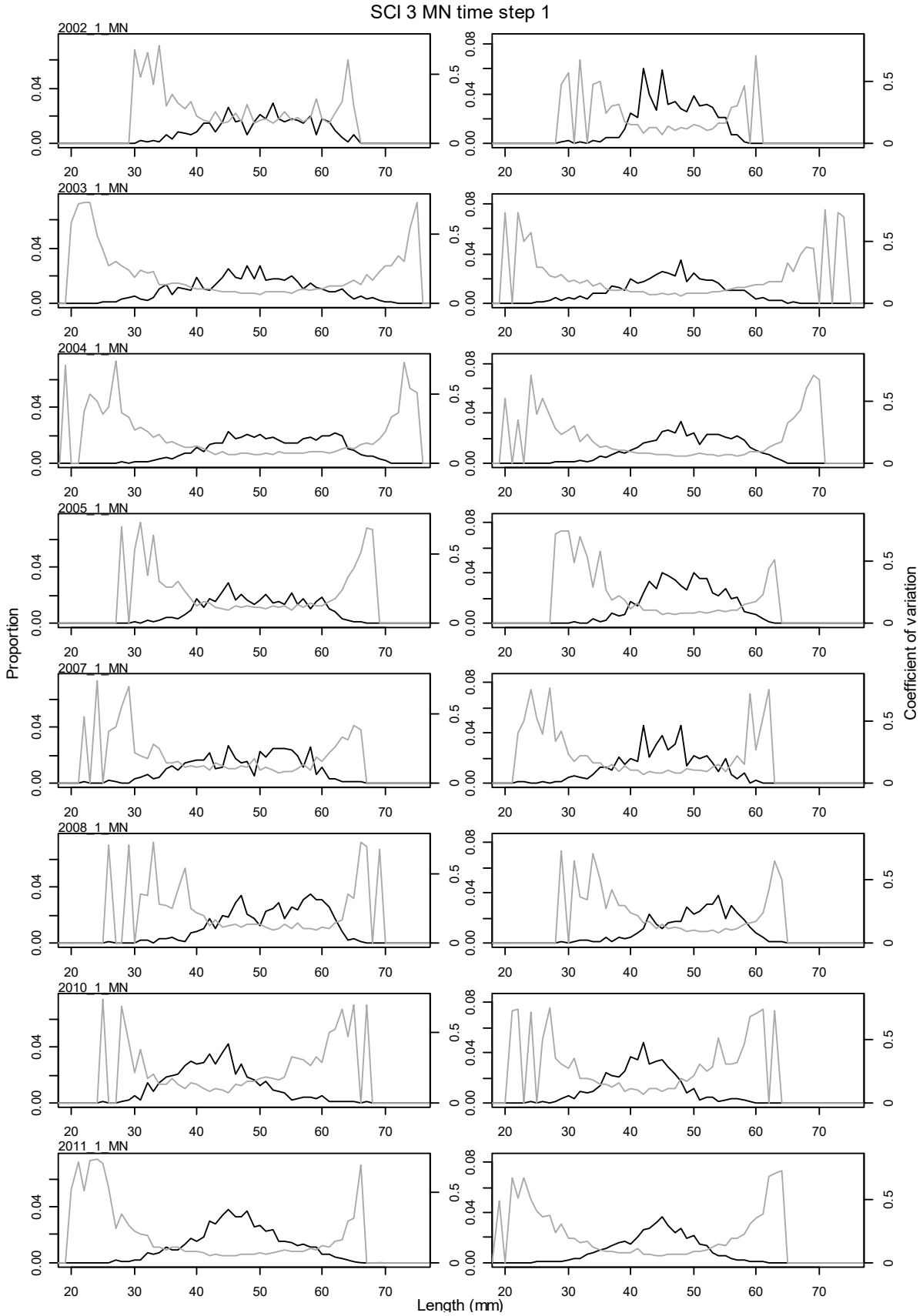

Figure 30: Proportional length frequency distributions (black line) and CVs (grey line) for commercial catches by model year for time step 1 (continued) for subarea MN of SCI 3. Males plotted on left, females on right.

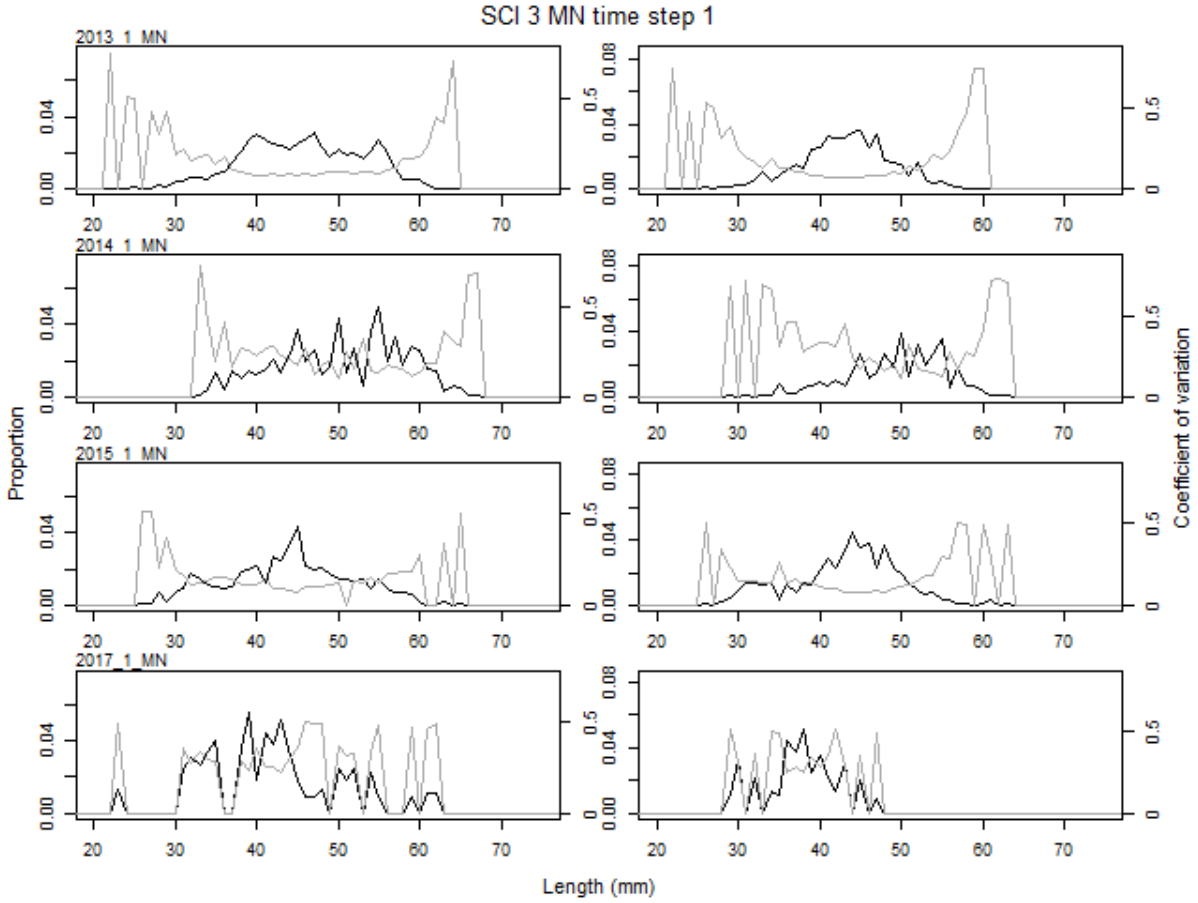

Figure 31: Proportional length frequency distributions (black line) and CVs (grey line) for commercial catches by model year for time step 1 (continued) for subarea MN of SCI 3. Males plotted on left, females on right.

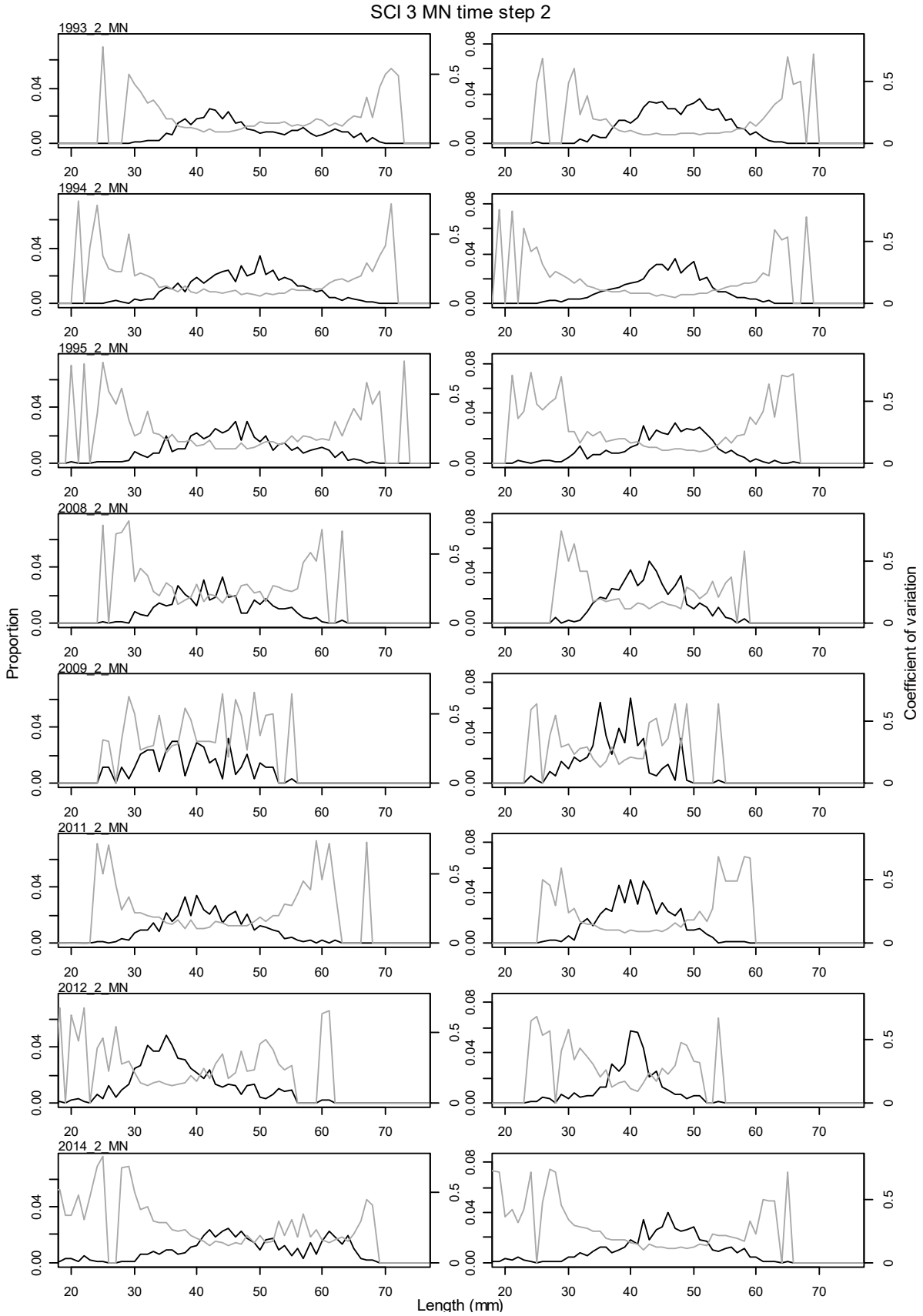

Figure 32: Proportional length frequency distributions (black line) and CVs (grey line) for commercial catches by model year for time step 2 for subarea MN of SCI 3. Males plotted on left, females on right.

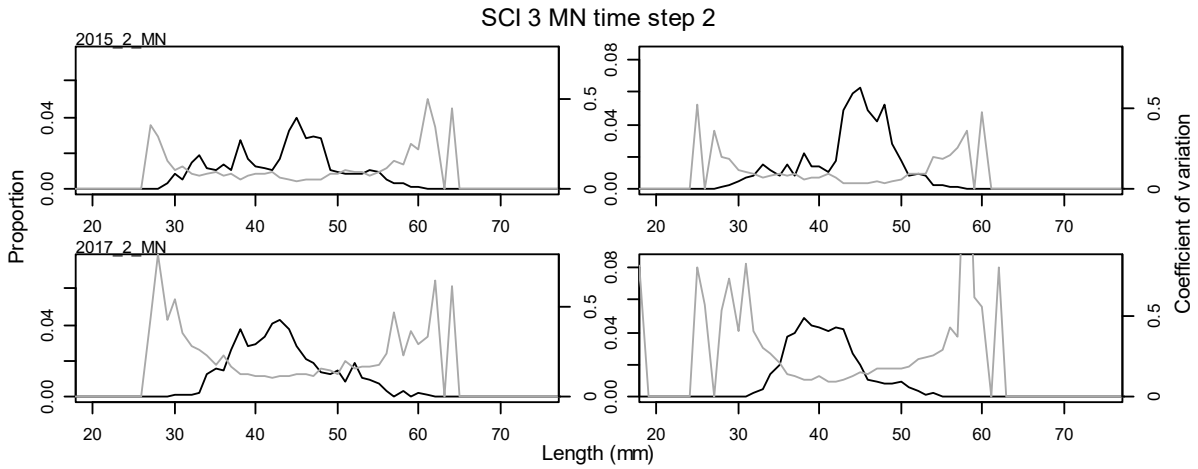

Figure 33: Proportional length frequency distributions (black line) and CVs (grey line) for commercial catches by model year for time step 2 (continued) for subarea MN of SCI 3. Males plotted on left, females on right.

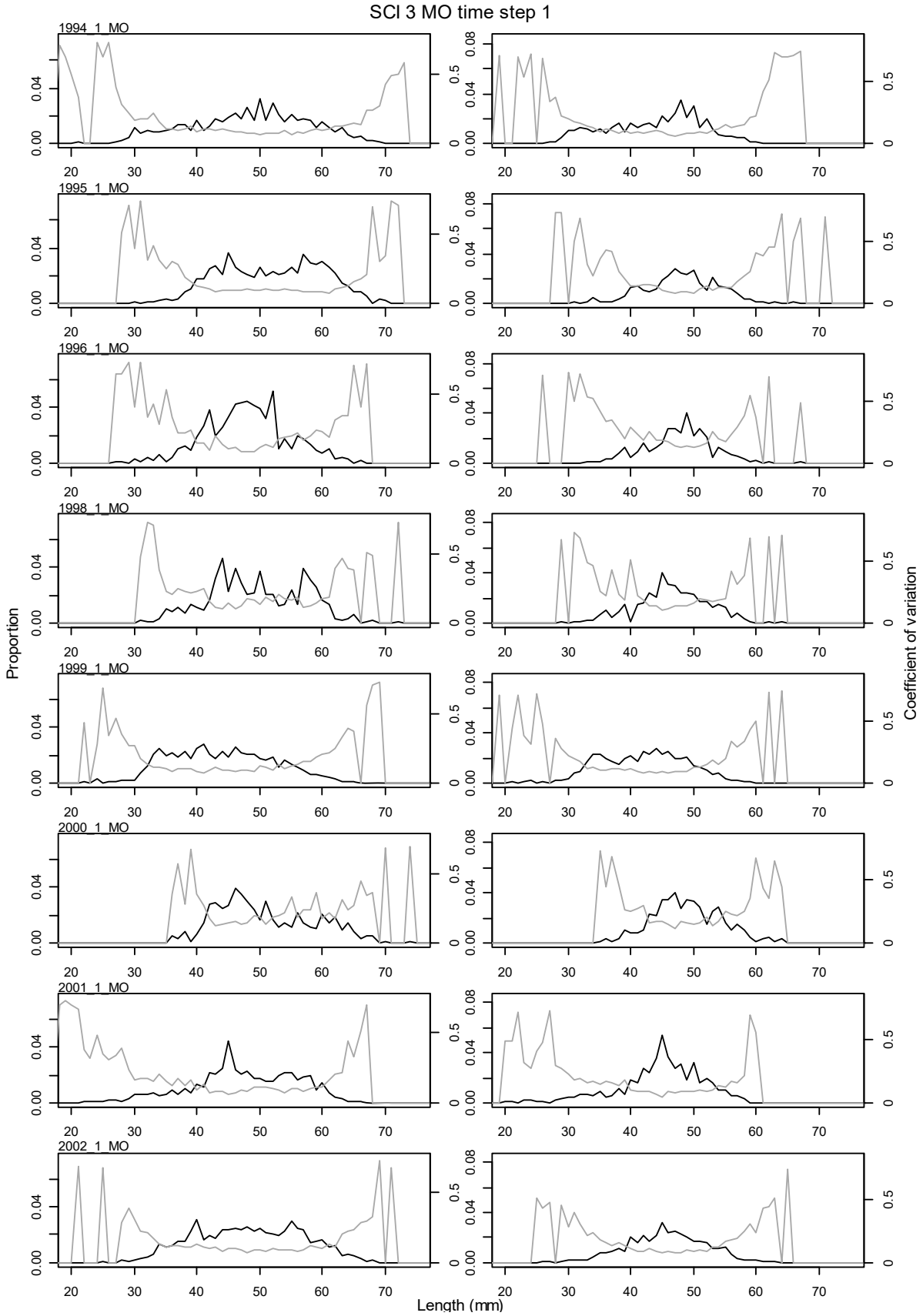

Figure 34: Proportional length frequency distributions (black line) and CVs (grey line) for commercial catches by model year for time step 1 for subarea MO SCI 3. Males plotted on left, females on right.

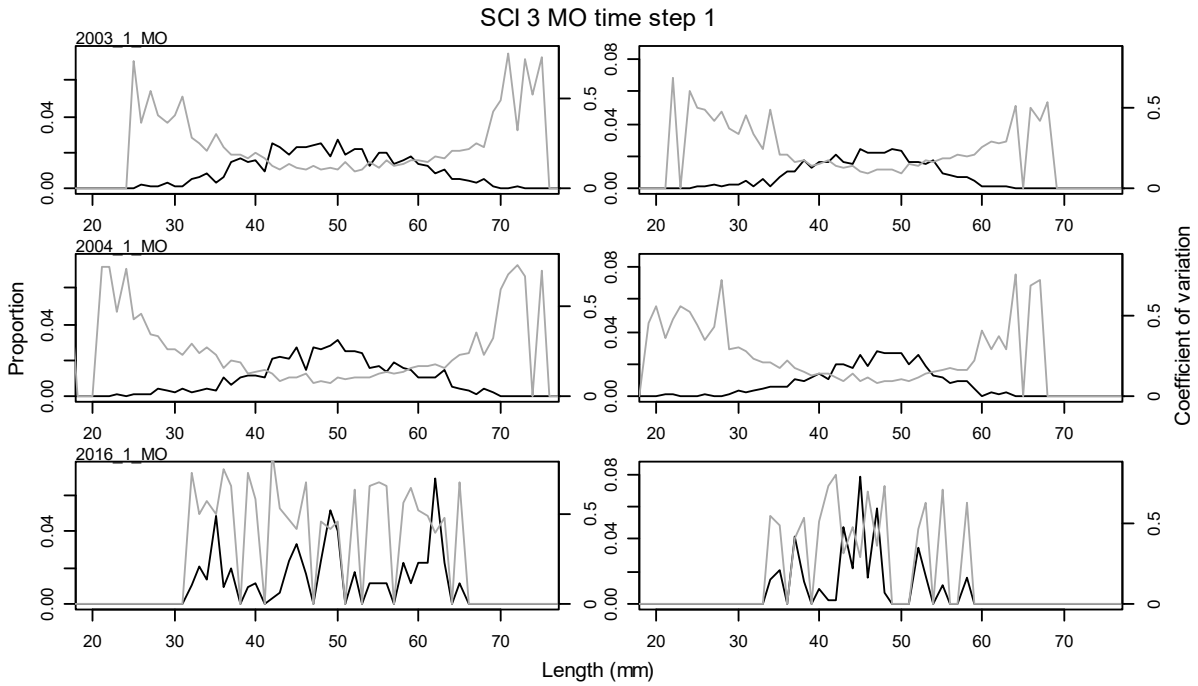

Figure 35: Proportional length frequency distributions (black line) and CVs (grey line) for commercial catches by model year for time step 1 (continued) for subarea MO SCI 3. Males plotted on left, females on right.

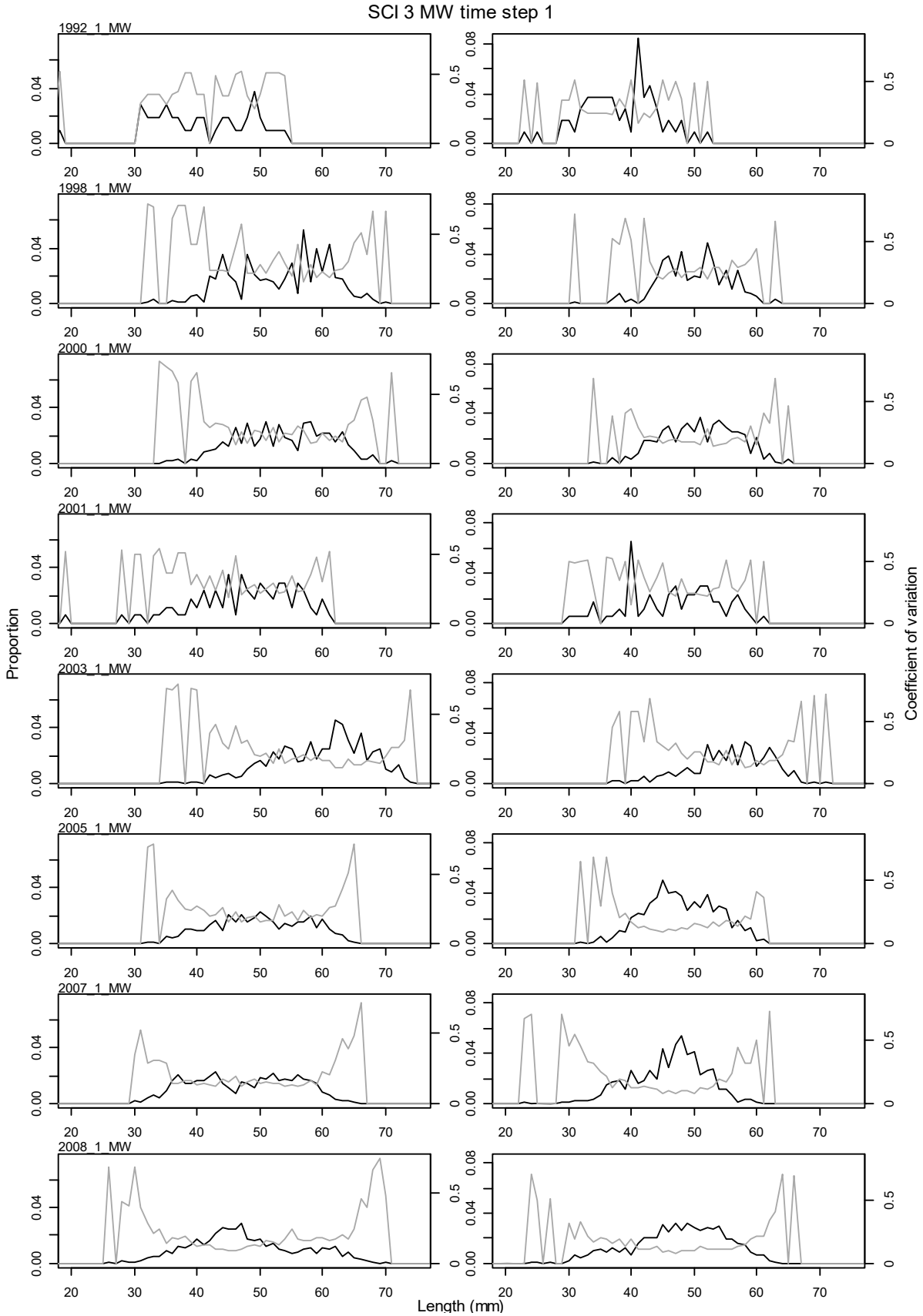

Figure 36: Proportional length frequency distributions (black line) and CVs (grey line) for commercial catches by model year for time step 1 for subarea MW SCI 3. Males plotted on left, females on right.

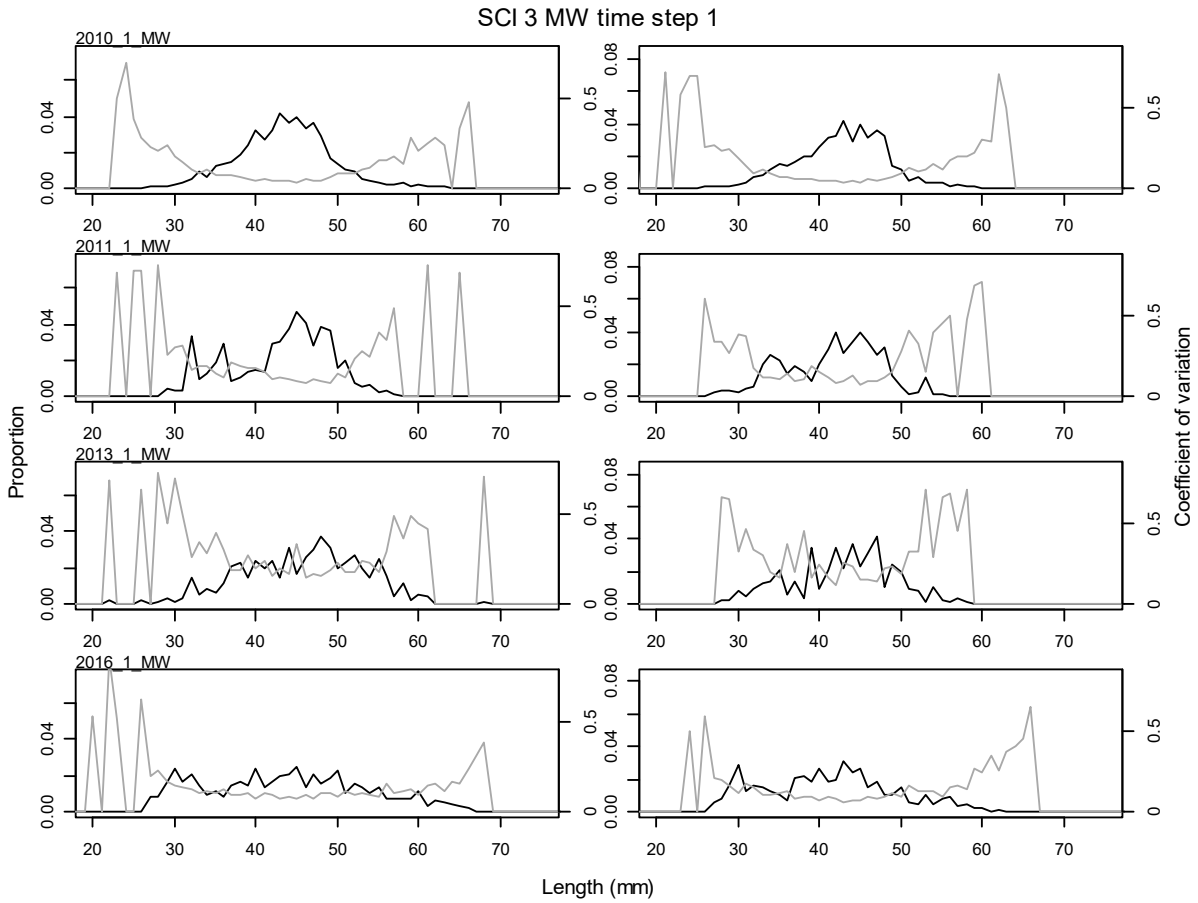

Figure 37: Proportional length frequency distributions (black line) and CVs (grey line) for commercial catches by model year for time step 1 (continued) for subarea MW SCI 3. Males plotted on left, females on right.

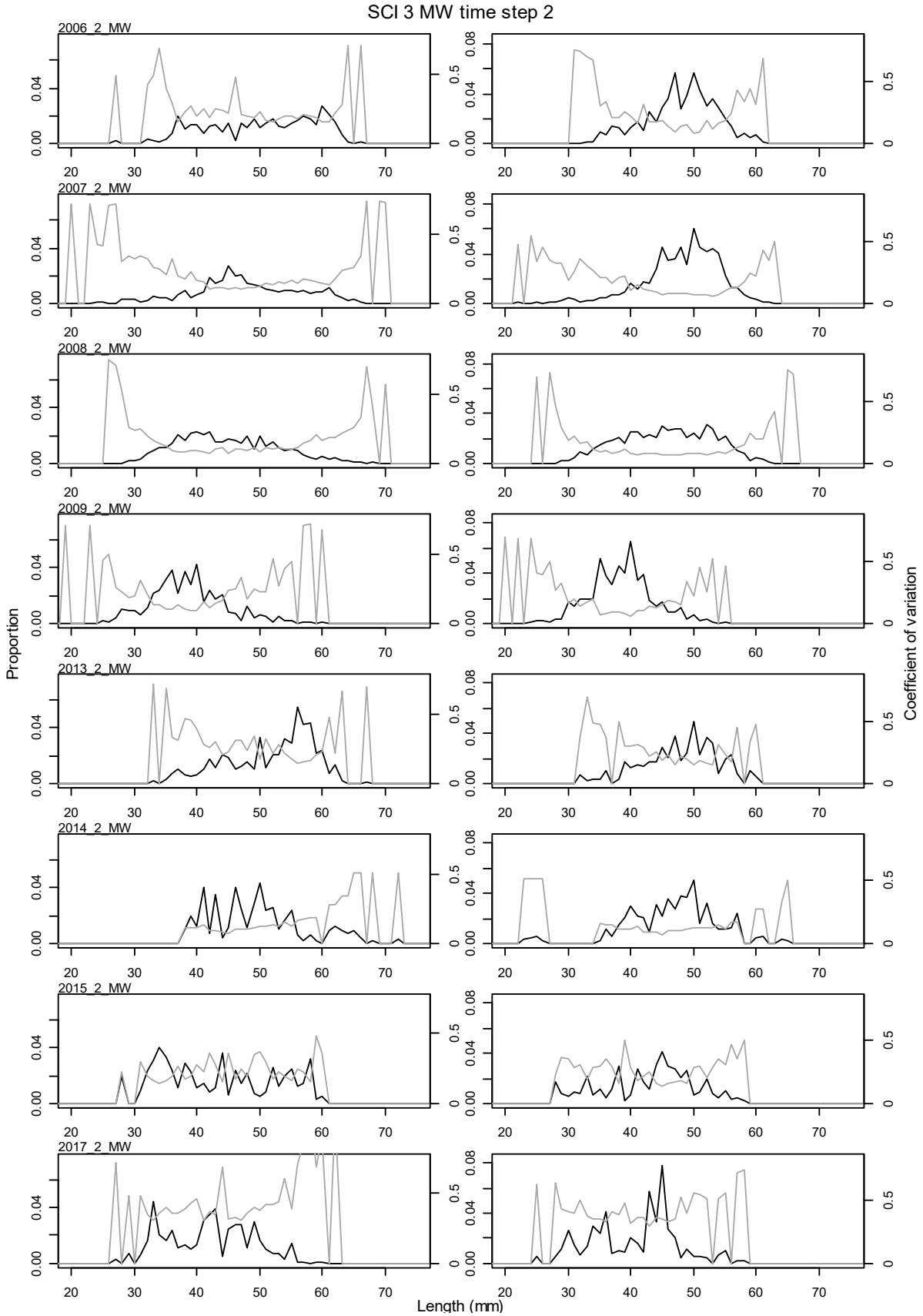

Figure 38: Proportional length frequency distributions (black line) and CVs (grey line) for commercial catches by model year for time step 2 for subarea MW SCI 3. Males plotted on left, females on right.

3.6.2 Trawl survey length distributions

Length frequency samples from research trawling have been taken by scientific staff on all surveys (Table 8). Estimated length frequency distributions (with associated CVs) were derived using NIWA's CALA software (Francis et al. 2016), using 1 mm OCL (Orbital Carapace Length) length classes by sex, and are presented in Figure 39 (MN), Figure 40 (MO), and Figure 41 (MW).

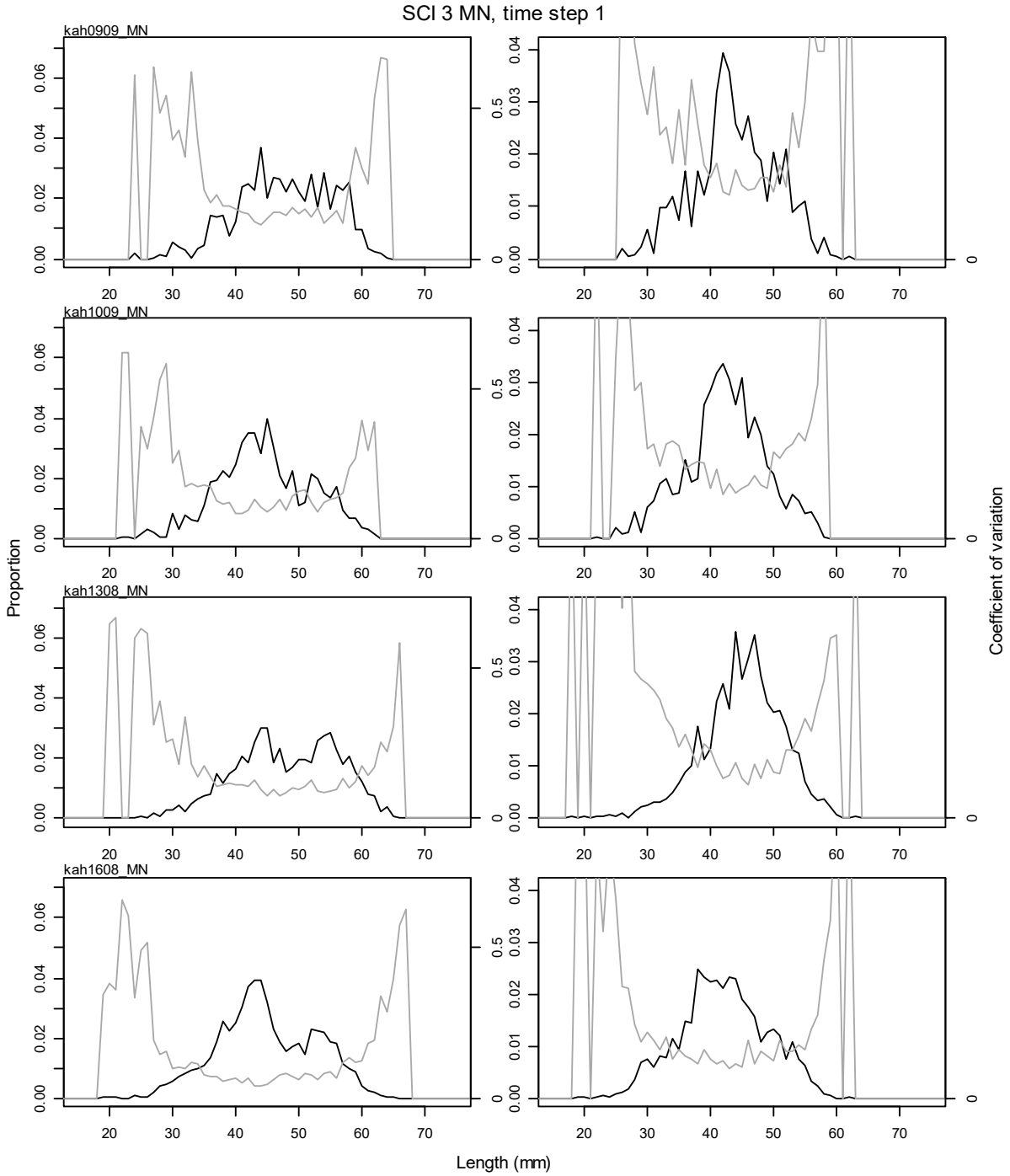

Figure 39: Proportional length frequency distributions (black line) and CVs (grey line) for research survey catches by model year for subarea MN of SCI 3. Males plotted on left, females on right.

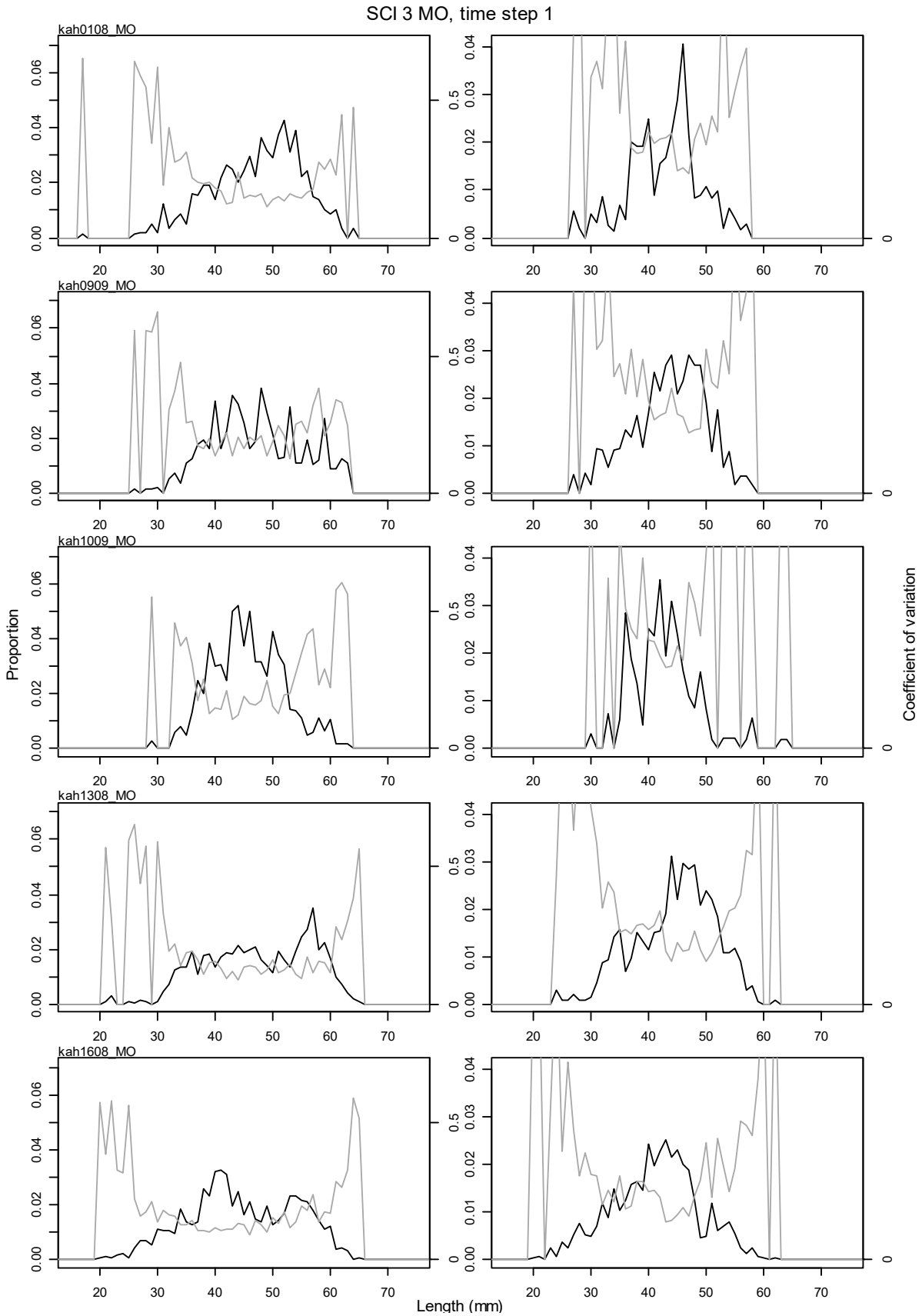

Figure 40: Proportional length frequency distributions (black line) and CVs (grey line) for research survey catches by model year for subarea MO of SCI 3. Males plotted on left, females on right.

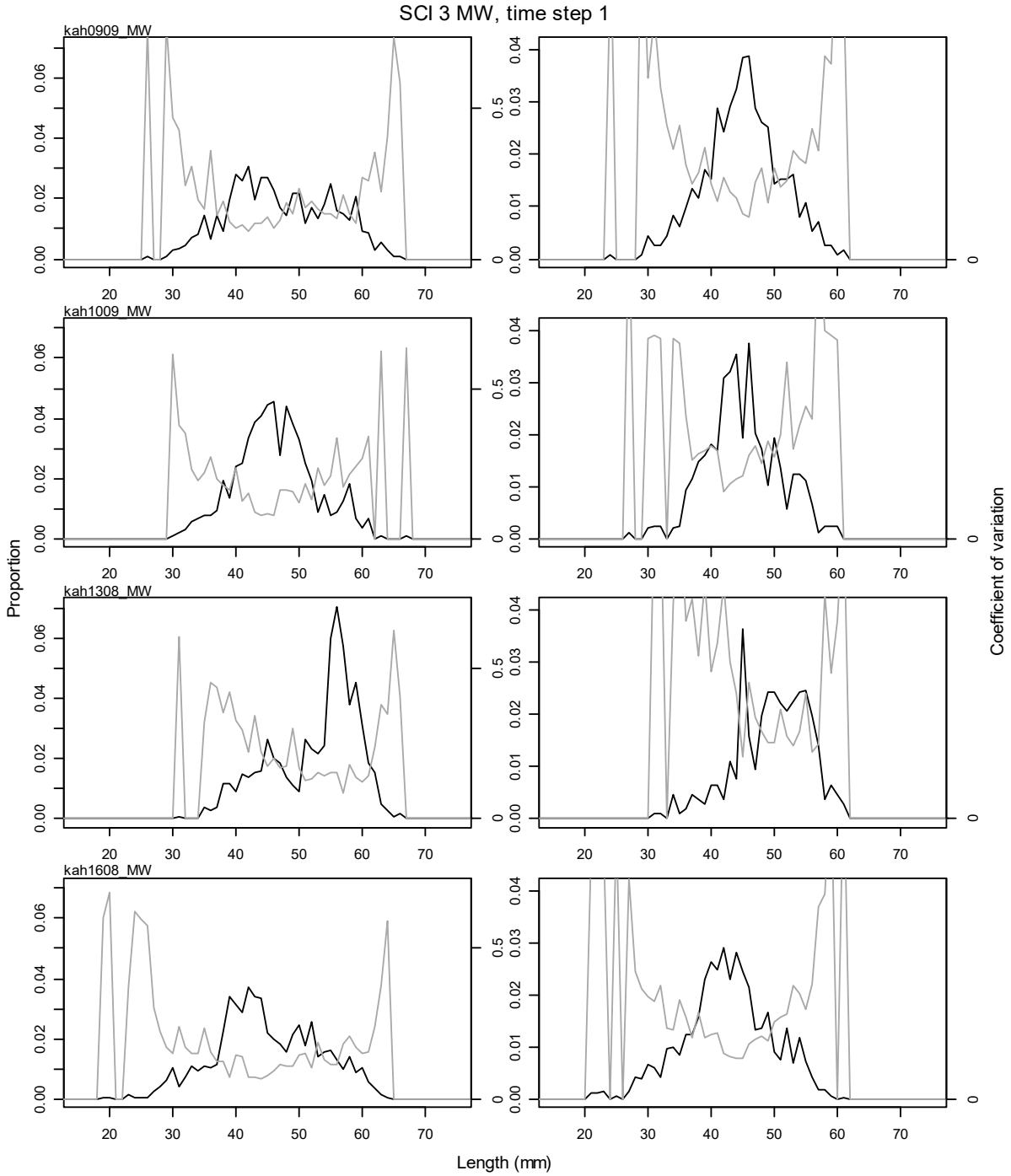

Figure 41: Proportional length frequency distributions (black line) and CVs (grey line) for research survey catches by model year for subarea MW of SCI 3. Males plotted on left, females on right.

3.6.3 Photo survey length distributions

Length frequency distributions were estimated for the relative photographic abundance series by measuring the widths of a large sample of major burrow openings in the images and converting these to orbital carapace lengths using a regression of OCL on major opening width (Cryer et al. 2005), augmented with additional data collected from more recent surveys. To estimate the CVs at length for each year, we used a bootstrap procedure, resampling with replacement from the original observations of burrow width, converting each observation to an estimated scampi size (in OCL), and using an error term sampled from a normal distribution fitted to the regression residuals. Compared with the length frequency distributions from trawl catches, this procedure gave very large CVs, but we think

this is realistic given the uncertainties involved in generating a length frequency distribution from burrow sizes. Estimates of the length frequency distributions (with associated CVs) for scampi generating burrows are presented in
Figure 42.

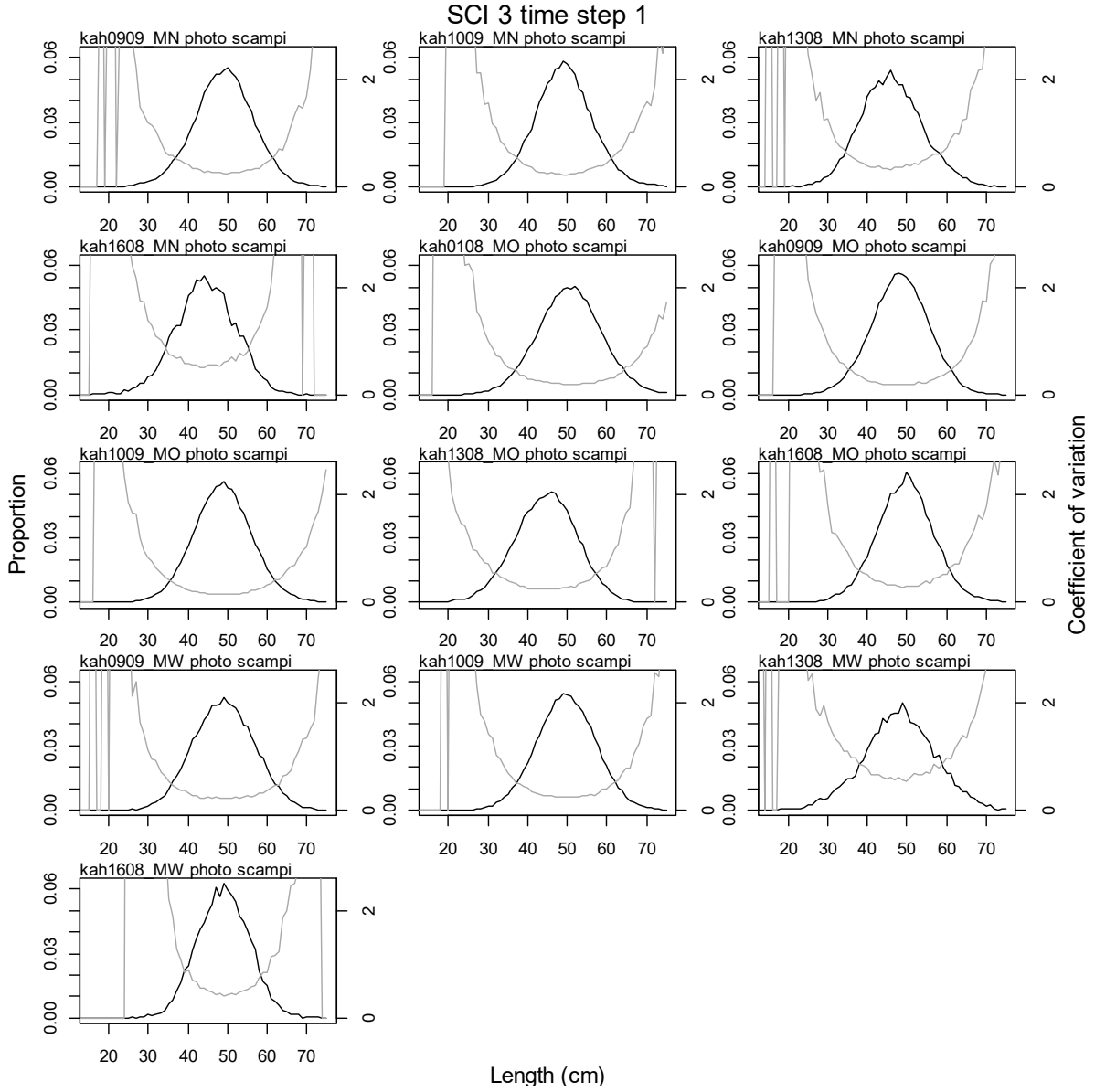

Figure 42: Proportional length frequency distributions (black line) and CVs (grey line) for photo survey observations of visible scampi by model year for SCI 3.

3.7 Model assumptions and priors

Maximum Posterior Density (MPD) fits were found within CASAL using a quasi-Newton optimiser and the BETADIFF automatic differentiation package (Bull et al. 2012). Fitting was done inside the model except for the weighting of the abundance and length frequency data. For the length frequency data, observation-error CVs were estimated using CALA, and then converted to equivalent observation-error multinomial Ns, which were used within the model. The appropriate multinomial Ns to account for both observation and process error were then calculated from the model residuals (method TA1.8), and these final Ns were used in all models (Francis 2011). This generally resulted in small Ns for the commercial length frequency data in particular, and therefore relatively low weighting

within the model. For the CPUE indices, the approach proposed by Clark & Hare (2006), and recommended by Francis (2011) was applied, to estimate the appropriate CV by fitting a smoother to the index. Process error for trawl and photo survey indices was estimated within preliminary runs of the model and, then on the basis of this, fixed at 0.25 and 0.2 respectively. CASAL was also used to generate Markov chain Monte-Carlo (MCMC) for the base models. MPD output was analysed using the extract and plot utilities in the CASAL library running under the general analytical package R.

The initial model was based on that described previously (Tuck & Dunn 2009; Tuck & Dunn 2012; Tuck 2014; Tuck 2015). The model inputs include catch data, abundance indices (CPUE, trawl, and photo surveys), and associated length frequency distributions. The parameters estimated by the base model include SSB_0 and R_0, and time series of *SSB* and year class strength; selectivity parameters for commercial and research trawling, and the photo survey; and associated catchability coefficients. To reduce the number of fitted parameters, the catchability coefficients (*q*s) for commercial fishing, research trawling, and photographic surveys have previously been assumed to be "nuisance" rather than free parameters. At the request of the SFAWG, models were also run with the *q*s as free parameters. The only informative priors used in the initial model were for *q-Photo*, *q-Trawl*, and the YCS vector (which constrains the variability of recruitment).

3.7.1 Scampi catchability

Previous priors for scampi catchability have been largely based on information on *Nephrops* emergence and occupancy rates from European studies conducted in far shallower waters than *Metanephrops* populations inhabit (Tuck & Dunn 2012), but the acoustic tagging study conducted at the Mernoo Bank in October 2010 offered an opportunity to estimate priors for occupancy and emergence from New Zealand data (Tuck 2013). Acoustic tagging was repeated successfully within the SCI 1 and SCI 2 surveys in 2012 (Tuck et al. 2015b) and was also conducted within the SCI 6A and SCI 3 surveys in 2013 (although less successfully). The data collected within these studies have been used to estimate catchability priors (Tuck et al. 2015a).

Acoustic tags were fitted to scampi, which were released with a moored hydrophone which recorded tag detections and, hence, when animals were emerged from burrows. Data were recorded over a period of up to 106 days (Tuck et al. 2015a). Some tag detections showed distinct cyclical patterns (12.6 hour cycle), but most animals showed no clear patterns, and the proportion of scampi detectable over the duration of the studies varied from 20 to 80% (2.5th to 97.5th percentile of range), with a median detection of 53%.

In previous analysis, the density of all visible scampi (ranging from those walking free on the surface to those within burrows, where only the tips of claws can be seen) is scaled by emergence. Before conducting emergence trials with live scampi, scuba divers activated and placed tags in burrows in shallow waters to confirm whether they became undetectable when they were acoustically obscured by the burrow. This showed that tags were detected on the surface of the seabed, and in the entrance to burrows, but not within a burrow.

Scampi are thought to spend a considerable amount of time within the burrow entrance, "door keeping", and inclusion of all these individuals in the density of scampi to be scaled up by the emergence rate is likely to overestimate the population density. When "door keeping", a scampi's position (and the likelihood of it being acoustically detectable if it carried a tag) can range from only just in the burrow (Figure 43, left, very likely to be detected), to about half in (Figure 43, centre, as likely or not to be detected), or almost fully in, with only the claws visible (Figure 43, right, very unlikely to be detected). Therefore, acoustically detectable scampi are considered those walking free on the surface (emerged) and a proportion of door keepers.

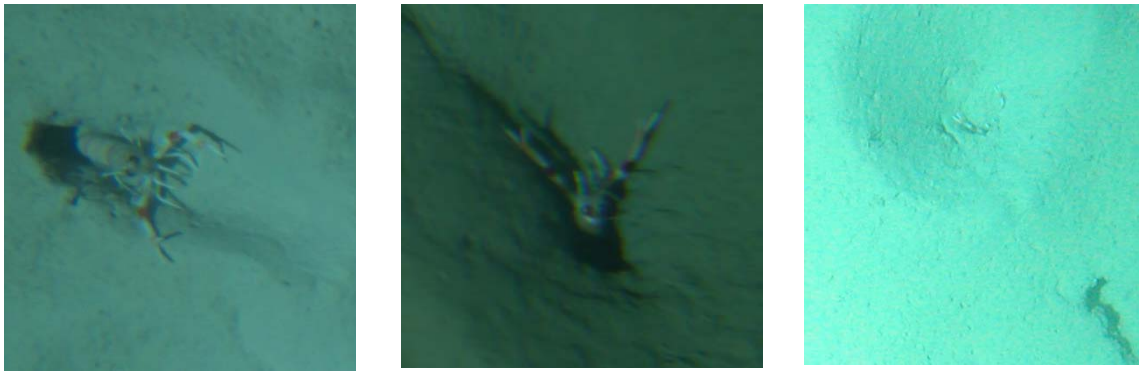

Figure 43: Examples of scampi within the entrance to burrows (door keeping).

On the basis of the data available for SCI 3, estimated population density would vary from 0.0330 m^{-2} to 0.0068 m^{-2}, depending on the proportion of tagged scampi within burrow entrances (door keepers) assumed to be acoustically detectable (Table 10). The number of detectable animals is then used in conjunction with the emergence and burrow count data to provide an estimate for *q-Photo* (the catchability for the burrow index, the number of major burrow openings per scampi).

Table 10: Examination of implications of acoustic detectability of door keeping scampi on estimated scampi population density and *q_photo*, based on median estimates from SCI 3 studies.

	% of door keepers detectable acoustically							Source
	0%	5%	30%	50%	70%	95%	100%	
Major opening density (m^{-2})	0.0794	0.0794	0.0794	0.0794	0.0794	0.0794	0.0794	From survey
Visible scampi density (m^{-2})	0.0175	0.0175	0.0175	0.0175	0.0175	0.0175	0.0175	From survey
Emerged scampi density (m^{-2})	0.0036	0.0036	0.0036	0.0036	0.0036	0.0036	0.0036	From survey
Door keeping density (m^{-2})	0.0139	0.0139	0.0139	0.0139	0.0139	0.0139	0.0139	Visible - emerged
Detectable scampi density (m^{-2})	0.0036	0.0043	0.0078	0.0105	0.0133	0.0168	0.0175	Emerged + (door keepers * % detectable)
Emergence rate	53%	53%	53%	53%	53%	53%	53%	From acoustic tags
Estimated population density (m^{-2})	0. 0068	0. 0081	0. 0147	0. 0199	0. 0252	0. 0317	0. 0330	Detectable / emergence
q_photo	11.69	9.80	5.41	3.99	3.15	2.51	2.40	Major openings * emergence / detectable

* - multiplied by

Once the emergence rate and detectable scampi density were used to estimate scampi population density, the density of scampi seen (that are likely to be caught in a trawl) is then used to estimate trawl catchability. In previous analyses the density of all scampi out of burrows was divided by the estimated scampi population density. However, examination of the relationship between estimates of scampi abundance (animals out of burrows) from photographic surveys and trawl sampling at a later date, during the same survey, suggests that although there is a noisy positive relationship (r^2=0.22), it is not a 1:1 slope, and, on average, the trawl catch estimates are a half to a third of the emerged scampi estimates (Figure 44). The pattern appears reasonably consistent between stocks.

Therefore, trawl survey catchability (*q-Trawl*) varies with both the percentage of door keepers that are acoustically detectable and the percentage of emerged scampi that would be caught if within the path of a trawl (Table 11).

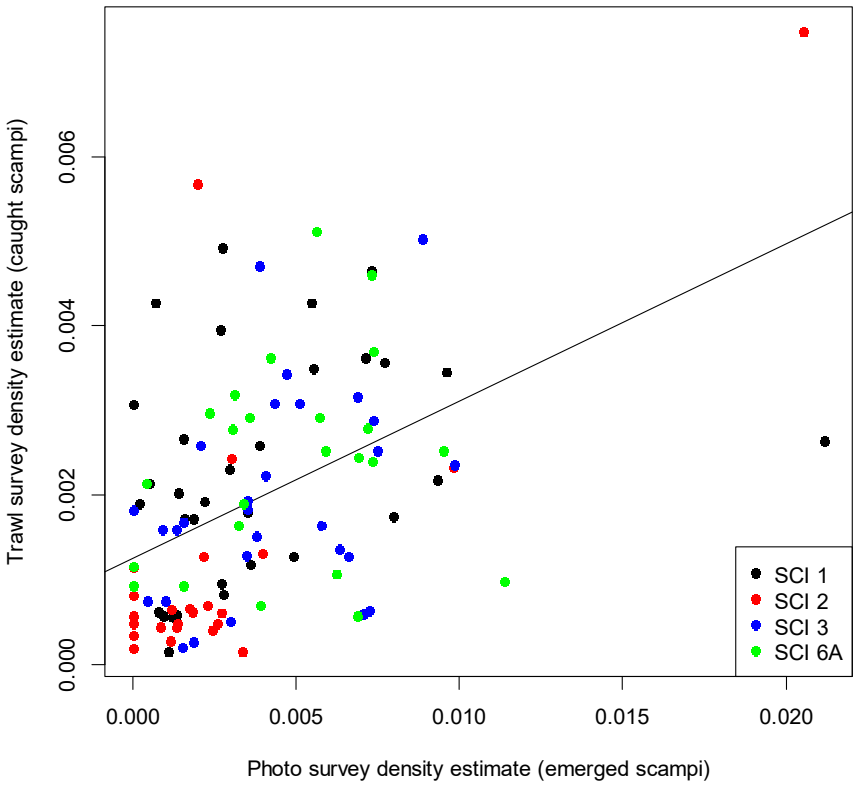

Figure 44: Relationship between strata level photographic survey estimate of emerged scampi density and trawl survey scampi density. Line represents best linear fit through all data (r^2=0.22).

Table 11: Estimated scampi density (on basis of observed data and assumptions on detectability of door keepers), the density of available scampi, and implied *q-Trawl*, on basis of assumptions on percentage of emerged scampi caught.

% of emerged scampi likely to be caught	Density of available scampi (m^{-2})	% of door keepers detectable acoustically						
		0%	5%	30%	50%	70%	95%	100%
Estimated density (m^{-2})		0.0068	0.0081	0.0147	0.0199	0.0252	0.0317	0.0330
10%	0.0004	0.0530	0.0444	0.0246	0.0181	0.0143	0.0114	0.0109
30%	0.0011	0.1590	0.1333	0.0737	0.0543	0.0429	0.0341	0.0327
40%	0.0014	0.2120	0.2221	0.0982	0.0723	0.0573	0.0454	0.0436
50%	0.0018	0.2650	0.2221	0.1228	0.0904	0.0716	0.0568	0.0545
70%	0.0025	0.3710	0.3110	0.1719	0.1266	0.1002	0.0795	0.0763
100%	0.0036	0.5300	0.4442	0.2456	0.1809	0.1431	0.1135	0.1090

3.7.2 Priors for *q*s

The emergence rate data and relative counts of emerged scampi, door keeping scampi, and scampi burrows are used to provide estimates of burrow, visible animal, and trawl survey catchability. Uncertainty in each component was accounted for by assumptions on the plausible range for percentage of door keepers that would be acoustically detectable (5–95%), the percentage of emerged scampi that would be caught in a trawl (10–70%), and resampling from the original distributions of emergence, and

animal and burrow counts (1000 iterations).The mean and upper and lower bound (2.5th and 97.5th quantiles) of the estimated catchability distributions were fitted within a binomial GLM (probit link) to estimate the slope and intercept of the cumulative frequency distribution, which in turn were used to estimate the mean and standard deviation of the lognormal distribution of the priors for the various catchability terms used in the assessment model.

q-Photo
This is the proportion of the scampi population represented by the count of major burrow openings. The best estimate is 3.99 (based on 50% detectability of door keepers; see Table 10). Upper and lower estimates are taken on the basis of 5% and 95% detectability and are assumed to reflect the 2.5th and 97.5th percentiles of the catchability distribution.

q-Trawl
This is the proportion of the scampi population represented by the trawl survey catches. The best estimate is 0.0723 (based on 50% detectability of door keepers and 40% of emerged scampi are caught; see Table 11). Upper and lower estimates are taken from the combination of 10–70% of emerged scampi being caught and 5–95% detectability of doorkeepers (see Table 11), as the 2.5th and 97.5th percentiles of the catchability distribution.

The distributions of the priors (Figure 45) are somewhat different to those previously used in the SCI 3 assessment (Tuck 2016b) and reflect an improved consideration of the data and factors contributing to scampi catchability.

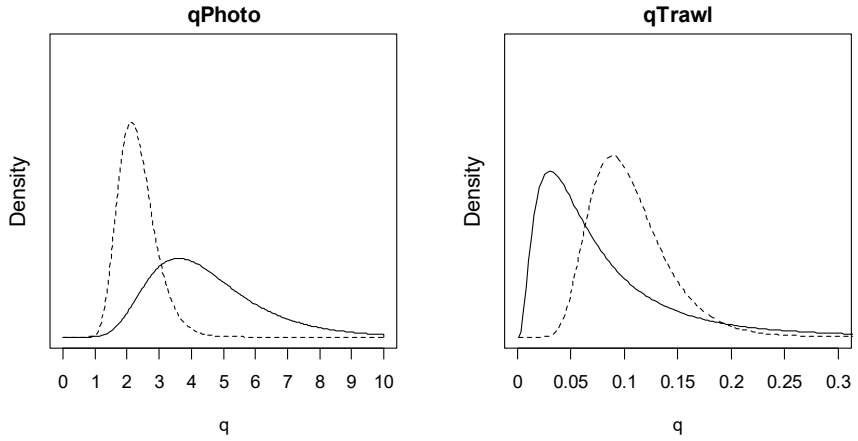

Figure 45: Estimated distribution of *q-Trawl* and *q-Photo* for SCI 3. Solid line represents the distribution of the prior as implemented in the current assessment; the dashed line represents the previous distribution (Tuck 2016b).

3.7.3 Recruitment

Few data are available on scampi recruitment. Relative year class strengths were fixed at 1 for the two most recent years and were assumed to average 1.0 over all other years. In the initial model development (Cryer et al. 2005), lognormal priors on relative year class strengths were assumed, with mean 1.0 and CV of 0.2. The sensitivity of year class strength (YCS) variation was examined in further developments (Tuck & Dunn 2006) and later increased to a CV of 1 (Tuck & Dunn 2012). Model explorations within the recent SCI 6A assessment (Tuck 2017) suggested that extreme YCS values estimated by the model were related to model structure rather than data. The preliminary model, and those applied to other scampi stocks, used the Haist parameterisation of YCS (Bull et al. 2012) where

$$YCS_i = \frac{y_i}{\bar{y}}$$

with a lognormal prior on y_i with mean of 1 and CV of 1, and a small penalty to ensure that the mean of YCS does not drift away from 1 ("a YCS average to 1 penalty"). Sensitivity trials (Tuck 2017) with the Haist parameterisation showed that both individually removing the penalty, and tightening the CV on the YCS prior, reduced the final YCS estimated by the model, but only removing the penalty and tightening the CV (to 0.7) generated a final YCS estimate of similar magnitude to previous good years. Further investigations examined the sensitivity to the CV on the YCS prior for models with the Haist parameterisation but no YCS average to 1 penalty, and also without the Haist parameterisation but with a YCS average to 1 penalty (Tuck 2017).

On the basis of these sensitivity analyses, the SFAWG agreed to proceed with a model structure implementing the Haist parameterisation, without the YCS average to 1 penalty, and with tighter CVs on the YCS prior. Preliminary examination of the implications of this parameterisation change to previously accepted stock assessment models for SCI 1 and SCI 2 did not suggest that perceptions of stock status would be altered, although this will be further examined as these assessments are updated.

The relationship between stock size and recruitment for scampi is unknown, and a Beverton Holt relationship with a steepness of 0.8 has been assumed. New Zealand scampi have very low fecundity (Wear 1976; Fenaughty 1989) (in the order of tens to hundreds of eggs carried by each female), so very successful recruitment is probably not plausible at low abundance. Recruitment enters the model partition as a year class, with a normally distributed OCL of mean 10 mm and CV of 0.4.

4. ASSESSMENT MODEL RESULTS

4.1 Initial models

As described in section 3.1, a three-stock three-area model was applied, with annual CPUE, photo, and trawl survey indices for each stock, and the same YCS pattern was shared by the three stocks. This model shared the photo survey catchability (*q-Photo*) between stocks (on the grounds that the camera survey should operate independently of seabed conditions), but estimated separate fishery and trawl survey (*q-Trawl*) catchability terms for each stock (on the basis of reports from the fishing industry that the areas "fished differently"). Preliminary model runs were based on the previous model successfully applied to SCI 3 (Tuck 2016b) and included the previously applied catchability priors to test sensitivities to some structural changes.

As described in section 3.7.3, the parameterisation of YCSs has been modified since the last assessment. Previous sensitivit conducted for SCI 1 and SCI 2 found that revising the YCS parameterisation did not change the perception of stock status (%SSB_0) (Tuck 2017). For SCI 3, the revised YCS parameterisation led to the estimation of a smaller peak YCS in the mid 1990s, but a generally similar pattern; above average YCS in the mid to late 1990s, a period of low recruitment through the 2000s, and above average YCS in the most recent years (Figure 46). The lower peak YCS in the mid 1990s led to a lower magnitude increase in biomass in the late 1990s and the estimation of a slightly higher stock status by 2014 (final assessment year). The SFAWG considered this to be a more realistic pattern in YCS than the previous model and agreed to proceed with the revised parameterisation.

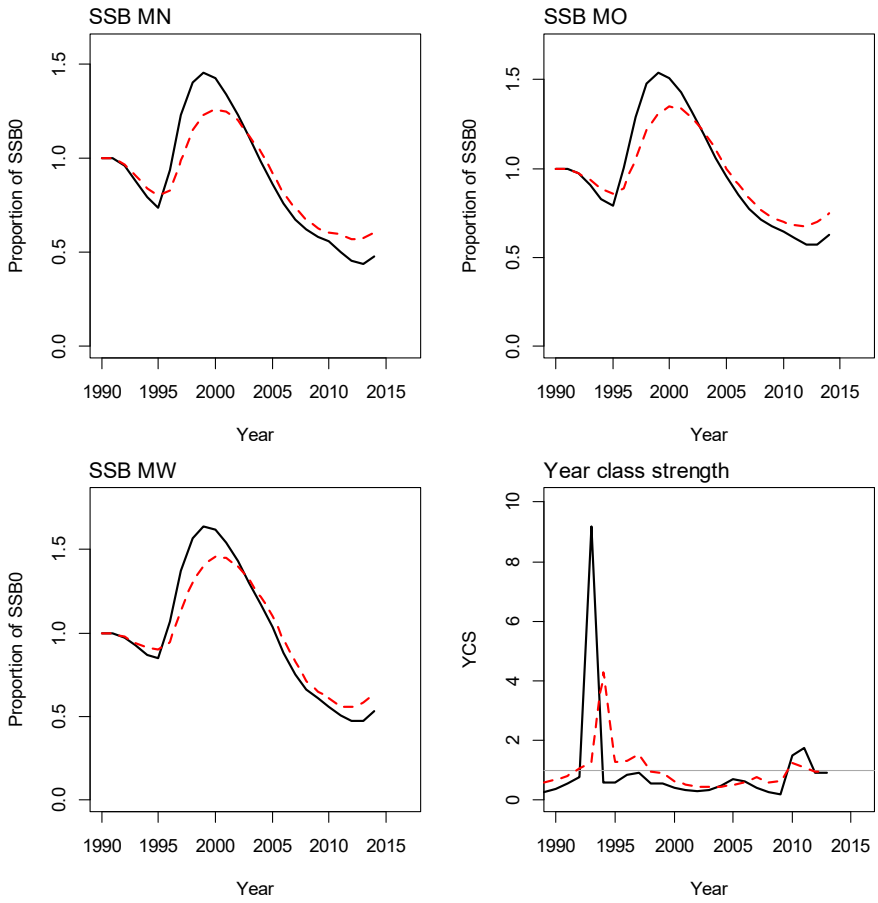

Figure 46: Sensitivity of previously accepted SCI 3 assessment model stock status trajectory and YCS (Tuck 2016b) to revised recruitment parameterisation (no YCS average to 1 penalty, CV on YCS prior = 0.4). Black line – previous parameterisation, red line – revised parameterisation.

New observer data on sex ratio in catches suggested a revision of the model year was appropriate (moving June from the start of time step 1 to the end of time step 2) (see section 2.3; Table 3). The effect of this change, and the extension of the assessment period to the end of the 2017 model year (June 2017), was to estimate a slightly lower peak YCS in the mid 1990s, resulting in a slightly lower stock trajectory subsequent to this (Figure 47). The above average YCS towards the end of the assessed period for the previous model (2010) was confirmed by the new model, and an above average YCS was also estimated for 2014.

Following updating of the model data, the influence of the revised catchability priors (see section 3.7.2) was examined. The revised priors (see Figure 45) suggest that *q-Trawl* is lower than previously expected (trawl survey catches represent a smaller proportion of the population), and *q-Photo* is higher (the ratio of burrow opening to scampi is higher). The revised priors led to the estimation of a greater B_0 (Figure 48), but had no effect on the perception of stock status or YCS patterns (Figure 49).

A range of further sensitivity analyses to some of the key parameter or structural assumptions of the model were also examined. These included treating the SCI 3 population as a single stock, sensitivities to natural mortality and the assumed process error on the CPUE indices, individual YCS patterns for each stock, and individual catchability terms for each stock.

The SCI 3 assessment has previously been undertaken as a three stock, three area model because of the differing fishing and management histories of the three distinct regions (see section 1.1, Table 1, Figure 4, and Figure 5), but the three stock model adds significant complexity. The SFAWG therefore requested a single stock model be developed, for comparison with the three stock, three area model.

The single stock model estimated a lower peak YCS in the mid 1990s, but had a very similar YCS pattern (Figure 50). Stock biomass and stock status show an increase in the late 1990s (following the peak YCS), but not to the extent estimated within the three stock model, although biomass and stock status are estimated at very similar levels in both models after about 2010.

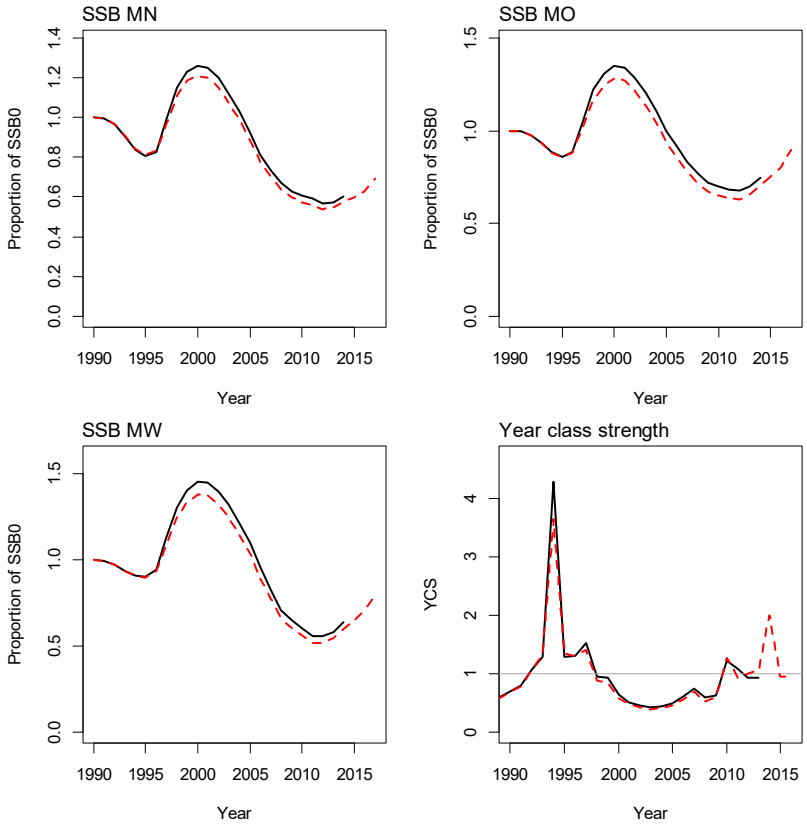

Figure 47: Sensitivity of the SCI 3 assessment model stock status trajectory and YCS with revised recruitment parameterisation to updating of the catch and abundance indices. Black line – model to 2014, red line – revised model year, model to 2017.

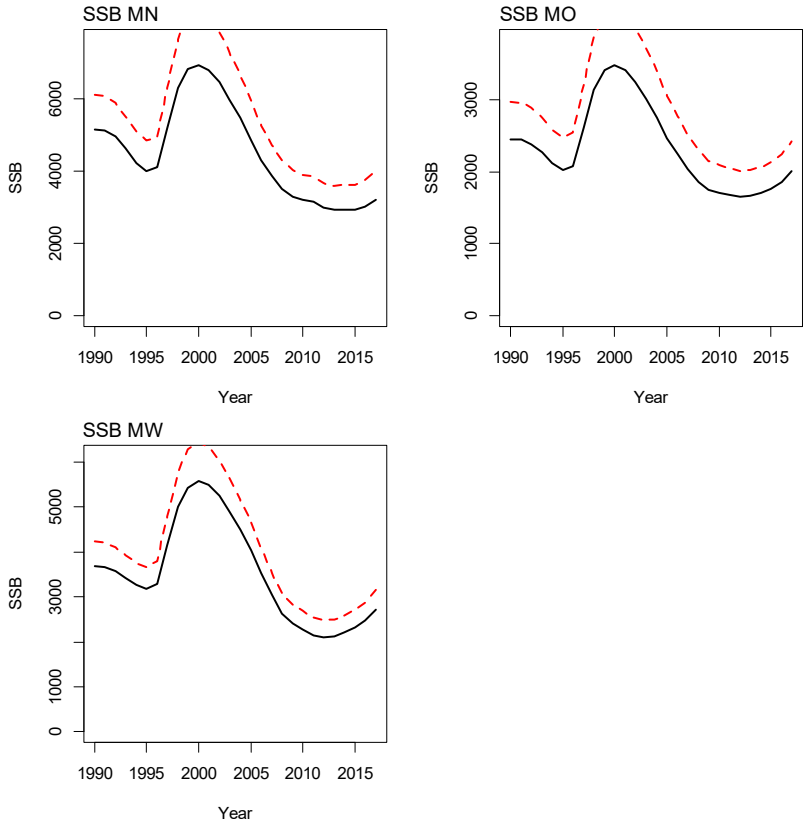

Figure 48: Sensitivity of the SCI 3 assessment model biomass trajectory to the revised catchability priors. Black line – old priors, red line – revised priors.

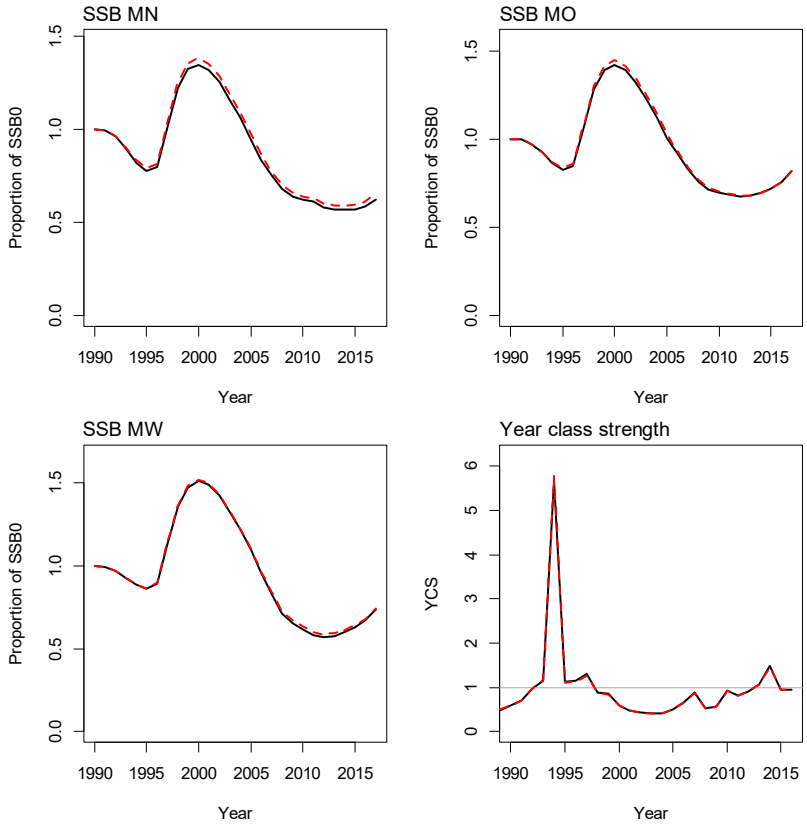

Figure 49: Sensitivity of the SCI 3 assessment model stock status trajectory and YCS to the revised catchability priors. Black line – old priors, red line – revised priors.

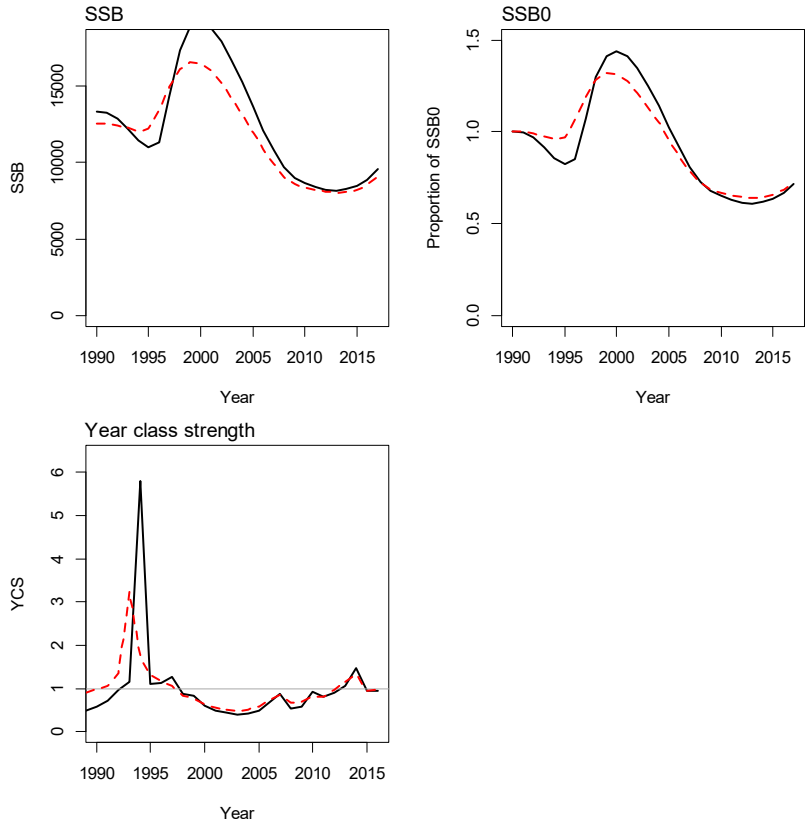

Figure 50: Comparison of the SCI 3 assessment model biomass, stock status, and YCS trajectory for three stock (shared YCS) and single stock models. Black line – three stock, red line – single stock.

Previous scampi assessment models for some stocks have attempted to estimate natural mortality, but the results have never been convincing, and so *M* has typically been assumed to be between 0.2 and 0.25. On the basis of the approach of Clark & Hare (2006), a CV of 0.20 was considered appropriate for each of the CPUE series, but sensitivities to both these were examined (*M* of 0.2 and 0.25, CV of 0.2 and 0.25). The higher natural mortality (0.25) resulted in a higher biomass trajectory across the whole model time series (Figure 51), with the models with the lower CV estimating a greater magnitude of biomass change (being more constrained to match the CPUE) between the late 1990s and mid-2000s. These model output differences resulted in different perceptions of the state of the stock around the year 2000, but very little difference since about 2005, with stock status declining to a minimum around 2011, and increasing in more recent years (Figure 52).

Adopting a shared YCS pattern between stocks (on the assumption that YCS patterns are probably strongly influenced by broad-scale environmental drivers) constrains the three stocks to have very similar trajectories over time, given that YCS is the only time varying parameter in the model. Although the CPUE indices show the same general pattern (increasing in late 1990s, declining through the 2000s, and increasing in the most recent years), the three areas show differences in the timing of peak CPUE, and estimation of individual YCS series for each stock allows the model to better account for this.

Estimating individual YCS series for each stock (while maintaining a shared *q-Photo*) allowed the model to estimate different patterns between areas (Figure 53). Although B_0 estimates and the magnitude of the peak YCS were lower in the individual YCS models, and the timing of the peak YCS and increase in biomass differed slightly between stocks, the stocks (and models) had the same general pattern, and current stock status was reasonably consistent between models (Figure 54). The shared *q-photo* between stocks does potentially constrain the model, and, when this is relaxed (all individual *q*s), there are slight shifts in the absolute biomass trajectories (Figure 55), although stock status trajectories are not affected (Figure 56).

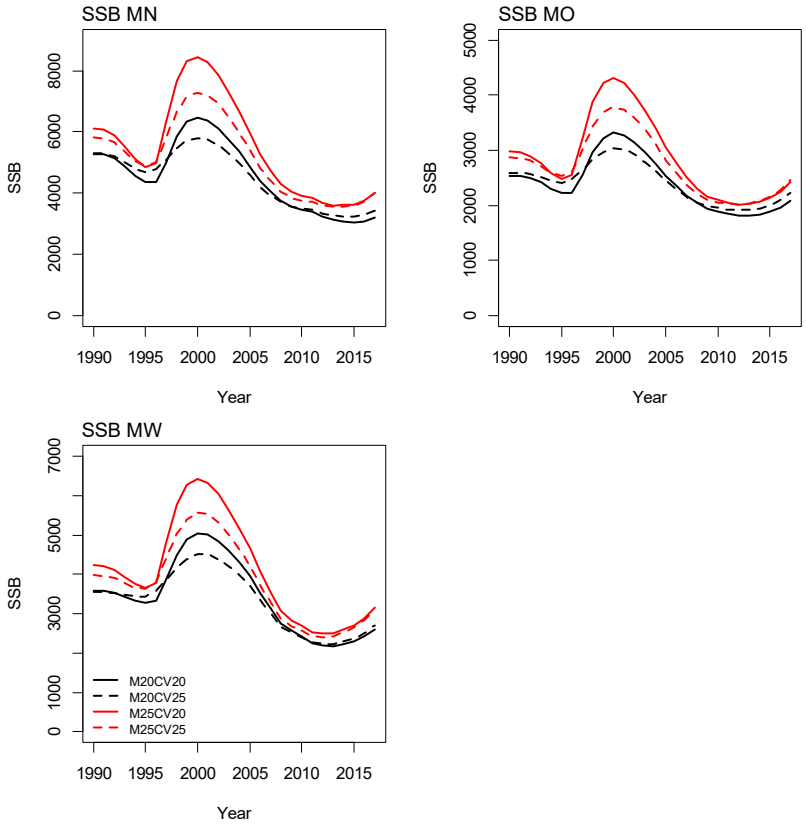

Figure 51: Sensitivity of the SCI 3 assessment model biomass trajectory to assumptions on natural mortality and CPUE process error.

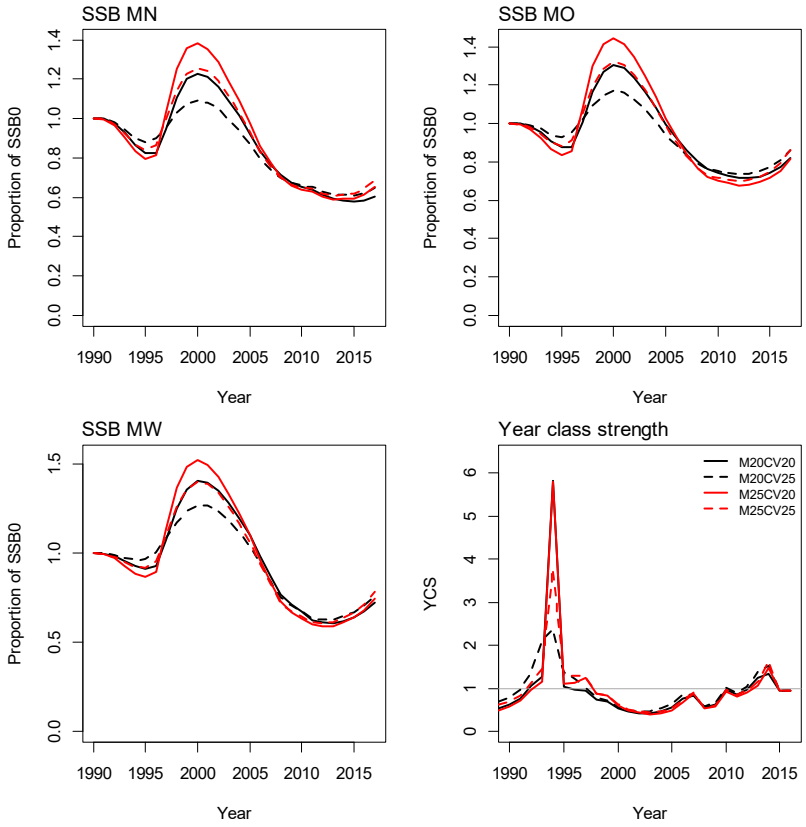

Figure 52: Sensitivity of the SCI 3 assessment model stock status and YCS trajectory to assumptions on natural mortality and CPUE process error.

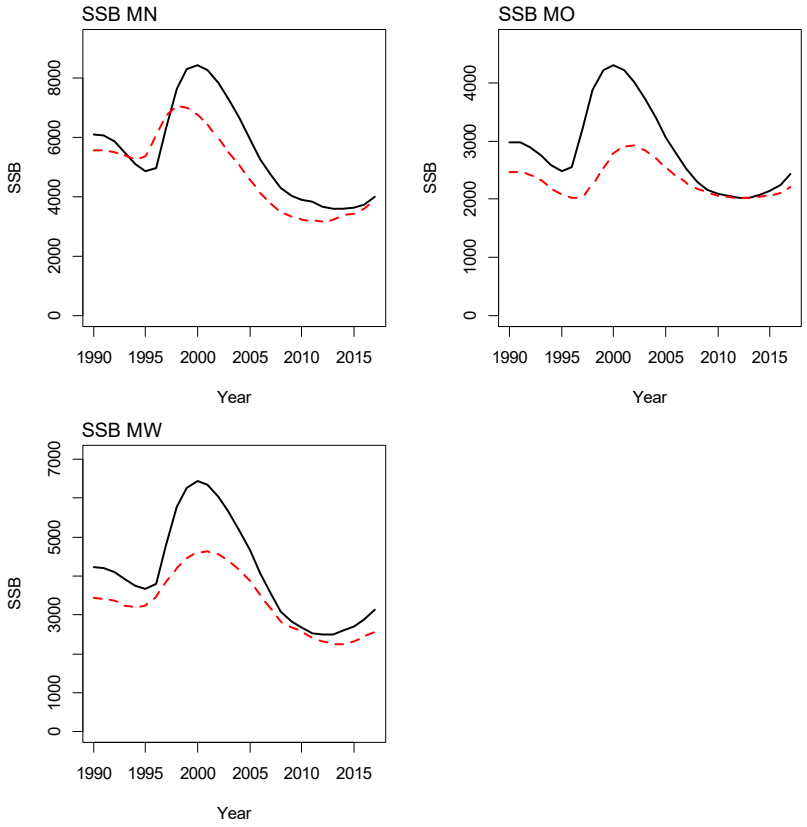

Figure 53: Sensitivity of the SCI 3 assessment model (sharing *q-Photo* between stocks) biomass trajectory to shared YCS patterns.

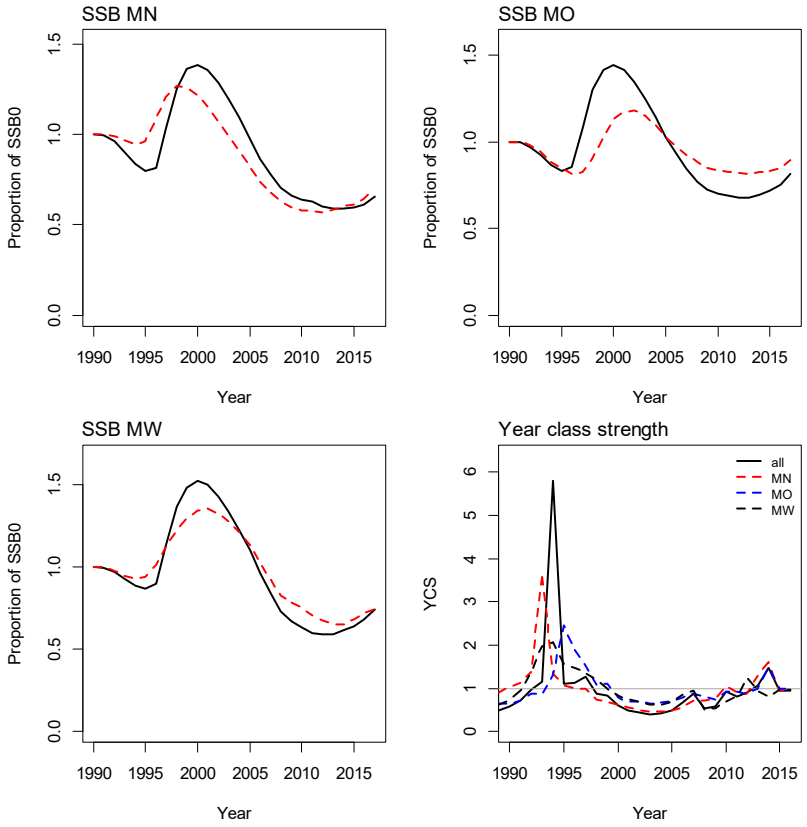

Figure 54: Sensitivity of the SCI 3 assessment model (sharing *q-Photo* between stocks) stock status and YCS trajectory to shared YCS patterns.

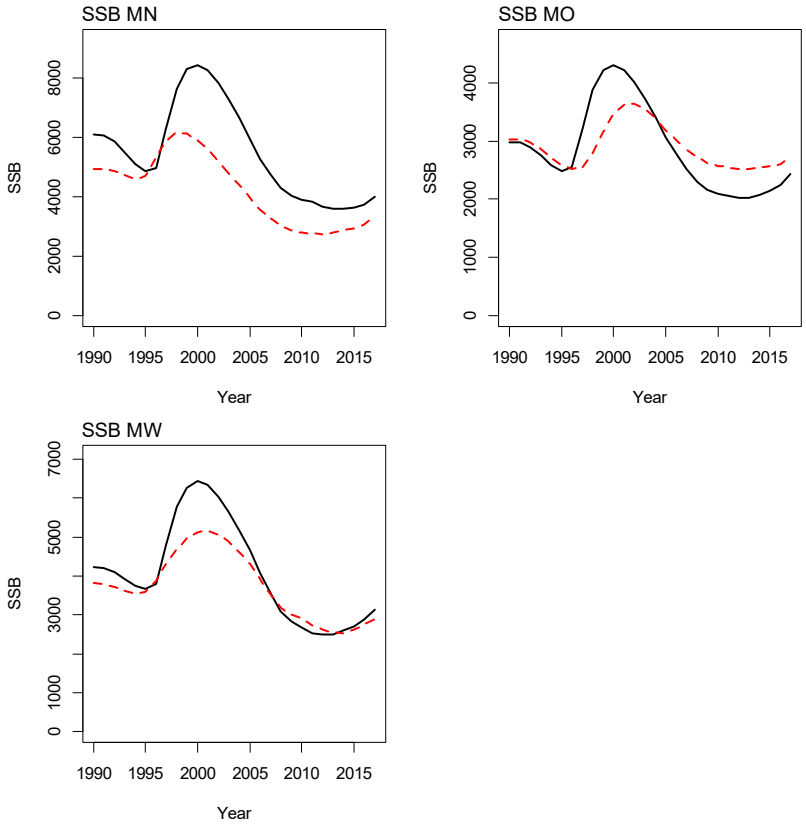

Figure 55: Sensitivity of the SCI 3 assessment model (all individual stock *q*s) biomass trajectory to shared YCS patterns.

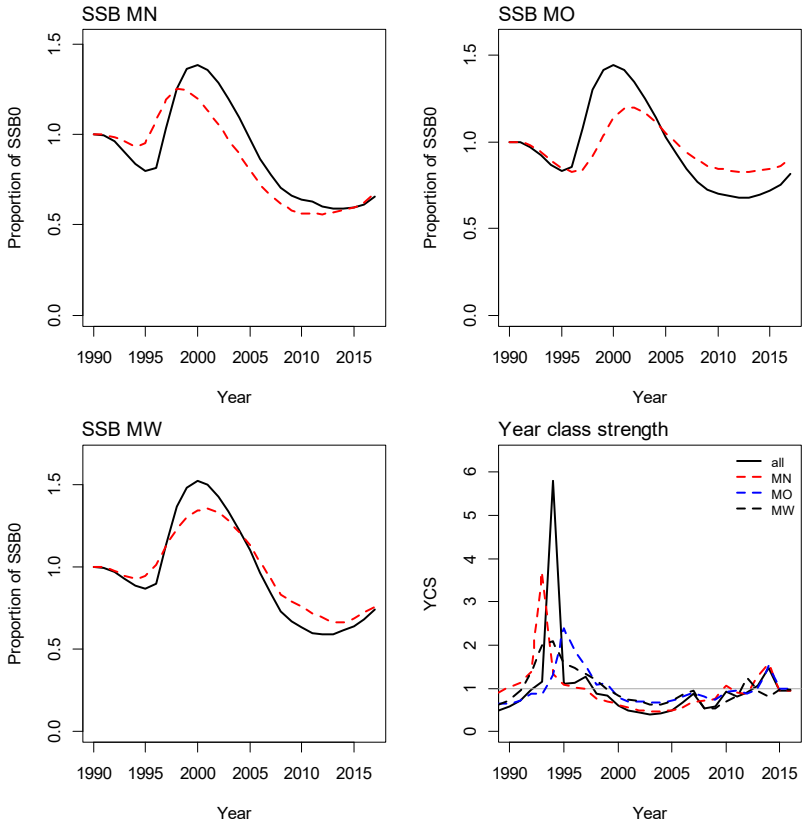

Figure 56: Sensitivity of the SCI 3 assessment model (all individual stock *q*s) stock status and YCS trajectory to shared YCS patterns.

Following presentation of these model sensitivities, the SFAWG considered the model outputs and determined base case and model sensitivities to be considered in more detail and taken to MCMC. Overall, the preliminary models suggest a stock status well above 50% B_0, with no apparent cause for concern. However, the single area model, while providing a very similar perception of stock status to the three stock model, hides any potential inter stock differences; although it may not be an issue under present conditions, it may hide individual stock declines in the future. The use of a shared YCS pattern may have a similar effect, forcing a similar trajectory for all three stocks. The preliminary model with individual YCS and *q*s for each stock was taken to MCMC to examine the posterior distribution of the catchabilities (Figure 57). There was reasonable overlap in the posterior distributions of the individual *q* terms between stocks, and the SFAWG did not consider that there was sufficient evidence to justify having different *q*s for each stock. Base models were therefore explored, with separate YCS estimated for each stock, but with shared *q*s between stocks. The Fisheries New Zealand Plenary Working Group did not agree with the SFAWG's conclusion over sharing *q*s and suggested that, though shared *q*s have been implemented within the current assessments, stock specific *q*s should be considered for future SCI 3 assessments.

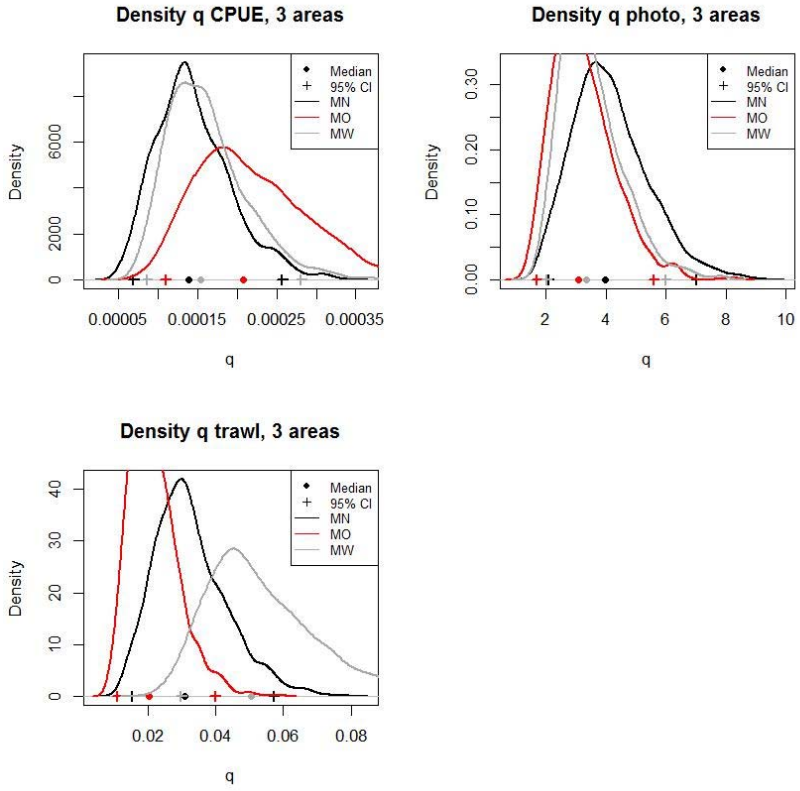

Figure 57: Posterior distribution of *q* terms estimated from the three stock model for SCI 3, with individual *q*s and YCS patterns for each stock.

4.2 Base models

On the basis of the preliminary sensitivity runs described above, the SFAWG requested a base model with M = 0.25 and CPUE process error = 0.2, with sensitivities to this (M = 0.2 and CV = 0.25). Each of the models was a three stock three area model, with stock specific YCS but shared qs. Details of the four models examined within the analyses are presented in Table 12. Key parameter and quantity estimates from the MPD fits for the models described in Table 13, and stock and recruitment trajectories, are presented in Figure 58. Models were developed with catchabilities as nuisance and free parameters. MPD outputs were very similar for the two versions of the same model, but free parameter models did not appear to converge at MCMC and so were not included. Various model output plots and diagnostics are presented in Appendices 3 to 6 for each of the models.

Table 12: General details of models examined within sensitivity analyses for SCI 3.

Model	M	CPUE process error
1	0.25	0.20
2	0.25	0.25
3	0.20	0.20
4	0.20	0.25

There was little difference between models in the fits to observed data. All the models showed an increase in biomass in the late 1990s, followed by a decline, and an increase in subareas MN and MW in the most recent years (Figure 58). SSB_0 was estimated to be slightly higher with a higher M (Table 13), SSB showed a greater magnitude of increase with lower CPUE process error, but overall patterns in SSB trajectory and YCS were very similar.

Table 13: Estimated key parameters and quantities from MPD fits for SCI 3 sensitivity model runs.

		Model 1	Model 2	Model 3	Model 4
M		0.25	0.25	0.2	0.2
CPUE process error		0.2	0.25	0.2	0.25
CPUE-Commercial$q$		0.0002	0.0002	0.0002	0.0002
TrawlSurvey$q$		0.0383	0.0381	0.0411	0.0397
PhotoSurvey$q$		4.4921	4.5596	4.6648	4.6921
MN.SSB_0		4613	4573	4403	4504
MW.SSB_0		3559	3520	3290	3370
MO.SSB_0		2900	2790	2768	2740
MN SSB_{2017}		3176	3362	2813	3081
MW SSB_{2017}		2706	2805	2446	2624
MO SSB_{2017}		2284	2289	2259	2287
MN SSB_{2017}/ SSB_0		0.69	0.74	0.64	0.68
MW SSB_{2017}/ SSB_0		0.76	0.80	0.74	0.78
MO SSB_{2017}/ SSB_0		0.79	0.82	0.82	0.83
maturity_props.all	a_{50}	43.34	43.34	43.34	43.34
	a_{to95}	7.04	7.04	7.04	7.04
selectivity[Fishing_1]	a_{50}	36.56	37.57	36.29	37.48
	a_{to95}	12.47	13.15	12.27	13.21
	amax M	1.11	1.10	1.13	1.11
selectivity[Fishing_2]	a_{50}	34.24	34.46	33.96	34.27
	a_{to95}	8.15	8.28	7.99	8.25
	amax M	0.82	0.82	0.83	0.83
selectivity[Survey_1]	a_{50}	32.74	33.31	32.34	33.02
	a_{to95}	10.17	10.31	9.53	9.81
	amax M	1.47	1.46	1.48	1.47
selectivity[Photo]	a_{50}	43.06	43.51	42.20	43.11
	a_{to95}	13.51	13.54	13.00	13.35
growth[1].g_male	g20	13.46	13.00	12.05	11.47
	g40	3.63	3.51	2.69	2.48
growth[1].g_female	g20	12.86	12.43	11.72	11.16
	g40	0.85	0.82	0.15	0.03

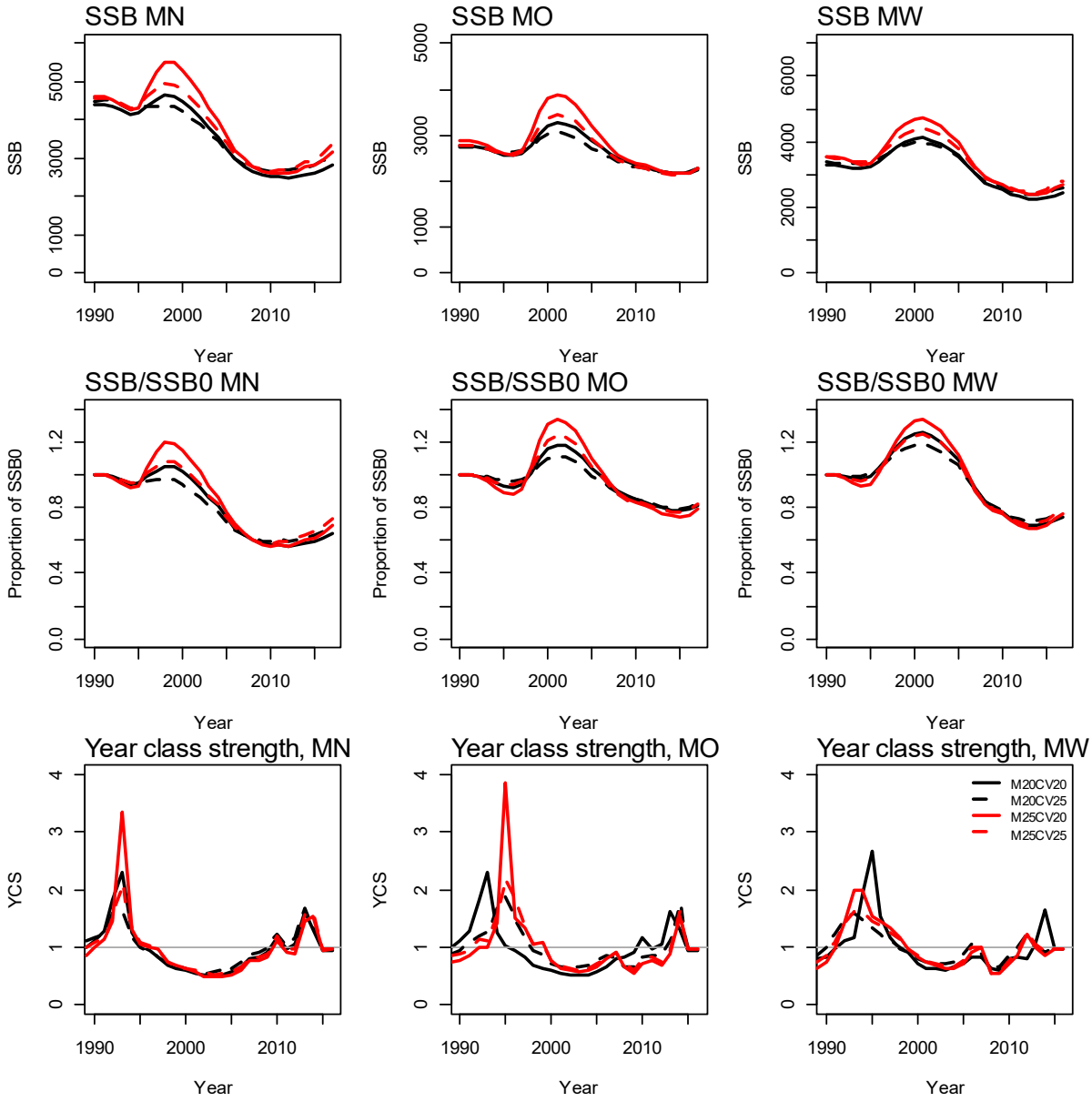

Figure 58: Plots of *SSB* (top row), *SSB* as a proportion of SSB_0 (middle row), and year class strength (YCS) (bottom row) by subarea for MPD fits to the SCI 3 sensitivity model runs.

4.2.1 Model 1: *M* fixed at 0.25, CPUE process error 0.2

The outputs and diagnostics for Model 1 (M = 0.25, CPUE process error = 0.2) are presented in Appendix 3. The estimated combined SSB_0 was 11 072 t (MN – 4613 t, MW – 3559 t, MO – 2900 t), with the combined SSB_{2017} estimated at 8166 t (MN – 3176 t, MW – 2706 t, MO – 2284 t), 74% of combined SSB_0 (MN – 69%, MW – 76%, MO – 79%). Fits to the indices and normalised residuals show that the model was not able to match the magnitude of the observed increase in CPUE in the late 1990s, but fitted the general trend in recent years reasonably well (A3. 1). The model followed the trend of increasing abundance in recent years shown by the trawl survey (
A3. 2) and photo survey (A3. 3), particularly for subarea MN, but was not able to match the magnitude of decline shown for both indices for subarea MO between 2001 and 2010. The *SSB* trajectories varied between subarea (MN showing a relatively smaller increase and a decline to a lower level by

the late 2000s), but all increased in the mid to late 1990s, declined to the late 2000s or early 2010s, and increased in the most recent years (A3. 4). Year class strengths were estimated to be above average during the 1990s, below average from 2000 to 2009 (or later in MO), and above average after this. Estimated selectivity curves (A3. 5) matched observed changes in sex ratio between time steps, with males more available to trawling during time step 1 and less available in time step 2. MPD estimates of trawl and photo survey catchability were within the prior distribution (A3. 6). Individual fits to the observer length frequency distributions were variable (A3. 7–A3. 8, A3. 25, A3. 39–A3. 40), with the data weighting giving observer length frequency samples low effective sample size (A3. 9–A3. 10, A3. 26, A3. 41–A3. 42). There is some evidence across all subareas of a slight pattern in the residuals from the fits to the length frequency distributions (A3. 12–A3. 15, A3. 28–A3. 29, A3. 44–A3. 47), which may suggest behavioural effects on availability, in addition to the size based logistic selectivity applied in the model, but the magnitude of the pattern is small (less than half a standard deviation). Fits to the trawl survey length frequency distributions were generally better (A3. 16, A3. 30, A3. 48), and effective sample size larger (A3. 17, A3. 31, A3. 49), but the fits showed a similar pattern in the residuals (A3. 19, A3. 44, A3. 51). Sample sizes for photo survey length frequency distributions were low, with high CVs, but the model estimated the average shape of the length distribution reasonably well (A3. 21, A3. 35, A3. 53).

The likelihood profile when B_0 is fixed shows a minimum at around 4500 t (just presented for subarea MN, but same pattern for all subareas; A3. 57), with the overall profile being quite flat. The priors are quite influential on the likelihood (particularly in avoiding lower SSB_0 values), and different data sets within the proportions at length give higher or lower SSB_0 values. The profiles for the abundance indices avoid lower SSB_0 values, but are otherwise very flat.

MCMC runs

Three independent MCMC chains were started a random step away from the MPD for the model, and run for 5 million simulations, with every one thousandth sample saved, giving a set of 5000 samples. Preliminary examination suggested that the individual chains had not converged, but were stabilising in their latter half. Therefore, the first 2500 were excluded as a burn in, and the three chains were concatenated to recalculate the covariance matrix. Three new chains were started a random step away from the MPD with the revised covariance matrix, and run for 2.6 million simulations, with every one thousandth sample saved, giving a set of 2600 samples. This same process was also followed for the other models.

The three chains from the model were examined for evidence of lack of convergence (A3. 58–A3. 61), and concatenated to produce a 7800 sample chain for projections. The three chains were very consistent (A3. 58–A3. 60), as were the distributions for SSB_0, SSB_{2017}, and SSB_{2017}/SSB_0, providing no evidence of lack of convergence (A3. 61). Posterior distributions of trawl and photo survey catchability were within the prior distribution (A3. 62), although had generally not explored the upper range of the prior distribution, with the MPD estimates also located within the posterior distributions. The posterior trajectory of combined *SSB* (Figure 59) suggests an increase during the late 1990s, a decline during the 2000s, and an increase in most recent years. The median estimate of current status (SSB_{2017}/SSB_0) is 76% (95% CI, 69–83%), with 0% probability that SSB_{2017} is below 40% SSB_0. The model estimates a period of above average recruitment in the mid to late 1990s, below average recruitment during the 2000s, and above average recruitment in most recent years (A3. 63–A3. 64).

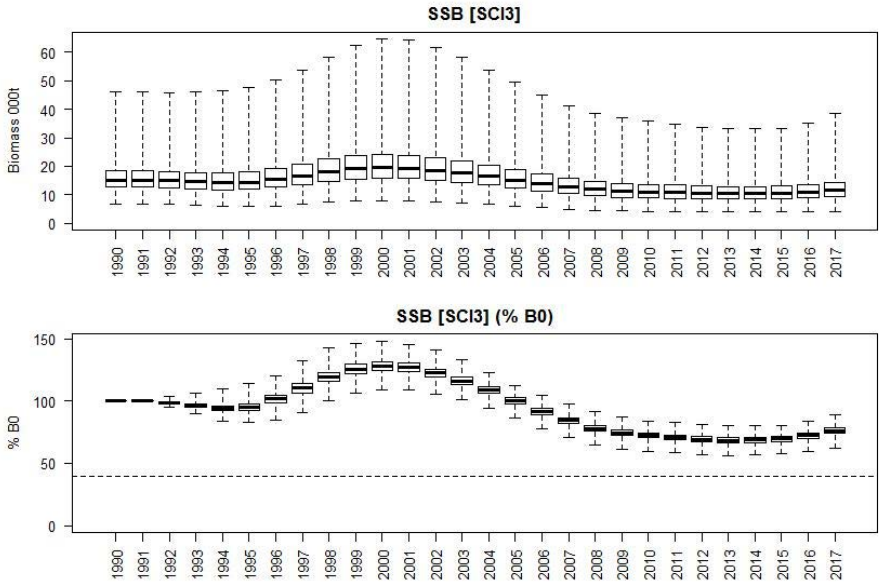

Figure 59: Posterior trajectory of combined *SSB* and SSB_{2017}/SSB_0 for Model 1.

4.2.2 Model 2: *M* fixed at 0.25, CPUE process error 0.25

The outputs and diagnostics for Model 2 (M = 0.25, CPUE process error = 0.25) are presented in Appendix 4. The estimated combined SSB_0 was 11 883 t (MN – 4573 t, MW – 3520 t, MO – 2790 t), with combined SSB_{2017} estimated at 8456 t (MN – 3362 t, MW – 2805 t, MO – 2289 t), 78% of combined SSB_0 (MN– 74%; MW– 80%; MO– 82%). Fits to the indices and normalised residuals show that the model was even less able than Model 1 to match the magnitude of the observed increase in CPUE in the late 1990s, but fitted the general trend in recent years reasonably well (A4. 1). As with Model 1, Model 2 followed the trend of increasing abundance in recent years shown by the trawl survey (A4. 2) and photo survey (A4. 3), particularly for subarea MN, but was not able to match the magnitude of decline shown for both indices for subarea MO between 2001 and 2010. The *SSB* trajectories varied between subarea, but showed a similar pattern: increase in the mid to late 1990s, decline to the late 2000s or early 2010s, and increase in the most recent years (A4. 4). Year class strengths showed smaller maximum values in the mid 1990s than Model 1, but a very similar overall pattern. As with Model 1, estimated selectivity curves (A4. 5) matched observed changes in sex ratio between time steps, with males more available to trawling during time step 1 and less available in time step 2. MPD estimates of trawl and photo survey catchability were within the prior distribution (A4. 6). Individual fits to the observer length frequency distributions were very similar to the previous model, and variable (A4. – A4. 8, A4. 25, A4. 39–A4. 40), with the data weighting giving observer length frequency samples low effective sample size (A4. 9–A4. 10, A4. 26, A4. 41–A4. 42). The slight pattern in the residuals from the fits to the length frequency distributions (A4. 12–A4. 15, A4. 28, A4. 44–A4. 47) is also present in this model. Fits to the trawl survey length frequency distributions were better (A4. 16, A4. 30, A4. 48) and effective sample size larger (A4. 17, A4. 31, A4. 49), but the fits showed the same pattern in the residuals (A4. 19, A4. 44, A4. 51) observed previously. The model fitted the shape of the photo survey length distribution reasonably well (A4. 21, A4. 35, A4. 53).

The likelihood profile when B_0 is fixed shows a minimum around 4500 t (for MN, A4. 57), with the overall profile being quite flat. Again, the priors be the most influential component on the likelihood.

MCMC runs

The three MCMC chains run with the revised covariance matrix were examined for evidence of lack of convergence (A4. 58–A4. 61) and concatenated to produce a 7800 sample chain for projections. The three chains were very consistent (A4. 58–A4. 60), as were the distributions for SSB_0, SSB_{2017}, and SSB_{2017}/SSB_0, providing no evidence of lack of convergence (A4. 61). Posterior distributions of trawl and photo survey catchability were within the prior distribution (A4. 62), with the MPD estimates also located within the posterior distributions. The posterior trajectory of combined *SSB* (Figure 60) suggests an increase through the late 1990s, a decline through the 2000s, and an increase most recently. The median estimate of current status (SSB_{2017}/SSB_0) is 81% (95% CI, 72–88%), with 0% probability that SSB_{2017} is below 40% SSB_0. The model estimated a period of above average recruitment in the mid to late 1990s, below average recruitment during the 2000s, and above average recruitment in most recent years (A4. 63–A4. 64).

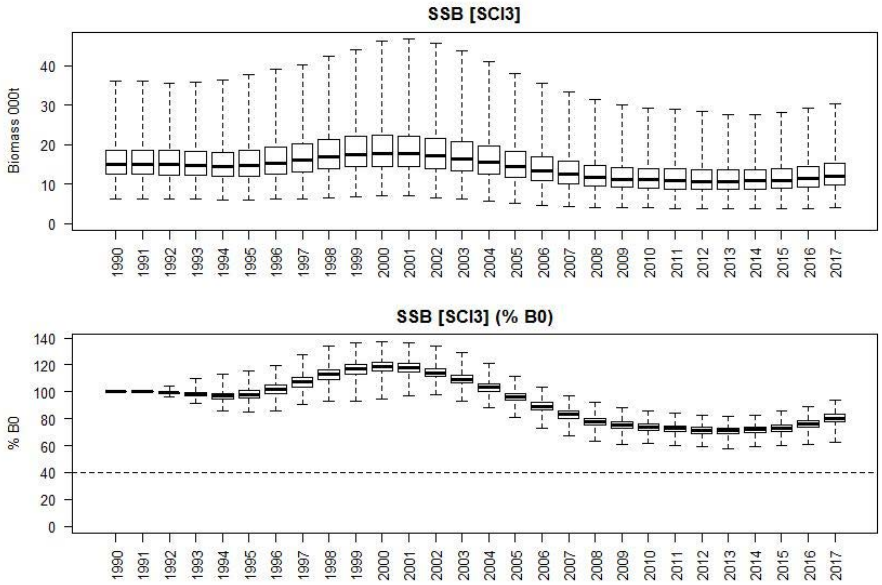

Figure 60: Posterior trajectory of *SSB* and SSB_{2017}/SSB_0 for Model 2.

4.2.3 Model 3: *M* fixed at 0.2, CPUE process error 0.2

The outputs and diagnostics for Model 3 ($M = 0.2$, CPUE process error = 0.2) are presented in Appendix 5. The estimated combined SSB_0 was 10 461 t (MN – 4403 t, MW – 3290 t, MO – 2768 t), with the combined SSB_{2017} at 7518 t (MN – 2813 t, MW – 2446 t, MO – 2259 t), 72% of combined SSB_0 (MN – 64%, MW – 74%, MO – 82%). Fits to the abundance indices and normalised residuals were similar to Model 1, in that they did not match the magnitude of the observed increase in CPUE in the late 1990s, but fitted the general trend in recent years reasonably well (A5. 1). As with the previous models, Model 3 followed the trend of increasing abundance in recent years shown by the trawl survey (A5. 2) and photo survey (A5. 3), particularly for subarea MN, but was not able to match the magnitude of decline shown for both indices for subarea MO between 2001 and 2010. The *SSB* trajectories were similar to previous models, varying between subarea, but showing a similar pattern, with an increase in the mid to late 1990s, a decline to the late 2000s or early 2010s, and an increase in the most recent years (A5. 4). Year class strengths showed a very similar overall pattern. Estimated selectivity curves (A5. 5) were similar to previous models and matched observed changes in sex ratio between time steps, and MPD estimates of trawl and photo survey catchability were within the prior distribution (A5. 6). Individual fits to the observer (A5. 7– A5. 8, A5. 25, A5. 39–A5. 40) and survey (A5. 16, A5. 30, A5. 48) length frequency distributions were very similar to the previous models, showing similar patterns in the residuals (A5. 12–A5. 15, A5. 28, A5. 44–A5. 47).

The likelihood profile was also very similar to previous models, with most influence from the catchability priors (A5. 57).

MCMC runs

The three MCMC chains run with the revised covariance matrix were examined for evidence of lack of convergence (A5. 58–A5. 61) and concatenated to produce a 7800 sample chain for projections. The three chains were very consistent (A5. 58–A5. 60), as were the distributions for SSB_0, SSB_{2017}, and SSB_{2017}/SSB_0, providing no evidence of lack of convergence (A5. 61). Posterior distributions of trawl and photo survey catchability were within the prior distribution (A5. 62), with the MPD estimates also located within the posterior distributions. The posterior trajectory of combined *SSB* (Figure 61) suggests an increase through the late 1990s, a decline through the 2000s, and an increase most recently. The median estimate of current status (SSB_{2017}/SSB_0) is 75% (95% CI, 67–82%), with 0% probability that SSB_{2017} is below 40% SSB_0. The model estimates a period of above average recruitment in the mid to late 1990s, below average recruitment during the 2000s, and above average recruitment in most recent years (A5. 63–A5. 64).

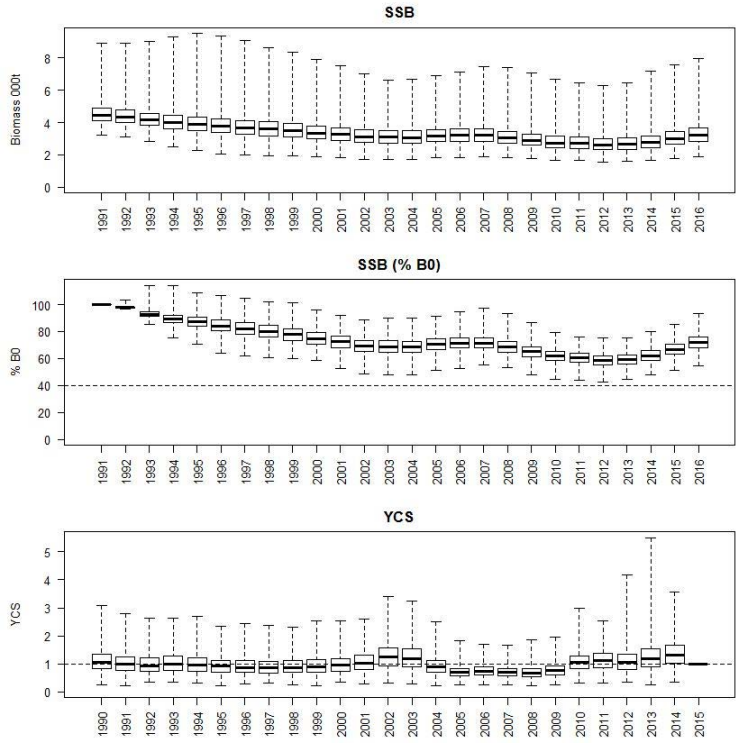

Figure 61: Posterior trajectory of *SSB* and SSB_{2017}/SSB_0 for Model 3.

4.2.4 Model 4: *M* fixed at 0.2, CPUE process error 0.25

The outputs and diagnostics for Model 4 (M = 0.2, CPUE process error = 0.25) are presented in Appendix 6. The estimated combined SSB_0 was 10 614 t (MN – 4504 t, MW – 3370 t, MO – 2740 t), with the combined SSB_{2017} estimated at 7992 t (MN – 3081 t, MW – 2624 t, MO – 2287 t), 75% of combined SSB_0 (MN – 68%, MW – 78%, MO – 83%). Fits to the abundance indices and normalised residuals were similar to previous models, in that they did not match the magnitude of the observed increase in CPUE in the late 1990s, but fitted the general trend in recent years reasonably well (A6. 1). As with the previous models, Model 4 followed the trend of increasing abundance in recent years shown by the trawl survey (A6. 2) and photo survey (A6. 3), particularly for subarea MN, but was not able to

match the magnitude of decline shown for both indices for subarea MO between 2001 and 2010. The *SSB* trajectories were again similar to previous models, varying between subarea, but showing a similar pattern, with an increase in the mid to late 1990s, a decline to the late 2000s or early 2010s, and an increase in the most recent years (A6. 4). Year class strengths were also similar to previous models, although, as with Model 2, maximum YCS values were lower than Model 1. Estimated selectivity curves (A6. 5) showed the same pattern as other models, and MPD estimates of trawl and photo survey catchability were within the prior distribution (A6. 6). Individual fits to the observer (A6. 7–A6. 8, A6. 25, A6. 39–A6. 40) and survey (A6. 16, A6. 30, A6. 48) length frequency distributions were very similar to the previous models, showing similar patterns in the residuals (A6. 12 – A6. 15, A6. 28, A6. 44 – A6. 47).

The likelihood profile was also very similar to previous models, with most influence from the catchability priors (A6. 57).

MCMC runs

The three MCMC chains run with the revised covariance matrix were examined for evidence of lack of convergence (A6. 58–A6. 61) and concatenated to produce a 7800 sample chain for projections. The three chains were very consistent (A6. 58–A6. 60), as were the distributions for SSB_0, SSB_{2017}, and SSB_{2017}/SSB_0 providing no evidence of lack of convergence (A6. 61). Posterior distributions of trawl and photo survey catchability were within the prior distribution (A6. 62), with the MPD estimates also located within the posterior distributions. The posterior trajectory of combined *SSB* (Figure 62) suggests an increase through the late 1990s, a decline through the 2000s, and an increase in most recent years. The median estimate of current status (SSB_{2017}/SSB_0) is 79% (95% CI, 70–86%), with 0% probability that SSB_{2017} is below 40% SSB_0. The model estimates a period of above average recruitment in the mid to late 1990s, below average recruitment through the 2000s, and above average recruitment in most recent years (A6. 63–A6. 64).

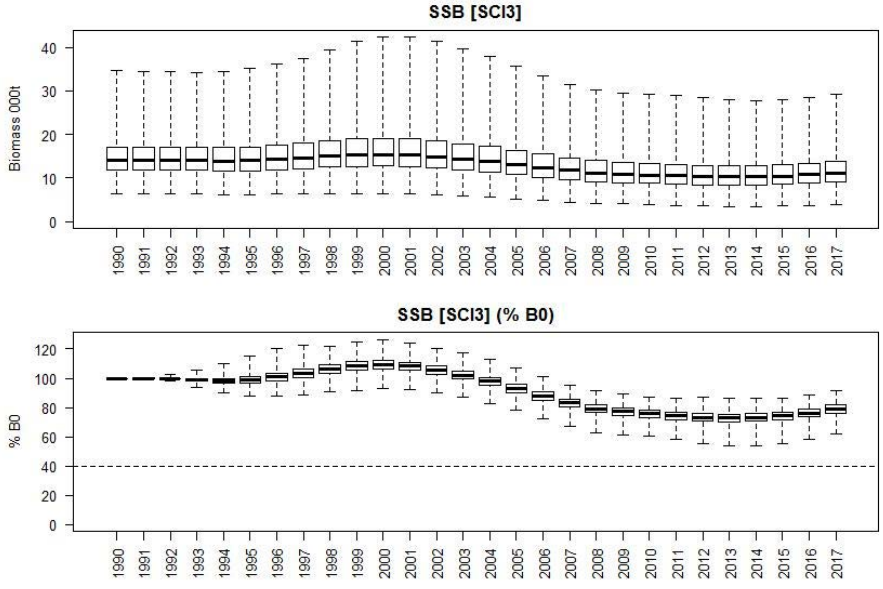

Figure 62: Posterior trajectory of *SSB* and SSB_{2017}/SSB_0 for Model 4.

4.3 Fishing pressure

Annual fishing intensity (equivalent annual F) and the level of fishing that, if applied forever, would result in an equilibrium biomass of 40% SSB_0 ($F_{40\%B0}$) were calculated using methods described by Cordue (2012). Estimates of annual fishing intensity and the Harvest Strategy Standard reference points were not sensitive to the choice of process error on the CPUE index, and so results are presented for Model 1 and Model 3, examining sensitivity to M (Figure 63 and Figure 64). Although the $F_{40\%B0}$ level differs between M assumptions, the overall pattern of the relationship between F and SSB relative to this reference point is similar. Initially SSB declined with the development of the fishery, but it increased to a maximum in 2000, then declined to a minimum around 2012, and has increased in more recent years. At all times throughout the fishery, SSB has remained well above the 40% SSB_0 target, and annual fishing intensity, at its peak in the most recent years, appears to be less than half the level estimated to result in an equilibrium biomass of 40% SSB_0, and thus remains well below $F_{40\%B0}$.

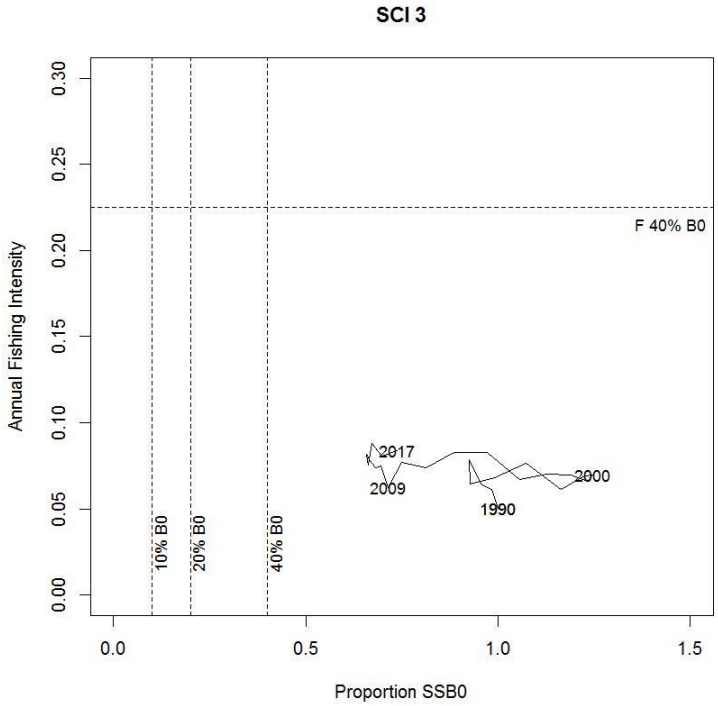

Figure 63: Trajectory of annual fishing intensity (equivalent annual F) plotted against proportion SSB_0 for the combined subareas for SCI 3 Model 1, in relation to Harvest Strategy Standard target and limit reference points.

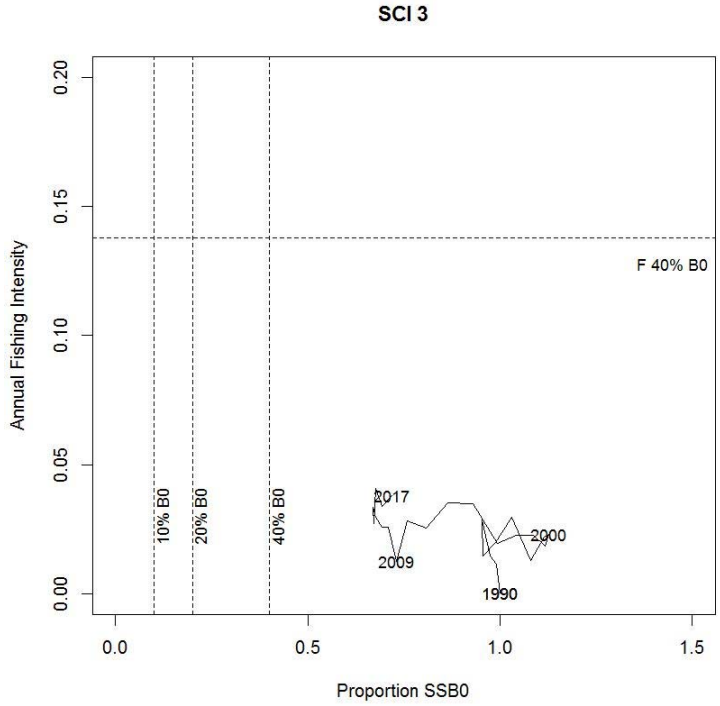

Figure 64: Trajectory of annual fishing intensity (equivalent annual *F*) plotted against proportion SSB_0 for the combined subareas for SCI 3 Model 3, in relation to Harvest Strategy Standard target and limit reference points.

4.4 Projections

The assessments reported SSB_0 and SSB_{2017} and used the ratio of current and projected *SSB* to SSB_0 as preferred indicators. Projections were conducted up to 2021 on the basis of catch scenarios proposed by Fisheries New Zealand (current average landings (current TACC of 340 t) and increases of 10 or 20%) (Table 14). Future catches were allocated to subarea on the basis of averages over the last 5 years; because this resulted in minimal allocation to subarea MO (less than 1%), the 20% increase projection was also run with all additional catch allocated to this subarea, to provide an alternative scenario. Projections have been conducted by randomly resampling year class strengths from the last decade estimated within the model (2005–14). The probabilities of exceeding the default Harvest Strategy Standard target and limit reference points are reported (Table 14). Projected stock trajectories are only shown for Model 1 (Figure 65–Figure 68), but are tabulated for all models (Table 14 and Table 15).

Very few differences were noted in the projections between models. For the most pessimistic case (Model 1; Table 14), current catches were projected to lead to a 5% increase in *SSB* across the SCI 3 area (1% decrease in MW, increases elsewhere), and a 20% increase in catches is projected to lead to a 4% increase in biomass. All projections examined for all models had a 100% probability of *SSB* exceeding 40% SSB_0 in 2021.

Table 14: SCI 3 projections for Model 1 and Model 2. Results from MCMC runs showing B_0, B_{2017}, and B_{2021} estimates at varying catch levels, and probabilities of projected spawning stock biomass exceeding the default Harvest Strategy Standard target and limit reference points.

		Model 1				Model 2			
	Subarea	MN	MW	MO	SCI 3	MN	MW	MO	SCI 3
	SSB_0	6 204	4 905	4 035	15 162	6 235	4 939	3 947	15 118
	SSB_{2017}	4 612	3 862	3 160	11 585	4 961	4 125	3 225	12 214
	SSB_{2017}/SSB_0	0.74	0.79	0.78	0.76	0.79	0.83	0.82	0.81
340 tonnes (current landings and TACC)	SSB_{2021}/SSB_0	0.78	0.78	0.84	0.81	0.85	0.84	0.89	0.86
	SSB_{2021}/SSB_{2017}	1.05	0.99	1.07	1.05	1.07	1	1.09	1.07
	$P\ SSB_{2021} < 10\%\ SSB_0$	0	0	0	0	0	0	0	0
	$P\ SSB_{2021} < 20\%\ SSB_0$	0	0	0	0	0	0	0	0
	$P\ SSB_{2021} > 40\%\ SSB_0$	1	1	1	1	1	1	1	1
	$P\ SSB_{2021} > SSB_{2017}$	0.684	0.465	0.819	0.821	0.742	0.5	0.871	0.88
375 tonnes (10% increase in TACC)	SSB_{2021}/SSB_0	0.77	0.78	0.84	0.8	0.84	0.83	0.89	0.86
	SSB_{2021}/SSB_{2017}	1.04	0.99	1.07	1.05	1.06	1	1.09	1.06
	$P\ SSB_{2021} < 10\%\ SSB_0$	0	0	0	0	0	0	0	0
	$P\ SSB_{2021} < 20\%\ SSB_0$	0	0	0	0	0	0	0	0
	$P\ SSB_{2021} > 40\%\ SSB_0$	0.999	1	1	1	1	1	1	1
	$P\ SSB_{2021} > SSB_{2017}$	0.63	0.456	0.819	0.781	0.688	0.489	0.871	0.851
408 tonnes (20% increase in TACC)	SSB_{2021}/SSB_0	0.76	0.77	0.84	0.79	0.83	0.83	0.89	0.85
	SSB_{2021}/SSB_{2017}	1.02	0.99	1.07	1.04	1.04	1	1.09	1.06
	$P\ SSB_{2021} < 10\%\ SSB_0$	0	0	0	0	0	0	0	0
	$P\ SSB_{2021} < 20\%\ SSB_0$	0	0	0	0	0	0	0	0
	$P\ SSB_{2021} > 40\%\ SSB_0$	0.999	1	1	1	0.999	1	1	1
	$P\ SSB_{2021} > SSB_{2017}$	0.577	0.445	0.819	0.741	0.639	0.478	0.871	0.819
408 tonnes (20% increase in TACC, extra taken in MO)	SSB_{2021}/SSB_0	0.78	0.78	0.8	0.79	0.85	0.84	0.84	0.85
	SSB_{2021}/SSB_{2017}	1.05	0.99	1.02	1.04	1.07	1	1.03	1.06
	$P\ SSB_{2021} < 10\%\ SSB_0$	0	0	0	0	0	0	0	0
	$P\ SSB_{2021} < 20\%\ SSB_0$	0	0	0	0	0	0	0	0
	$P\ SSB_{2021} > 40\%\ SSB_0$	1	1	1	1	1	1	1	1
	$P\ SSB_{2021} > SSB_{2017}$	0.684	0.465	0.574	0.741	0.742	0.5	0.659	0.819

Table 15: SCI 3 projections for Model 3 and Model 4. Results from MCMC runs showing B_0, B_{2017}, and B_{2021} estimates at varying catch levels, and probabilities of projected spawning stock biomass exceeding the default Harvest Strategy Standard target and limit reference points.

		Model 3				Model 4			
	Subarea	MN	MW	MO	SCI 3	MN	MW	MO	SCI 3
	SSB_0	5 625	4 335	3 668	13 643	5 910	4 546	3 728	14 168
	SSB_{2017}	3 943	3 373	3 000	10 246	4 451	3 760	3 127	11 222
	SSB_{2017}/SSB_0	0.7	0.78	0.82	0.75	0.75	0.82	0.84	0.79
340 tonnes (current landings and TACC)	SSB_{2021}/SSB_0	0.74	0.78	0.89	0.8	0.81	0.83	0.92	0.85
	SSB_{2021}/SSB_{2017}	1.05	1.01	1.08	1.06	1.07	1.01	1.1	1.07
	$P\ SSB_{2021} < 10\%\ SSB_0$	0	0	0	0	0	0	0	0
	$P\ SSB_{2021} < 20\%\ SSB_0$	0	0	0	0	0	0	0	0
	$P\ SSB_{2021} > 40\%\ SSB_0$	0.999	1	1	1	1	1	1	1
	$P\ SSB_{2021} > SSB_{2017}$	0.703	0.534	0.908	0.884	0.757	0.585	0.948	0.936
375 tonnes (10% increase in TACC)	SSB_{2021}/SSB_0	0.73	0.78	0.89	0.79	0.79	0.83	0.92	0.84
	SSB_{2021}/SSB_{2017}	1.04	1	1.08	1.05	1.05	1.01	1.1	1.07
	$P\ SSB_{2021} < 10\%\ SSB_0$	0	0	0	0	0	0	0	0
	$P\ SSB_{2021} < 20\%\ SSB_0$	0	0	0	0	0	0	0	0
	$P\ SSB_{2021} > 40\%\ SSB_0$	0.998	1	1	1	1	1	1	1
	$P\ SSB_{2021} > SSB_{2017}$	0.629	0.515	0.908	0.839	0.696	0.57	0.948	0.913
408 tonnes (20% increase in TACC)	SSB_{2021}/SSB_0	0.71	0.77	0.89	0.78	0.78	0.83	0.92	0.84
	SSB_{2021}/SSB_{2017}	1.02	1	1.08	1.04	1.04	1.01	1.1	1.06
	$P\ SSB_{2021} < 10\%\ SSB_0$	0	0	0	0	0	0	0	0
	$P\ SSB_{2021} < 20\%\ SSB_0$	0	0	0	0	0	0	0	0
	$P\ SSB_{2021} > 40\%\ SSB_0$	0.997	1	1	1	0.999	1	1	1
	$P\ SSB_{2021} > SSB_{2017}$	0.557	0.5	0.908	0.794	0.632	0.556	0.948	0.877
408 tonnes (20% increase in TACC, extra taken in MO)	SSB_{2021}/SSB_0	0.74	0.78	0.84	0.78	0.81	0.83	0.88	0.84
	SSB_{2021}/SSB_{2017}	1.05	1.01	1.02	1.04	1.07	1.01	1.04	1.06
	$P\ SSB_{2021} < 10\%\ SSB_0$	0	0	0	0	0	0	0	0
	$P\ SSB_{2021} < 20\%\ SSB_0$	0	0	0	0	0	0	0	0
	$P\ SSB_{2021} > 40\%\ SSB_0$	0.999	1	1	1	1	1	1	1
	$P\ SSB_{2021} > SSB_{2017}$	0.703	0.534	0.639	0.793	0.757	0.585	0.732	0.877

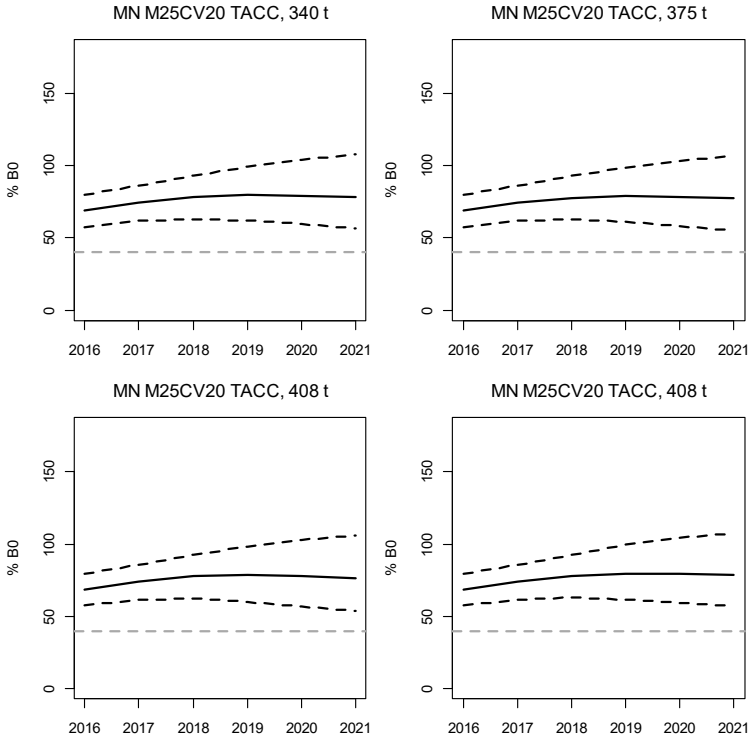

Figure 65: Projected stock trajectory (as a % of SSB_0) for subarea MN of SCI 3 from Model 1 for TACC (and current average) (top left), 10% increase in TACC (top right), 20% increase in TACC (bottom left), and 20% increase in TACC with all extra catch taken from MO (bottom right). Solid black line represents median of projections, and dashed black lines represent 2.5th and 97.5th quantiles. Horizontal dashed grey line represents 40% SSB_0.

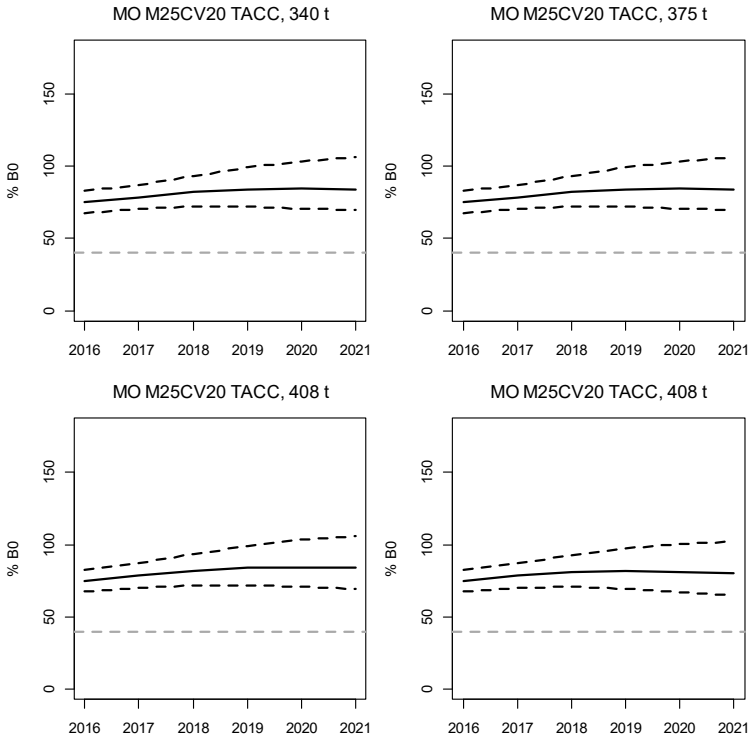

Figure 66: Projected stock trajectory (as a % of SSB_0) for subarea MO of SCI 3 from Model 1 for TACC (and current average) (top left), 10% increase in TACC (top right), 20% increase in TACC (bottom left), and 20% increase in TACC with all extra catch taken from MO (bottom right). Solid black line represents median of projections, and dashed black lines represent 2.5th and 97.5th quantiles. Horizontal dashed grey line represents 40% SSB_0.

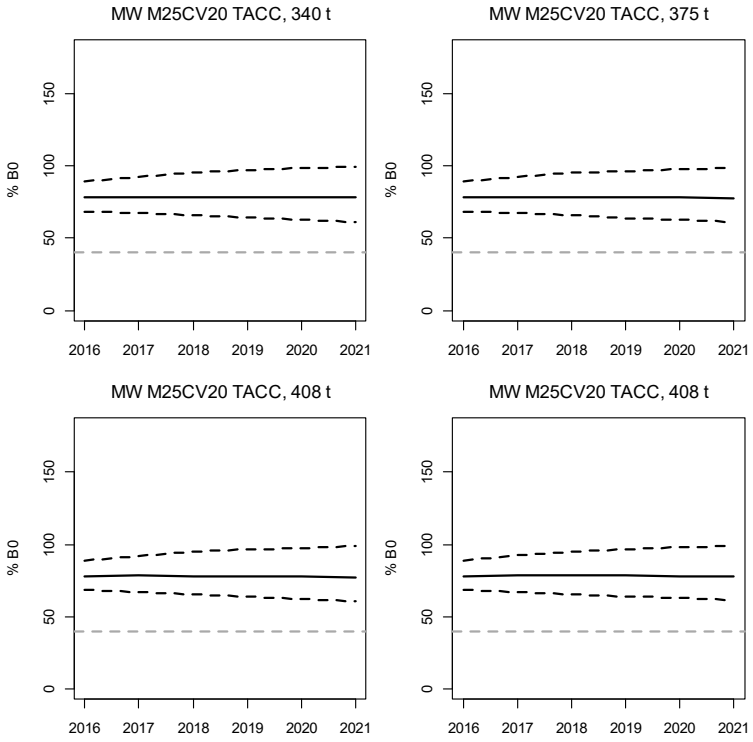

Figure 67: Projected stock trajectory (as a % of SSB_0) subarea MW of SCI 3 from Model 1 for TACC (and current average) (top left), 10% increase in TACC (top right), 20% increase in TACC (bottom left), and 20% increase in TACC with all extra catch taken from MO (bottom right). Solid black line represents median of projections, and dashed black lines represent 2.5th and 97.5th quantiles. Horizontal dashed grey line represents 40% SSB_0.

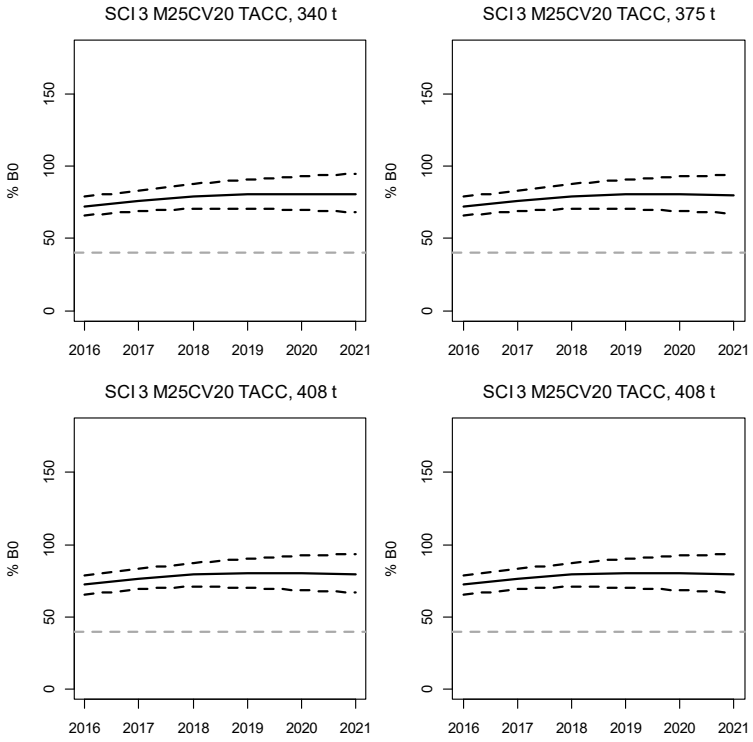

Figure 68: Projected stock trajectory (as a % of SSB_0) for the combined modelled area of SCI 3 from Model 1 for TACC (and current average) (top left), 10% increase in TACC (top right), 20% increase in TACC (bottom left), and 20% increase in TACC with all extra catch taken from MO (bottom right). Solid black line represents median of projections, and dashed black lines represent 2.5th and 97.5th quantiles. Horizontal dashed grey line represents 40% SSB_0.

5. DISCUSSION

An assessment of the SCI 3 stock was last conducted in 2015 (Tuck 2016b), and the current study has implemented progress made in the SCI 6A assessment in YCS parameterisation (Tuck 2017) and updated the catchability priors. The assessment was accepted.

Base models were developed, with *M* fixed at 0.2 and 0.25, and sensitivity to the process error on CPUE was investigated. Annual standardised CPUE indices and trawl and photographic survey series were calculated for each subarea and fitted within the assessment model. Projections were conducted up to 2021 on the basis of recent average landings (TACC) and 10% and 20% increases in future constant catch scenarios.

SSB_0 showed some sensitivity to *M* and the process error on CPUE, but overall the models were very consistent in their estimated stock trajectory and current stock status, with median estimates of SSB_{2017}/SSB_0 for the combined SCI 3 area ranging from 62% to 78%. Overall patterns of estimated YCS were similar between models, all of which estimated a series of above average YCSs in the mid 1990s, lower YCS during the 2000s, and improved YCS in more recent years. The model suggests slight differences in YCSs between subareas. Projections out to 2021 suggested that *SSB* would remain well above 40% SSB_0 with future catches representing up to a 20% increase in TACC (the most pessimistic prediction giving a 100% probability of SSB_{2021} exceeding 40% SSB_0, and 74% probability of SSB_{2021} exceeding SSB_{2017}).

6. ACKNOWLEDGEMENTS

This work was funded by the Ministry for Primary Industries under project SCI2017-02 and builds on a series of scampi assessment projects funded by the Ministry. We thank the many NIWA, Ministry of Fisheries, and MPI staff who measured scampi over the years, and the members of the NIWA scampi image reading team. Development of the catchability priors implemented this year benefitted greatly from comments by members of the Shellfish Fisheries Assessment Working Group. This report was reviewed by Bruce Hartill (NIWA, Auckland).

7. REFERENCES

Bell, M.C.; Redant, F.; Tuck, I.D. (2006). Nephrops species. In: B. Phillips (Ed). *Lobsters: Biology, management, Aquaculture and Fisheries*. Blackwell Publishing, Oxford: 412–461.

Bell, M.C.; Tuck, I.D.; Dobby, H. (2013). *Nephrops* species. In: B. Phillips (Ed). *Lobsters: biology, management, aquaculture and fisheries*. John Wiley & Sons: 357–413.

Bentley, N.; Kendrick, T.H.; Starr, P.J.; Breen, P.A. (2012). Influence plots and metrics: tools for better understanding fisheries catch-per-unit-effort standardisations. *ICES Journal of Marine Science*, 69: 84–88.

Bivand, R.; Lewin-Koh, N. (2019). maptools: Tools for Handling Spatial Objects.Software v 0.9-5. https://CRAN.R-project.org/package=maptools

Bull, B.; Dunn, A. (2002). Catch-at-age: User manual v 1.06.2002/09/12. *NIWA Internal Report*, 114: 23 p.

Bull, B.; Francis, R.I.C.C.; Dunn, A.; McKenzie, A.; Gilbert, D.J.; Smith, M.H. (2004). CASAL (C++ algorithmic stock assessment laboratory): CASAL user manual v2.06-2004/09/26. *NIWA Technical Report No.*, 126: 261 p.

Bull, B.; Francis, R.I.C.C.; Dunn, A.; McKenzie, A.; Gilbert, D.J.; Smith, M.H.; Bian, R.; Fu, D. (2012). CASAL (C++ algorithmic stock assessment laboratory): CASAL user manual v2.30-2012/03/21. *NIWA Technical Report No.*, 135: 280 p.

Chapman, C.J.; Johnstone, A.D.F.; Urquhart, G.G. (1974). Preliminary acoustic tracking studies on *Nephrops norvegicus*. Department of Agriculture and Fisheries for Scotland, Marine Laboratory Internal Report. 15 p.

Charnov, E.L.; Berrigan, D.; Shine, R. (1983). The M/*k* ratio is the same for fish and reptiles. *Amer Naturalist*, 142: 707-711.

Clark, W.G.; Hare, S.R. (2006). Assessment and management of Pacific halibut: data, methods, and policy. International Pacific Halibut Commission Scientific Report. 111 p.

Cordue, P.L. (2012). Fishing intensity metrics for use in overfishing determination. *ICES Journal of Marine Science: Journal du Conseil*, 69(4): 615-623. 10.1093/icesjms/fss036

Cryer, M. (2000). A consideration of current management areas for scampi in QMAs 3, 4, 6A and 6B. Final Research Report for Ministry of Research Project MOF199904K Objective 1. 52 p.

Cryer, M.; Coburn, R. (2000). Scampi stock assessment for 1999. *New Zealand Fisheries Assessment Report*, 2000/7: 61 p.

Cryer, M.; Dunn, A.; Hartill, B. (2005). Length-based population model for scampi (Metanephrops challengeri) in the Bay of Plenty (QMA 1). *New Zealand Fisheries Assessment Report*, 2005/27: 56 p.

Cryer, M.; Hartill, B.; Drury, J.; Tuck, I.D.; Armiger, H.; Smith, M.; Middleton, C. (2003). Indices of relative abundance for scampi, *Metanephrops challengeri*, based on photographic surveys before and after fishing in QMA 3, 2001. Final Research Report for Ministry of Fisheries Research Project SCI2000-02 Obj 3. 33 p.

Cryer, M.; Stotter, D.R. (1999). Movement and growth rates of scampi inferred from tagging, Alderman Islands, western Bay of Plenty. *NIWA Technical Report*, No 49: 36 p.

Fenaughty, C. (1989). Reproduction in *Metanephrops challengeri*. Unpubl. Rep. MAF Fisheries, Wellington. 46 p.

Francis, R.I.C.C. (1999). The impact of correlations in standardised CPUE indices. New Zealand Fisheries Assessment Research Document 99/42. 31 p.

Francis, R.I.C.C. (2011). Data weighting in statistical fisheries stock assessment models. *Canadian Journal Fisheries and Aquatic Science*, 68: 1124–1138.

Francis, R.I.C.C.; Rasmussen, S.; Fu, D.; Dunn, A. (2016). CALA: Catch-at-length and -age user manual, CALA v. *National Institute of Water & Atmospheric Research Ltd. Unpublished report.*: 92 p.

Lazaridis, E. (2014). lunar: Lunar Phase & Distance, Seasons and Other Environmental Factors.Software v 0.1-04. http://statistics.lazaridis.eu

McCullagh, P.; Nelder, J.A. (1989). *Generalised Linear Models*. Chapman and Hall, London: 511 p.

Morizur, Y. (1982). Estimation de la mortalité pour quelques stocks de langoustine, *Nephrops norvegicus*. *ICES CM*, 1982/K:10.

Pauly, D. (1980). On the interrelationships between natural mortality, growth parameters, and mean environmental temperature in 175 fish stocks. *Journal du Conseil International pour l'Exloration du Mer*, 39: 175-192.

R Development Core Team (2018). R: A language and environment for statistical computing.Software. https://www.R-project.org/

Smith, P.J. (1999). Allozyme variation in scampi (*Metanephrops challengeri*) fisheries in New Zealand. *New Zealand journal of Marien and Freshwater Research*, 33: 491-497.

Starr, P.J. (2009). Rock lobster catch and effort data: summaries and CPUE standardisations, 1979–80 to 2007–08. *New Zealand Fisheries Assessment Report*, 2009/38: 73 p.

Starr, P.J.; Breen, P.A.; Kendrick, T.H.; Haist, V. (2009). Model and data used for the 2008 stock assessment of rock lobsters (*Jasus edwardsii*) in CRA 3. *New Zealand Fisheries Assessment Report*, 2009/22: 62 p.

Tuck, I.D. (2009). Characterisation of scampi fisheries and the examination of catch at length and spatial distribution of scampi in SCI 1, 2, 3, 4A and 6A. *New Zealand Fisheries Assessment Report*, 2009/27: 102 p.

Tuck, I.D. (2010). Scampi burrow occupancy, burrow emergence and catchability. *New Zealand Fisheries Assessment Report*, 2010/13: 58 p.

Tuck, I.D. (2013). Characterisation and length-based population model for scampi (*Metanephrops challengeri*) on the Mernoo Bank (SCI 3). *New Zealand Fisheries Assessment Report*, 2013/24: 165 p.

Tuck, I.D. (2014). Characterisation and length-based population model for scampi (*Metanephrops challengeri*) in the Bay of Plenty (SCI 1) and Hawke Bay/Wairarapa (SCI 2). *New Zealand Fisheries Assessment Report*, 2014/33: 172 p.

Tuck, I.D. (2015). Characterisation and length-based population model for scampi (*Metanephrops challengeri*) at the Auckland Islands (SCI 6A). *New Zealand Fisheries Assessment Report*, 2015/21: 164 p.

Tuck, I.D. (2016a). Characterisation and length-based assessment model for scampi (*Metanephrops challengeri*) in the Bay of Plenty (SCI 1) and Hawke Bay– Wairarapa (SCI 2). *New Zealand Fisheries Assessment Report*, 2016/51: 194 p.

Tuck, I.D. (2016b). Characterisation and length-based population model for scampi (*Metanephrops challengeri*) on the Mernoo Bank (SCI 3). *New Zealand Fisheries Assessment Report*, 2016/55: 221 p.

Tuck, I.D. (2017). Characterisation and length-based population model for scampi (*Metanephrops challengeri*) at the Auckland Islands (SCI 6A). *New Zealand Fisheries Assessment Report*, 2017/56: 180 p.

Tuck, I.D. (in prep). Characterisation and CPUE standardisation of scampi in SCI 4A. *New Zealand Fisheries Assessment Report*.

Tuck, I.D.; Atkinson, R.J.A.; Chapman, C.J. (2000). Population biology of the Norway lobster, *Nephrops norvegicus* (L.) in the Firth of Clyde, Scotland. II. Fecundity and size at onset of maturity. *ICES Journal of Marine Science*, 57: 1222-1237.

Tuck, I.D.; Dunn, A. (2006). Length based population model for scampi (*Metanephrops challengeri*) in the Bay of Plenty (SCI 1) and Wairarapa / Hawke Bay (SCI 2). Final Research Report for Ministry of Research Project SCI200501 (Objectives 2 & 3). 42 p.

Tuck, I.D.; Dunn, A. (2009). Length-based population model for scampi (*Metanephrops challengeri*) in the Bay of Plenty (SCI 1) and Wairarapa / Hawke Bay (SCI 2). Final Research Report for Ministry of Fisheries research project SCI2008-03 (Objective 1). 30 p.

Tuck, I.D.; Dunn, A. (2012). Length-based population model for scampi (*Metanephrops challengeri*) in the Bay of Plenty (SCI 1), Wairarapa / Hawke Bay (SCI 2) and Auckland Islands (SCI 6A). *New Zealand Fisheries Assessment Report*, 2012/1: 125 p.

Tuck, I.D.; Hartill, B.; Parkinson, D.; Drury, J.; Smith, M.; Armiger, H. (2009). Estimating the abundance of scampi - Relative abundance of scampi, *Metanephrops challengeri*, from a photographic survey in SCI 6A (2009). Final Research Report for Ministry of Fisheries research project SCI2008-01 Objectives 1 & 2. 26 p.

Tuck, I.D.; Hartill, B.; Parkinson, D.; Smith, M.; Armiger, H.; Rush, N.; Drury, J. (2011). Estimating the abundance of scampi - Relative abundance of scampi, *Metanephrops challengeri*, from photographic surveys in SCI 3 (2009 & 2010). Final Research Report for Ministry of Fisheries research projects SCI200901 & SCI 201001. 29 p.

Tuck, I.D.; Parkinson, D.; Armiger, H.; Smith, M.; Miller, A.; Rush, N.; Spong, K. (2015a). Estimating the abundance of scampi in SCI 3 (Mernoo Bank) in 2013. *New Zealand Fisheries Assessment Report*, 2015/23: 49 p.

Tuck, I.D.; Parkinson, D.; Armiger, H.; Smith, M.; Miller, A.; Rush, N.; Spong, K. (in press). Estimating the abundance of scampi in SCI 3 (Mernoo Bank) in 2016. *New Zealand Fisheries Assessment Report*: 36 p.

Tuck, I.D.; Parkinson, D.; Hartill, B.; Drury, J.; Smith, M.; Armiger, H. (2007). Estimating the abundance of scampi - relative abundance of scampi, *Metanephrops challengeri*, from a photographic survey in SCI 6A (2007). Final Research Report for Ministry of Fisheries Research Project SCI2006/02 Objectives 1 & 2. 29 p.

Tuck, I.D.; Parsons, D.M.; Hartill, B.W.; Chiswell, S.M. (2015b). Scampi (*Metanephrops challengeri*) emergence patterns and catchability. *ICES Journal of Marine Science*, 72 (Supplement 1): i199-i210. http://icesjms.oxfordjournals.org/content/early/2015/01/08/icesjms.fsu244.abstract

Verry, A. (2017). Population genetics of New Zealand Scampi (Metanephrops challengeri). Victoria University of Wellington, Wellington: 84 p.

Vignaux, M. (1994). Catch per unit effort (CPUE) analysis of west coast South Island and Cook Strait spawning hoki fisheries, 1987–93. New Zealand Fisheries Assessment Research Document. 29 p.

Wear, R.G. (1976). Studies on the larval development of *Metanephrops challengeri* (Balss, 1914) (Decapoda, Nephropidae). *Crustaceana*, 30: 113-122.

Zacarais, L.D. (2013). Genetic population structure of deep-water prawns *Haliporoides triarthrus* and langoustines *Metanephrops mozambicus* in the South West Indian Ocean: use of mitochondrial DNA

to investigate metapopulation structure. *School of Life Sciences*. University of KwaZulu-Natal, Durban: 87 p.

APPENDIX 1: CPUE STANDARDISATION DIAGNOSTICS

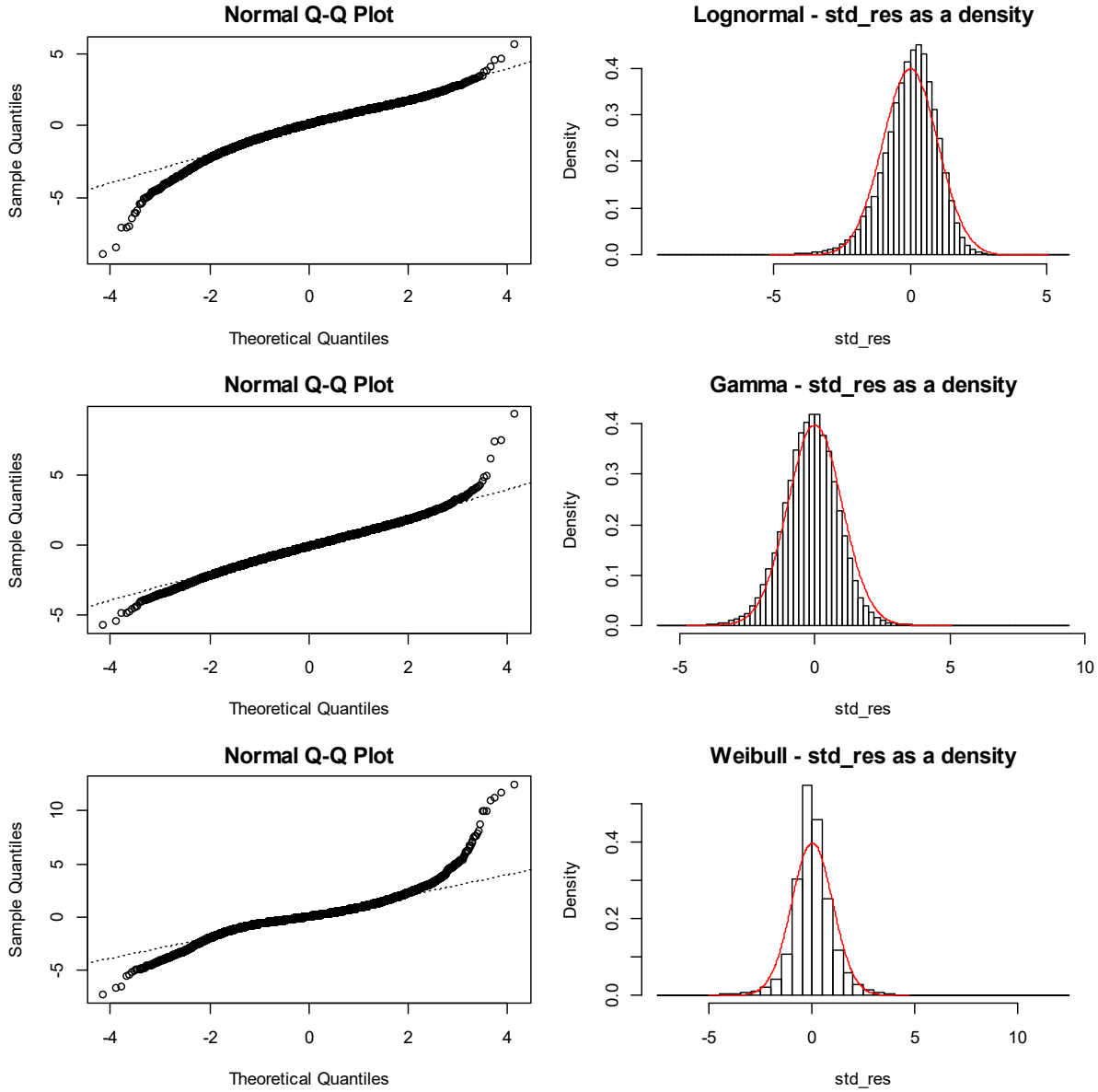

A1. 1: Plots of the distributions of standardised residuals for simple standardised CPUE models for SCI 3 with log normal (top panel), gamma (middle panel), and Weibull (bottom panel) error distributions.

Annual CPUE index

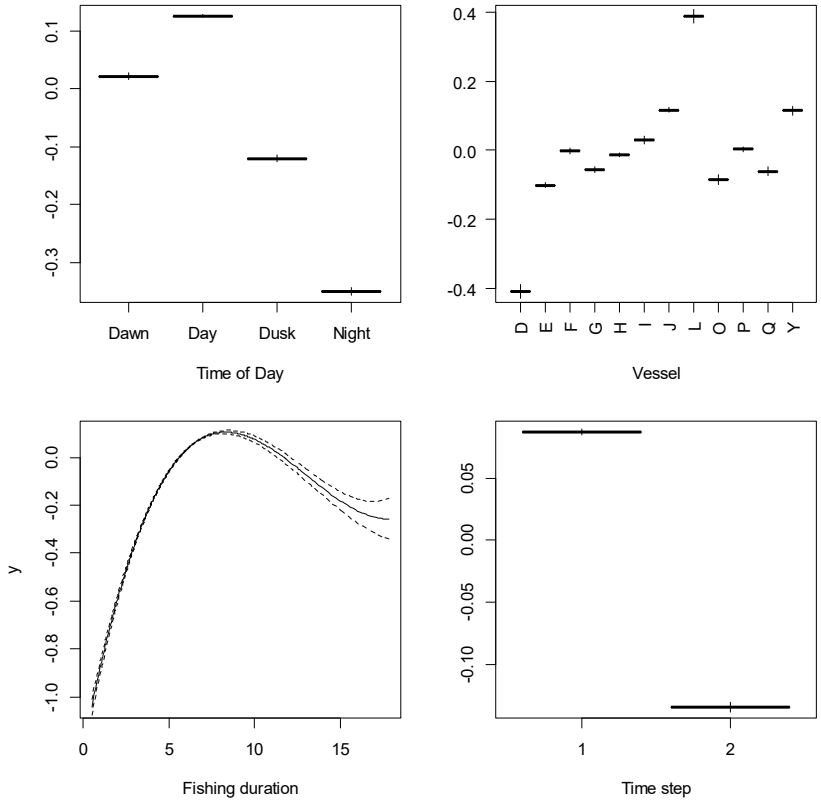

A1. 2: Term plot for final SCI 3 CPUE standardisation model.

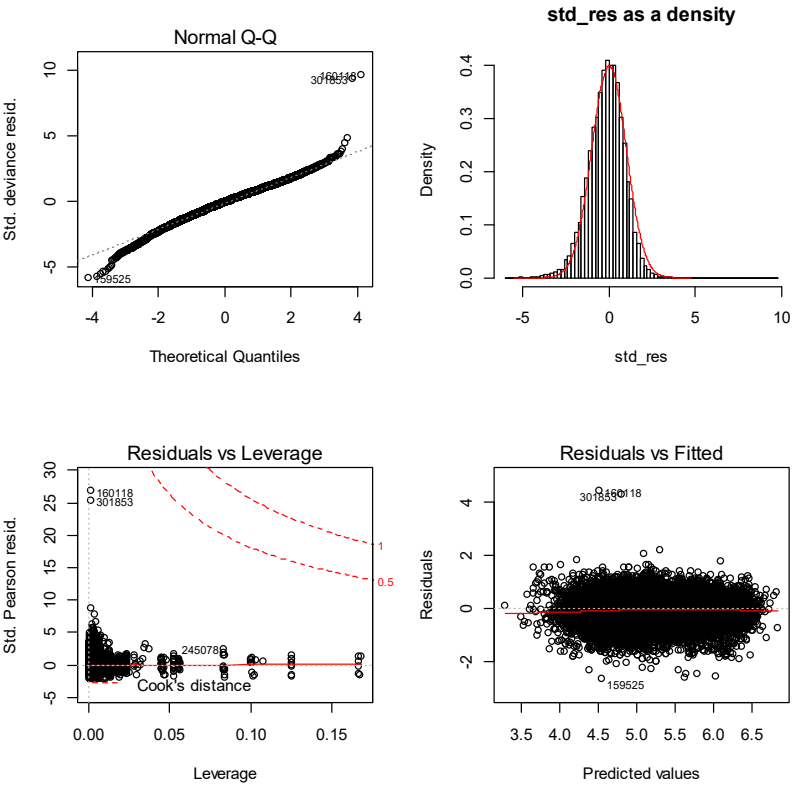

A1. 3: Diagnostic plots for final SCI 3 CPUE standardisation model.

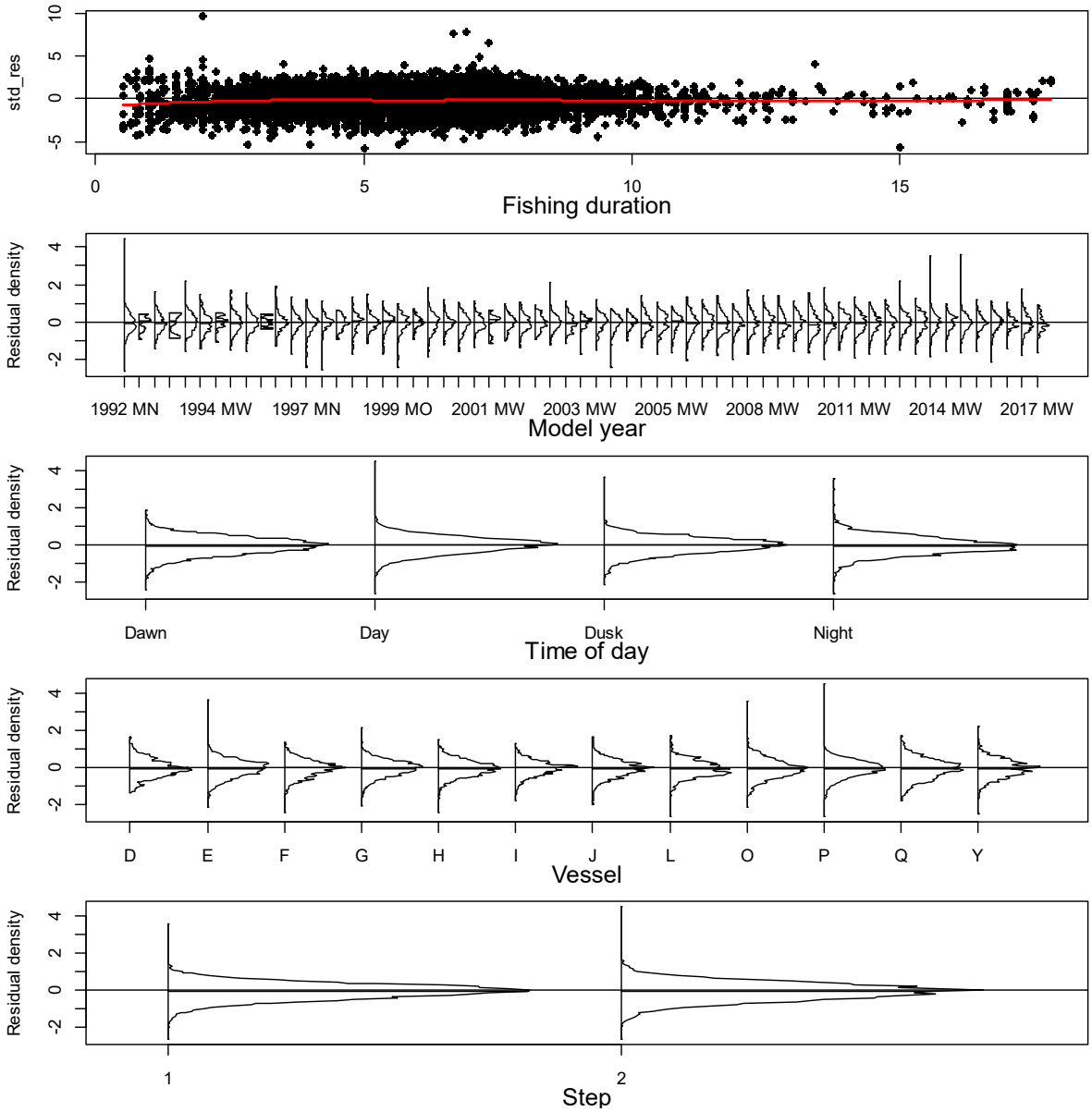

A1. 4: Distributions of residuals for final SCI 3 CPUE standardisation model.

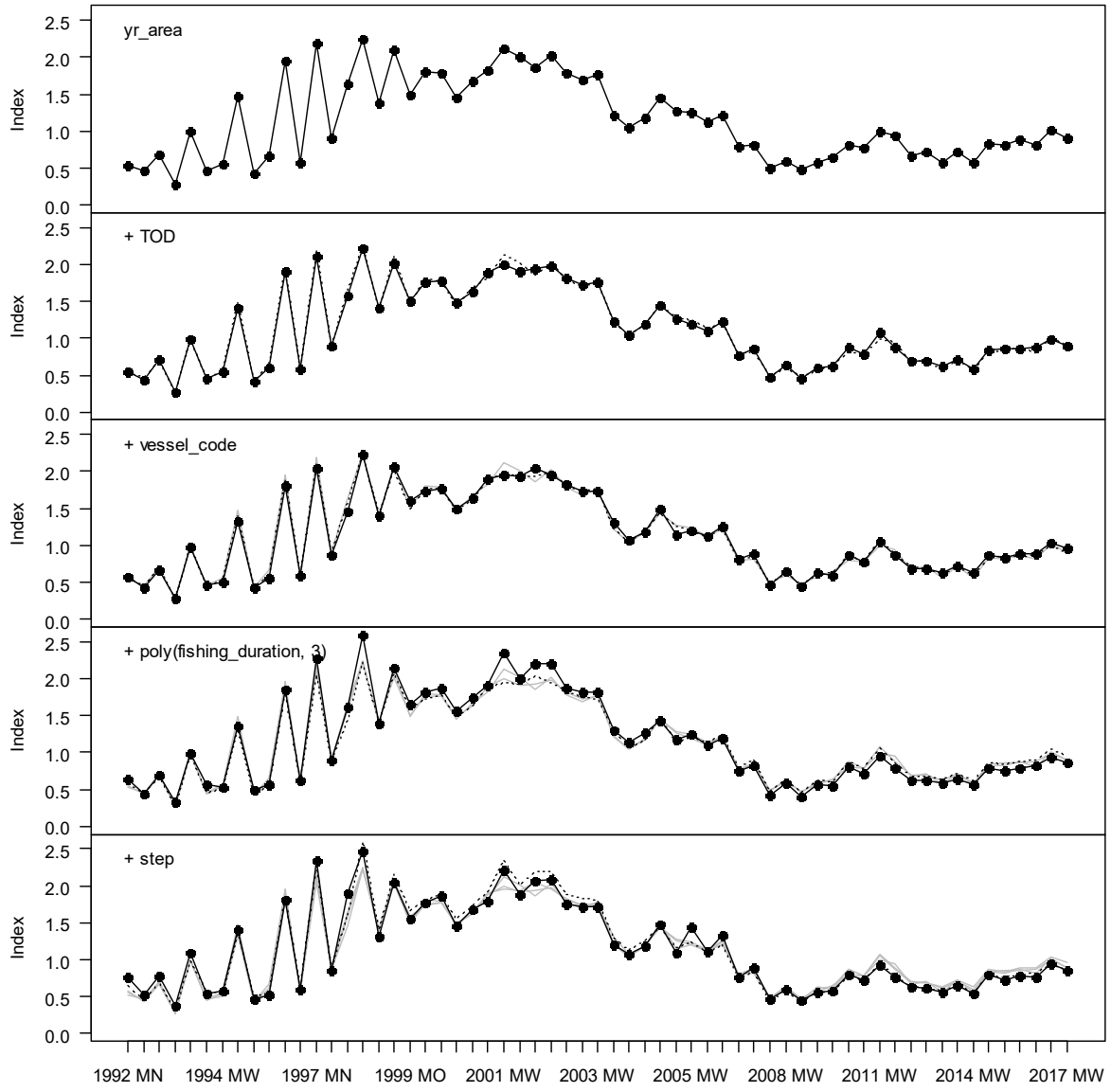

A1. 5: Step influence plot for final SCI 3 CPUE standardisation model. TOD is time of day.

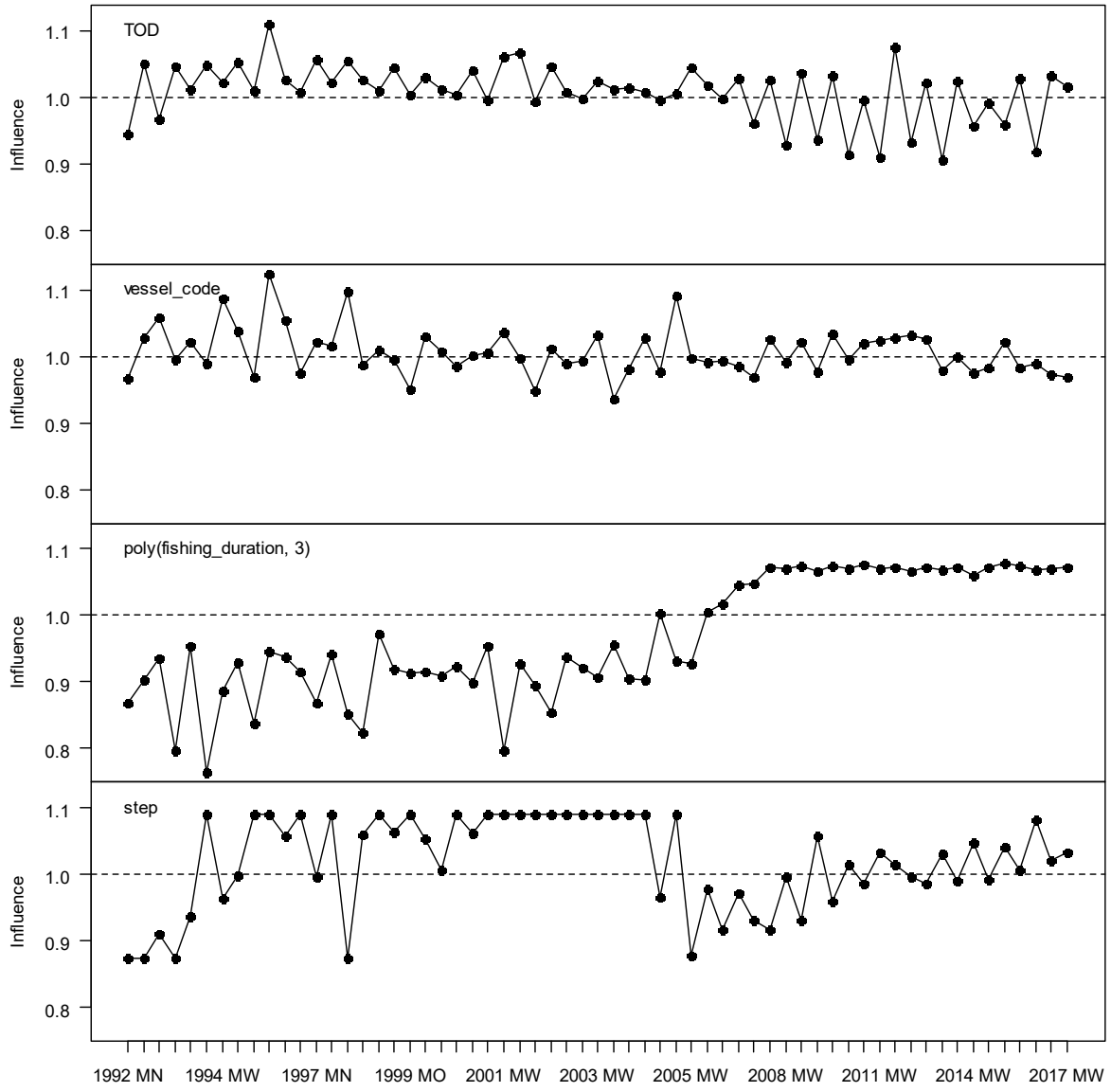

A1. 6: Year influence plots for each explanatory variable for final SCI 3 CPUE standardisation model. TOD is time of day.

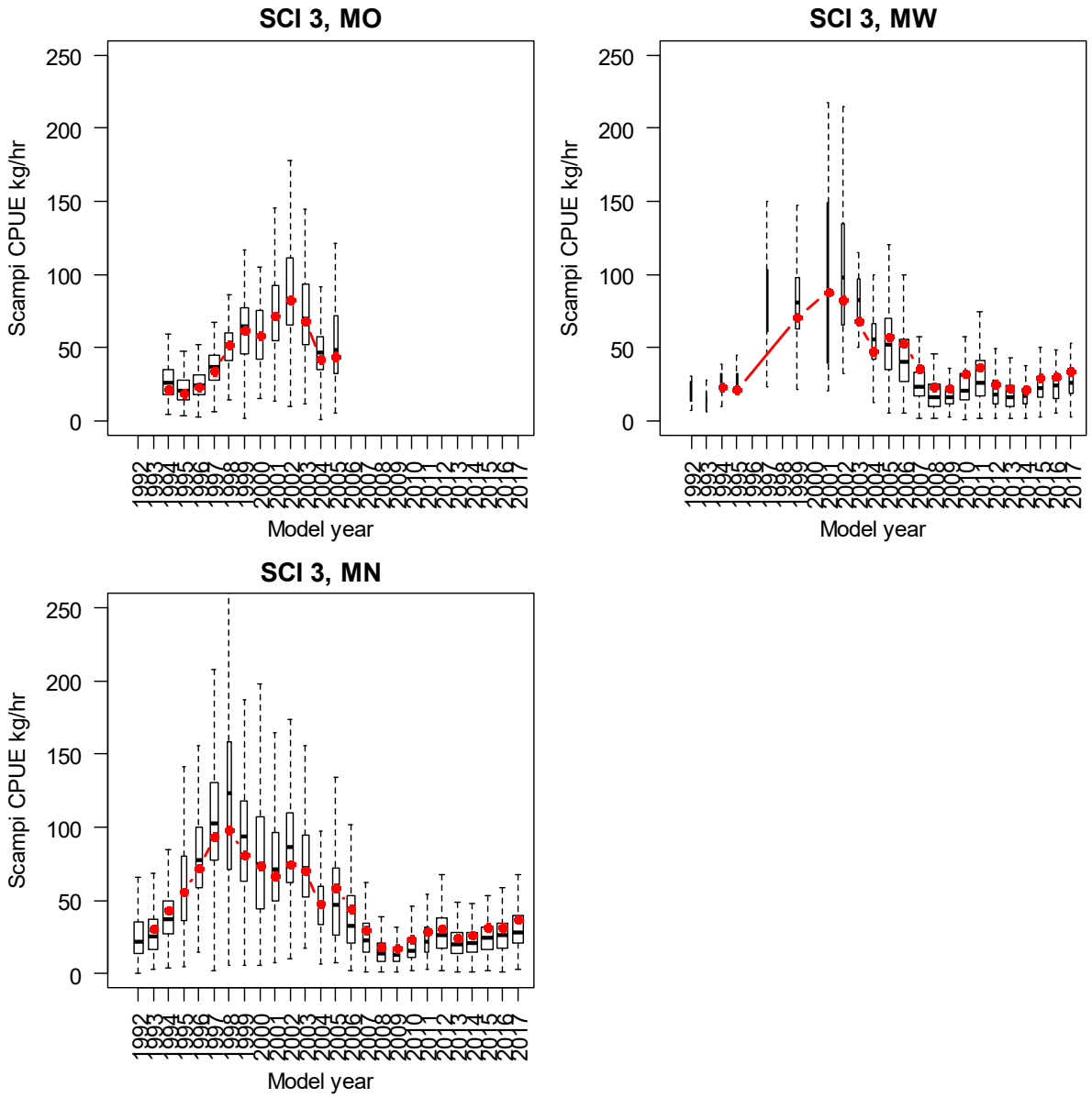

A1. 7: Plot of standardised and unstandardised CPUE indices for SCI 3.

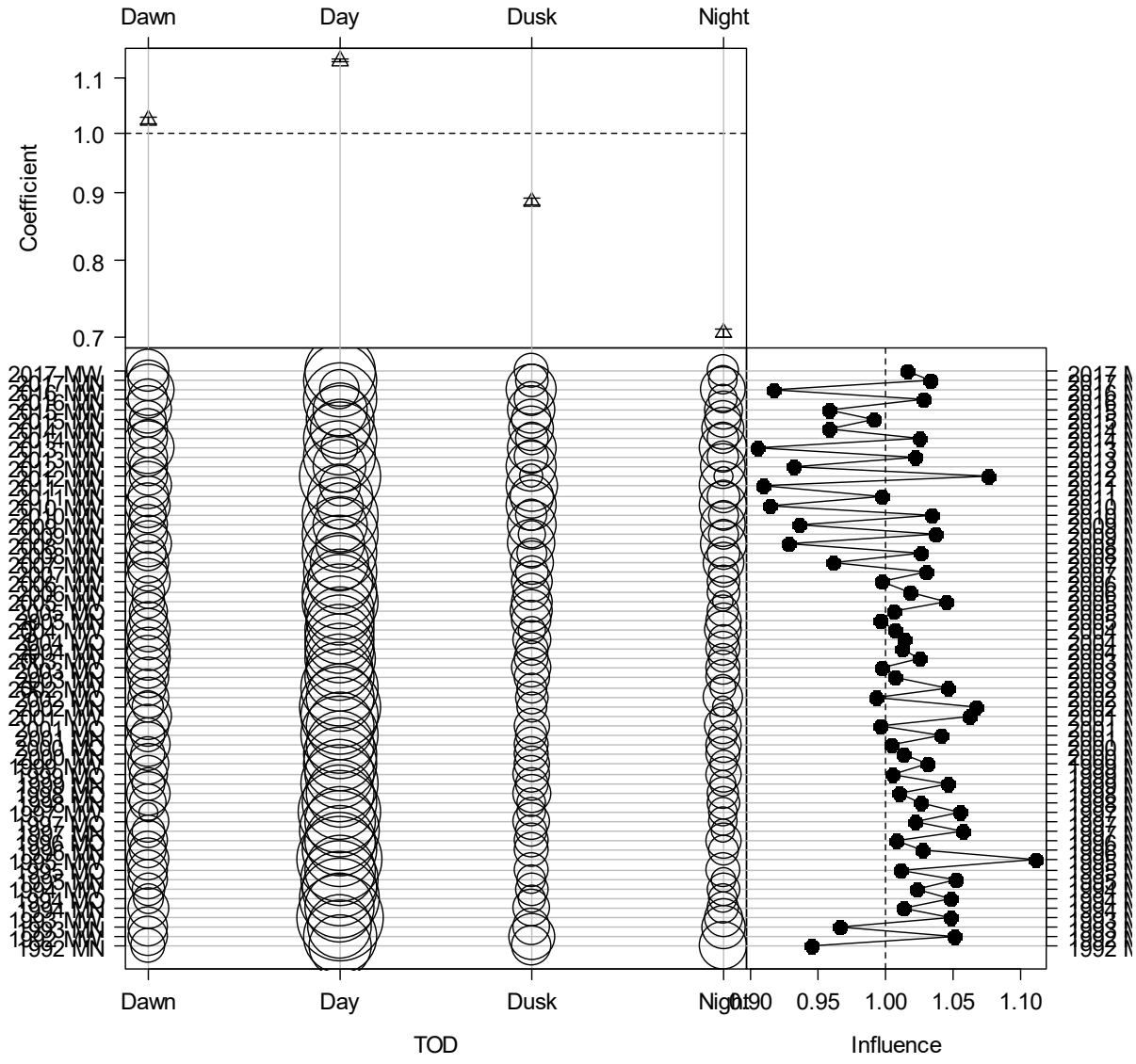

A1. 8: Coefficient-distribution influence plot for time of day (TOD) for final SCI 3 CPUE standardisation model.

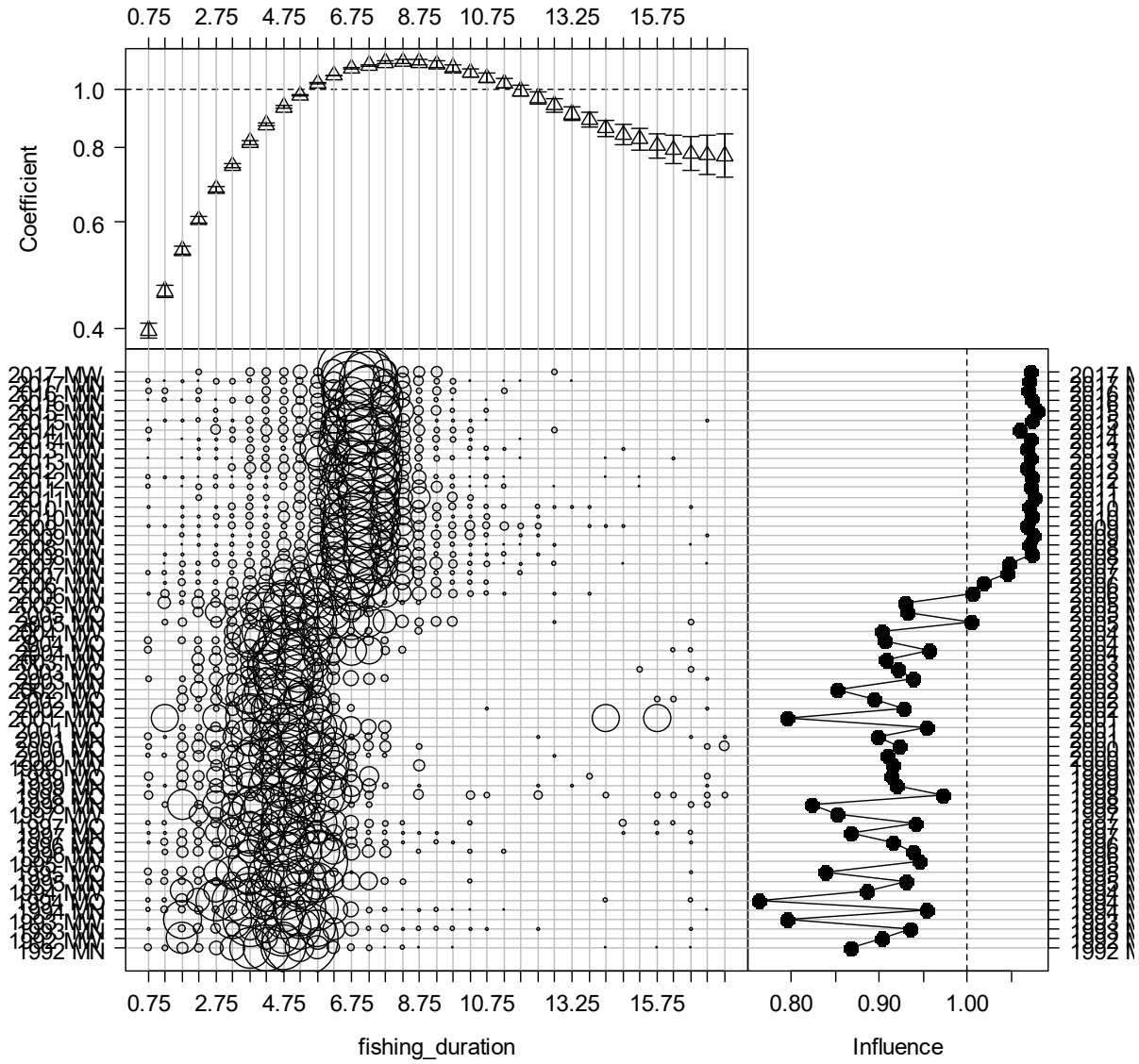

A1. 9: Coefficient-distribution influence plot for fishing duration for final SCI 3 CPUE standardisation model.

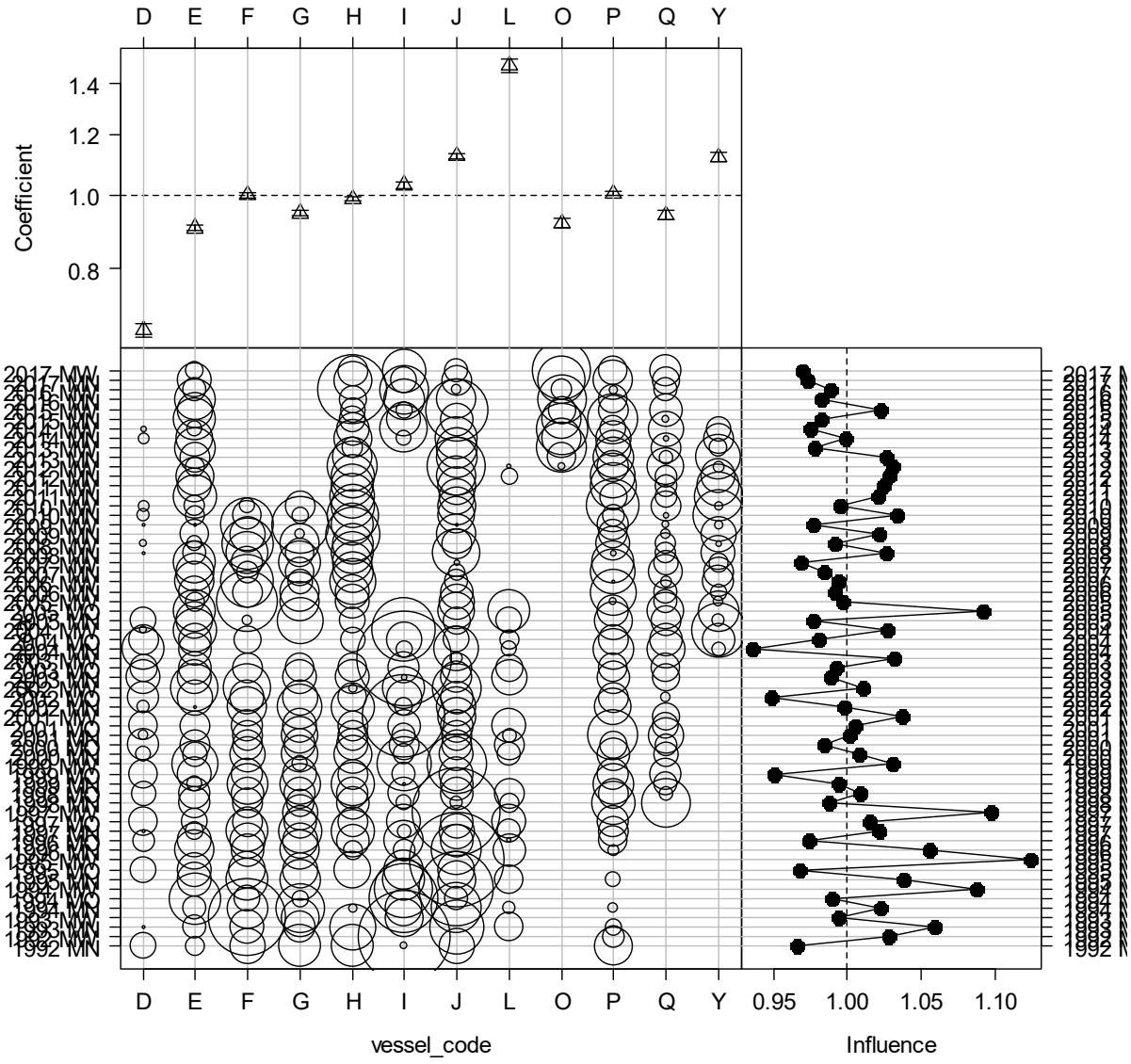

A1. 10: Coefficient-distribution influence plot for vessel for final SCI 3 CPUE standardisation model.

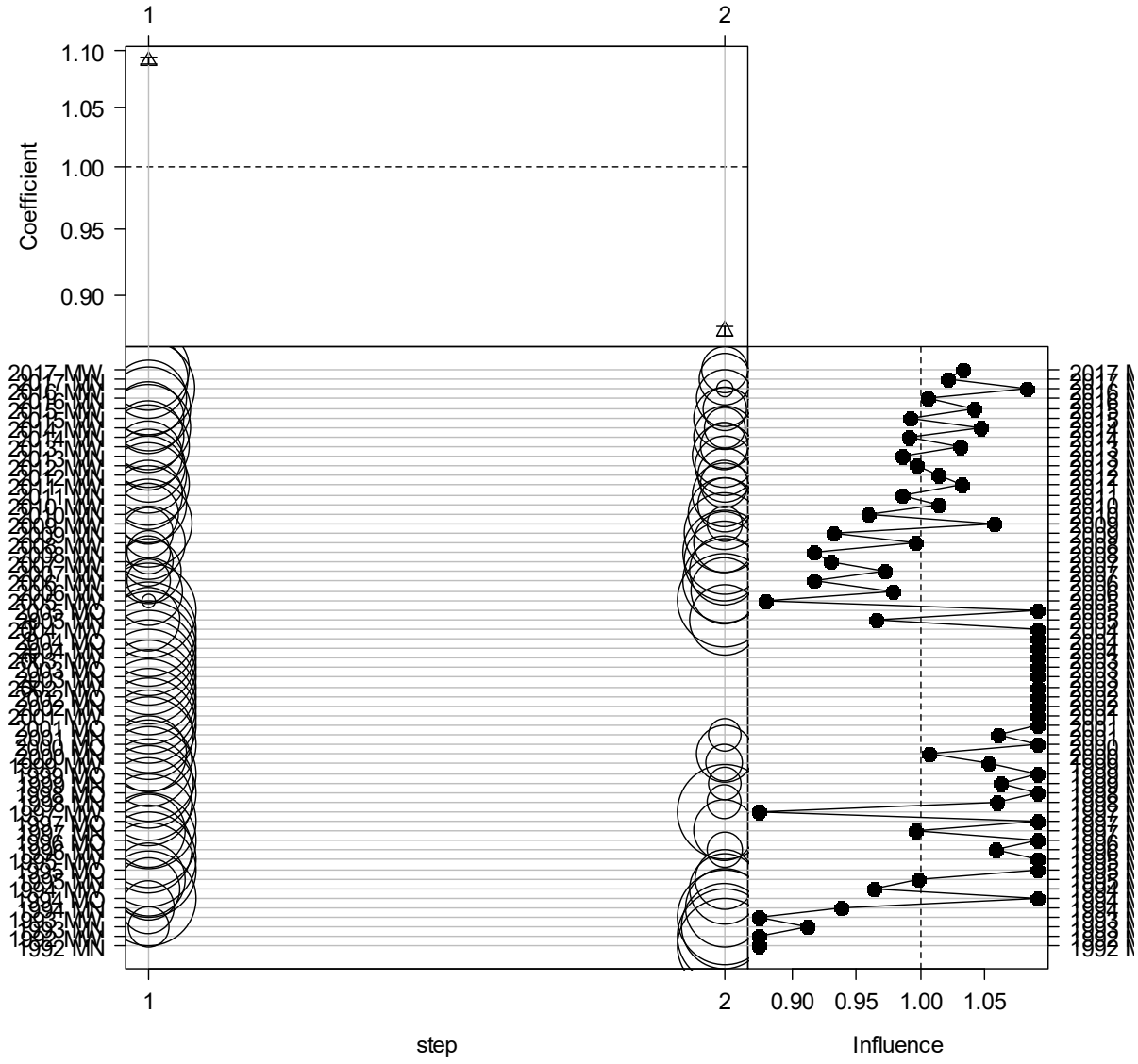

A1. 11: Coefficient-distribution influence plot for time step for final SCI 3 CPUE standardisation model.

APPENDIX 2: ANALYSIS OF LENGTH COMPOSITION DATA

Trawl survey length frequency data

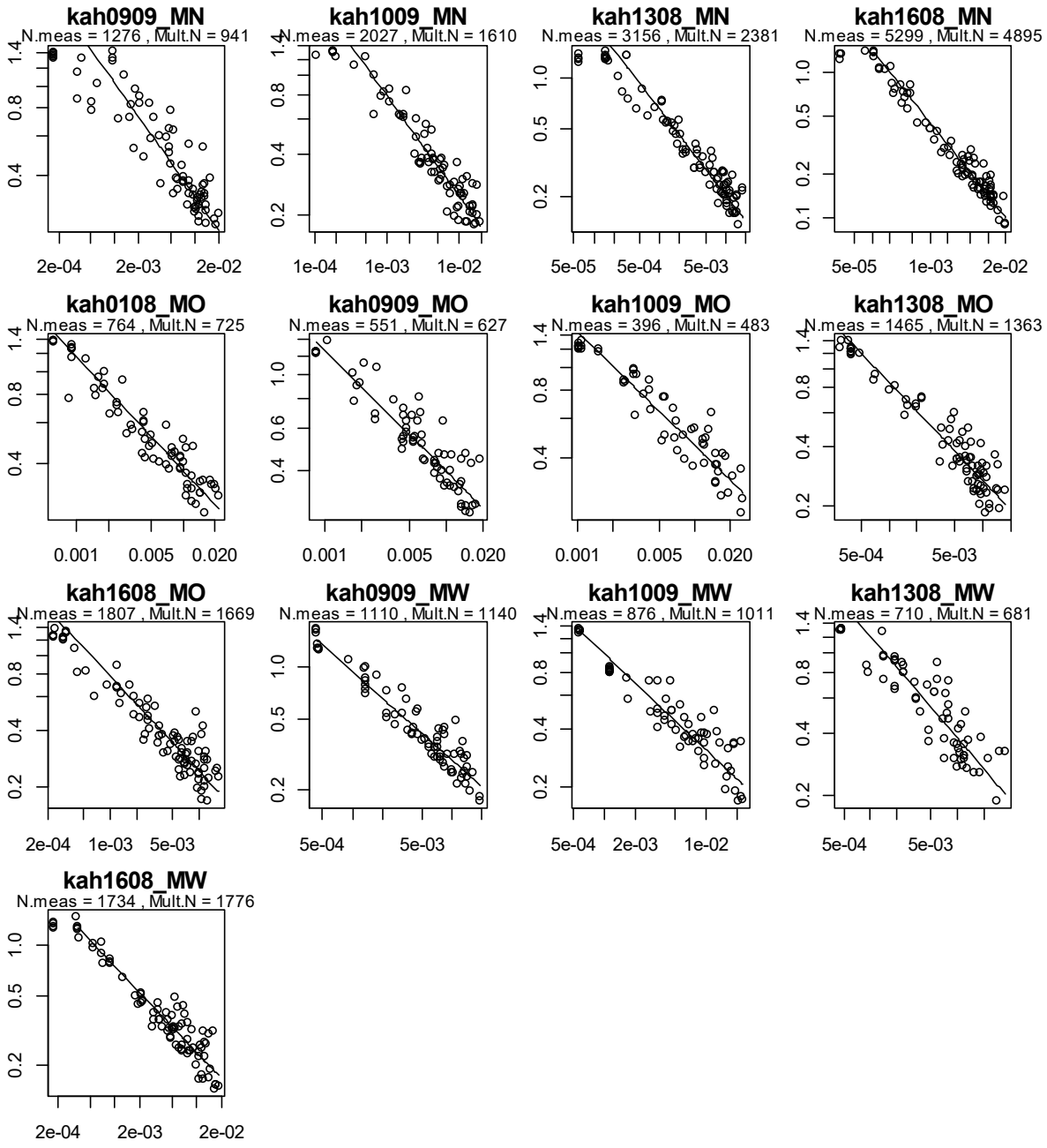

A2. 1: Observation-error CVs for the trawl survey proportions-at-length data sets for each subarea surveyed. Trawl surveys were carried out in time step 1. Each point represents a proportion at a specific length and sex for a given year. The diagonal line, which is the same in each panel, is added to aid comparison between panels; it shows the relationship between proportion and CV that would hold with simple multinomial sampling with sample size 500.

Observer length frequency data

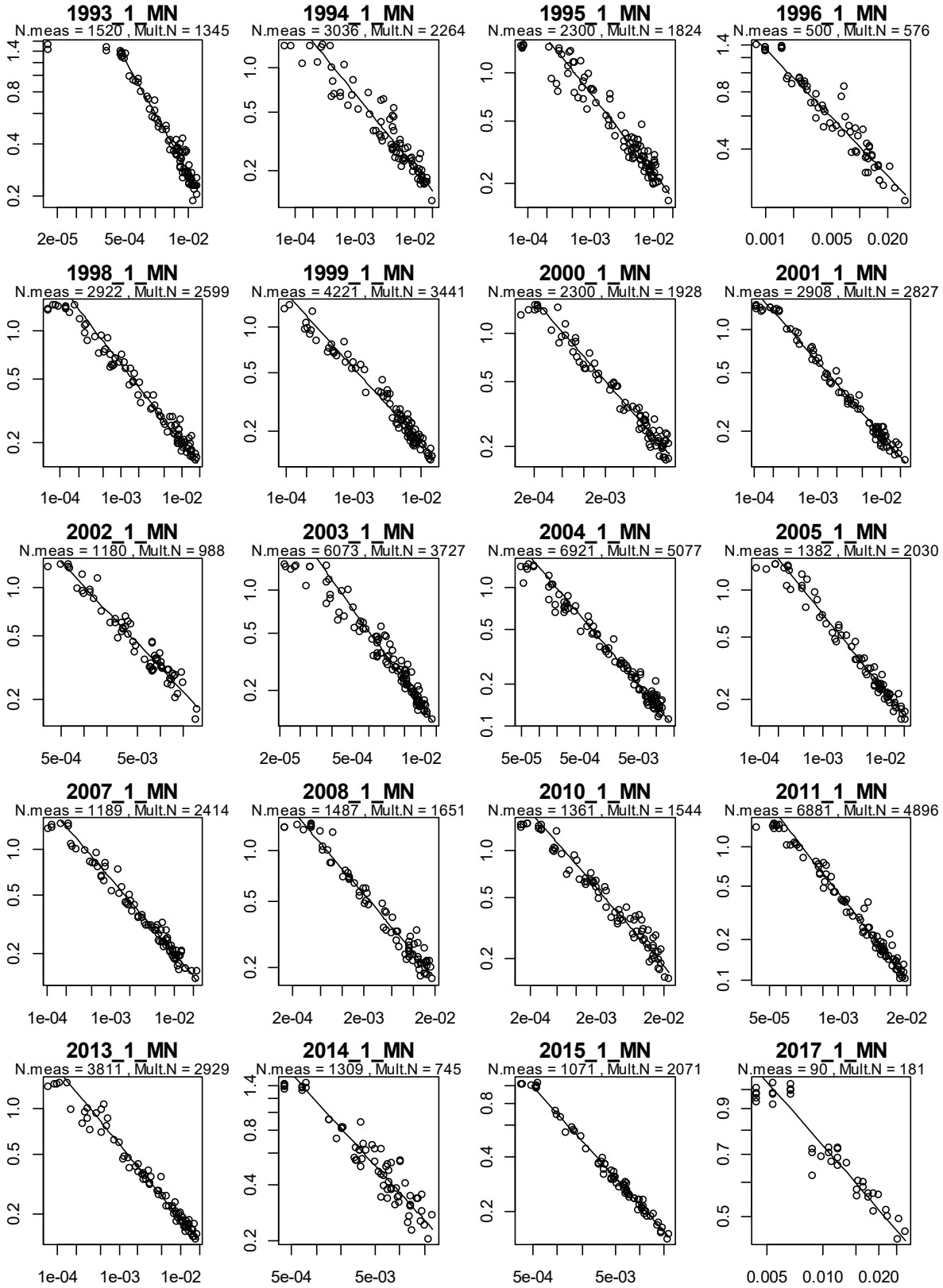

A2. 2: Observation-error CVs for the observer proportions-at-length data sets for subarea MN in time step 1. Each point represents a proportion at a specific length and sex for a given year. The diagonal line, which is the same in each panel, is added to aid comparison between panels; it shows the relationship between proportion and CV that would hold with simple multinomial sampling with sample size 500.

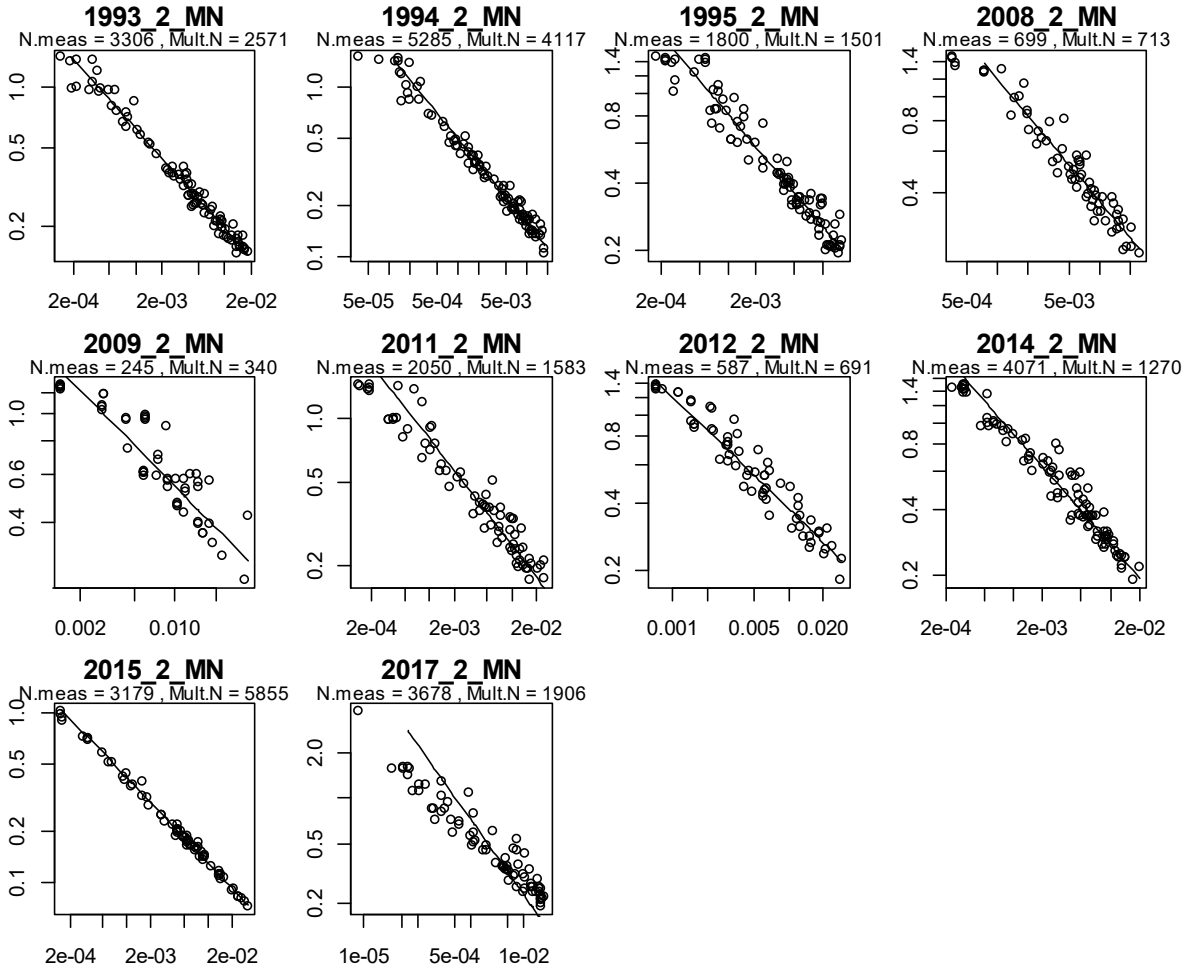

A2. 3: Observation-error CVs for the observer proportions-at-length data sets for subarea MN in time step 2. Each point represents a proportion at a specific length and sex for a given year. The diagonal line, which is the same in each panel, is added to aid comparison between panels; it shows the relationship between proportion and CV that would hold with simple multinomial sampling with sample size 500.

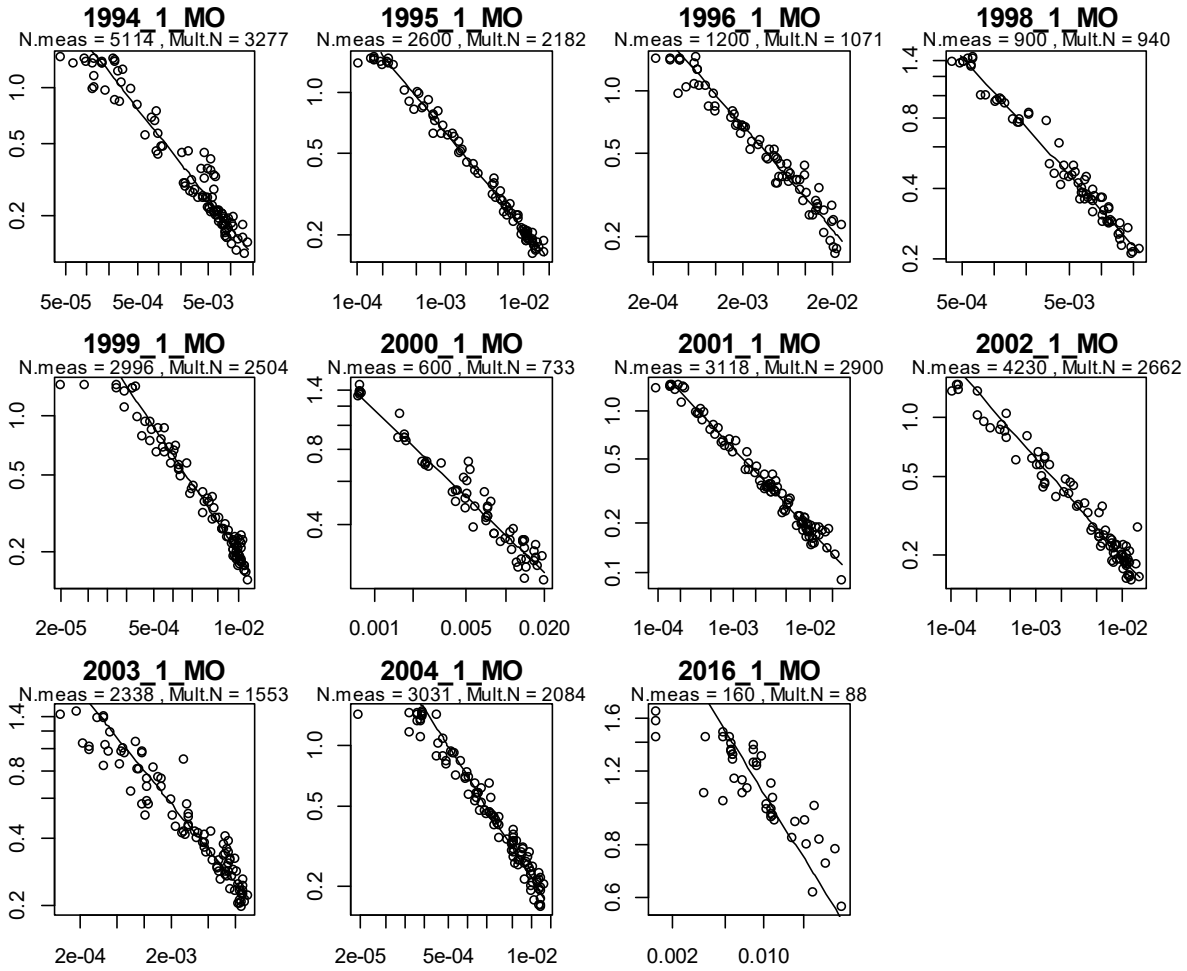

A2. 4: Observation-error CVs for the observer proportions-at-length data sets for subarea MO in time step 1. Each point represents a proportion at a specific length and sex for a given year. The diagonal line, which is the same in each panel, is added to aid comparison between panels; it shows the relationship between proportion and CV that would hold with simple multinomial sampling with sample size 500.

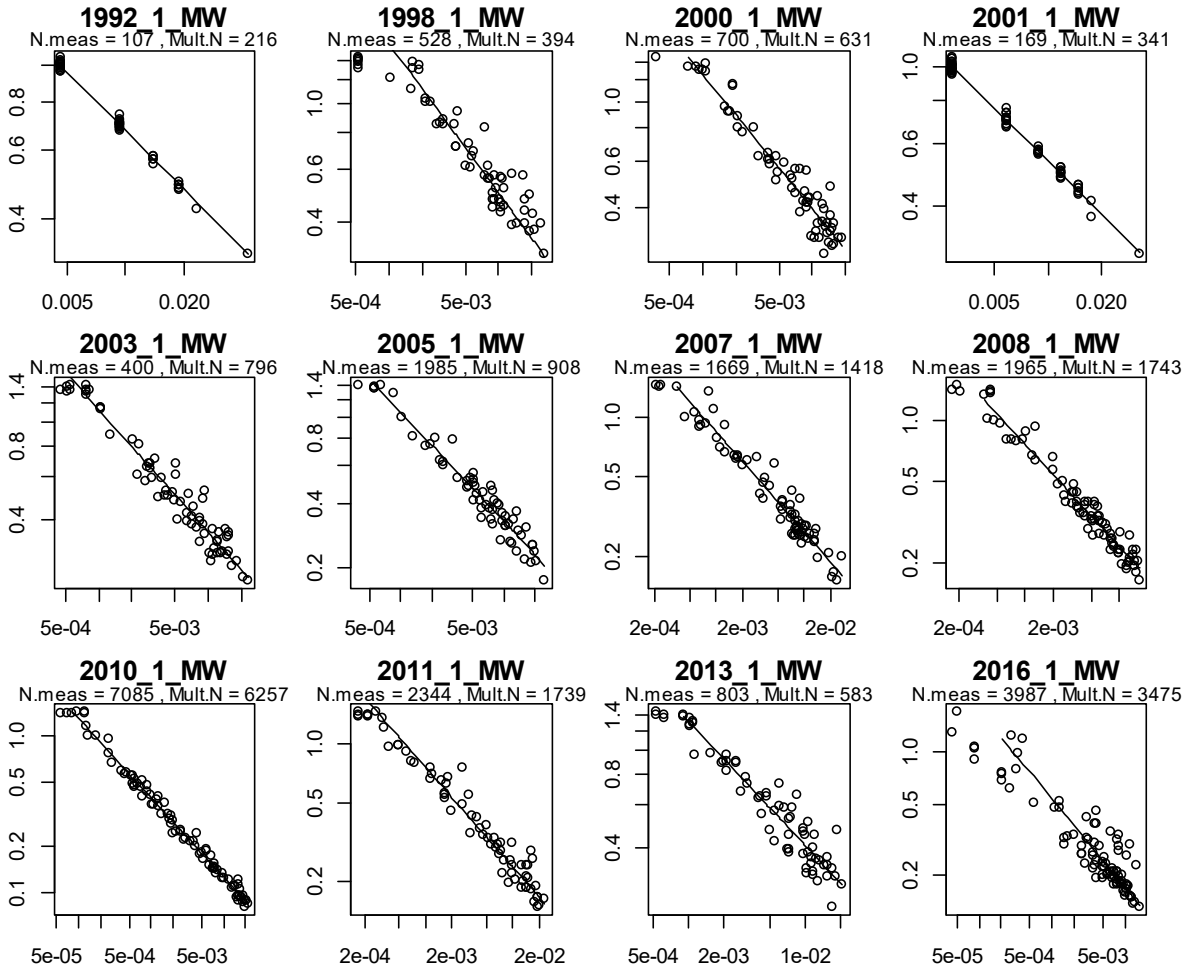

A2. 5: Observation-error CVs for the observer proportions-at-length data sets for subarea MW in time step 1. Each point represents a proportion at a specific length and sex for a given year. The diagonal line, which is the same in each panel, is added to aid comparison between panels; it shows the relationship between proportion and CV that would hold with simple multinomial sampling with sample size 500.

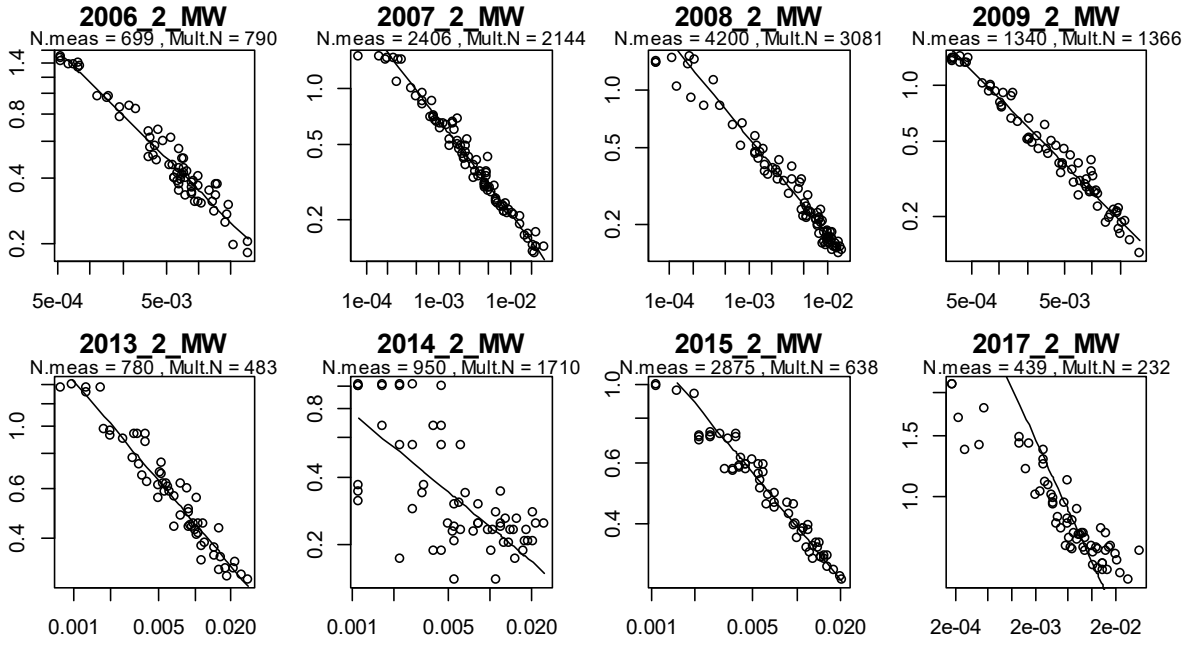

A2. 6: Observation-error CVs for the observer proportions-at-length data sets for subarea MW in time step 2. Each point represents a proportion at a specific length and sex for a given year. The diagonal line, which is the same in each panel, is added to aid comparison between panels; it shows the relationship between proportion and CV that would hold with simple multinomial sampling with sample size 500.

Photo survey data

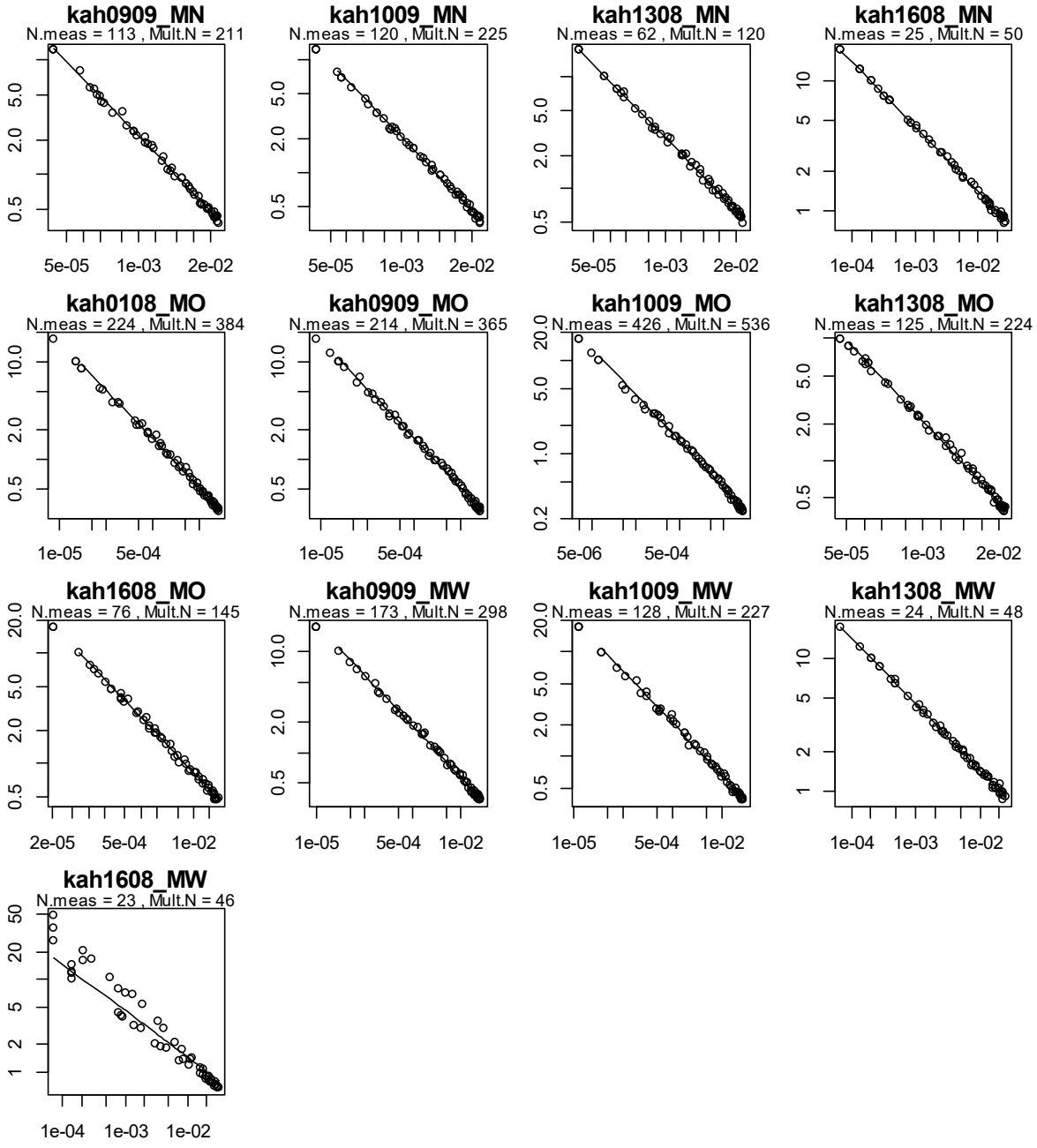

A2. 7: Observation-error CVs for the photo survey proportions-at-length data sets for each subarea surveyed. Trawl surveys were carried out in time step 1. Each point represents a proportion at a specific length and sex for a given year. The diagonal line, which is the same in each panel, is added to aid comparison between panels; it shows the relationship between proportion and CV that would hold with simple multinomial sampling with sample size 500.

APPENDIX 3: MODEL 1, *M* fixed at 0.25, CPUE process error 0.2

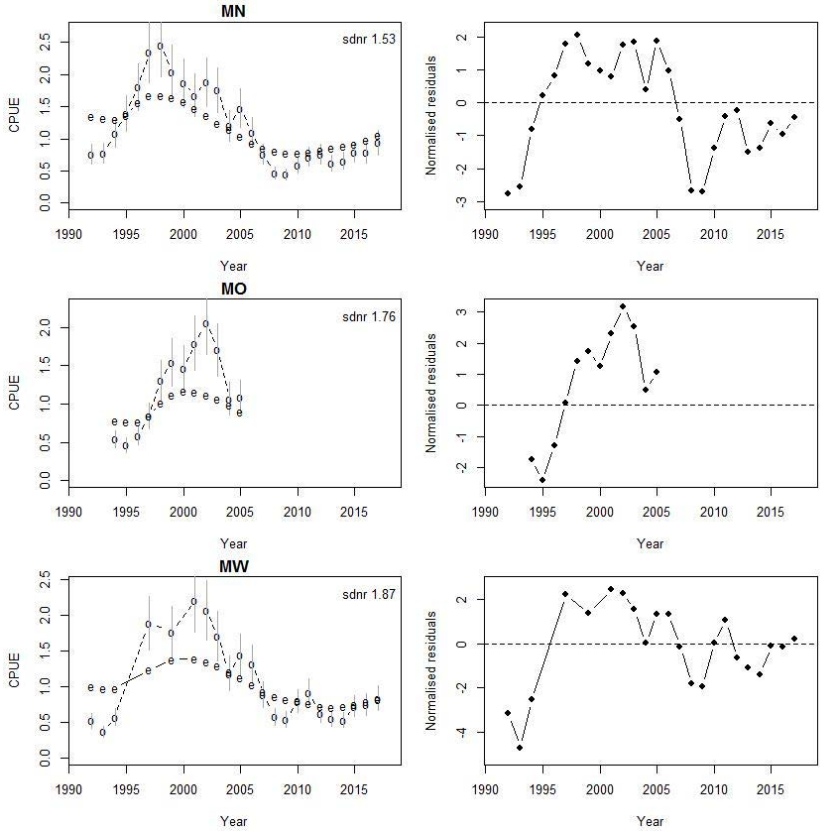

A3. 1: Fits to CPUE indices (left column) and normalised residuals (right column) by subarea (MN - top row, MO - middle row, MW - bottom row) for SCI 3 Model 1.

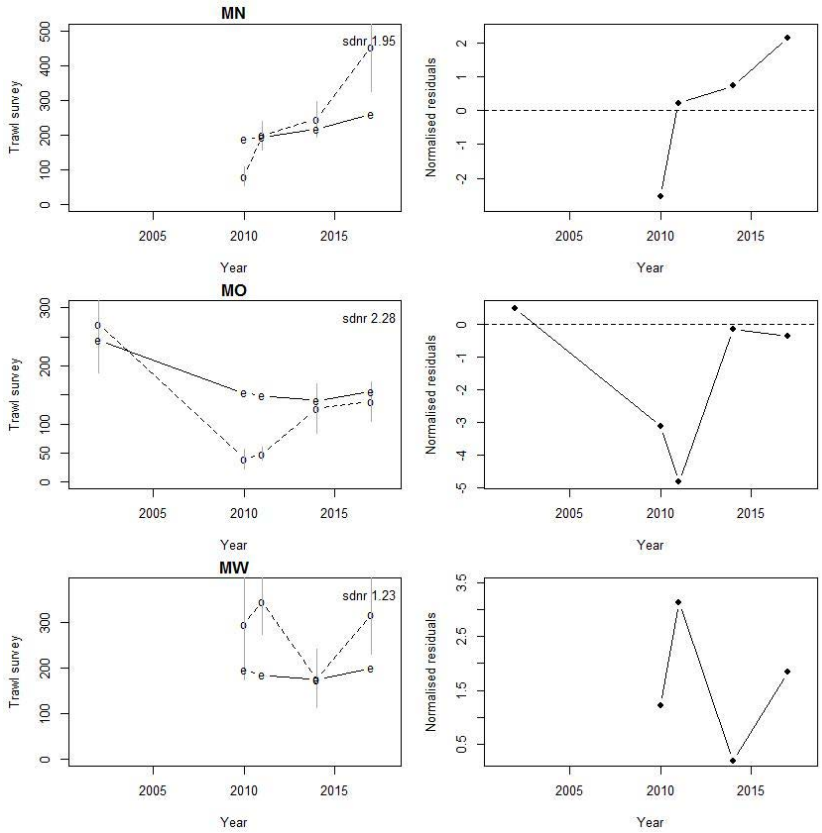

A3. 2: Fits to trawl survey indices (left column) and normalised residuals (right column) by subarea (MN - top row, MO - middle row, MW - bottom row) for SCI 3 Model 1.

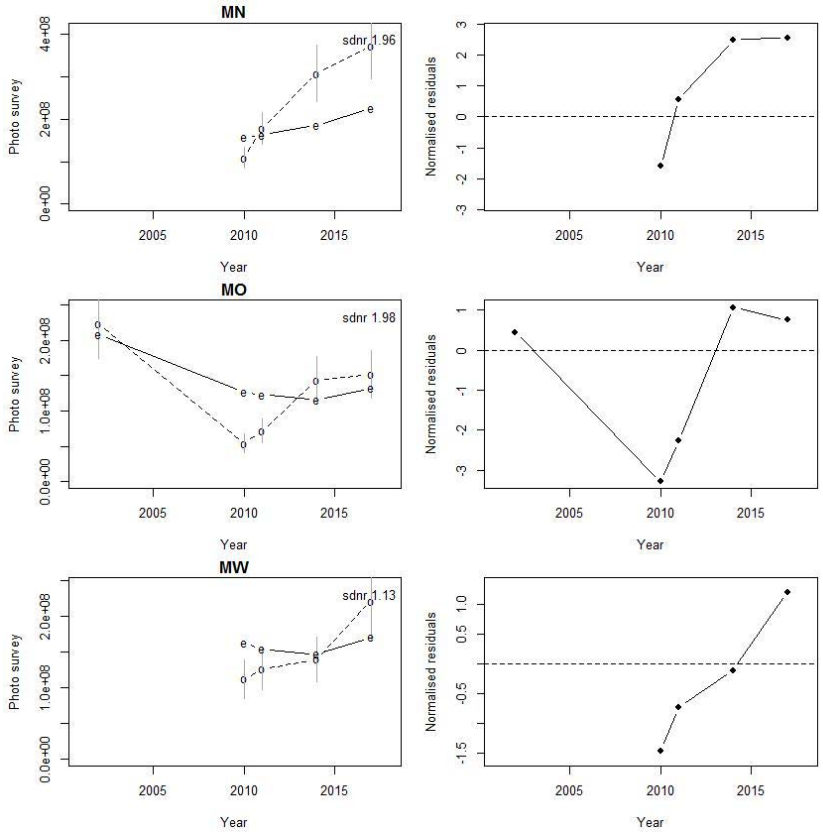

A3. 3: Fits to photo survey indices (left column) and normalised residuals (right column) by subarea (MN - top row, MO - middle row, MW - bottom row) for SCI 3 Model 1.

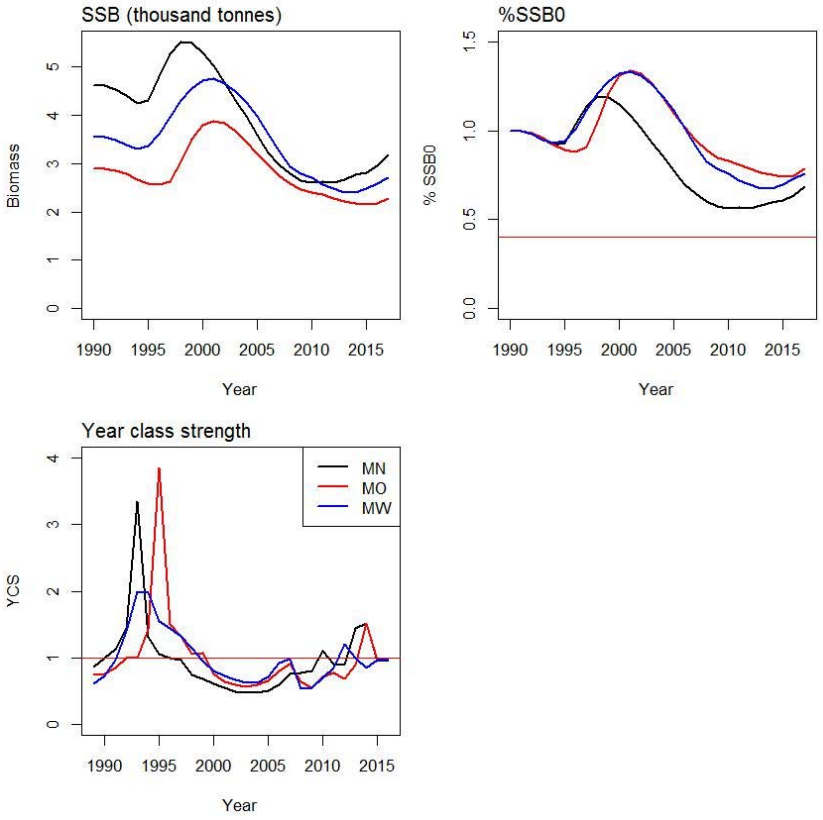

A3. 4: Spawning stock biomass trajectory (upper left), spawning stock biomass as a percentage of SSB_0 (upper right), and year class strength (lower plot) by subarea for SCI 3 Model 1.

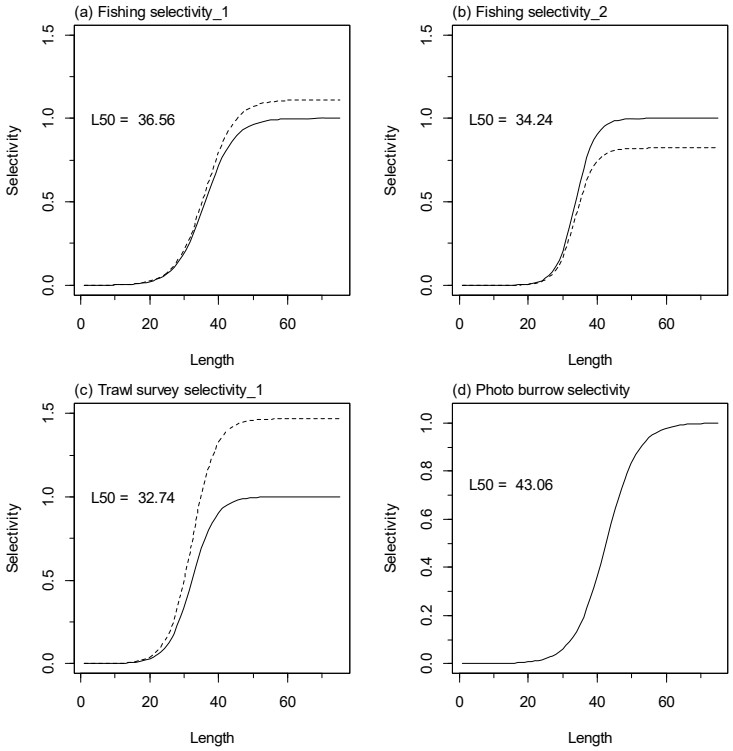

A3. 5: Fishery and photo survey selectivity curves for SCI 3 Model 1. Solid line – females, dotted line – males. The scampi photo index is not sexed, and a single selectivity applies.

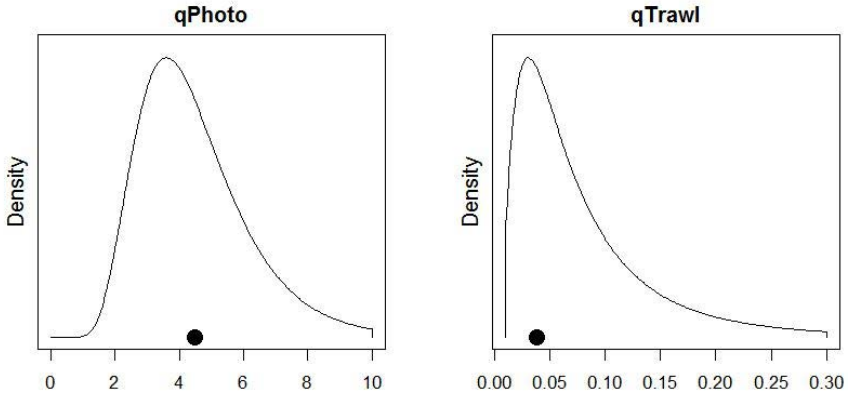

A3. 6: Catchability estimates from MPD model run for SCI 3 Model 1, plotted in relation to prior distribution.

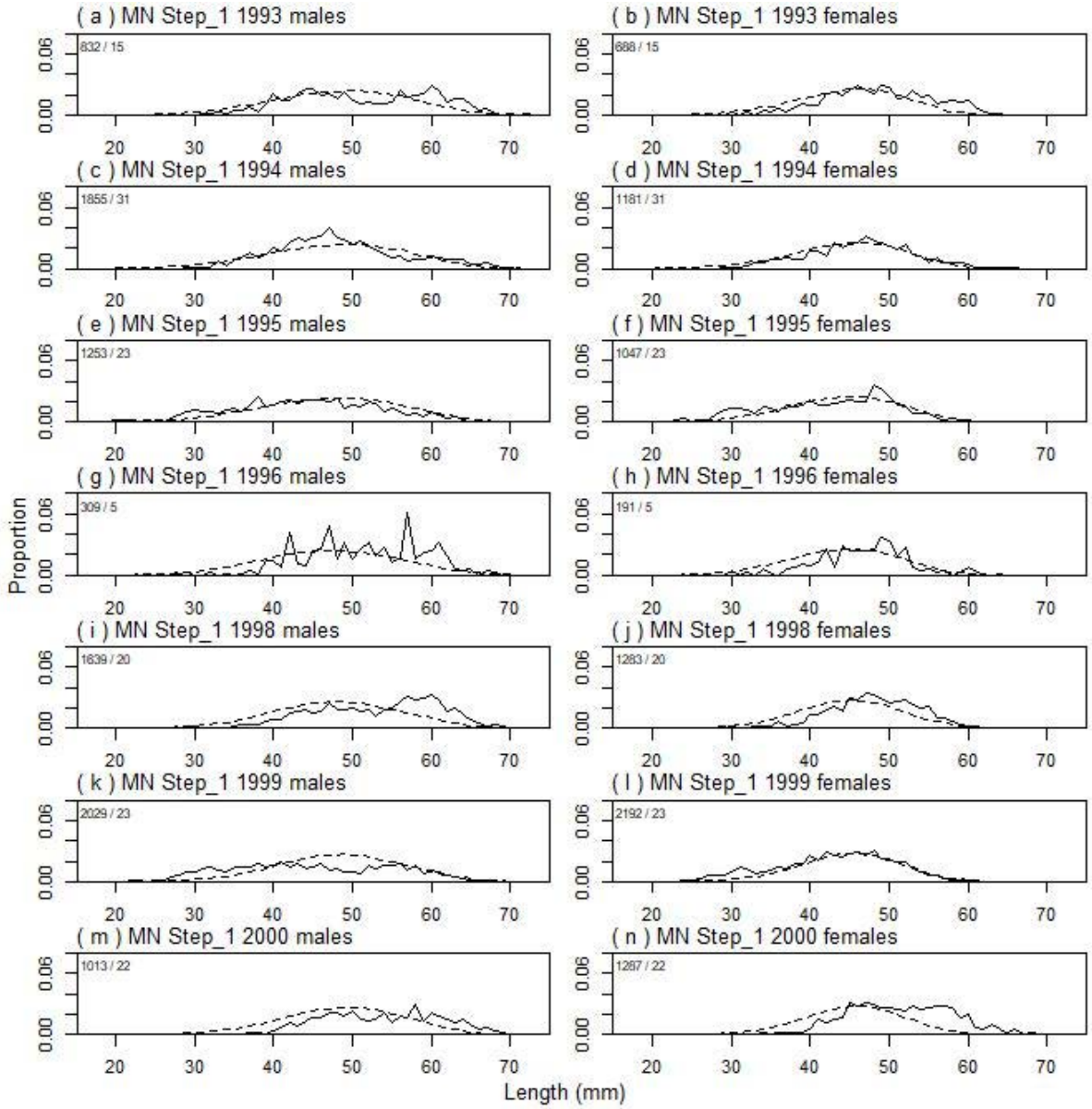

A3. 7: Observed (solid line) and fitted (dashed line) length frequency distributions for observer samples, MN time step 1. Numbers in top left corner of each plot represent number of scampi measured / number of events sampled.

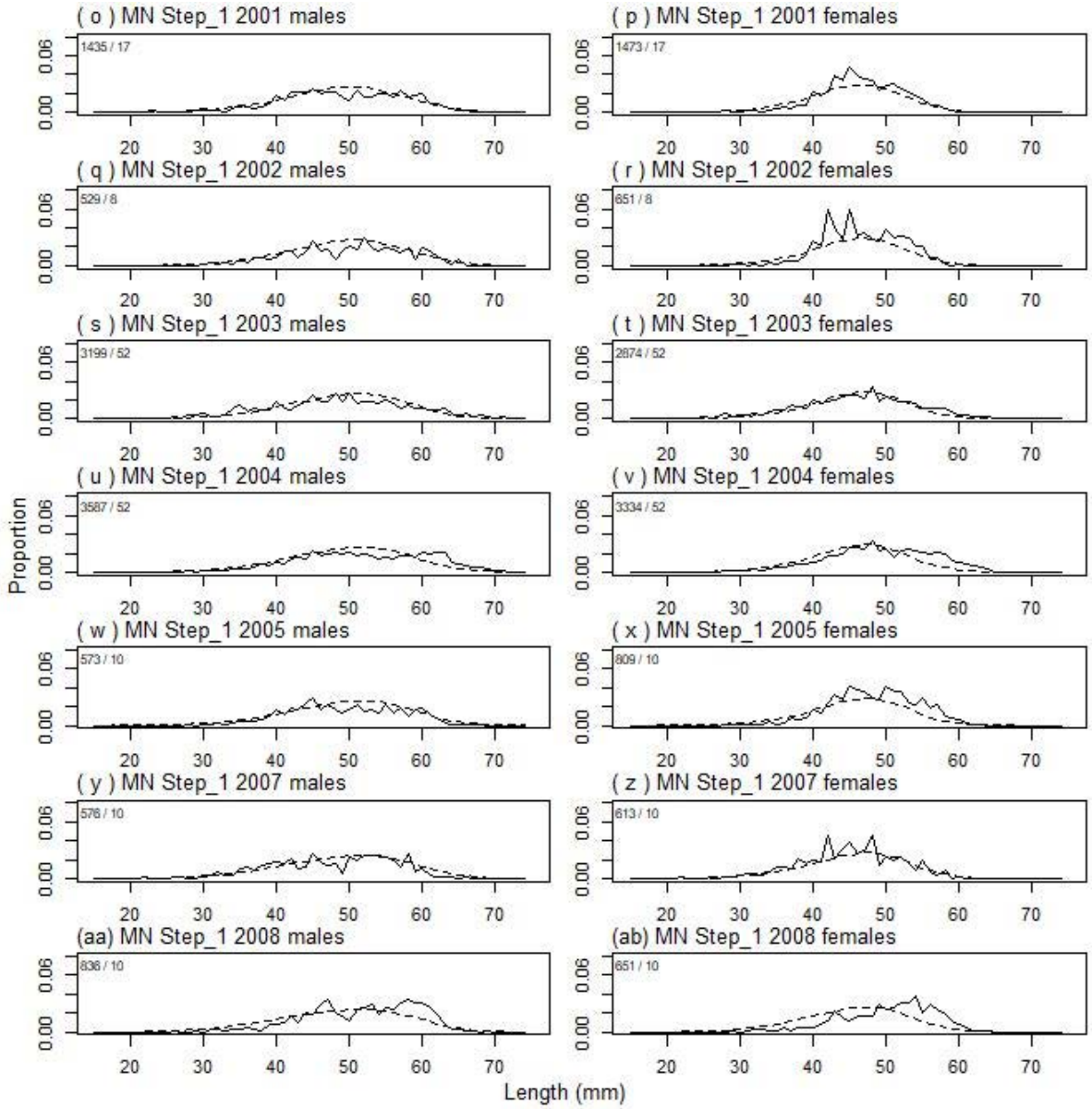

A3. 7 *continued*: Observed (solid line) and fitted (dashed line) length frequency distributions for observer samples, MN time step 1. Numbers in top left corner of each plot represent number of scampi measured / number of events sampled.

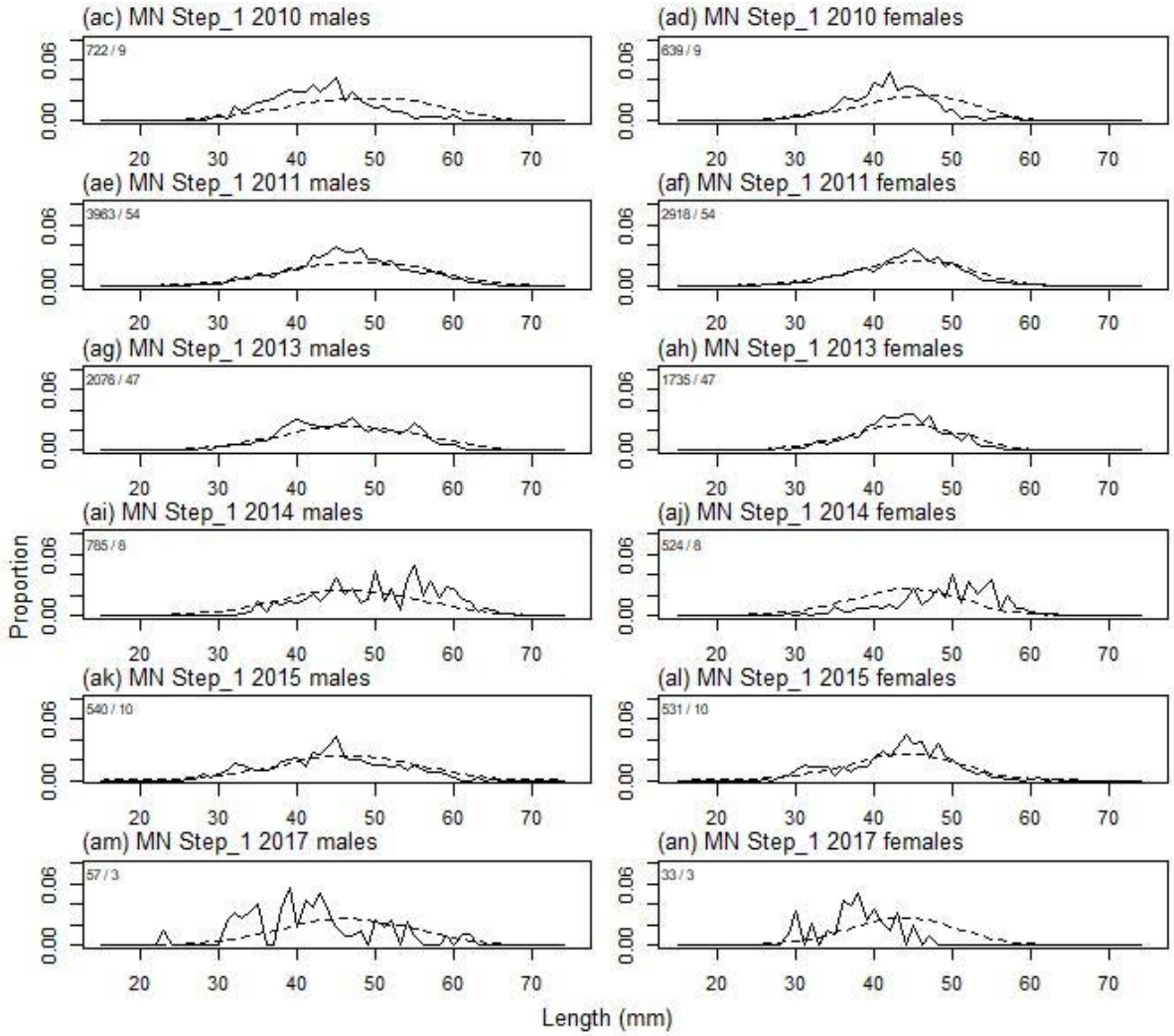

A3. 7 *continued*: Observed (solid line) and fitted (dashed line) length frequency distributions for observer samples, MN time step 1. Numbers in top left corner of each plot represent number of scampi measured / number of events sampled.

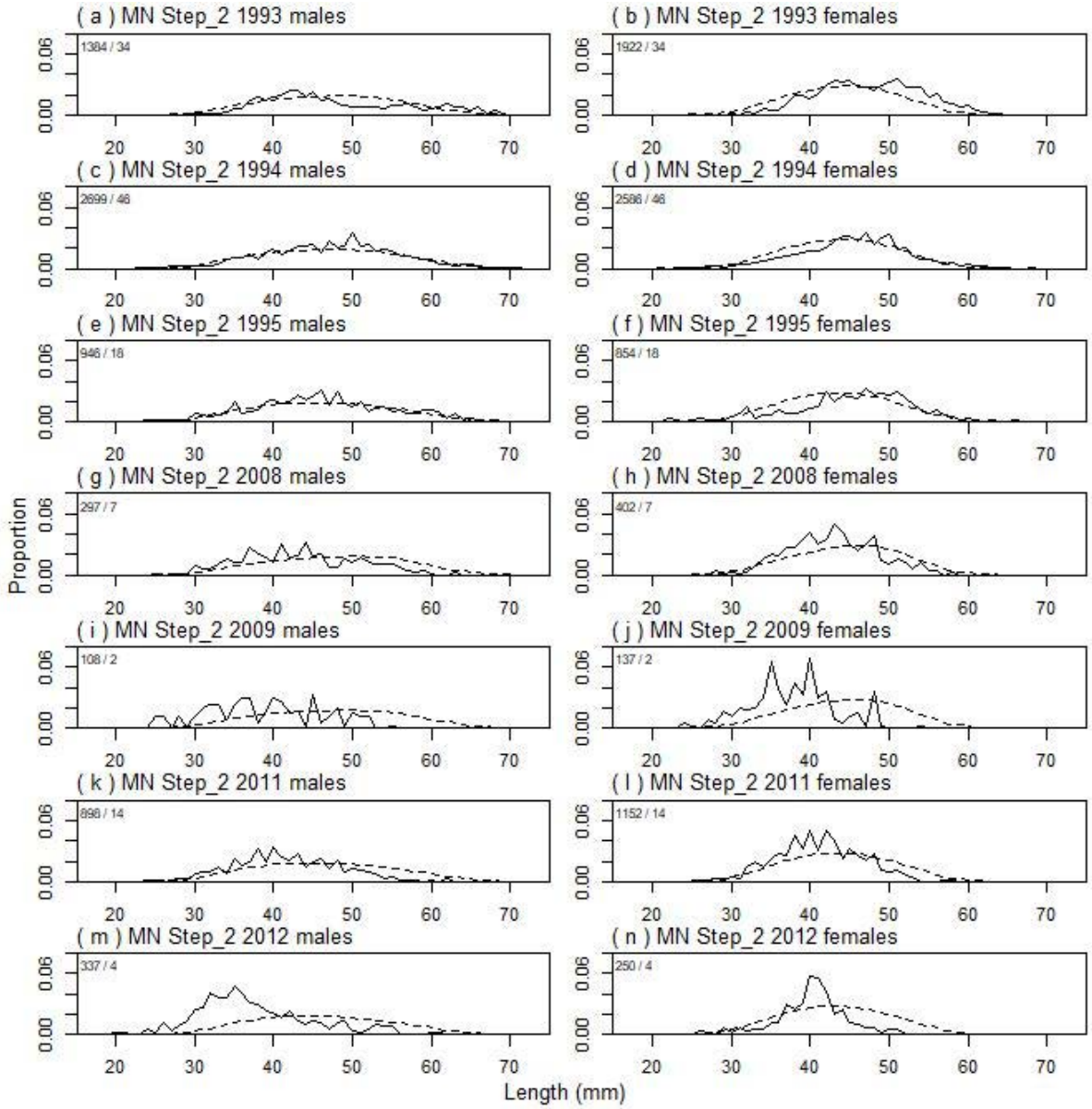

A3. 8: Observed (solid line) and fitted (dashed line) length frequency distributions for observer samples, MN time step 2. Numbers in top left corner of each plot represent number of scampi measured / number of events sampled.

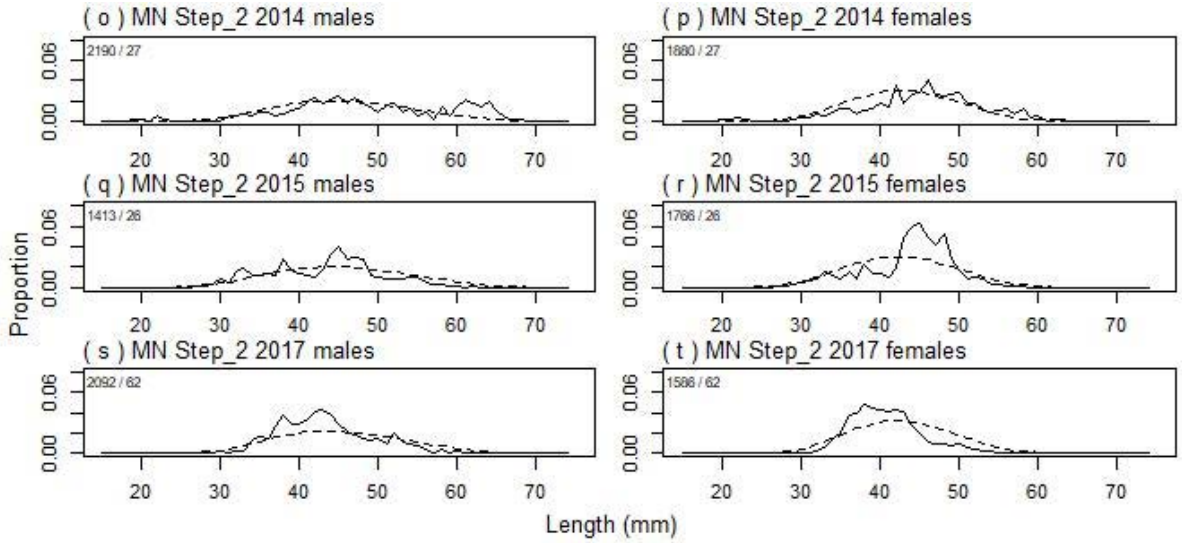

A3. 8 *continued*: Observed (solid line) and fitted (dashed line) length frequency distributions for observer samples, MN time step 2. Numbers in top left corner of each plot represent number of scampi measured / number of events sampled.

A3. 9: Numbers of scampi measured, estimated multinomial N sample size, and effective sample size used within the model for length frequency distributions for observer samples, MN time step 1.

	Measured	Multinomial N	Effective sample size
N_1993	1 520	1 345	5.96
N_1994	3 036	2 264	10.04
N_1995	2 300	1 824	8.09
N_1996	500	576	2.55
N_1998	2 922	2 599	11.53
N_1999	4 221	3 441	15.26
N_2000	2 300	1 928	8.55
N_2001	2 908	2 827	12.54
N_2002	1 180	988	4.38
N_2003	6 073	3 727	16.53
N_2004	6 921	5 077	22.51
N_2005	1 382	2 030	9.00
N_2007	1 189	2 414	10.70
N_2008	1 487	1 651	7.32
N_2010	1 361	1 544	6.85
N_2011	6 881	4 896	21.71
N_2013	3 811	2 929	12.99
N_2014	1 309	745	3.30
N_2015	1 071	2 071	9.18
N_2017	90	181	0.80

A3. 10: Numbers of scampi measured, estimated multinomial N sample size, and effective sample size used within the model for length frequency distributions for observer samples, MN time step 2.

	Measured	Multinomial N	Effective sample size
N_1993	3 306	2 571	15.01
N_1994	5 285	4 117	24.03
N_1995	1 800	1 501	8.76
N_2008	699	713	4.16
N_2009	245	340	1.98
N_2011	2 050	1 583	9.24
N_2012	587	691	4.03
N_2014	4 071	1 270	7.41
N_2015	3 179	5 855	34.18
N_2017	3 678	1 906	11.13

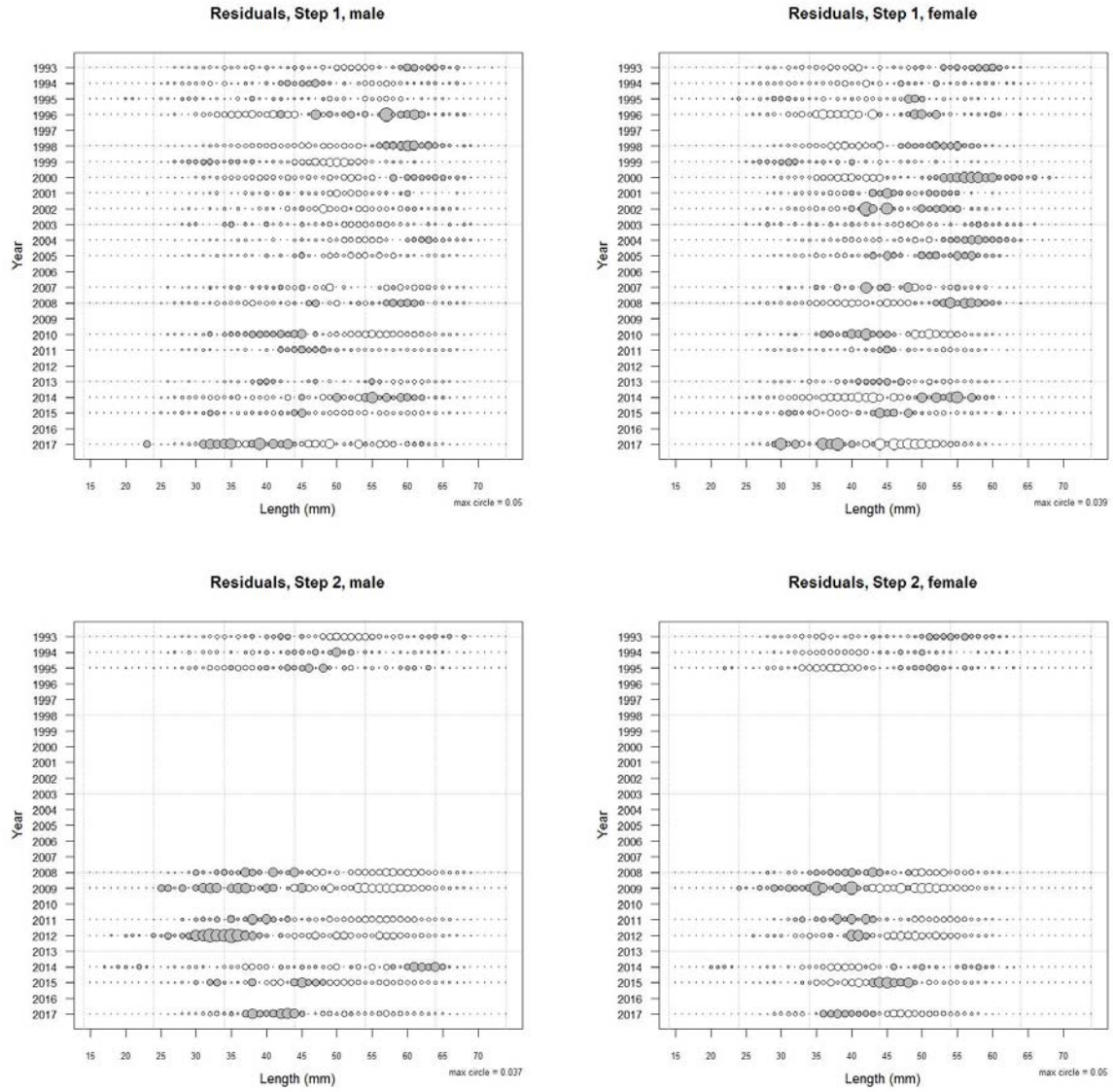

A3. 11: Bubble plots of residuals for fits to length frequency distributions for MN observer sampling.

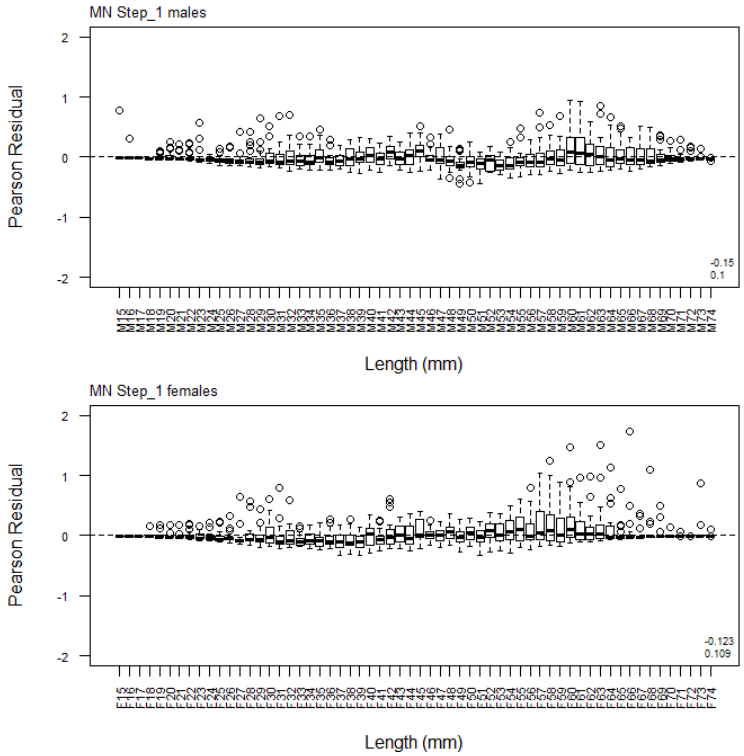

A3. 12: Box plots of Pearson residuals from the fit to length frequency distributions by length from observer sampling by sex for MN time step 1.

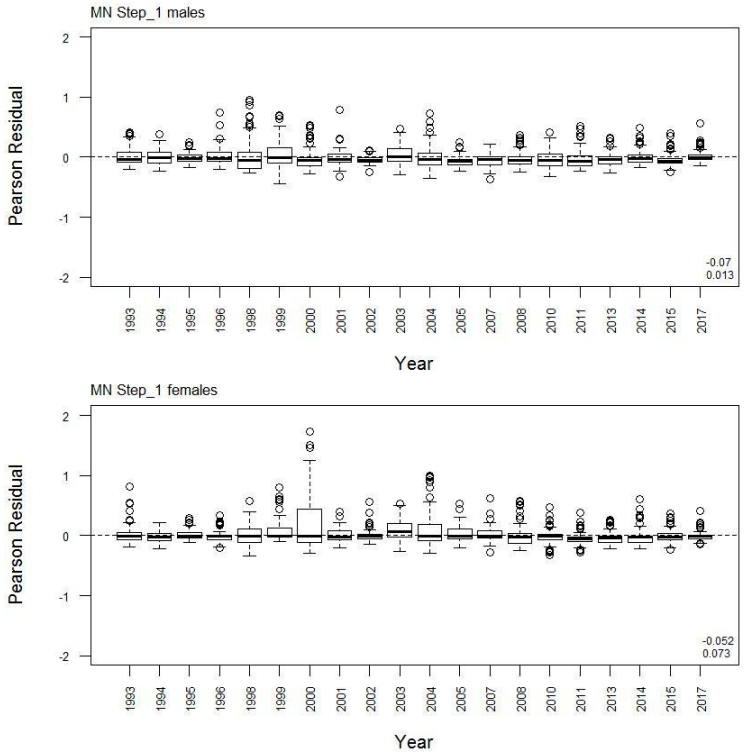

A3. 13: Box plots of Pearson residuals from the fit to length frequency distributions by year from observer sampling by sex for MN time step 1.

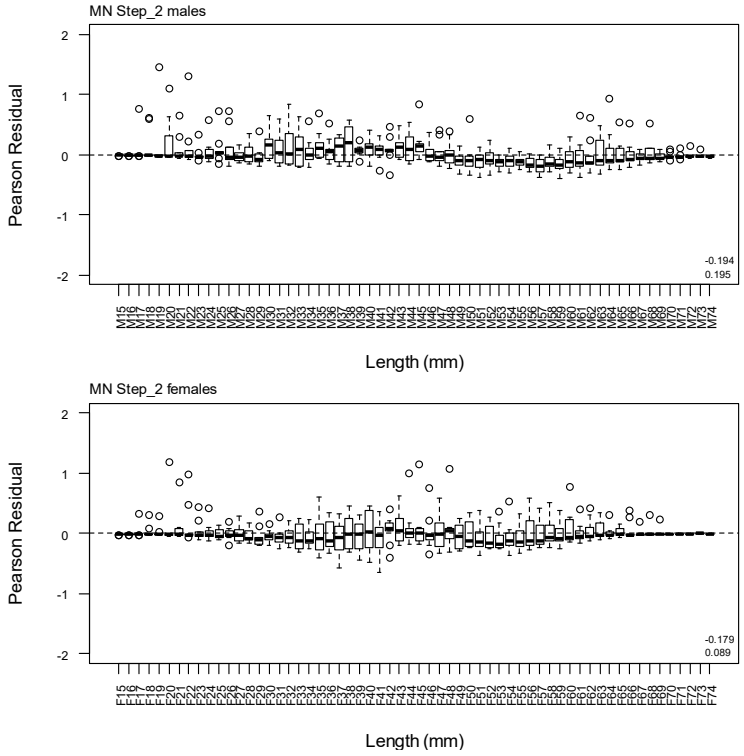

A3. 14: Box plots of Pearson residuals from the fit to length frequency distributions by length from observer sampling by sex for MN time step 2.

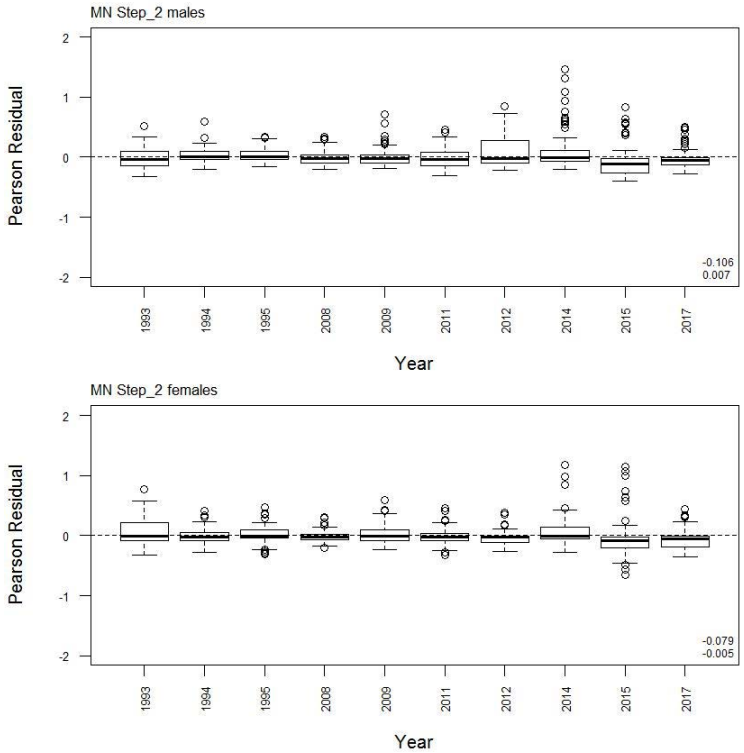

A3. 15: Box plots of Pearson residuals from the fit to length frequency distributions by year from observer sampling by sex for MN time step 2.

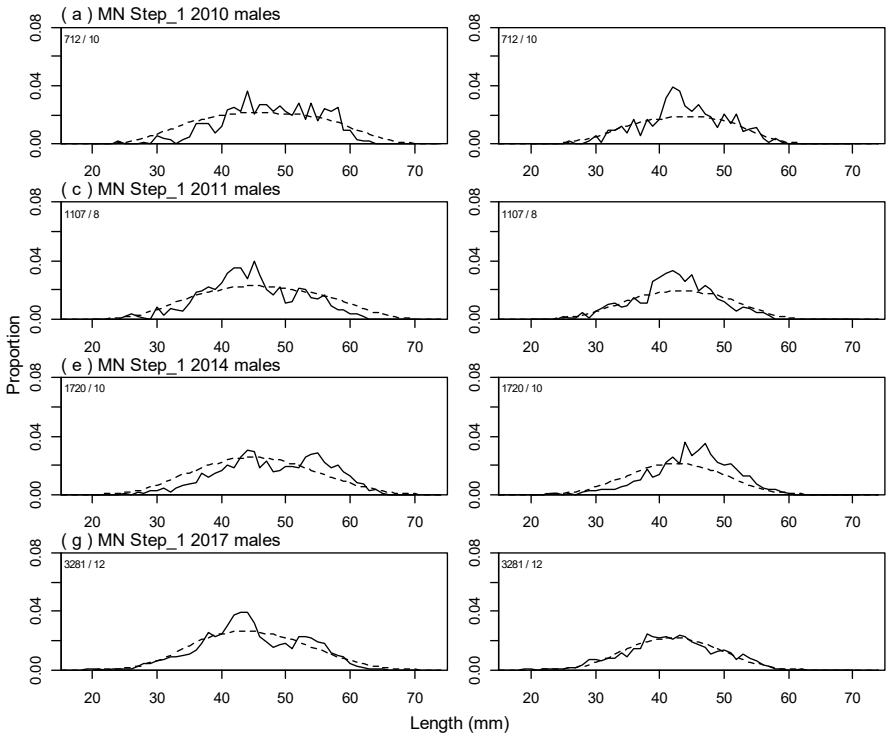

A3. 16: Observed (solid line) and fitted (dashed line) length frequency distributions for MN research survey samples.

A3. 17: Numbers of scampi measured, estimated multinomial N sample size, and effective sample size used within the model for length frequency distributions for MN research survey samples.

	Measured	Multinomial N	Effective sample size
N_2010	1 276	941	13.73
N_2011	2 027	1 610	23.49
N_2014	3 156	2 381	34.75
N_2017	5 299	4 895	71.43

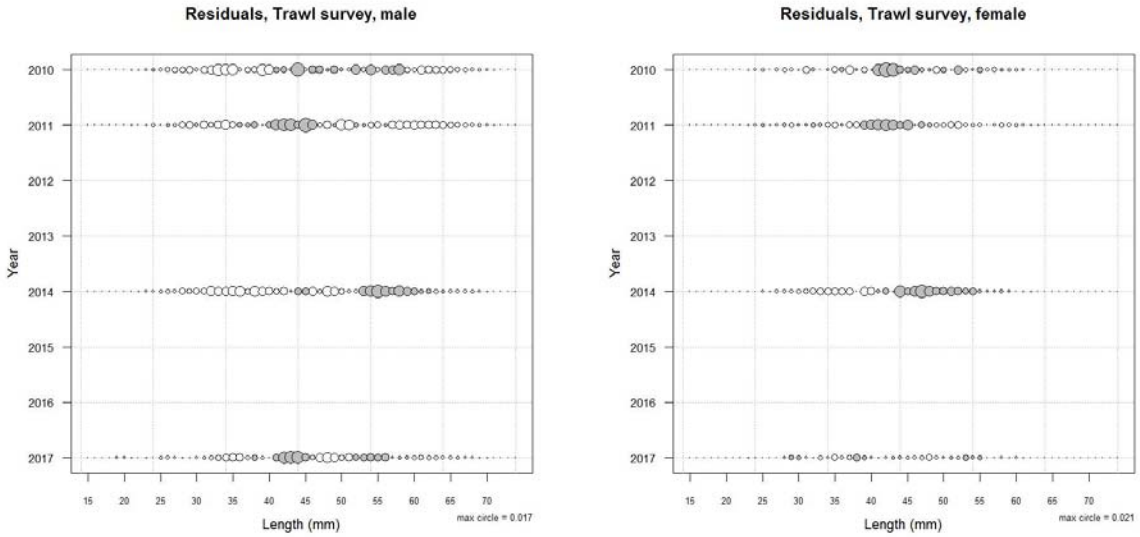

A3. 18: Bubble plots of residuals for fits to length frequency distributions for MN trawl sampling.

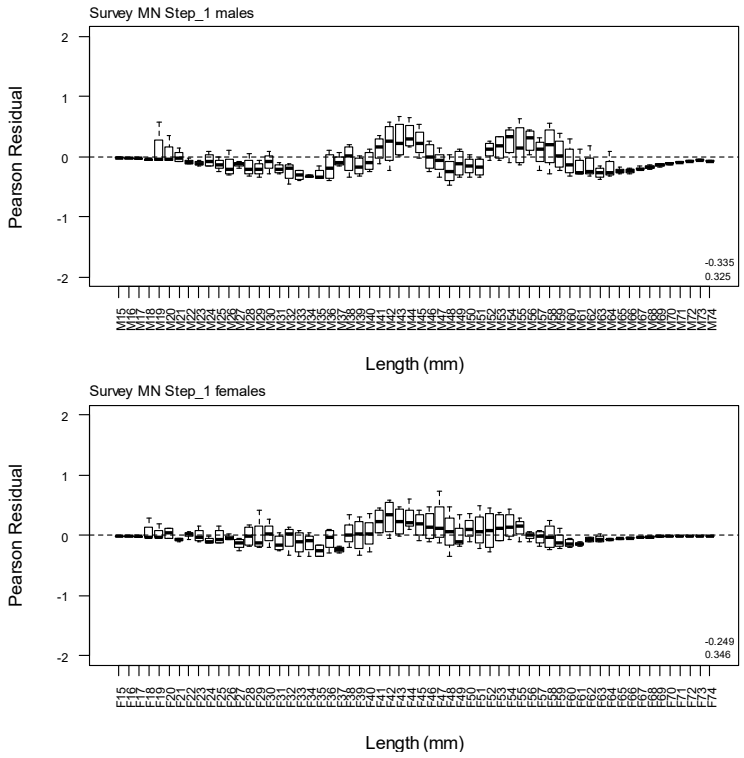

A3. 19: Box plots of Pearson residuals from the fit to length frequency distributions by length from MN trawl sampling.

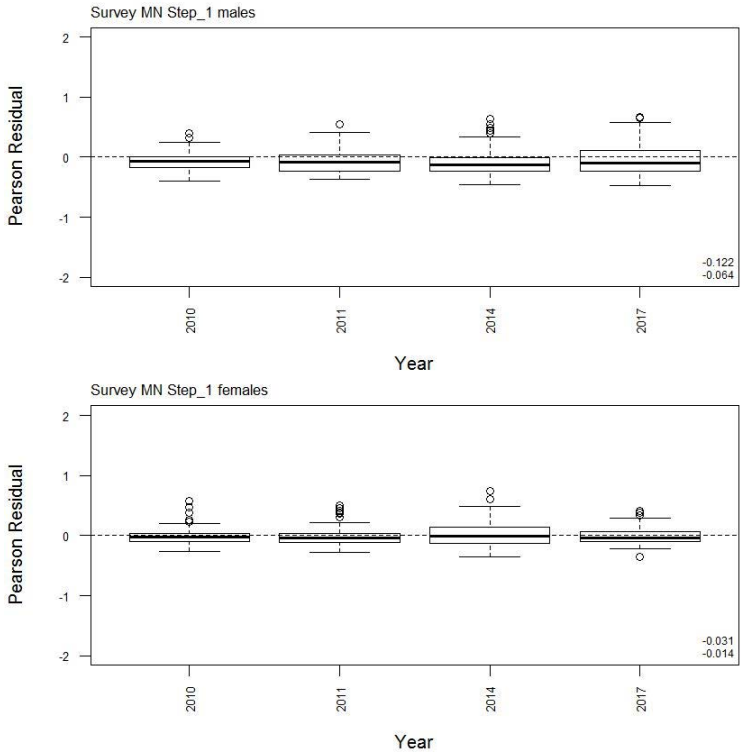

A3. 20: Box plots of Pearson residuals from the fit to length frequency distributions by year from MN trawl sampling.

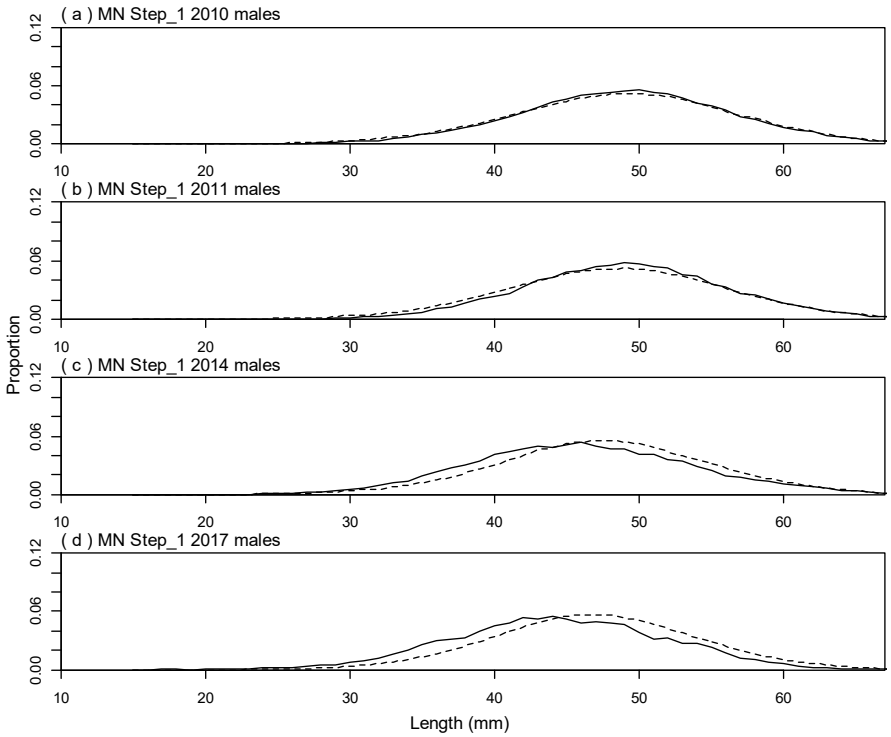

A3. 21: Observed (solid line) and fitted (dashed line) length frequency distributions for MN photographic survey scampi size estimation.

A3. 22: Numbers of scampi measured, estimated multinomial N sample size, and effective sample size used within the model for length frequency distributions for MN photographic survey samples.

	Measured	Multinomial N	Effective sample size
N_2010	113	211	56.48
N_2011	120	225	60.23
N_2014	62	120	32.12
N_2017	25	50	13.38

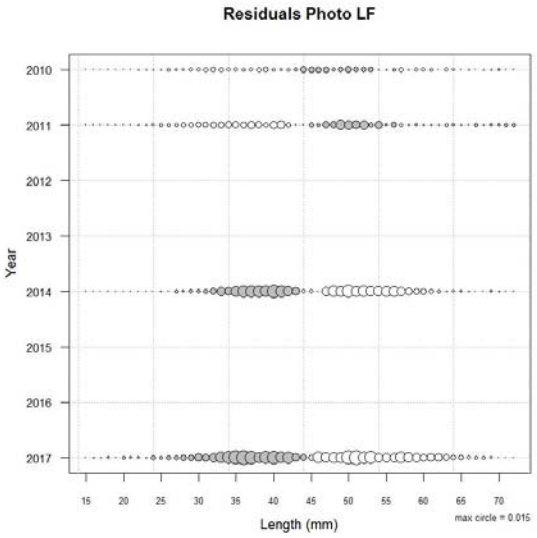

A3. 23: Bubble plots of residuals for fits to length frequency distributions for MN photographic sampling.

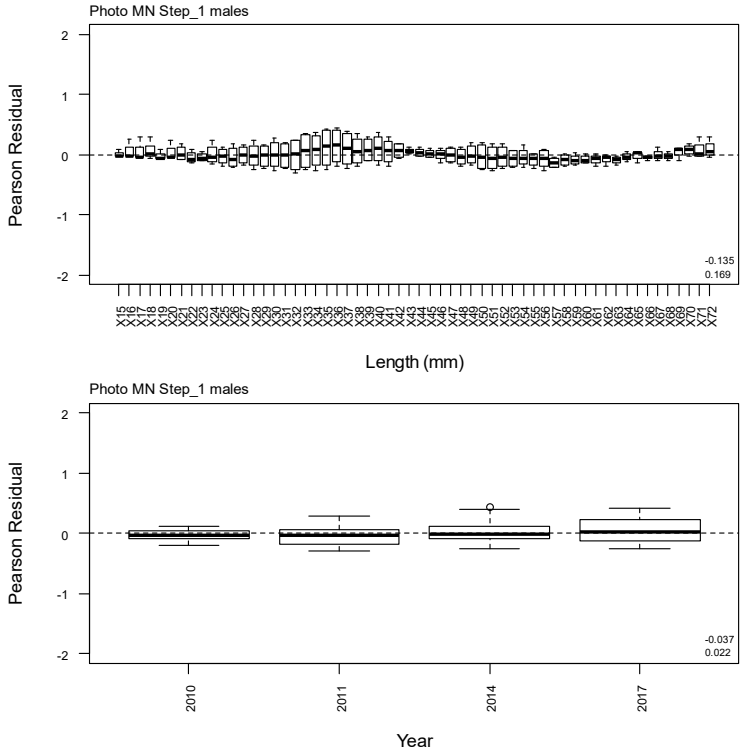

A3. 24: Box plots of Pearson residuals from the fit to length frequency distributions by length and year for MN photographic sampling.

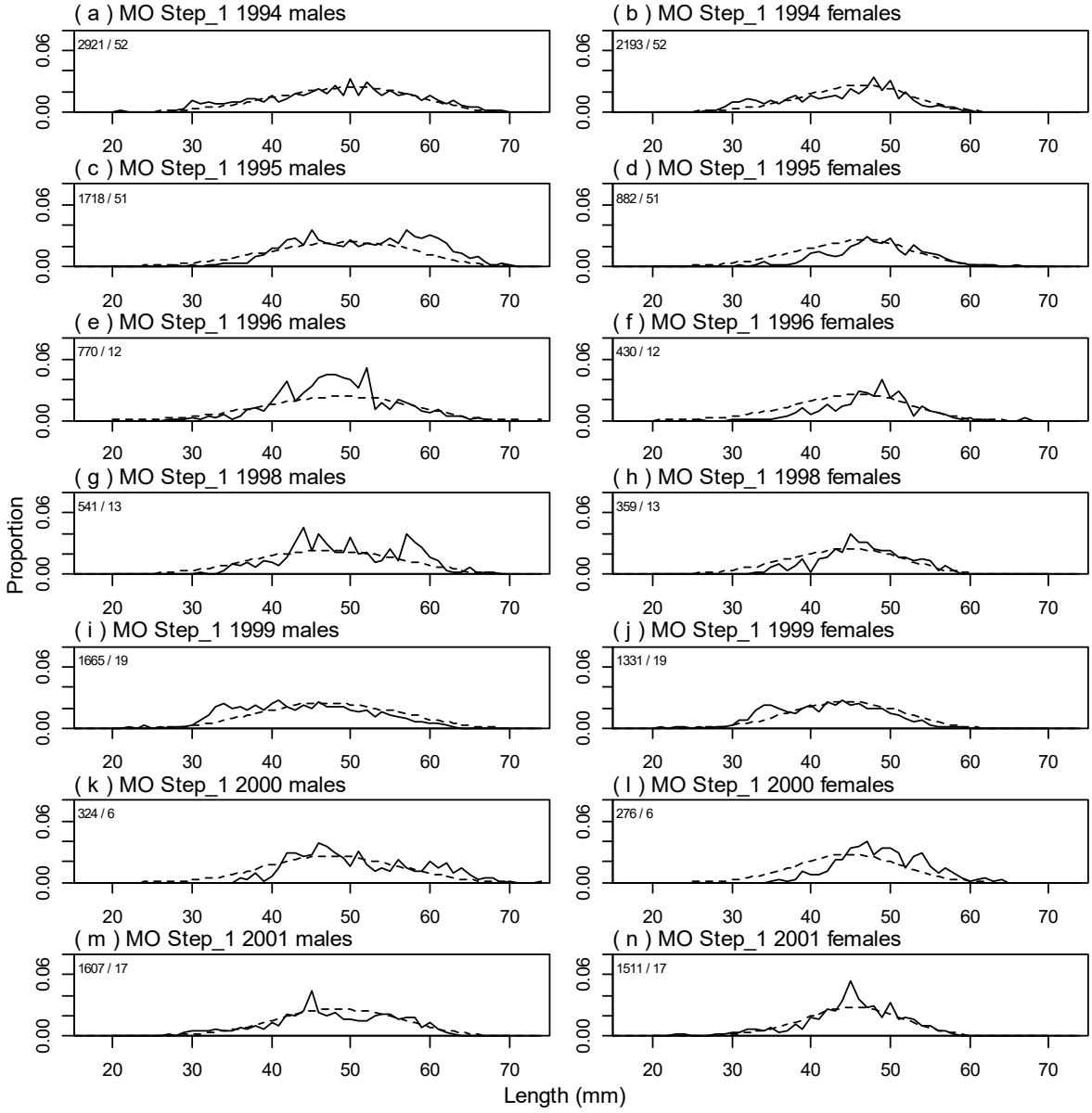

A3. 25: Observed (solid line) and fitted (dashed line) length frequency distributions for observer samples, MO time step 1. Numbers in top left corner of each plot represent number of scampi measured / number of events sampled.

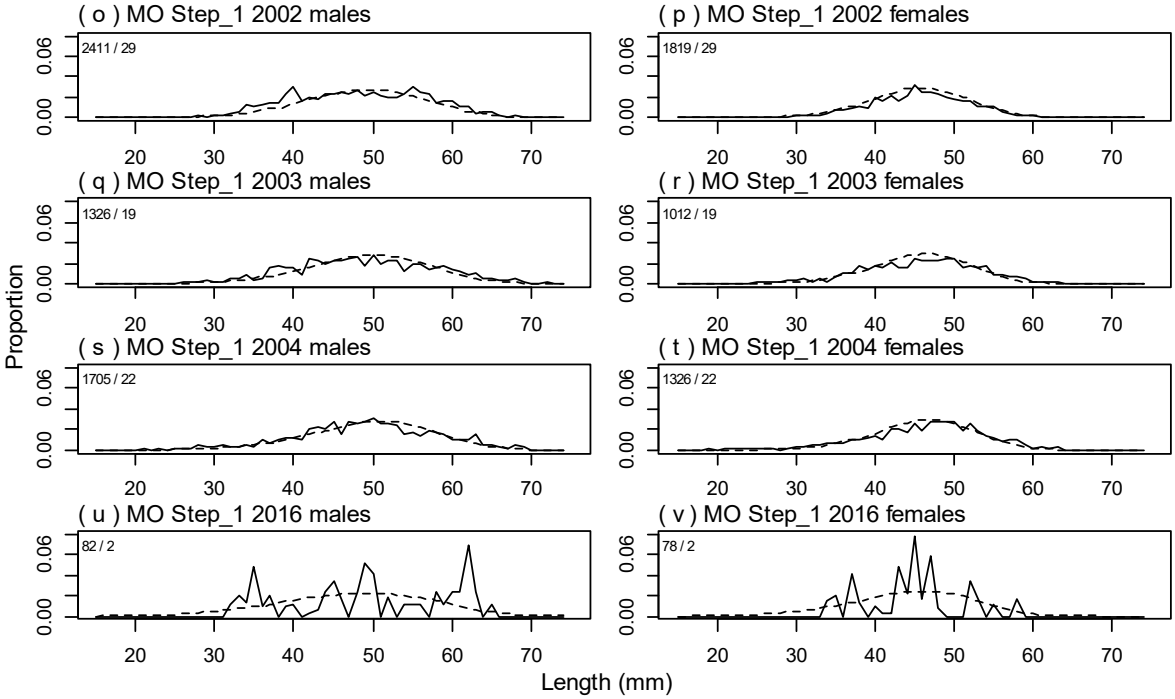

A3. 25 *continued*: Observed (solid line) and fitted (dashed line) length frequency distributions for observer samples, MO time step 1. Numbers in top left corner of each plot represent number of scampi measured / number of events sampled.

A3. 26: Numbers of scampi measured, estimated multinomial N sample size, and effective sample size used within the model for length frequency distributions for observer samples, MO time step 1.

	Measured	Multinomial N	Effective sample size
N_1994	5 114	3 277	29.51
N_1995	2 600	2 182	19.65
N_1996	1 200	1 071	9.64
N_1998	900	940	8.46
N_1999	2 996	2 504	22.55
N_2000	600	733	6.60
N_2001	3 118	2 900	26.12
N_2002	4 230	2 662	23.17
N_2003	2 338	1 553	13.99
N_2004	3 031	2084	18.77
N_2016	160	88	0.79

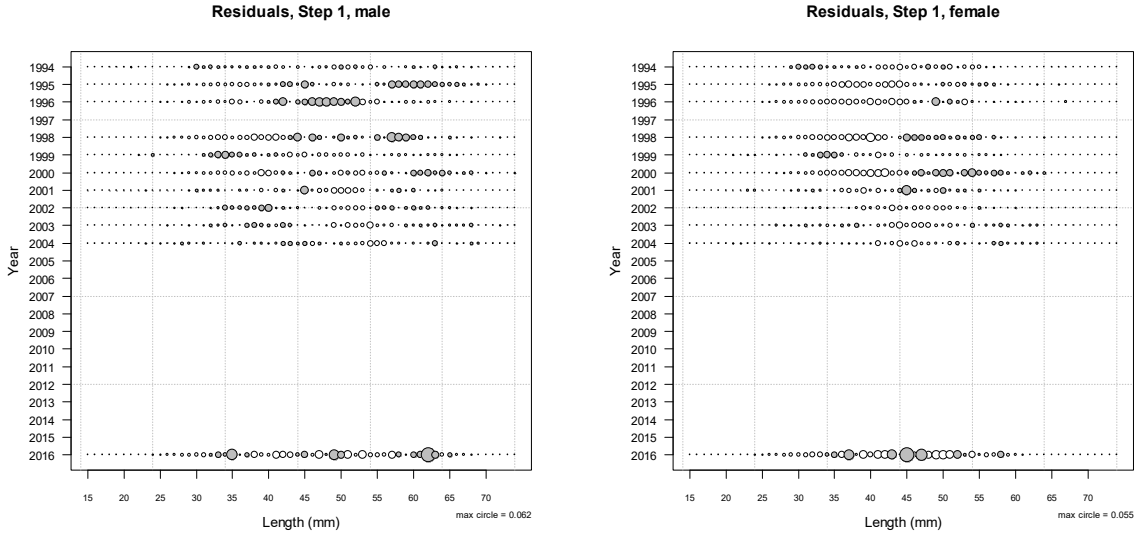

A3. 27: Bubble plots of residuals for fits to length frequency distributions for MO observer sampling.

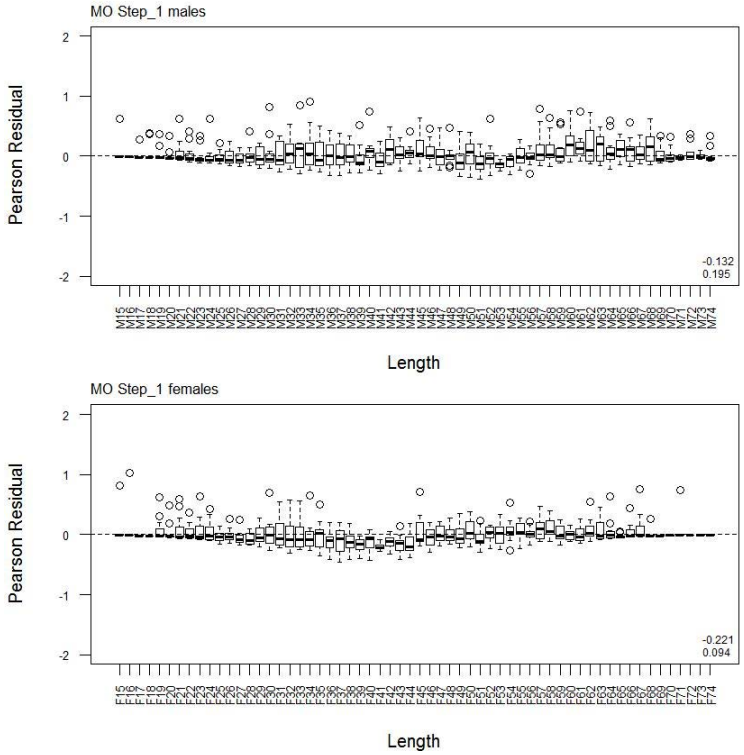

A3. 28: Box plots of Pearson residuals from the fit to length frequency distributions by length from observer sampling by sex for MO time step 1.

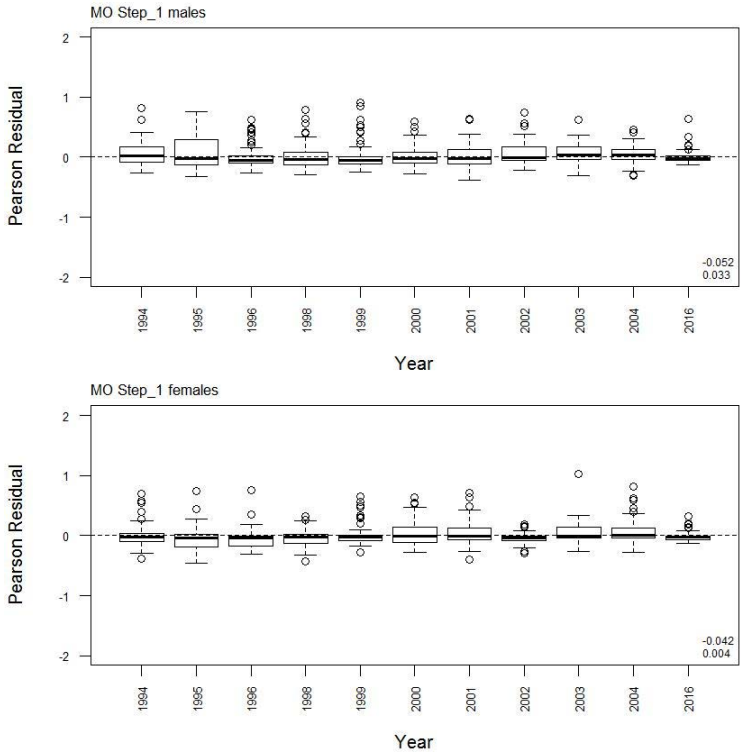

A3. 29: Box plots of Pearson residuals from the fit to length frequency distributions by year from observer sampling by sex for MO time step 1.

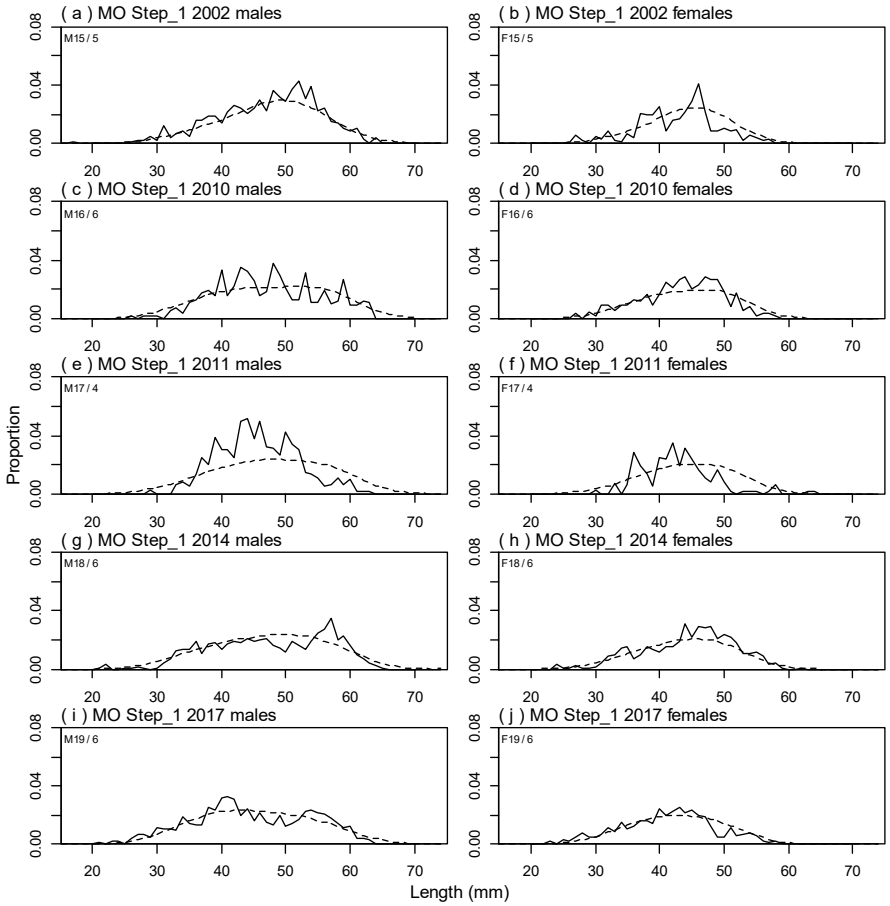

A3. 30: Observed (solid line) and fitted (dashed line) length frequency distributions for MO research survey samples.

A3. 31: Numbers of scampi measured, estimated multinomial N sample size, and effective sample size used within the model for length frequency distributions for MO research survey samples.

	Measured	Multinomial N	Effective sample size
N_2002	764	725	117.30
N_2010	551	627	101.45
N_2011	396	483	78.15
N_2014	1 465	1 363	220.53
N_2017	1 807	1 669	270.04

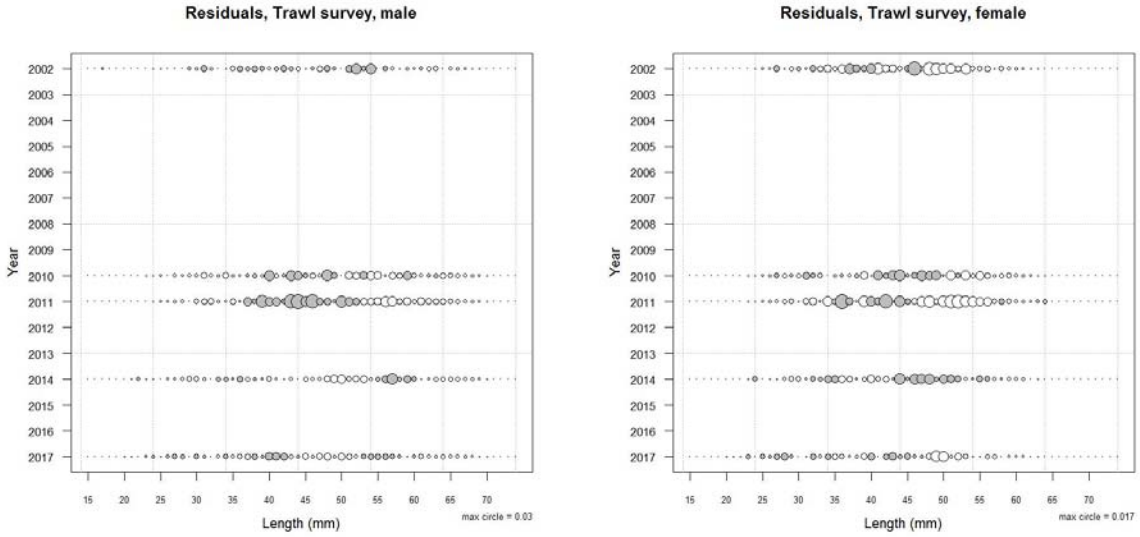

A3. 32: Bubble plots of residuals for fits to length frequency distributions for MO trawl sampling.

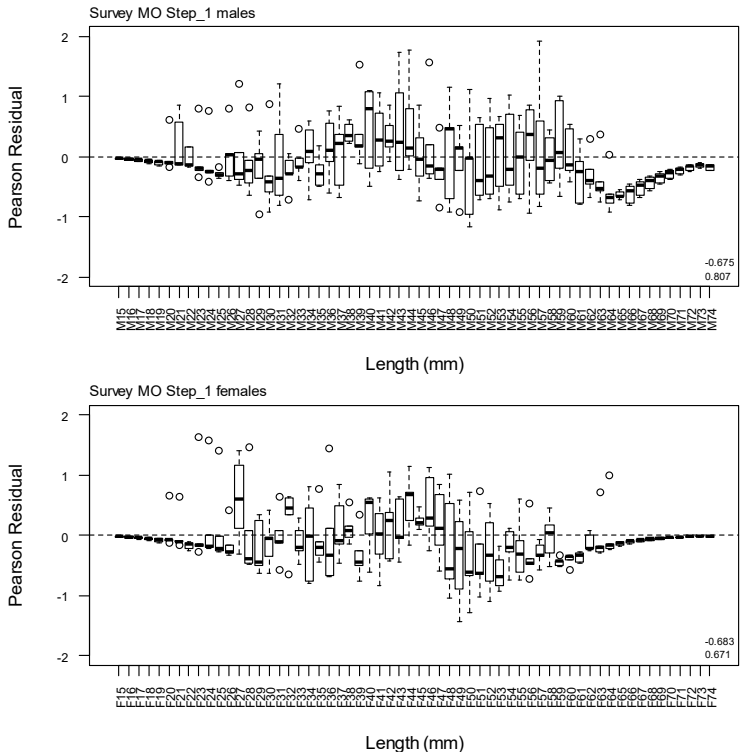

A3. 33: Box plots of Pearson residuals from the fit to length frequency distributions by length from MO trawl sampling.

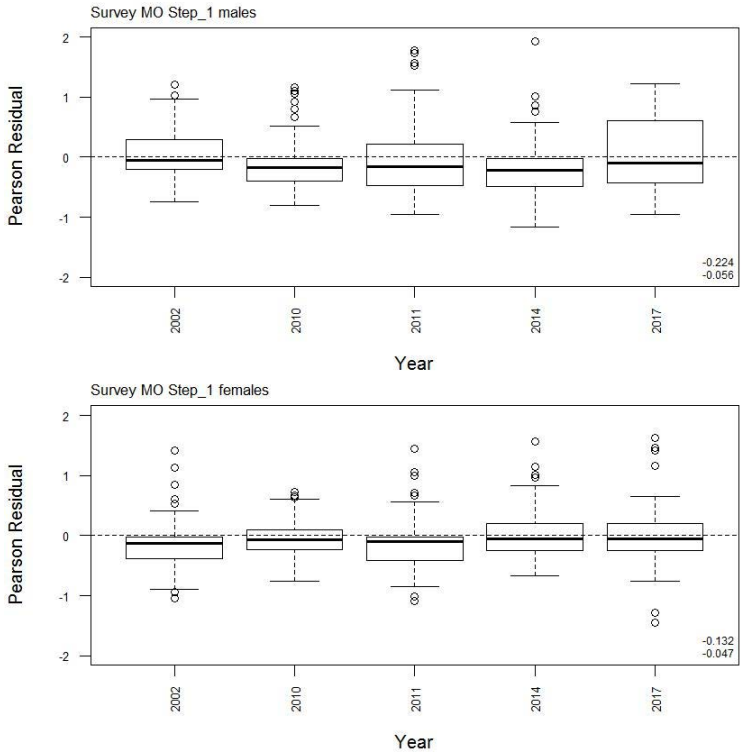

A3. 34: Box plots of Pearson residuals from the fit to length frequency distributions by year from MO trawl sampling.

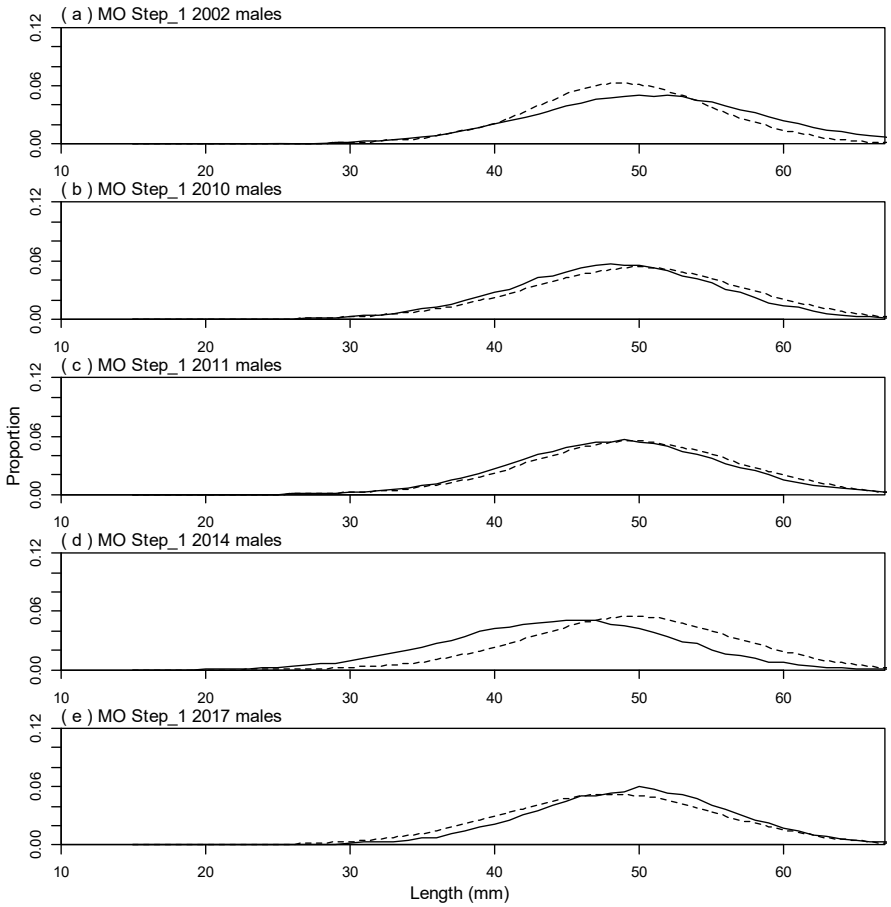

A3. 35: Observed (solid line) and fitted (dashed line) length frequency distributions for MO photographic survey scampi size estimation.

A3. 36: Numbers of scampi measured, estimated multinomial N sample size, and effective sample size used within the model for length frequency distributions for MO photographic survey samples.

	Measured	Multinomial N	Effective sample size
N_2002	224	384	12.59
N_2010	214	365	11.97
N_2011	426	536	17.57
N_2014	125	224	7.34
N_2017	76	145	4.75

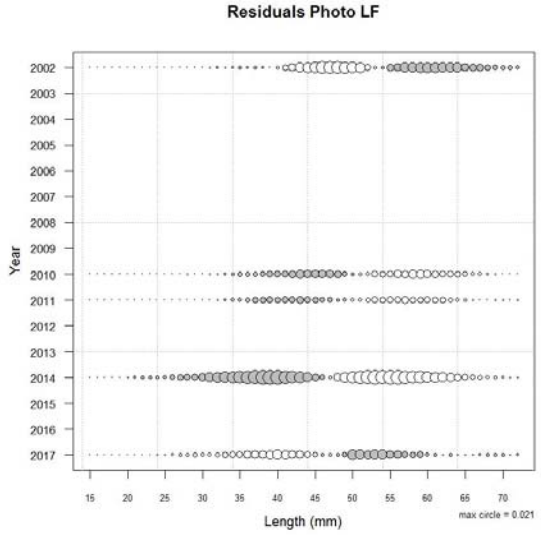

A3. 37: Bubble plots of residuals for fits to length frequency distributions for MO photographic sampling.

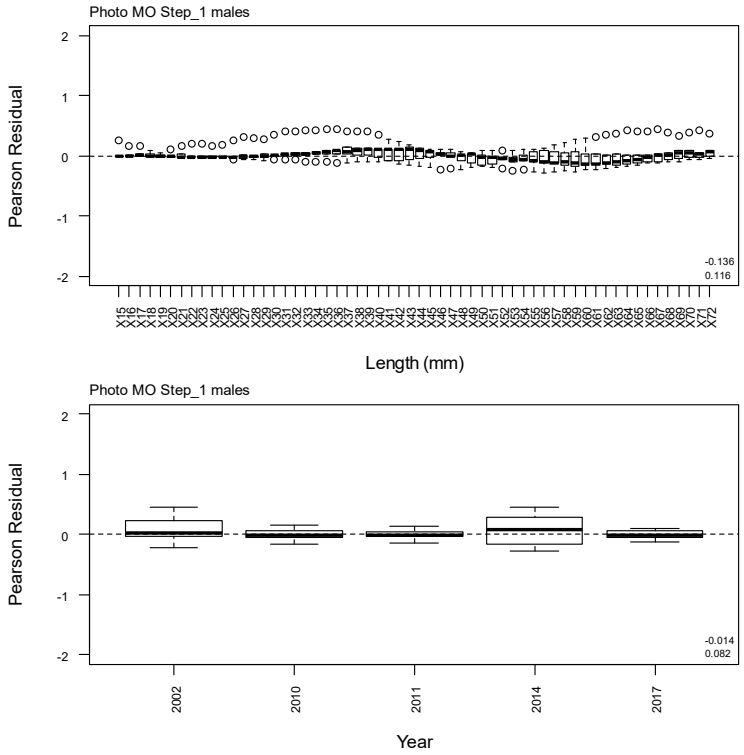

A3. 38: Box plots of Pearson residuals from the fit to length frequency distributions by length and year for MO photographic sampling.

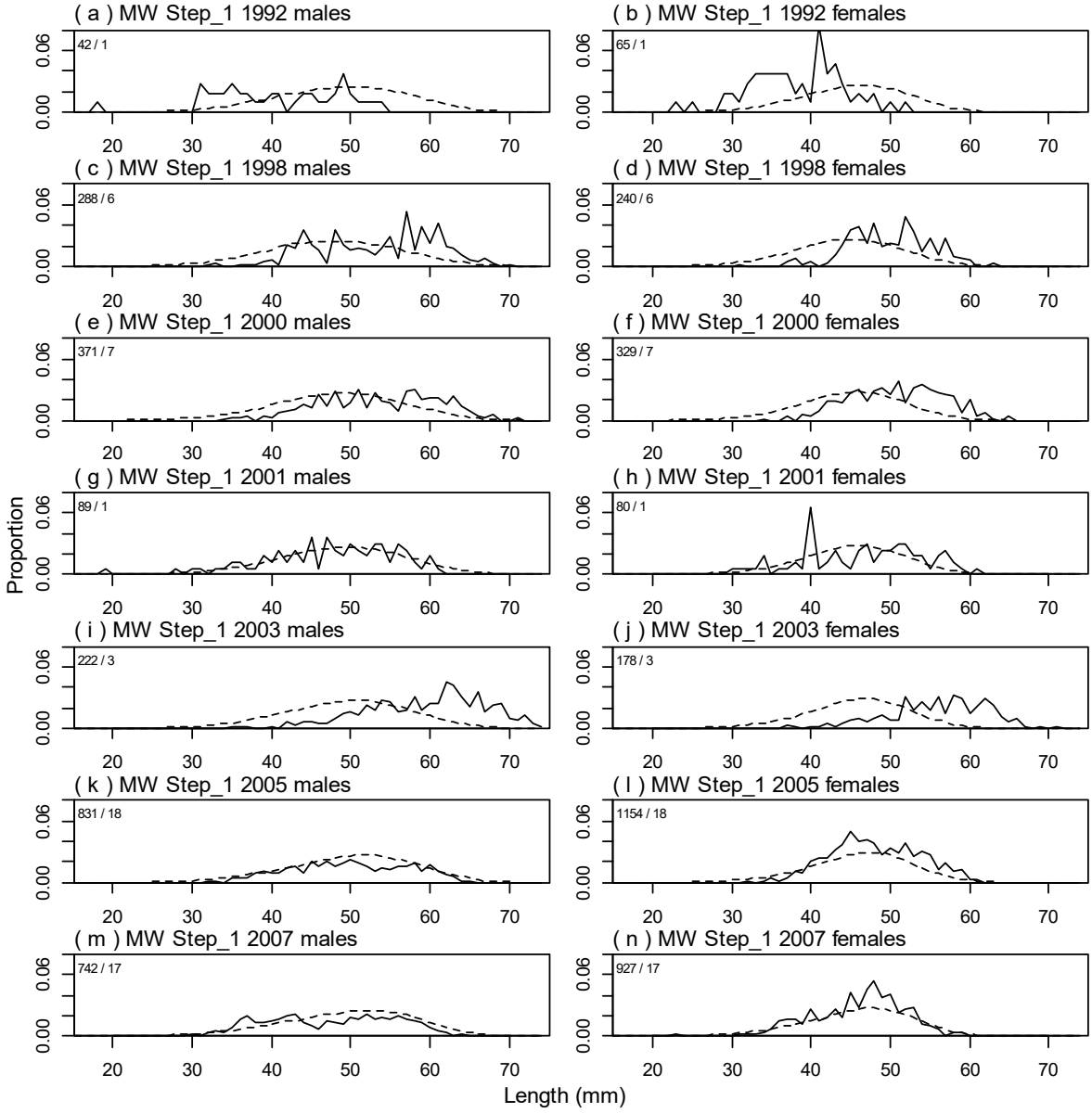

A3. 39: Observed (solid line) and fitted (dashed line) length frequency distributions for observer samples, MW time step 1. Numbers in top left corner of each plot represent number of scampi measured / number of events sampled.

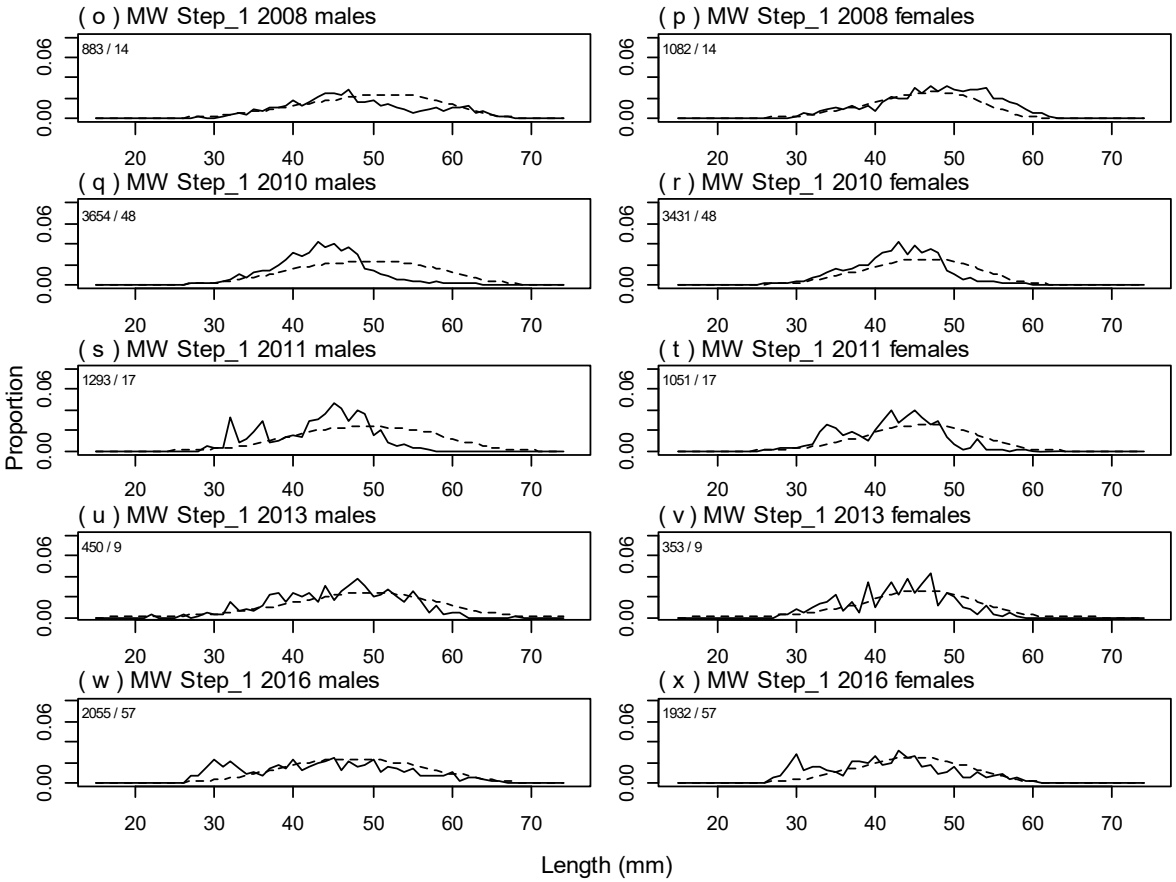

A3. 39 *continued*: Observed (solid line) and fitted (dashed line) length frequency distributions for observer samples, MW time step 1. Numbers in top left corner of each plot represent number of scampi measured / number of events sampled.

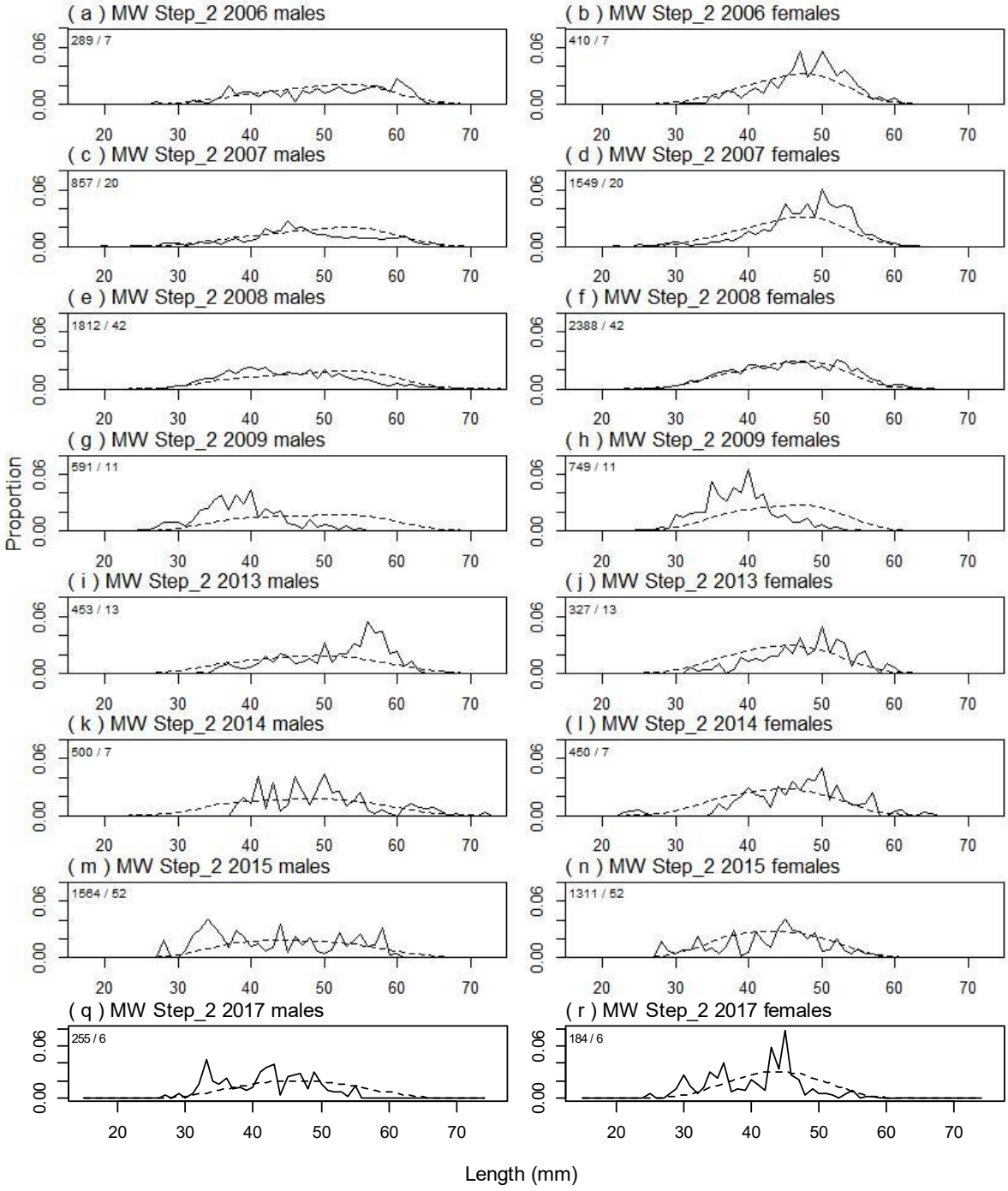

A3. 40: Observed (solid line) and fitted (dashed line) length frequency distributions for observer samples, MW time step 2. Numbers in top left corner of each plot represent number of scampi measured / number of events sampled.

A3. 41: Numbers of scampi measured, estimated multinomial N sample size, and effective sample size used within the model for length frequency distributions for observer samples, MW time step 1.

	Measured	Multinomial N	Effective sample size
N_1992	107	216	0.50
N_1998	528	394	0.91
N_2000	700	631	1.45
N_2001	169	341	0.78
N_2003	400	796	1.83
N_2005	1 985	908	2.09
N_2007	1 669	1 418	3.26
N_2008	1 965	1 743	4.01
N_2010	7 085	6 257	14.38
N_2011	2 344	1 739	4.00
N_2013	803	583	1.34
N_2016	3 987	3 475	7.99

A3. 42: Numbers of scampi measured, estimated multinomial N sample size, and effective sample size used within the model for length frequency distributions for observer samples, MW time step 2.

	Measured	Multinomial N	Effective sample size
N_2006	699	790	3.59
N_2007	2 406	2 144	9.74
N_2008	4 200	3 081	14.00
N_2009	1 340	1 366	6.21
N_2013	780	483	2.19
N_2014	950	1 710	7.77
N_2015	2 875	638	2.90
N_2017	439	232	1.05

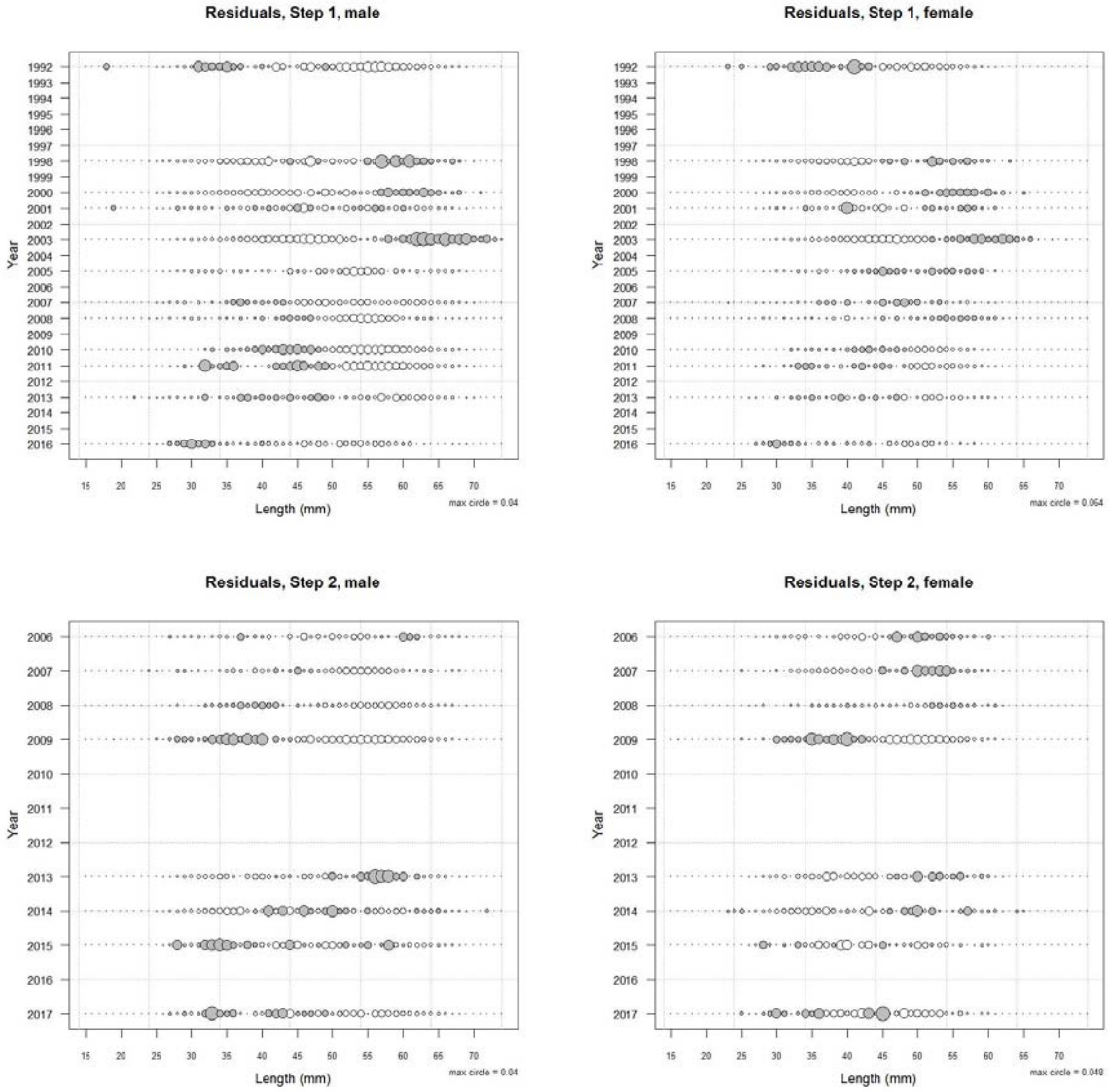

A3. 43: Bubble plots of residuals for fits to length frequency distributions for MW observer sampling.

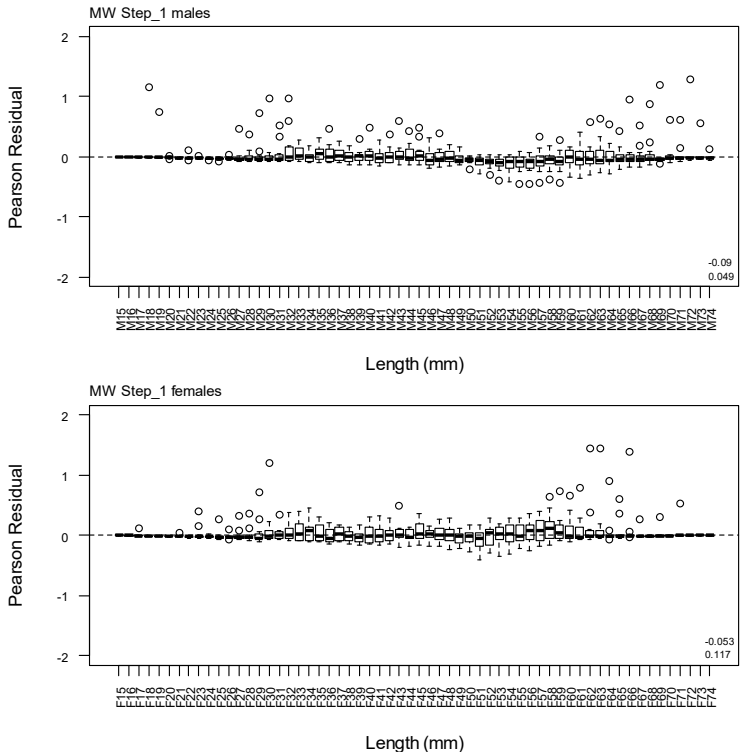

A3. 44: Box plots of Pearson residuals from the fit to length frequency distributions by length from observer sampling by sex for MW time step 1.

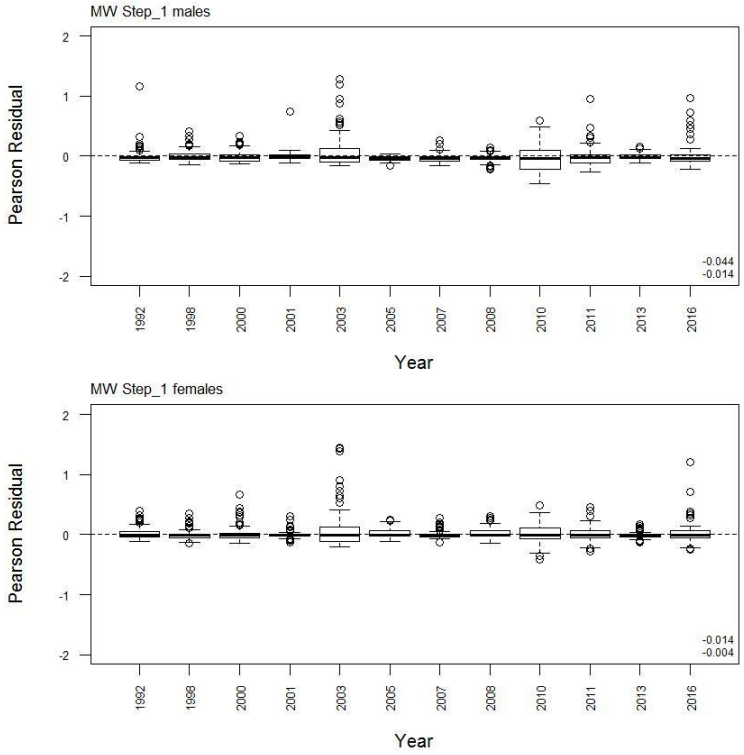

A3. 45: Box plots of Pearson residuals from the fit to length frequency distributions by year from observer sampling by sex for MW time step 1.

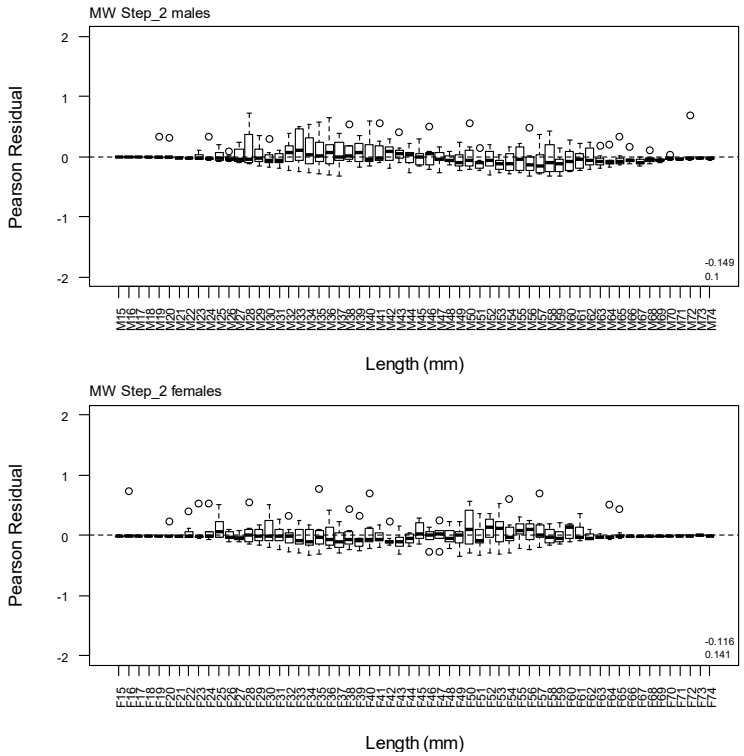

A3. 46: Box plots of Pearson residuals from the fit to length frequency distributions by length from observer sampling by sex for MW time step 2.

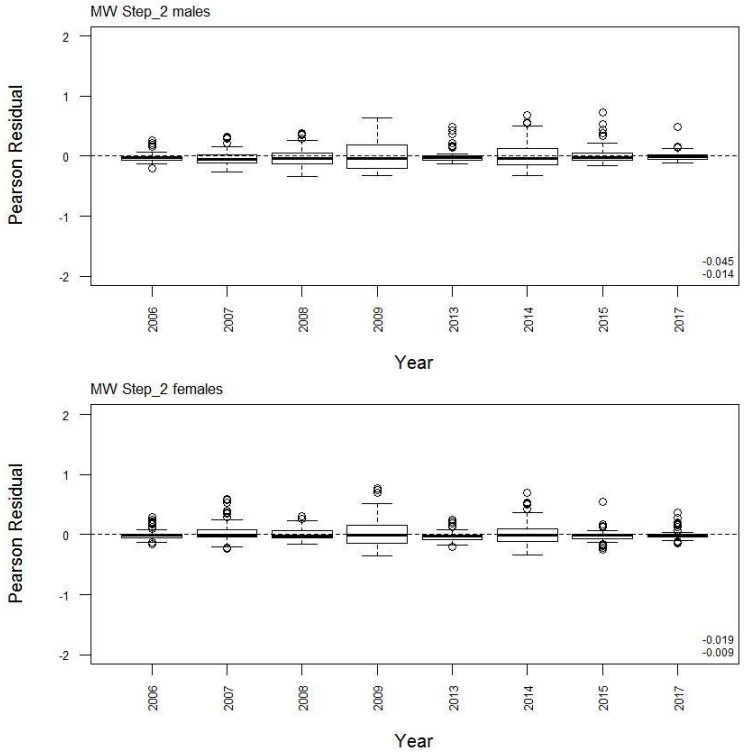

A3. 47: Box plots of Pearson residuals from the fit to length frequency distributions by year from observer sampling by sex for MW time step 2.

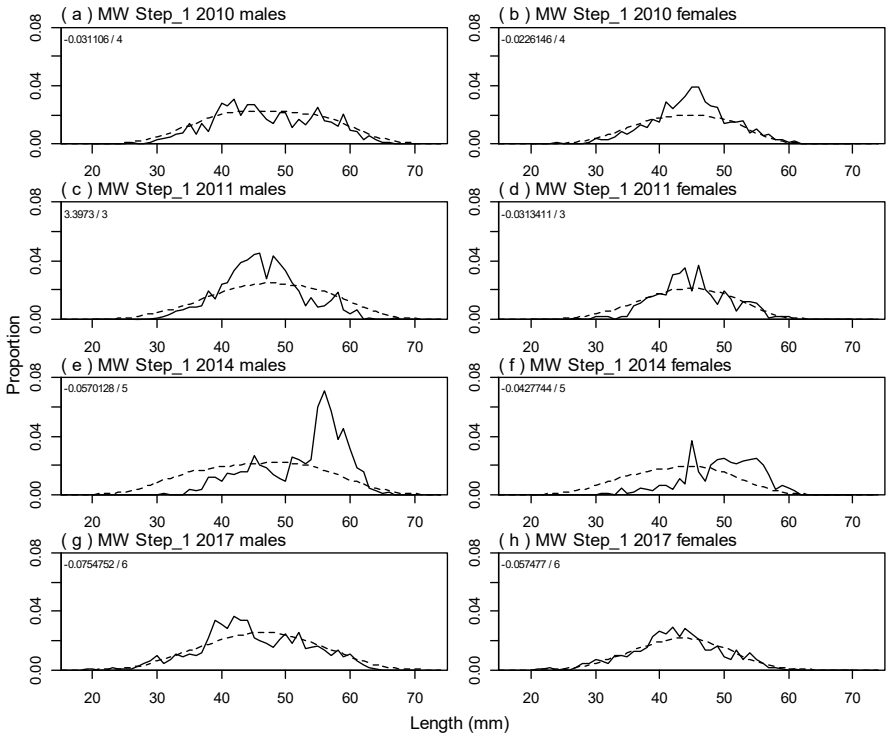

A3. 48: Observed (solid line) and fitted (dashed line) length frequency distributions for MW research survey samples.

A3. 49: Numbers of scampi measured, estimated multinomial N sample size, and effective sample size used within the model for length frequency distributions for MW research survey samples.

	Measured	Multinomial N	Effective sample size
N_2010	1 110	1 140	9.51
N_2011	876	1 011	8.44
N_2014	710	681	5.68
N_2017	1 734	1 776	14.82

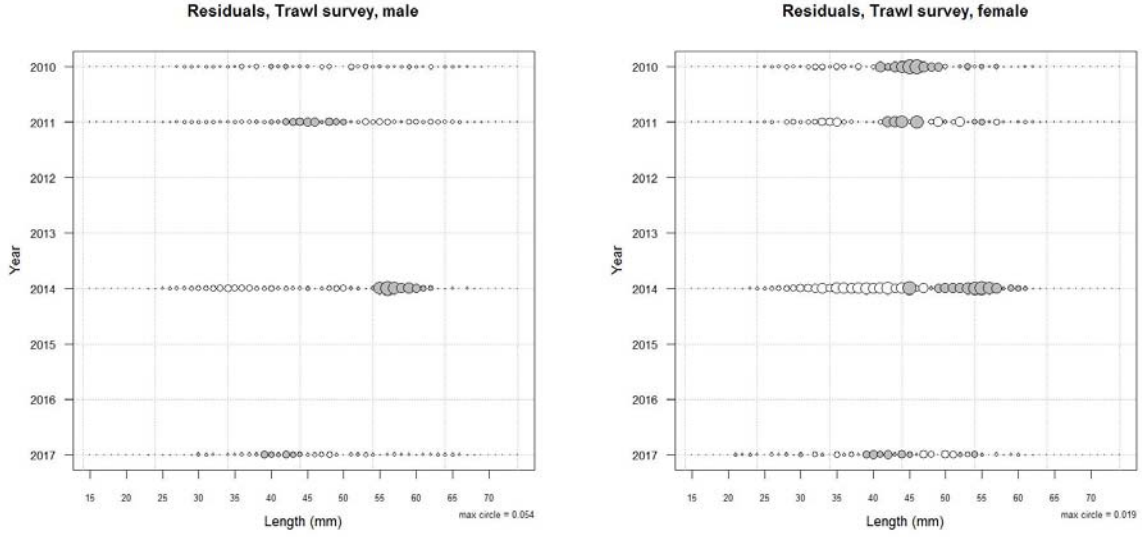

A3. 50: Bubble plots of residuals for fits to length frequency distributions for MW trawl sampling.

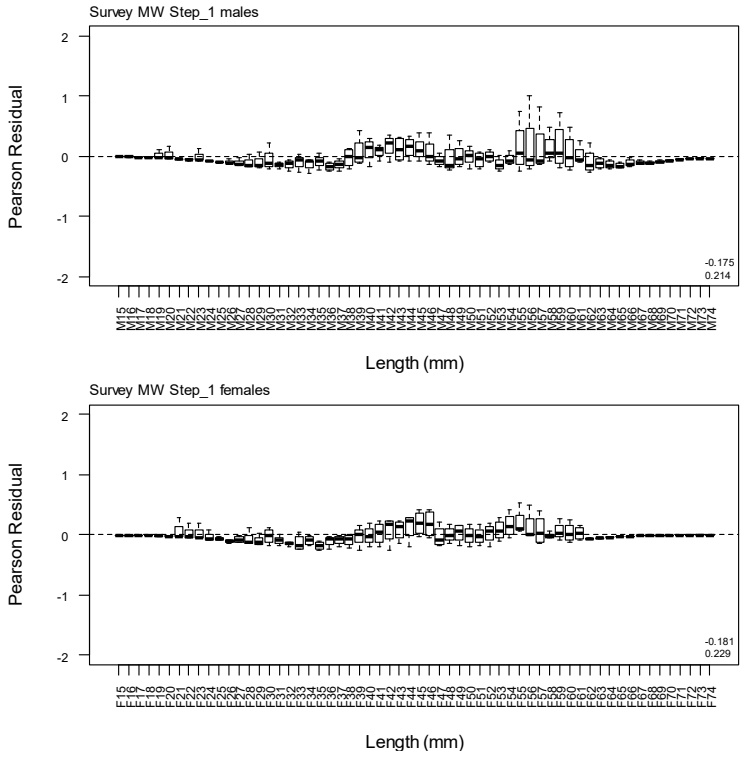

A3. 51: Box plots of Pearson residuals from the fit to length frequency distributions by length from MW trawl sampling.

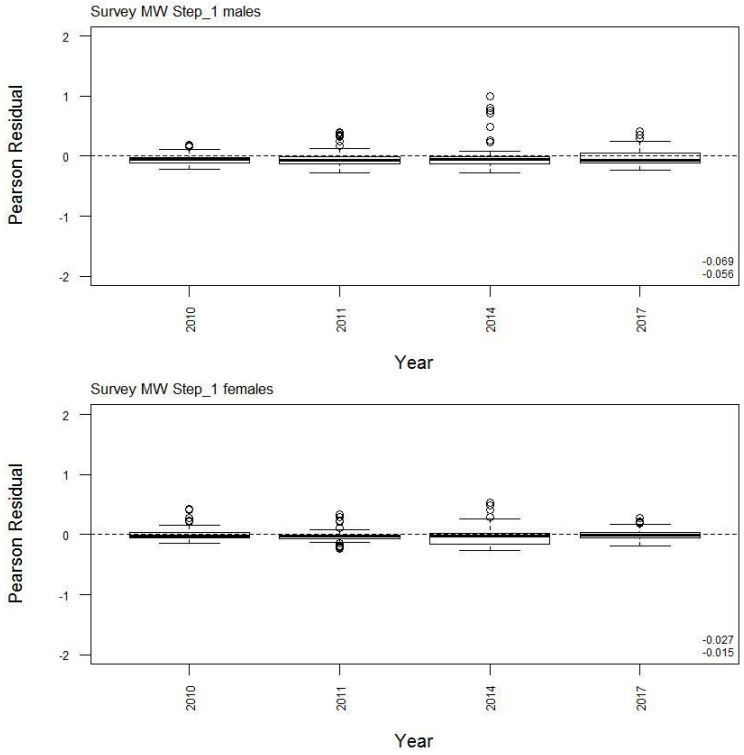

A3. 52: Box plots of Pearson residuals from the fit to length frequency distributions by year from MW trawl sampling.

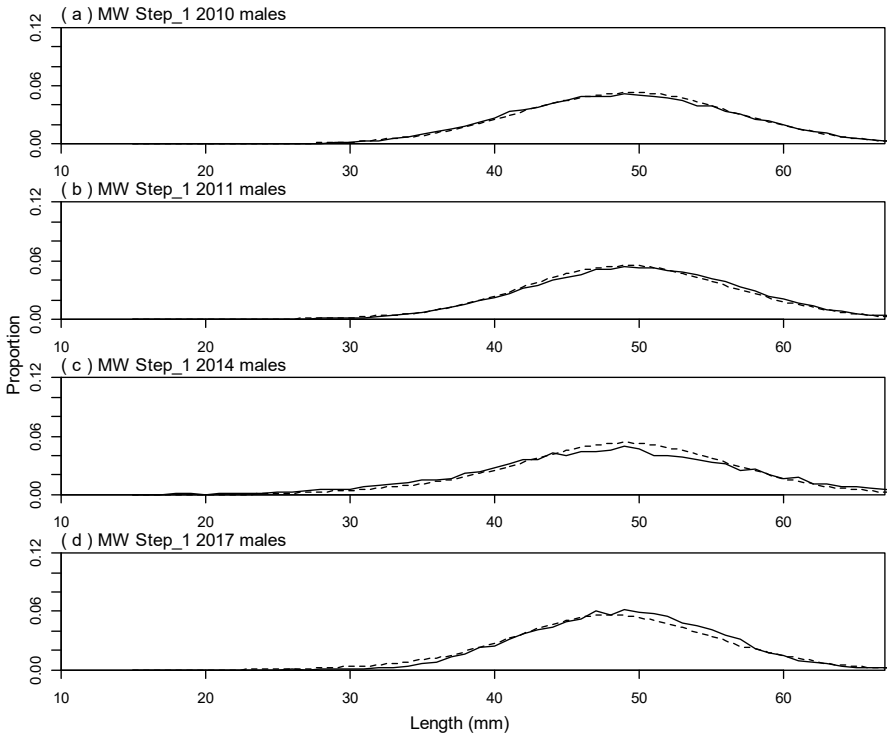

A3. 53: Observed (solid line) and fitted (dashed line) length frequency distributions for MW photographic survey scampi size estimation.

A3. 54: Numbers of scampi measured, estimated multinomial N sample size, and effective sample size used within the model for length frequency distributions for MW photographic survey samples.

	Measured	Multinomial N	Effective sample size
N_2010	173	298	707.92
N_2011	128	227	539.26
N_2014	24	48	114.03
N_2017	23	46	109.28

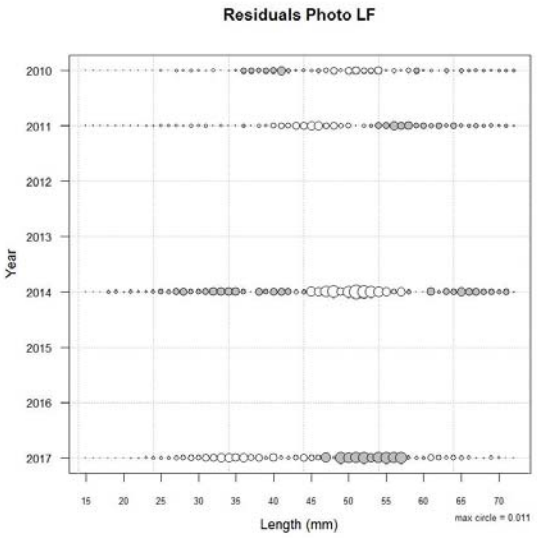

A3. 55: Bubble plots of residuals for fits to length frequency distributions for MW photographic sampling.

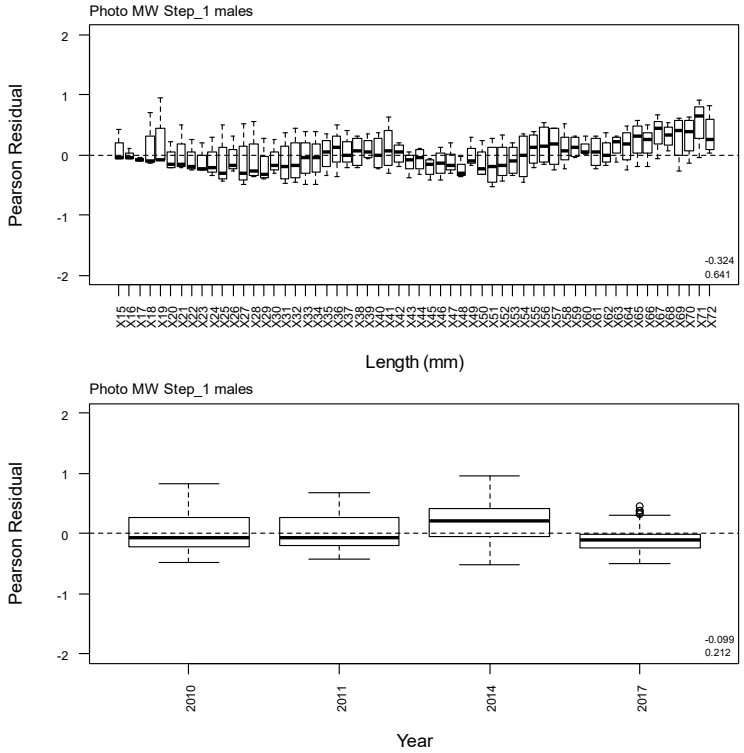

A3. 56: Box plots of Pearson residuals from the fit to length frequency distributions by length and year for MW photographic sampling.

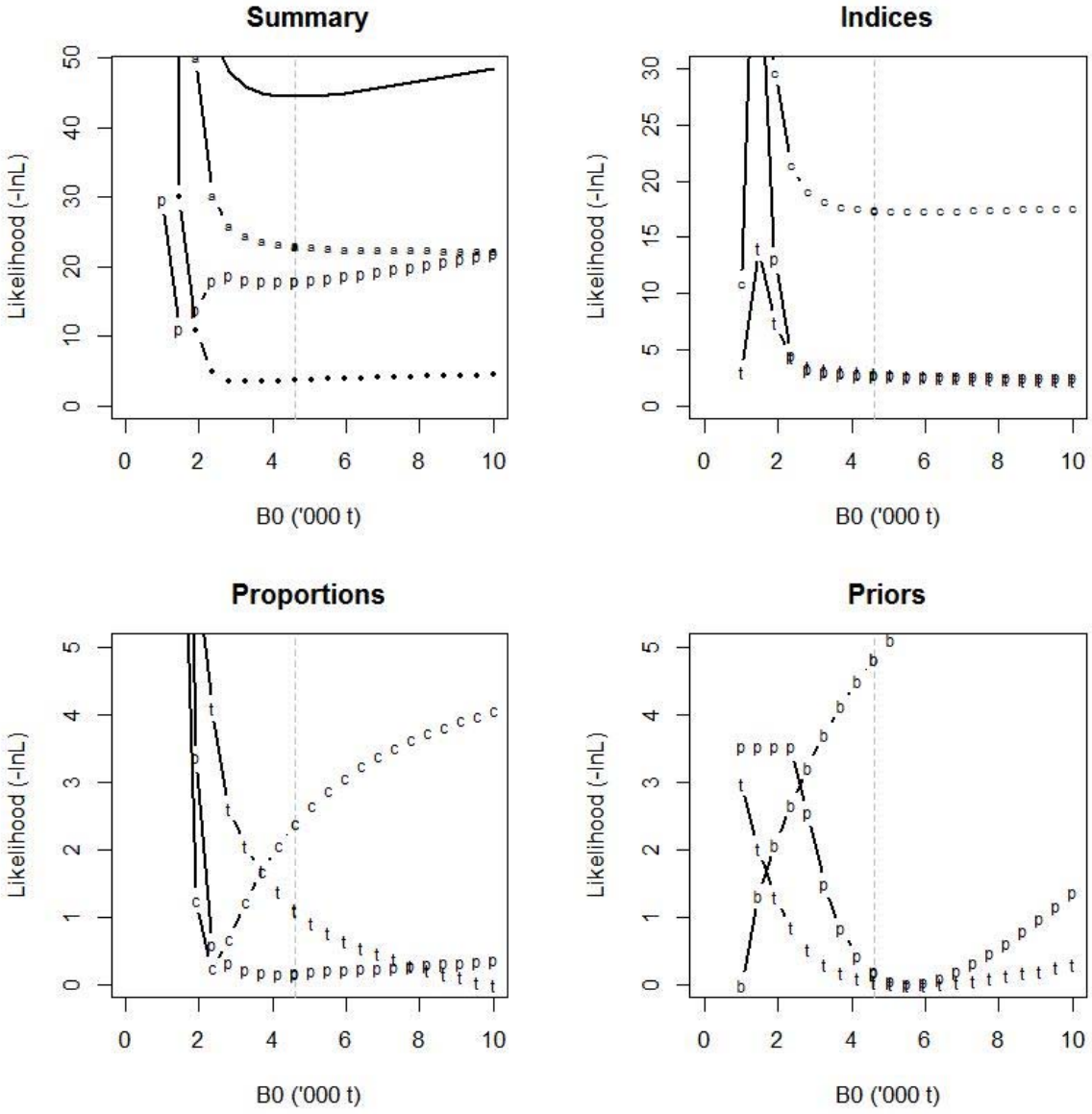

A3. 57: Likelihood profiles for SCI 3 Model 1 when B_0 is fixed in the model. Figures show profiles for main priors (top left, p – priors, a – abundance indices, • – proportions at length), abundance indices (top right, t – trawl survey, c – CPUE, p – photo survey), proportion at length data (bottom left, t – trawl, c – observer, p – photo) and priors (bottom right, b – B_0, p – *q-Photo*, t – *q-Trawl*). Vertical dashed line represents MPD.

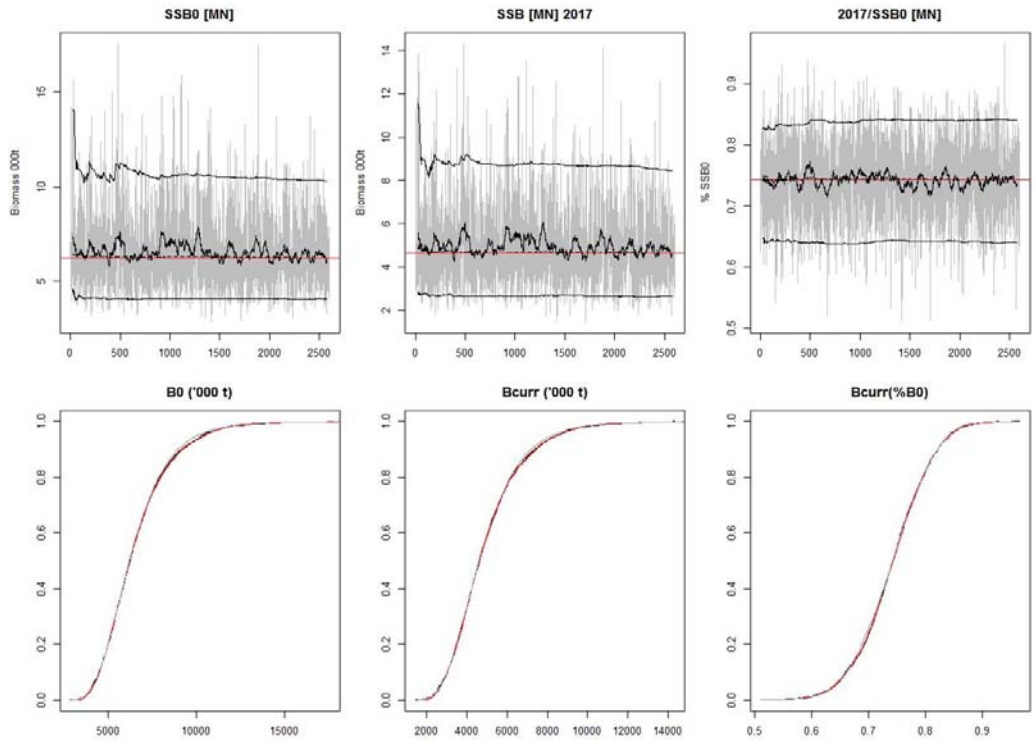

A3. 58: MCMC traces for MN SSB_0, SSB_{2017}, and SSB_{2017}/SSB_0 terms for SCI 3 Model 1 (nuisance q)(trace – grey line, cumulative moving median – dashed black line, moving average and cumulative moving 2.5%, 97.5% quantiles – solid black lines, overall median – solid red line, left plots); and cumulative frequency distributions for three independent MCMC chains (shown as red, grey, and black lines, right plots).

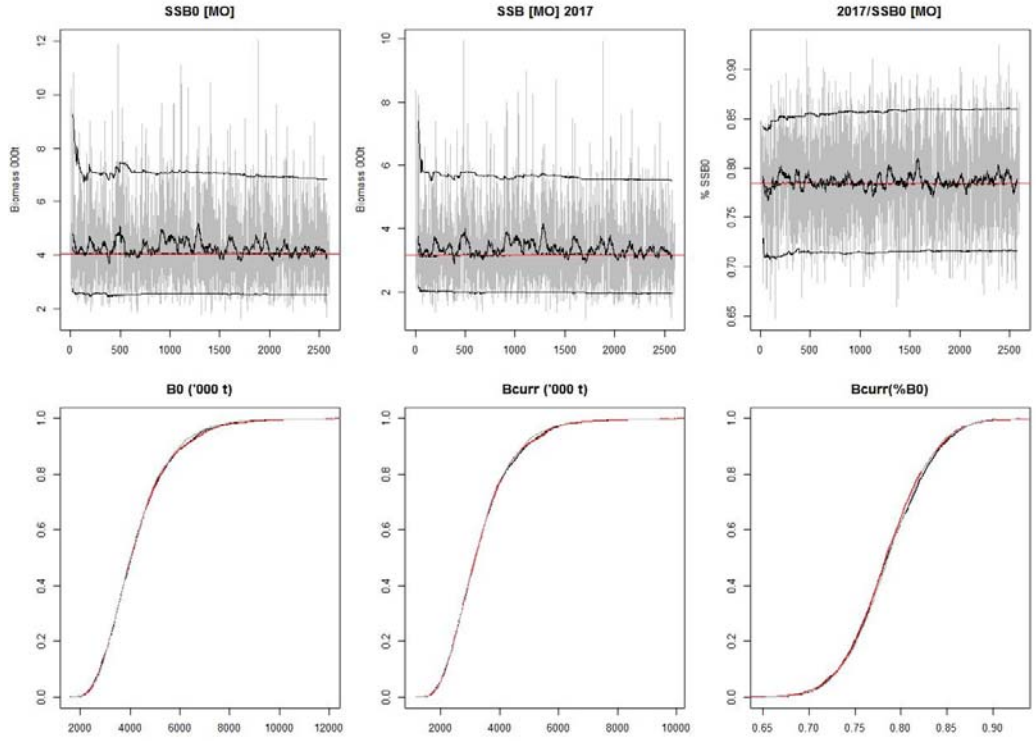

A3. 59: MCMC traces for MO SSB_0, SSB_{2017}, and SSB_{2017}/SSB_0 terms for SCI 3 Model 1 (nuisance q)(trace – grey line, cumulative moving median – dashed black line, moving average and cumulative moving 2.5%, 97.5% quantiles – solid black lines, overall median – solid red line, left plots); and cumulative frequency distributions for three independent MCMC chains (shown as red, grey, and black lines, right plots).

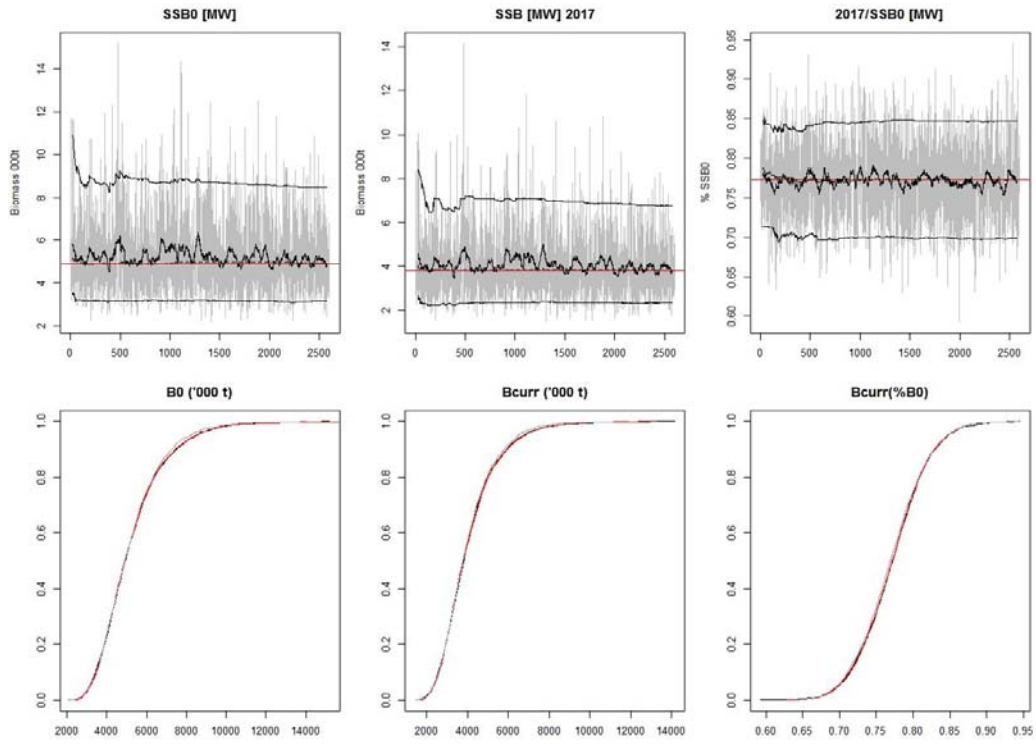

A3. 60: MCMC traces for MW SSB_0, SSB_{2017}, and SSB_{2017}/SSB_0 terms for SCI 3 Model 1 (nuisance q)(trace – grey line, cumulative moving median – dashed black line, moving average and cumulative moving 2.5%, 97.5% quantiles – solid black lines, overall median – solid red line, left plots); and cumulative frequency distributions for three independent MCMC chains (shown as red, grey and black lines, right plots).

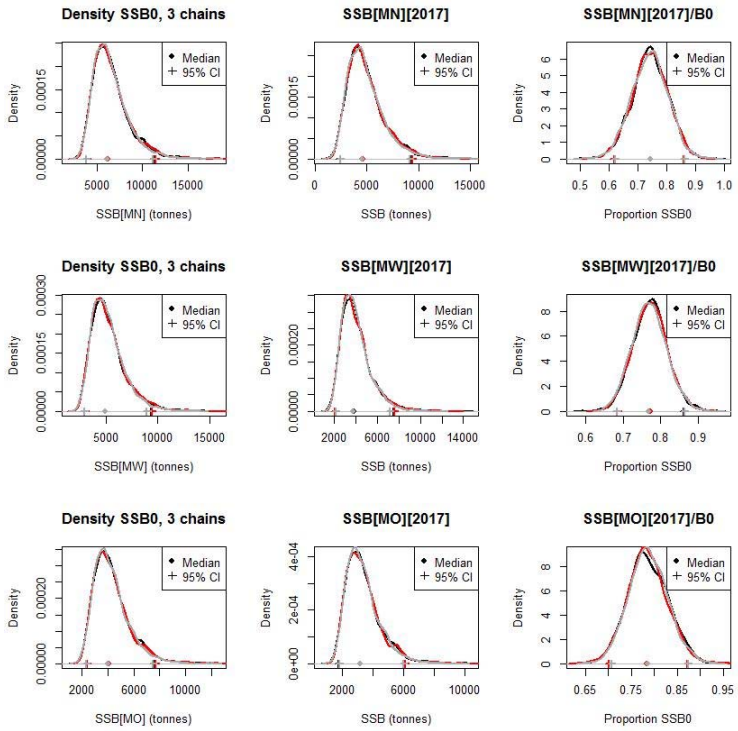

A3. 61: Density plots for SSB_0, SSB_{2017}, and SSB_{2017}/SSB_0 terms for each subarea of SCI 3 Model 1 for three independent MCMC chains, with median and 95% confidence intervals.

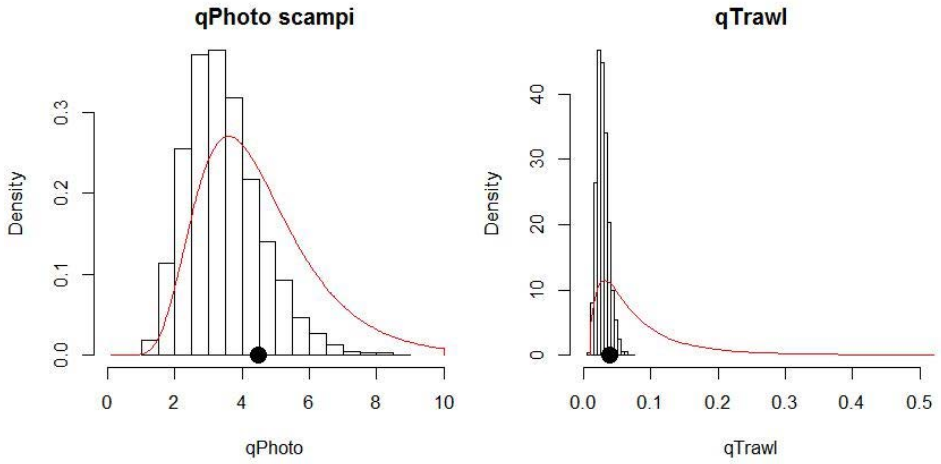

A3. 62: Marginal posterior distributions (histograms), MPD estimates (solid symbols), and distributions of priors (lines) for catchability terms.

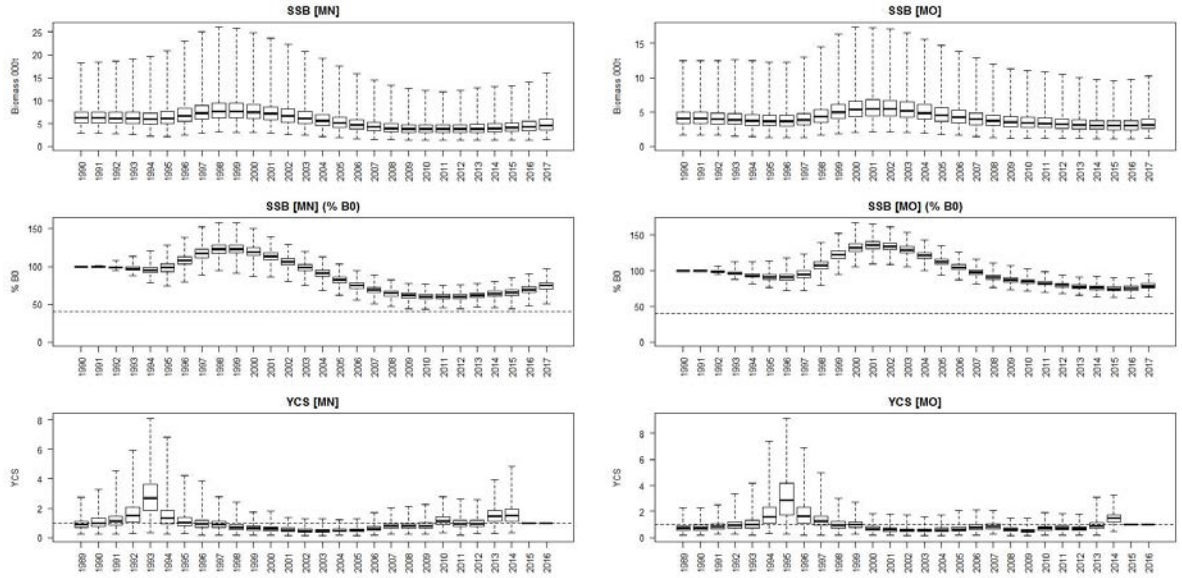

A3. 63: Posterior trajectory of *SSB*, SSB_{2016}/SSB_0 and YCS for subareas MN and MO.

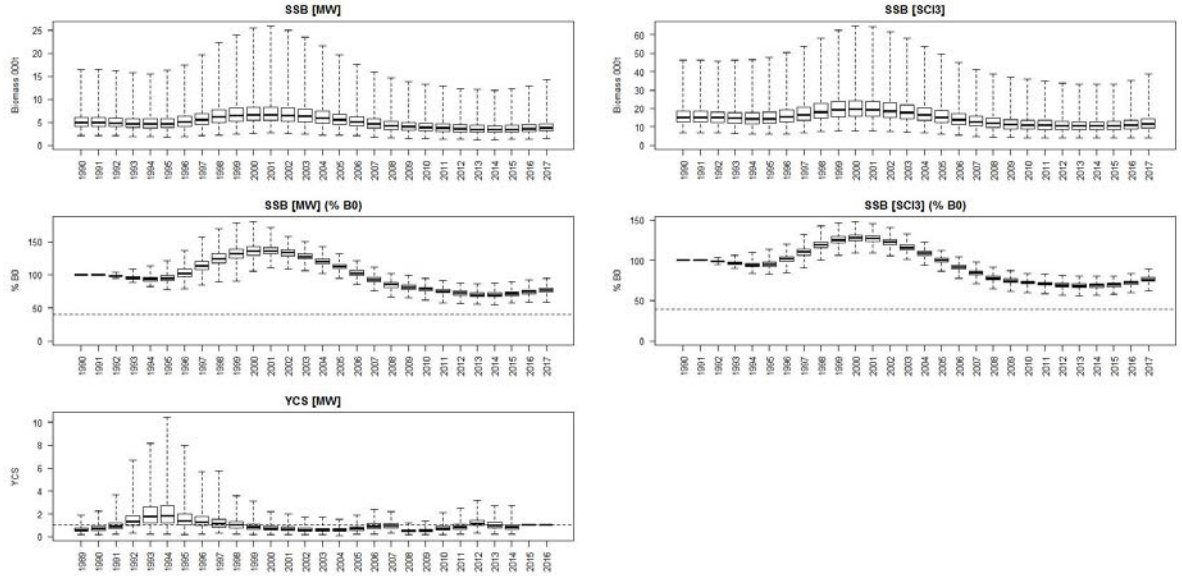

A3. 64: Posterior trajectory of *SSB*, SSB_{2016}/SSB_0, and YCS for subareas MW and the combined SCI 3 modelled area.

APPENDIX 4: MODEL 2, *M* fixed at 0.25, CPUE process error 0.25

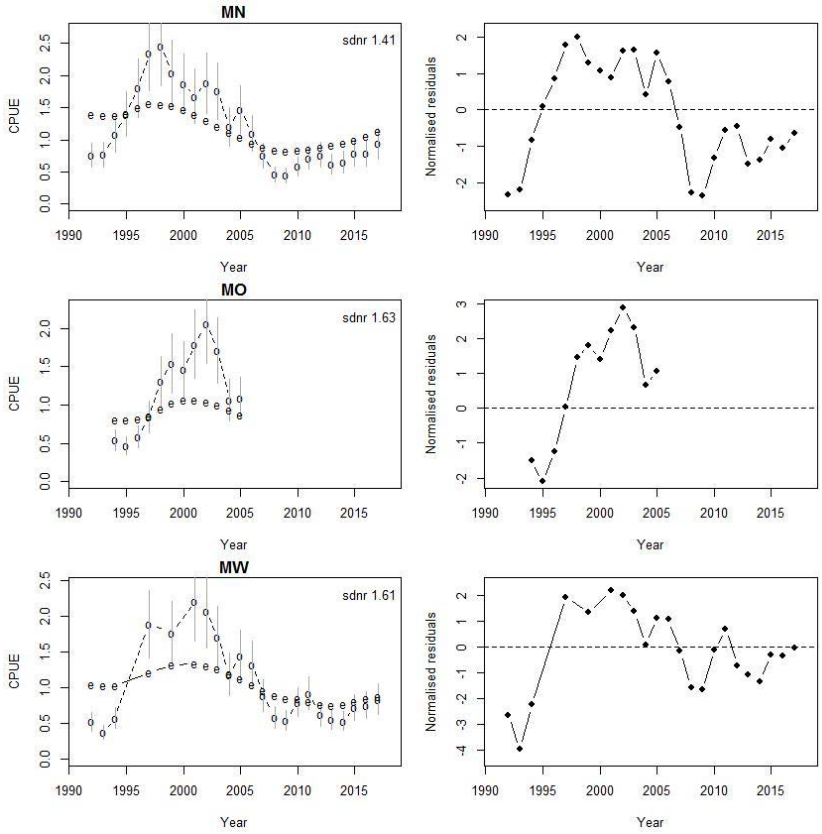

A4. 1: Fits to CPUE indices (left column) and normalised residuals (right column) by subarea (MN - top row, MO - middle row, MW - bottom row) for SCI 3 Model 2.

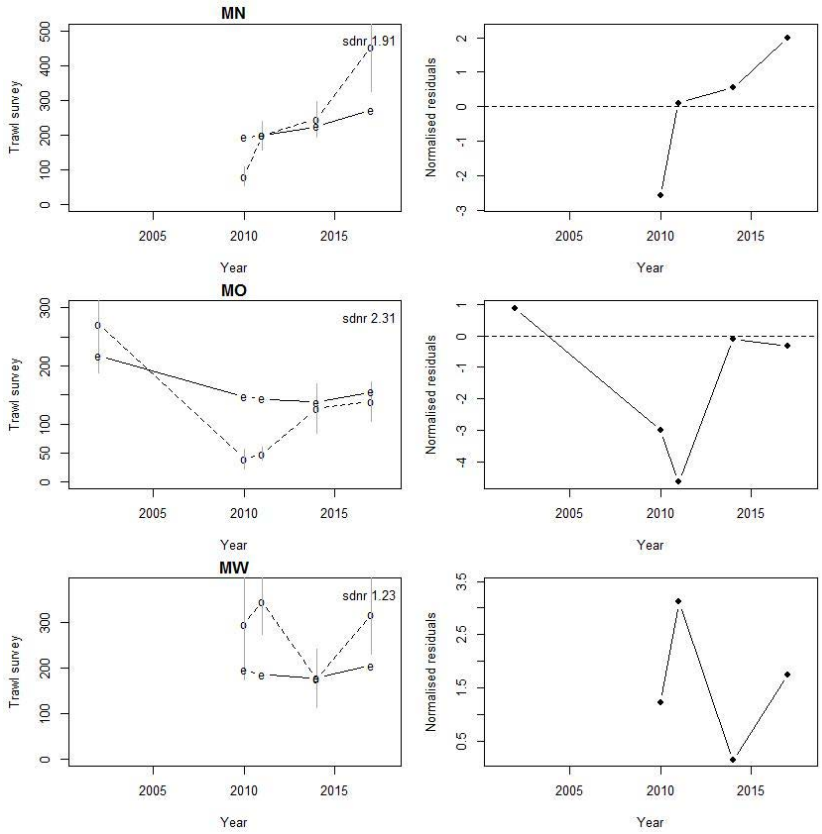

A4. 2: Fits to trawl survey indices (left column) and normalised residuals (right column) by subarea (MN - top row, MO - middle row, MW - bottom row) for SCI 3 Model 2.

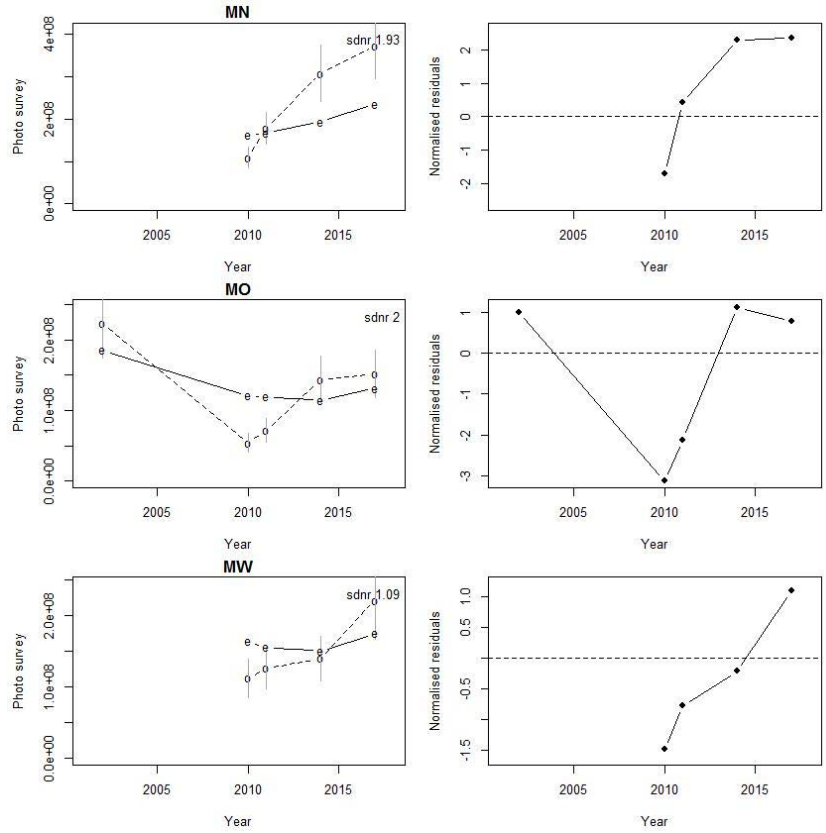

A4. 3: Fits to photo survey indices (left column) and normalised residuals (right column) by subarea (MN - top row, MO - middle row, MW - bottom row) for SCI 3 Model 2.

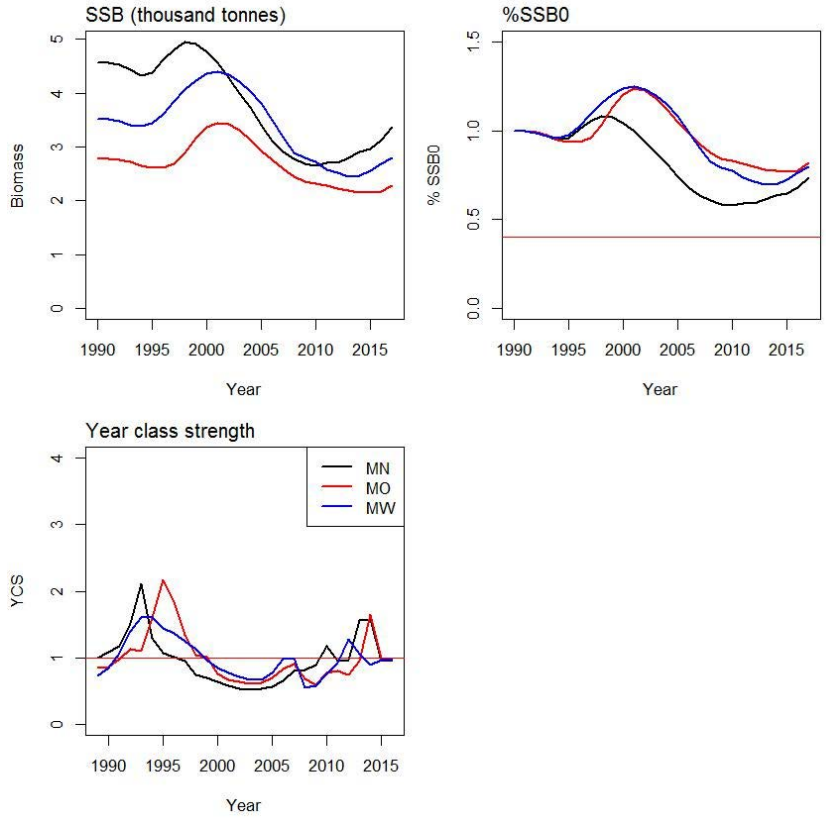

A4. 4: Spawning stock biomass trajectory (upper left), Spawning stock biomass as a percentage of SSB_0 (upper right), and year class strength (lower plot) by subarea for SCI 3 Model 2.

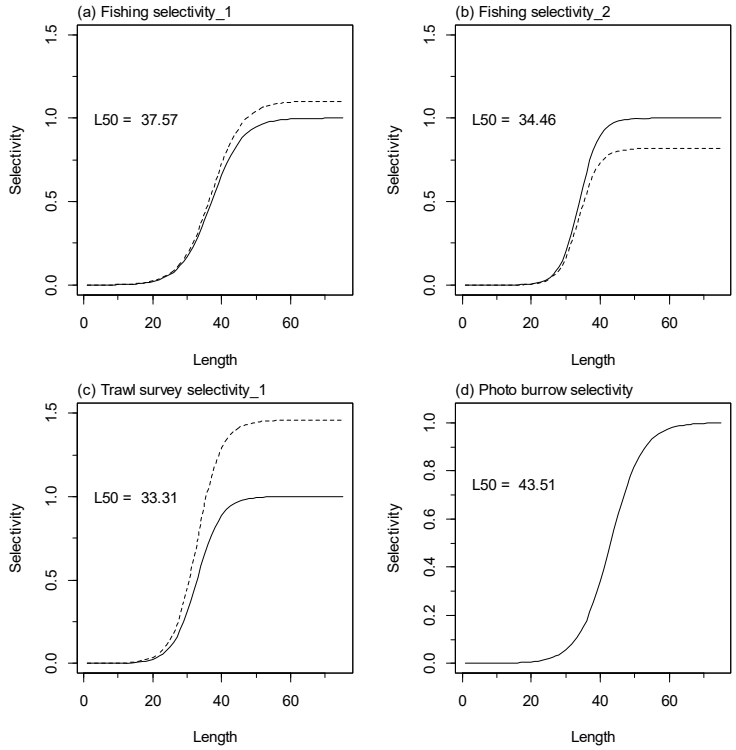

A4. 5: Fishery and photo survey selectivity curves for SCI 3 Model 2. Solid line – females, dotted line – males. The scampi photo index is not sexed, and a single selectivity applies.

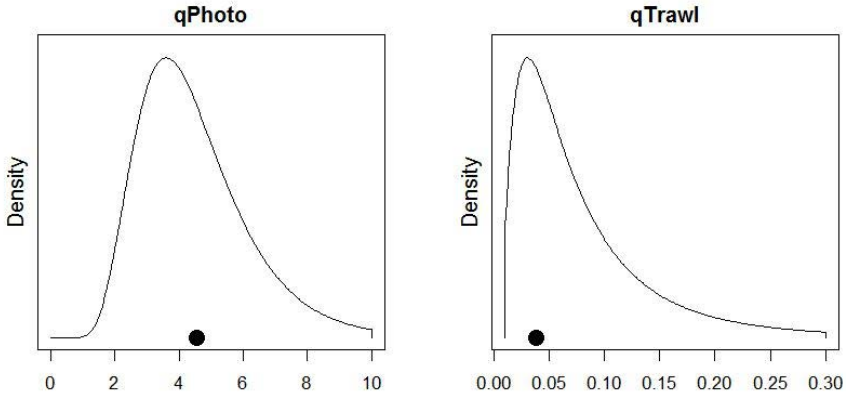

A4. 6: Catchability estimates from MPD model run for SCI 3 Model 2, plotted in relation to prior distribution.

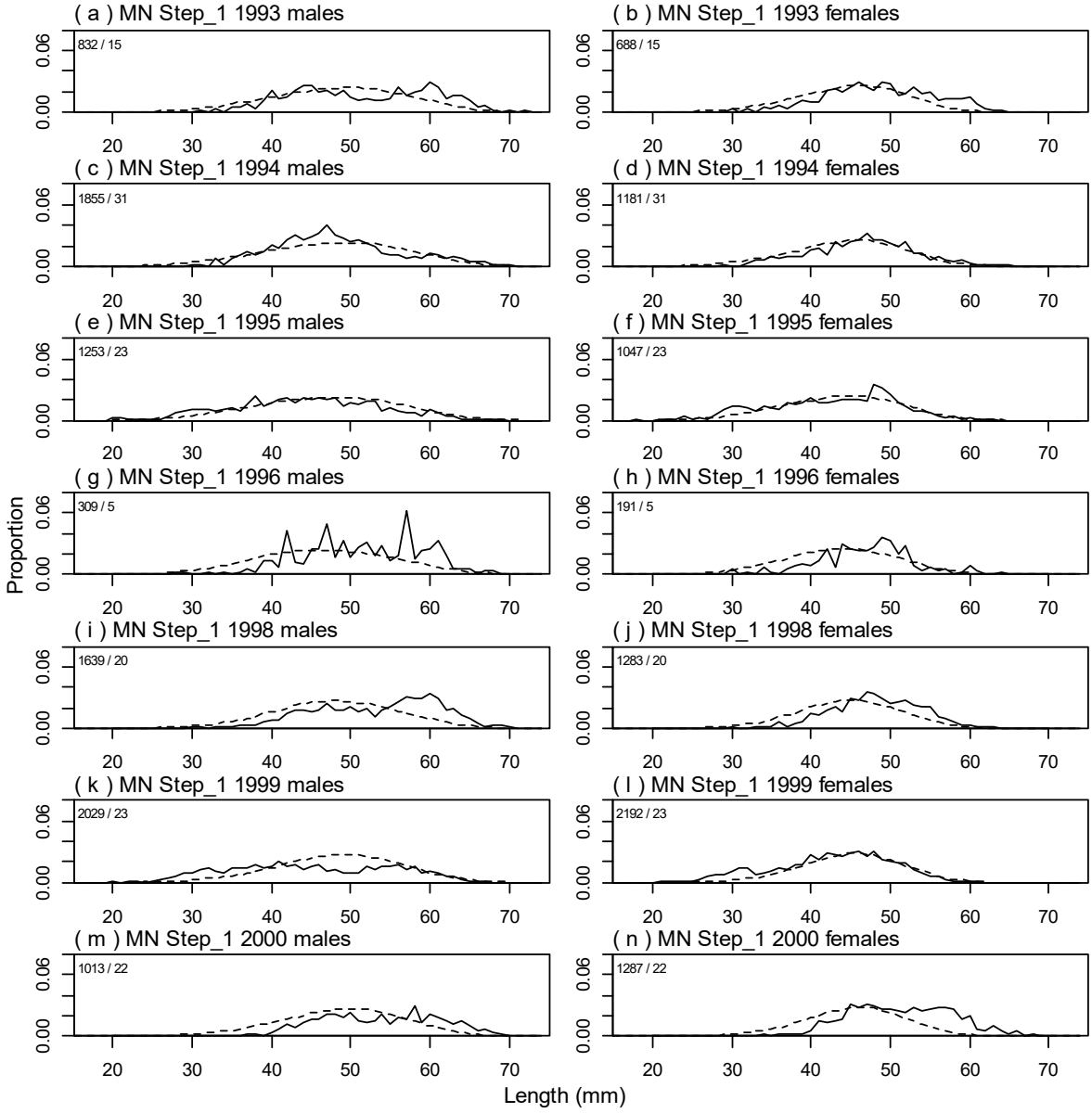

A4. 7: Observed (solid line) and fitted (dashed line) length frequency distributions for observer samples, MN time step 1. Numbers in top left corner of each plot represent number of scampi measured / number of events sampled.

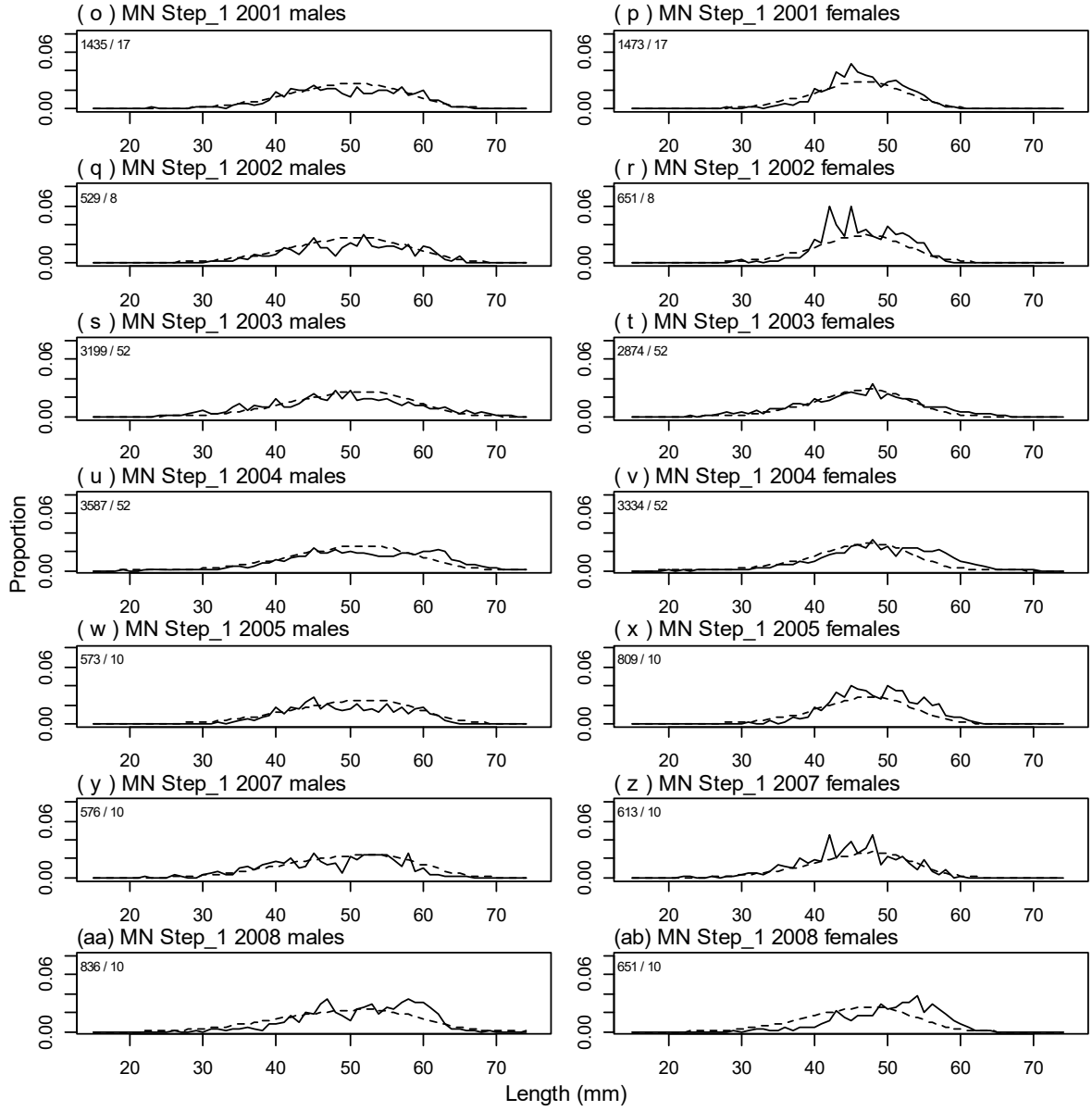

A4. 7 *continued*: Observed (solid line) and fitted (dashed line) length frequency distributions for observer samples, MN time step 1. Numbers in top left corner of each plot represent number of scampi measured / number of events sampled.

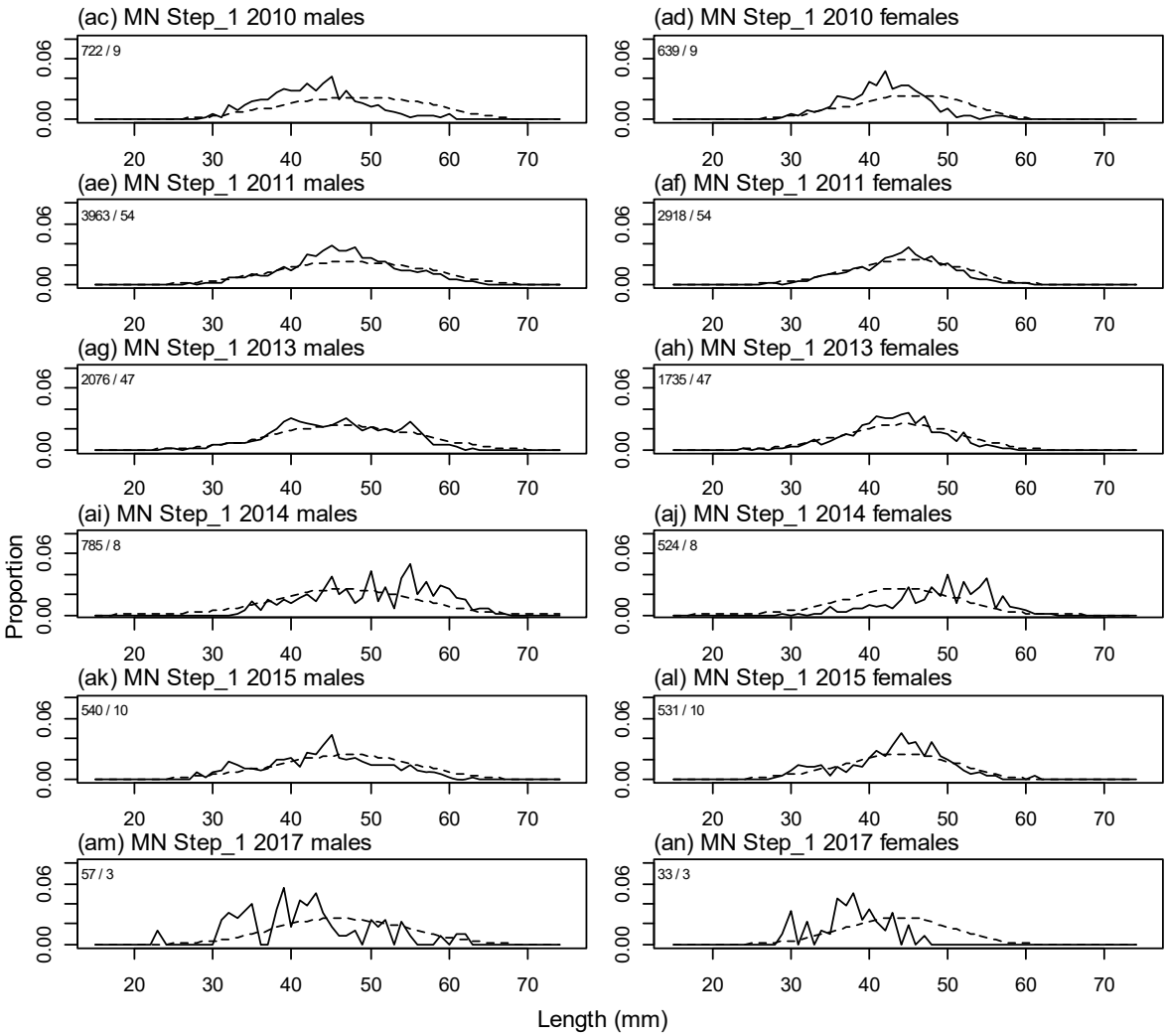

A4. 7 *continued*: Observed (solid line) and fitted (dashed line) length frequency distributions for observer samples, MN time step 1. Numbers in top left corner of each plot represent number of scampi measured / number of events sampled.

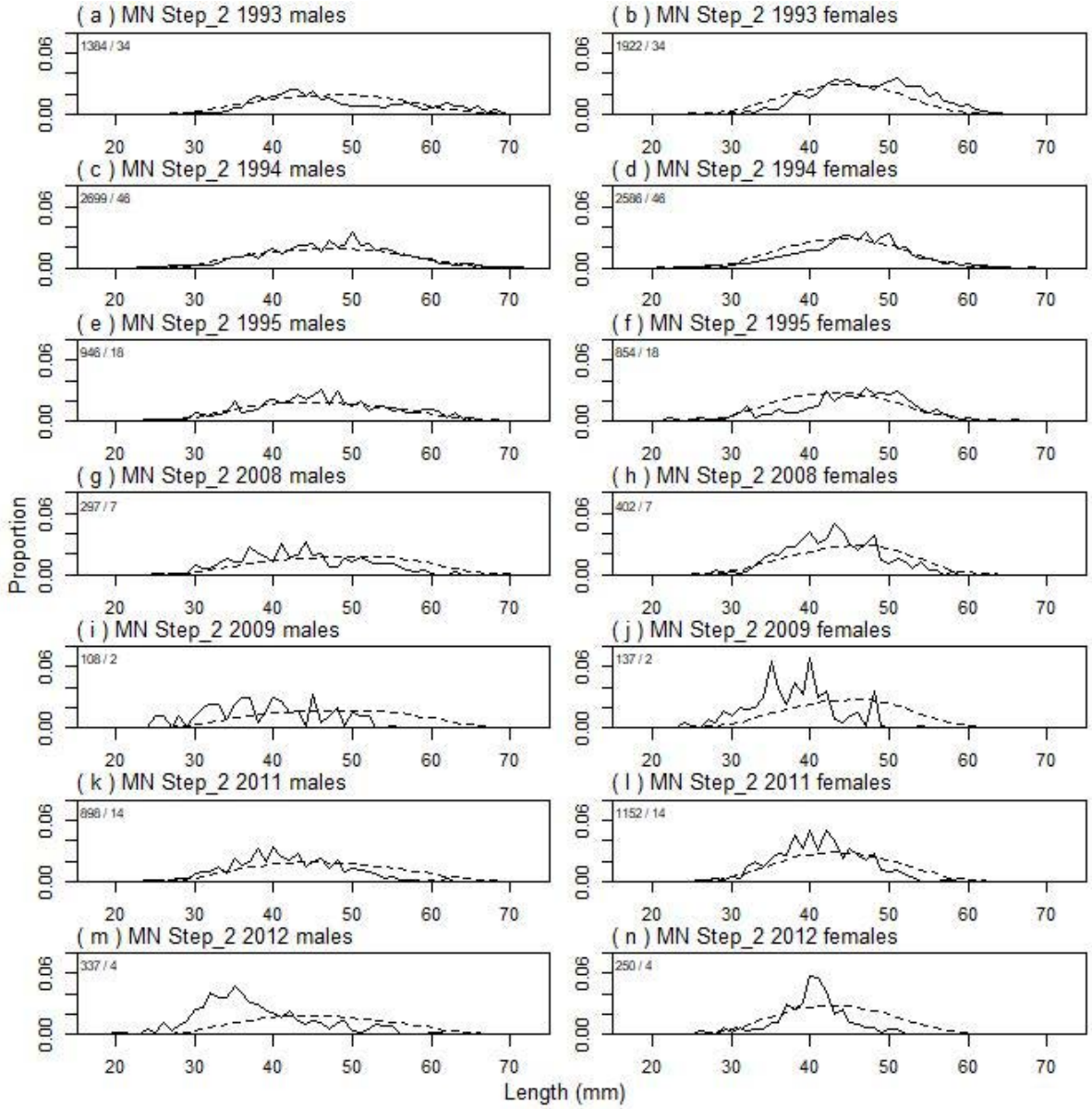

A4. 8: Observed (solid line) and fitted (dashed line) length frequency distributions for observer samples, MN time step 2. Numbers in top left corner of each plot represent number of scampi measured / number of events sampled.

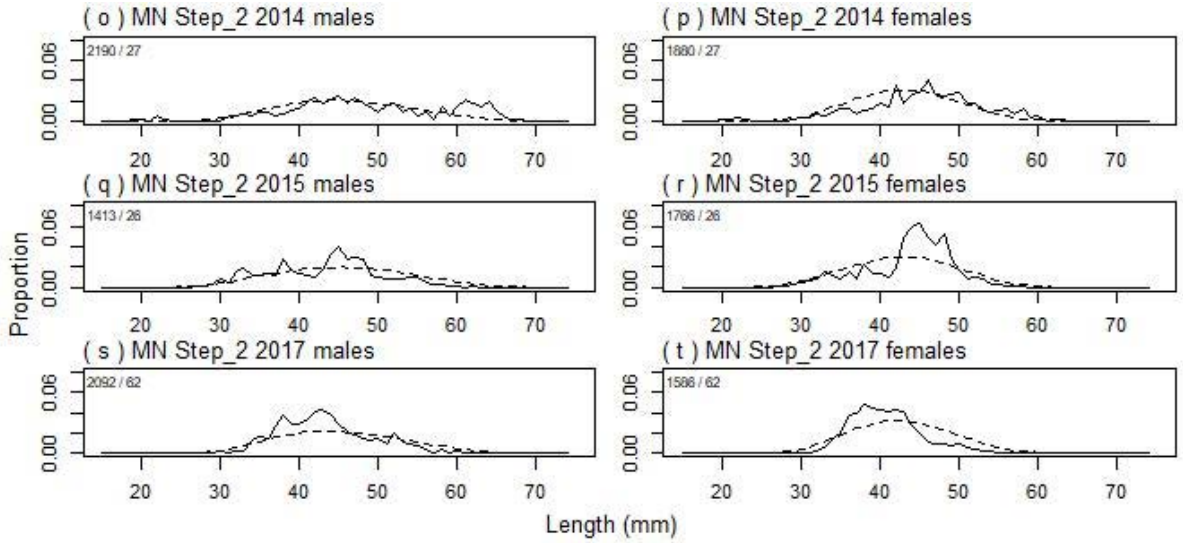

A4. 8 *continued*: Observed (solid line) and fitted (dashed line) length frequency distributions for observer samples, MN time step 2. Numbers in top left corner of each plot represent number of scampi measured / number of events sampled.

A4. 9: Numbers of scampi measured, estimated multinomial N sample size, and effective sample size used within the model for length frequency distributions for observer samples, time step 1.

	Measured	Multinomial N	Effective sample size
N_1993	1 520	1 345	6.03
N_1994	3 036	2 264	10.14
N_1995	2 300	1 824	8.17
N_1996	500	576	2.58
N_1998	2 922	2 599	11.65
N_1999	4 221	3 441	15.42
N_2000	2 300	1 928	8.64
N_2001	2 908	2 827	12.67
N_2002	1 180	988	4.43
N_2003	6 073	3 727	16.70
N_2004	6 921	5 077	22.75
N_2005	1 382	2 030	9.10
N_2007	1 189	2 414	10.82
N_2008	1 487	1 651	7.40
N_2010	1 361	1 544	6.92
N_2011	6 881	4 896	21.94
N_2013	3 811	2 929	13.12
N_2014	1 309	745	3.34
N_2015	1 071	2 071	9.28
N_2017	90	181	0.81

A4. 10: Numbers of scampi measured, estimated multinomial N sample size, and effective sample size used within the model for length frequency distributions for observer samples, MN time step 2.

	Measured	Multinomial N	Effective sample size
N_1993	3 306	2 571	15.56
N_1994	5 285	4 117	24.92
N_1995	1 800	1 501	9.09
N_2008	699	713	4.32
N_2009	245	340	2.06
N_2011	2 050	1 583	9.58
N_2012	587	691	4.18
N_2014	4 071	1 270	7.69
N_2015	3 179	5 855	35.44
N_2017	3 678	1906	11.54

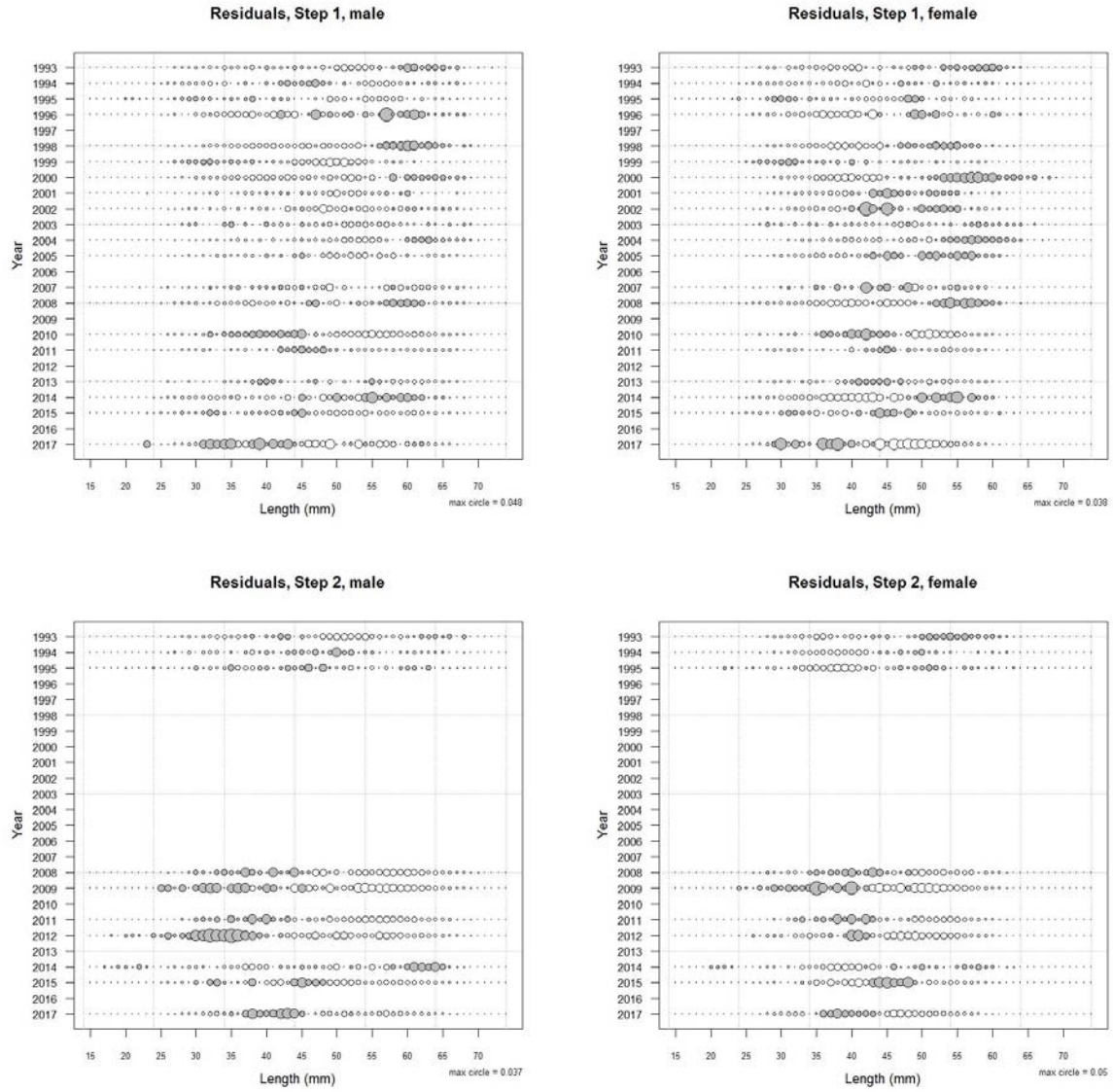

A4. 11: Bubble plots of residuals for fits to length frequency distributions for MN observer sampling.

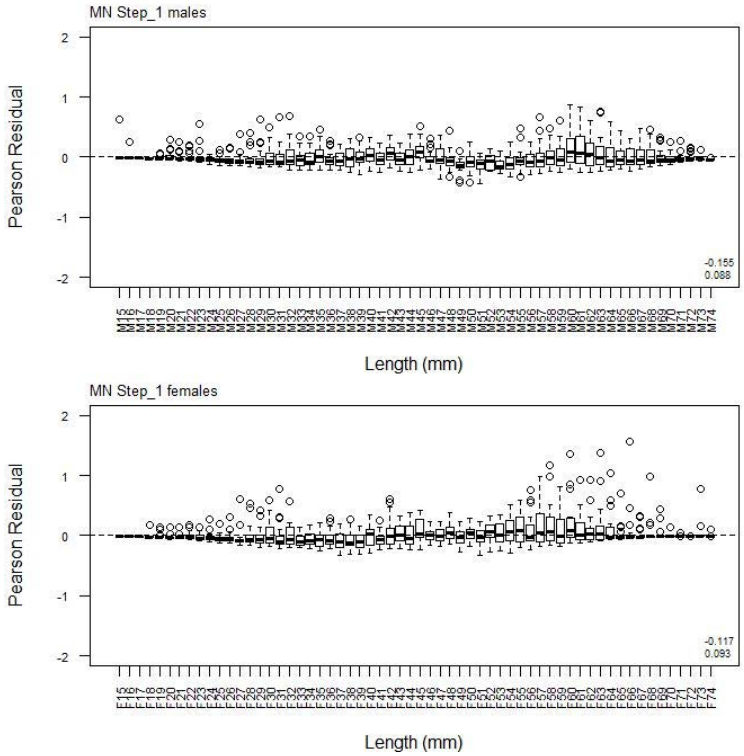

A4. 12: Box plots of Pearson residuals from the fit to length frequency distributions by length from observer sampling by sex for MN time step 1.

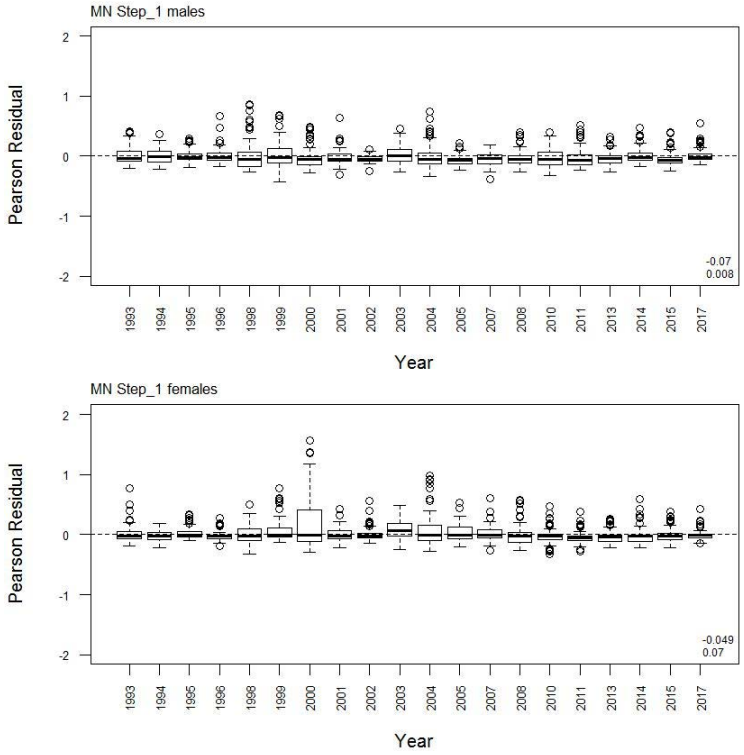

A4. 13: Box plots of Pearson residuals from the fit to length frequency distributions by year from observer sampling by sex for MN time step 1.

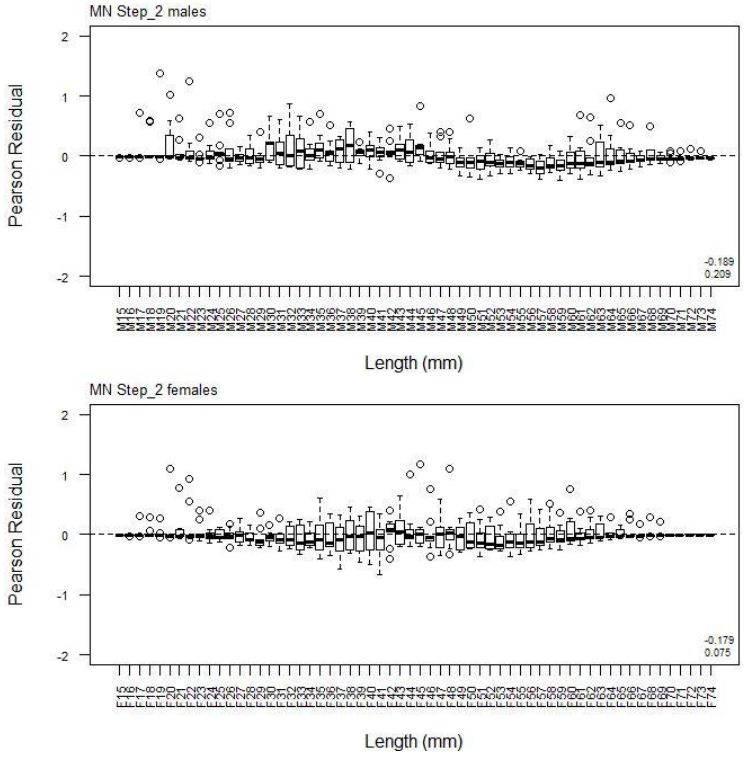

A4. 14: Box plots of Pearson residuals from the fit to length frequency distributions by length from observer sampling by sex for MN time step 2.

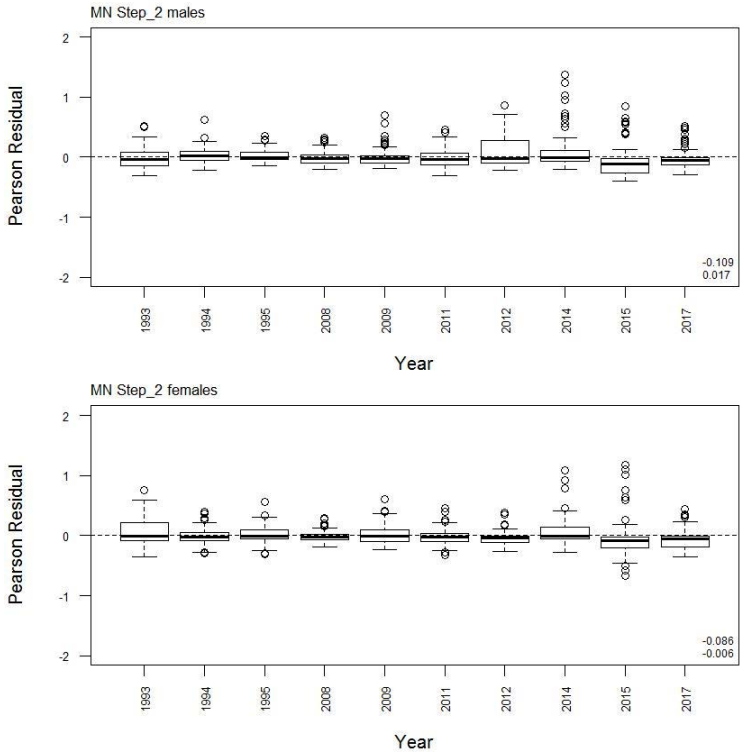

A4. 15: Box plots of Pearson residuals from the fit to length frequency distributions by year from observer sampling by sex for MN time step 2.

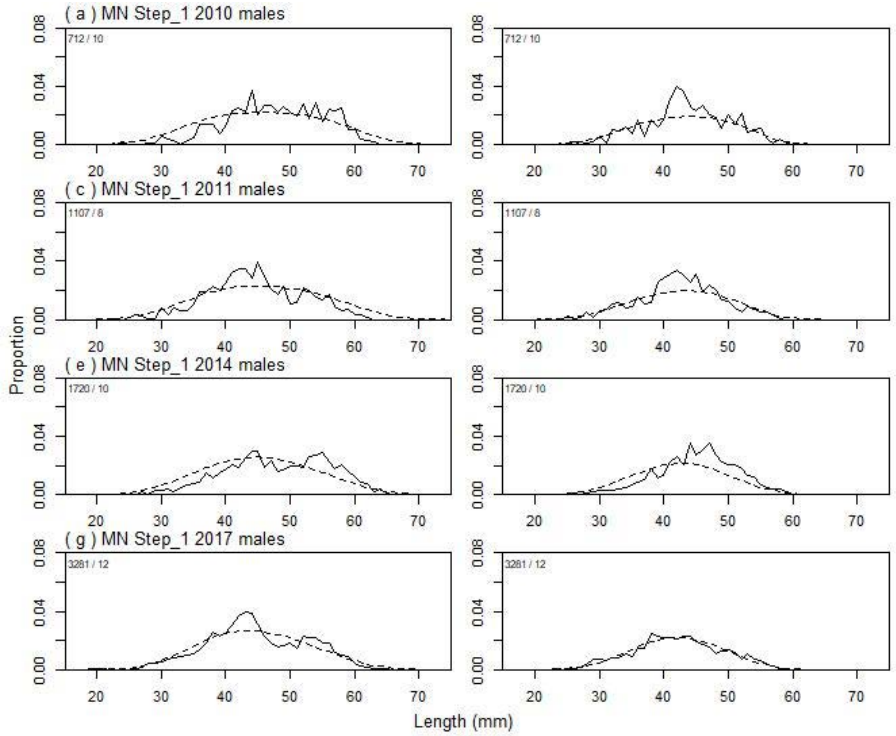

A4. 16: Observed (solid line) and fitted (dashed line) length frequency distributions for MN research survey samples.

A4. 17: Numbers of scampi measured, estimated multinomial N sample size, and effective sample size used within the model for length frequency distributions for MN research survey samples.

	Measured	Multinomial N	Effective sample size
N_2010	1 276	941	13.70
N_2011	2 027	1 610	23.43
N_2014	3 156	2 381	34.66
N_2017	5 299	4 895	71.25

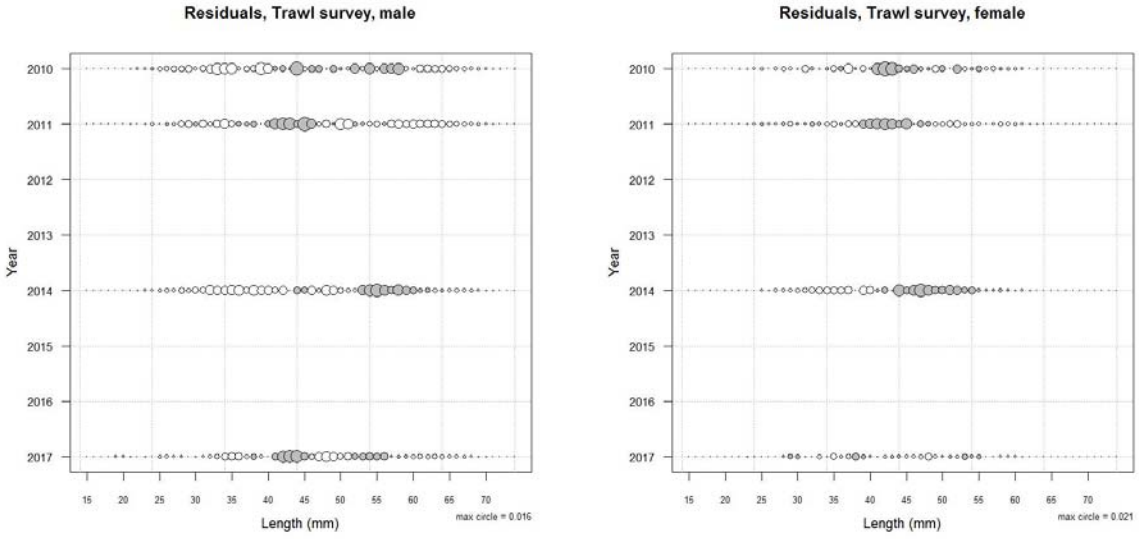

A4. 18: Bubble plots of residuals for fits to length frequency distributions for MN trawl sampling.

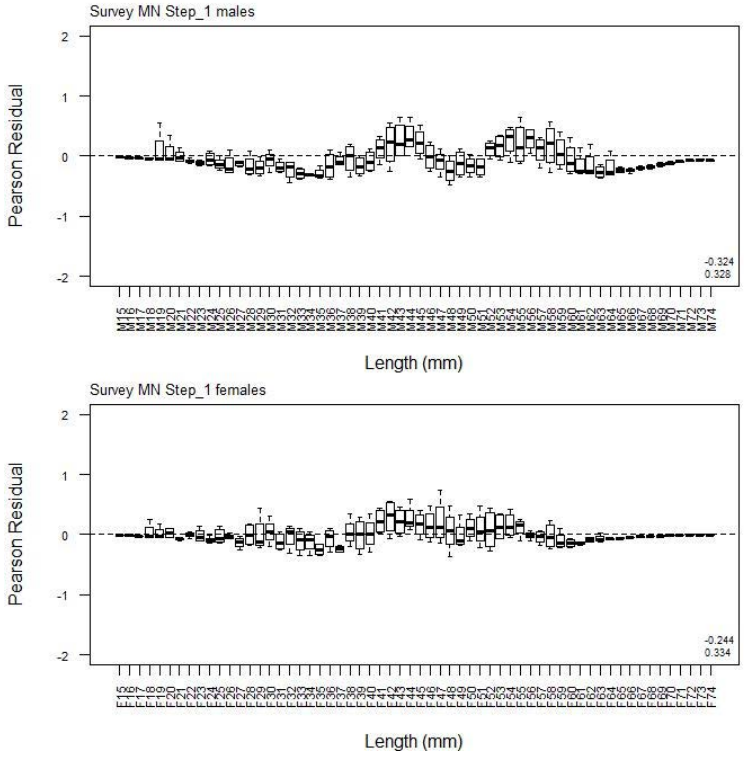

A4. 19: Box plots of Pearson residuals from the fit to length frequency distributions by length from MN trawl sampling.

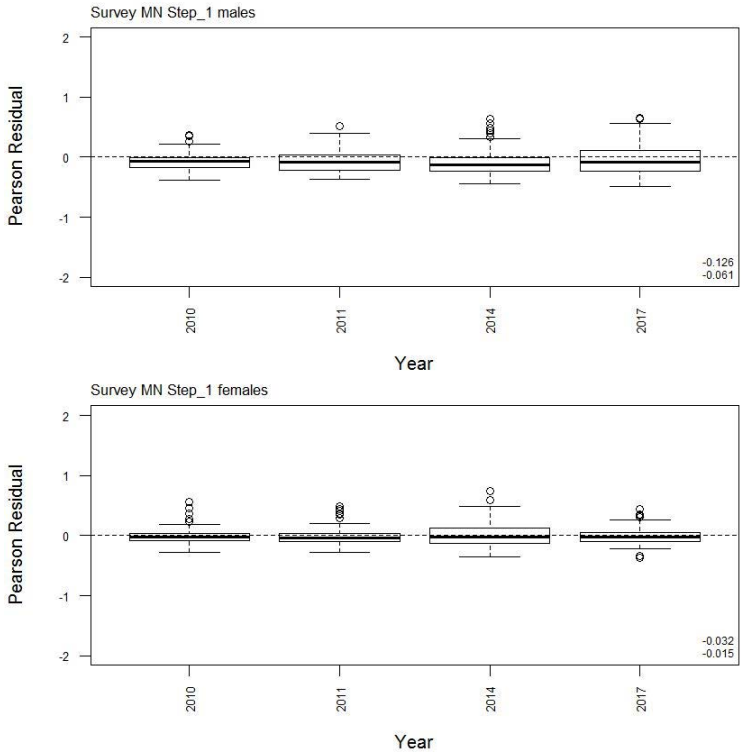

A4. 20: Box plots of Pearson residuals from the fit to length frequency distributions by year from MN trawl sampling.

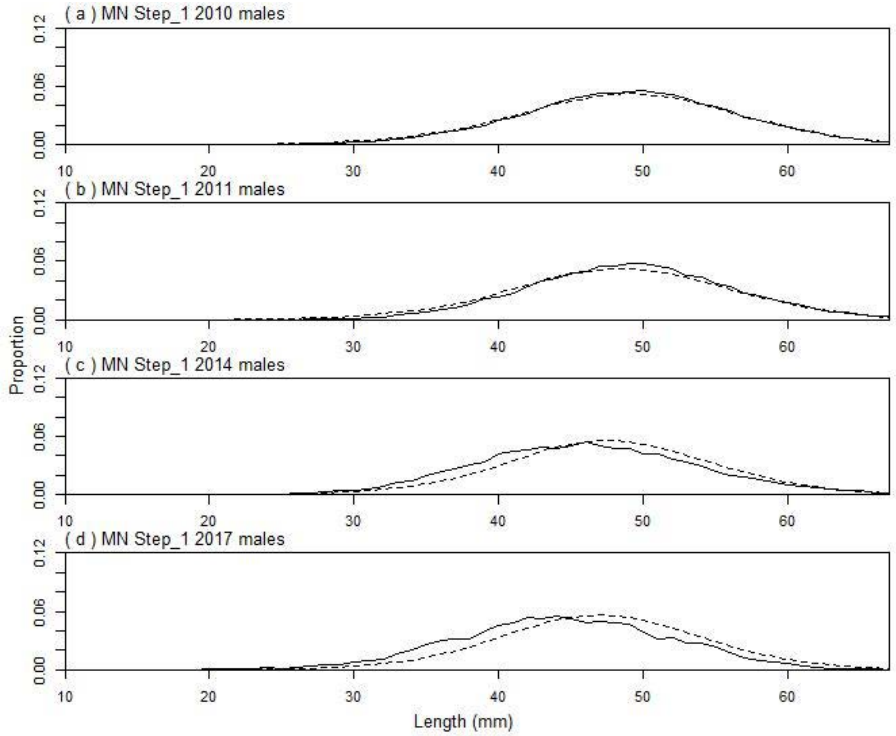

A4. 21: Observed (solid line) and fitted (dashed line) length frequency distributions for MN photographic survey scampi size estimation.

A4. 22: Numbers of scampi measured, estimated multinomial N sample size, and effective sample size used within the model for length frequency distributions for MN photographic survey samples.

	Measured	Multinomial N	Effective sample size
N_2010	113	211	50.96
N_2011	120	225	54.34
N_2014	62	120	28.98
N_2017	25	50	12.08

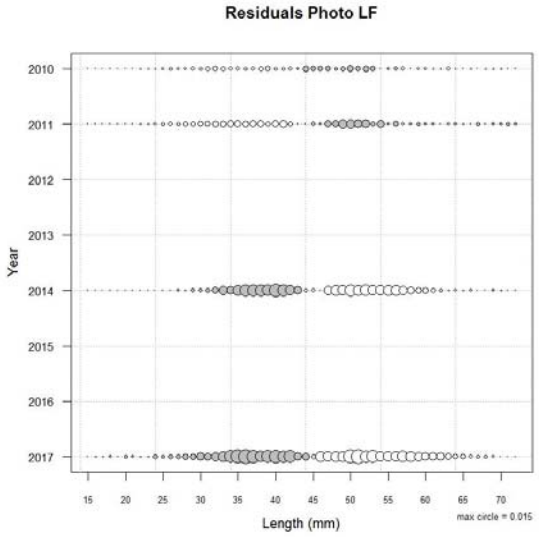

A4. 23: Bubble plots of residuals for fits to length frequency distributions for MN photographic sampling.

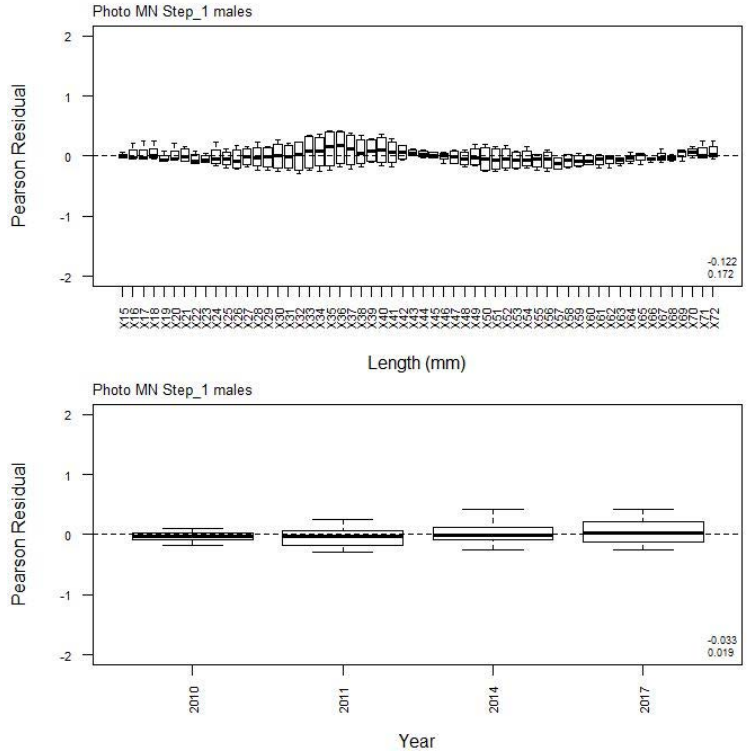

A4. 24: Box plots of Pearson residuals from the fit to length frequency distributions by length and year for MN photographic sampling.

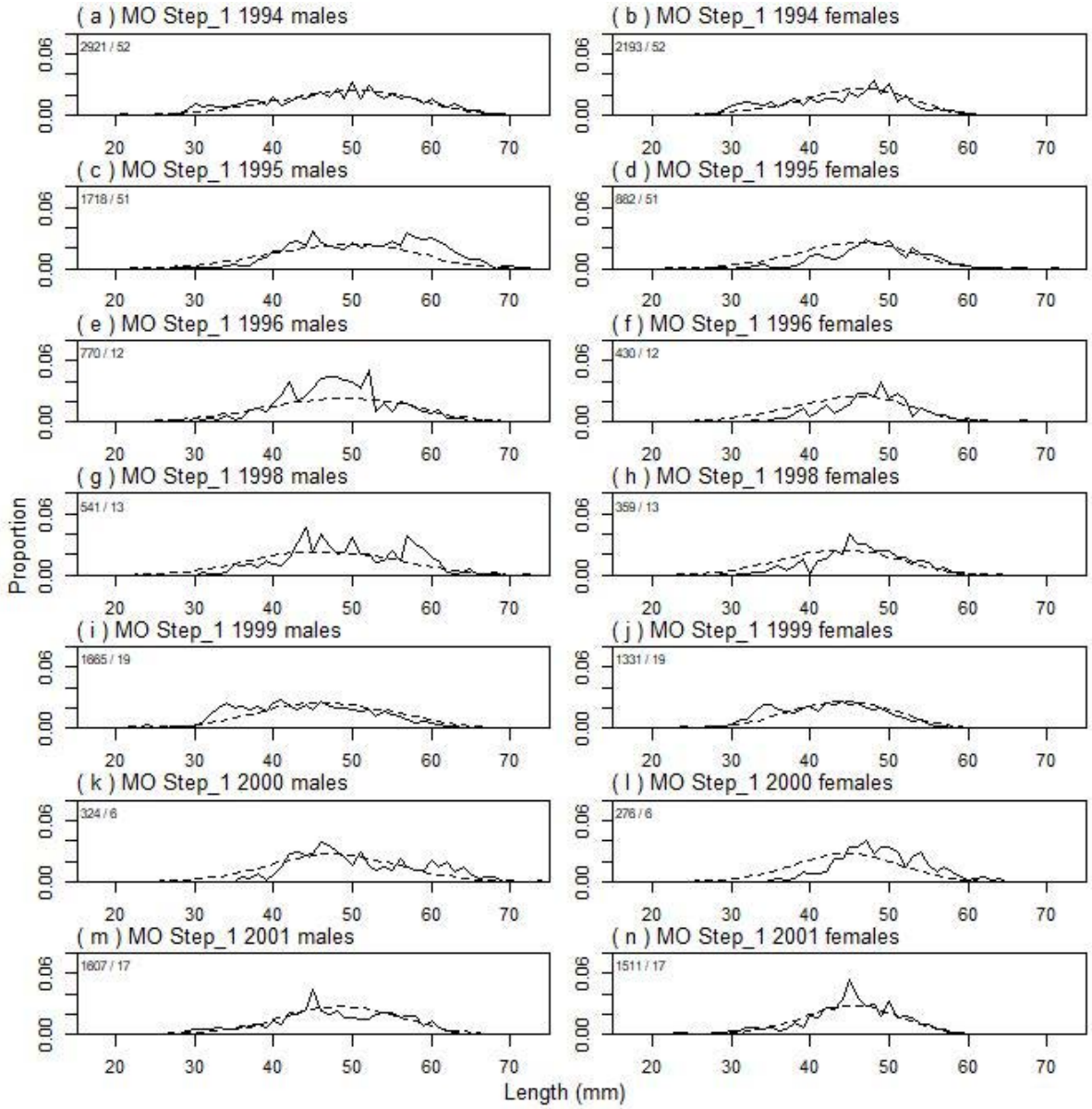

A4. 25: Observed (solid line) and fitted (dashed line) length frequency distributions for observer samples, MO time step 1. Numbers in top left corner of each plot represent number of scampi measured / number of events sampled.

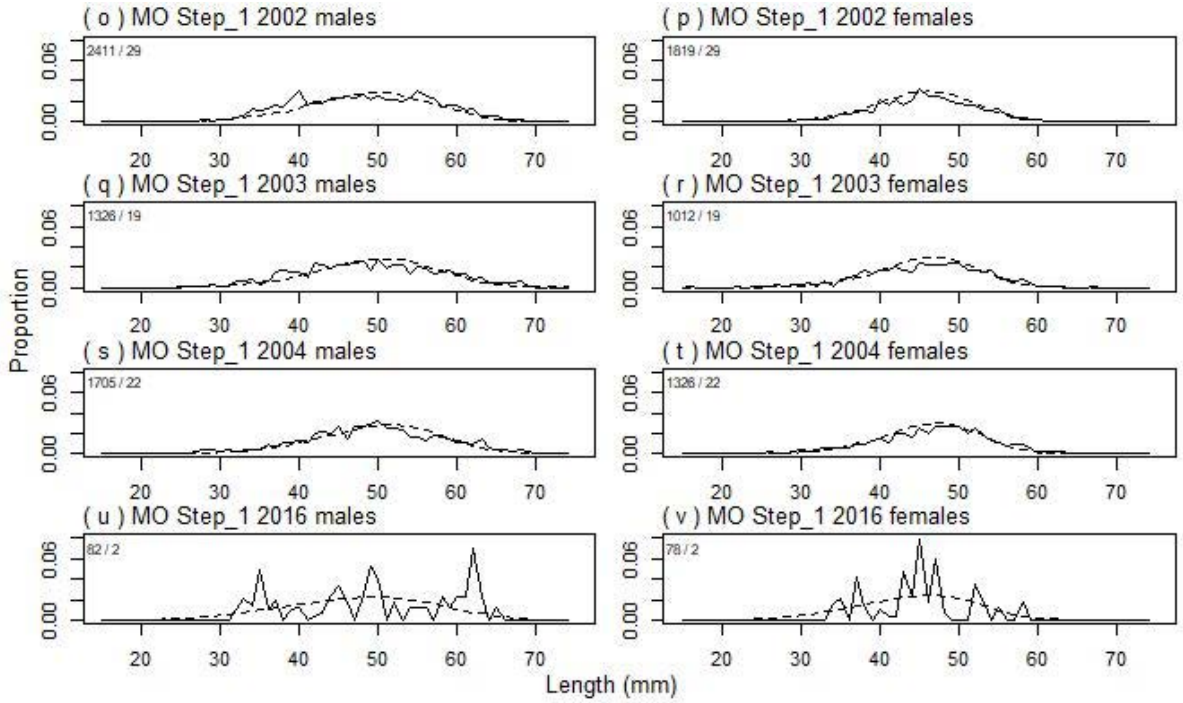

A4. 25 *continued*: Observed (solid line) and fitted (dashed line) length frequency distributions for observer samples, MO time step 1. Numbers in top left corner of each plot represent number of scampi measured / number of events sampled.

A4. 26: Numbers of scampi measured, estimated multinomial N sample size, and effective sample size used within the model for length frequency distributions for observer samples, MO time step 1.

	Measured	Multinomial N	Effective sample size
N_1994	5 114	3 277	30.58
N_1995	2 600	2 182	20.36
N_1996	1 200	1 071	9.99
N_1998	900	940	8.77
N_1999	2 996	2 504	23.36
N_2000	600	733	6.84
N_2001	3 118	2 900	27.06
N_2002	4 230	2 662	24.01
N_2003	2 338	1 553	14.49
N_2004	3 031	2 084	19.45
N_2016	160	88	0.82

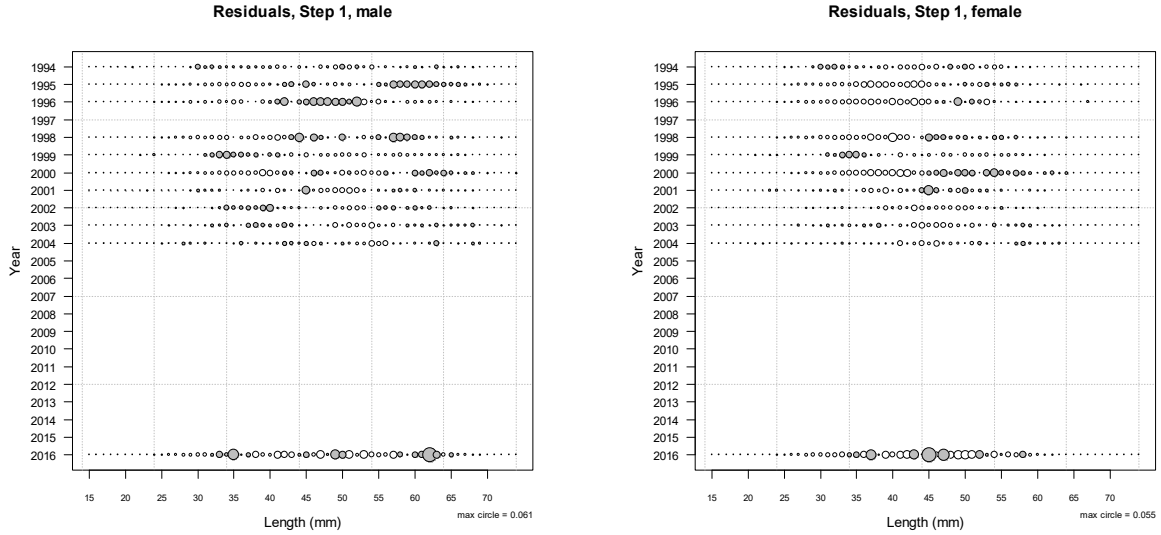

A4. 27: Bubble plots of residuals for fits to length frequency distributions for MO observer sampling.

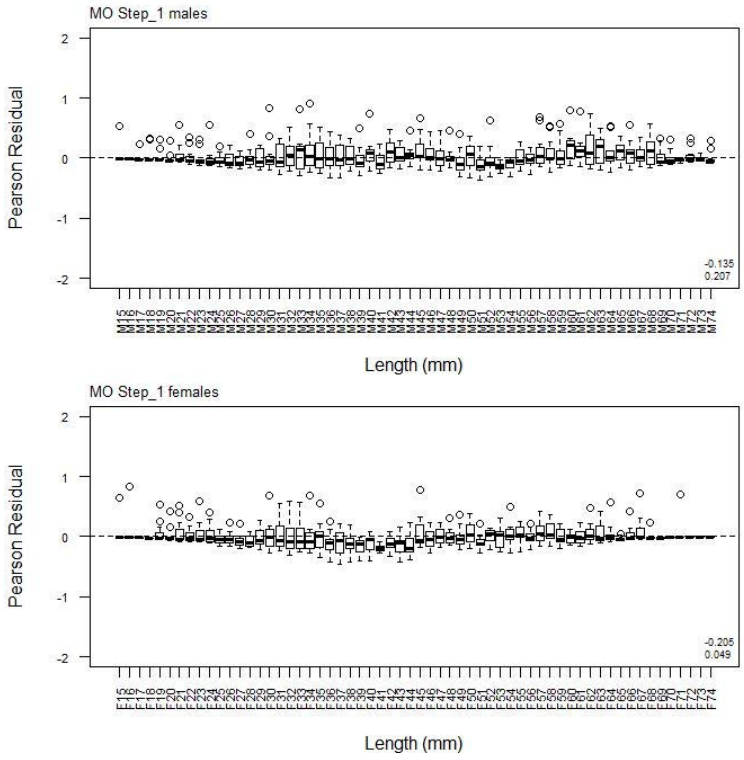

A4. 28: Box plots of Pearson residuals from the fit to length frequency distributions by length from observer sampling by sex for MO time step 1.

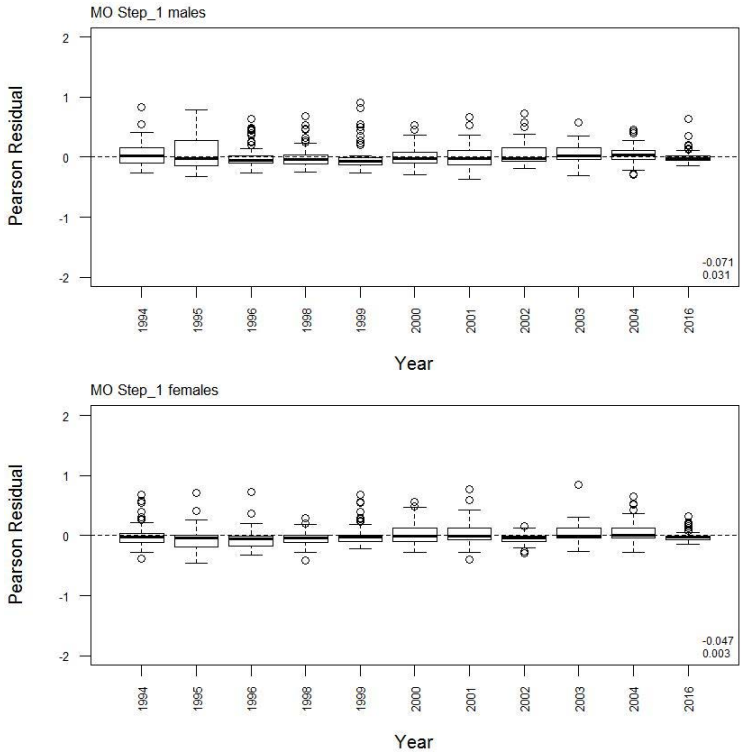

A4. 29: Box plots of Pearson residuals from the fit to length frequency distributions by year from observer sampling by sex for MO time step 1.

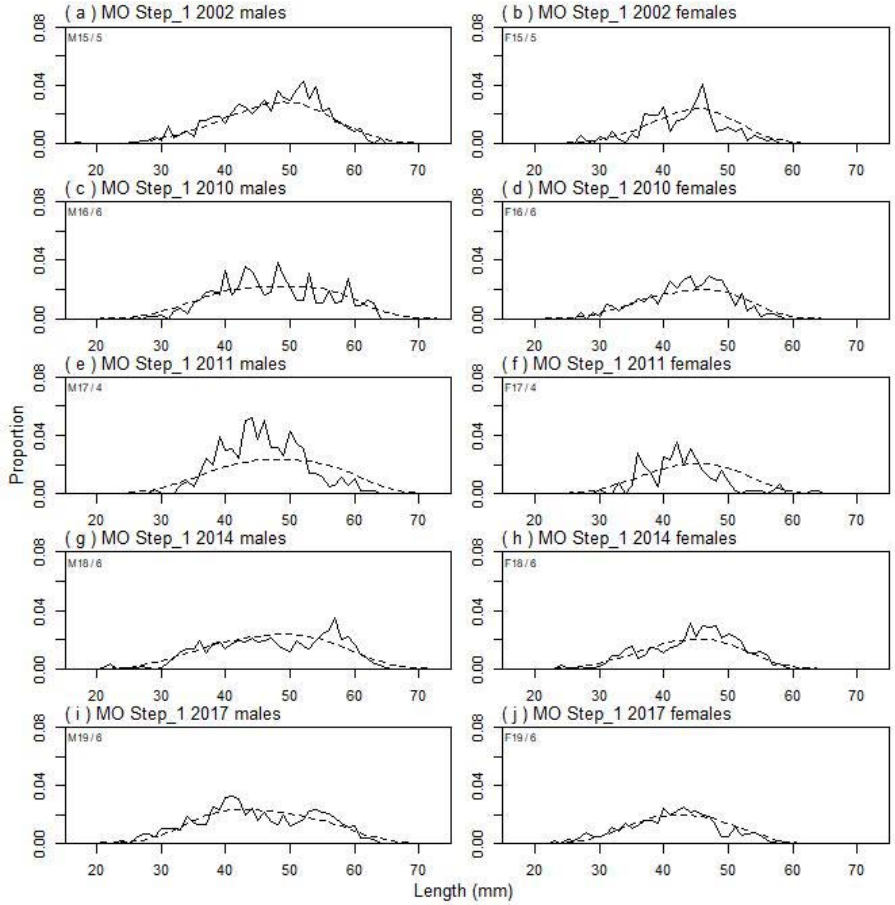

A4. 30: Observed (solid line) and fitted (dashed line) length frequency distributions for MO research survey samples.

A4. 31: Numbers of scampi measured, estimated multinomial N sample size, and effective sample size used within the model for length frequency distributions for MO research survey samples.

	Measured	Multinomial N	Effective sample size
N_2002	764	725	105.63
N_2010	551	627	91.35
N_2011	396	483	70.37
N_2014	1 465	1 363	198.58
N_2017	1 807	1 669	243.17

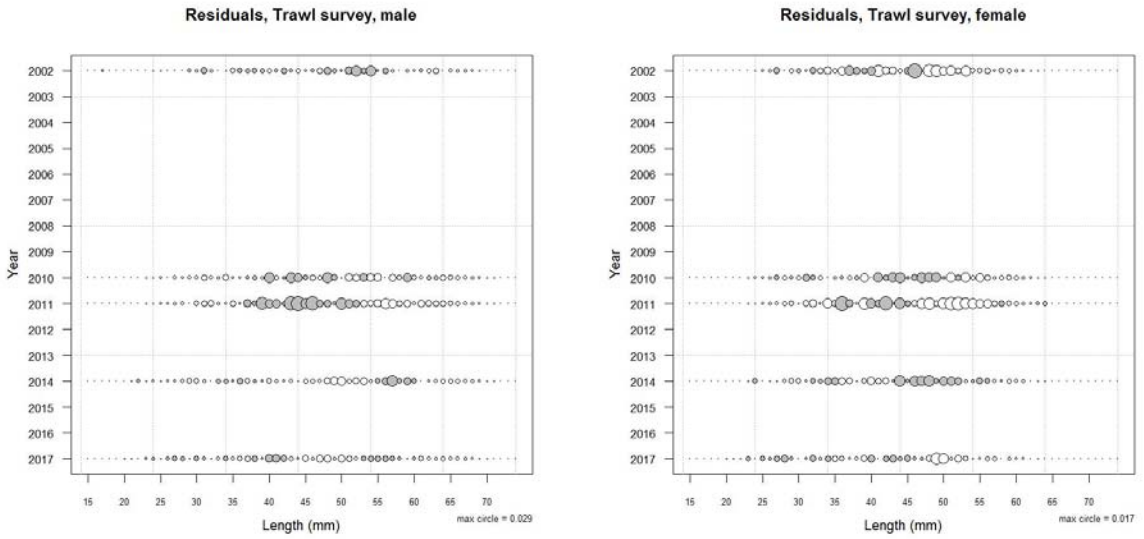

A4. 32: Bubble plots of residuals for fits to length frequency distributions for MO trawl sampling.

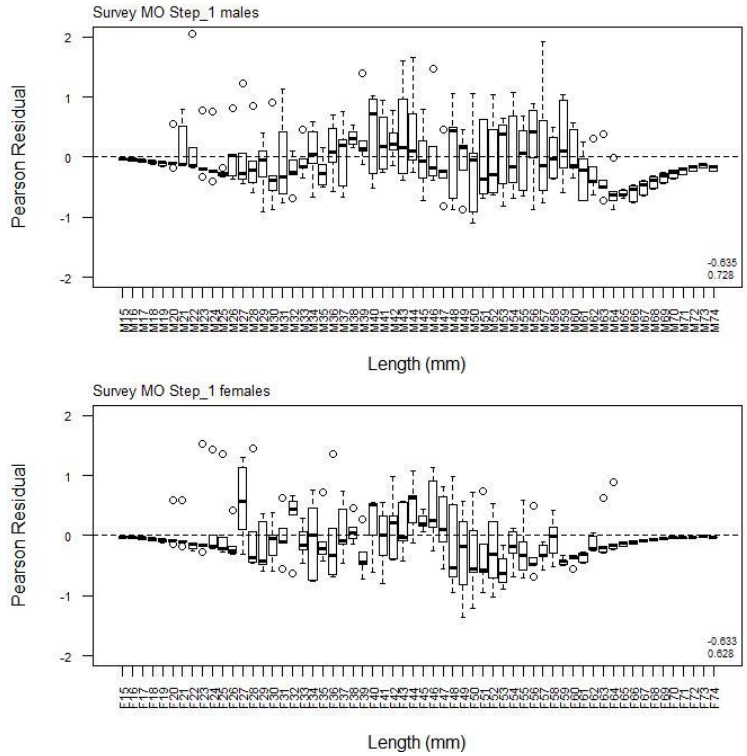

A4. 33: Box plots of Pearson residuals from the fit to length frequency distributions by length from MO trawl sampling.

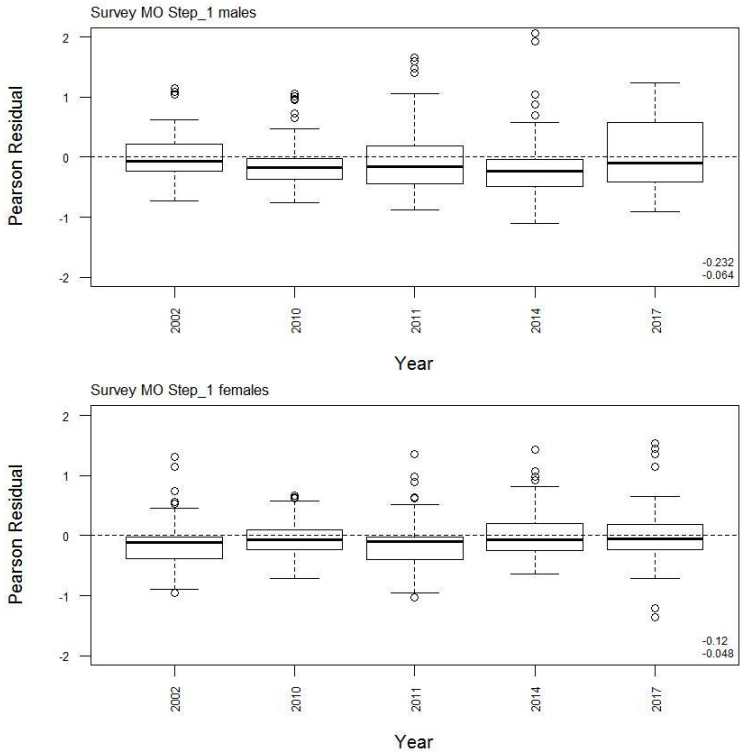

A4. 34: Box plots of Pearson residuals from the fit to length frequency distributions by year from MO trawl sampling.

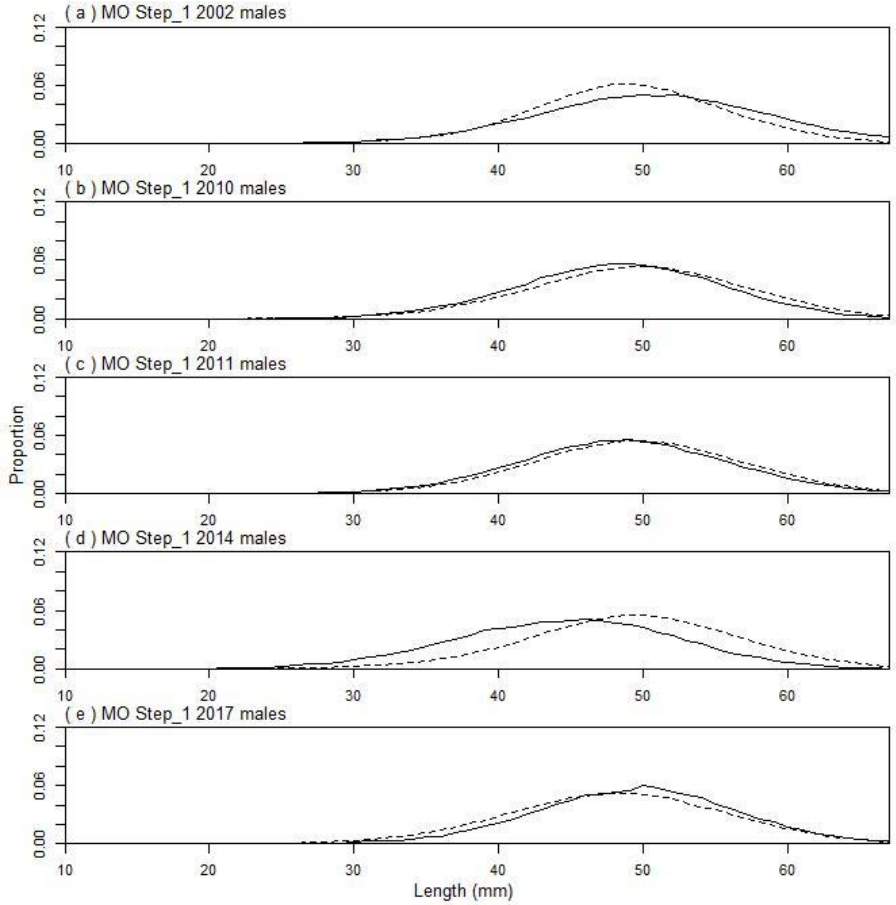

A4. 35: Observed (solid line) and fitted (dashed line) length frequency distributions for MO photographic survey scampi size estimation.

A4. 36: Numbers of scampi measured, estimated multinomial N sample size, and effective sample size used within the model for length frequency distributions for MO photographic survey samples.

	Measured	Multinomial N	Effective sample size
N_2002	224	384	12.99
N_2010	214	365	12.35
N_2011	426	536	18.14
N_2014	125	224	7.58
N_2017	76	145	4.91

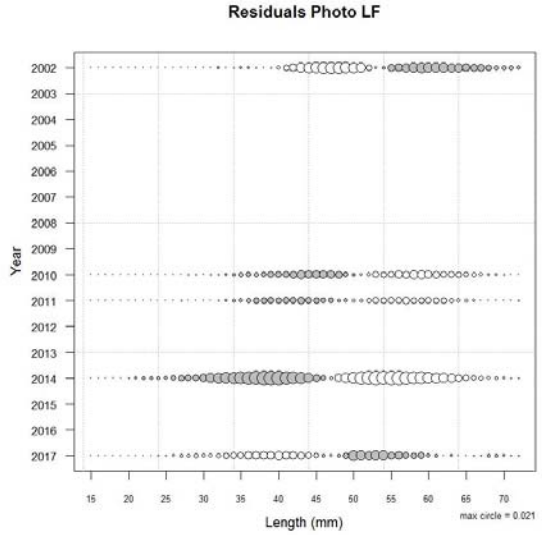

A4. 37: Bubble plots of residuals for fits to length frequency distributions for MO photographic sampling.

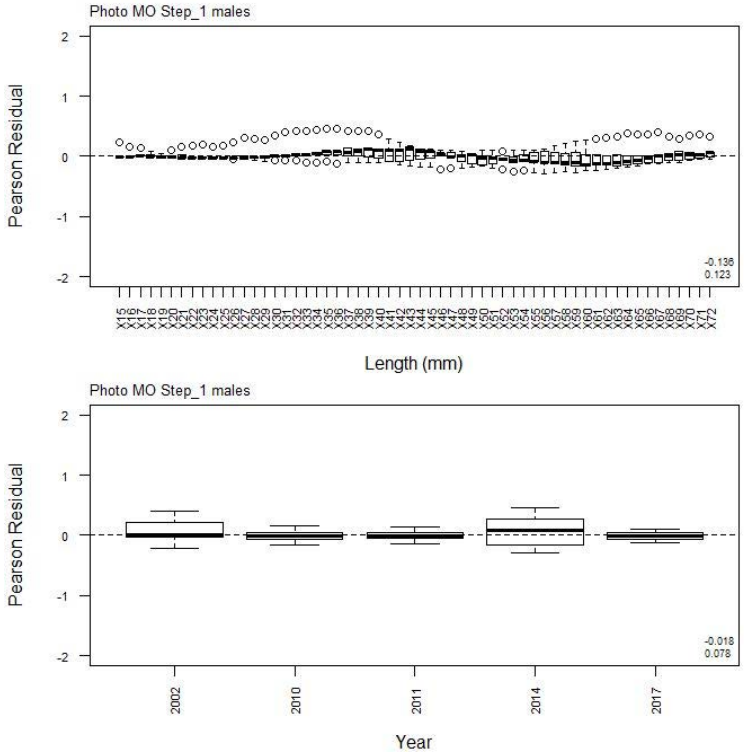

A4. 38: Box plots of Pearson residuals from the fit to length frequency distributions by length and year for MO photographic sampling.

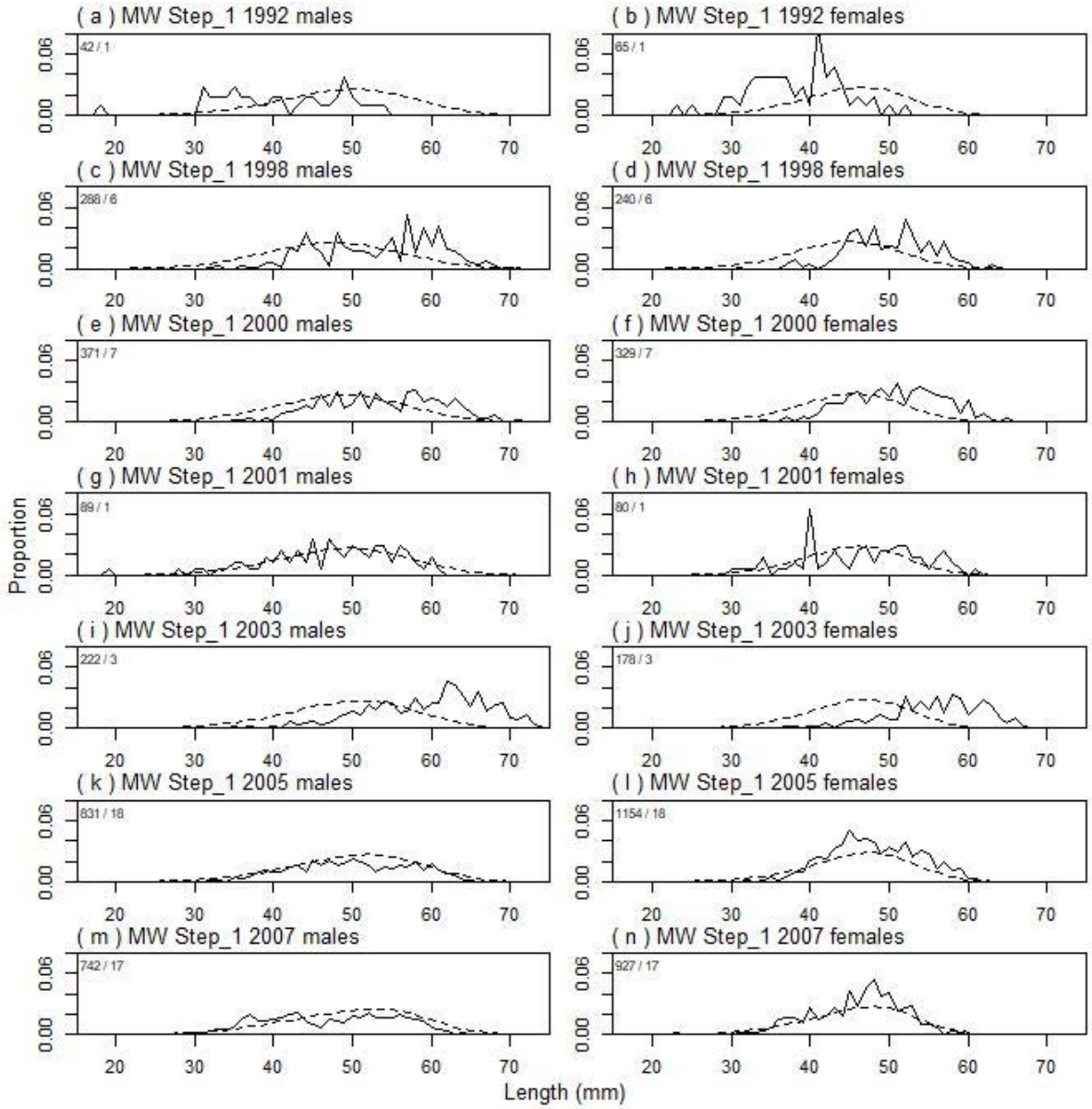

A4. 39: Observed (solid line) and fitted (dashed line) length frequency distributions for observer samples, MW time step 1. Numbers in top left corner of each plot represent number of scampi measured / number of events sampled.

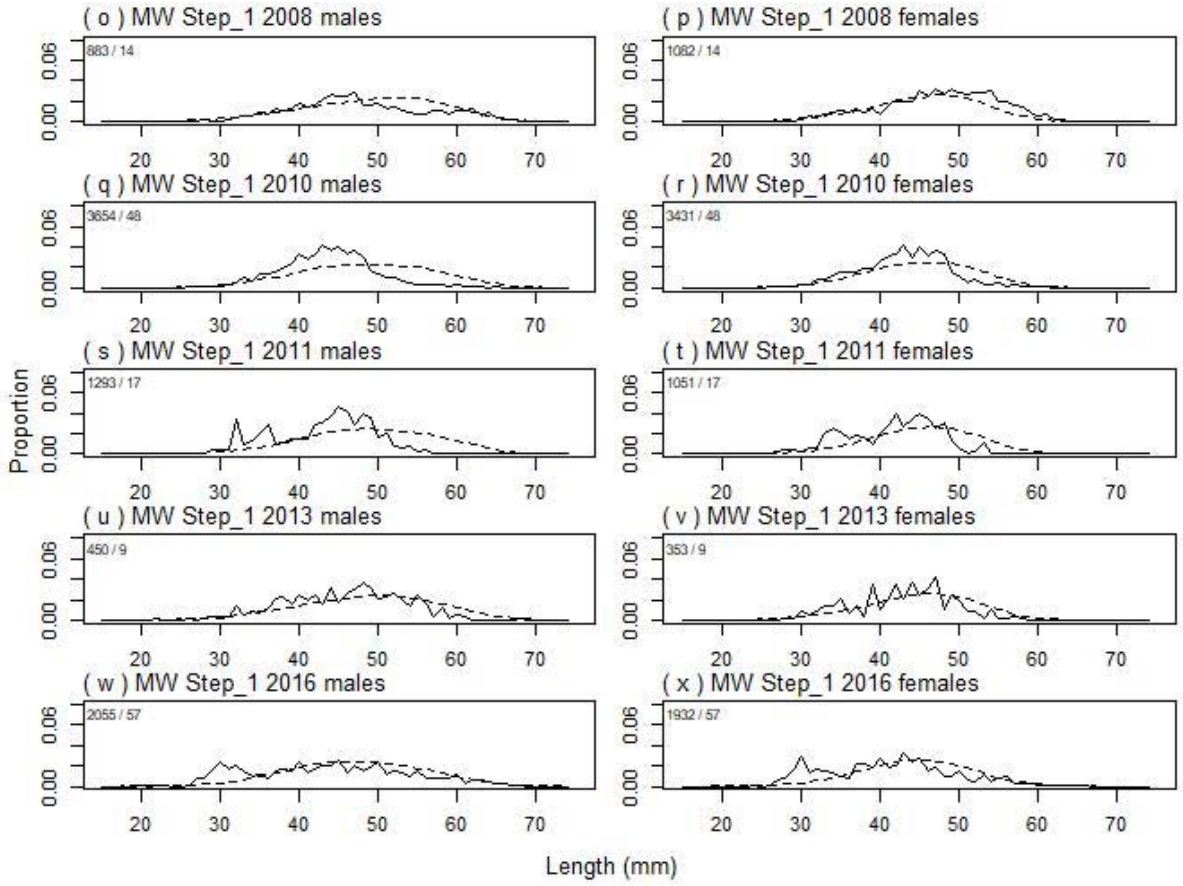

A4. 39 *continued*: Observed (solid line) and fitted (dashed line) length frequency distributions for observer samples, MW time step 1. Numbers in top left corner of each plot represent number of scampi measured / number of events sampled.

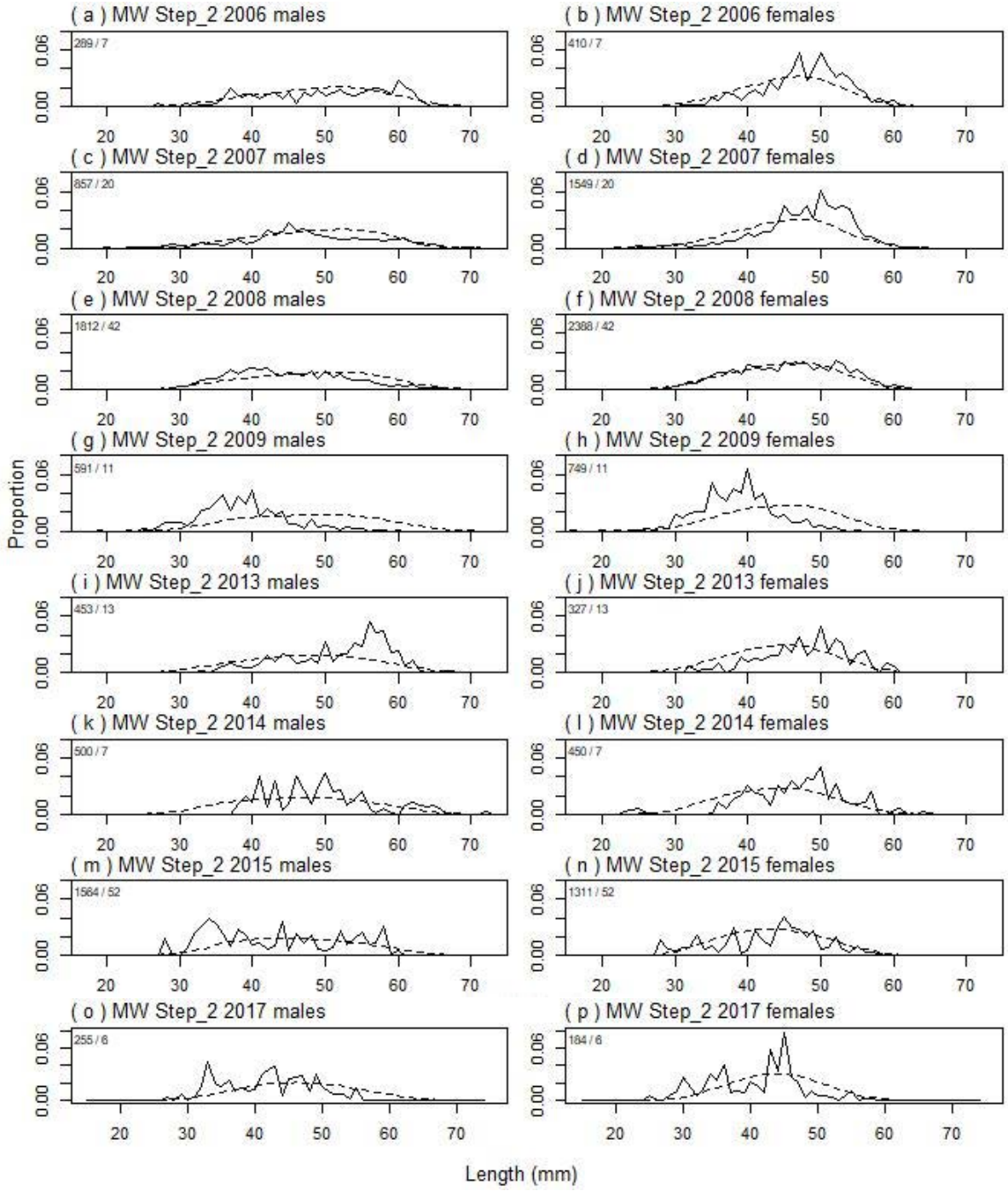

A4. 40: Observed (solid line) and fitted (dashed line) length frequency distributions for observer samples, MW time step 2. Numbers in top left corner of each plot represent number of scampi measured / number of events sampled.

A4. 41: Numbers of scampi measured, estimated multinomial N sample size, and effective sample size used within the model for length frequency distributions for observer samples, MW time step 1.

	Measured	Multinomial N	Effective sample size
N_1992	107	216	0.50
N_1998	528	394	0.91
N_2000	700	631	1.46
N_2001	169	341	0.79
N_2003	400	796	1.84
N_2005	1 985	908	2.10
N_2007	1 669	1 418	3.27
N_2008	1 965	1 743	4.03
N_2010	7 085	6 257	14.45
N_2011	2 344	1 739	4.02
N_2013	803	583	1.35
N_2016	3 987	3 475	8.03

A4. 42: Numbers of scampi measured, estimated multinomial N sample size, and effective sample size used within the model for length frequency distributions for observer samples, MW time step 2.

	Measured	Multinomial N	Effective sample size
N_2006	699	790	3.59
N_2007	2 406	2 144	9.75
N_2008	4 200	3 081	14.01
N_2009	1 340	1 366	6.21
N_2013	780	483	2.20
N_2014	950	1 710	7.78
N_2015	2 875	638	2.90
N_2017	439	232	1.06

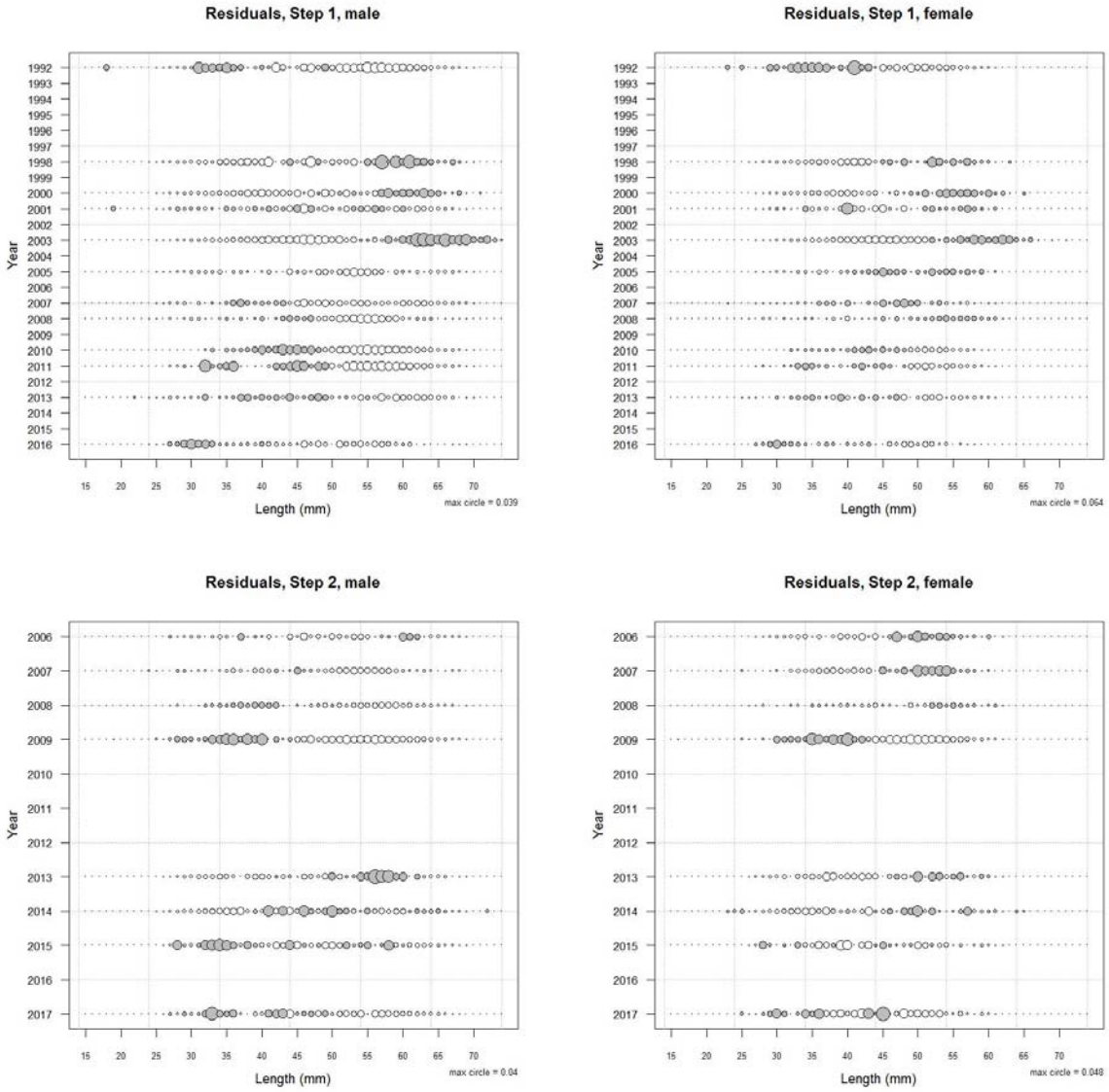

A4. 43: Bubble plots of residuals for fits to length frequency distributions for MW observer sampling.

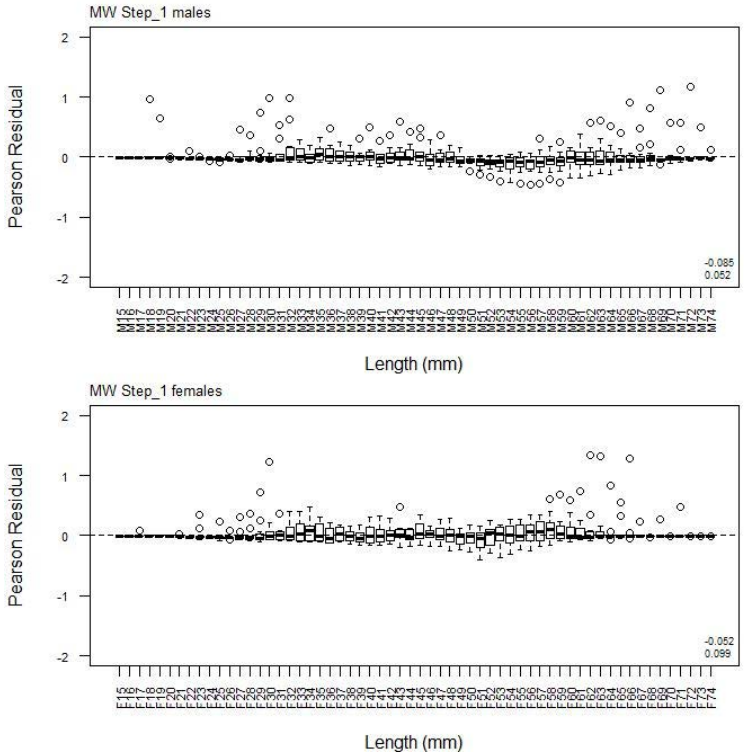

A4. 44: Box plots of Pearson residuals from the fit to length frequency distributions by length from observer sampling by sex for MW time step 1.

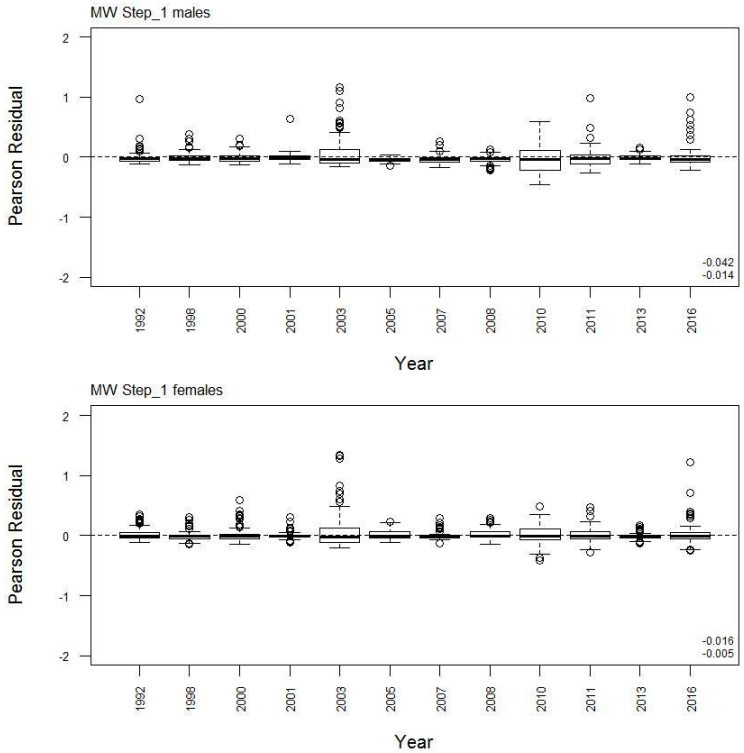

A4. 45: Box plots of Pearson residuals from the fit to length frequency distributions by year from observer sampling by sex for MW time step 1.

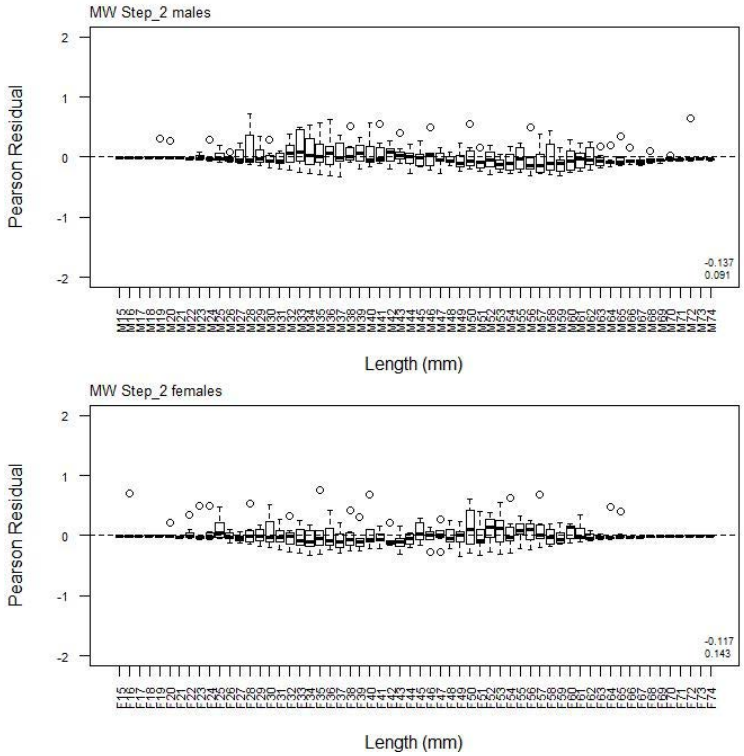

A4. 46: Box plots of Pearson residuals from the fit to length frequency distributions by length from observer sampling by sex for MW time step 2.

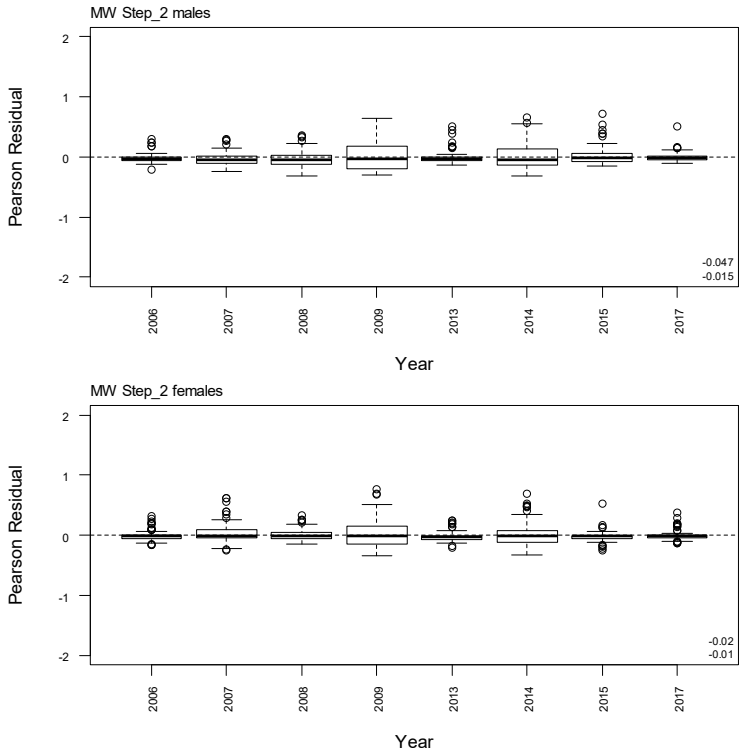

A4. 47: Box plots of Pearson residuals from the fit to length frequency distributions by year from observer sampling by sex for MW time step 2.

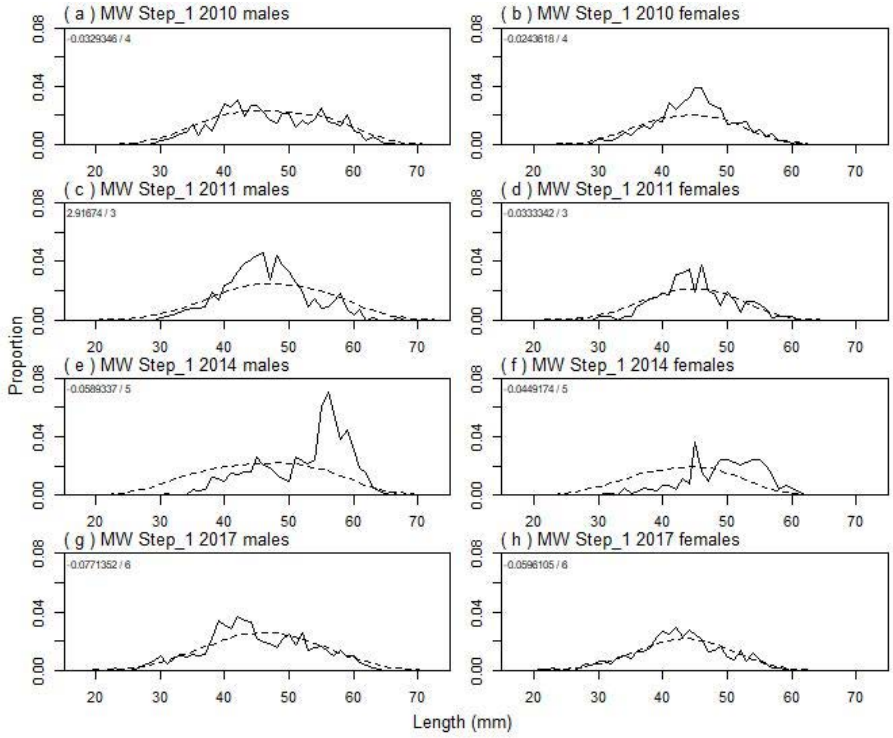

A4. 48: Observed (solid line) and fitted (dashed line) length frequency distributions for MW research survey samples.

A4. 49: Numbers of scampi measured, estimated multinomial N sample size, and effective sample size used within the model for length frequency distributions for MW research survey samples.

	Measured	Multinomial N	Effective sample size
N_2010	1 110	1 140	9.41
N_2011	876	1 011	8.35
N_2014	710	681	5.62
N_2017	1 734	1 776	14.66

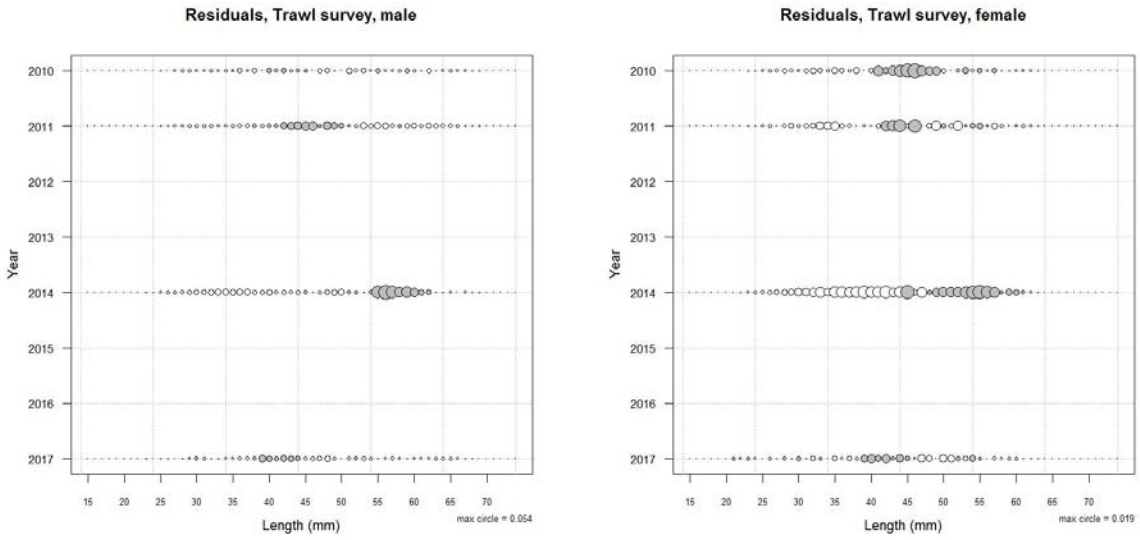

A4. 50: Bubble plots of residuals for fits to length frequency distributions for MW trawl sampling.

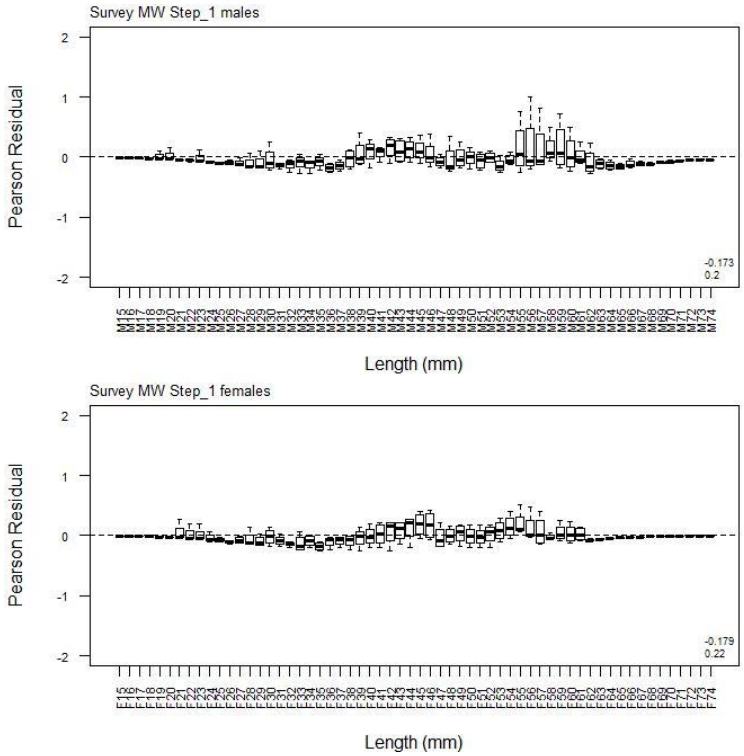

A4. 51: Box plots of Pearson residuals from the fit to length frequency distributions by length from MW trawl sampling.

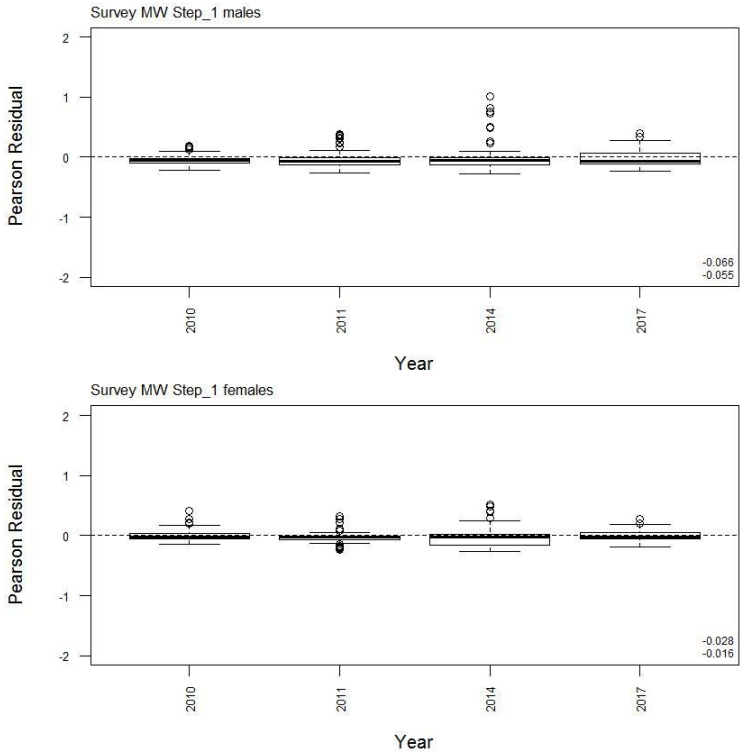

A4. 52: Box plots of Pearson residuals from the fit to length frequency distributions by year from MW trawl sampling.

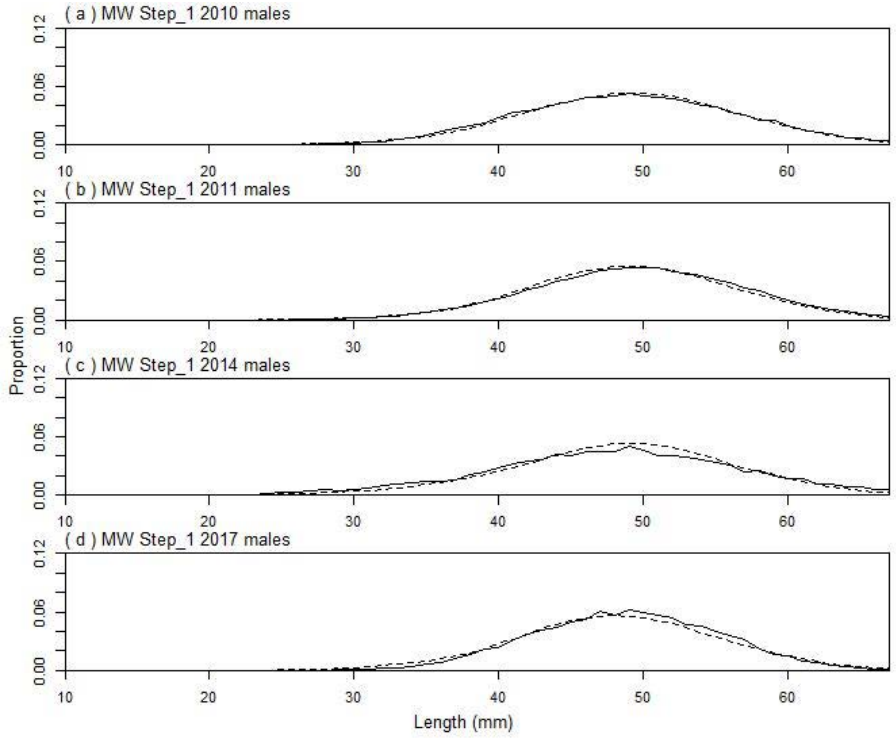

A4. 53: Observed (solid line) and fitted (dashed line) length frequency distributions for MW photographic survey scampi size estimation.

A4. 54: Numbers of scampi measured, estimated multinomial N sample size, and effective sample size used within the model for length frequency distributions for MW photographic survey samples.

	Measured	Multinomial N	Effective sample size
N_2010	173	298	722.80
N_2011	128	227	550.59
N_2014	24	48	116.42
N_2017	23	46	111.57

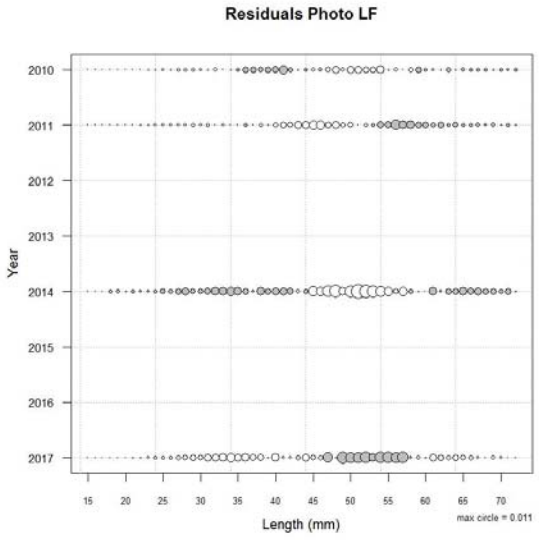

A4. 55: Bubble plots of residuals for fits to length frequency distributions for MW photographic sampling.

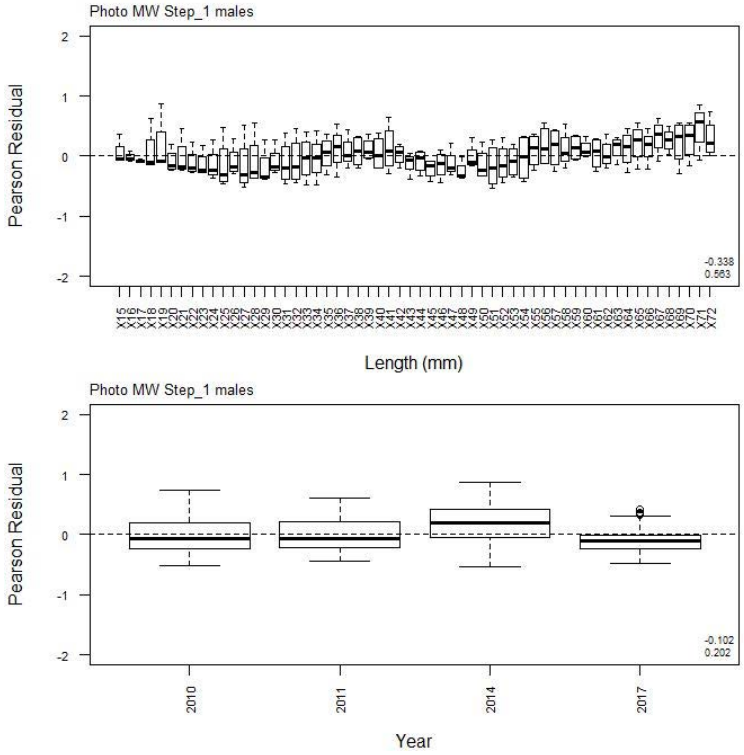

A4. 56: Box plots of Pearson residuals from the fit to length frequency distributions by length and year for MW photographic sampling.

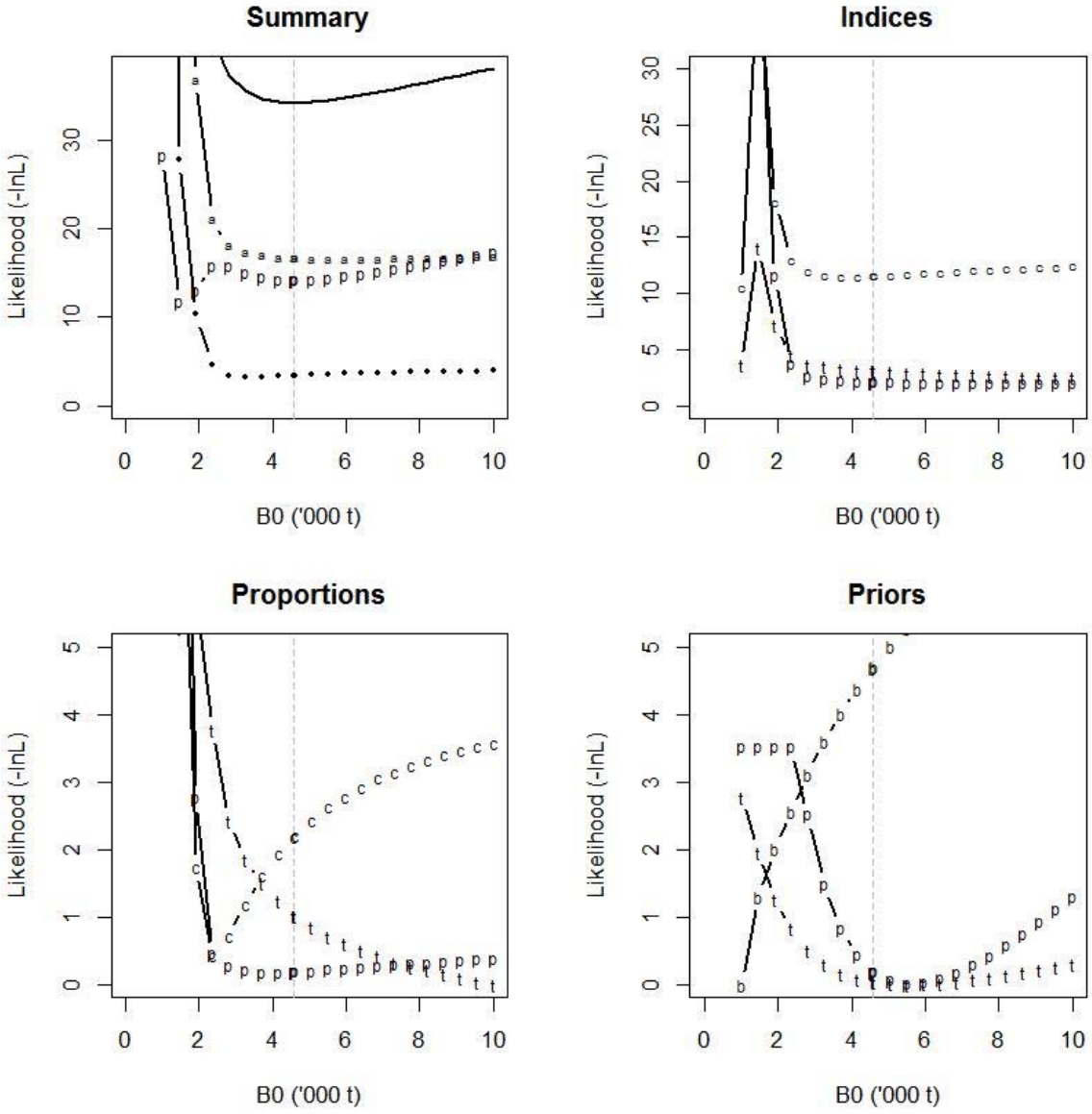

A4. 57: Likelihood profiles for SCI 3 Model 2 when B_0 is fixed in the model. Figures show profiles for main priors (top left, p – priors, a – abundance indices, • – proportions at length), abundance indices (top right, t – trawl survey, c – CPUE, p – photo survey), proportion at length data (bottom left, t–trawl, c – observer, p – photo) and priors (bottom right, b – B_0, p – *q-Photo*, t – *q-Trawl*). Vertical dashed line represents MPD.

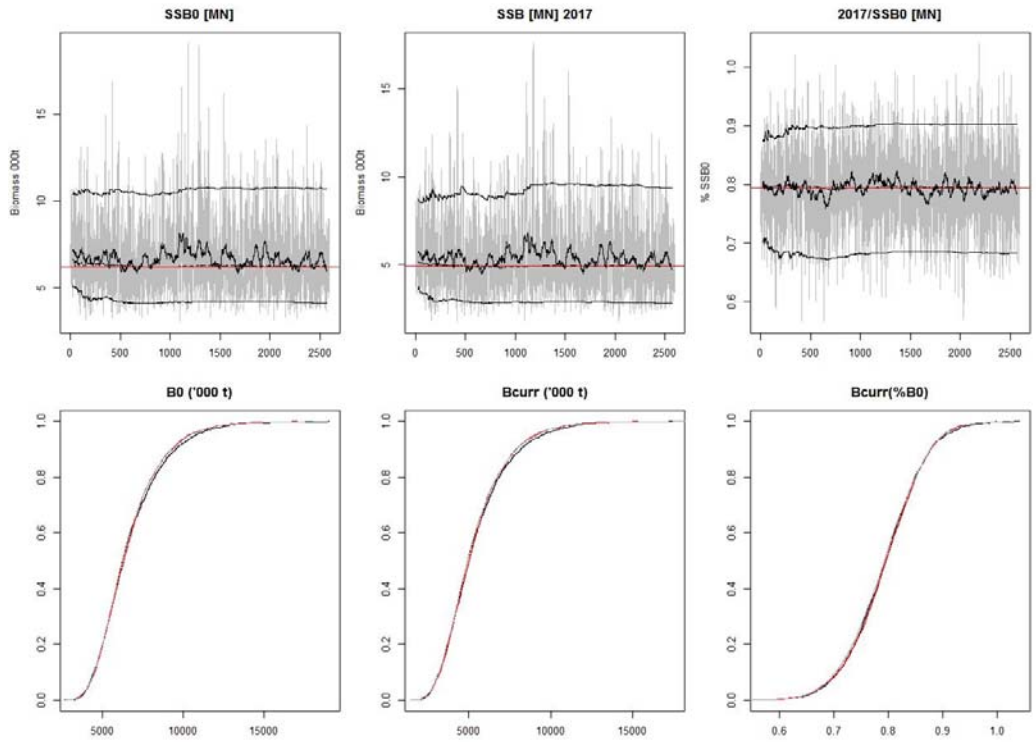

A4. 58: MCMC traces for MN SSB_0, SSB_{2017}, and SSB_{2017}/SSB_0 terms for SCI 3 Model 2 (nuisance q)(trace – grey line, cumulative moving median – dashed black line, moving average and cumulative moving 2.5%, 97.5% quantiles – solid black lines, overall median – solid red line, left plots); and cumulative frequency distributions for three independent MCMC chains (shown as red, grey, and black lines, right plots).

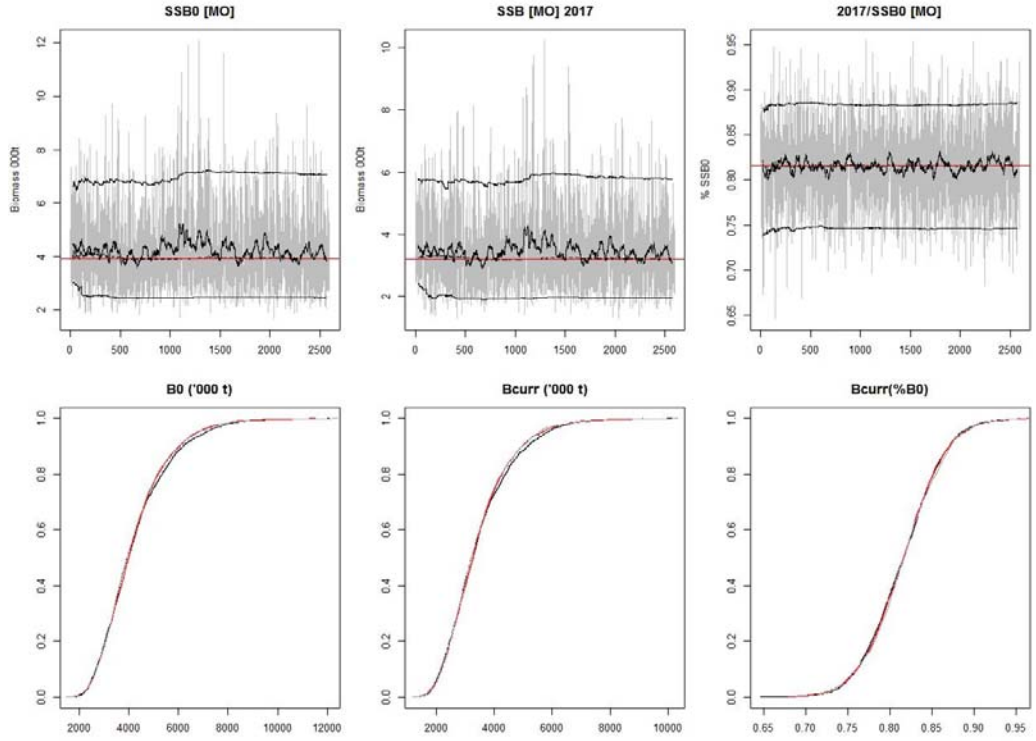

A4. 59: MCMC traces for MO SSB_0, SSB_{2017}, and SSB_{2017}/SSB_0 terms for SCI 3 Model 2 (nuisance q)(trace – grey line, cumulative moving median – dashed black line, moving average and cumulative moving 2.5%, 97.5% quantiles – solid black lines, overall median – solid red line, left plots); and cumulative frequency distributions for three independent MCMC chains (shown as red, grey, and black lines, right plots).

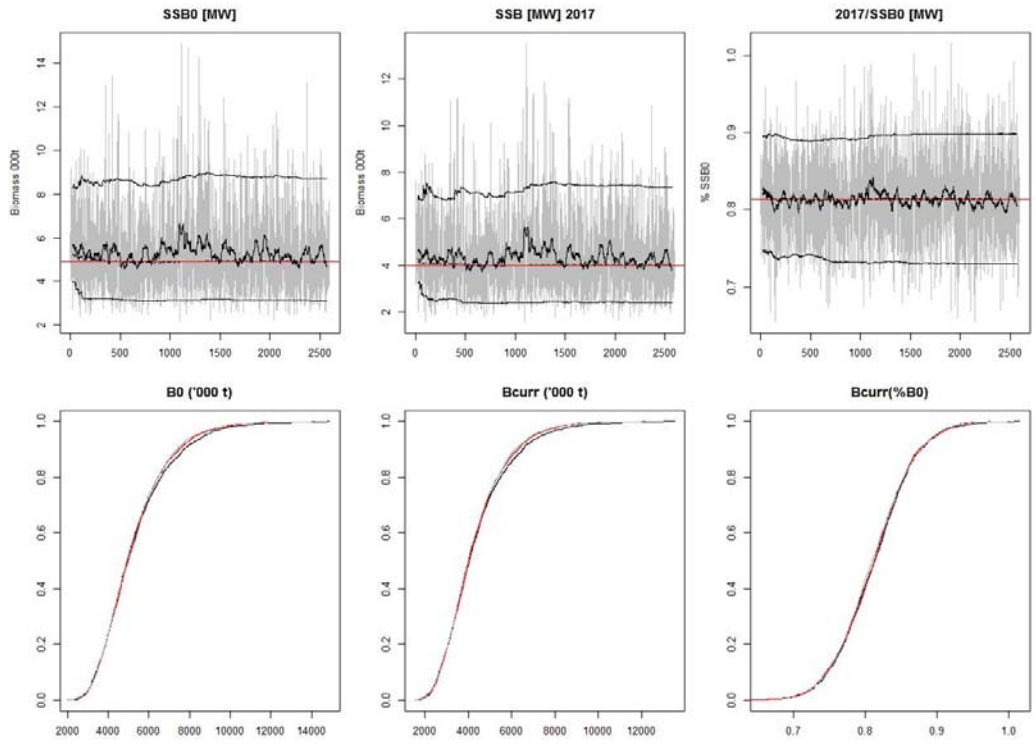

A4. 60: MCMC traces for MW SSB_0, SSB_{2017}, and SSB_{2017}/SSB_0 terms for SCI 3 Model 2 (nuisance q)(trace – grey line, cumulative moving median – dashed black line, moving average and cumulative moving 2.5%, 97.5% quantiles – solid black lines, overall median – solid red line, left plots); along with cumulative frequency distributions for three independent MCMC chains (shown as red, grey, and black lines, right plots).

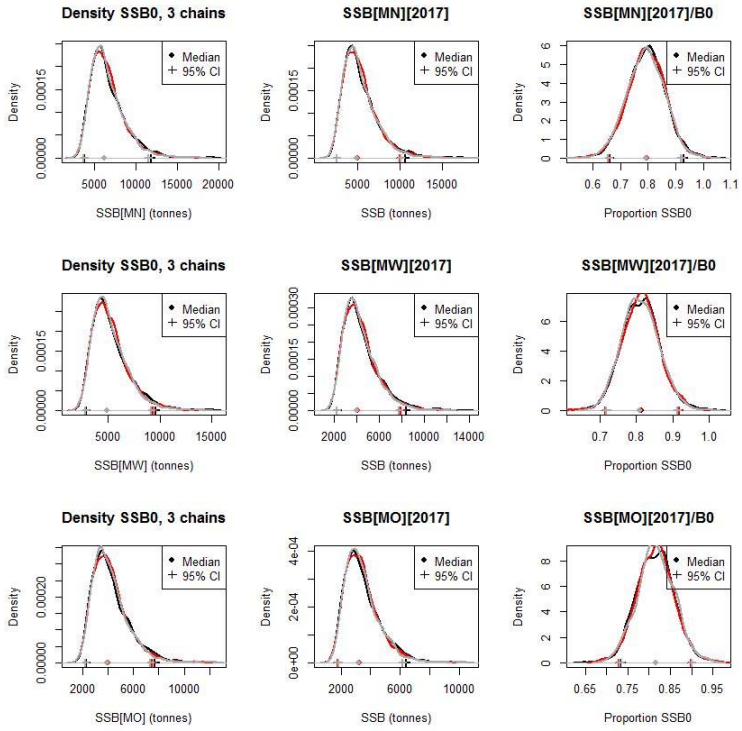

A4. 61: Density plots for SSB_0, SSB_{2017}, and SSB_{2017}/SSB_0 terms for each subarea of SCI 3 Model 2 for three independent MCMC chains, with median and 95% confidence intervals.

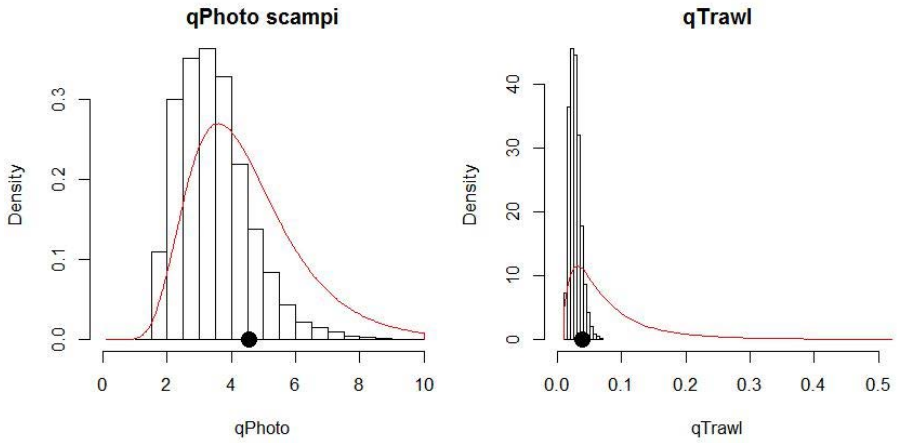

A4. 62: Marginal posterior distributions (histograms), MPD estimates (solid symbols), and distributions of priors (lines) for catchability terms.

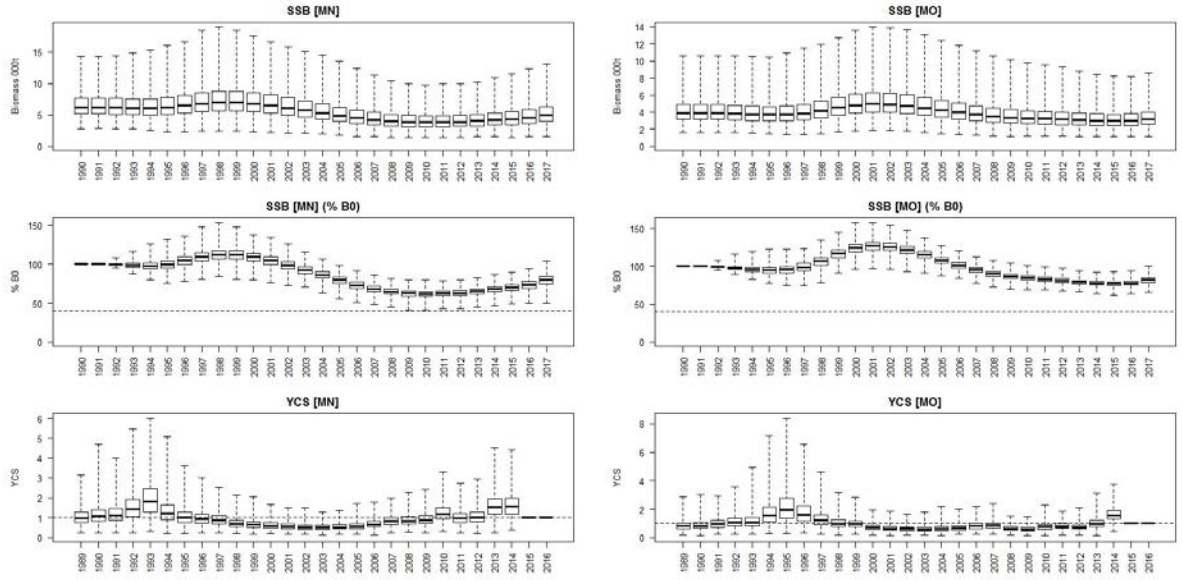

A4. 63: Posterior trajectory of *SSB*, SSB_{2016}/SSB_0, and YCS for subareas MN and MO.

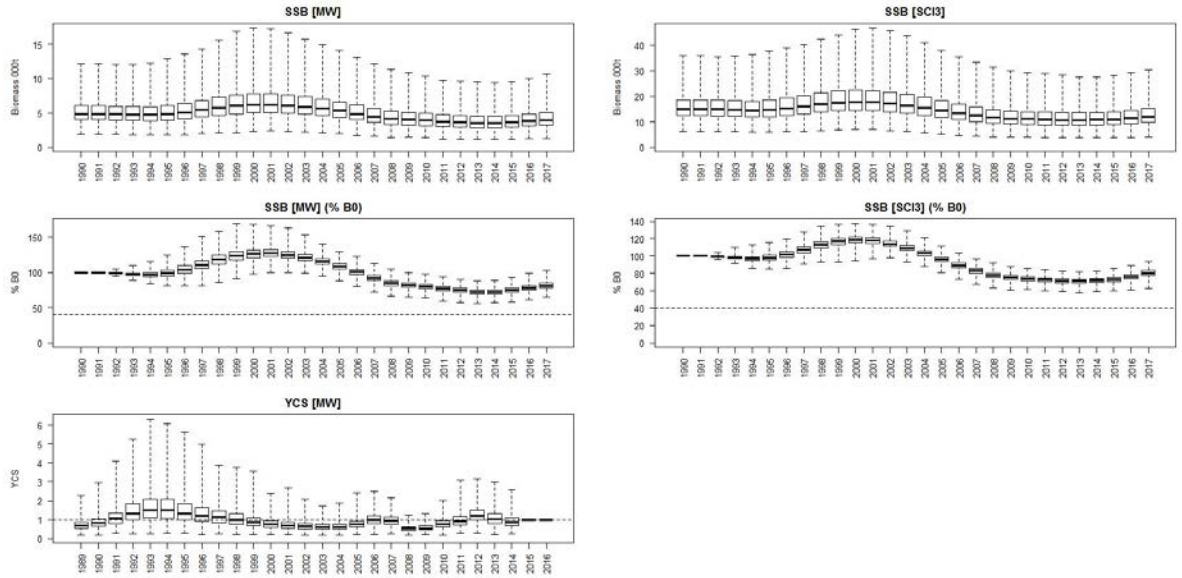

A4. 64: Posterior trajectory of *SSB*, SSB_{2016}/SSB_0, and YCS for subareas MW and the combined SCI 3 modelled area.

APPENDIX 5: MODEL 3, *M* fixed at 0.20, CPUE process error 0.2

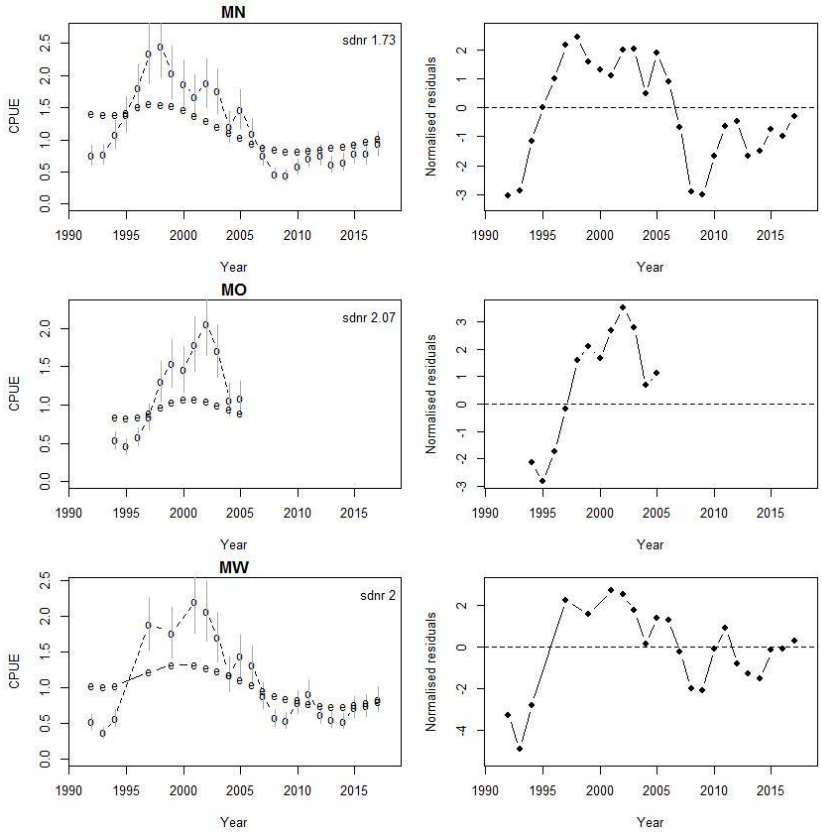

A5. 1: Fits to CPUE indices (left column) and normalised residuals (right column) by subarea (MN - top row, MO - middle row, MW - bottom row) for SCI 3 Model 3.

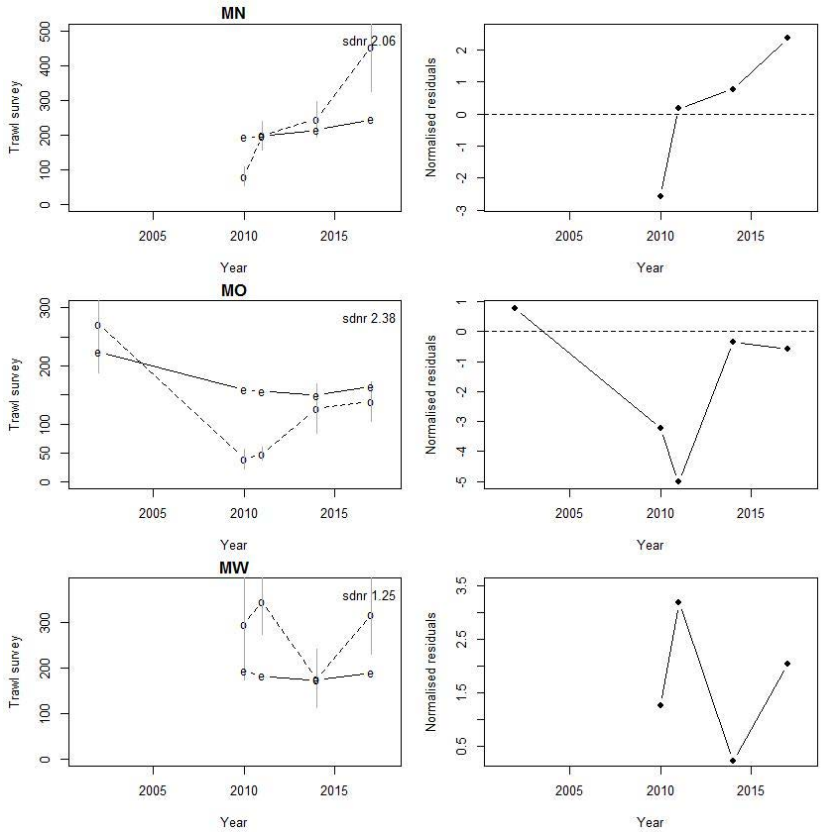

A5. 2: Fits to trawl survey indices (left column) and normalised residuals (right column) by subarea (MN - top row, MO - middle row, MW - bottom row) for SCI 3 Model 3.

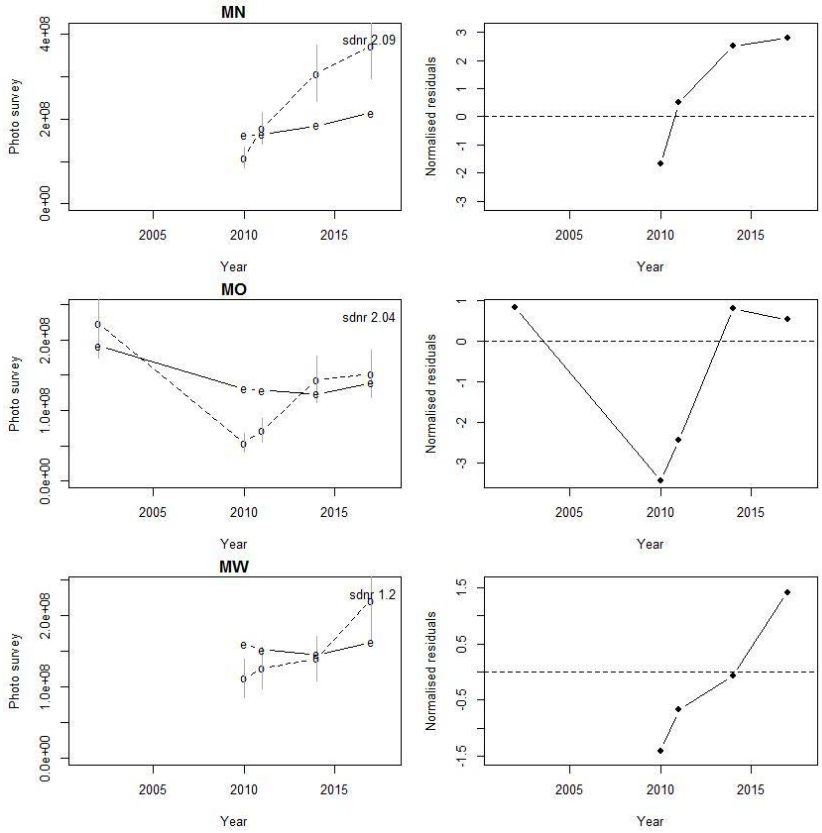

A5. 3: Fits to photo survey indices (left column) and normalised residuals (right column) by subarea (MN - top row, MO - middle row, MW - bottom row) for SCI 3 Model 3.

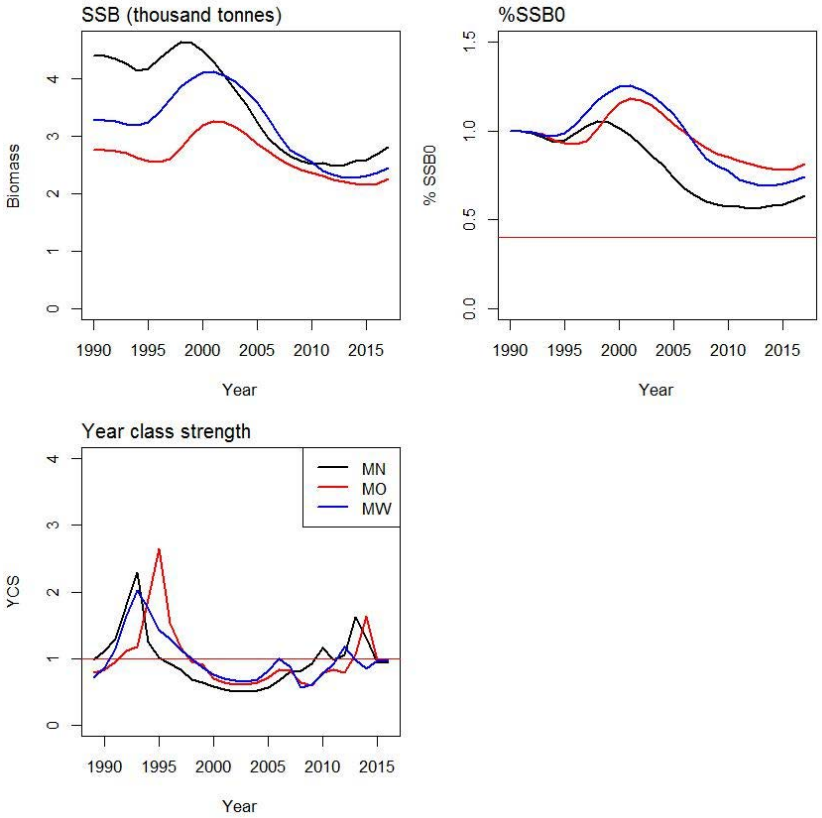

A5. 4: Spawning stock biomass trajectory (upper left), Spawning stock biomass as a percentage of SSB_0 (upper right), and year class strength (lower plot) by subarea for SCI 3 Model 3.

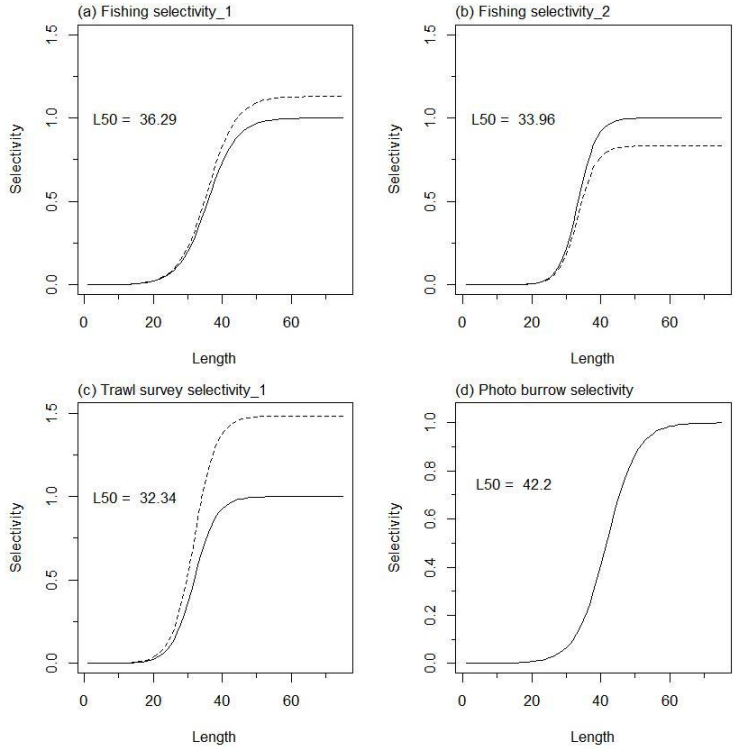

A5. 5: Spawning stock biomass trajectory (upper left), Spawning stock biomass as a percentage of SSB_0 (upper right), and year class strength (lower plot) by subarea for SCI 3 Model 3.

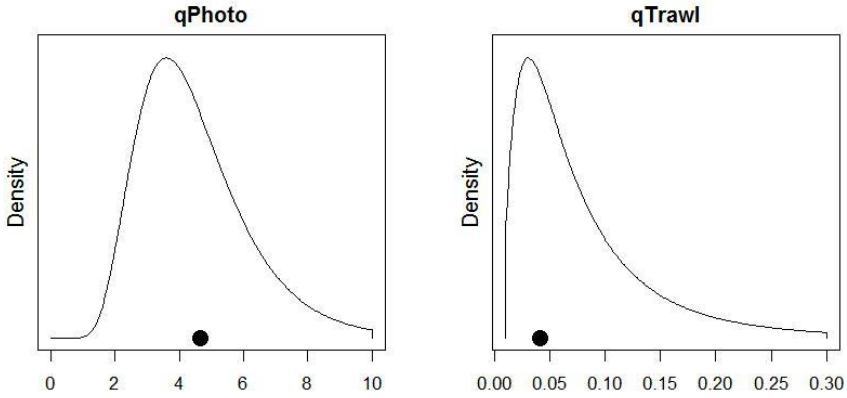

A5. 6: Catchability estimates from MPD model run for SCI 3 Model 3, plotted in relation to prior distribution.

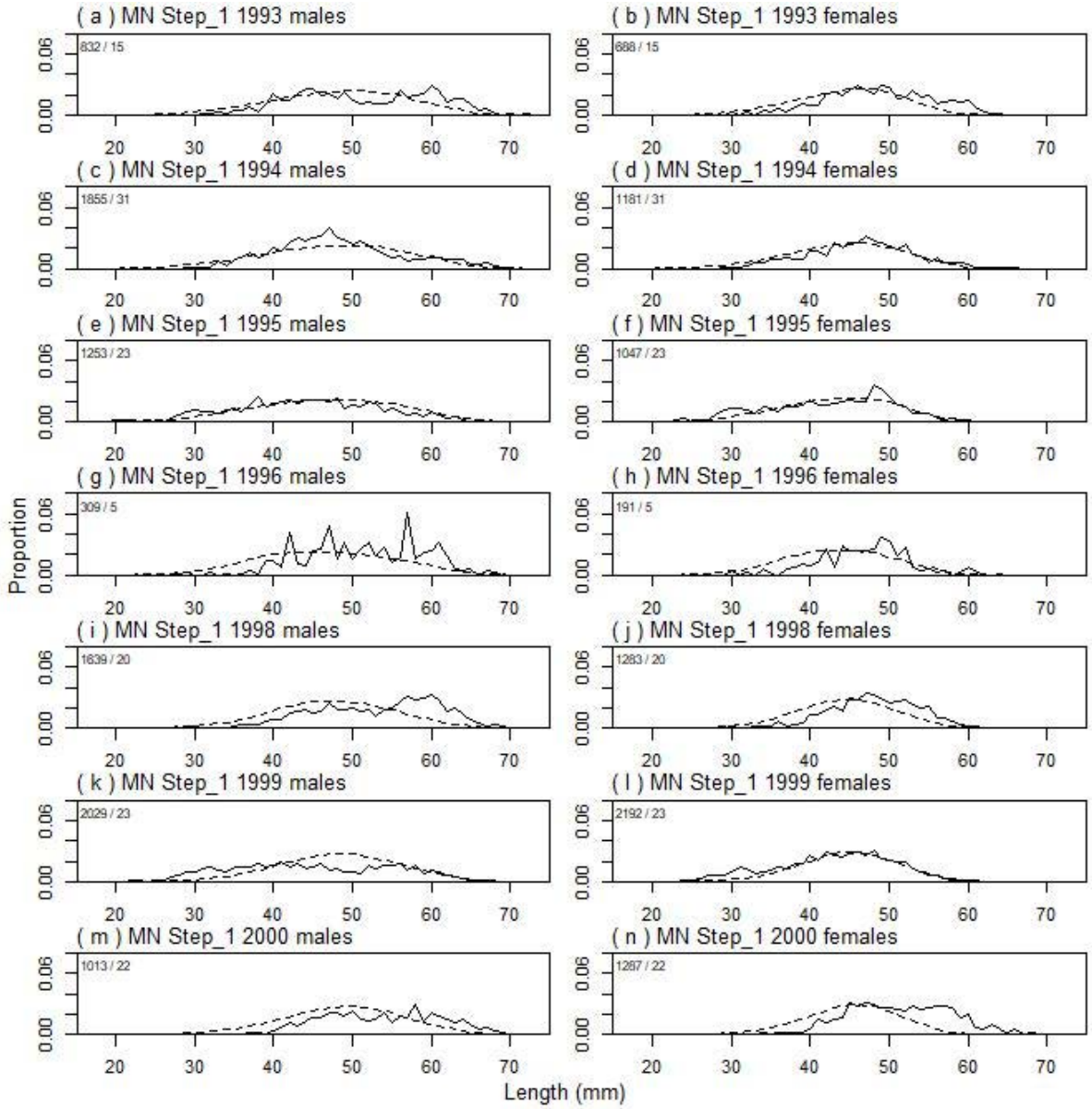

A5. 7: Observed (solid line) and fitted (dashed line) length frequency distributions for observer samples, MN time step 1. Numbers in top left corner of each plot represent number of scampi measured / number of events sampled.

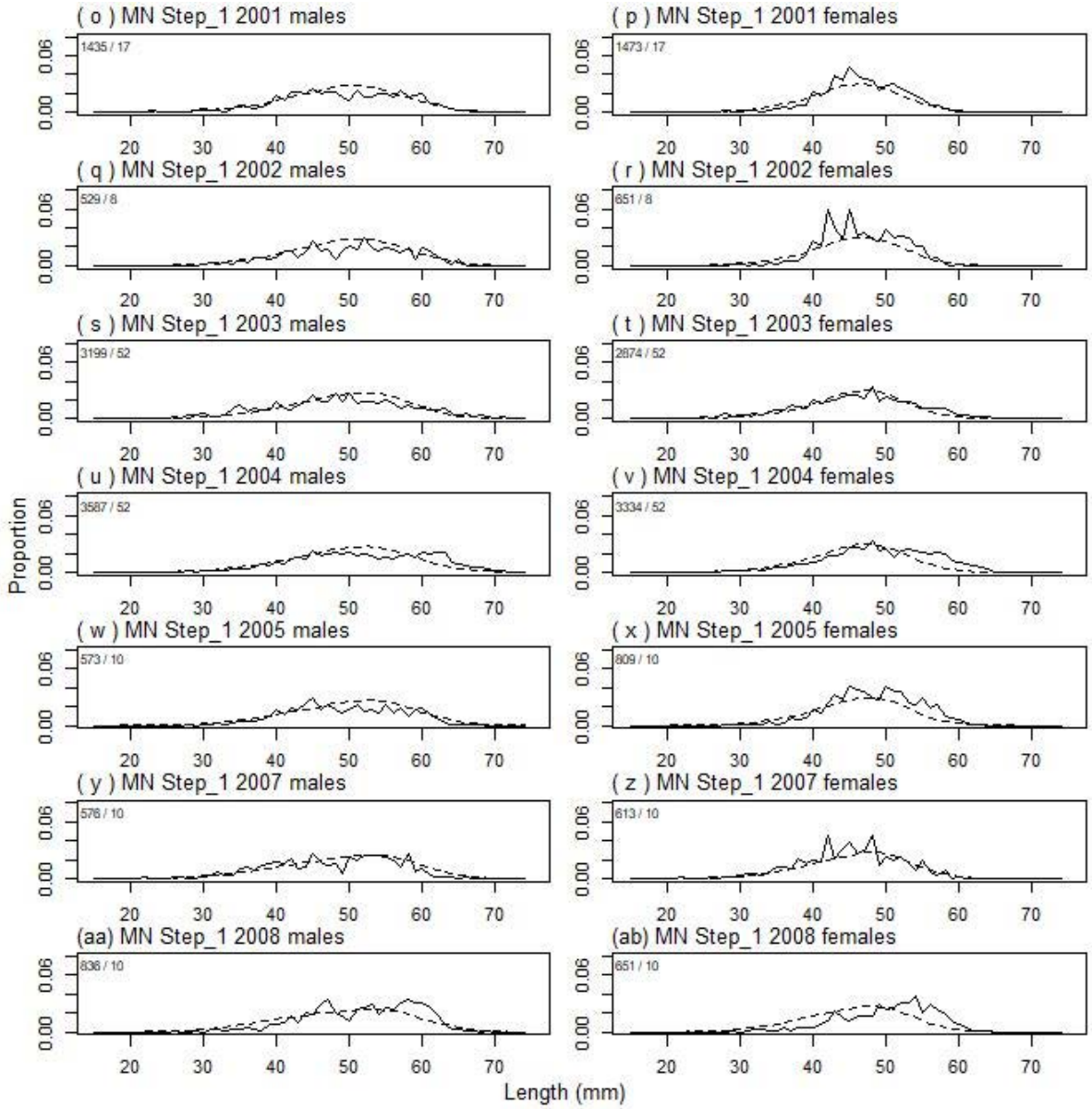

A5. 7 *continued*: Observed (solid line) and fitted (dashed line) length frequency distributions for observer samples, MN time step 1. Numbers in top left corner of each plot represent number of scampi measured / number of events sampled.

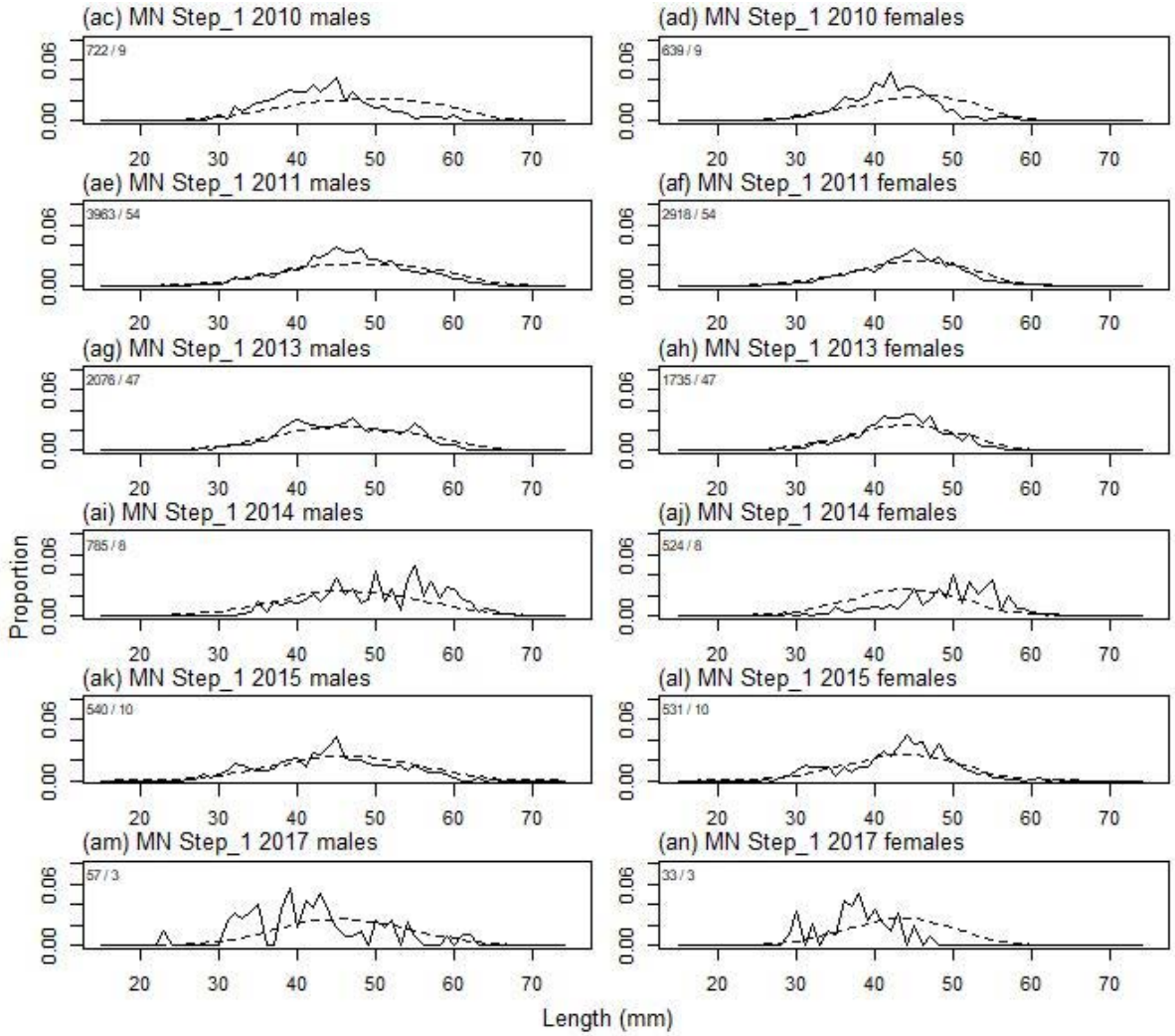

A5. 7 *continued*: Observed (solid line) and fitted (dashed line) length frequency distributions for observer samples, MN time step 1. Numbers in top left corner of each plot represent number of scampi measured / number of events sampled.

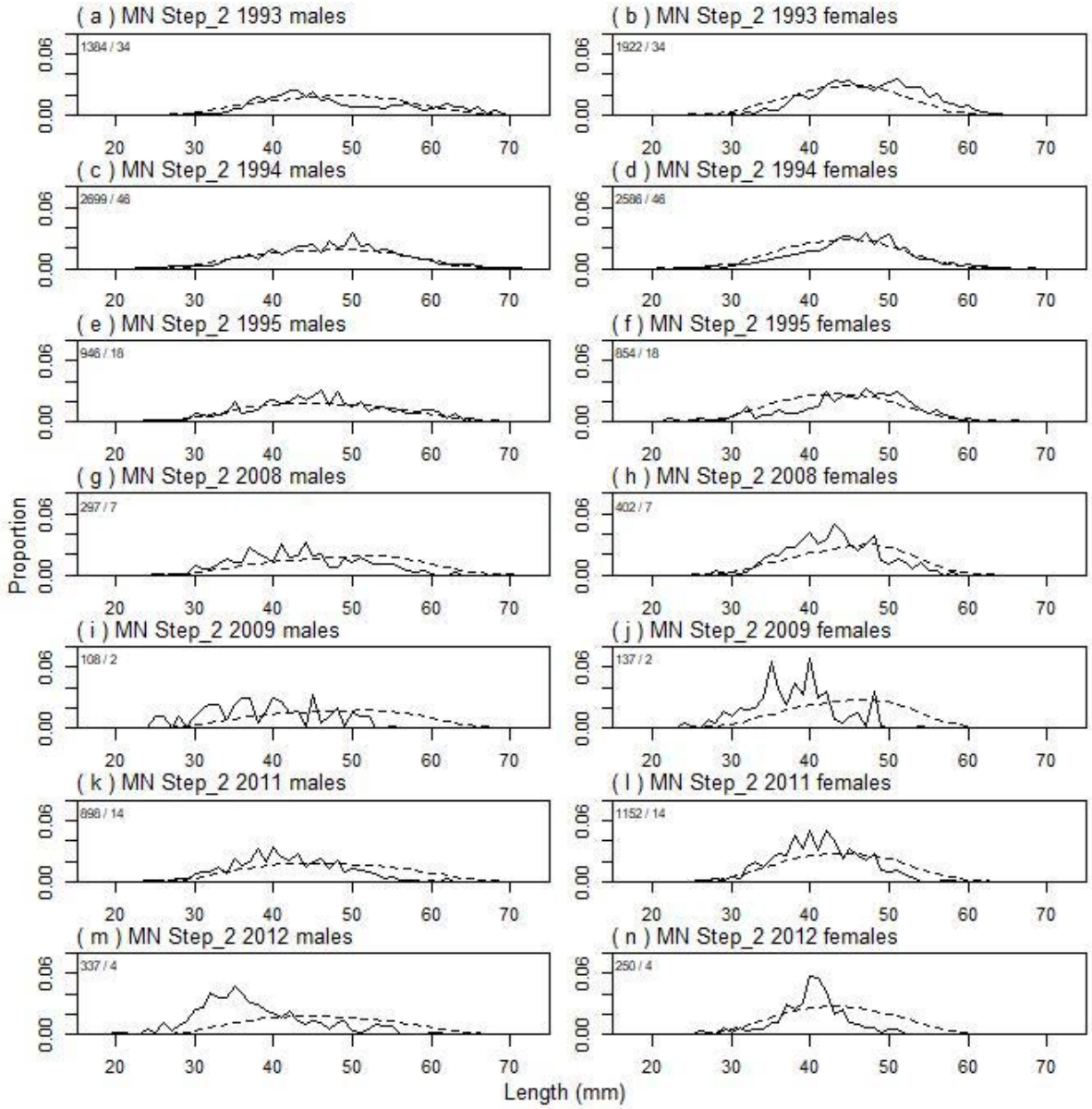

A5. 8: Observed (solid line) and fitted (dashed line) length frequency distributions for observer samples, MN time step 2. Numbers in top left corner of each plot represent number of scampi measured / number of events sampled.

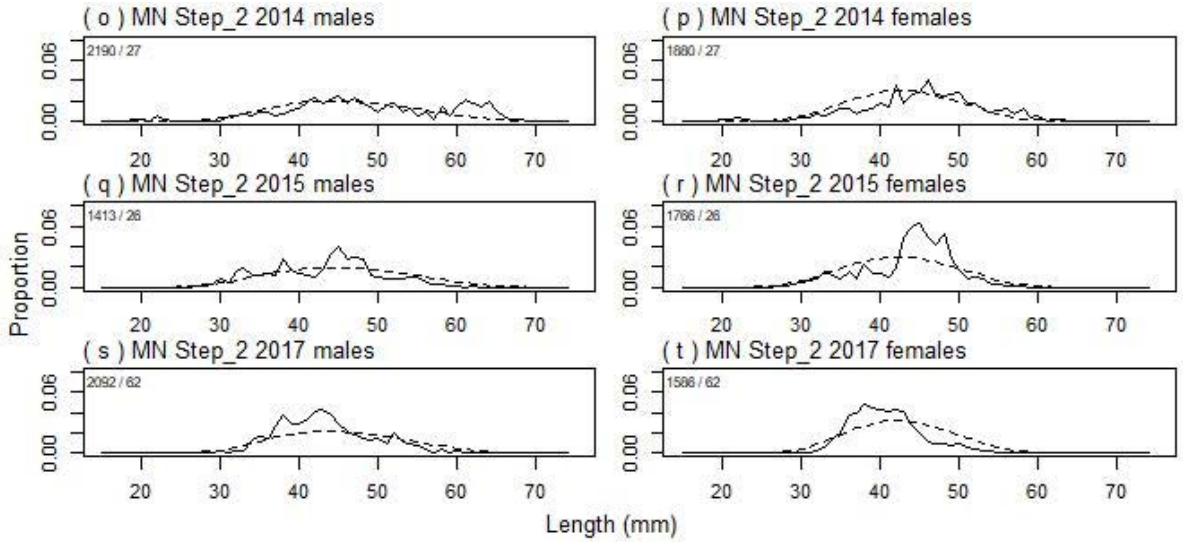

A5. 8 *continued*: Observed (solid line) and fitted (dashed line) length frequency distributions for observer samples, MN time step 2. Numbers in top left corner of each plot represent number of scampi measured / number of events sampled.

A5. 9: Numbers of scampi measured, estimated multinomial N sample size, and effective sample size used within the model for length frequency distributions for observer samples, time step 1.

	Measured	Multinomial N	Effective sample size
N_1993	1 520	1 345	5.87
N_1994	3 036	2 264	9.88
N_1995	2 300	1 824	7.96
N_1996	500	576	2.51
N_1998	2 922	2 599	11.35
N_1999	4 221	3 441	15.02
N_2000	2 300	1 928	8.42
N_2001	2 908	2 827	12.34
N_2002	1 180	988	4.31
N_2003	6 073	3 727	16.27
N_2004	6 921	5 077	22.16
N_2005	1 382	2 030	8.86
N_2007	1 189	2 414	10.54
N_2008	1 487	1 651	7.21
N_2010	1 361	1 544	6.74
N_2011	6 881	4 896	21.37
N_2013	3 811	2 929	12.79
N_2014	1 309	745	3.25
N_2015	1 071	2 071	9.04
N_2017	90	181	0.79

A5. 10: Numbers of scampi measured, estimated multinomial N sample size, and effective sample size used within the model for length frequency distributions for observer samples, MN time step 2.

	Measured	Multinomial N	Effective sample size
N_1993	3 306	2 571	15.26
N_1994	5 285	4 117	24.44
N_1995	1 800	1 501	8.91
N_2008	699	713	4.23
N_2009	245	340	2.02
N_2011	2 050	1 583	9.40
N_2012	587	691	4.10
N_2014	4 071	1 270	7.54
N_2015	3 179	5 855	34.76
N_2017	3 678	1 906	11.31

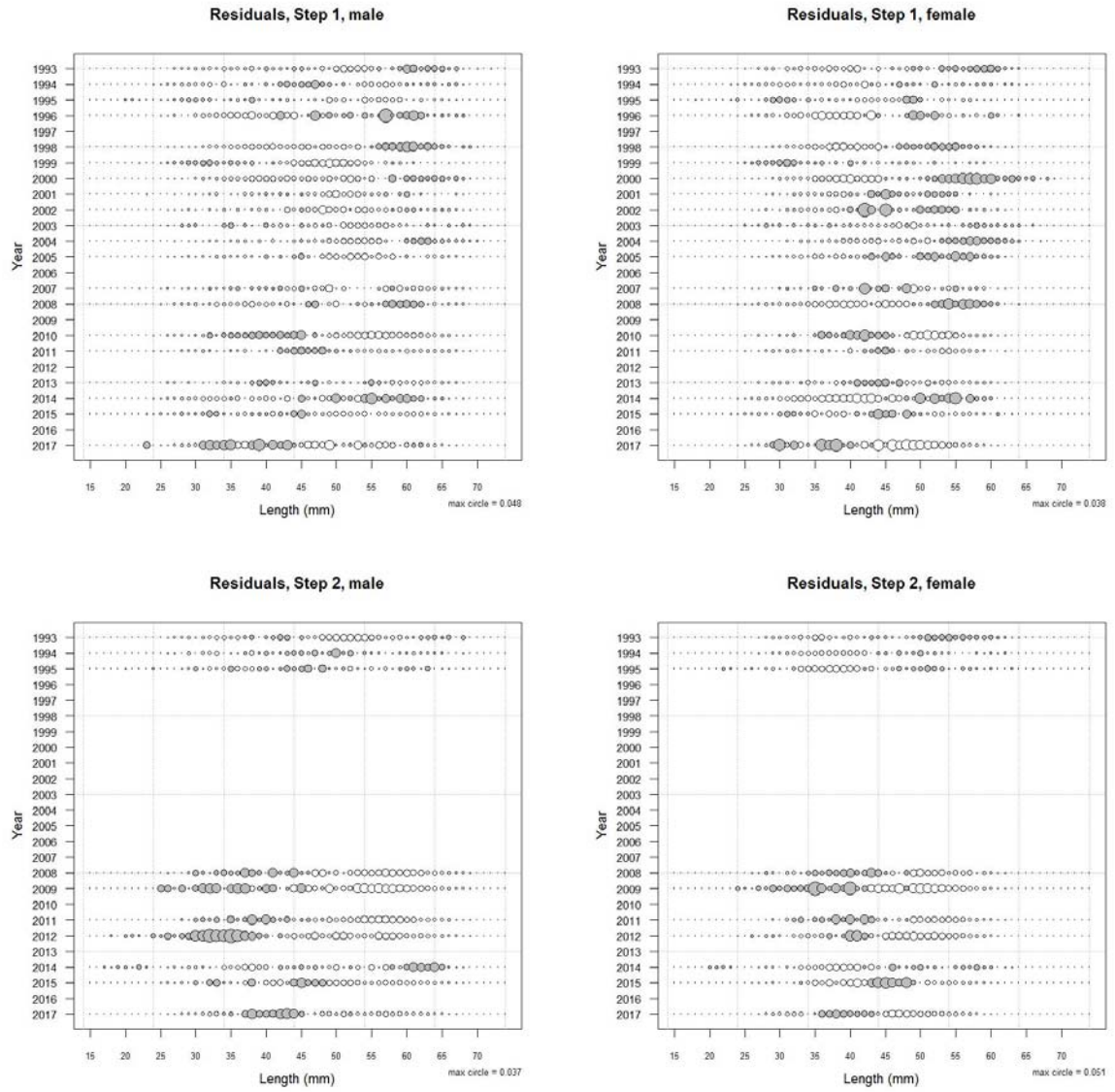

A5. 11: Bubble plots of residuals for fits to length frequency distributions for MN observer sampling.

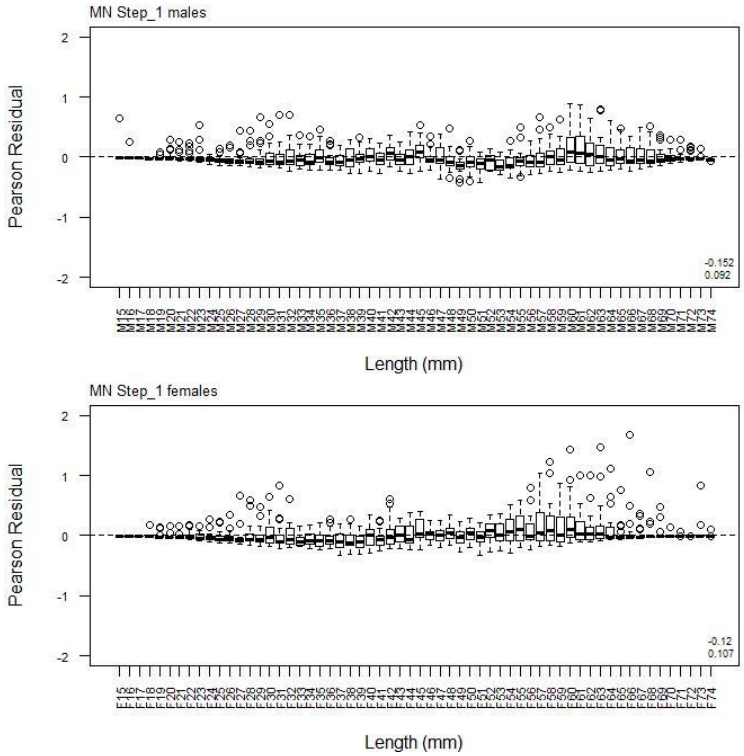

A5. 12: Box plots of Pearson residuals from the fit to length frequency distributions by length from observer sampling by sex for MN time step 1.

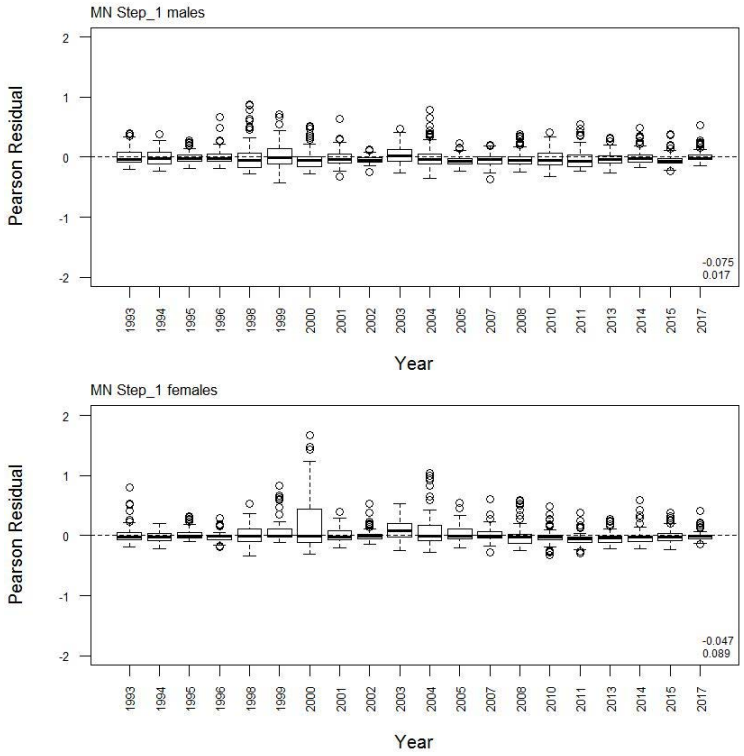

A5. 13: Box plots of Pearson residuals from the fit to length frequency distributions by year from observer sampling by sex for MN time step 1.

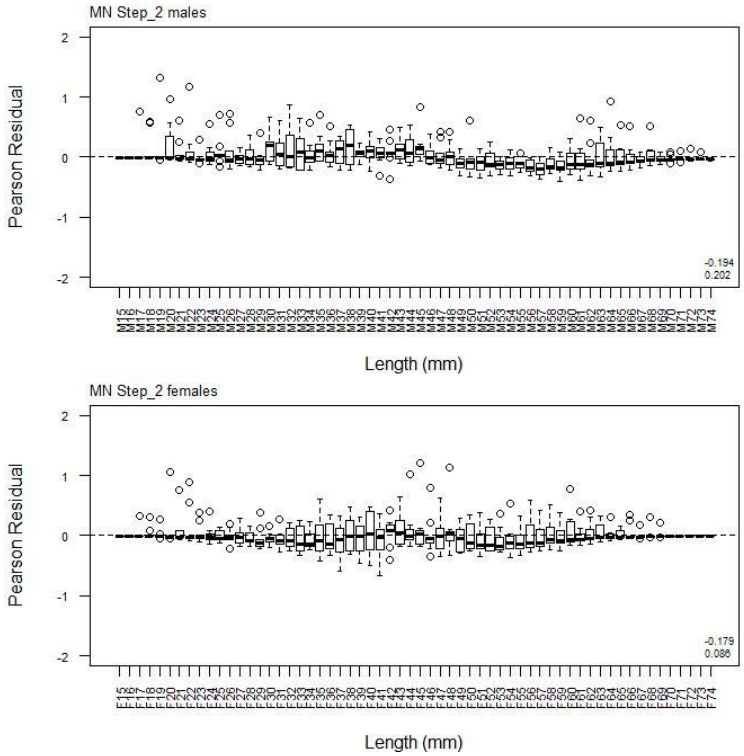

A5. 14: Box plots of Pearson residuals from the fit to length frequency distributions by length from observer sampling by sex for MN time step 2.

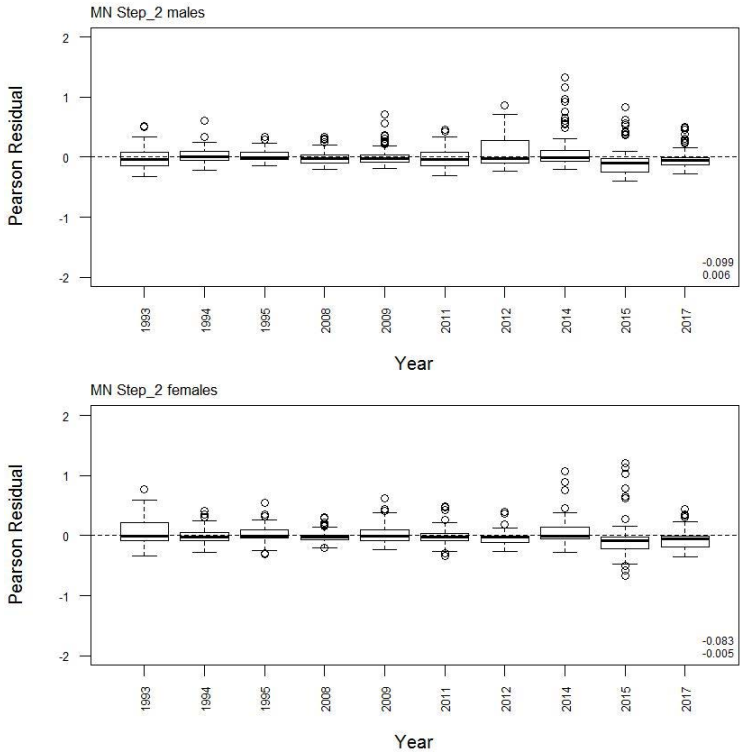

A5. 15: Box plots of Pearson residuals from the fit to length frequency distributions by year from observer sampling by sex for MN time step 2.

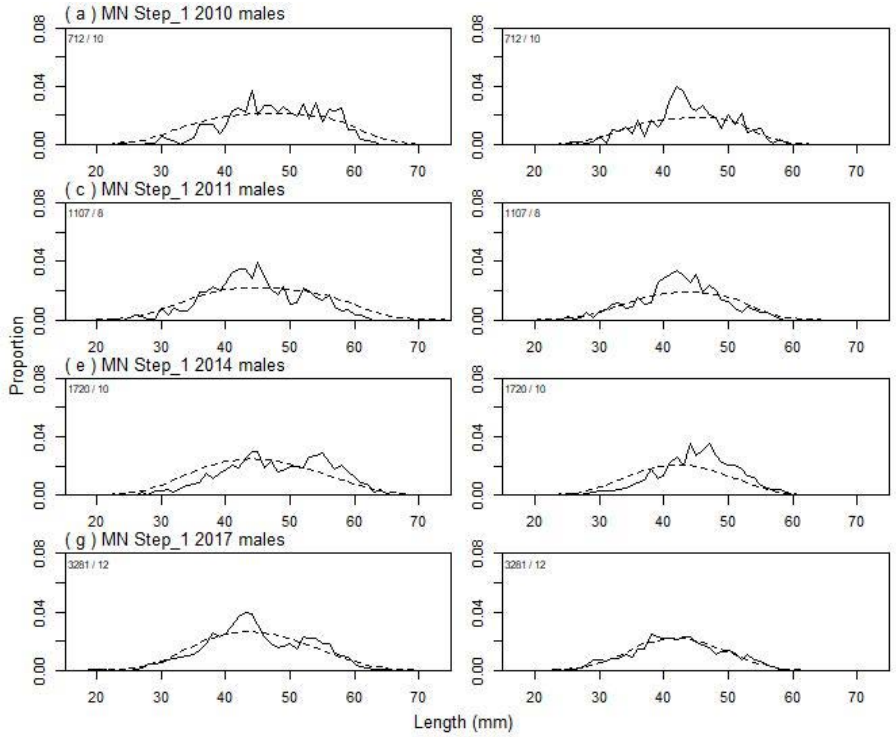

A5. 16: Observed (solid line) and fitted (dashed line) length frequency distributions for MN research survey samples.

A5. 17: Numbers of scampi measured, estimated multinomial N sample size, and effective sample size used within the model for length frequency distributions for MN research survey samples.

	Measured	Multinomial N	Effective sample size
N_2010	1 276	941	12.10
N_2011	2 027	1 610	20.71
N_2014	3 156	2 381	30.63
N_2017	5 299	4 895	62.96

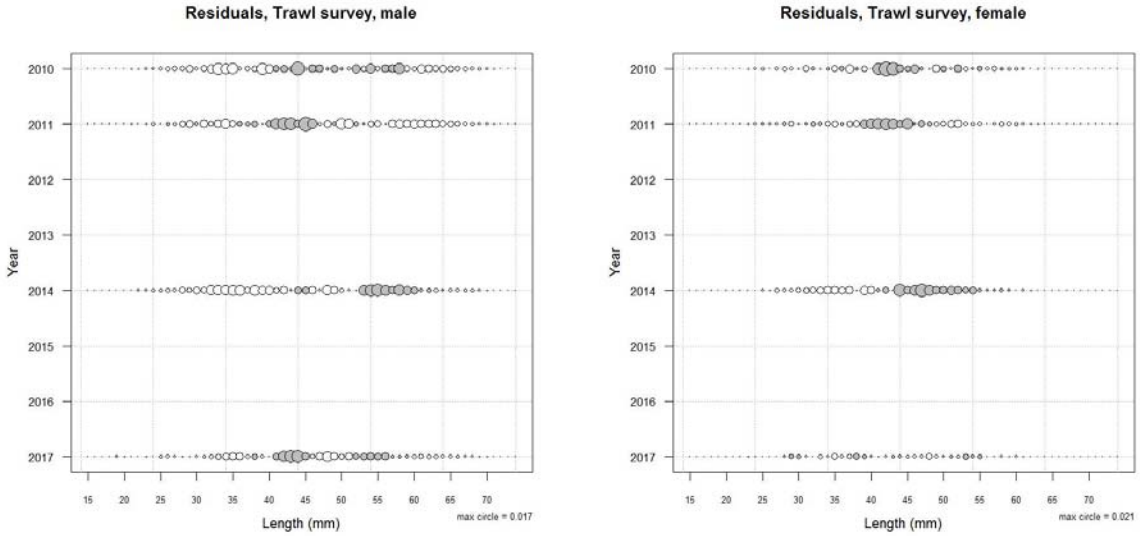

A5. 18: Bubble plots of residuals for fits to length frequency distributions for MN trawl sampling.

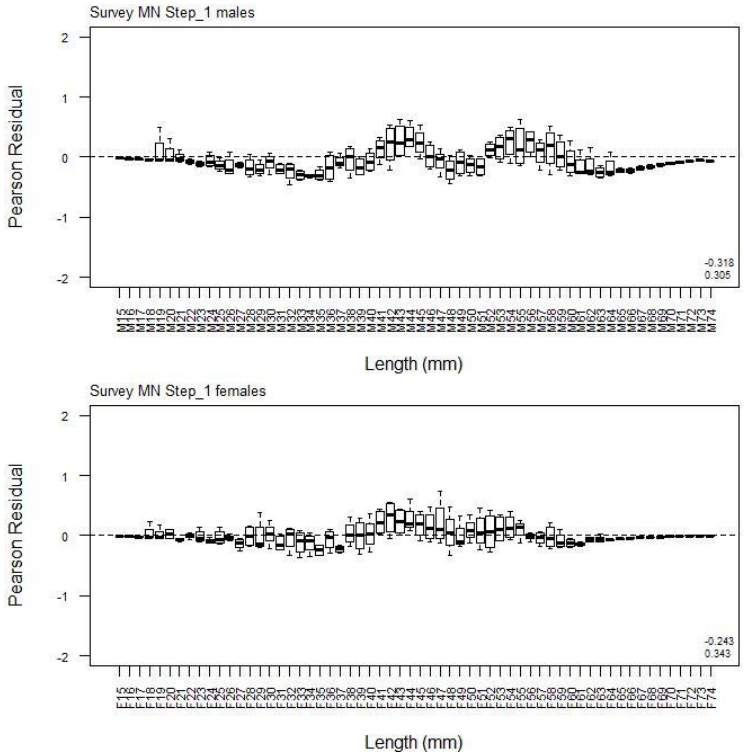

A5. 19: Box plots of Pearson residuals from the fit to length frequency distributions by length from MN trawl sampling.

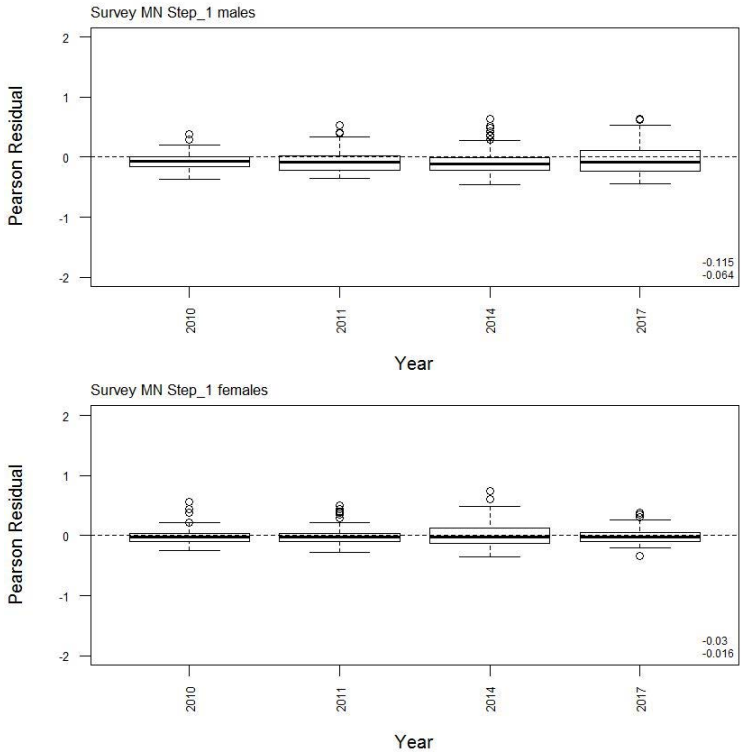

A5. 20: Box plots of Pearson residuals from the fit to length frequency distributions by year from MN trawl sampling.

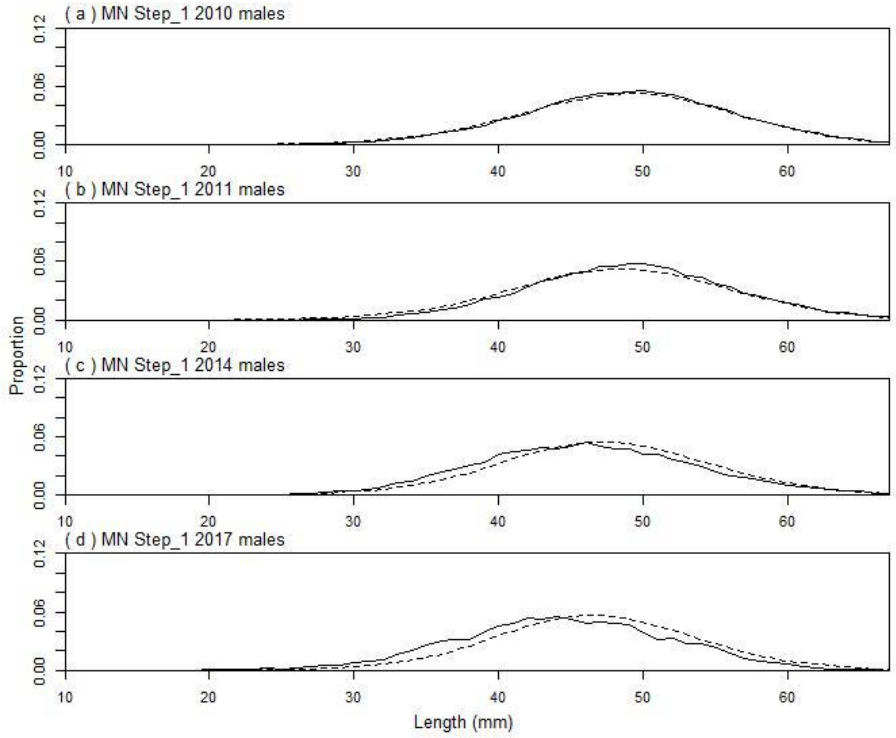

A5. 21: Observed (solid line) and fitted (dashed line) length frequency distributions for MN photographic survey scampi size estimation.

A5. 22: Numbers of scampi measured, estimated multinomial N sample size, and effective sample size used within the model for length frequency distributions for MN photographic survey samples.

	Measured	Multinomial N	Effective sample size
N_2010	113	211	57.65
N_2011	120	225	61.48
N_2014	62	120	32.79
N_2017	25	50	13.66

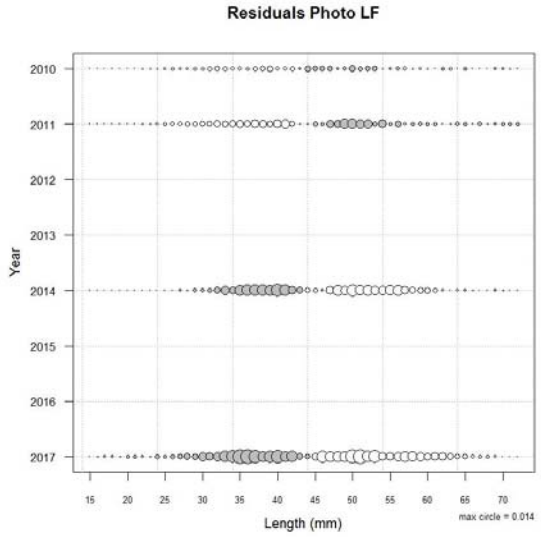

A5. 23: Bubble plots of residuals for fits to length frequency distributions for MN photographic sampling.

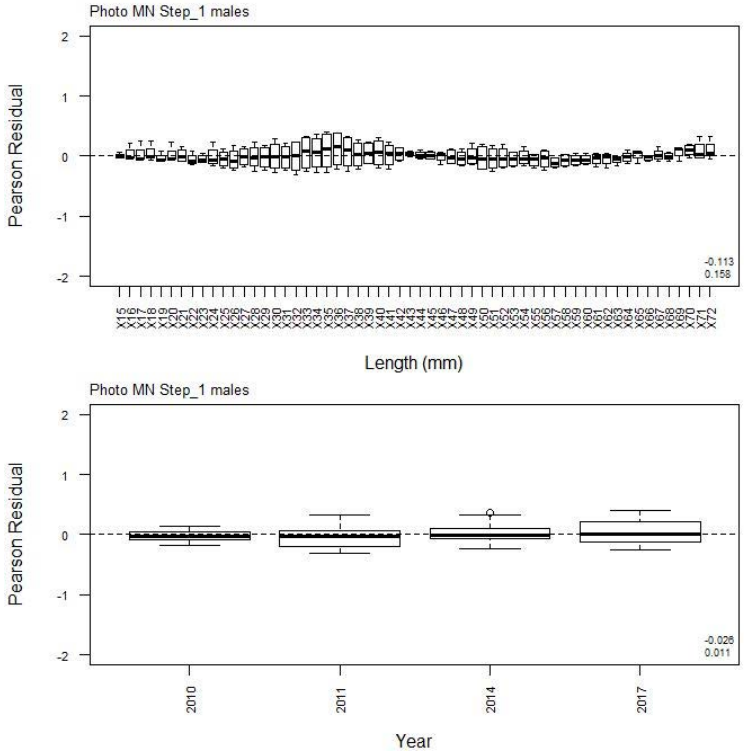

A5. 24: Box plots of Pearson residuals from the fit to length frequency distributions by length and year for MN photographic sampling.

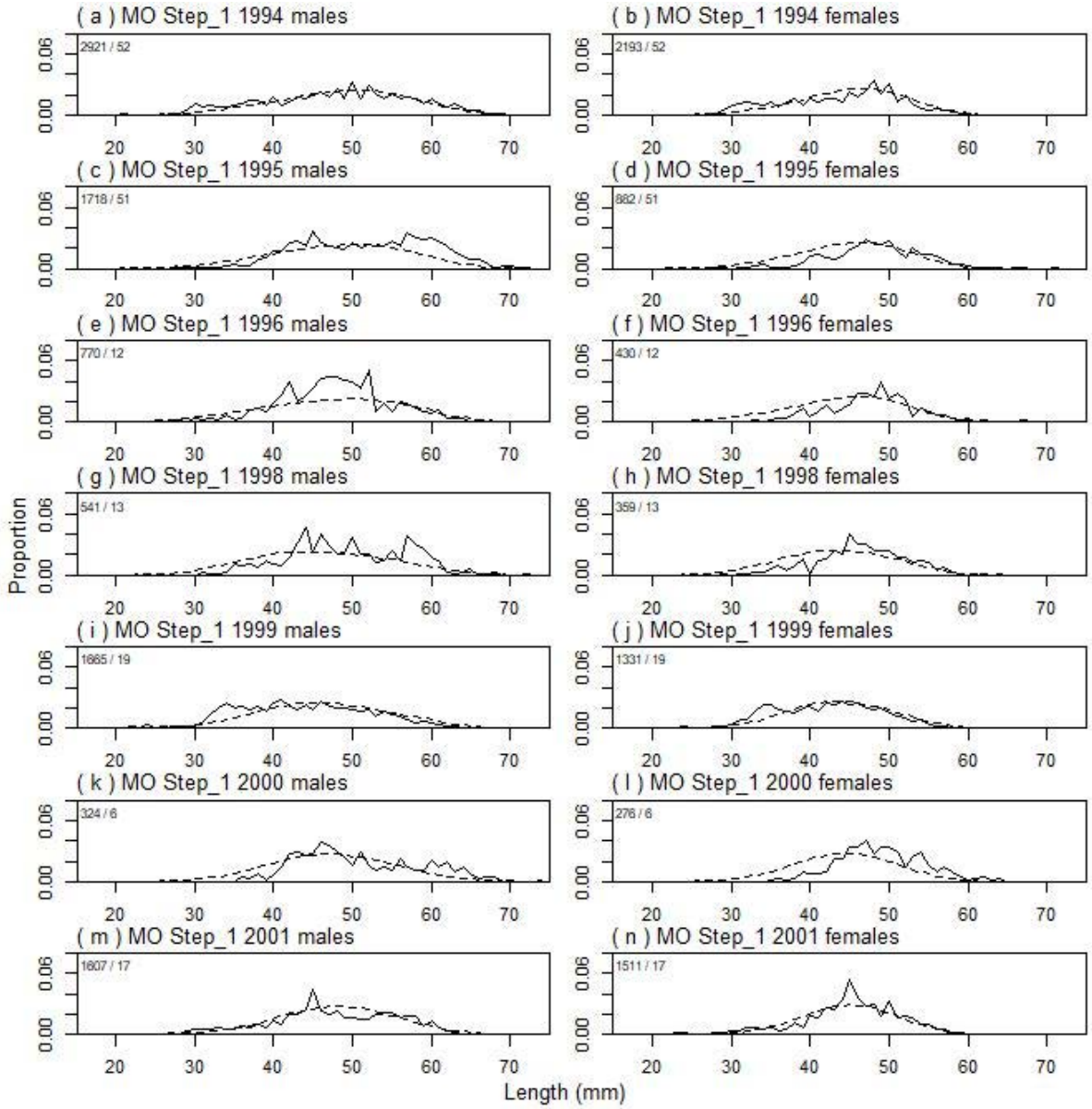

A5. 25: Observed (solid line) and fitted (dashed line) length frequency distributions for observer samples, MO time step 1. Numbers in top left corner of each plot represent number of scampi measured / number of events sampled.

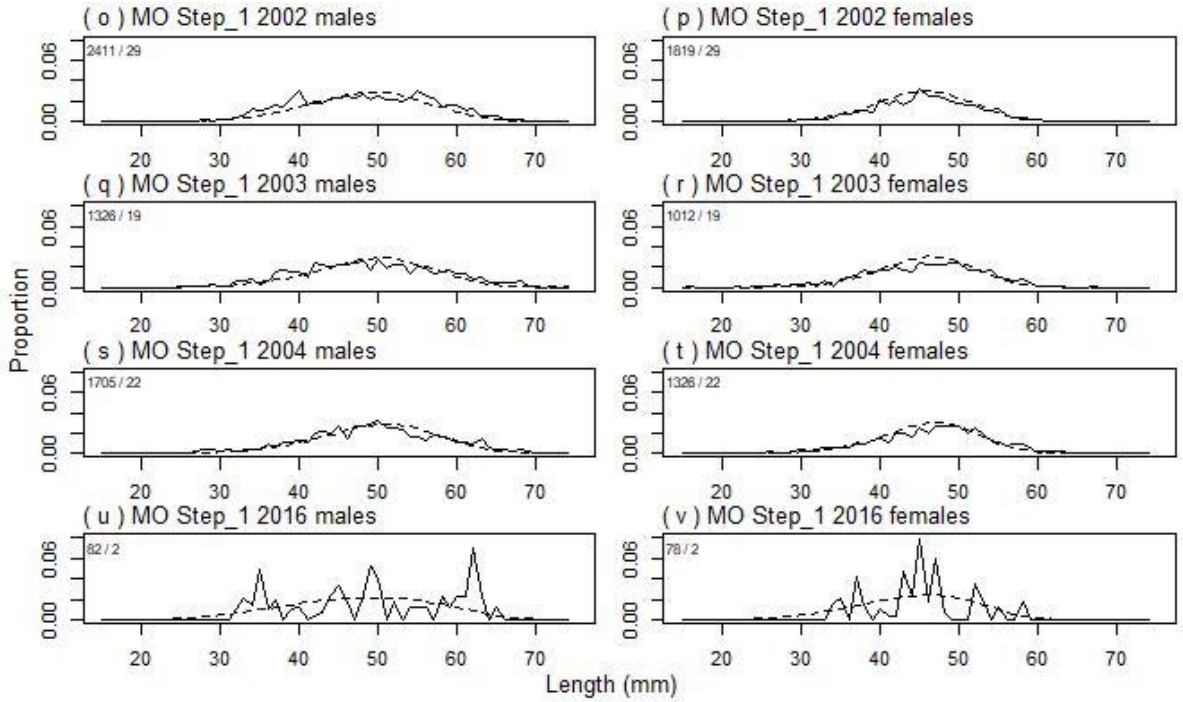

A5. 25 *continued*: Observed (solid line) and fitted (dashed line) length frequency distributions for observer samples, MO time step 1. Numbers in top left corner of each plot represent number of scampi measured / number of events sampled.

A5. 26: Numbers of scampi measured, estimated multinomial N sample size, and effective sample size used within the model for length frequency distributions for observer samples, MO time step 1.

	Measured	Multinomial N	Effective sample size
N_1994	5 114	3 277	30.84
N_1995	2 600	2 182	20.54
N_1996	1 200	1 071	10.08
N_1998	900	940	8.85
N_1999	2 996	2 504	23.57
N_2000	600	733	6.90
N_2001	3 118	2 900	27.29
N_2002	4 230	2 662	24.21
N_2003	2 338	1 553	14.62
N_2004	3 031	2 084	19.61
N_2016	160	88	0.83

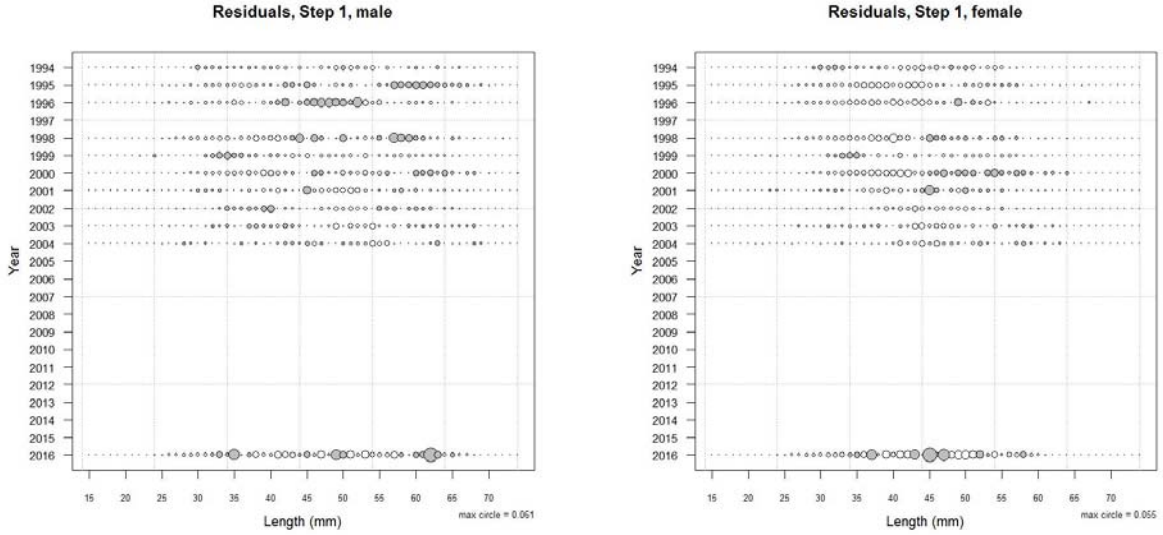

A5. 27: Bubble plots of residuals for fits to length frequency distributions for MO observer sampling.

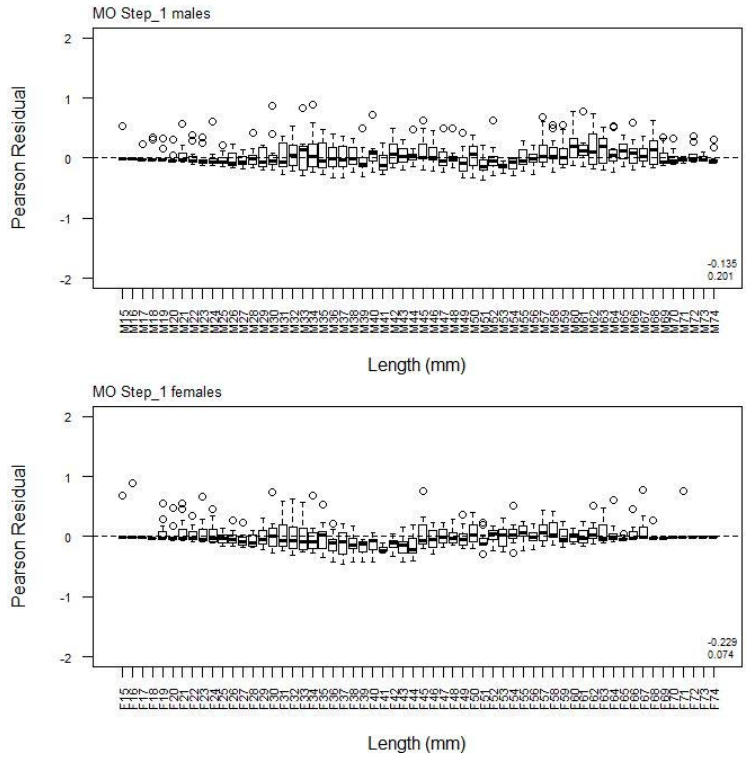

A5. 28: Box plots of Pearson residuals from the fit to length frequency distributions by length from observer sampling by sex for MO time step 1.

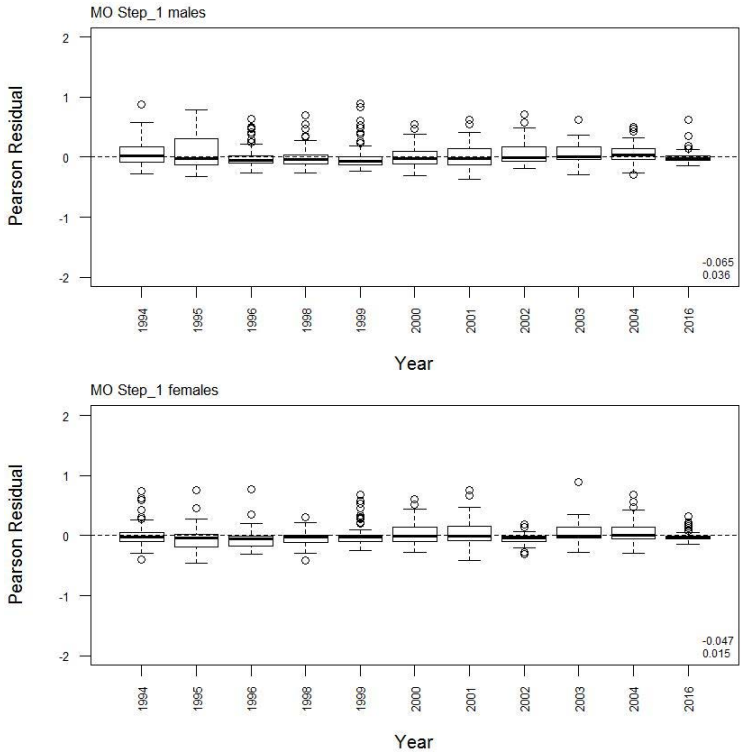

A5. 29: Box plots of Pearson residuals from the fit to length frequency distributions by year from observer sampling by sex for MO time step 1.

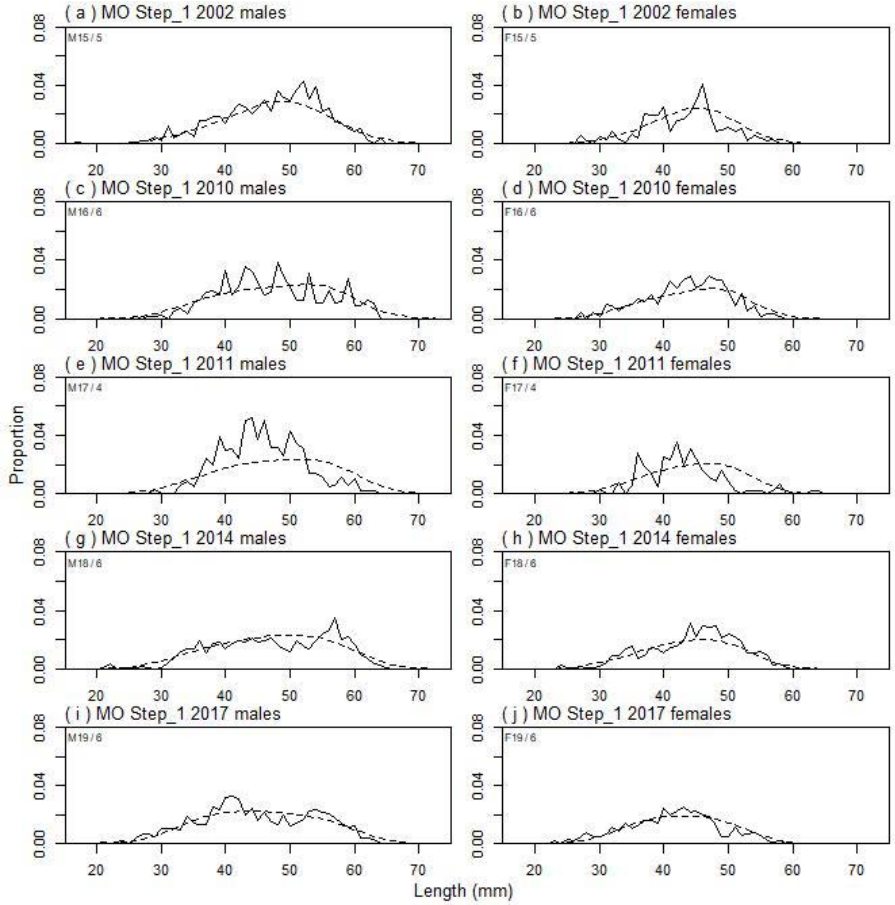

A5. 30: Observed (solid line) and fitted (dashed line) length frequency distributions for MO research survey samples.

A5. 31: Numbers of scampi measured, estimated multinomial N sample size, and effective sample size used within the model for length frequency distributions for MO research survey samples.

	Measured	Multinomial N	Effective sample size
N_2002	764	725	100.77
N_2010	551	627	87.15
N_2011	396	483	67.13
N_2014	1 465	1 363	189.45
N_2017	1 807	1 669	231.98

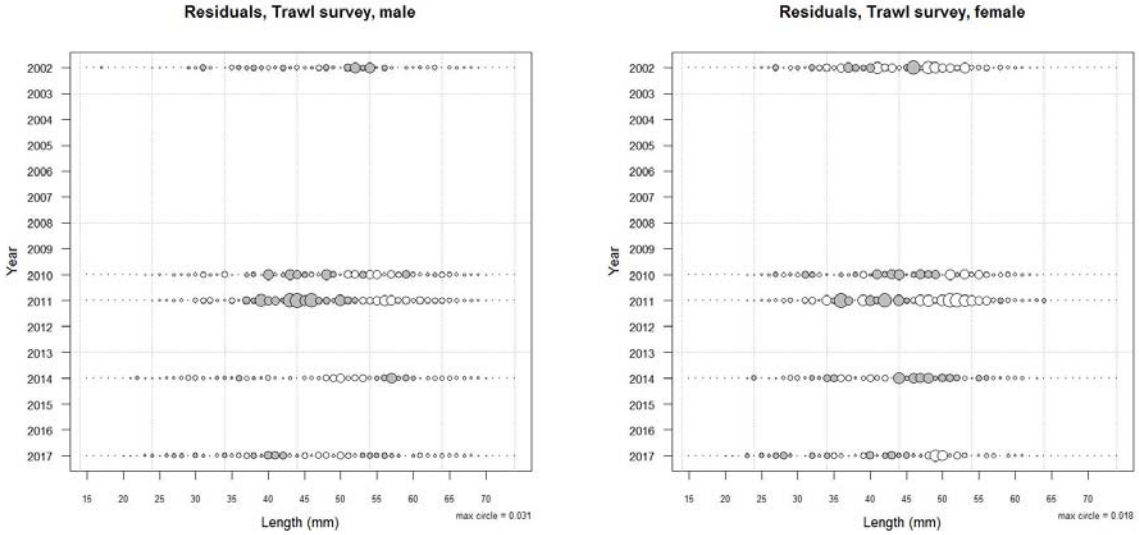

A5. 32: Bubble plots of residuals for fits to length frequency distributions for MO trawl sampling.

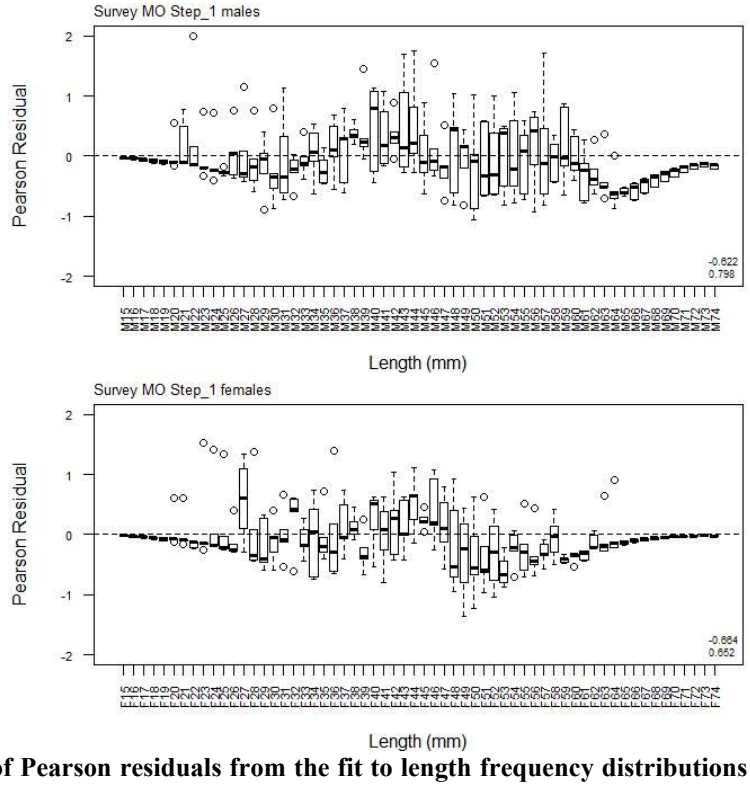

A5. 33: Box plots of Pearson residuals from the fit to length frequency distributions by length from MO trawl sampling.

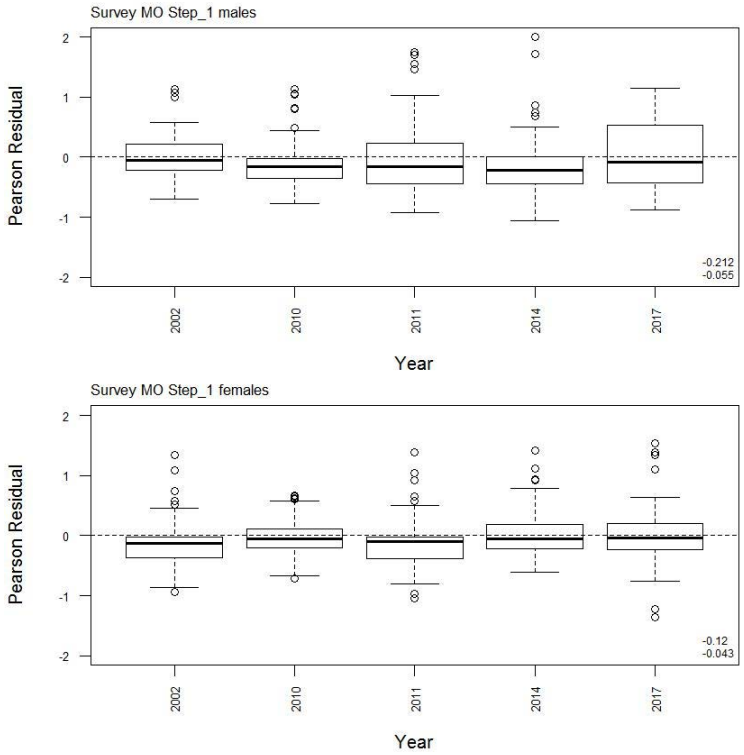

A5. 34: Box plots of Pearson residuals from the fit to length frequency distributions by year from MO trawl sampling.

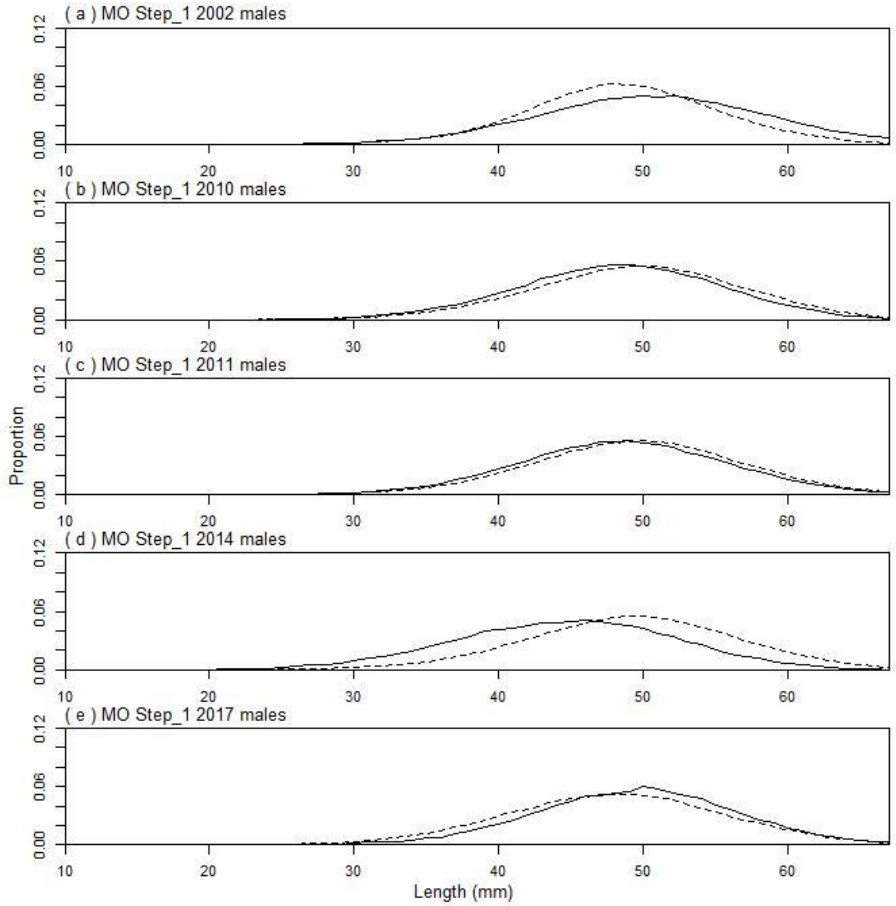

A5. 35: Observed (solid line) and fitted (dashed line) length frequency distributions for MO photographic survey scampi size estimation.

A5. 36: Numbers of scampi measured, estimated multinomial N sample size, and effective sample size used within the model for length frequency distributions for MO photographic survey samples.

	Measured	Multinomial N	Effective sample size
N_2002	224	384	11.98
N_2010	214	365	11.39
N_2011	426	536	16.73
N_2014	125	224	6.99
N_2017	76	145	4.52

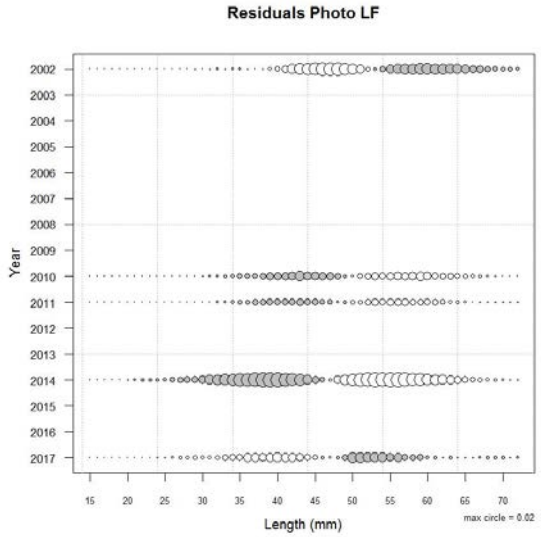

A5. 37: Bubble plots of residuals for fits to length frequency distributions for MO photographic sampling.

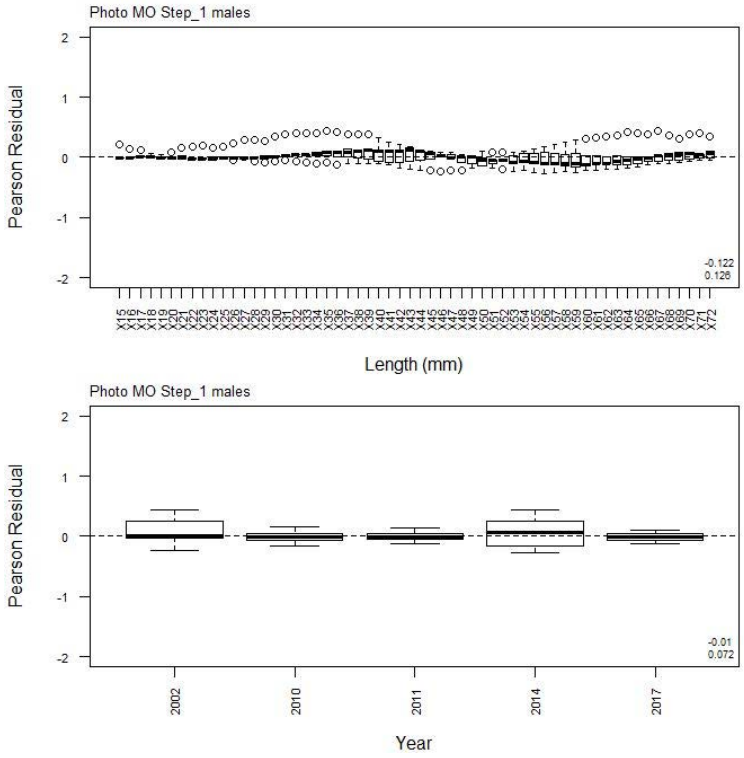

A5. 38: Box plots of Pearson residuals from the fit to length frequency distributions by length and year for MO photographic sampling.

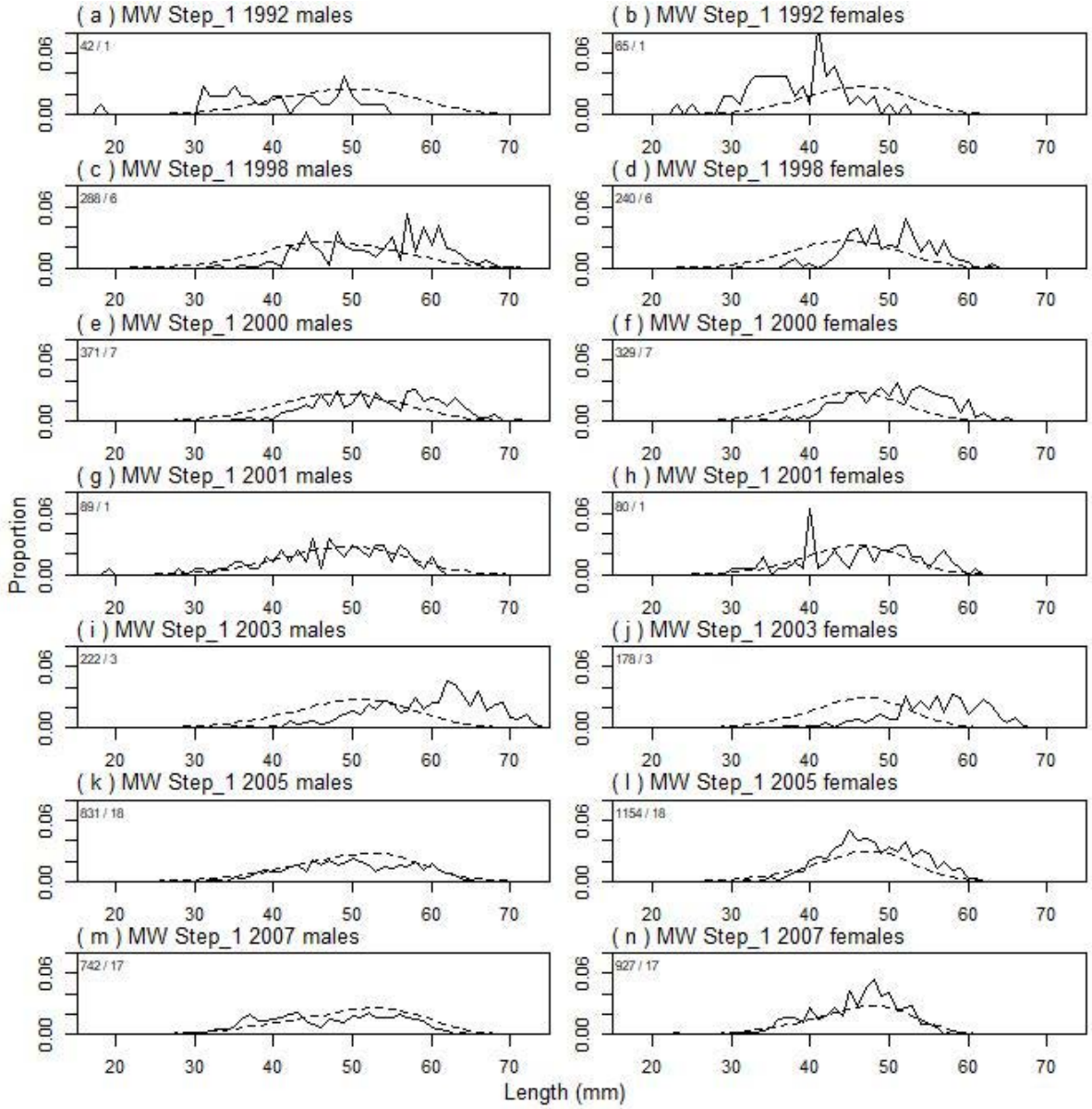

A5. 39: Observed (solid line) and fitted (dashed line) length frequency distributions for observer samples, MW time step 1. Numbers in top left corner of each plot represent number of scampi measured / number of events sampled.

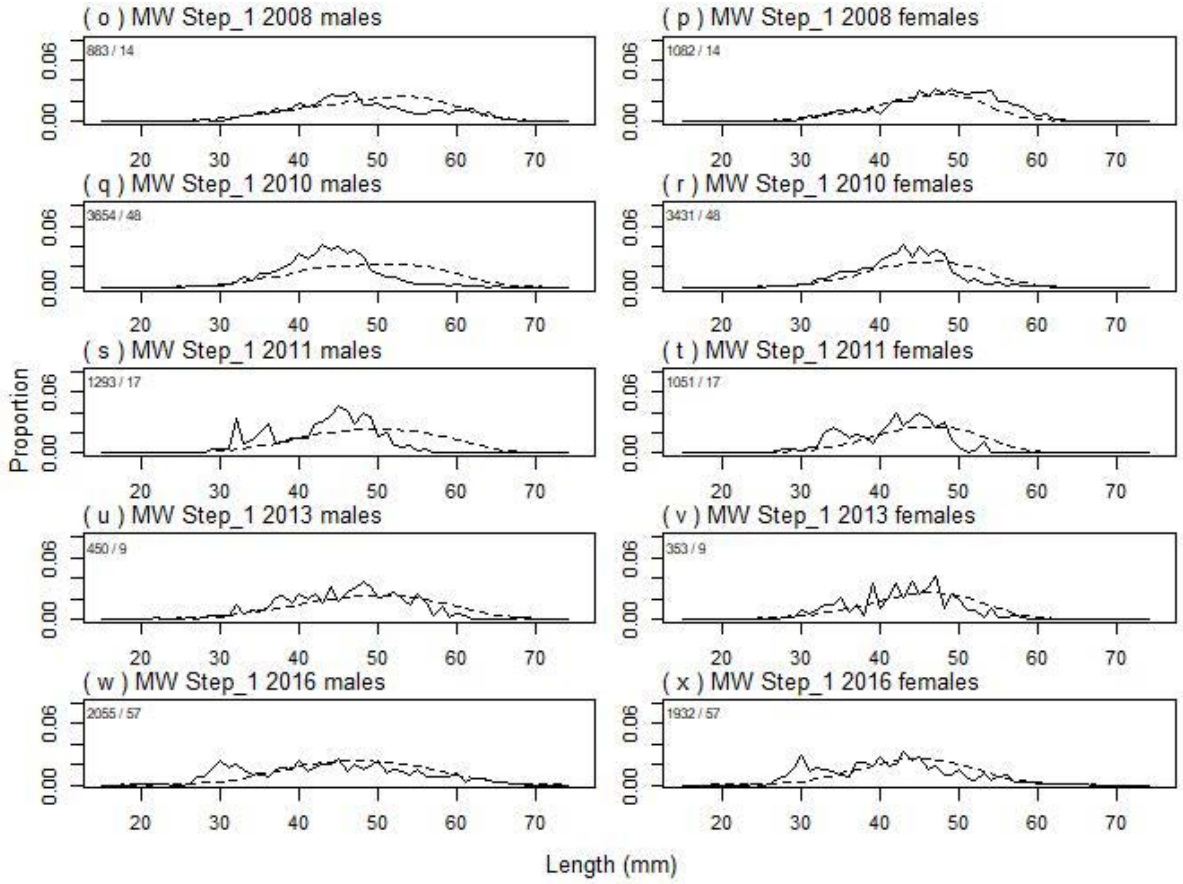

A5. 39 *continued*: Observed (solid line) and fitted (dashed line) length frequency distributions for observer samples, MW time step 1. Numbers in top left corner of each plot represent number of scampi measured / number of events sampled.

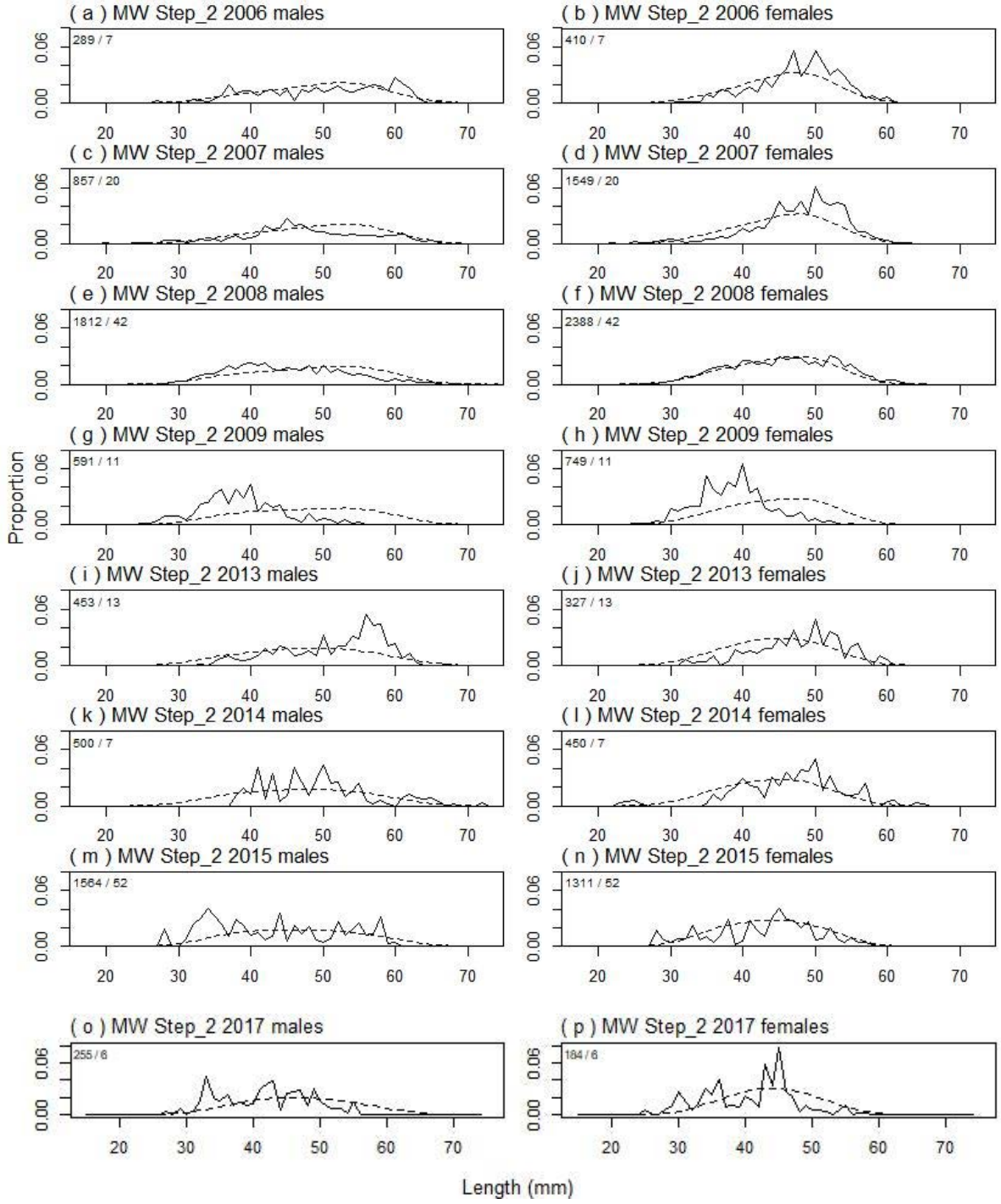

A5. 40: Observed (solid line) and fitted (dashed line) length frequency distributions for observer samples, MW time step 2. Numbers in top left corner of each plot represent number of scampi measured / number of events sampled.

A5. 41: Numbers of scampi measured, estimated multinomial N sample size, and effective sample size used within the model for length frequency distributions for observer samples, MW time step 1.

	Measured	Multinomial N	Effective sample size
N_1992	107	216	0.48
N_1998	528	394	0.88
N_2000	700	631	1.41
N_2001	169	341	0.76
N_2003	400	796	1.78
N_2005	1 985	908	2.03
N_2007	1 669	1 418	3.18
N_2008	1 965	1 743	3.91
N_2010	7 085	6 257	14.02
N_2011	2 344	1 739	3.90
N_2013	803	583	1.31
N_2016	3 987	3 475	7.79

A5. 42: Numbers of scampi measured, estimated multinomial N sample size, and effective sample size used within the model for length frequency distributions for observer samples, MW time step 2.

	Measured	Multinomial N	Effective sample size
N_2006	699	790	3.45
N_2007	2 406	2 144	9.37
N_2008	4 200	3 081	13.46
N_2009	1 340	1 366	5.97
N_2013	780	483	2.11
N_2014	950	1 710	7.47
N_2015	2 875	638	2.79
N_2017	439	232	1.01

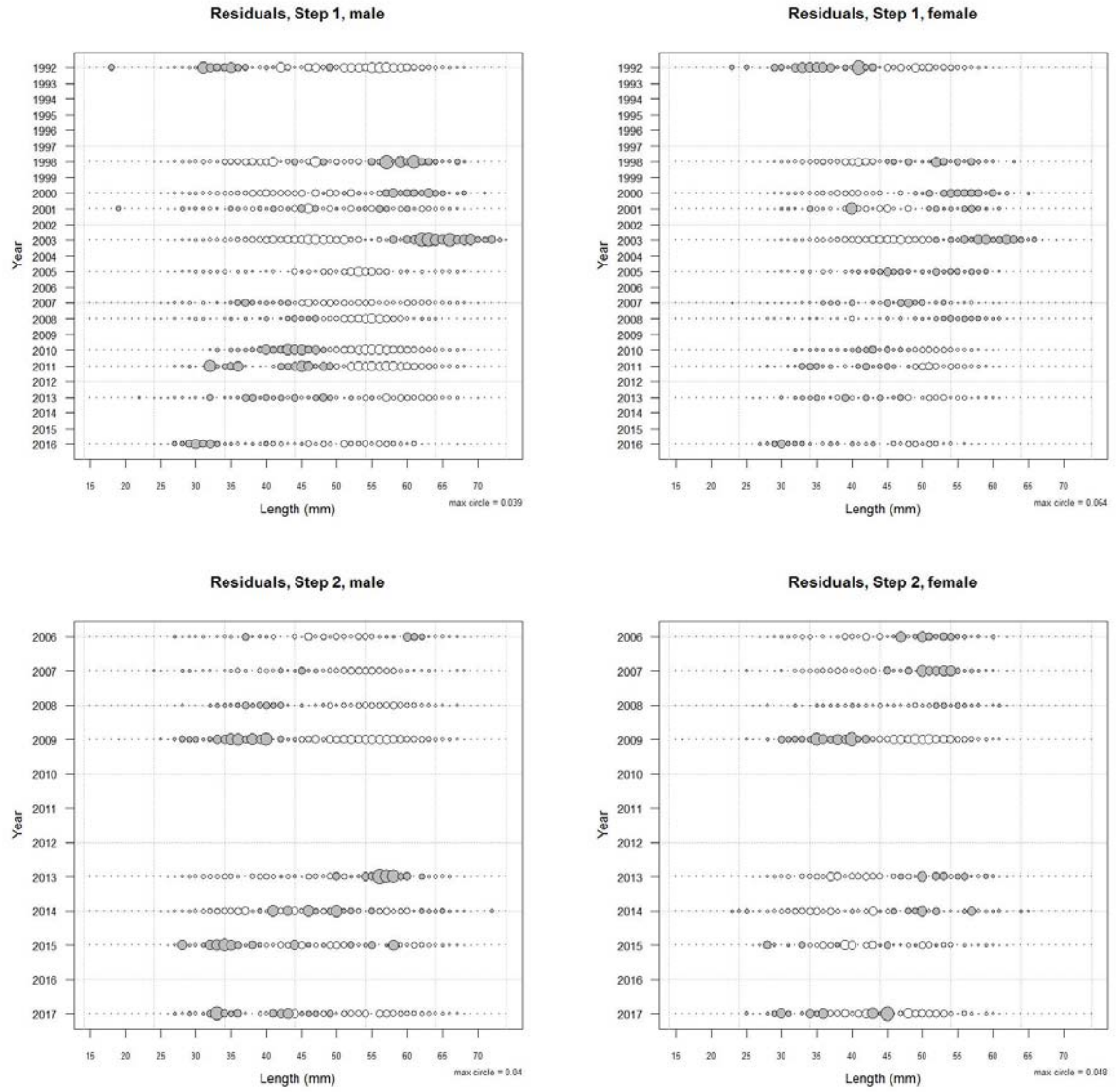

A5. 43: Bubble plots of residuals for fits to length frequency distributions for MW observer sampling.

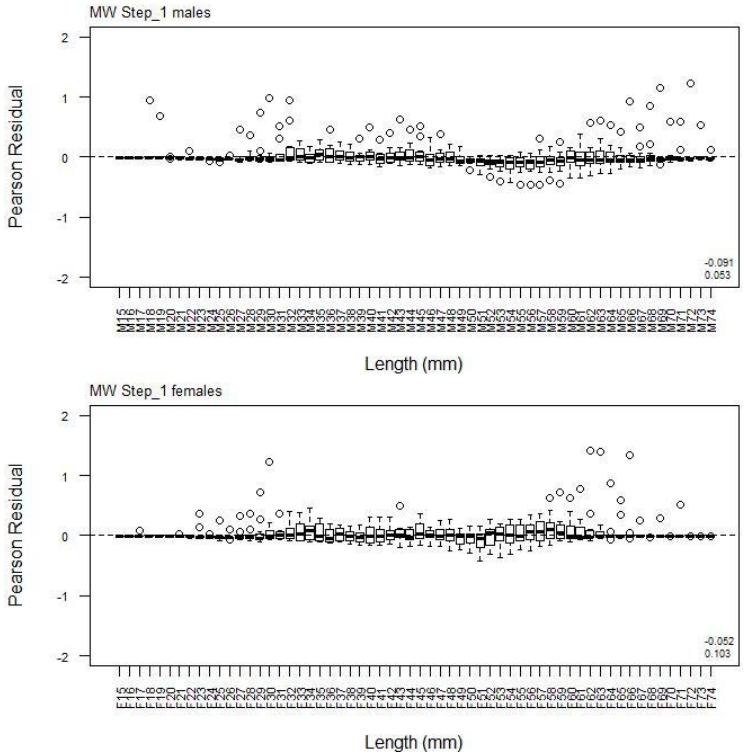

A5. 44: Box plots of Pearson residuals from the fit to length frequency distributions by length from observer sampling by sex for MW time step 1.

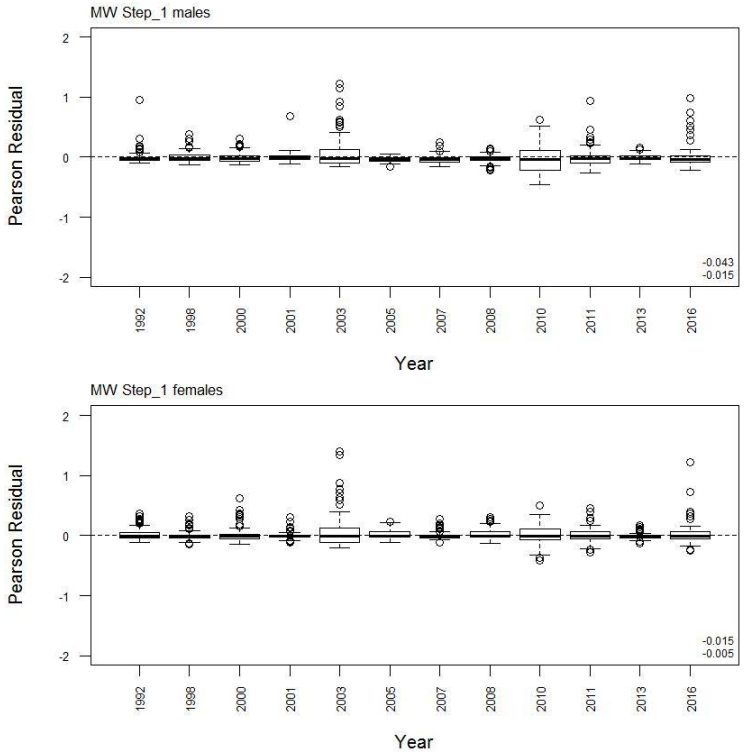

A5. 45: Box plots of Pearson residuals from the fit to length frequency distributions by year from observer sampling by sex for MW time step 1.

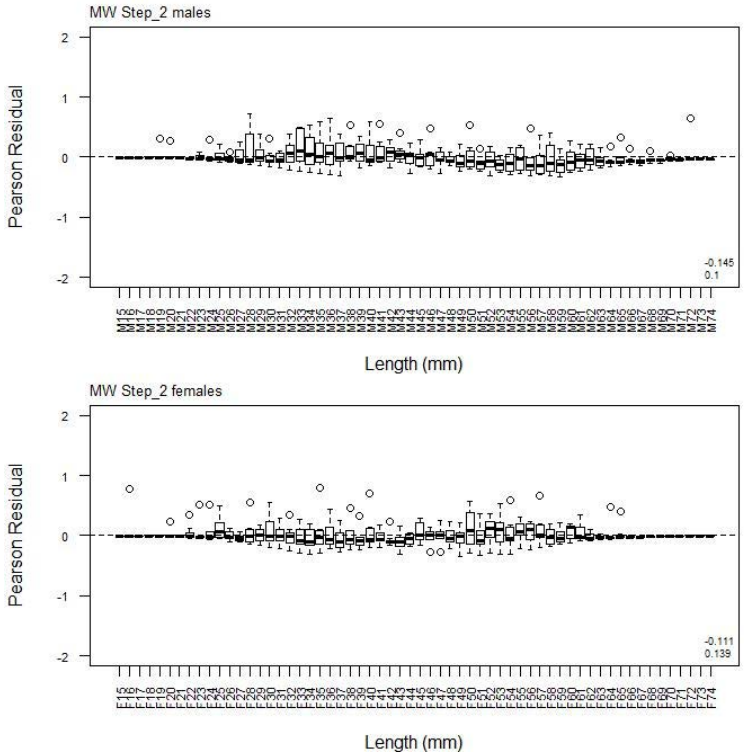

A5. 46: Box plots of Pearson residuals from the fit to length frequency distributions by length from observer sampling by sex for MW time step 2.

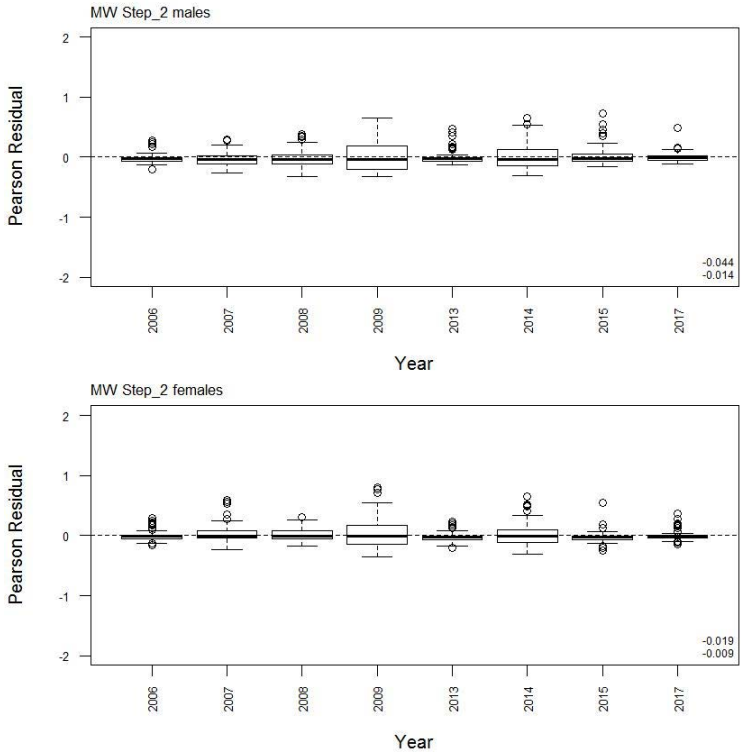

A5. 47: Box plots of Pearson residuals from the fit to length frequency distributions by year from observer sampling by sex for MW time step 2.

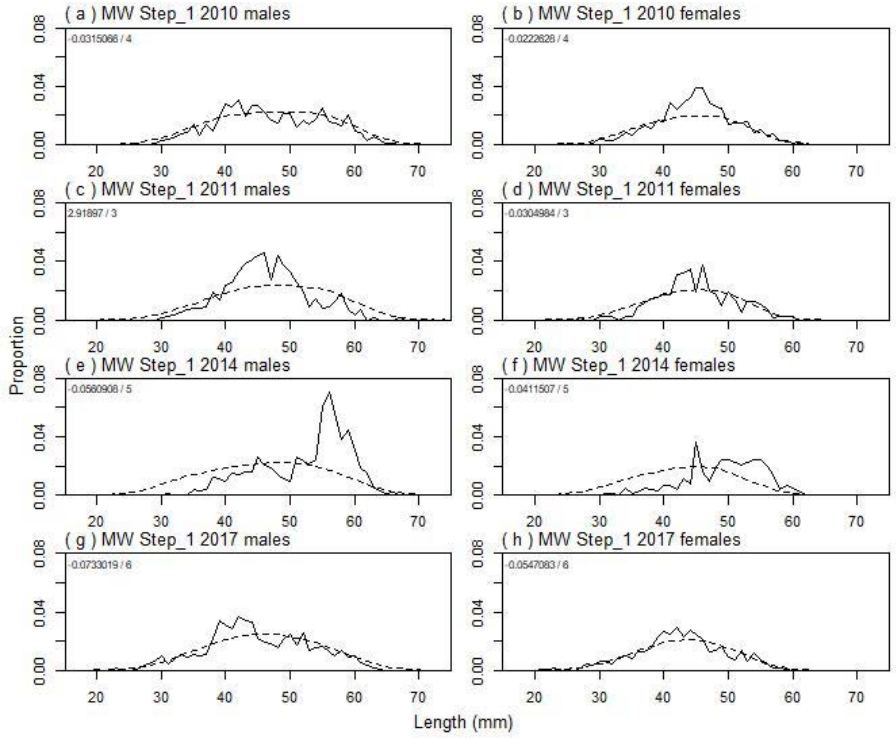

A5. 48: Observed (solid line) and fitted (dashed line) length frequency distributions for MW research survey samples.

A5. 49: Numbers of scampi measured, estimated multinomial N sample size, and effective sample size used within the model for length frequency distributions for MW research survey samples.

	Measured	Multinomial N	Effective sample size
N_2010	1 110	1 140	9.86
N_2011	876	1 011	8.74
N_2014	710	681	5.89
N_2017	1 734	1 776	15.36

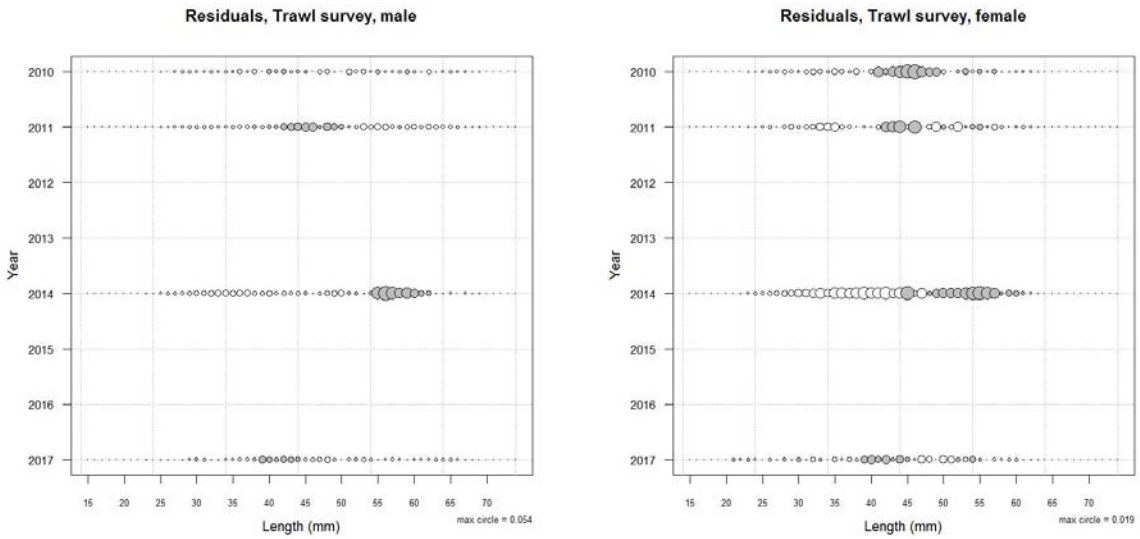

A5. 50: Bubble plots of residuals for fits to length frequency distributions for MW trawl sampling.

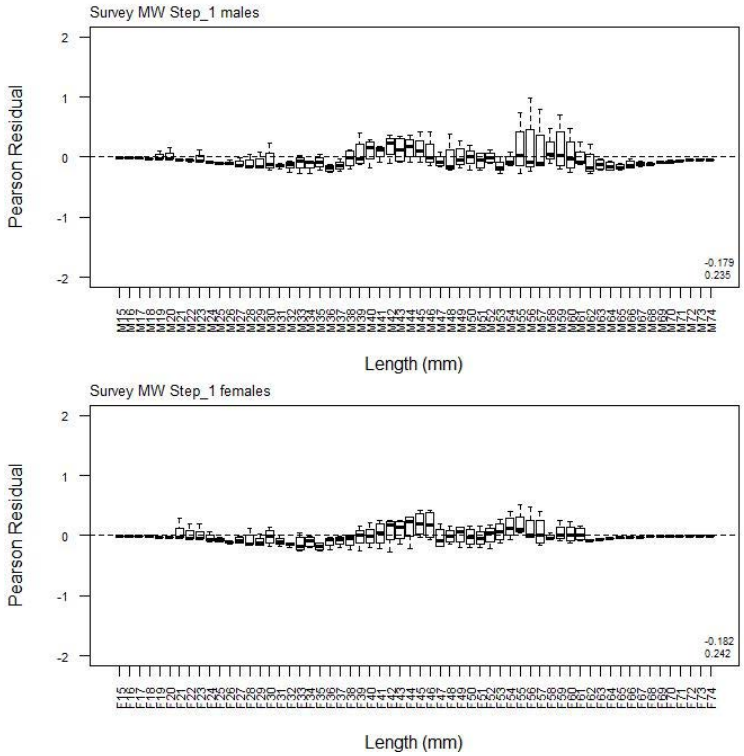

A5. 51: Box plots of Pearson residuals from the fit to length frequency distributions by length from MW trawl sampling.

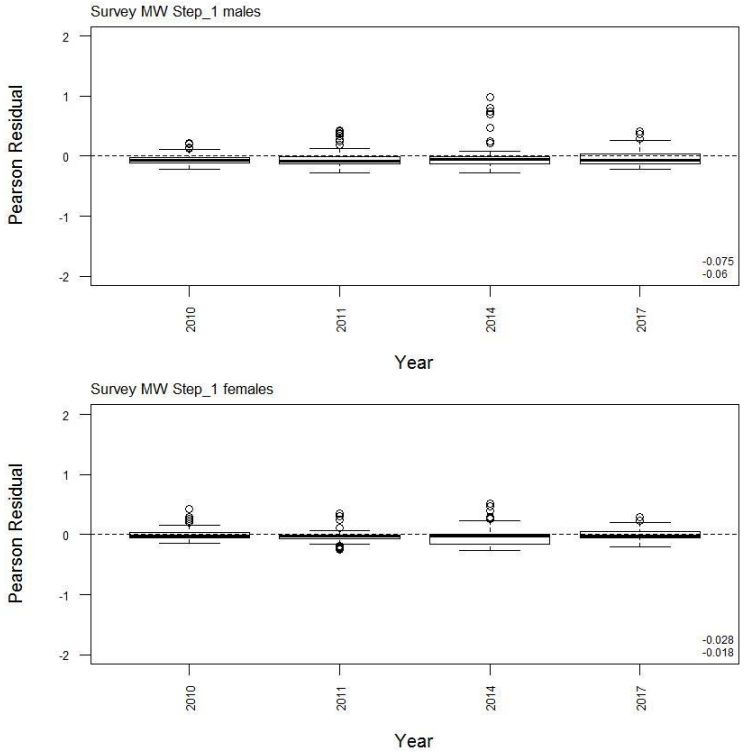

A5. 52: Box plots of Pearson residuals from the fit to length frequency distributions by year from MW trawl sampling.

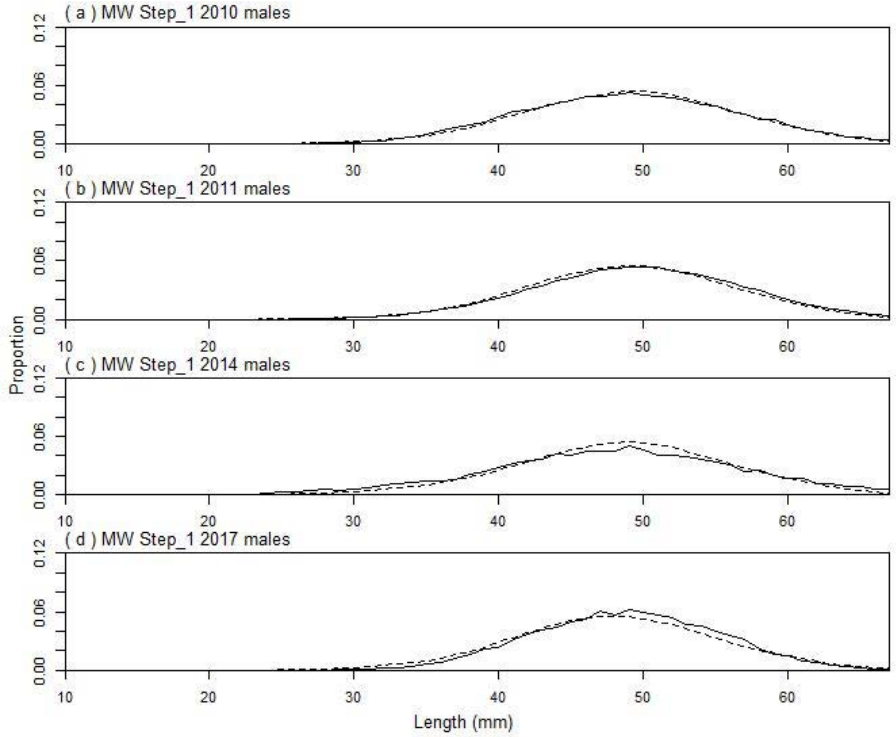

A5. 53: Observed (solid line) and fitted (dashed line) length frequency distributions for MW photographic survey scampi size estimation.

A5. 54: Numbers of scampi measured, estimated multinomial N sample size, and effective sample size used within the model for length frequency distributions for MW photographic survey samples.

	Measured	Multinomial N	Effective sample size
N_2010	173	298	543.74
N_2011	128	227	414.19
N_2014	24	48	87.58
N_2017	23	46	83.93

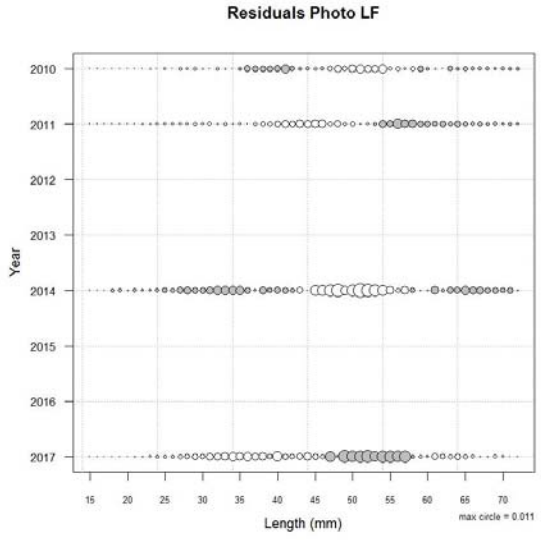

A5. 55: Bubble plots of residuals for fits to length frequency distributions for MW photographic sampling.

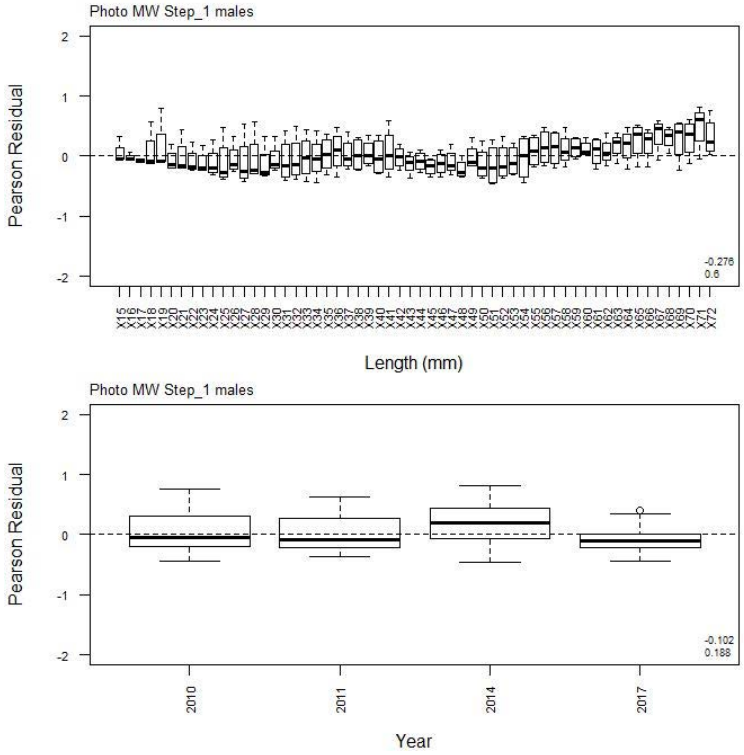

A5. 56: Box plots of Pearson residuals from the fit to length frequency distributions by length and year for MW photographic sampling.

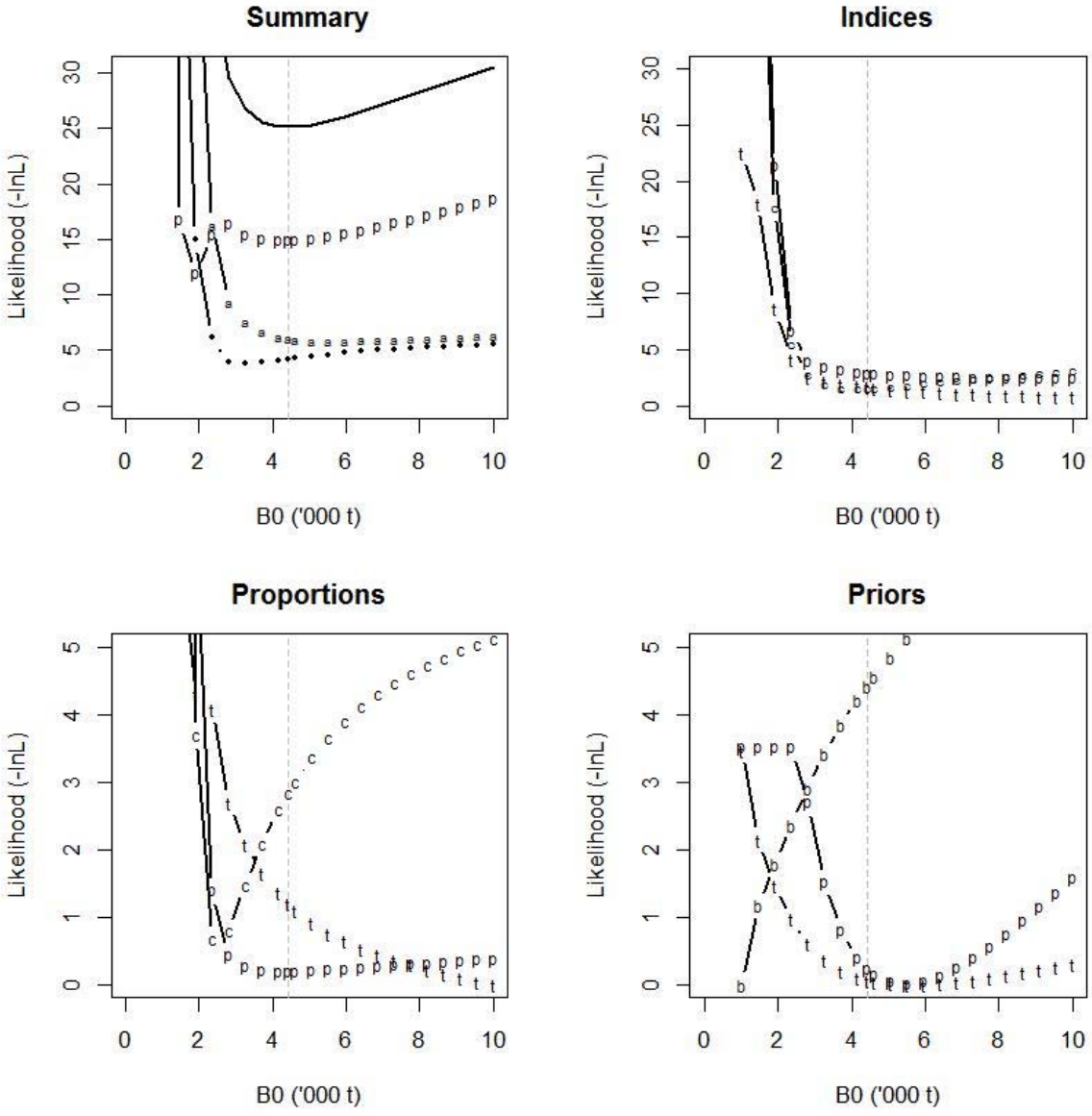

A5. 57: Likelihood profiles for SCI 3 Model 3 when B_0 is fixed in the model. Figures show profiles for main priors (top left, p – priors, a – abundance indices, • – proportions at length), abundance indices (top right, t – trawl survey, c – CPUE, p – photo survey), proportion at length data (bottom left, t – trawl, c – observer, p – photo) and priors (bottom right, b – B_0, p – *q-Photo*, t – *q-Trawl*). Vertical dashed line represents MPD.

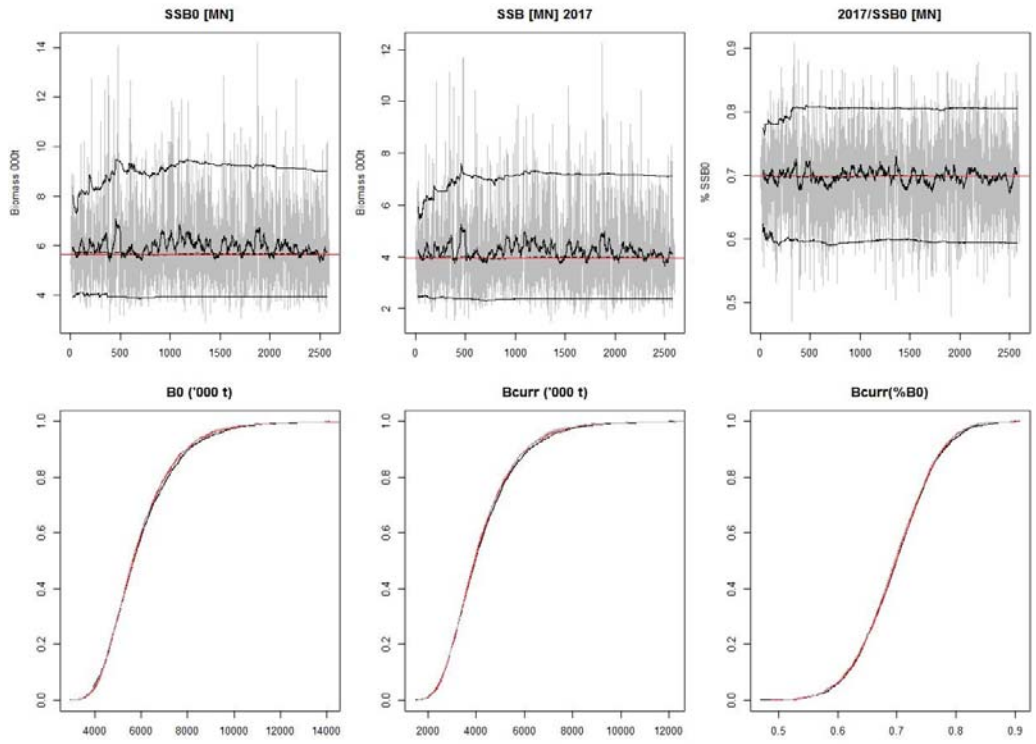

A5. 58: MCMC traces for MN SSB_0, SSB_{2017}, and SSB_{2017}/SSB_0 terms for SCI 3 Model 3 (nuisance *q*)(trace – grey line, cumulative moving median – dashed black line, moving average and cumulative moving 2.5%, 97.5% quantiles – solid black lines, overall median – solid red line, left plots); and cumulative frequency distributions for three independent MCMC chains (shown as red, grey, and black lines, right plots).

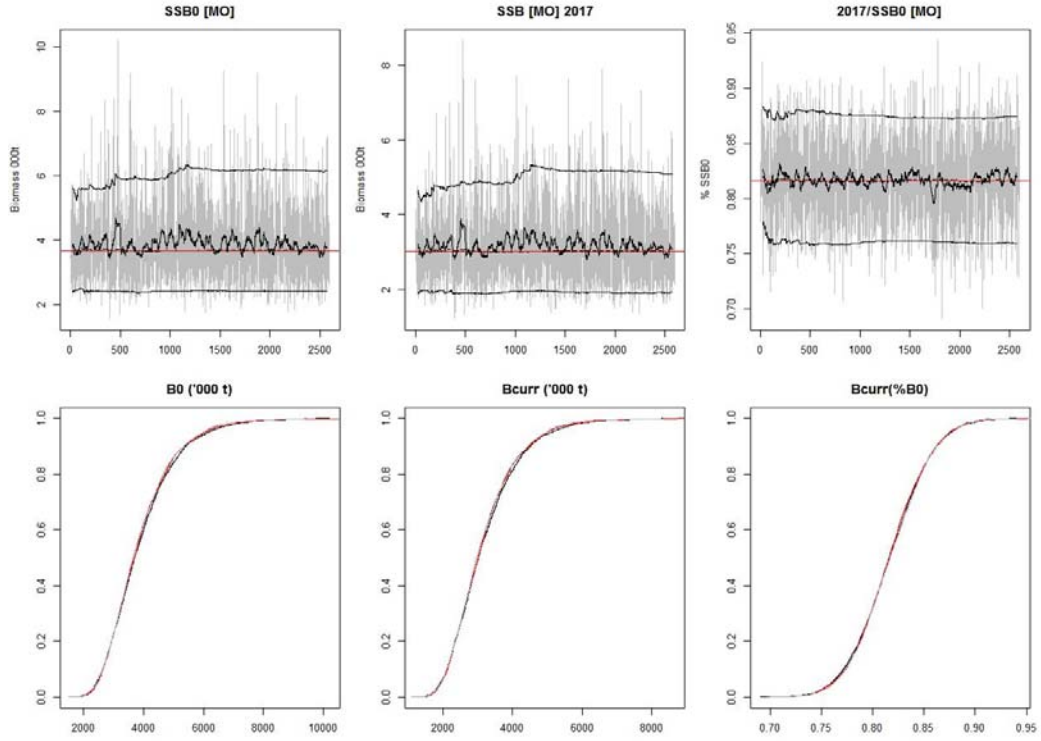

A5. 59: MCMC traces for MO SSB_0, SSB_{2017}, and SSB_{2017}/SSB_0 terms for SCI 3 Model 3 (nuisance *q*)(trace – grey line, cumulative moving median – dashed black line, moving average and cumulative moving 2.5%, 97.5% quantiles – solid black lines, overall median – solid red line, left plots); and cumulative frequency distributions for three independent MCMC chains (shown as red, grey, and black lines, right plots).

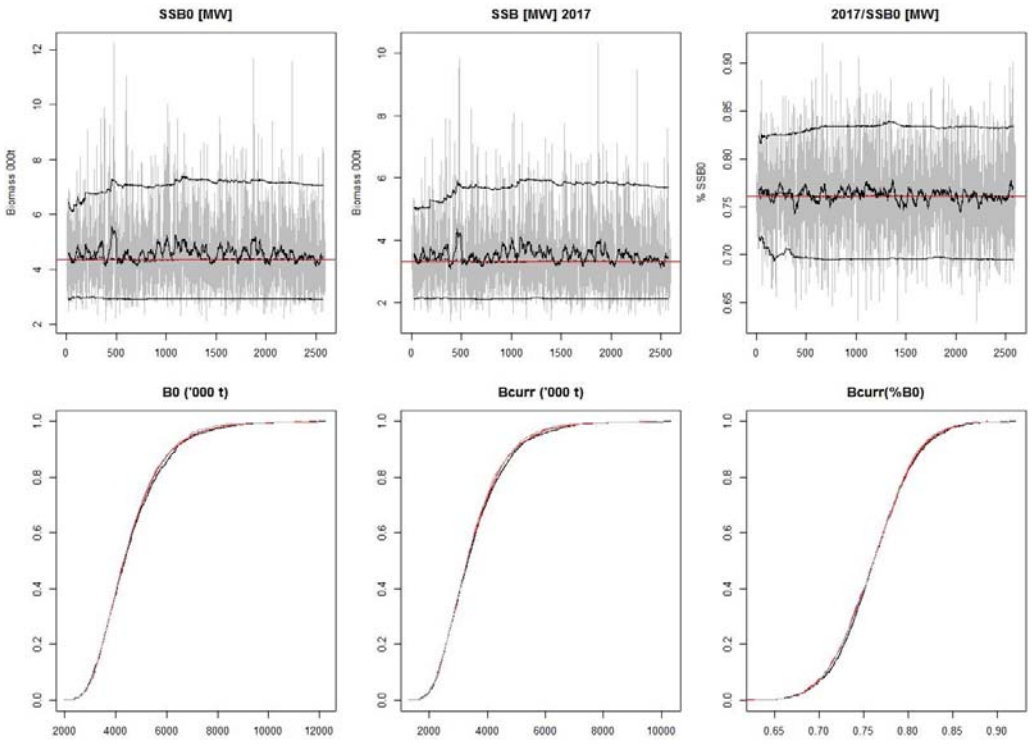

A5. 60: MCMC traces for MW SSB_0, SSB_{2017}, and SSB_{2017}/SSB_0 terms for SCI 3 Model 3 (nuisance q)(trace – grey line, cumulative moving median – dashed black line, moving average and cumulative moving 2.5%, 97.5% quantiles – solid black lines, overall median – solid red line, left plots); and cumulative frequency distributions for three independent MCMC chains (shown as red, grey and black lines, right plots).

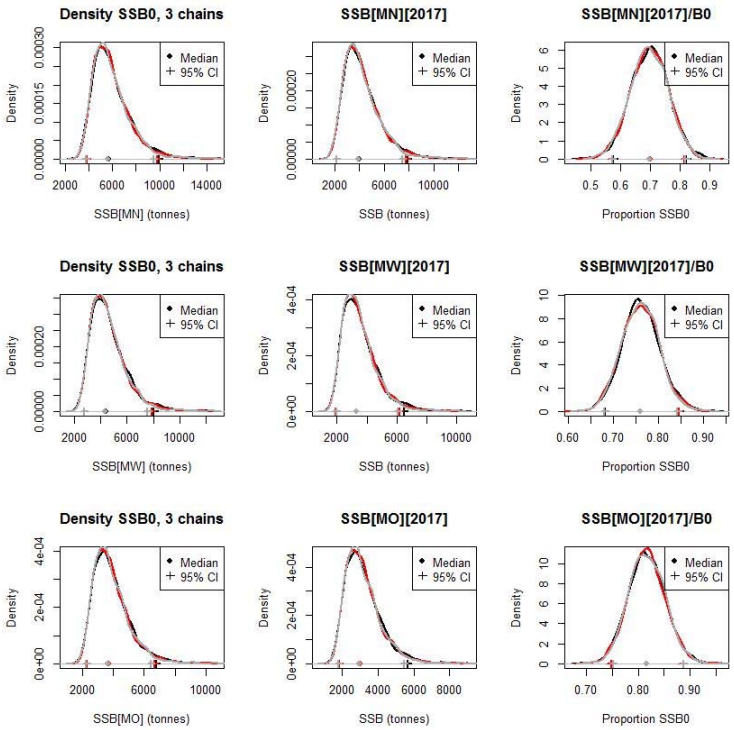

A5. 61: Density plots for SSB_0, SSB_{2017}, and SSB_{2017}/SSB_0 terms for each subarea of SCI 3 Model 3 for three independent MCMC chains, with median and 95% confidence intervals.

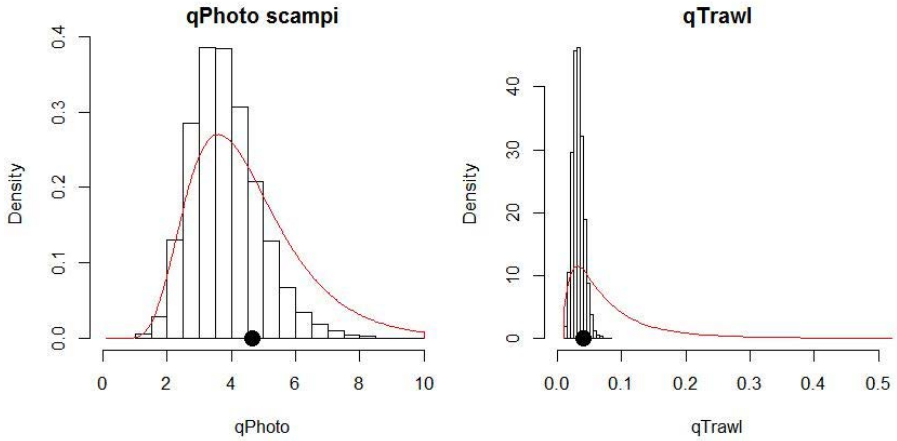

A5. 62: Marginal posterior distributions (histograms), MPD estimates (solid symbols), and distributions of priors (lines) for catchability terms.

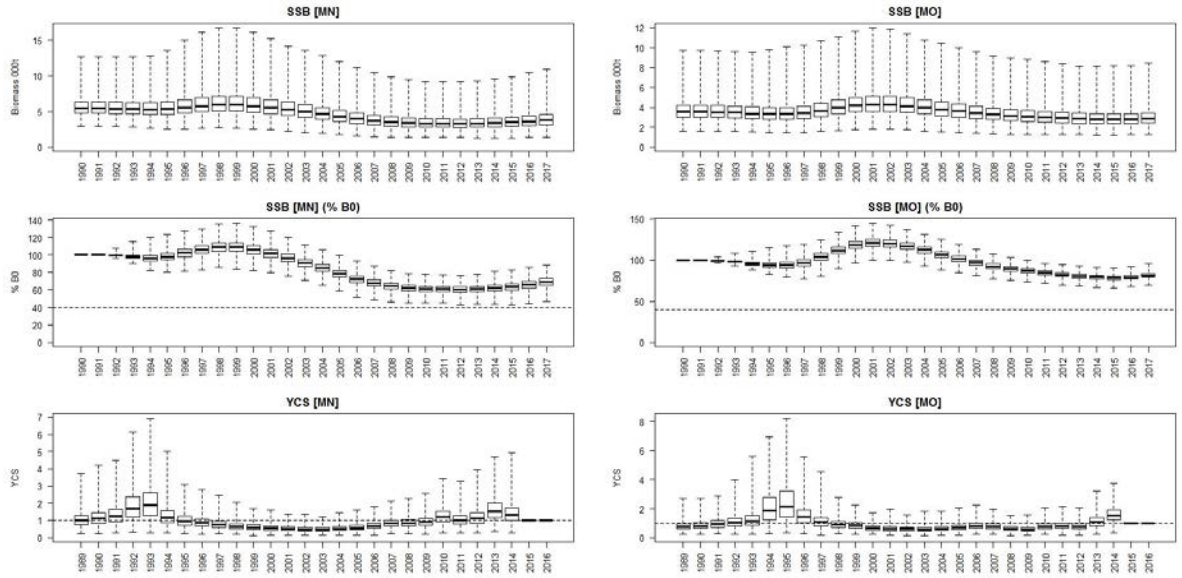

A5. 63: Posterior trajectory of *SSB*, SSB_{2016}/SSB_0, and YCS for subareas MN and MO.

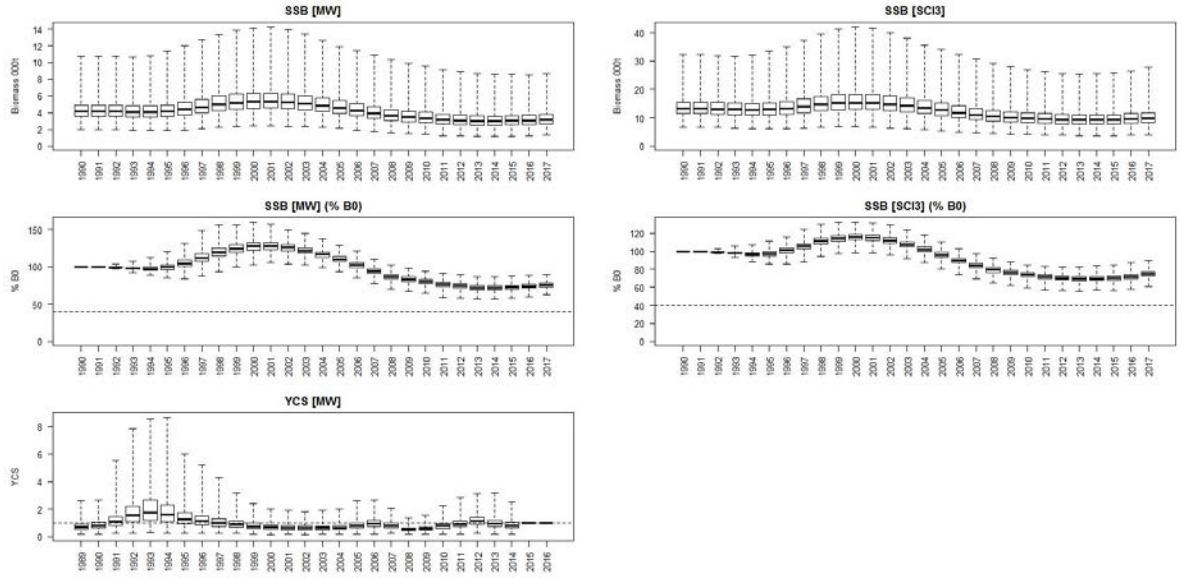

A5. 64: Posterior trajectory of *SSB*, SSB_{2016}/SSB_0, and YCS for subareas MW and the combined SCI 3 modelled area.

APPENDIX 6: MODEL 4, *M* fixed at 0.20, CPUE process error 0.25

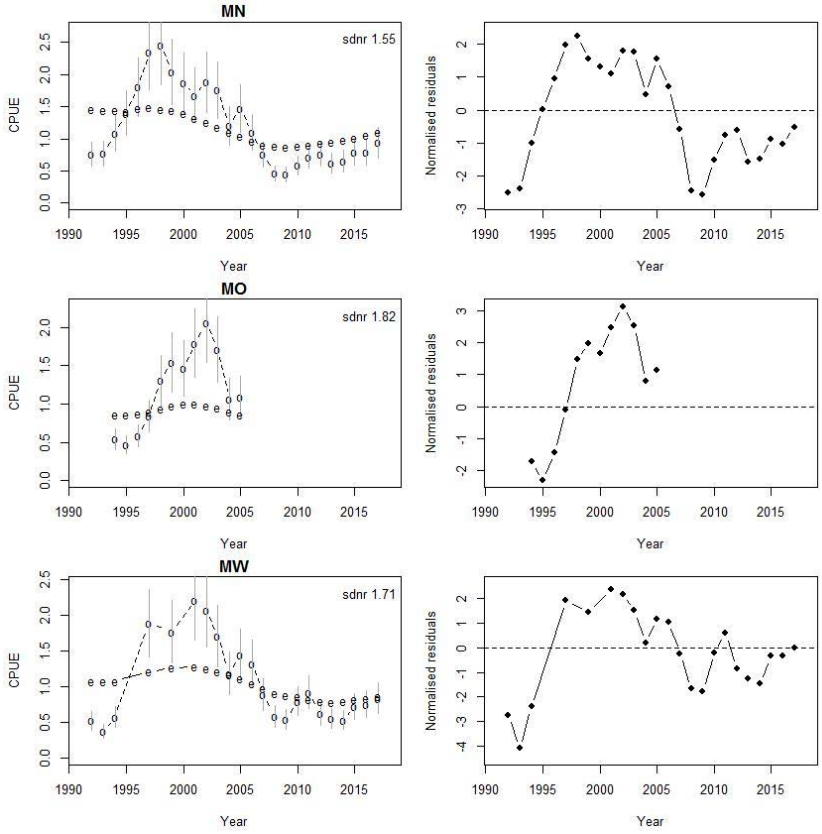

A6. 1: Fits to CPUE indices (left column) and normalised residuals (right column) by subarea (MN - top row, MO - middle row, MW - bottom row) for SCI 3 Model 4.

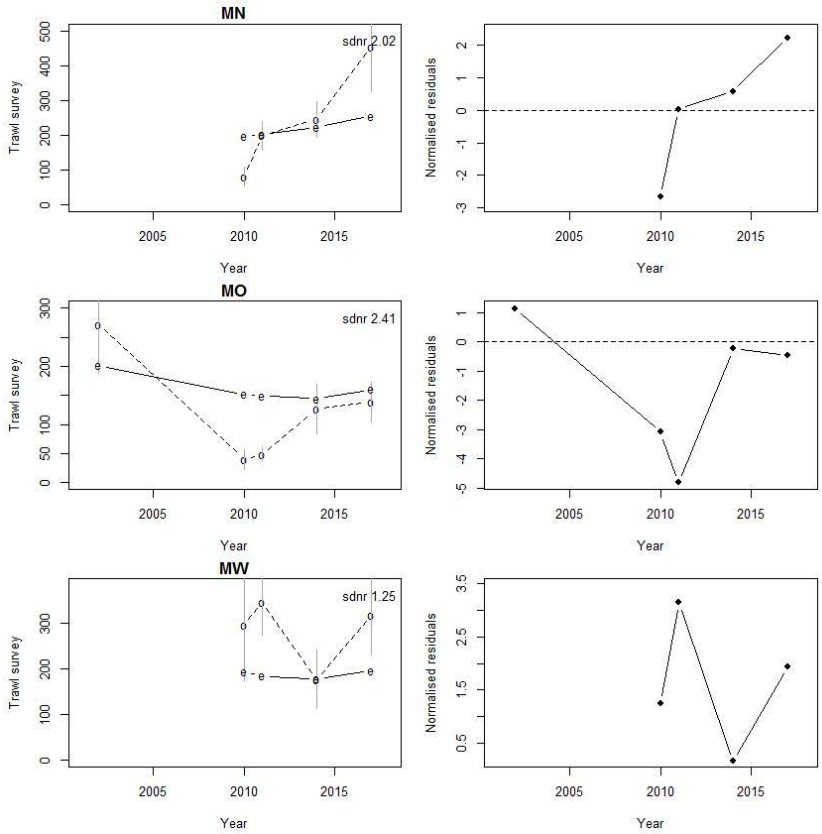

A6. 2: Fits to trawl survey indices (left column) and normalised residuals (right column) by subarea (MN - top row, MO - middle row, MW - bottom row) for SCI 3 Model 4.

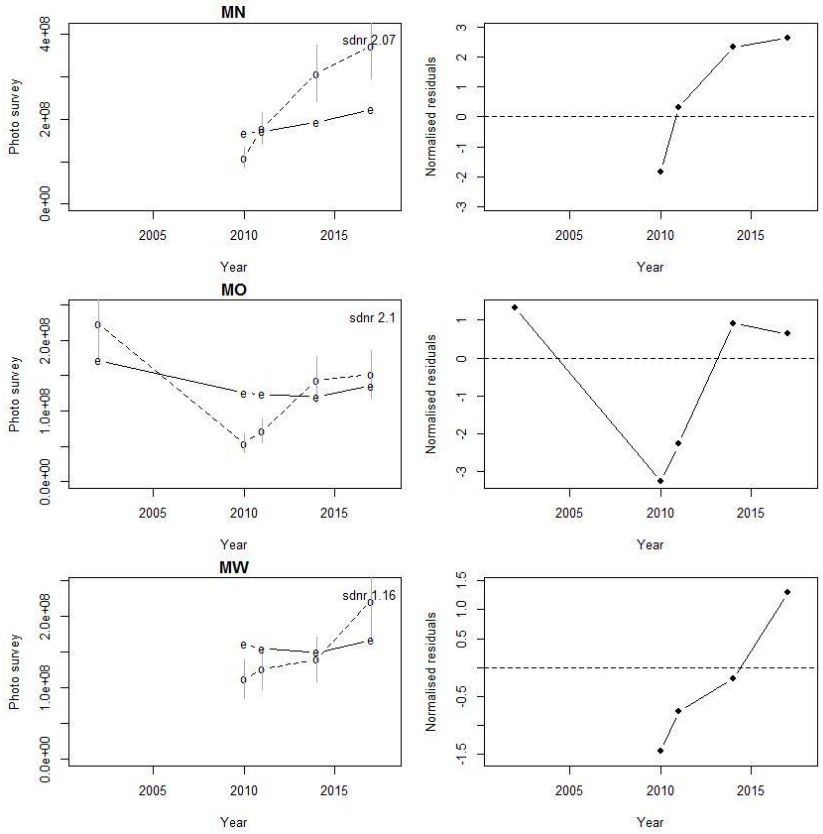

A6. 3: Fits to photo survey indices (left column) and normalised residuals (right column) by subarea (MN - top row, MO - middle row, MW - bottom row) for SCI 3 Model 4.

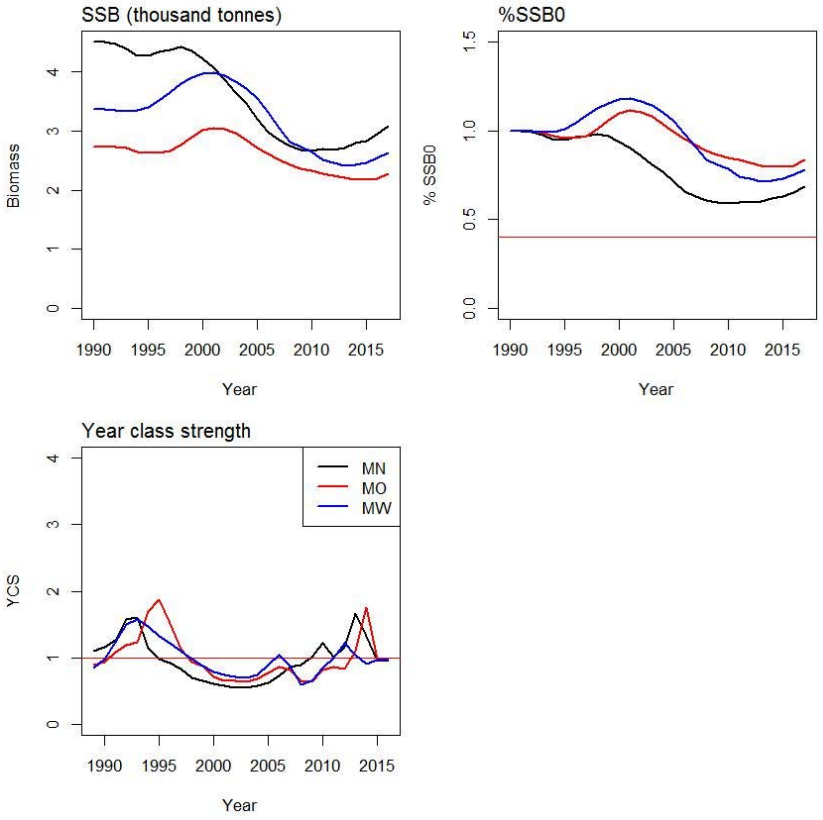

A6. 4: Spawning stock biomass trajectory (upper left), spawning stock biomass as a percentage of SSB_0 (upper right), and year class strength (lower plot) by subarea for SCI 3 Model 4.

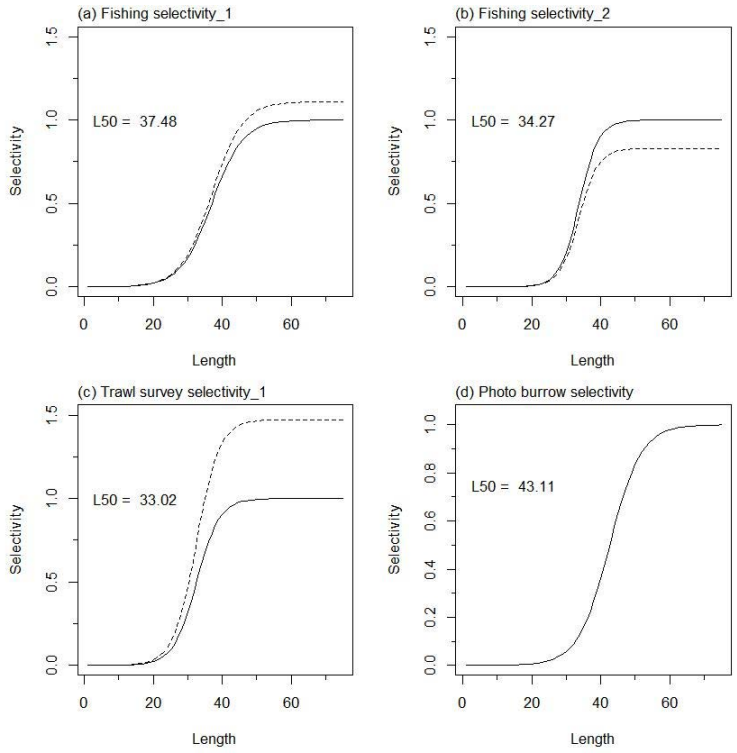

A6. 5: Spawning stock biomass trajectory (upper left), spawning stock biomass as a percentage of SSB_0 (upper right), and year class strength (lower plot) by subarea for SCI 3 Model 4.

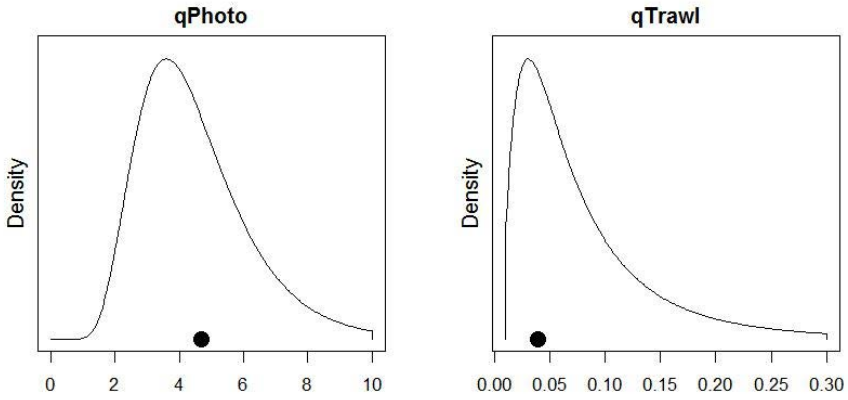

A6. 6: Catchability estimates from MPD model run for SCI 3 Model 3, plotted in relation to prior distribution.

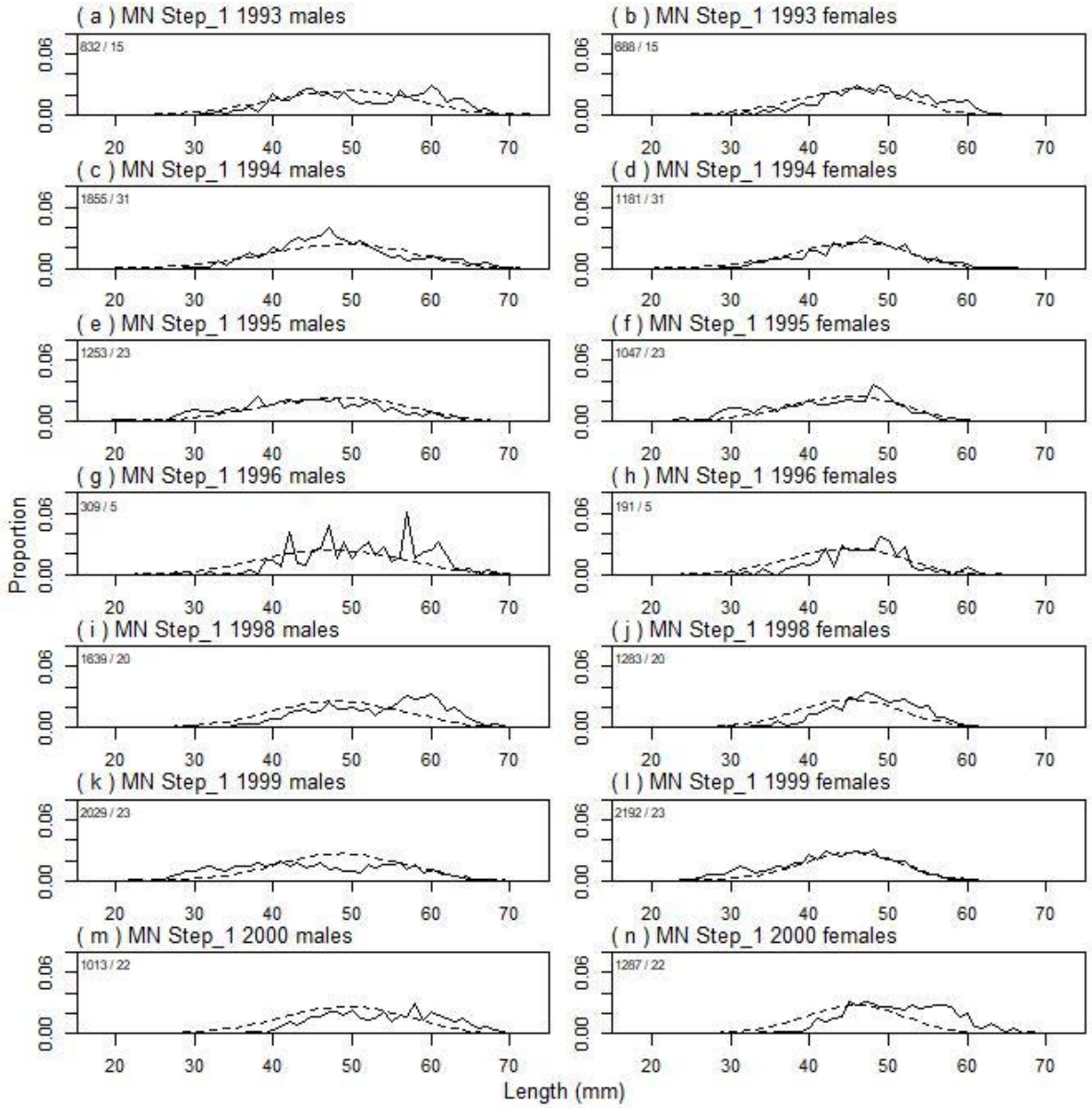

A6. 7: Observed (solid line) and fitted (dashed line) length frequency distributions for observer samples, MN time step 1. Numbers in top left corner of each plot represent number of scampi measured / number of events sampled.

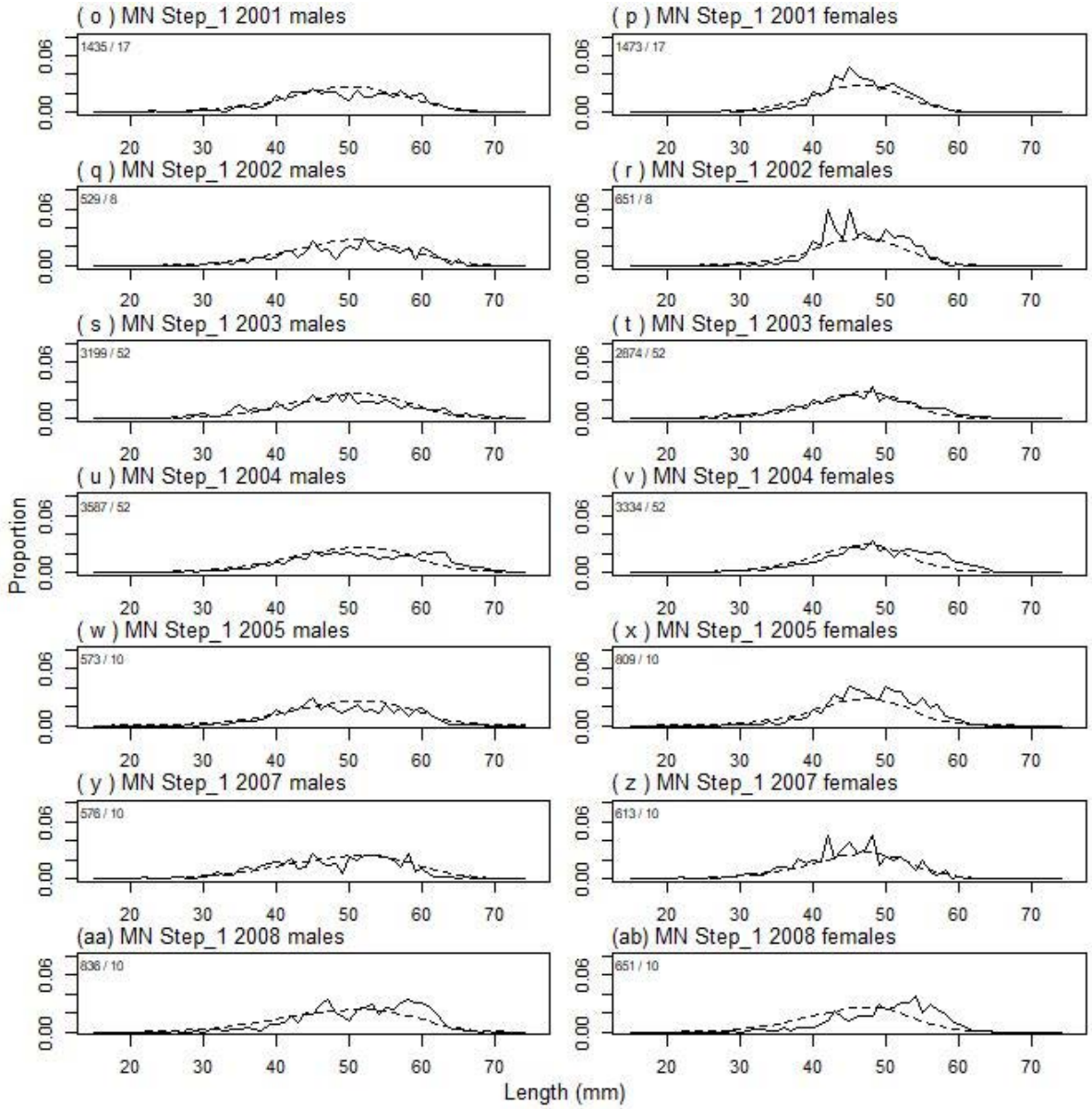

A6. 7 *continued*: Observed (solid line) and fitted (dashed line) length frequency distributions for observer samples, MN time step 1. Numbers in top left corner of each plot represent number of scampi measured / number of events sampled.

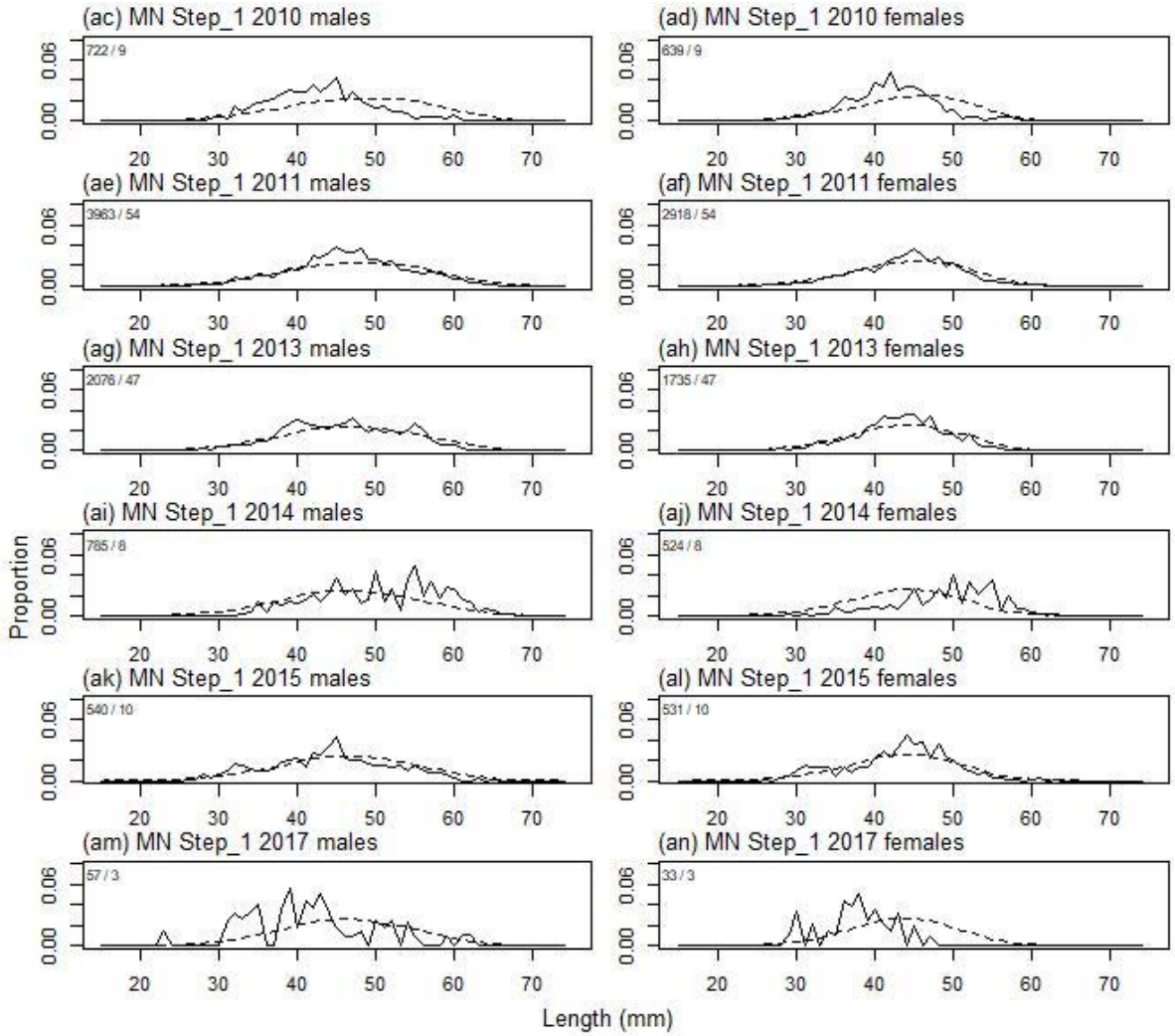

A6. 7 *continued*: Observed (solid line) and fitted (dashed line) length frequency distributions for observer samples, MN time step 1. Numbers in top left corner of each plot represent number of scampi measured / number of events sampled.

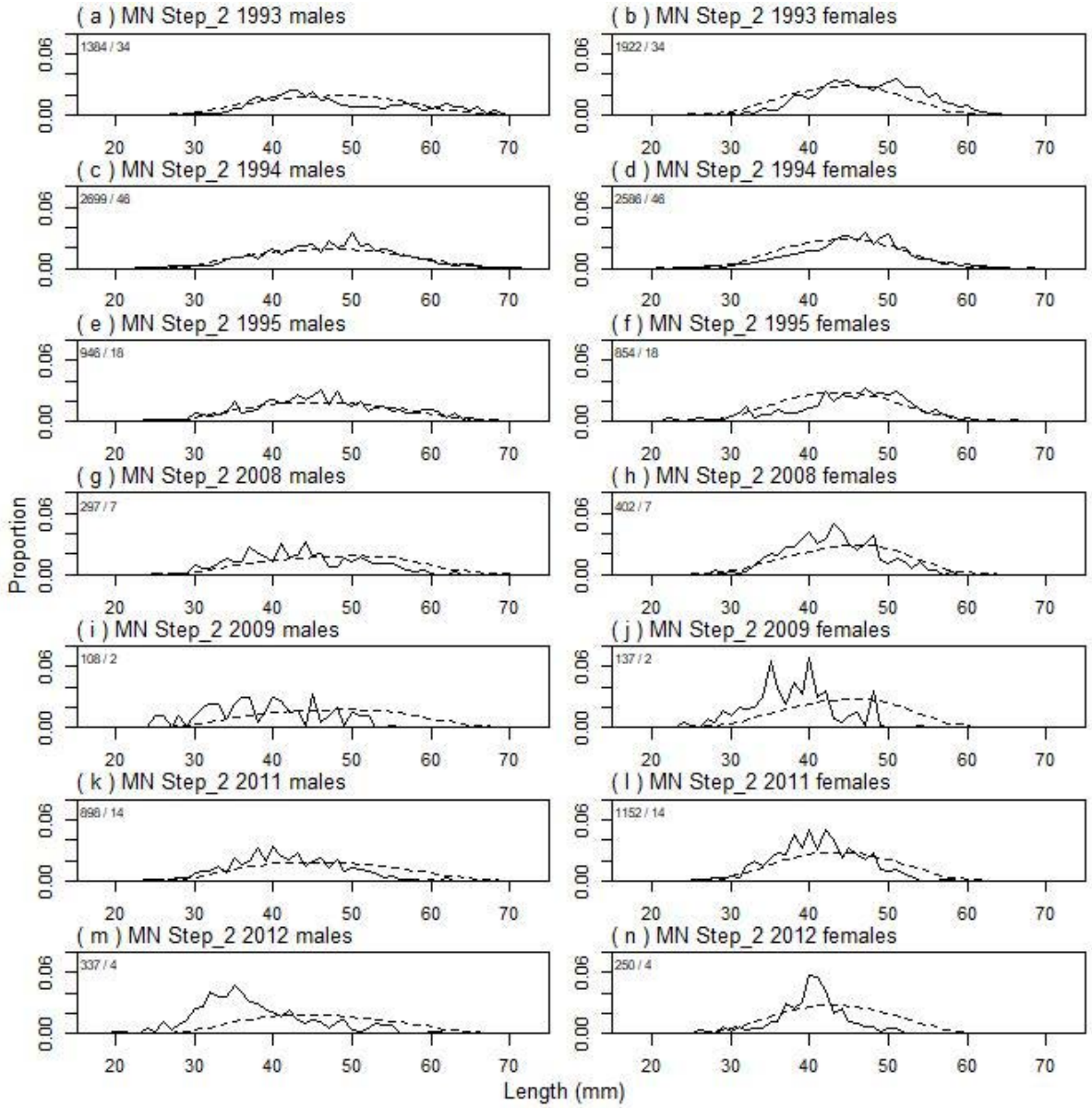

A6. 8: Observed (solid line) and fitted (dashed line) length frequency distributions for observer samples, MN time step 2. Numbers in top left corner of each plot represent number of scampi measured / number of events sampled.

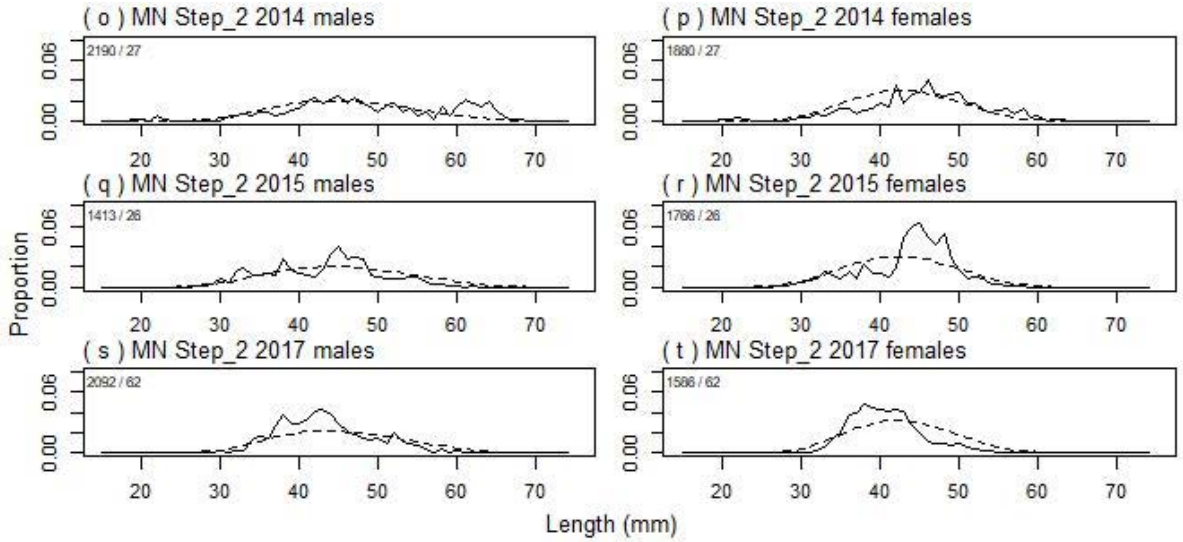

A6. 8 *continued*: Observed (solid line) and fitted (dashed line) length frequency distributions for observer samples, MN time step 2. Numbers in top left corner of each plot represent number of scampi measured / number of events sampled.

A6. 9: Numbers of scampi measured, estimated multinomial N sample size, and effective sample size used within the model for length frequency distributions for observer samples, time step 1.

	Measured	Multinomial N	Effective sample size
N_1993	1 520	1 345	5.94
N_1994	3 036	2 264	10.00
N_1995	2 300	1 824	8.05
N_1996	500	576	2.54
N_1998	2 922	2 599	11.48
N_1999	4 221	3 441	15.19
N_2000	2 300	1 928	8.51
N_2001	2 908	2 827	12.48
N_2002	1 180	988	4.36
N_2003	6 073	3 727	16.46
N_2004	6 921	5 077	22.42
N_2005	1 382	2 030	8.96
N_2007	1 189	2 414	10.66
N_2008	1 487	1 651	7.29
N_2010	1 361	1 544	6.82
N_2011	6 881	4 896	21.62
N_2013	3 811	2 929	12.93
N_2014	1 309	745	3.29
N_2015	1 071	2 071	9.14
N_2017	90	181	0.80

A6. 10: Numbers of scampi measured, estimated multinomial N sample size, and effective sample size used within the model for length frequency distributions for observer samples, MN time step 2.

	Measured	Multinomial N	Effective sample size
N_1993	3 306	2 571	16.03
N_1994	5 285	4 117	25.68
N_1995	1 800	1 501	9.36
N_2008	699	713	4.45
N_2009	245	340	2.12
N_2011	2 050	1 583	9.87
N_2012	587	691	4.31
N_2014	4 071	1 270	7.92
N_2015	3 179	5 855	36.52
N_2017	3 678	1 906	11.89

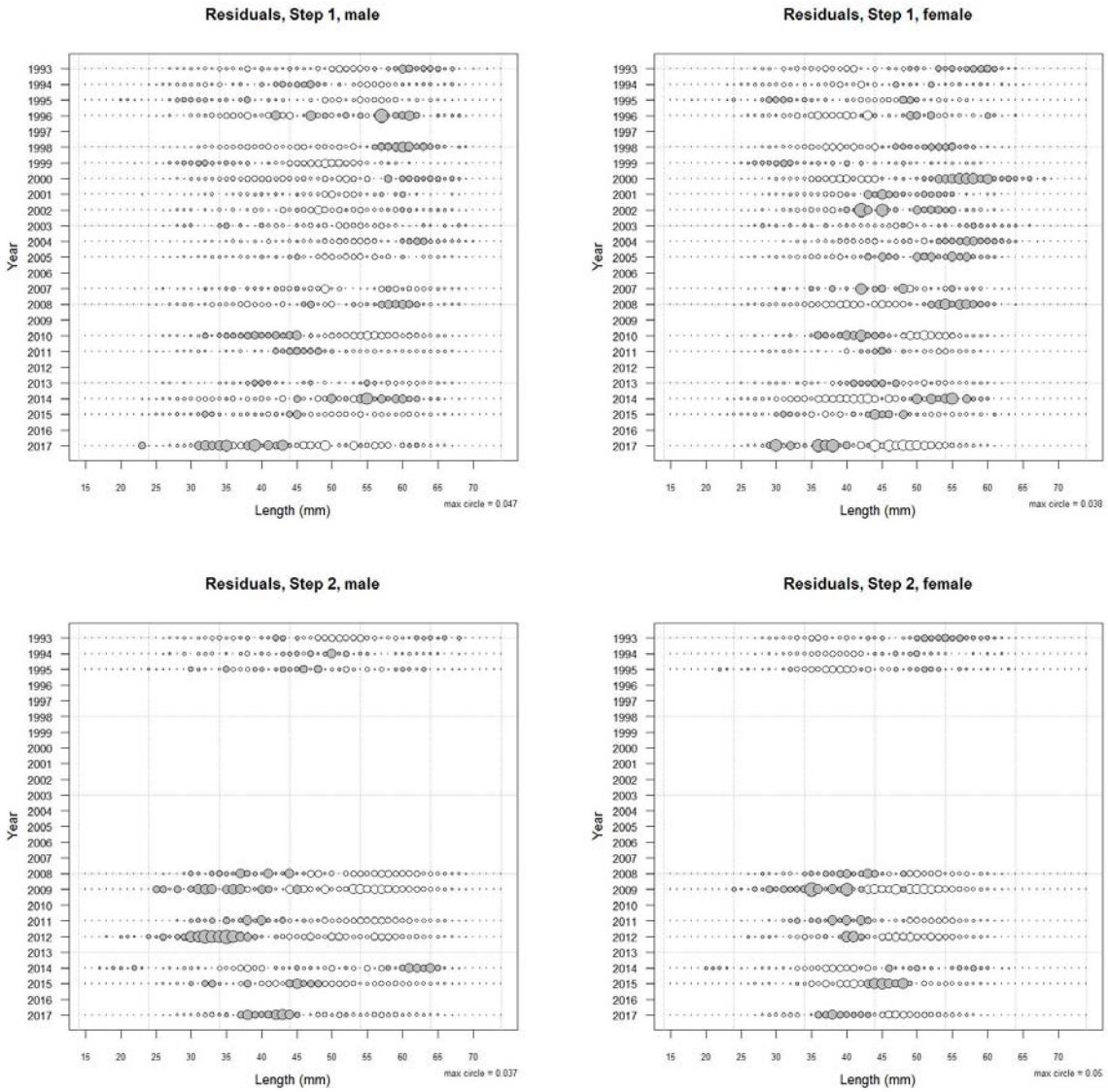

A6. 11: Bubble plots of residuals for fits to length frequency distributions for MN observer sampling.

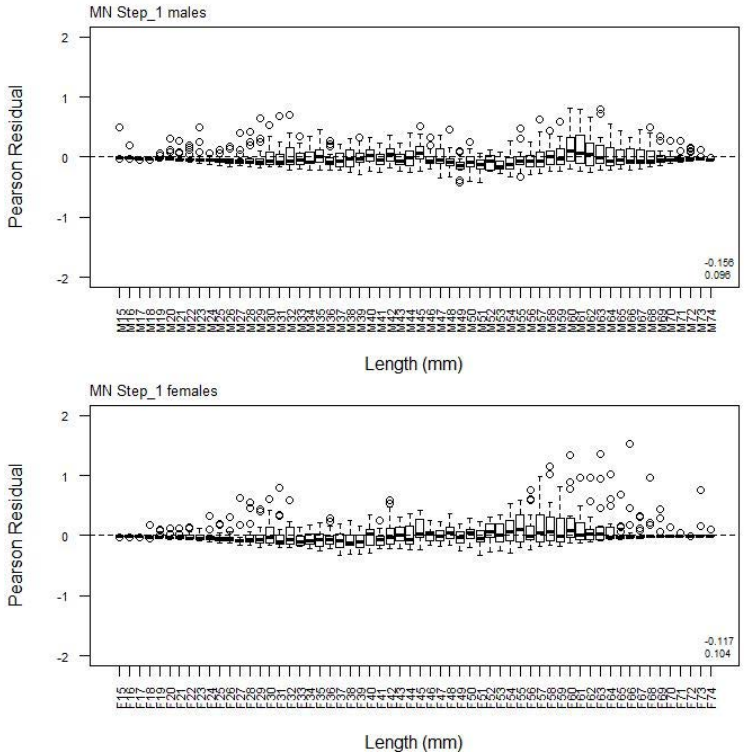

A6. 12: Box plots of Pearson residuals from the fit to length frequency distributions by length from observer sampling by sex for MN time step 1.

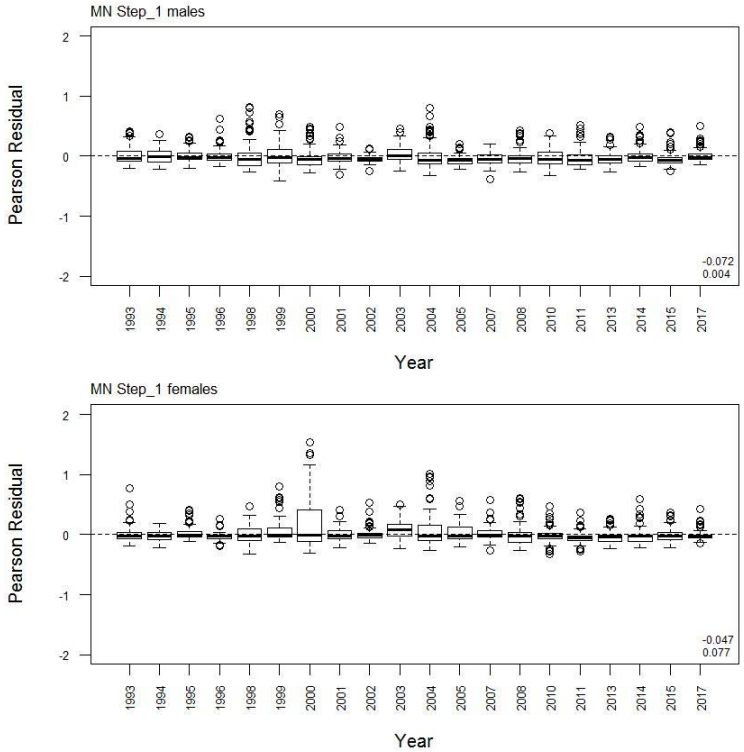

A6. 13: Box plots of Pearson residuals from the fit to length frequency distributions by year from observer sampling by sex for MN time step 2.

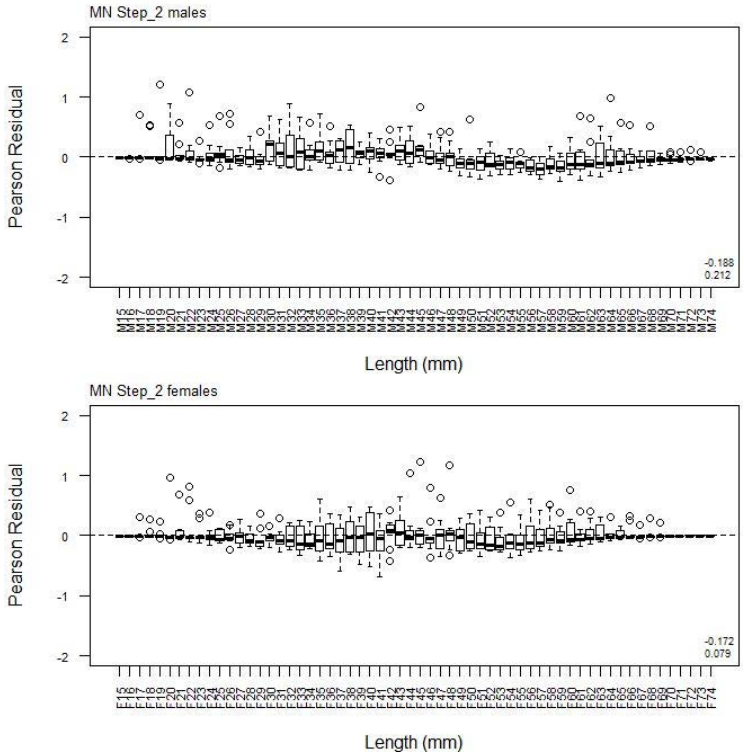

A6. 14: Box plots of Pearson residuals from the fit to length frequency distributions by length from observer sampling by sex for MN time step 2.

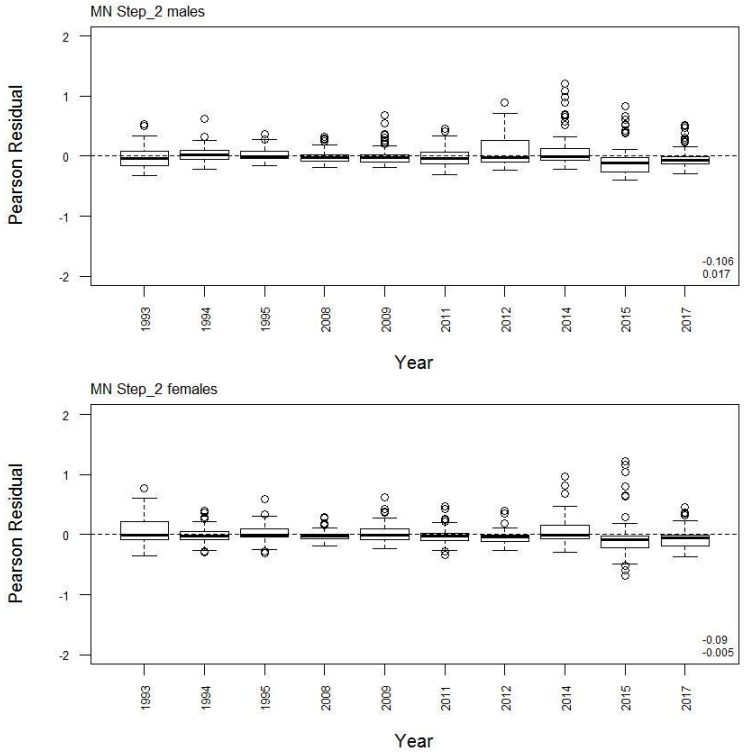

A6. 15: Box plots of Pearson residuals from the fit to length frequency distributions by year from observer sampling by sex for MN time step 2.

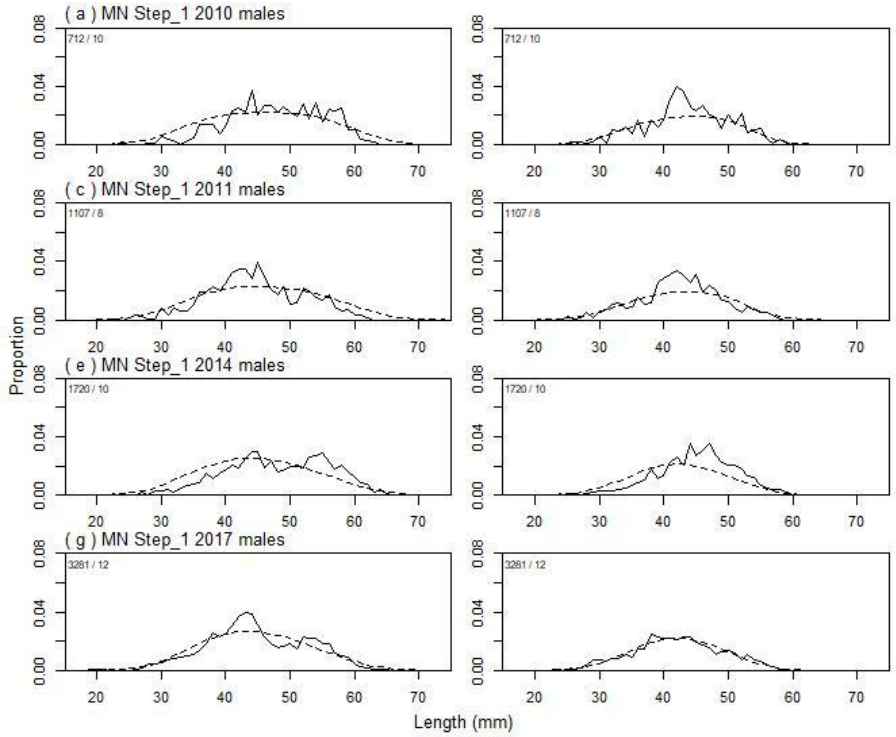

A6. 16: Observed (solid line) and fitted (dashed line) length frequency distributions for MN research survey samples.

A6. 17: Numbers of scampi measured, estimated multinomial N sample size, and effective sample size used within the model for length frequency distributions for MN research survey samples.

	Measured	Multinomial N	Effective sample size
N_2010	1 276	941	12.17
N_2011	2 027	1 610	20.82
N_2014	3 156	2 381	30.78
N_2017	5 299	4 895	63.29

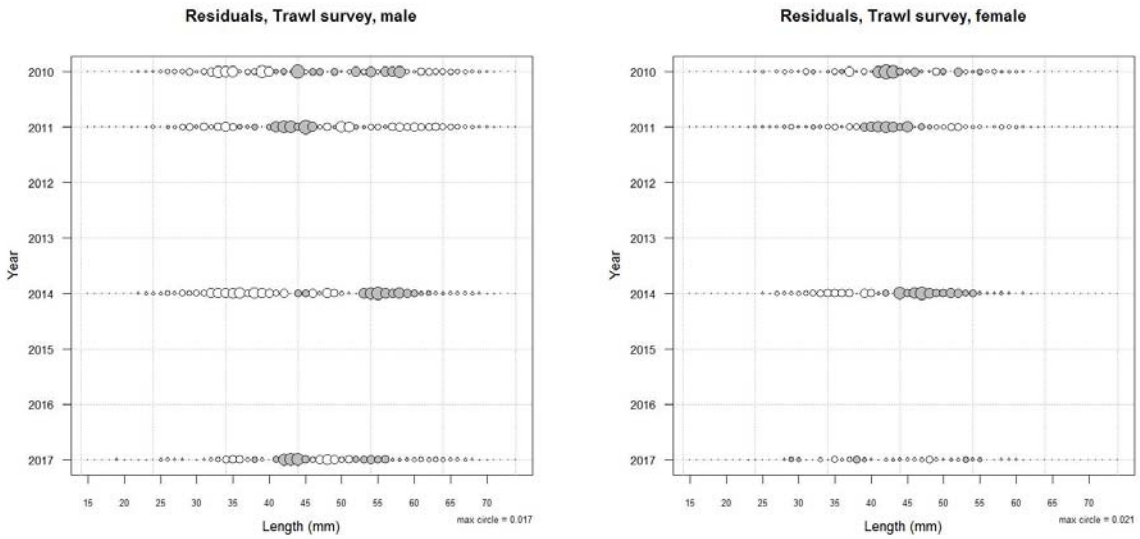

A6. 18: Bubble plots of residuals for fits to length frequency distributions for MN trawl sampling.

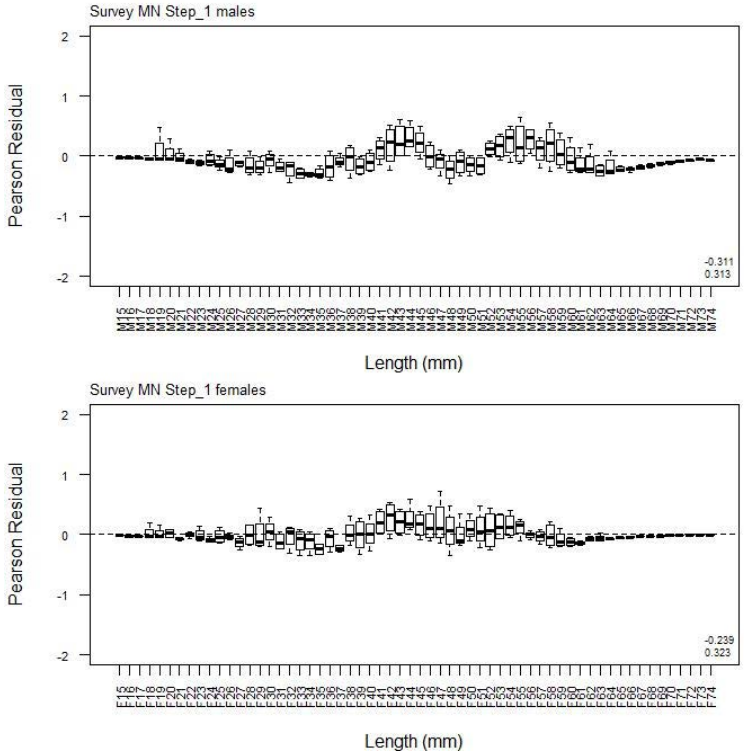

A6. 19: Box plots of Pearson residuals from the fit to length frequency distributions by length from MN trawl sampling.

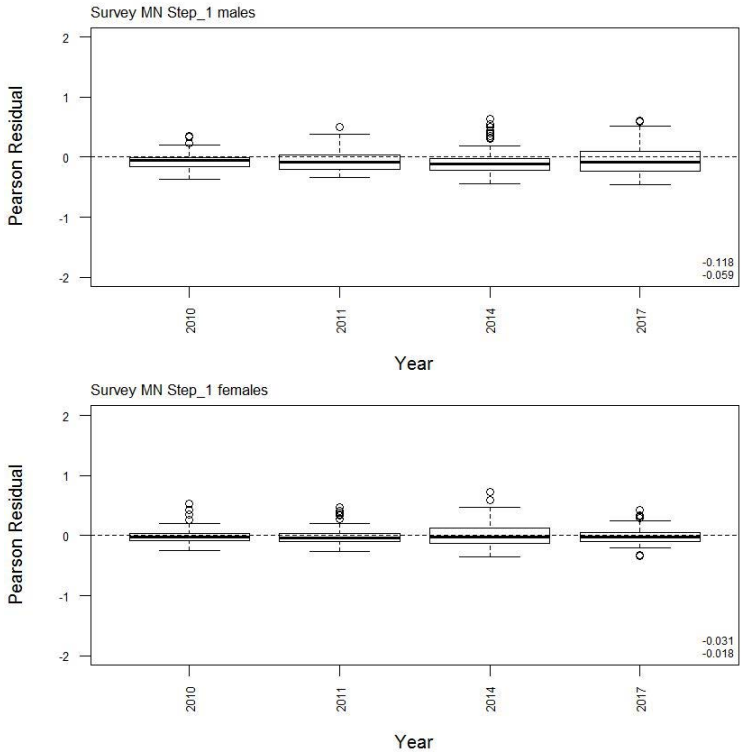

A6. 20: Box plots of Pearson residuals from the fit to length frequency distributions by year from for MN trawl sampling.

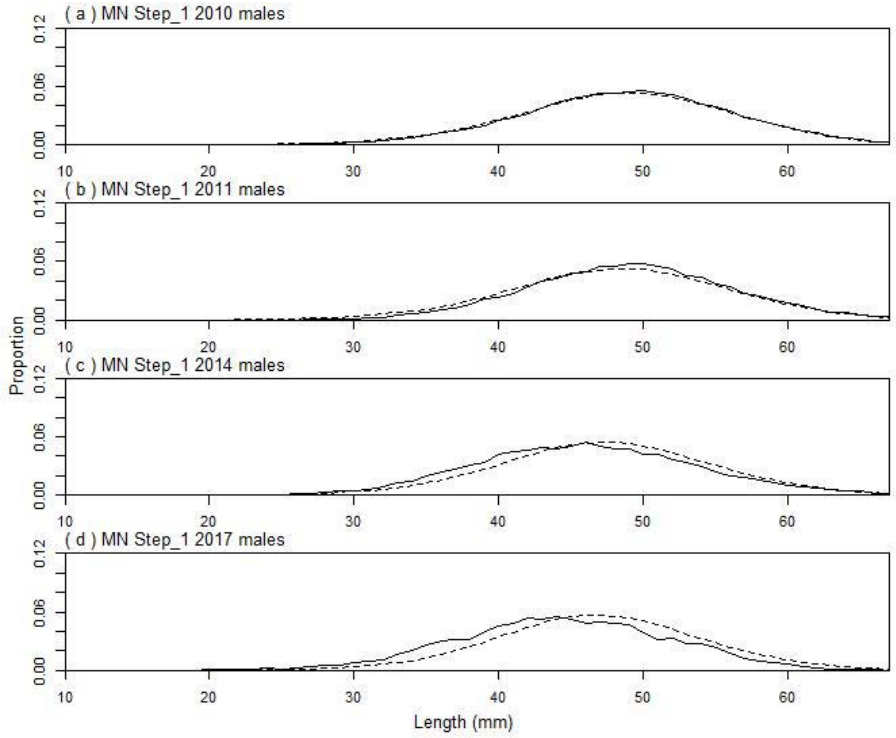

A6. 21: Observed (solid line) and fitted (dashed line) length frequency distributions for MN photographic survey scampi size estimation.

A6. 22: Numbers of scampi measured, estimated multinomial N sample size, and effective sample size used within the model for length frequency distributions for MN photographic survey samples.

	Measured	Multinomial N	Effective sample size
N_2010	113	211	50.25
N_2011	120	225	53.58
N_2014	62	120	28.58
N_2017	25	50	11.91

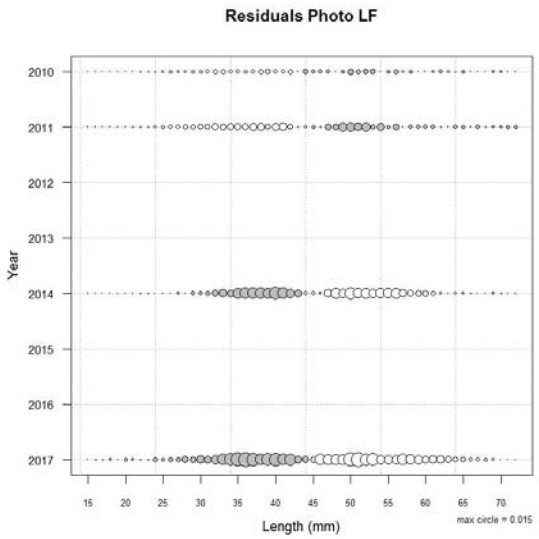

A6. 23: Bubble plots of residuals for fits to length frequency distributions for MN photographic sampling.

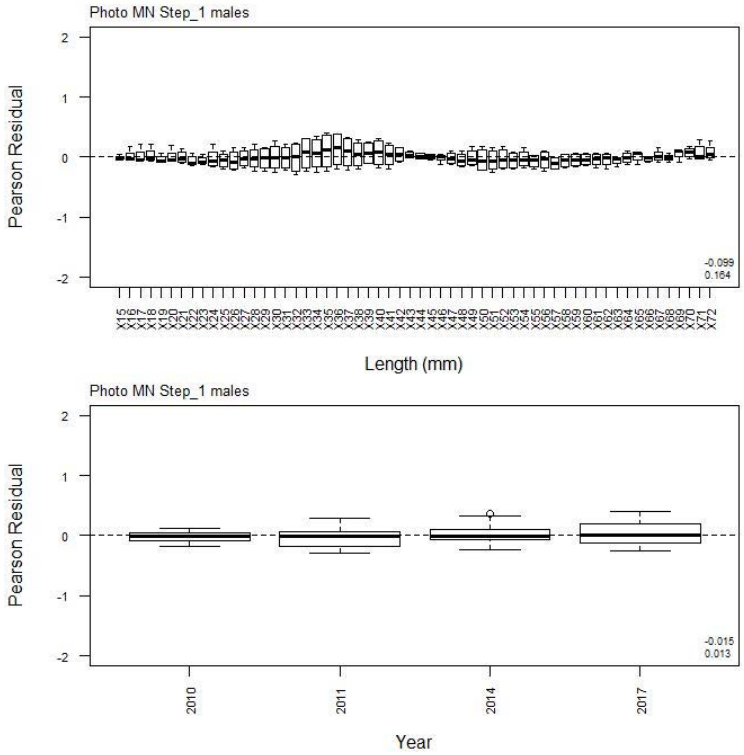

A6. 24: Box plots of Pearson residuals from the fit to length frequency distributions by length and year for MN photographic sampling.

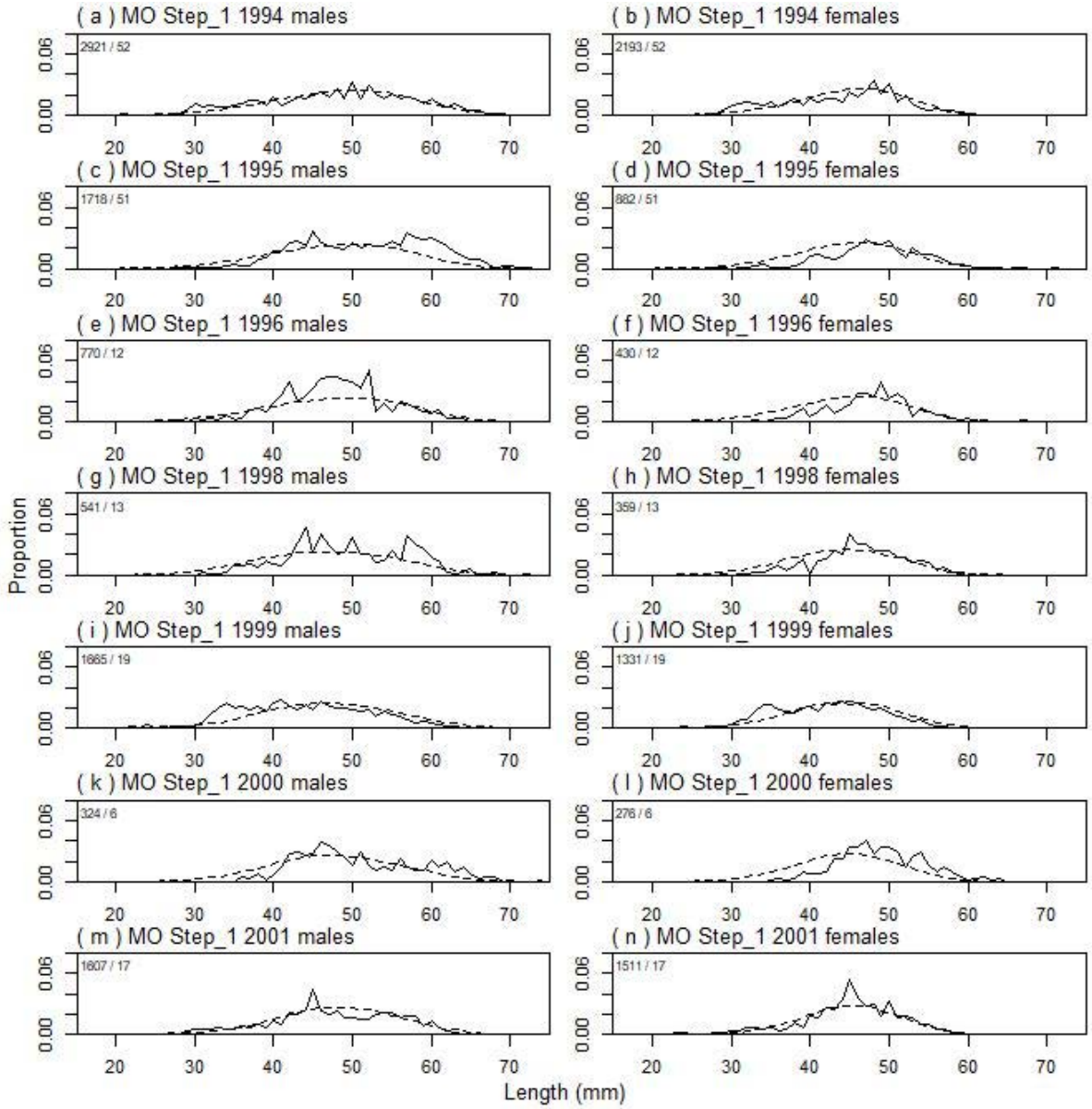

A6. 25: Observed (solid line) and fitted (dashed line) length frequency distributions for observer samples, MO time step 1. Numbers in top left corner of each plot represent number of scampi measured / number of events sampled.

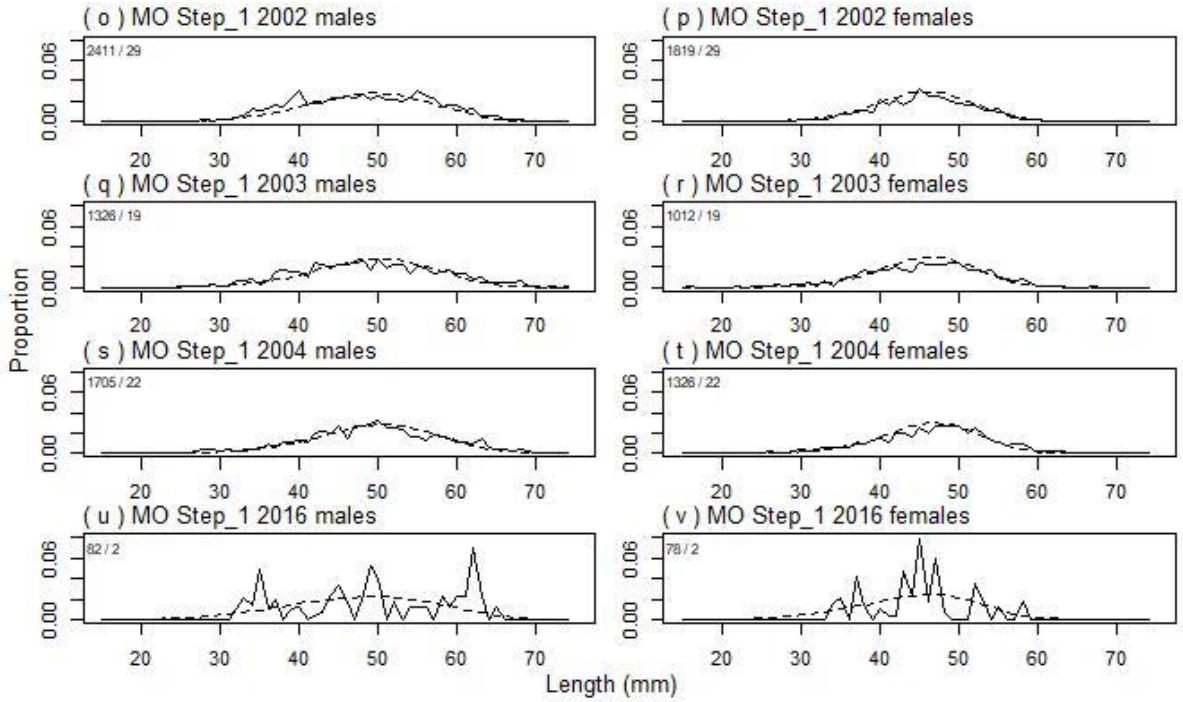

A6. 25 *continued*: Observed (solid line) and fitted (dashed line) length frequency distributions for observer samples, MO time step 1. Numbers in top left corner of each plot represent number of scampi measured / number of events sampled.

A6. 26: Numbers of scampi measured, estimated multinomial N sample size, and effective sample size used within the model for length frequency distributions for observer samples, MO time step 1.

	Measured	Multinomial N	Effective sample size
N_1994	5 114	3 277	29.92
N_1995	2 600	2 182	19.92
N_1996	1 200	1 071	9.78
N_1998	900	940	8.58
N_1999	2 996	2 504	22.86
N_2000	600	733	6.69
N_2001	3 118	2 900	26.48
N_2002	4 230	2 662	23.49
N_2003	2 338	1 553	14.18
N_2004	3 031	2 084	19.03
N_2016	160	88	0.80

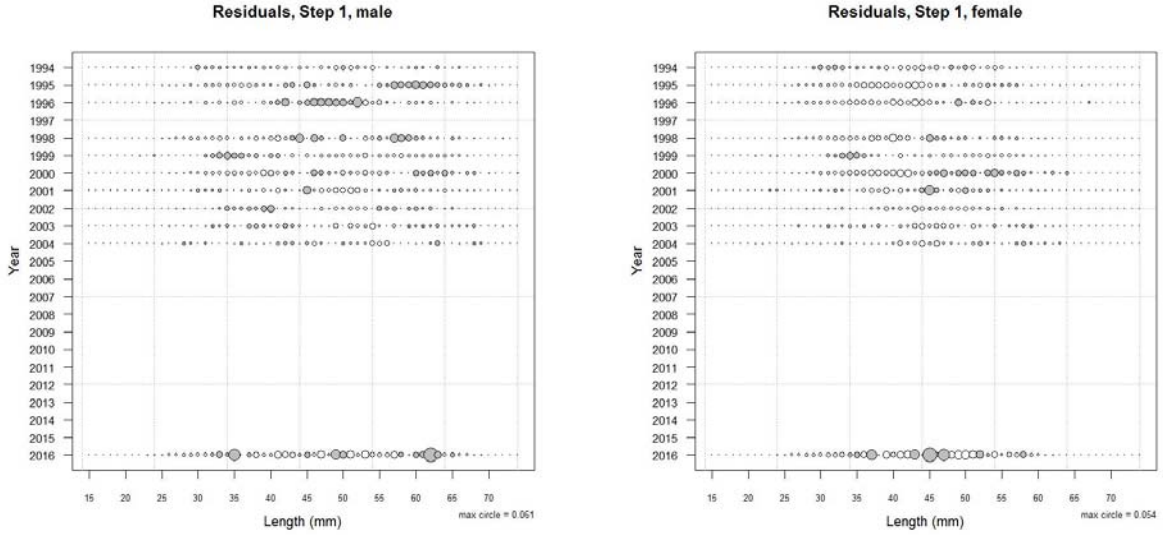

A6. 27: Bubble plots of residuals for fits to length frequency distributions for MO observer sampling.

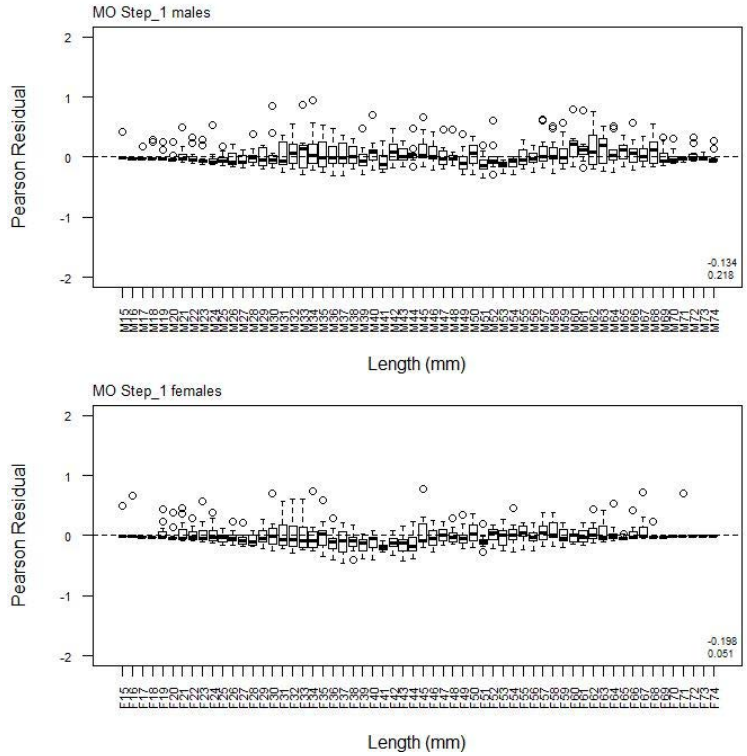

A6. 28: Box plots of Pearson residuals from the fit to length frequency distributions by length from observer sampling by sex for MO time step 1.

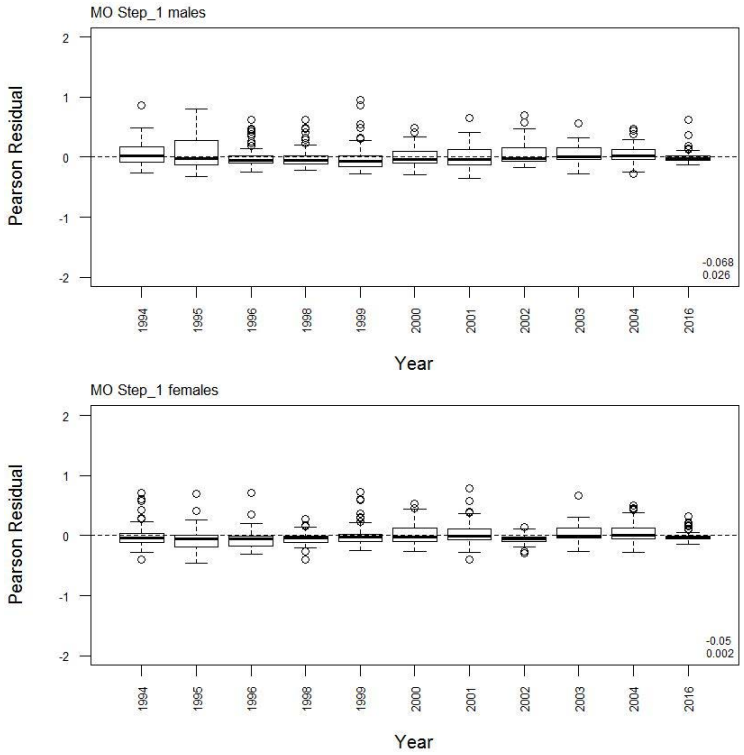

A6. 29: Box plots of Pearson residuals from the fit to length frequency distributions by year from observer sampling by sex for MO time step 1.

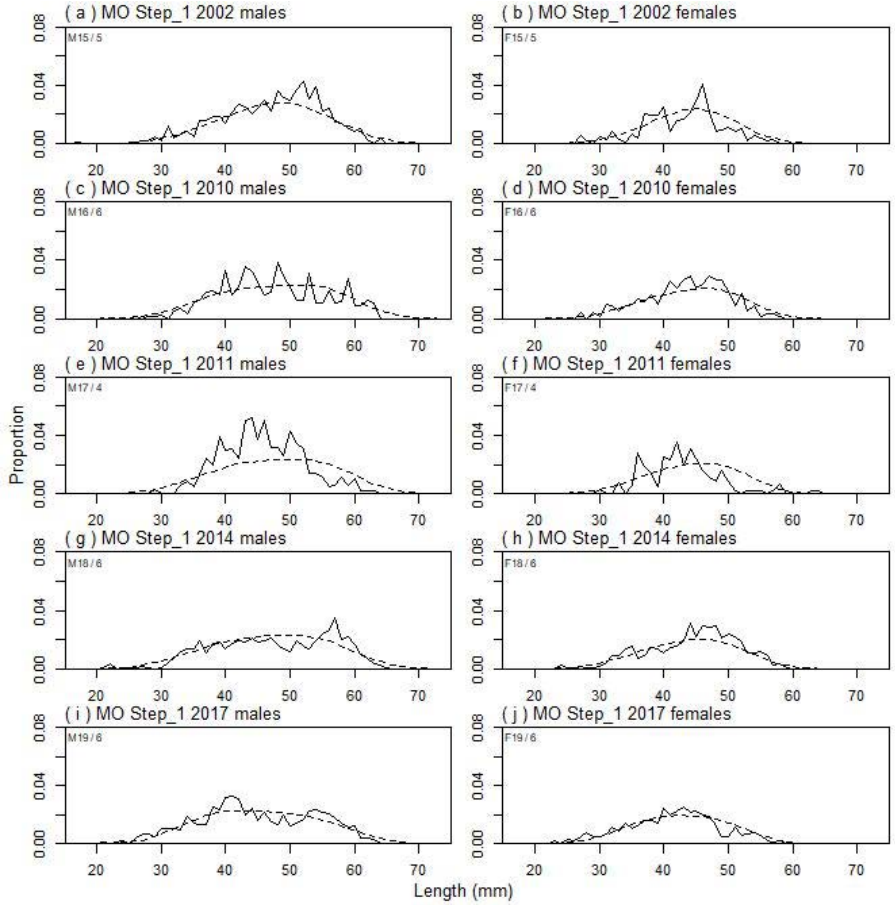

A6. 30: Observed (solid line) and fitted (dashed line) length frequency distributions for MO research survey samples.

A6. 31: Numbers of scampi measured, estimated multinomial N sample size, and effective sample size used within the model for length frequency distributions for MO research survey samples.

	Measured	Multinomial N	Effective sample size
N_2002	764	725	98.50
N_2010	551	627	85.19
N_2011	396	483	65.62
N_2014	1 465	1 363	185.19
N_2017	1 807	1 669	226.76

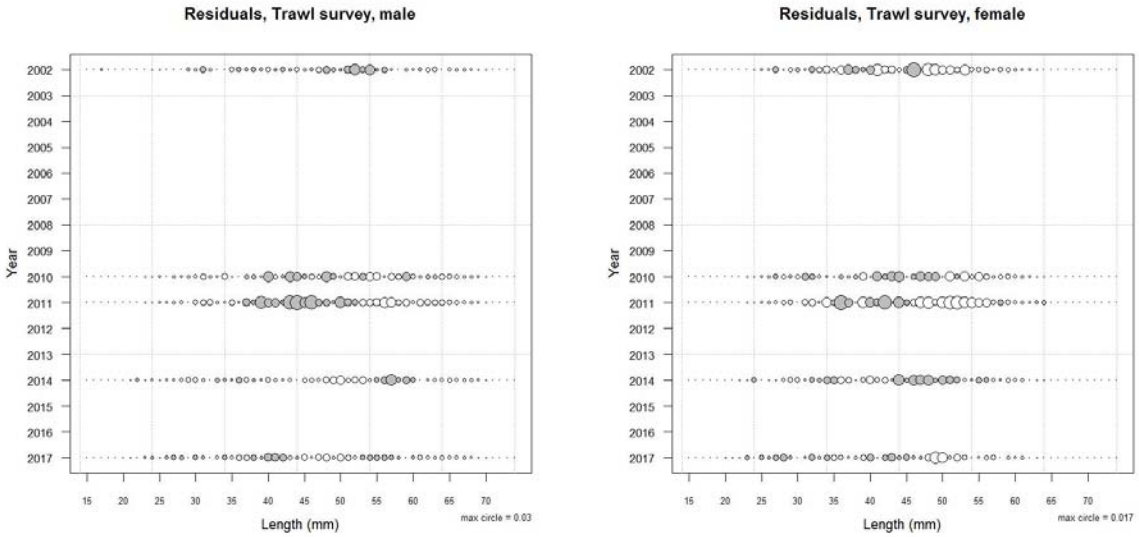

A6. 32: Bubble plots of residuals for fits to length frequency distributions for MO trawl sampling.

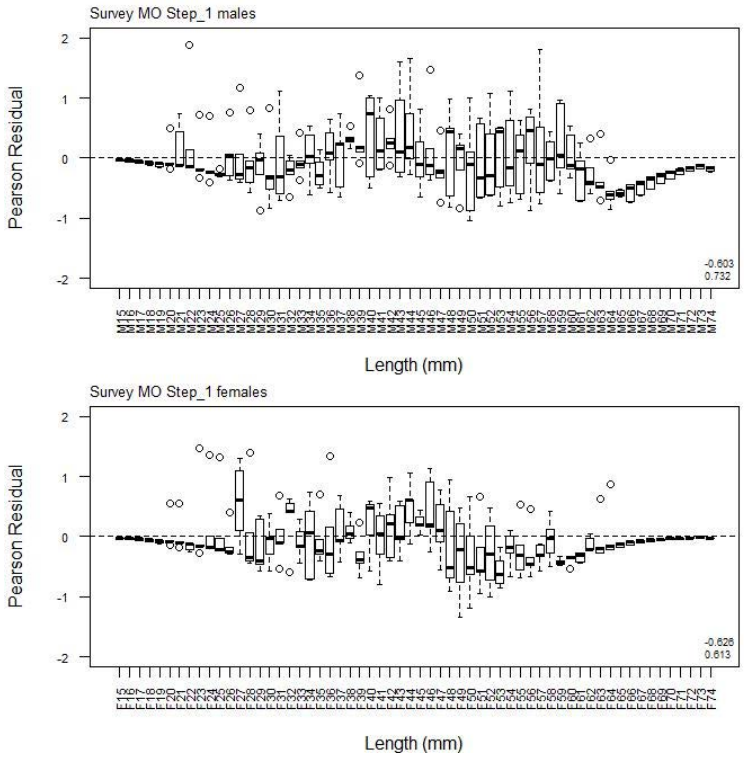

A6. 33: Box plots of Pearson residuals from the fit to length frequency distributions by length from MO trawl sampling.

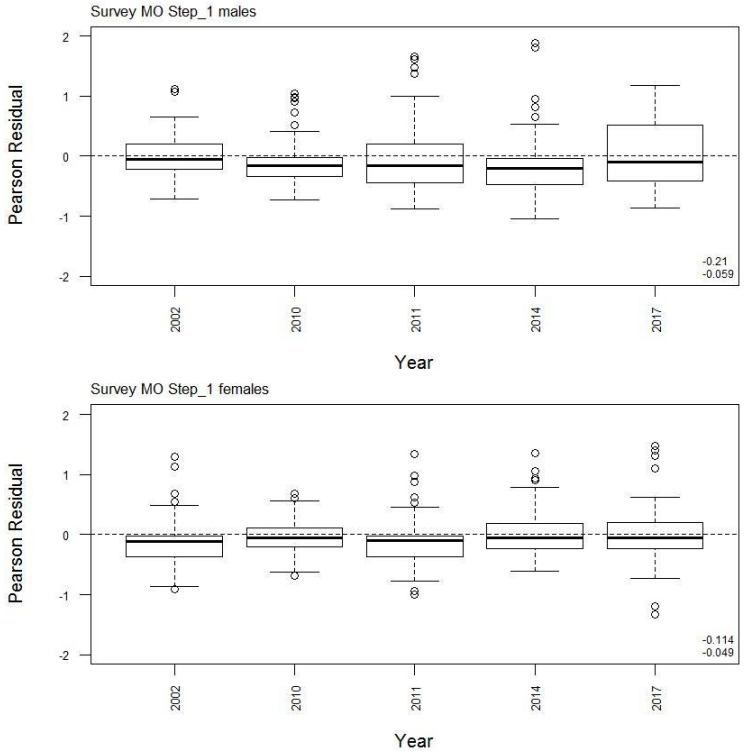

A6. 34: Box plots of Pearson residuals from the fit to length frequency distributions by year from MO trawl sampling.

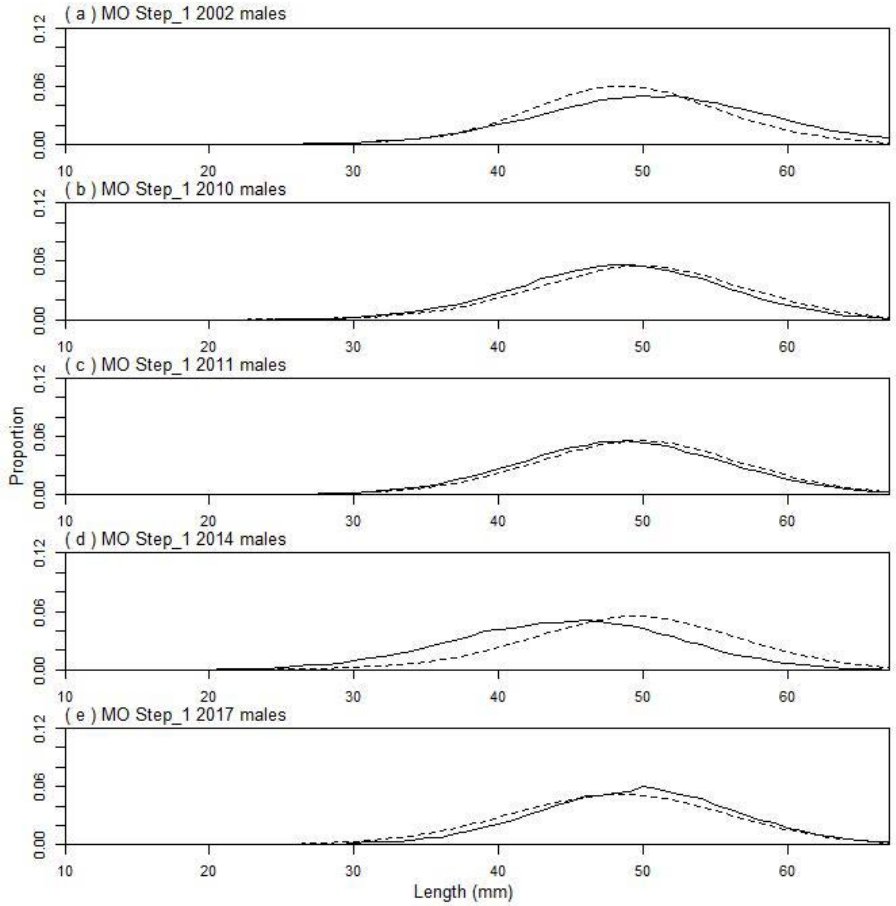

A6. 35: Observed (solid line) and fitted (dashed line) length frequency distributions for MO photographic survey scampi size estimation.

A6. 36: Numbers of scampi measured, estimated multinomial N sample size, and effective sample size used within the model for length frequency distributions for MO photographic survey samples.

	Measured	Multinomial N	Effective sample size
N_2002	224	384	12.67
N_2010	214	365	12.04
N_2011	426	536	17.69
N_2014	125	224	7.39
N_2017	76	145	4.78

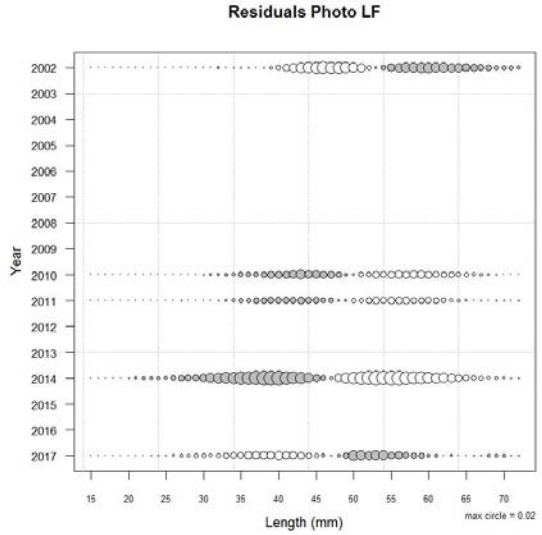

A6. 37: Bubble plots of residuals for fits to length frequency distributions for MO photographic sampling.

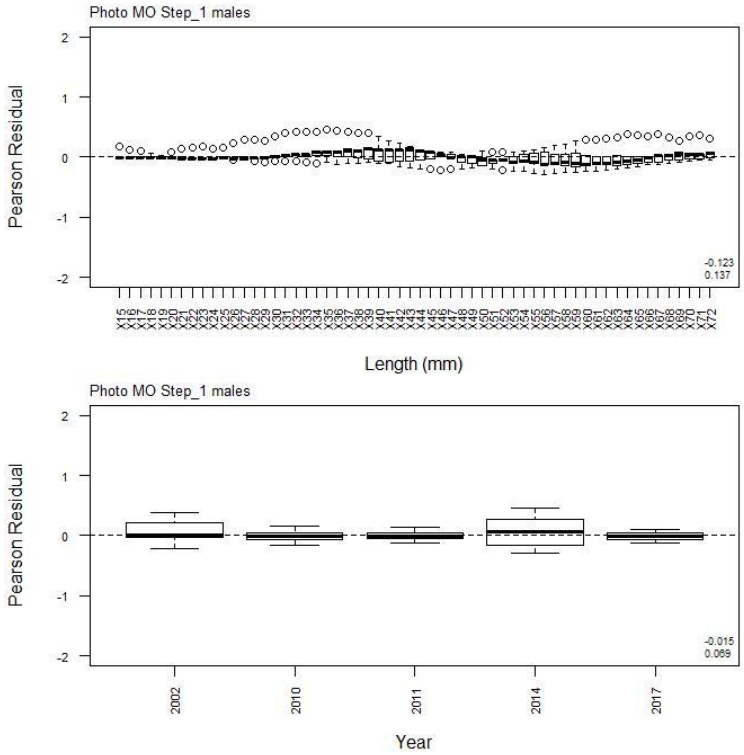

A6. 38: Box plots of Pearson residuals from the fit to length frequency distributions by length and year for MO photographic sampling.

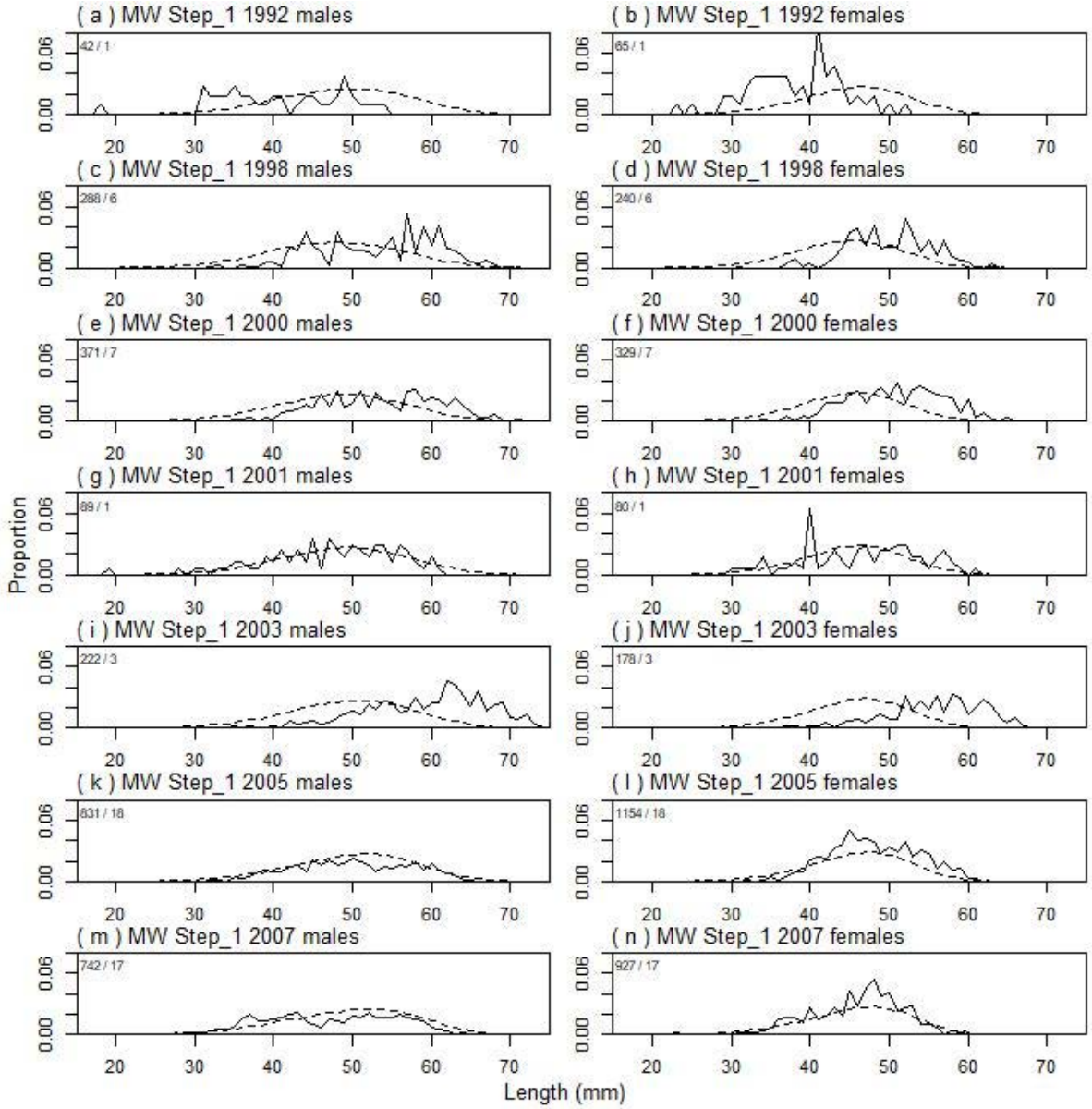

A6. 39: Observed (solid line) and fitted (dashed line) length frequency distributions for observer samples, MW time step 1. Numbers in top left corner of each plot represent number of scampi measured / number of events sampled.

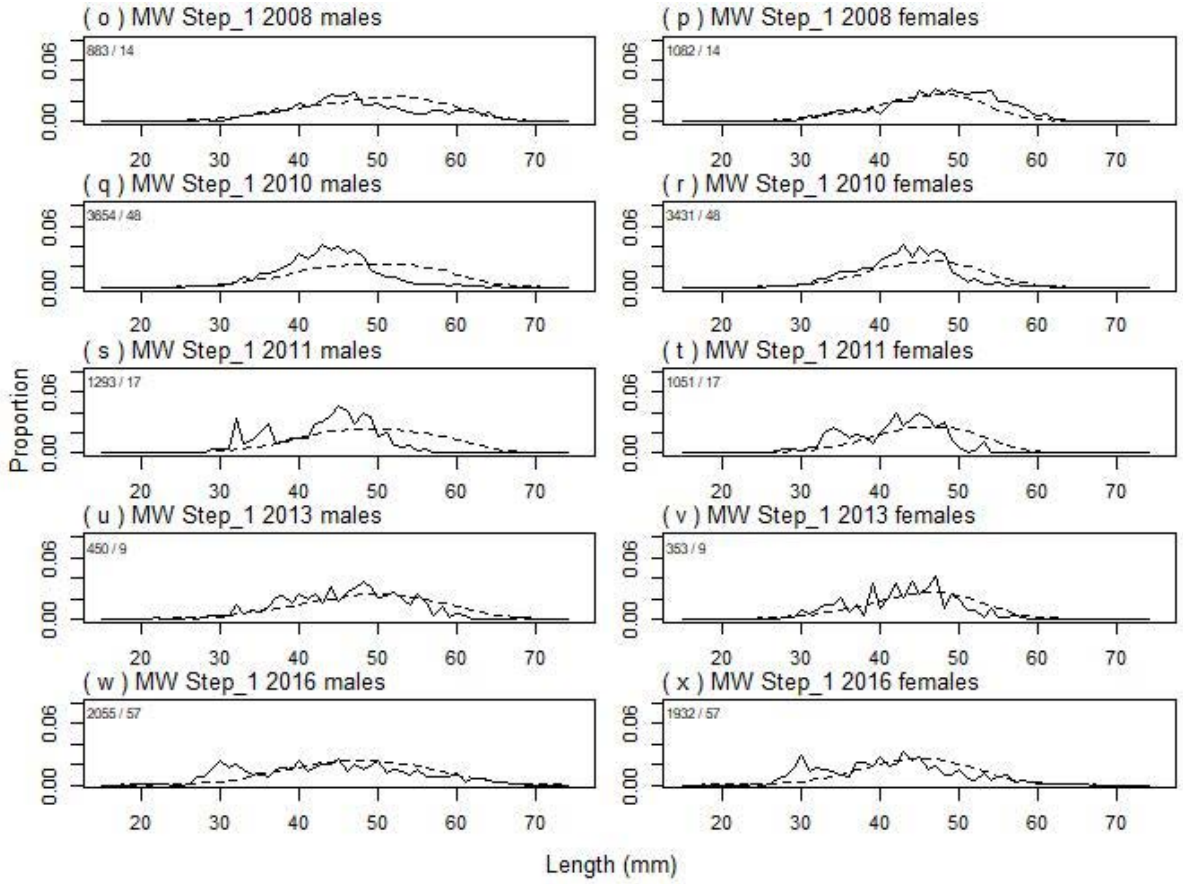

A6. 39 *continued*: Observed (solid line) and fitted (dashed line) length frequency distributions for observer samples, MW time step 1. Numbers in top left corner of each plot represent number of scampi measured / number of events sampled.

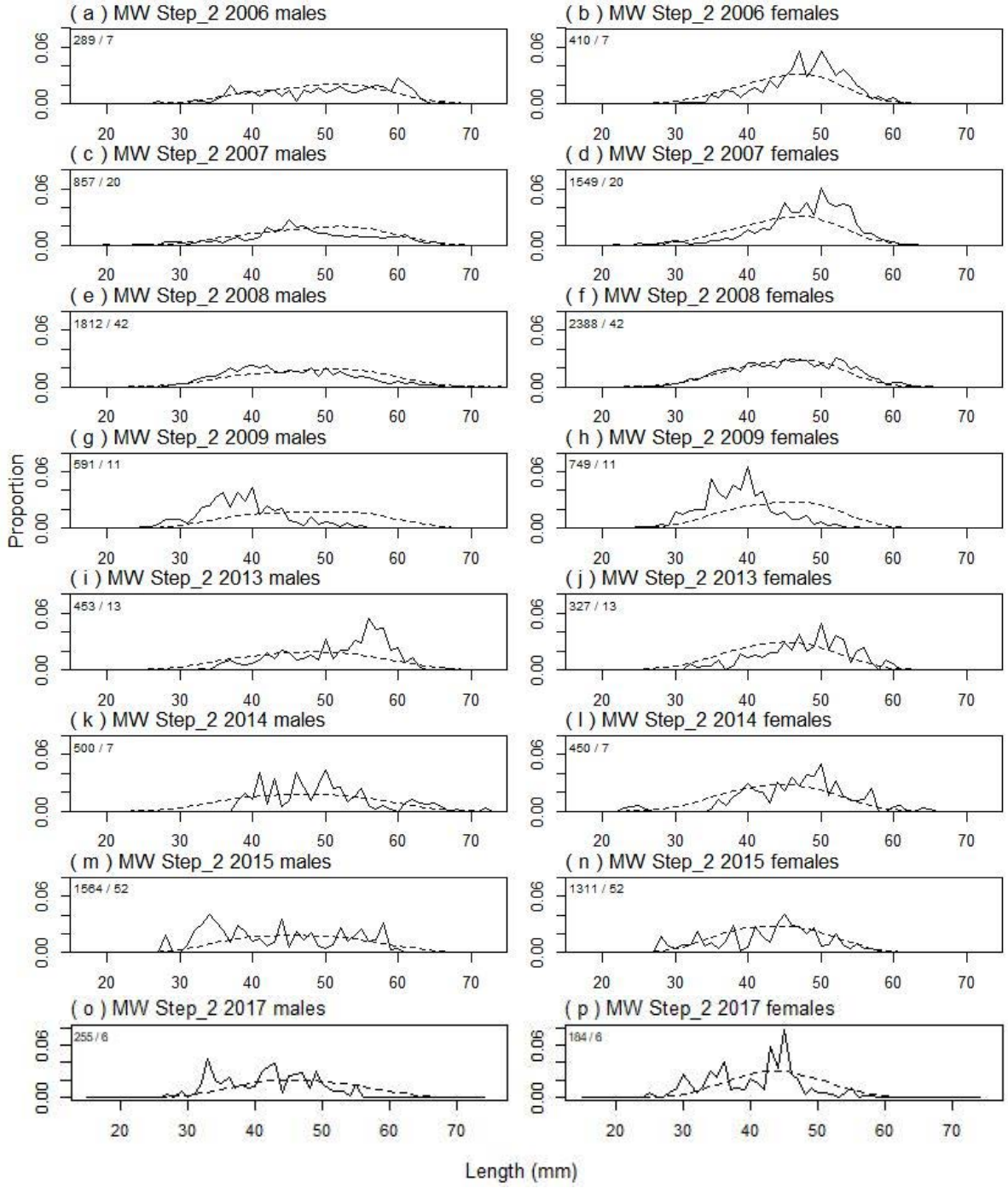

A6. 40: Observed (solid line) and fitted (dashed line) length frequency distributions for observer samples, MW time step 2. Numbers in top left corner of each plot represent number of scampi measured / number of events sampled.

A6. 41: Numbers of scampi measured, estimated multinomial N sample size, and effective sample size used within the model for length frequency distributions for observer samples, MW time step 1.

	Measured	Multinomial N	Effective sample size
N_1992	107	216	0.50
N_1998	528	394	0.90
N_2000	700	631	1.45
N_2001	169	341	0.78
N_2003	400	796	1.83
N_2005	1 985	908	2.09
N_2007	1 669	1 418	3.26
N_2008	1 965	1 743	4.00
N_2010	7 085	6 257	14.37
N_2011	2 344	1 739	3.99
N_2013	803	583	1.34
N_2016	3 987	3 475	7.98

A6. 42: Numbers of scampi measured, estimated multinomial N sample size, and effective sample size used within the model for length frequency distributions for observer samples, MW time step 2.

	Measured	Multinomial N	Effective sample size
N_2006	699	790	3.47
N_2007	2 406	2 144	9.41
N_2008	4 200	3 081	13.52
N_2009	1 340	1 366	5.99
N_2013	780	483	2.12
N_2014	950	1 710	7.50
N_2015	2 875	638	2.80
N_2017	439	232	1.02

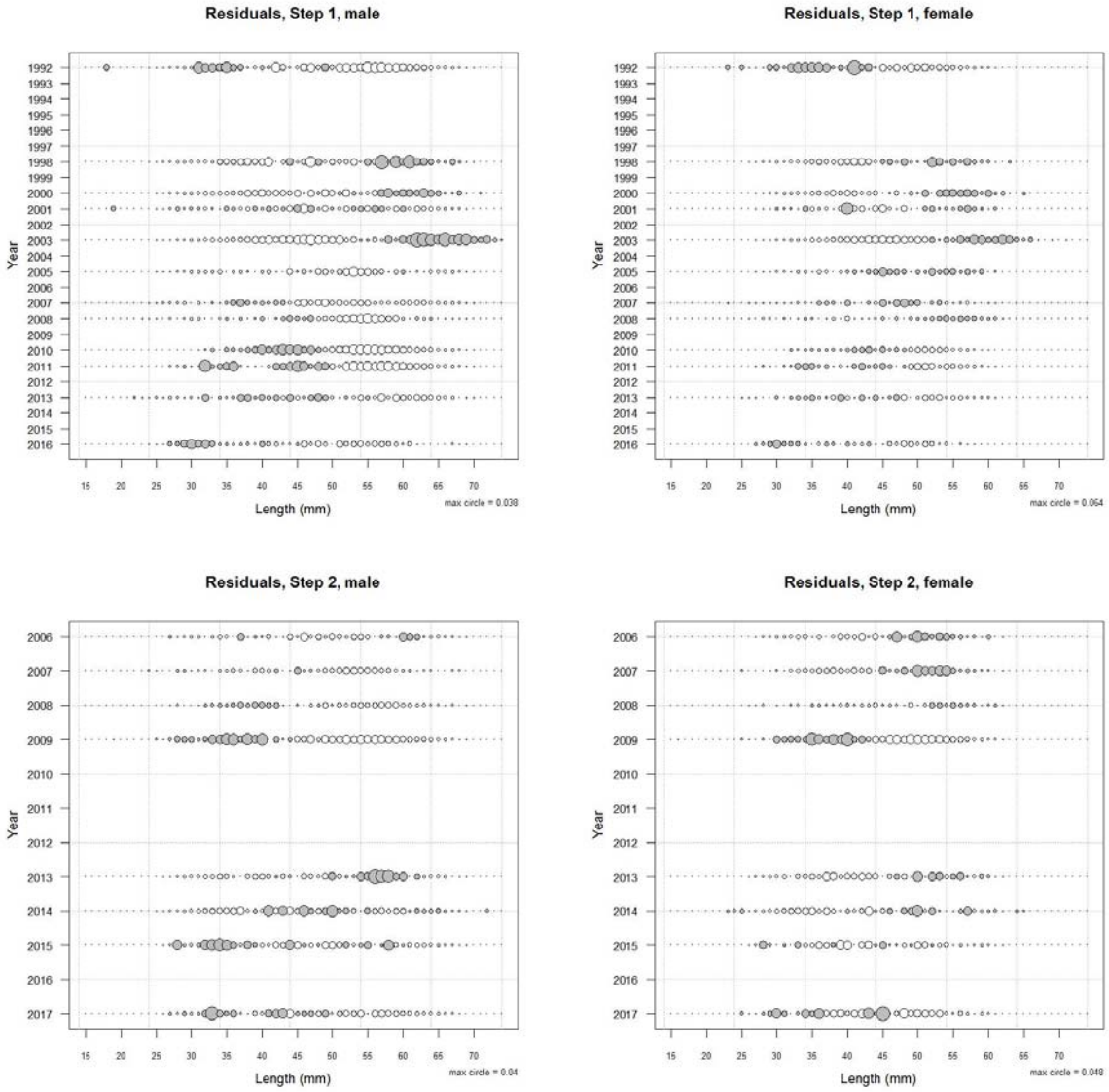

A6. 43: Bubble plots of residuals for fits to length frequency distributions for MW observer sampling.

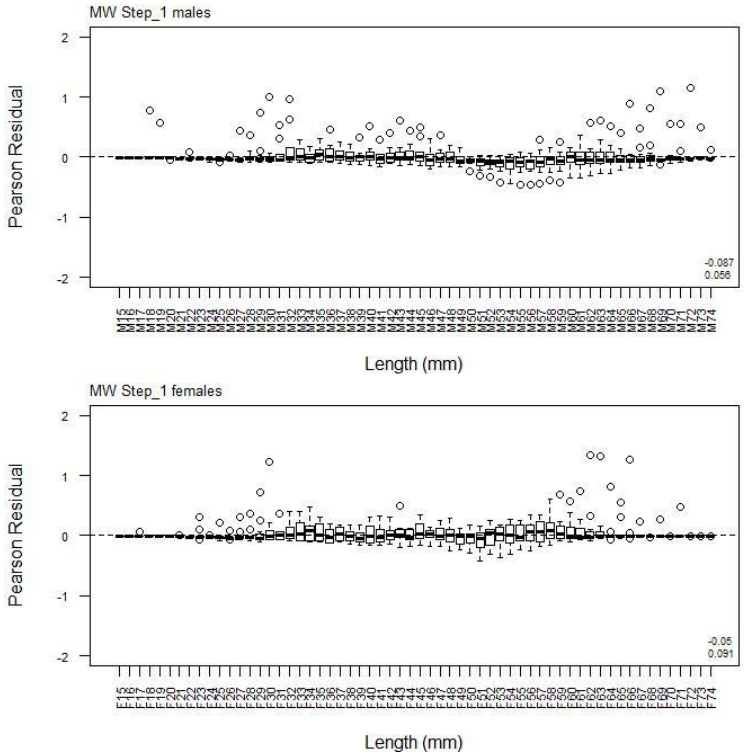

A6. 44: Box plots of Pearson residuals from the fit to length frequency distributions by length from observer sampling by sex for MW time step 1.

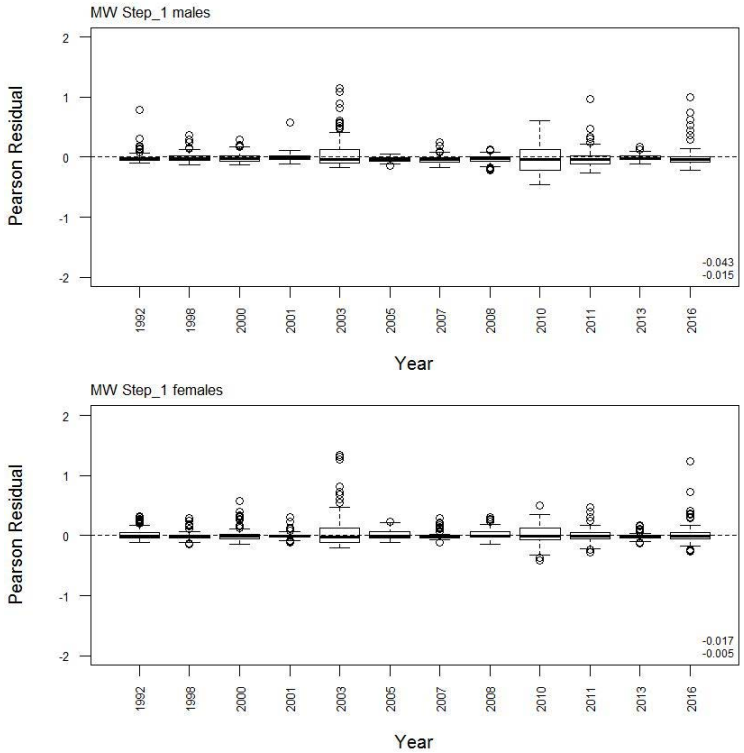

A6. 45: Box plots of Pearson residuals from the fit to length frequency distributions by year from observer sampling by sex for MW time step 1.

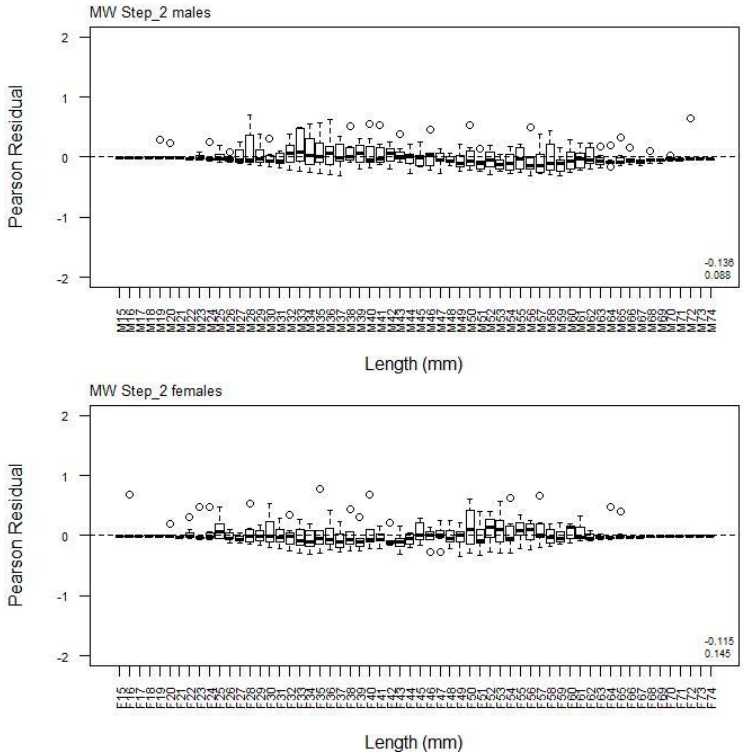

A6. 46: Box plots of Pearson residuals from the fit to length frequency distributions by length from observer sampling by sex for MW time step 2.

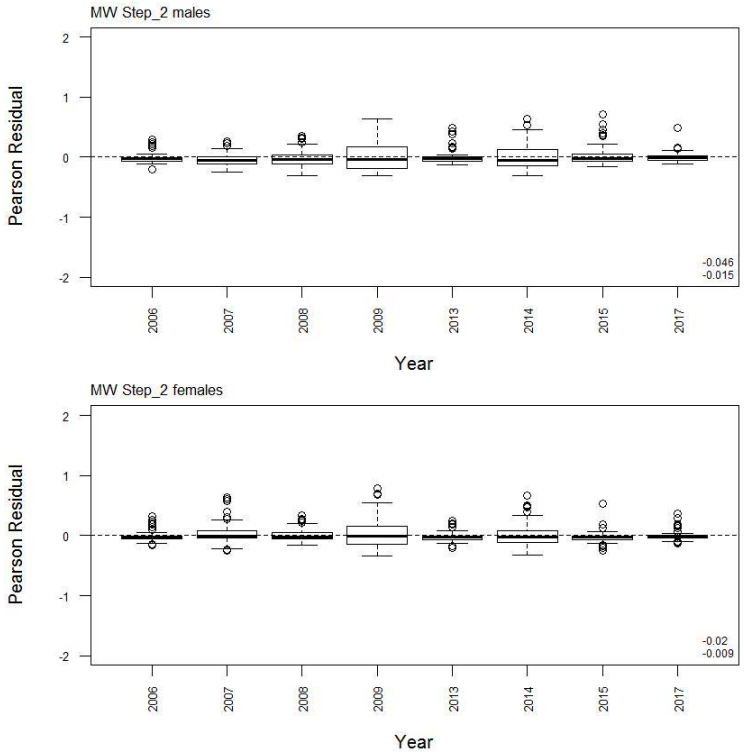

A6. 47: Box plots of Pearson residuals from the fit to length frequency distributions by year from observer sampling by sex for MW time step 2.

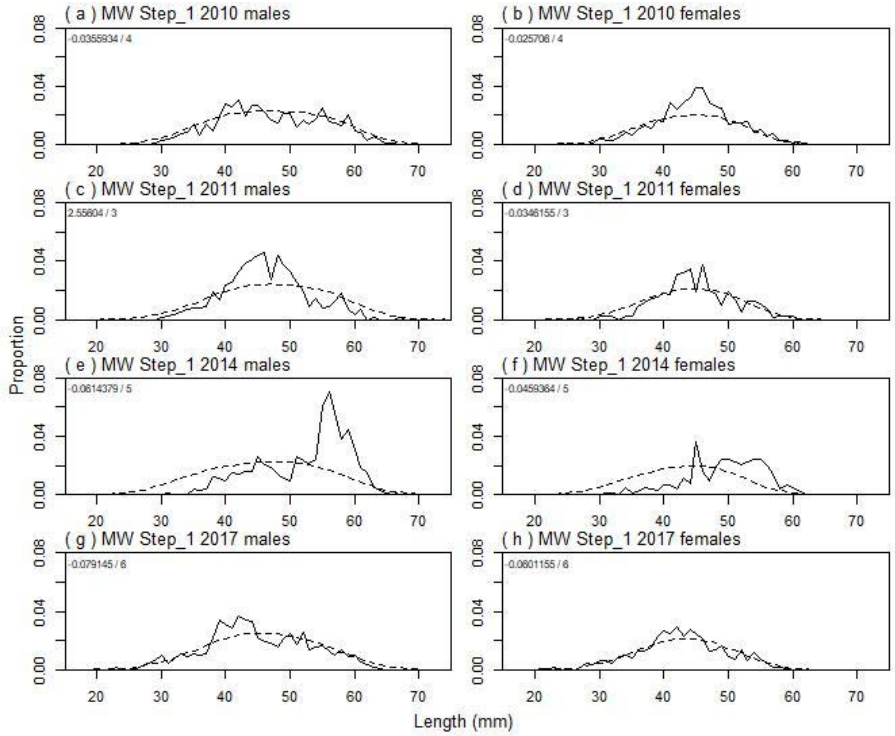

A6. 48: Observed (solid line) and fitted (dashed line) length frequency distributions for MW research survey samples.

A6. 49: Numbers of scampi measured, estimated multinomial N sample size, and effective sample size used within the model for length frequency distributions for MW research survey samples.

	Measured	Multinomial N	Effective sample size
N_2010	1 110	1 140	9.88
N_2011	876	1 011	8.76
N_2014	710	681	5.90
N_2017	1 734	1 776	15.38

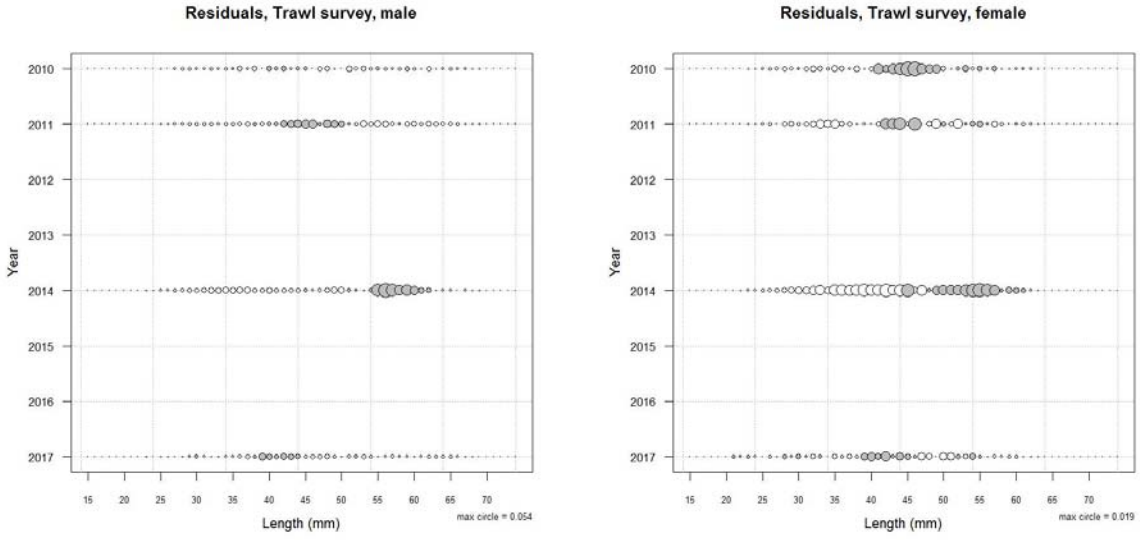

A6. 50: Bubble plots of residuals for fits to length frequency distributions for MW trawl sampling.

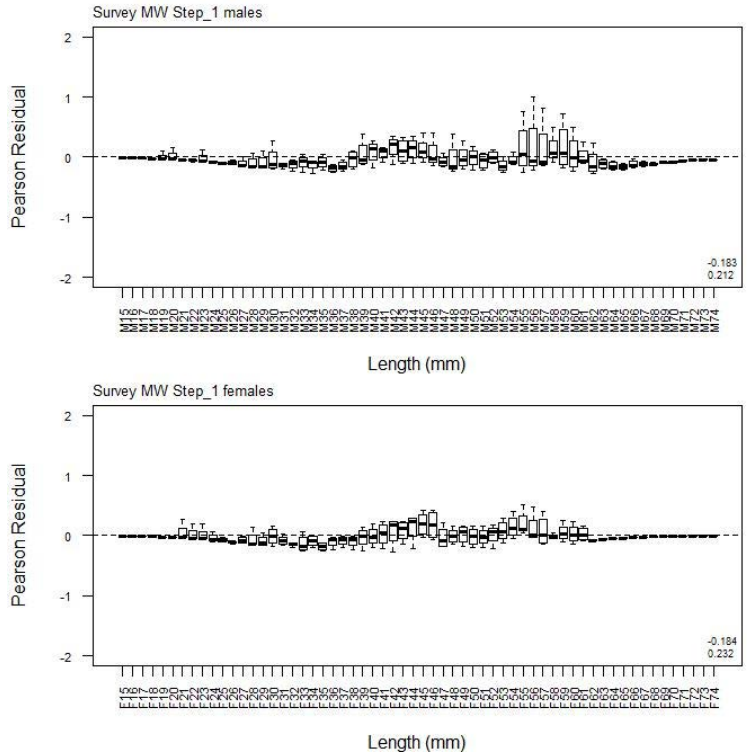

A6. 51: Box plots of Pearson residuals from the fit to length frequency distributions by length from MW trawl sampling.

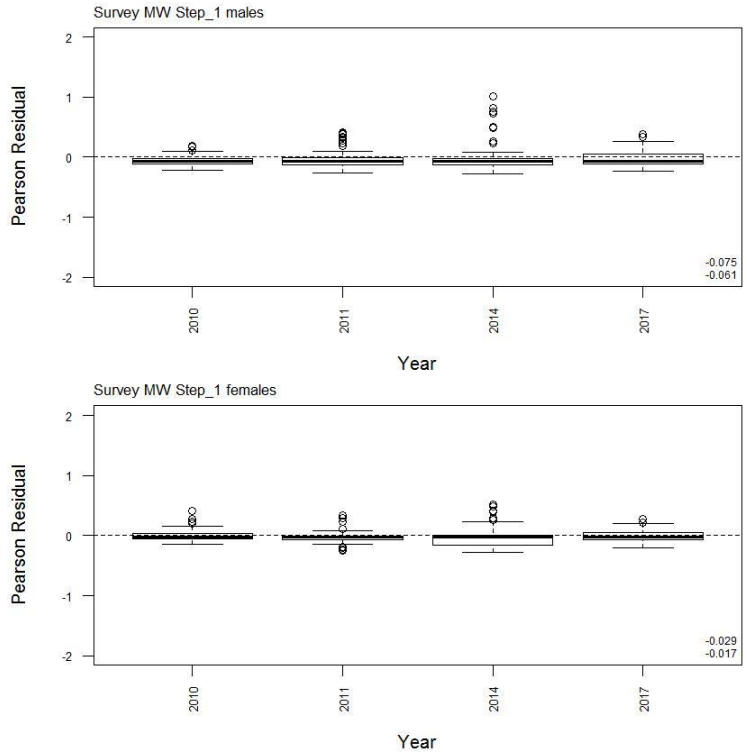

A6. 52: Box plots of Pearson residuals from the fit to length frequency distributions by year from MW trawl sampling.

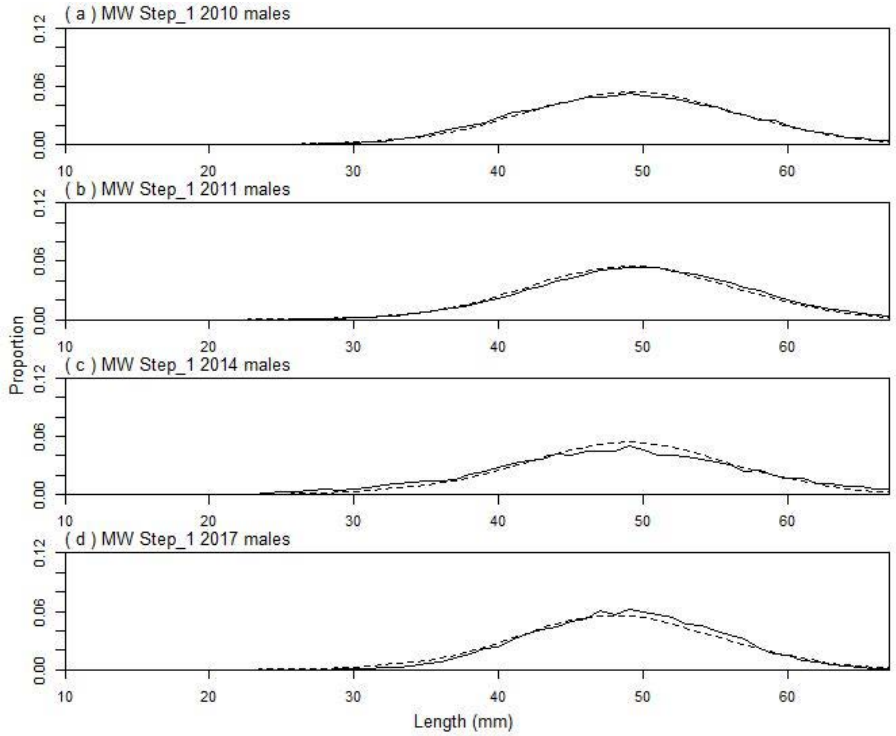

A6. 53: Observed (solid line) and fitted (dashed line) length frequency distributions for MW photographic survey scampi size estimation.

A6. 54: Numbers of scampi measured, estimated multinomial N sample size, and effective sample size used within the model for length frequency distributions for MW photographic survey samples.

	Measured	Multinomial N	Effective sample size
N_2010	173	298	533.11
N_2011	128	227	406.09
N_2014	24	48	85.87
N_2017	23	46	82.29

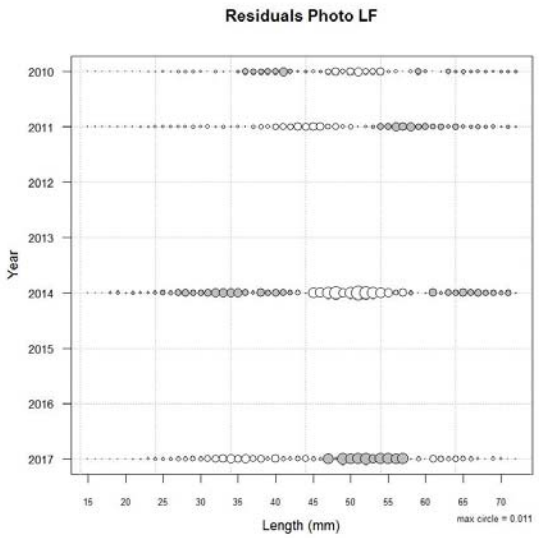

A6. 55: Numbers of scampi measured, estimated multinomial N sample size, and effective sample size used within the model for length frequency distributions for MW photographic survey samples.

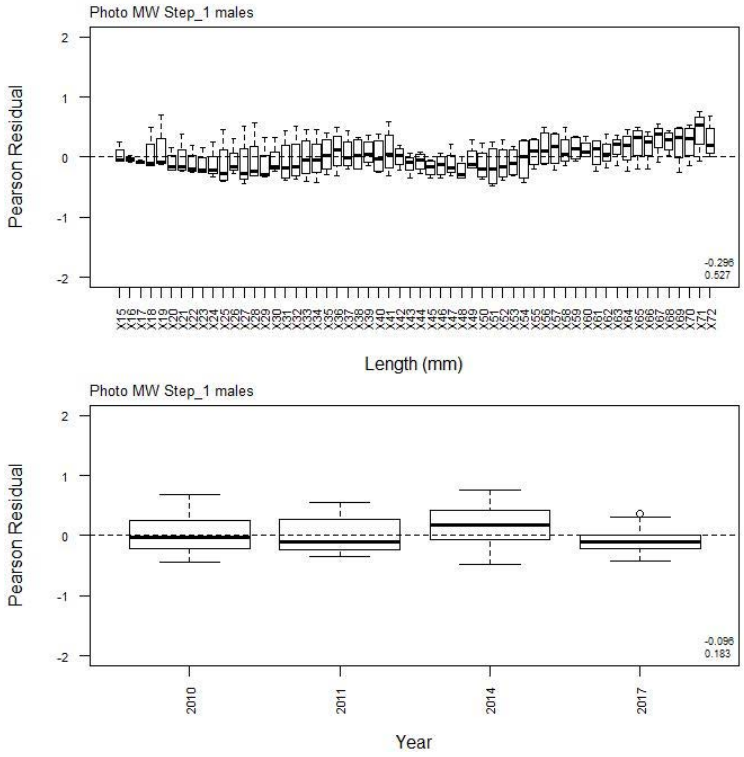

A6. 56: Box plots of Pearson residuals from the fit to length frequency distributions by length and year for MW photographic sampling.

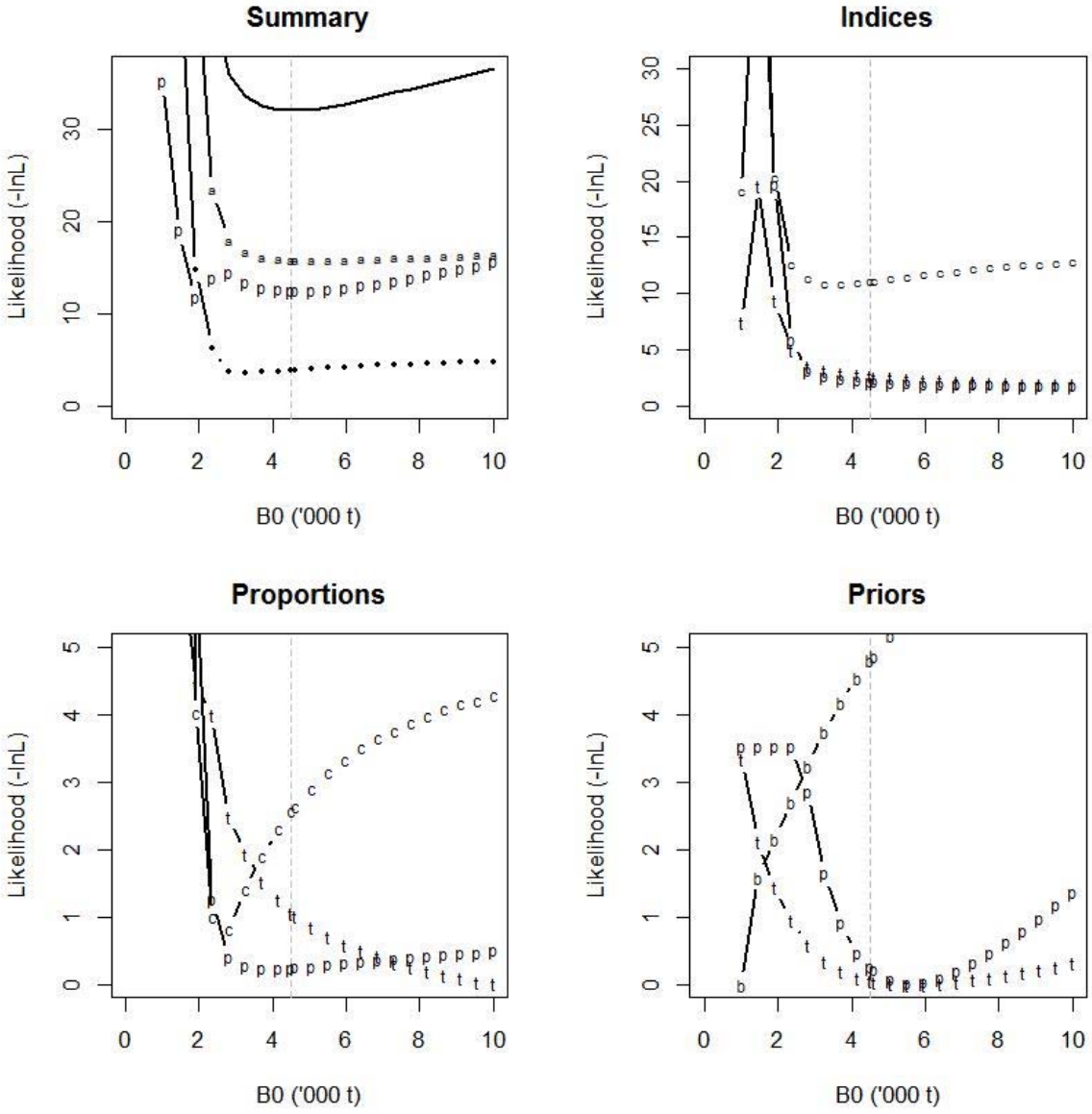

A6. 57: Likelihood profiles for SCI 3 Model 4 when B_0 is fixed in the model. Figures show profiles for main priors (top left, p – priors, a – abundance indices, • – proportions at length), abundance indices (top right, t – trawl survey, c – CPUE, p – photo survey), proportion at length data (bottom left, t –trawl, c – observer, p – photo) and priors (bottom right, b – B_0, p – *q-Photo*, t – *q-Trawl*). Vertical dashed line represents MPD.

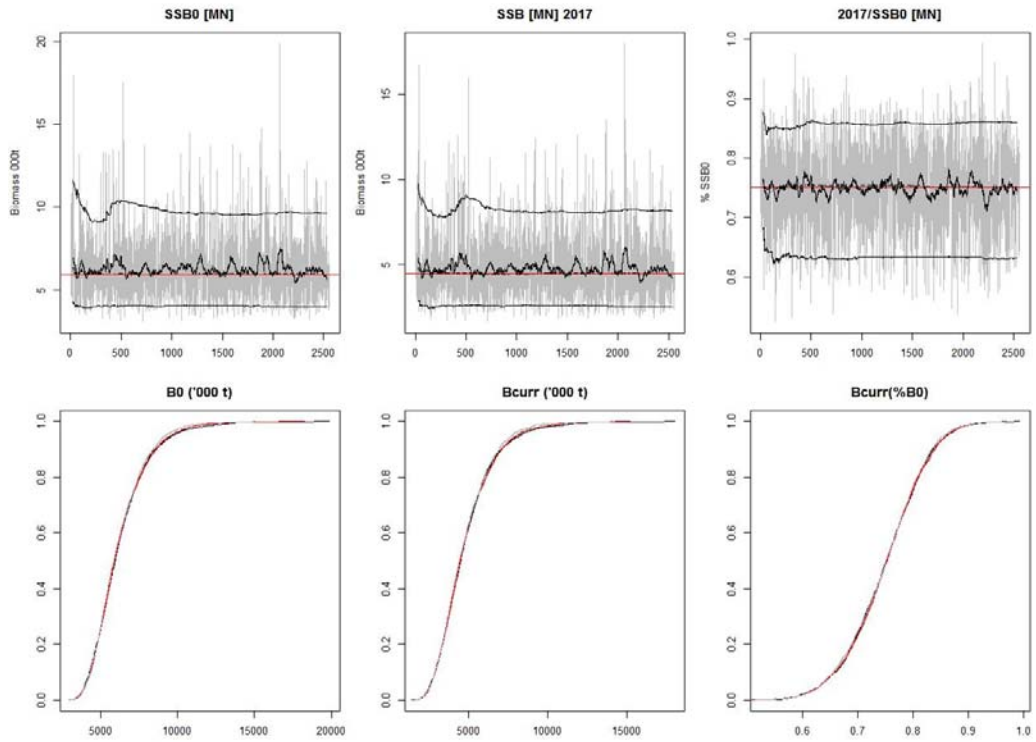

A6. 58: MCMC traces for MN SSB_0, SSB_{2017}, and SSB_{2017}/SSB_0 terms for SCI 3 Model 4 (nuisance q)(trace – grey line, cumulative moving median – dashed black line, moving average and cumulative moving 2.5%, 97.5% quantiles – solid black lines, overall median – solid red line, left plots); and cumulative frequency distributions for three independent MCMC chains (shown as red, grey, and black lines, right plots).

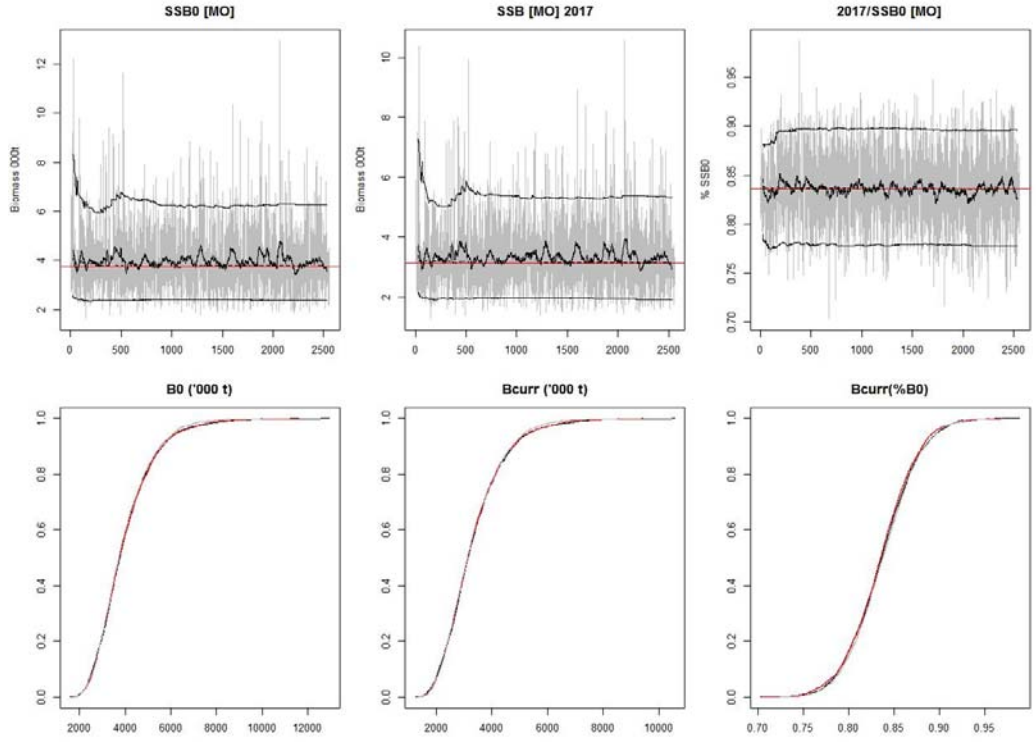

A6. 59: MCMC traces for MO SSB_0, SSB_{2017}, and SSB_{2017}/SSB_0 terms for SCI 3 Model 4 (nuisance q)(trace – grey line, cumulative moving median – dashed black line, moving average and cumulative moving 2.5%, 97.5% quantiles – solid black lines, overall median – solid red line, left plots); and cumulative frequency distributions for three independent MCMC chains (shown as red, grey, and black lines, right plots).

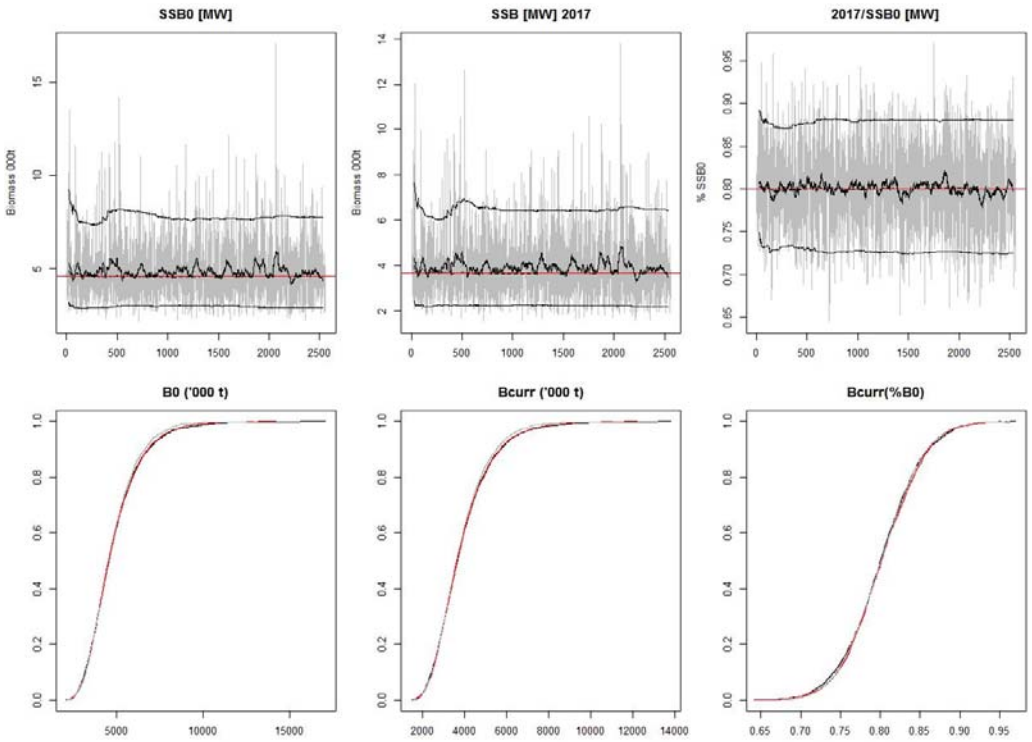

A6. 60: MCMC traces for MW SSB_0, SSB_{2017}, and SSB_{2017}/SSB_0 terms for SCI 3 Model 4 (nuisance q)(trace – grey line, cumulative moving median – dashed black line, moving average and cumulative moving 2.5%, 97.5% quantiles – solid black lines, overall median – solid red line, left plots); and cumulative frequency distributions for three independent MCMC chains (shown as red, grey, and black lines, right plots).

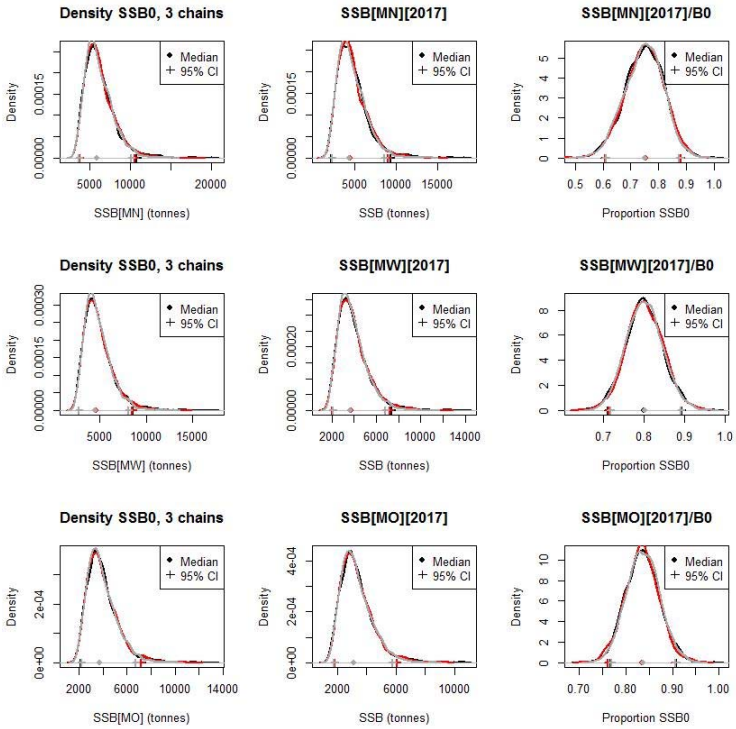

A6. 61: Density plots for SSB_0, SSB_{2017}, and SSB_{2017}/SSB_0 terms for each subarea of SCI 3 Model 4 for three independent MCMC chains, with median and 95% confidence intervals.

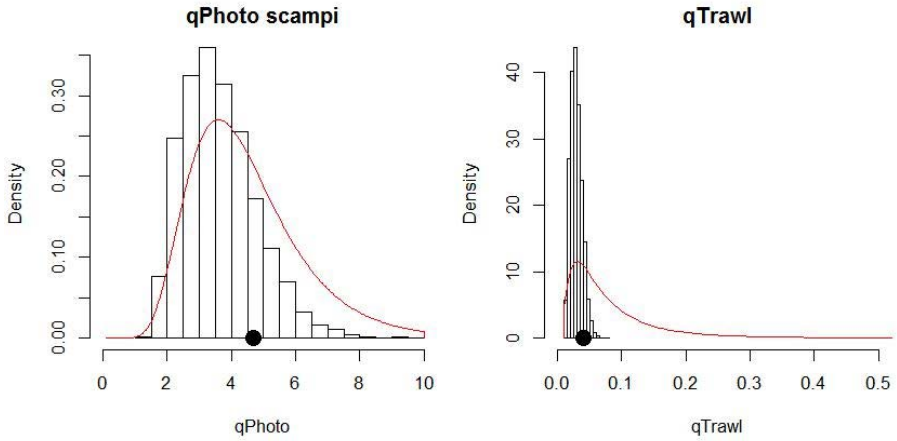

A6. 62: Marginal posterior distributions (histograms), MPD estimates (solid symbols), and distributions of priors (lines) for catchability terms.

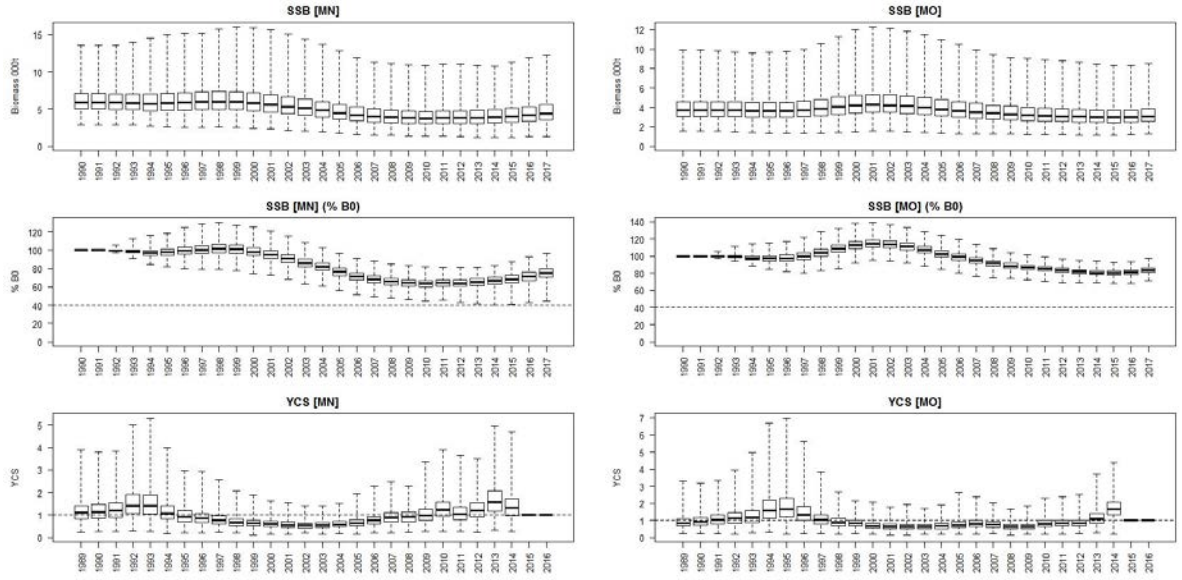

A6. 63: Posterior trajectory of *SSB*, SSB_{2016}/SSB_0, and YCS for subareas MN and MO.

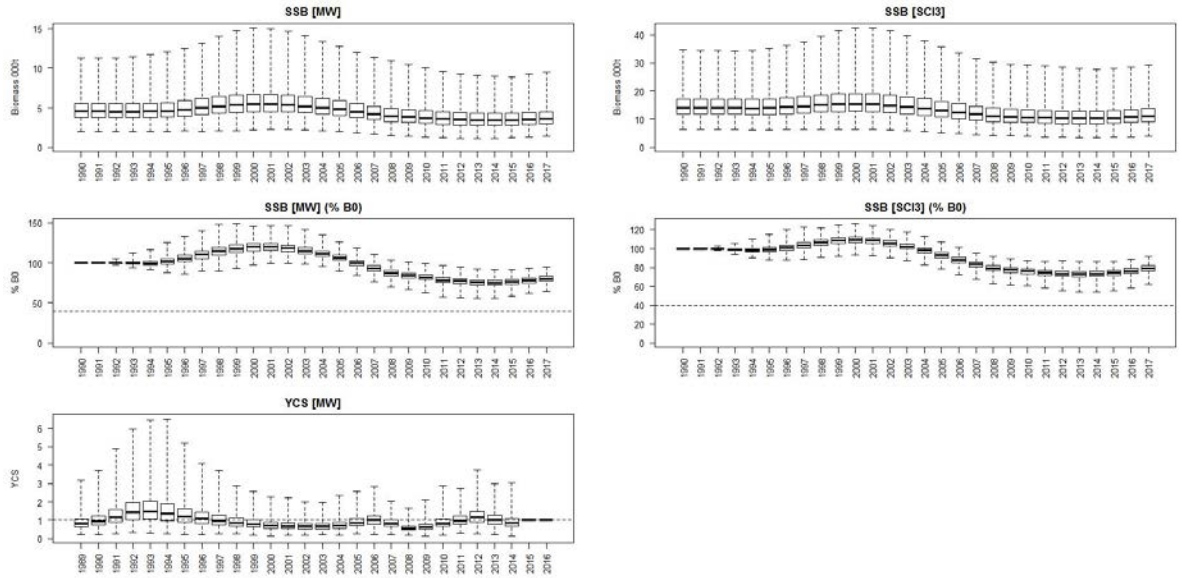

A6. 64: Posterior trajectory of *SSB*, SSB_{2016}/SSB_0, and YCS for subareas MW and the combined SCI 3 modelled area.